PHYSICAL VOLCANOLOGY, STRATIGRAPHY, AND LITHOGEOCHEMISTRY OF AN ARCHEAN VOLCANIC ARC: EVOLUTION FROM PLUME-RELATED VOLCANISM TO ARC RIFTING WITHIN THE SE ABITIBI GREENSTONE BELT, VAL D'OR, QUÉBEC, CANADA

By

Craig Russell Scott

Submitted in partial fulfillment of the Requirements
For the Degree of Doctor of Philosophy

at

Université de Québec à Chicoutimi
Chicoutimi, Québec

ABSTRACT

The 2714-2702 Ma eastern segment of the Southern Volcanic Zone (SVZ) of the Abitibi Greenstone Belt is a complex sequence of volcano-sedimentary rocks cut by syn- to post-volcanic plutonic suites. This segment can be subdivided into two stratigraphic groups based on regional tectonics and volcano-sedimentary stratigraphy: the basal Malartic Group, composed of the La Motte-Vassan, Dubuisson, and Jacola formations, and the overlying Louvicourt Group, containing the Val d'Or and Héva formations. The Malartic Group represents an Archean oceanic floor controlled by extensional mantle plume tectonics and characterized by effusive komatiites and basalts and intrusive dykes and sills. The Louvicourt Group marked a change to subduction-related processes; whereby incipient arc construction, represented by the lower Val d'Or Formation, overlapped with the waning stages of plume-generated volcanism, represented by the Jacola Formation. This contemporaneous volcanic activity indicates a conformable relationship. Subsequent rifting, represented by the Héva Formation, formed voluminous lavas that flooded the arc-related lavas.

The Jacola Formation is characterized by komatiitic and Mg-rich basalt, which is related to a mantle-plume source, that formed an extensive tholeiitic submarine lava plain. The contact between the mafic-ultramafic Jacola Formation and the intermediate-felsic Val d'Or Formation is gradational and indicated by the first appearance of voluminous volcaniclastic (i.e., fragmental) deposits that are tholeiitic to transitional and have a geochemical arc-signature.

The 3-5 km-thick Val d'Or Formation is a complex subaqueous volcano-sedimentary arc composed of numerous sequences of discontinuous and laterally interstratified intermediate to felsic lavas and their associated volcaniclastic deposits that evolved from tholeiitic to calc-alkaline. These small volume sequences are composed of

1-100 m-thick massive, pillowed/lobate, and brecciated lavas flows that are variably vesicular (1-30-vol%) and interstratified with 1-50 m-thick amalgamated volcaniclastic deposits of normal- to reverse-graded beds composed of angular to subrounded tuff- to breccia-sized clasts and a vesicularity index between 15 to 35-vol%. In addition, numerous small felsic-dominated volcanic centers of limited areal extent, containing massive sulfide deposits, define the Val d'Or Arc. Contact between the Val d'Or and Héva formations is defined by the abrupt appearance of tholeiitic lavas, represented by a tholeiitic spherulitic felsic unit at the base of the Héva Formation.

The 2-3 km-thick tholeiitic Héva Formation is characterized by effusive mafic and felsic volcanism with local volcaniclastic deposits. The basal spherulitic unit is traceable for 40 km along strike, thereby serving as a marker horizon for the base of Louvicourt Group. A polymictic tuff breccia sequence, located stratigraphically above the spherulitic unit, is composed of reworked mafic to felsic fragments that have a geochemical arc-signature, suggesting they originated from the underlying Val d'Or Formation. This implies that the Val d'Or Formation is younger and has a conformable relationship with the Héva Formation. Up-section, massive to pillowed mafic flows with gabbroic dykes and sills are dominant, suggesting more fissural-type volcanism. Local tuff turbidites and reworked scoriaous pyroclastic deposits attest to explosive eruption(s).

The Jacola Formation represents a deep marine, ridge-like oceanic setting controlled by mantle plume volcanism, which formed the base for arc construction, as well as contaminating the early lavas. Intermediate volcaniclastic rocks and lavas at the base of the Val d'Or Formation indicate subduction-related volcanism. The tholeiitic Héva Formation indicates a return to an extensional regime with fissure-type volcanism during arc dissection. The Val d'Or Arc forms a monocline, south-facing volcano-sedimentary succession evolving from plume- to subduction-related volcanism.

RÉSUMÉ

Le segment Est (2714-2702 Ma) de la Zone Volcanique Sud (ZVS) dans la ceinture de roches vertes de l'Abitibi est une séquence complexe de roches volcano-sédimentaires coupées par les suites plutoniques syn- et post-volcaniques. Ce segment peut être subdivisé en deux groupes stratigraphiques basés sur la tectonique régionale et la stratigraphie volcano-sédimentaire : le Groupe de Malartic à la base, composé des formations de La Motte-Vassan, de Dubuisson, et de Jacola, et au-dessus, le Groupe de Louvicourt, contenant les formations de Val-d'Or et d'Héva. Le Groupe de Malartic représente une plate-forme océanique archéenne contrôlée par l'extension tectonique due à une plume du manteau et caractérisée par les komatiites et les basaltes effusifs et les filons-couches et dykes. Le Groupe de Louvicourt a marqué un changement vers des processus associés à une subduction; le début de la construction d'arc, représentée par la Formation de Val-d'Or inférieure, s'est produit simultanément avec les étapes d'affaiblissement du volcanisme de plume, représentées par la Formation de Jacola. Cette activité volcanique contemporaine indique une relation conforme. L'extention qui suivit, représentée par la Formation d'Héva, a formé les laves volumineuses qui ont inondé les laves associées au volcanisme d'arc.

La Formation de Jacola est caractérisée par des komatiitiques et basaltes riches en Mg, liés à une source de plume du manteau, qui ont formé une grande plaine sous-marine de lave tholéiitique. Le contact entre la Formation de Jacola mafique-ultramafique et la Formation de Val-d'Or intermédiaire-felsique est graduel et indiqué par l'apparition (i.e.,

fragmentaire) de dépôts volcaniclastiques volumineux qui sont tholéiitiques à transitoires et qui ont une signature géochimique d'arc.

La Formation de Val-d'Or de 3-5 km d'épaisseur est un arc volcano-sédimentaire subaquatique complexe composé de nombreuses séquences de laves intermédiaires à felsiques discontinues et latéralement interstratifiées et de leurs dépôts volcaniclastiques associés qui ont évolué de tholeiitique à calco-alkalins. Ces petites sequences se composent de coulées de laves massives, coussinées/lobées, et bréchifiées, de 1 à 100 m d'épaisseur, qui sont vésiculaires de façon variable (1-30-vol%) et interstratifiées avec des dépôts volcaniclastiques amalgamés, 1 à 50 m d'épaisseur, de lits normal à renversé composés de fragments angulaires à subarrondis de grosseur tuff à brèche et un indice de vésicularité entre 15 et 35-vol%. De plus, de nombreux petits centres volcaniques à dominance felsiques d'ampleur régionale limitée, contenant les gisements massifs de sulfures, définissent l' Arc de Val-d'Or. Le contact entre les formations de Val-d'Or et d'Héva est défini par l'apparition soudaine de laves tholeiitiques, et est représenté par une unité felsique sphérulitique tholeiitique à la base de la Formation d'Héva.

La Formation d'Héva tholeiitique de 2 à 3 km d'épaisseur est définie par le volcanisme mafique effusif et felsique avec des dépôts volcaniclastiques locaux. L'unité sphérulitique à la base de la Formation d'Héva est décelable pour 40 kilomètres, servant (de ce fait) d'horizon-repère au Groupe de Louvicourt. Une séquence de tufs bréchiques polymictiques, située stratigraphiquement au-dessus de l'unité sphérulitique, se compose de fragments mafiques et felsiques remoblisés qui ont une signature géochimique d'arc, suggérant qu'ils sont provenus de la Formation de Val-d'Or sous-jacente. Ceci implique

que la Formation de Val-d'Or est plus jeune et a une relation conforme avec la Formation d'Héva. Vers le haut de la stratigraphie, des coulées de lave mafique massives à coussinées avec des dykes et filons-couches de gabbro dominent, suggérant des éruptions plus fissurales. Les tufs turbiditiques locaux et les dépôts pyroclastiques scorieux remoblisés certifient une/deséruption(s) explosif(ves).

La Formation de Jacola représente un environnement marin profond semblable à une dorsale médio-océanique, controlé par le volcanisme de plume de manteau, qui a formé la base pour la construction d'un arc, et a contaminé les premières laves. Les roches volcaniclastiques intermédiaires et les laves à la base de la Formation de Val-d'Or indiquent le volcanisme relié à une subduction. La Formation d'Héva tholéiitique indique un retour à un régime d'extension avec le volcanisme fissural pendant la dissection d'arc. L'Arc de Val-d'Or forme une séquence monoclinale volcano-sédimentaire, de polarité vers le sud, évoluant du volcanisme associé à une plume au volcanisme associé à une subduction.

Quotation:

I learned this, at least, by my experiment; that if one advances confidently in the direction of one's dreams, and endeavors to live the life which he has imagined, he will meet with a success unexpected in common hours.

From Walden: Henry David Thoreau

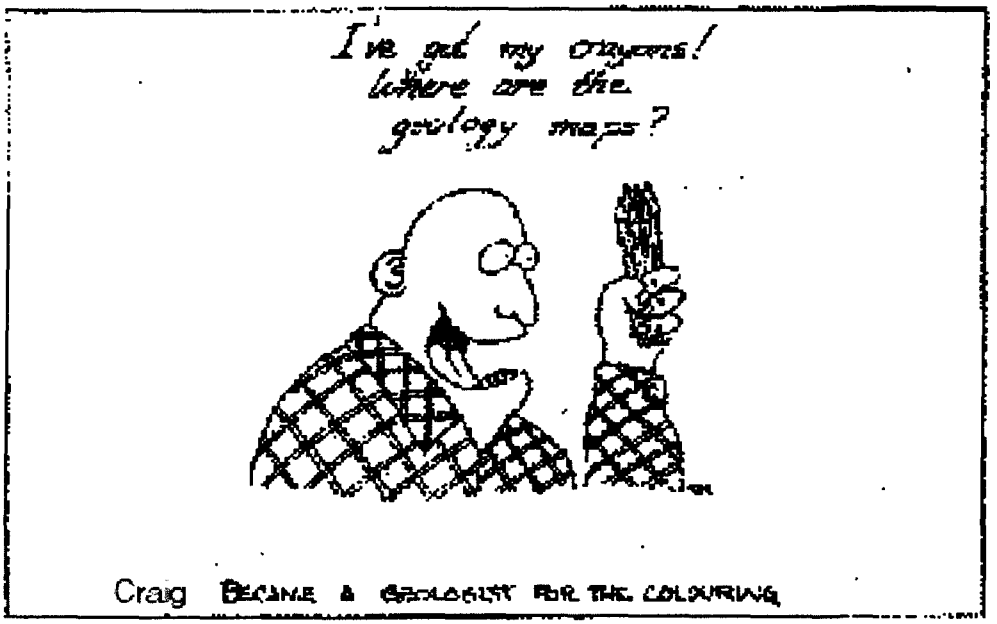

Table of Contents

Title page..... i
Signature Page..... ii
Copyright agreement form..... iii
Abstract..... iv
Résumé..... vi
Table of Contents..... x
List of Figures xiv
List of Tables xxiii
Acknowledgements..... xxiv

1 INTRODUCTION..... 1
1.1 Statement of Purpose..... 3
1.2 Aims and Objectives..... 6
1.3 Methodology..... 7
1.4 Terminology..... 9
1.5 Organization..... 14
1.6 Corroboration..... 14

2 GEOLOGY..... 16
2.1 Abitibi Geology..... 16
2.2 Malartic Block of the SVZ..... 21
2.2.1 Southern Malartic Block: formations within the study area..... 26
2.3 Geodynamic Models for the Malartic Block..... 30

3 JACOLA FORMATION: AN OCEANIC PLATFORM..... 35
3.1 Reasoning..... 37
3.2 Characteristics of the Jacola Formation..... 37

3.3	Interpretation	50
4	VAL D'OR FORMATION: ARC CONSTRUCTION	55
4.1	Lower Val d'Or Formation	57
4.1.1	Base of the sequence; Val d'Or Playground (ROI 1)	57
4.1.1.1	Description of playground stratigraphy	57
4.1.1.2	Interpretation of playground stratigraphy	68
4.1.2	Placer Dome North (ROI 2)	73
4.1.2.1	Description of outcrop characteristics	75
4.1.2.2	Interpretation of Placer Dome North stratigraphy	93
4.1.3	East Sullivan Outcrops (ROI 3)	101
4.1.3.1	Lithology of outcrops	101
4.1.3.2	Pole Line Deposits	119
4.1.3.3	Interpretation of lithofacies	126
4.1.4	Manitou Area (ROI 4)	130
4.1.4.1	Interpretation of Manitou area	135
4.1.5	Camnet Area (ROI 5)	136
4.1.5.1	Lithology and Stratigraphy of Camnet Area	138
4.1.5.2	Interpretation of Camnet area	152
4.2	Upper Val d'Or Formation	155
4.2.1	Study of Relais area (ROI 6)	155
4.2.1.1	Lithology and stratigraphy of Relais area	157
4.2.1.2	Interpretation of Relais area (ROI 6)	166
4.2.2	Dunraine east (ROI 7)	169
4.2.2.1	Lithology and stratigraphy of Dunraine east area	170
4.2.2.2	Interpretation of Dunraine East	182
4.2.3	Abitibi Copper area (ROI 8)	184
4.2.3.1	Lithology and stratigraphy of Abitibi Copper	184
4.2.3.2	Interpretation of Abitibi Copper stratigraphy	194

4.2.4	Sleepy Lake Area (ROI 9)	196
4.2.4.1	Lithology and stratigraphy of Sleepy Lake area	196
4.2.4.2	Interpretation of Sleepy Lake area	206
4.2.5	Dunraine west area (ROI 10)	212
4.2.5.1	Lithology and stratigraphy of Dunraine west	212
4.2.5.2	Interpretation of Dunraine west area	221
4.3	Stratigraphic Top: South or North?	223
4.4	Subaqueous volcanism – explosive or non-explosive behavior	224
4.4.1	Subaqueous phreatomagmatic eruptions	226
4.4.2	Archean subaqueous phreatomagmatic examples	228
4.4.3	Subaqueous magmatic eruptions	231
5	HÉVA FORMATION: ARC RIFTING	236
5.1	Felsic spherulitic unit	239
5.1.1	Lithology of felsic spherulitic unit	241
5.1.2	Interpretation of felsic spherulitic unit	255
5.1.3	Model of emplacement	257
5.2	Tex-Sol area (volcaniclastic facies)	262
5.2.1	Lithology of Tex-Sol area	262
5.2.2	Interpretation of Tex-Sol area	268
5.3	Akasaba North area (ROI 3)	272
5.3.1	Lithology of Akasaba North	273
5.3.2	Interpretation	291
5.4	Akasaba South (ROI 4)	297
5.4.1	Lithology of Akasaba South	299
5.4.2	Interpretation of Akasaba South	306
6	GEOCHEMISTRY & GEOCHRONOLOGY	309
6.1	Geochemical Characteristics	310

6.2	Major Element Geochemistry	313
6.3	Geochemical Trends	319
6.4	Rare Earth and Trace Elements	323
6.4.1	Discussion of REE and multi-element diagrams	330
6.5	Discrimination Diagrams	334
6.4	Geochronology	336
7	DISCUSSION	337
7.1	Subaqueous Volcanism	338
7.2	Geochemical and Geochronological Support	340
7.3	Paleogeographic Reconstruction	346
7.4	VMS Deposition	354
7.5	Comparison between Modern and Archean Arc Systems	356
7.6	Autochthonous or Allochthonous? A final Word	358
8	CONCLUSIONS	361
	BIBLIOGRAPHY	368
	APPENDICES	391

List of Figures

Chapter 1		
Figure 1:	Proposed stratigraphy of the Malartic Block	5
Chapter 2		
Figure 2:	Superior Province Map	17
Figure 3:	Abitibi Geology Map	18
Figure 4:	Map of metamorphic grade within the Abitibi Greenstone Belt	22
Figure 5A:	Various stratigraphic interpretations of Malartic Block	24
Figure 5B:	Imreh correlation of the Malartic Block	27
Figure 6:	Regional geology map of the Val d'Or region	28
Figure 7:	Block diagram outlining the comparable formations/domains	29
Figure 8:	Geodynamic models of Desrochers	31
Figure 9:	Geodynamic model of Dimroth	33
Chapter 3		
Figure 10:	Regional geology map outlining areas of interest within JF	36
Figure 11:	Location map of area studied in JF for thesis with formational contacts	38
Figure 12:	Local geology map of JF (after Champagne 2003)	39
Figure 13:	Spinifex veins	41
Figure 14:	Spinifex in brecciated units	41
Figure 15A:	Photomicrograph of re-crystallized groundmass of komatiitic basalt	42
Figure 15B:	Photomicrograph of relict bladed pyroxene phenocryst	42
Figure 16:	Map of New Bidlamaque illustrating the transition form pillowed to massive architecture	44
Figure 17:	Photo of hyaloclastites fragments mantling tongue-like termination of mafic lava	45
Figure 18:	Photos of pillow showing younging direction	45
Figure 19:	Photo of hyaloclastites observed between pillows at New Bidlamaque – several shots of small angular fragments and elongated, tabular fragments	46
Figure 20:	Close up shot of chilled margins with varioles	46
Figure 21:	Photo of BP dykes cross-cutting stratigraphy of JF	48
Figure 22:	Age date of volcaniclastic facies – JF	48
Figure 23:	Lateral variations in effusive mafic volcanism	53
Figure 24:	Omarau pillows	53
Chapter 4		
Figure 25:	Regional geology map outlining areas of interest within the VDF	56

Figure 26:	Stratigraphy section from playground, lower VDF	59
Figure 27A:	Field photo of erosional features in tuff facies and isolated subrounded breccia-sized fragments.	61
Figure 27B:	Sketch of photo in A.	61
Figure 28:	Contact relationship between stratified tuff facies and feldspar-phyric facies.	62
Figure 29:	Diffuse contact between tuff and clast-supported tuff breccia facies.	62
Figure 30A:	Clast-supported nature of monolithic, weakly vesicular tuff breccia facies.	63
Figure 30B:	Sketch of figure 32A illustrating plastic deformation textures	63
Figure 31A:	Photomicrograph: chloritized chilled margin of fragment	65
Figure 31B:	Macroscopic photo of molded contact between fragment and matrix.	65
Figure 32A:	Photomicrograph: wispy, vitrophyric shards	66
Figure 32B:	Photomicrograph: wispy, vitrophyric shards	66
Figure 33:	Photomicrograph: oval, partially flattened amygdules	67
Figure 34:	Comparison to Mueller and White fire-fountain section	71
Figure 35:	Outline of outcrops of Place Dome North	74
Figure 36:	Simplified geology of PDN	76
Figure 37:	Correlated stratigraphic sections from PDN	78
Figure 38A:	Vertical transition from amoeboidal to bun-shaped pillows	79
Figure 38B:	Amoeboidal pillows from PDN	79
Figure 38C:	Spatter-like lava morphology	80
Figure 38D:	Amoeboid morphology	80
Figure 39:	Vertical and lateral transition from tube-like pillows to breccia	82
Figure 40:	Microphotograph of pillow core of fine-grained feldspar with single quartz amygdules	82
Figure 41A:	Simplified geology of PDN reversed	83
Figure 41B:	Detailed geology showing the various volcaniclastic facies	83
Figure 41C:	One flow unit from PDN	83
Figure 42A:	Tuff strat from PDN	85
Figure 42B:	Photo of tuff facies	85
Figure 43:	Four photomicrographs of textural features of tuff and lapilli tuff facies	86
Figure 44:	Idealized debris flow section	87
Figure 45A:	Outcrop shot illustrating stratigraphy of one depositional unit	88
Figure 45B:	Close up of amoeboidal fragments at base of depositional unit	88
Figure 45C:	Flattened chloritized lapilli fragments	89
Figure 45D:	Flattened fragments and breccia-sized vesicular fragment with a possible chilled margin.	89
Figure 46:	Lateral variation in stratigraphy as illustrated by two composed stratigraphic sections.	90

Figure 47:	Sketch of possible mechanism for the formation of pillow spatter lenses.	94
Figure 48:	Monsterrat photo showing channel-like morphology of pyroclastic flow	100
Figure 49:	Correlated East Sullivan outcrops	102
Figure 50:	Western outcrop – ES	105
Figure 51:	Eastern Outcrop – ES	106
Figure 52A:	Bun-shaped pillowed from ES-west	107
Figure 52B:	Irregular shaped pillows from ES-east	107
Figure 53:	Erosive contact between irregular pillows and lapilli tuff – ES-east	108
Figure 54:	General stratigraphy documenting the relationship between tuff breccias and amoeboidal lava facies	108
Figure 55A:	Amalgamated volcaniclastic beds	109
Figure 55B:	Normally graded, clast-supported, high concentration turbidity flow (R3) composed of vesicular breccia-sized fragments that are plastically deformed when in contact with adjacent fragments.	109
Figure 56:	Stratigraphic sections from eastern outcrops	111
Figure 57:	Examples of vesicularity of fragments	112
Figure 58:	Hornblende-rich, non-vesicular fragment	113
Figure 59A/B:	Subrounded, plastically deformed breccia-sized fragments	115
Figure 59A/B:	Subrounded, plastically deformed breccia-sized fragments	116
Figure 60:	In situ brecciated fragments	118
Figure 61:	Photomicrograph of crystal tuff	118
Figure 62:	Sketch of outcrops in the area and lateral and vertical transitions	120
Figure 63A:	Bun-shaped pillows indicating southward younging direction – Pole Line	122
Figure 63B:	Lateral transition from pillowed to brecciated facies – Pole Line	122
Figure 64A:	Microphotograph of lapilli-sized, feldspar-phyric fragment	124
Figure 64B:	Microphotograph of broken, euhedral feldspar phenocrysts in matrix	124
Figure 65:	*In situ* brecciation of breccia-sized fragments.	125
Figure 66:	Field photography of lapilli tuff with larger fragments being epidotized	133
Figure 67:	Detailed map and stratigraphic section from a doubly graded tuff breccia series	134
Figure 68:	Close up of regional geology within the Camnet area.	137
Figure 69:	Massive felsic lava with *in situ* brecciation whereby fractures are filled by sericite	140
Figure 70:	Flow banded massive felsic lava.	140
Figure 71:	Amoeboidal breccia fragments in proximity to intermediate	142

	pillowed facies.	
Figure 72:	Angular to subangular mafic hyaloclastites.	142
Figure 73:	Tube-like mafic pillows	143
Figure 74:	Field sketch of small stripped outcrop illustrating contact relationships between the various facies.	145
Figure 75:	Field map of Hollow showing	146
Figure 76:	Erosive behavior of tuff breccia indicating younging direction towards the south.	147
Figure 77:	Flow banded, sericitized subangular felsic fragment	147
Figure 78:	Subrounded, lapilli-sized vesicular fragments with epidotized cores host in feldspar-phyric matrix.	148
Figure 79:	Vesicular-rich, flattened breccia-sized intermediate fragment	148
Figure 80:	Field photo of lapilli tuff facies showing vesicular fragments and liberated feldspar phenocrysts in matrix.	150
Figure 81:	Kink banding in shear zone within lapilli tuff bed	150
Figure 82:	Field photo of contact relationship between feldspar-phyric facies and brecciated facies as outlined by a possible chilled margin.	151
Figure 83:	*In situ* brecciation of feldspar-phyric facies showing jigsaw patterns.	151
Figure 84:	Abundant quartz amygdules within feldspar-phyric facies.	151
Figure 85:	Simplified geology map of study area.	156
Figure 86A:	Geology of Relais region	158
Figure 86B:	Cartoon of possible overlap between two felsic dome complexes	158
Figure 87A:	Felsic lobe extending into breccia carapace	160
Figure 87B:	Lobe-hyaloclastite	160
Figure 87C:	Small lobe closure defined by flow banded margin	160
Figure 88A:	Polygonal fracture pattern in massive felsic lava	162
Figure 88B:	Columnar jointed massive felsic lava	162
Figure 89:	Flow banding in felsic lava	163
Figure 90A:	Microphotograph of blocky euhedral feldspar in re-crystallized groundmass of felsic facies.	164
Figure 90B:	Microphotograph of tabular euhedral feldspar and anhedral quartz in re-crystallized vesicular groundmass of felsic facies.	164
Figure 91:	Pillowed intermediate lava indicating tops to the south	165
Figure 92:	Laminated tuff turbidite sequence indicating tops to the south	165
Figure 93:	Cartoon of felsic dome complex by Gibson (1997)	168
Figure 94:	Simplified geology of Dunraine east region	171
Figure 95A:	Sheared nature of felsic facies	173
Figure 95B:	Contact between two felsic facies.	173
Figure 96:	Plane polarized microphotograph of *in situ* brecciation of felsic facies	175

Figure 97:	Dunraine stratigraphic column of volcaniclastic sequence	177
Figure 98:	Erosive contact between lapilli tuff and tuff breccia indicating tops to the south	178
Figure 99:	Flow-banded subrounded breccia-sized fragment.	178
Figure 100:	Subrounded, vesicular breccia-sized fragment	179
Figure 101:	Jigsaw pattern of breccia-sized fragments indicating *in situ* brecciation.	179
Figure 102:	Microphotograph of serrated feldspar-phyric fragment.	181
Figure 103:	Gossan zone in volcaniclastic sequence.	181
Figure 104A:	Simplified geology of Abitibi Copper region	185
Figure 104B:	Simplified stratigraphic column of volcaniclastic sequence	185
Figure 105A:	Field photo of *in situ* brecciation of felsic lava	188
Figure 105B:	Photomicrograph of *in situ* and feldspar-phyric nature of felsic facies	188
Figure 106:	Field photo of meter-sized bun-shaped intermediate pillows indicating younging direction towards the south.	189
Figure 107:	Series of finely bedded tiff turbidities indicating tops to the south.	189
Figure 108:	Clast-supported nature of tuff breccia facies	191
Figure 109:	Close-up of clast-supported breccia fragments that are jigsaw fitting and vesicular	192
Figure 110:	Subrounded, vesicular breccia-sized fragment where vesicles are perpendicular to margin.	192
Figure 111A:	Plane polarized light image of serrated, vesicular lapilli fragment.	193
Figure 111B:	Cross-Nicols image of same field of view as (A).	193
Figure 112:	Generalized stratigraphic section for Sleepy Lake area	198
Figure 113A:	Field photo of pipe vesicles and lobate felsic lava	199
Figure 113B:	Cartoon of field photo in (A).	199
Figure 114:	Stripped outcrop where felsic lobe has intruded and disturbed bedding within tuff turbidite and lapilli tuff sequences.	200
Figure 115:	*In situ* brecciation of flow banded felsic lava.	201
Figure 116:	Irregular contact between flow banded felsic lava and felsic breccia, where flow bands are contorted near the contact.	201
Figure 117:	Clast-supported nature felsic tuff breccia, composed of subrounded, flow banded felsic lava.	203
Figure 118:	Subrounded to subangular, chloritized lapilli-sized fragments, part of felsic tuff breccia.	203
Figure 119:	Detailed map of autoclastic felsic tuff breccia.	204
Figure 120:	Meter-sized flow banded raft within autoclastic tuff breccia.	205
Figure 121:	Photomicrograph of vesicular lapilli-sized fragment from intermediate volcaniclastic sequence.	205
Figure 122A:	Stratigraphic section I of tuff turbidite.	207

Figure 122B:	Stratigraphic section II of tuff turbidite.	208
Figure 122C:	Ball and pillow textures within tuff turbidities.	208
Figure 122D:	Flame structures within tuff turbidities.	208
Figure 122E:	Syn-sedimentary faults in tuff turbidities.	208
Figure 123:	Generalized geology map of Dunraine west region.	213
Figure 124:	Photomicrograph of tabular, euhedral feldspar in intermediate massive lava.	215
Figure 125:	Field photo of vesicular, bun-shaped pillows of intermediate lava.	215
Figure 126:	Erosive contacts in a series a tuff turbidities indicating younging direction to the south.	216
Figure 127:	Field photo showing mineralized bands cutting tuff turbidite sequence.	216
Figure 128:	Crossed-Nicols photomicrograph of broken feldspar phenocryst in tuff turbidite.	217
Figure 129:	Plastic autoclastic fragmentation of massive to pillow intermediate lava forming pillow breccia.	217
Figure 130:	Subrounded, plastically deformed, breccia-sized fragments from clast-supported tuff breccia with 15-20-vol% quartz amygdules.	219
Figure 131:	Subrounded, breccia-sized fragment with epidotized core.	219
Figure 132A:	Crossed-Nicols photomicrograph of breccia fragment composed of quartz and carbonate amygdules and relict feldspar phenocrysts.	220
Figure 132B:	Crossed-Nicols photomicrograph of matrix illustrating the feldspar-phyric nature.	220
Figure 133:	Field photo showing feldspar-phyric nature of QFP facies.	222
Figure 134A/B:	Model of phreatomagmatic eruption for Placer Dome North	229
Figure 135:	Model of subaqueous fire fountain eruption for East Sullivan outcrops.	233

Chapter 5

Figure 136:	Regional geology with emphasis on Héva Formation.	237
Figure 137	Detailed area mapped within Héva Formation	238
Figure 138A:	Aeromagnetic map outlining the lateral extent of the spherulitic unit	240
Figure 138B:	Aerial photo mosaic outlining outcrops of the spherulitic unit	240
Figure 139:	Simplified stratigraphic column of felsic spherulitic unit	243
Figure 140A:	Massive zone of coalesced spherulites	244
Figure 140B:	Thin zone of isolated spherulites within massive spherulitic facies	244
Figure 141:	Photo of polished slab illustrating banding of spherulites	245
Figure 142:	Outcrop shot of cm-sized isolated spherulites in dark	245

	groundmass	
Figure 143:	Possible basal breccia facies associated with massive spherulitic facies	246
Figure 144:	Contact relationship between gabbro and massive spherulitic facies	246
Figure 145A:	Finely crystalline nature of intergrown spherulites, PPL	247
Figure 145B:	Finely crystalline nature of intergrown spherulites, crossed nicols	247
Figure 145C:	Spherulitic bands, PPL	247
Figure 145D:	Isolated spherulites with arrested spherulitic development in groundmass, PPL	247
Figure 146:	Photo and sketch of lobe-hyaloclastite facies	249
Figure 147:	Map of lobe-hyaloclastite facies	250
Figure 148A:	Microphotograph of fine crystalline nature of spherulites within lobes	251
Figure 148B:	Microphotograph of lobe margin with recognizable spherulites	251
Figure 149A:	*In situ* brecciation and jigsaw texture of hyaloclastite, PPL	253
Figure 149B:	*In situ* brecciation minus jigsaw texture of hyaloclastite, PPL	253
Figure 149C:	*In situ* brecciation minus jigsaw texture of hyaloclastite, crossed nicols	253
Figure 149D:	Perlitic texture of hyaloclastite, PPL	253
Figure 150:	Fibroradial character of albite, crossed nicols	254
Figure 151:	Photomicrograph of capping hyaloclastite facies, PPL	254
Figure 152:	Detailed map of Tex-Sol outcrop	264
Figure 153A:	Field photo of subangular vesicular mafic fragment	266
Figure 153B:	Crossed nicols microphotograph of feldspar-phyric nature of mafic fragment	266
Figure 154A:	Field photo of rounded vesicular felsic fragment	267
Figure 154B:	PPL microphotography of vesicular felsic fragment	267
Figure 155:	Varioles developed along gabbro margin	269
Figure 156:	Peperitic texture between intruded gabbro and volcaniclastic sediment	269
Figure 157A:	Crossed nicols image of isolated sub-spherical spherulite of fibrous feldspar	270
Figure 157B:	PPL image of amalgamated mat of acicular feldspar	270
Figure 158:	Detailed map of lowermost part of stratigraphy within the Akasaba region	275
Figure 159:	Stratigraphic section of lowermost part of Akasaka region	276
Figure 160A:	Truncated laminae in tuff facies beds	278
Figure 160B:	Rip up clasts of tuff in overlying lapilli tuff	278
Figure 160C:	Flame structures in tuff	278
Figure 160D:	Grading of lapilli tuff – tuff beds	278
Figure 161:	Detailed map of western most part of the stratigraphy	279

Figure 162:	Detailed map of central part of the stratigraphy	280
Figure 163A:	Disturbed bedding of tuff in proximity to gabbro	281
Figure 163B:	Massive homogeneous tuff in proximity to gabbro	281
Figure 163C:	Fragments of bedded tuff in gabbro	281
Figure 163D:	Brecciation of gabbro in proximity to tuff	281
Figure 163E:	Penetrating fingers of gabbro into featureless sediment	282
Figure 163F:	Amoeboidal forms of gabbro in sediment	282
Figure 163G:	Amoeboidal forms of gabbro in sediment	282
Figure 163H:	Amoeboidal forms of gabbro in sediment	282
Figure 164A:	PPL microphotography of lapilli tuff characterized by broken feldspar phenocrysts	283
Figure 164B:	PPL microphotography of peperite, with sediment and gabbro	283
Figure 165A:	Angular bedded tuff fragment in pyroclastic lapilli tuff facies	285
Figure 165B:	Subrounded, vesicular fragment that is recessively weathered, with broken feldspar crystals in matrix	285
Figure 165C:	Flattened fragment with broken feldspar crystals in matrix	285
Figure 165D:	Armored fragment with broken feldspar crystals in matrix	285
Figure 165E:	Crossed-nicols microphotography of broken euhedral feldspar phenocrysts	286
Figure 165F:	Orange stained tuff megablock in pyroclastic lapilli tuff	286
Figure 166A:	Linear, fine laminations in gabbro in proximity to pyroclastic lapilli tuff	289
Figure 166B:	Irregular blebs of dark green gabbro (?) hosted in featureless homogeneous phase	289
Figure 166C:	Close-up of irregular blebs characterized by a whitish and fractured contact zone in homogeneous host	289
Figure 167:	Cross-polarized microphotograph of sub-spherical forms in fine-grained gabbro	290
Figure 168:	Contact between felsic sediments and mineralized zone	290
Figure 169:	Cartoon depicting different stages of interaction between felsic sediments and gabbro forming peperite	295
Figure 170:	Cartoon illustrating temporal and spatial relationships between sediments and intrusions	298
Figure 171:	Detailed map of outcrops at the top of Héva Formation, part of Akasaba South	300
Figure 172A:	Feldspar glomerocrysts in massive mafic facies	302
Figure 172B:	Bun-shaped mafic pillows with feldspar glomerocrysts	302
Figure 172C:	Perpendicular fractures extending from tuff into underlying massive mafic facies	304
Figure 172D:	Intermixed fluidal and blocky peperite developed below laminated tuff	304
Figure 172E:	Fluidal peperite developed below thin laminated tuff	305

Figure 172F:	Millimeter-sized garnet crystals in granodiorite intrusion	305
Chapter 6		
Figure 173A:	SiO_2 vs. Zr/TiO_2 * 0.0001 rock classification	311
Figure 173B:	Jensen cation plot for rock classification	312
Figure 174:	SiO_2 vs. Zr/TiO_2 * 0.0001 rock classification for the HF	320
Figure 175A:	Y vs. Zr plot for geochemical affinity of JF	321
Figure 175B:	Y vs. Zr plot for geochemical affinity of VDF	321
Figure 175C:	Y vs. Zr plot for geochemical affinity of HF	321
Figure 176:	Chondrite-normalized REE plot for the Jacola Formation	324
Figure 177A/D:	Chondrite-normalized REE plots for the Val d'Or Formation	325
Figure 178A/C:	Chondrite-normalized REE plots for the Héva Formation	326
Figure 179A/D:	Primordial-normalized trace element plots for the Val d'Or Formation	328
Figure 180A/C:	Primordial-normalized trace element plots for the Héva Formation	329
Figure 181A:	REE profiles for upper VDF and volcaniclastic deposits from the HF	333
Figure 181B:	Multi-element profiles for upper VDF and volcaniclastic deposits from the HF	333
Figure 182:	Tectonomagmatic diagrams for Jacola, Val d'Or and Héva formations	335
Chapter 7		
Figure 183:	Geology with correlated stratigraphic columns	347
Figure 184A/C:	3-D block diagrams for the paleogeographic reconstruction of the Val d'Or Arc	350
Figure 184D/E:	3-D block diagrams for the paleogeographic reconstruction of the Val d'Or Arc	353
Figure 185:	Stratigraphic column comparisons between previous interpretations and this study	355

List of Tables

Chapter 1		
Table 1:	List of nomenclature concerned with subaqueous processes and their deposits	11
Table 2:	Classification of turbidity currents	15
Chapter 3		
Table 3:	Pillow sizes	47
Table 4:	Structural info	49
Chapter 4		
Table 5:	Playground stratigraphy (ROI 1)	58
Table 6:	Placer Dome North stratigraphy (ROI 2)	77
Table 7:	East Sullivan stratigraphy (ROI 3)	103
Table 8:	Vesicularity of breccia-sized pumice fragments	114
Table 9:	Pole Line stratigraphy (ROI 3)	121
Table 10:	Manitou stratigraphy (ROI 4)	132
Table 11:	Camnet stratigraphy (ROI 5)	139
Table 12:	Relais stratigraphy (ROI 6)	159
Table 13:	East Dunraine stratigraphy (ROI 7)	172
Table 14:	Abitibi copper stratigraphy (ROI 8)	186
Table 15:	Sleepy Lake stratigraphy (ROI 9)	197
Table 16:	Schistosity vs. bedding	225
Chapter 5		
Table 17:	Felsic spherulitic unit stratigraphy	242
Table 18:	Tex-Sol stratigraphy	265
Table 19:	Akasaba North stratigraphy	274
Table 20:	Akasaba South stratigraphy	301
Chapter 6		
Table 21	Representative major and trace elements for study area	314
Chapter 7		
Table 22:	Comparison of geochemical characteristics of formations	341
Table 23:	Geologic characteristics of the Val d'Or Arc	348
Table 24:	Comparison between modern and Archean Island Arcs	357

ACKNOWLEDGEMENTS

As with any thesis there are numerous people that worked behind the scenes to make this piece of work possible. And of course as it dragged out to an astonishing seven years that list is very long indeed and I already have a 400+ page thesis, so this is the abridged version. Seven years….. I guess you might consider this a lucky thesis then? Time will tell.

Well academically there have been many people involved in my progression from a Bachelors Degree back in Newfoundland to this large volume now completed under the auspicious guidance of Dr. Wulf U. Mueller at the Université du Québec à Chicoutimi. From Drs. Roger Mason and Toby Rivers at MUN, in writing referral letters that spoke of my potential and again Dr. Wulf. U. Mueller. I only have a vague idea of the pressure that Wulf was under by his peers at UQAC after that debacle called a devis de recherché. He had tremendous patience and his "tough love" pushed many students to the edge, myself included. They say 'what doesn't kill us makes us stronger' well I would just like to say – who are "they"! Seriously, I would not be the field geologist I am today without his vision and direction. And an honorable mention goes out to Dr. Tony D. Fowler. He was my original mentor and continues to be a source of strength. No statement of acknowledgements would be complete without mentioning his name.

On a professional side, the government of Québec was instrumental in providing all the resources necessary for this thesis. With the Ministere there would have been no thesis in the first place. Mr. Pierre Pilote was the irreplaceable field guide to Val d'Or geology as well as serving as a sometimes necessary filter and protective barrier from undue distractions in the field. To the pig (Clarence), Joe (Seb or Zeb), and Red (Christine), united we stood and as the three little pigs and lil' red riding hood withstood the wrath of the big bad Wulf (sometimes). To Gabe, thanks for getting me to UQAC (I think?). I like to extend a hardy thank you to Cal State Northridge. They gave me access to microscopes to finish off some loose ends. And of course paper and printers that helped print several versions of this thesis. They also facilitated my love of teaching, which I wasn't too sure I wanted to do initially. And of course they introduce me to a good friend – Karen.

On a more personal side. I would like to thank my mother for being another source of support behind the scenes. Her door is always open and I have frequently walked through it countless times during the course of this and my last thesis. While she doesn't know exactly what I do, she knows that it involves rocks and I know I have her love and support. And a special thanks to my surrogate mother Nicole, as she had to put up with my coming and going through my mother's open door! And last but certainty not least – my wife. Just enough pressure to write without cracking the whip while offering loving support. With her I see my future, which allowed me to get the drive and energy to write this thesis so that any future "chapters" will be written together!!

CHAPTER 1

INTRODUCTION

Paleogeographic reconstruction of Archean terranes must consider not only Archean continental growth models, which include subduction and mantle plume processes (Abbott and Isley, 2002; Campbell et al., 1989; Kusky and Polat, 1999; Mueller et al., 1996; Polat et al., 1998), but must also determine if these terranes were allochthonous, autochthonous, or parautochthonous. These issues are not limited to geologic provinces, such as the Superior Province, where growth is regarded as progressive or episodic or due to accretion of ocean plateaus (cf. Polat and Kerrich, 2001; Thurston, 2002).

Greenstone belts, Archean supracrustal sequences, are composed of volcano-sedimentary rocks and coeval granitic intrusions produced by divergent and/or convergent plate tectonic processes (Helmstaedt et al., 1986; Mueller et al., 1996; Polat et al., 1998; Kusky and Polat, 1999), or possibly mantle plumes (Campbell et al., 1989; Abbott and Isley, 2002). They are typically greenschist grade terranes that form 10-25 km wide, 100-300 km long, elongated synclinal keels of felsic to ultramafic volcanic and associated sedimentary rocks (Taira et al., 1992). Komatiites, an Archean phenomenon, are primitive, high temperature lavas thought to be derived from a mantle plume (Campbell et al., 1989; Abbott and Isley, 2002), and are used to infer a higher heat flow during this period of the Earth's geologic history (Bickle, 1978; Sleep and Windley, 1982; Abbott and Hoffman, 1984). Divergent plate boundaries are characterized by fissure-fed effusive volcanism forming thin, areally extensive komatiite to tholeiitic basalt lava flows (Hill et al., 1995)

that construct large oceanic platforms (Dimroth et al., 1982). Convergent boundaries are typified by subduction-related volcanism, which constructed complex, central volcanic edifices up to 30-km in diameter. The edifices are composed of abundant felsic to intermediate fragmental debris interstratified with calc-alkaline basalt and dacite-rhyolite lavas (Dimroth et al., 1982; Card, 1990), together with tholeiitic basalt erupted from penecontemporaneous extension-related volcanism (Hamilton, 1995). Recent stratigraphic and volcanic facies analysis (Dostal and Mueller, 1997; Wyman et al., 1999a; Mueller and Mortensen, 2002), geochemical (Hollings et al., 1999; Wyman et al., 1999b; Polat and Kerrich, 2001), and structural (Desrochers et al., 1993; Polat and Kerrich, 2001; Daigneault et al., 2002) studies have illustrated a spatial relationship between plume- and subduction-related volcanism.

Wyman (1999) inferred a progressive transition from plume- to arc-dominated volcanism based on geochemical evidence of komatiites and depleted, low-Ti tholeiitic basalts, covered by subsequent eruptions of calc-alkaline lavas. Depleted, low-Ti tholeiitic lavas are generated during mantle melting associated with initial subsidence forming a proto-arc or juvenile subduction zone (Stern and Bloomer, 1992; Wharton et al., 1995). Most volcanic arcs are spatially restricted successions composed of lavas and fragmental flow units that form central volcanic complexes (Dimroth et al., 1982; Lafrance et al., 2000), stratovolcanoes with multiple vents (Riggs and Busby-Spera, 1990) or caldera complexes (Fiske, 1994). In addition, arc complexes typically evolve geochemically from tholeiitic to calc-alkaline during arc evolution, or maturation (Wilson, 1989, pp. 167).

1.1 Statement of Problem

Archean greenstone belts (evolution) can be allochthonous, autochthonous, or parautochthonous. Past and present workers have tackled this problem from a structural, stratigraphic, volcanological, geochemical and geochronological aspect at the scale of geologic provinces (Kimura et al., 1993; Thurston, 2002), subprovinces (Chown et al., 1992; Mueller et al., 1996; Polat et al., 1998; Calvert and Ludden, 1999), and formations (Lafrance et al., 2000; Legault et al., 2002). Several studies have attempted to incorporate more than one aspect, such as structural and geochemical or stratigraphic and volcanological studies, with rare studies utilizing more than two (e.g., Corcoran, 2000; Dostal and Mueller, 1997; Scott et al., 2002). The Superior Province is probably one of the most studied Archean supracrustal cratons in the world due to its accessibility, economic potential, and overall size. Within this framework, the Abitibi greenstone belt (Subprovince), represents several well-known volcano-sedimentary sequences with two volcanic zones (Chown et al., 1992), but in which the southern segment has diverse interpretations.

Geochemical, structural, and stratigraphic studies have documented general evolutionary trends within greenstone belts, whereby the geodynamic setting has changed from plume-generated to arc-related volcanism (Desrochers et al., 1993; Hollings et al., 1999; Wyman, 1999; Wyman et al., 1999b); however they have not focused on field relationships with regard to style of volcanism between formations/groups. This is a fundamental problem in any study attempting to assess whether crustal evolution is

allochthonous or autochthonous. This study focuses on formational contacts and assesses the change in volcanism, such as plume-generated komatiite or subduction-related calc-alkaline rocks. A volcanological approach is important because: (1) of the predominance of volcanic and volcaniclastic rocks in the field area; and (2) the style of volcanism (Wilson, 1989) and sedimentation (Fisher and Smith, 1991a, b; Orton, 1996) are controlled by the geodynamic setting. Volcanology of this region can be subdivided into physical characteristics and geochemical attributes. The physical characteristics describe the morphology of lava flows, or volcaniclastic-pyroclastic deposits, and hence constrain the depositional setting. The geochemistry defines the composition of explosive or effusive magmatic products, but more importantly can be used to constrain the overall geodynamic setting. Discrimination diagrams can be employed to identify an arc, or continental setting for example.

The relationship between plume-generated and subduction-related volcanic rocks has become an important issue for the Archean. Is there a temporal and/or spatial relationship between these two magma-generating systems? The constant interaction between these two magma-generating systems may suggest that Archean evolution was quite different.

Another complication of working within a well-documented region is the assimilation of a vast amount of past work without becoming biased toward a previous interpretation. The initial idea in this study was to incorporate the existing formational nomenclature, but the recognition of two distinct magma types favored the division into

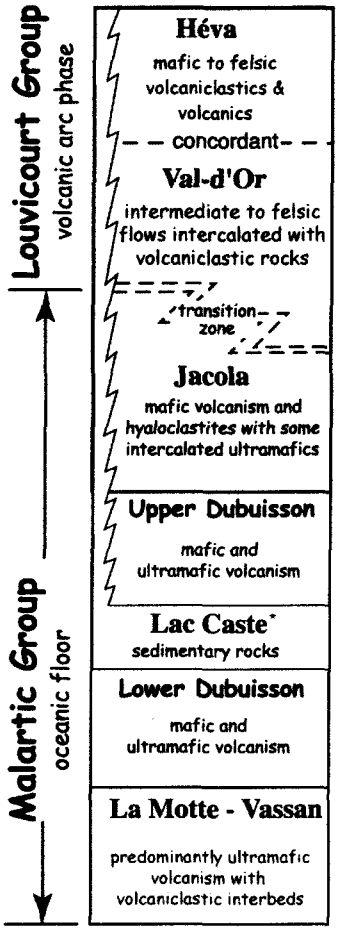

Figure 1: Composite stratigraphic column for the Malartic Block. Organization in the Malartic and Louvicourt Groups based on proposed tectonic enivironments. Studied formations in gray. Stratigraphic setting of Lac Caste Formation after Mueller and Donaldson (1992).

two groups. Original formation names were retained, but were re-organized into the previous Malartic Group and the new Louvicourt Group (**Figure 1**; Scott et al., 2002).

Oceans were prominent during Archean greenstone belt evolution, as suggested by a lack of isotopic inheritance in the southern Abitibi greenstone belt (Ayer et al., 2002), prominent pillowed sequences, and therefore subaqueous volcanic eruptions, from initial emission to final deposition (Cas and Wright, 1991; Stix, 1991), were greatly influenced by the effects of water. Thus, it is essential to understand the role water plays during volcanic activity. A problem facing research involving subaqueous processes is: to what degree does the water depth affect explosive submarine volcanism? In the past, certain depth limits were placed on explosive subaqueous eruptions. The basis of which was on the exsolution of dissolved magmatic volatiles and generation of steam (McBirney, 1963; Cas and Wright, 1987). However, the recent discovery of pumice, deep-sea scoria and vesiculated lava at depths in excess of 2000m (Smith and Batiza, 1989; Gill et al., 1990; Batiza and White, 2000; Hekinian et al., 2000) have questioned their validity. Such concepts to inferred deep-water conditions in relation to phreatomagmatic and magmatic eruptions have recently been discussed at a Chapman Meeting in 2002 (Dunedin, New Zealand). The study of ancient, and especially

Archean deposits offer a distinct advantage, as exposed facies associations can be correlated, whereas modern submarine deposits are restricted by their accessibility. Ancillary to ancient subaqueous volcanism is the exploration for volcanogenic massive sulfide (VMS) deposits. Hydrothermal venting of metal-rich brines is intimately associated with subaqueous volcanic vents (Doucet et al., 1994; Wright et al., 1998; Iizasa et al., 1999; Gibson et al., 2000), so that the identification of proximal volcanic facies offers an additional exploration tool for VMS-type deposits, particularly in areas of vertical bedding.

The final step in any mapping program is the compilation and correlation of small and large-scale work. Regional and local mapping of the complex inter- and intra-formational relationships permits the reconstruction of the paleogeographic setting, whereby a new stratigraphic framework for the region can be proposed. This thesis is the result of a 3 year mapping project in the Val d'Or Mining Camp, which was generously supported by the Ministere des Ressources naturelles, Québec.

1.2 Aims and objectives

The principal aim of this thesis is to reconstruct the geodynamic environment for the southeastern part of the Abitibi Greenstone Belt, which encompasses the Jacola, Val d'Or and Héva formations, using a modern volcano-sedimentary facies analysis approach. Defining the geotectonic setting requires the examination of each formation and understanding both spatial and temporal relationships. Such a paleogeographic model reflecting a distinct geodynamic setting will be derived from the construction of a series of

stratigraphic sections based on the physical volcanology and sedimentology (facies analysis), as well as petrography and geochemistry. Culmination of work from these various geologic applications into a 'global' model facilitates the reconstruction of the geodynamic environment.

In order to establish a well-defined stratigraphy it is necessary to identify the: 1) nature of contacts; 2) structural relationships; 3) younging direction(s); and 4) lateral facies changes of the various lithological units comprising the study area. In addition to the tectonic evolution, the economic potential of this segment of the Val d'Or Mining Camp will be evaluated. To accomplish these goals, the following short term objectives were followed: 1) evaluation of previous stratigraphic/model(s) for the Malartic Group; 2) determination of fragmentation mechanism (i.e., pyroclastic, hydroclastic, autoclastic); 3) volcano-sedimentary facies of volcanic-volcaniclastic rocks; 3) determination of the prevalent transport processes of volcanic deposits in a subaqueous setting; 5) identification of proximal and distal subaqueous deposits with regard to volcanic edifices; 6) utilization of the geochemistry of various lithological units, together which facilitate defining a possible geotectonic setting; and 7) structural measurements of selected areas.

1.3 Methodology

Synthesis of previous work, quality and quantity of outcrops, and size of the field area, together with geochemical and geochronological analyses, required three field seasons of detailed lithological field mapping and laboratory work. Previous work came in the form of

lithological and structural work by the provincial and federal governments along with extensive gold and base metal exploration by industry. Work concentrated on constructing the stratigraphy of the Val d'Or (VDF) and Héva (HF) formations, but was extended to include the upper part of the Jacola Formation (JF) based on volcanic and geochemical analysis that suggested an evolutionary trend from the JF to the HF. Mapping was conducted at the: (1) regional or small-scale, in order to define the stratigraphy, and (2) detailed or large-scale volcano-sedimentary analysis.

Regional 1:1000 to 1:10 000 scale mapping included company maps. Company maps were useful as outcrops were located along N-S grids at 50-100 m-thick spacing. This provided the necessary coverage to outline lithological variation as well as any geochemical disparity between formations. A series of regional stratigraphic sections were constructed at a scale of 1:20 000 in order to document any small-scale lateral variations in lithofacies to help identify volcanic vents. Every outcrop zone was investigated in detail, whereby volcanic textures and structures permitted facies analysis at scales of 1:10, 1:25, 1:100, and 1:200. Detailed mapping concentrated on recognizing fragmentation and flow processes of stratified to massive volcaniclastic deposits and their association with intercalated pillowed to massive lavas. This, in turn, is used to distinguish between proximal versus distal with respect to the volcanic vent or fissure source. At outcrop scales, stratigraphic sections were constructed at scales of 1:20 and 1:200 in order to characterize lateral and vertical facies variations. This work included sedimentological characteristics such as grading, crossbeds, and sorting, but also to determine interbedding relationships. Description of individual clasts in beds, including morphology, vesicularity, size, and crystallinity are considered. A

total of 852 samples were collected over three summer field programs to examine primary volcanic textures, with 479 thin sections prepared to examine mineralogical and textural features. Vesicularity was determined through point counting, using 1 mm, 5 mm, and 1 cm spaced grids on photos and digital images, as well as 500 points in thin section.

Geochemical analyses were conducted on 183 samples from the Jacola, Val d'Or, and Héva formations at the Centre de Recherche Minérale (Sainte-Foy, Québec) for major and certain trace elements (Ga, Nb, Rb, Sr, Y, Zr) by X-ray fluorescence (XRF), except for Zn and Cu (ICP-AES). Supplemental analyses are provided by Champagne (2002) for ultramafic lavas from the Jacola Formation. Eighty-four representative samples were originally chosen for analysis of rare earth elements by the Sainte-Foy lab, but lack of precision and accuracy for all samples precluded their use. Forty-seven samples were then picked for rare earth elements (REE) by instrument neutron activation analysis (INAA) at the Université de Québec à Chicoutimi (UQAC) following the procedure of Bédard and Barnes (1990). Precision and accuracy for both XRF and INAA are presented in chapter 6.

1.4 Volcanic Terminology

This section considers the terminology of subaqueous volcaniclastic deposits. Depending on an individual's *school of thought*, a reworked deposit composed of formerly **unconsolidated** volcanic fragments could be classified by a sedimentary (Cas and Wright, 1987; McPhie et al., 1993) or volcanic (Fisher, 1961; Fisher and Smith, 1991b) scheme. The former concept, advocated by the *Australian* school (Cas and Wright, 1987; McPhie et

al., 1993), considers reworking of juvenile pyroclastic particles by any process other than the gas-support (e.g., pyroclastic flows) should be classified by a sedimentary size scheme (i.e., crystal-rich sandstone). The *American* view argues that transporting agents, such as water and wind, do not change the origin of the components (Fisher and Smith, 1991). This is a crucial point, because in a submarine environment, water is incorporated into freshly erupted volcanic particles, whereby the complete mélange (water + volcanic particles) can be transported and deposited without an intervening stage of repose.

Fisher (1961) introduced the term volcaniclastic to describe flow deposits of fragmented volcanic material without reference to its mode of fragmentation or transportation processes. Moreover, Bates and Jackson (1987) defined a volcaniclastic rock as a "sedimentary rock" composed of abundant volcanic material "irrespective" of their mode of origin or environment. Thus, the term "volcaniclastic" includes pyroclastic, autoclastic, and epiclastic rocks, which is useful in describing ancient rocks where irrefutable evidence of particle origin is difficult to ascertain. This thesis embraces the concepts put forth by Fisher (1961) in describing the volcano-sedimentary facies.

Table 1 gives an overview of subaqueous deposits and their origin. The submarine environment affects volcaniclastic deposits, particularly for finer grained units where explosive fragmentation is commonly implied. The notion of efficient, explosive disintegration of lava (or magma) with abundant water at elevated pressures is a contentious issue. In addition, the prevalence of water ingestion not only influences fragmentation (i.e., phreatomagmatism), it controls the subsequent transportation and deposition of volcanic material. It is the ingestion of water that *fuels* the debate on

Table 1: Subaqueous pyroclastic flows and their subaqueous deposits.

Subaqueous pyroclastic flows	
Fiske & Matsuda 1964	A warm or cold contemporaneous flow composed of pyroclastic aggregates from a subaqueous eruption
Fisher & Schmincke 1984	A contemporaneous flow consisting of pyroclasts formed by direct volcanic activity that origins or flows into water
Yamada 1984	Near shore to shallow water eruption generates a high density current similar to subaerial pyroclastic flows but they incorporate steam not air.
Cas & Wright 1987	High temperature flow that is equivalent to subaerial pyroclastic flow
Stix 1991	Primary products of explosive magmatic eruptions that are hot and may be gas-supported
White 2000	A high particle density current with a continuous gas phase formed from a sustained explosive eruption
Other subaqueous flows	
Carey & Sigurdsson 1980	**Subaqueous pyroclastic debris flows** are water-supported equivalents to subaqueous pyroclastic flows that lack evidence of hot emplacement
Cas & Wright 1987	**Water-particle debris flow** or **granular mass-flows** are water-supported, high concentration debris flows of pyroclastic material
Stix 1991	**Mass flows of pyroclastic debris** are not emplaced in a hot state but are primary in the sense that they are direct products of an eruptions and are deposited essentially immediately after the eruption
Stix 1991	"**Mass flows of volcaniclastic debris** are secondary flows not necessarily synchronous with, nor genetically related to, an explosive eruption"
White 2000	**Eruption-fed turbidity currents** are low to high particle density currents with a continuous water phase formed from tephra jets of intermediate explosivity
Subaqueous deposits	
Cas & Wright 1987	**Subaqueous pyroclastic flow deposit** is emplaced under high temperature conditions that are equivalent to subaerial pyroclastic flows
Fisher and Schmincke 1984	**Subaqueous pyroclastic flow deposit** is from a syneruptive, hot or cold flow consisting of pyroclasts formed by volcanic activity
Cas and Wright 1987	**Volcaniclastic debris flow** or **volcaniclastic granular mass-flow deposits** are subaqueously deposited flows that are deposited in a cold state
McPhie et al. 1993	**Subaqueously-erupted volcaniclastic deposits** are water-supported, volcaniclastic mass flow deposits produced by subaqueous explosive eruptions
Carey & Sigurdsson 1980	**Subaqueous pyroclastic debris flow deposit** describes deposition from a high-concentration debris flow of pyroclastic material

subaqueous pyroclastic processes. Recent reviews have focused on re-examining interpreted subaqueous pyroclastic flow deposits in the literature (Cas, 1992), along with examining how external water affects pyroclastic processes (Stix, 1991). The argument can be subdivided into two questions: (1) are deep-water explosive eruptions possible?, and (2) can primary *pyroclastic* material be transported and deposited by a hot, gas-supported, high concentration laminar flow in a submarine environment? The former debate has subsided with the observation of fresh vesicular scoria to depths in excess of 1800m during submersible dives (Smith and Batiza, 1989; Gill et al., 1990; White et al., 2003) and observed surface discoloration accompanied by large rafts of hot pumice fragments from submerged vents at Surtsey (Kokelaar and Durant, 1983), and Myojin Knoll (Fiske et al., 2001). The latter is more subjective, as alteration/deformation of ancient deposits typically destroys one or more clues of the thermal character and transporting medium. In younger deposits it is possible to use paleomagnetic indicators and sedimentology (Mandeville et al., 1994; Mandeville et al., 1996), but in ancient deposits, textural evidence, such as eutaxitic textures, fiamme, and jointing, is necessary (Schneider et al., 1992; Fritz and Stillman, 1996; Scott et al., 2003).

The term hyaloclastite was introduced to describe deposits composed of glass fragments produced by non-explosive spalling and granulation of pillow margins (Rittman, 1962), and now includes all vitroclastic tephra produced by the interaction between water and hot lava/magma (Fisher, 1984). Hydroclastite processes, which include hyaloclastite, are defined as explosive/non-explosive fragmentation due to magma interaction with water. Alternatively, the term hyaloclastite is restricted to non-explosive or weakly explosive

granulation of volcanic glass due to quenching with external water (Heiken and Wohletz, 1985; Yamagishi, 1987), which is the definition followed in this thesis.

The standard granulometric classification scheme used for describing ancient volcaniclastic deposits are: (1) breccia or block, > 64 mm; (2) lapilli, 2-64 mm; and (3) tuff, < 2 mm (Fisher, 1961, 1966). Depending on the modal percentage of fragments (≥ 25%), volcaniclastic deposits are termed lapilli tuff, tuff breccia, lapilli tuff breccia, or lapillistone. Genetic terms such as hyaloclastic, pyroclastic, and autoclastic should be reserved for deposits where the mode of fragmentation is known. For example, a hyaloclastic tuff breccia represents a deposit composed of breccia-sized fragments (> 25%) supported by tuff (> 25%) that originated from water-lava interaction, in which contact relationships between the coherent lava flow and associated brecciated facies are observed.

The mapped volcano-sedimentary sequences can be described using sedimentological terminology in regard to transportation and deposition processes, because the supporting medium was probably water. Furthermore, most of the deposits can be interpreted as some variant of a sedimentary gravity flow deposit, or low- to high-concentration turbidity flow. Thus, interpreted turbulent-type flow deposits are classified according to the scheme devised by Lowe (1982), based on grain size and structure (**Table 2**). Grain-size is divided into gravel- (breccia), sand- (lapilli), or mud-dominated (tuff) beds, corresponding to R-, S-, or T-types, respectively. Structure is concerned with grading and stratification with each bed-type.

1.5 Organization

Organization of this dissertation is based on an initial assessment of the physical characteristics of each formation in their order of deposition, beginning with the Jacola Formation at the base, the Val d'Or Formation, and ending with the Héva Formation. Each formation is examined with regard to outcrops that characterize the style and composition of volcanic activity. Detailed volcanological analyses document inter- and intra-bedding relationships in order to elucidate the eruptive mechanisms and possible proximity to the source. Particular eruptive processes are outlined at the end of each chapter in relation to effusive activity or magmatic to phreatomagmatic explosive fragmentation processes and their restrictions in a subaqueous environment. In addition, the geochemistry of each formation is presented in Chapter 6 and subsequently discussed. Chapter 7 combines the geochemistry and the regional stratigraphy so that a model of the paleogeographic environment can be constructed. Detailed petrographic analyses of type sections are documented in appendix A.

1.6 Corroboration

This dissertation represents a contribution to better understand the geodynamic environment within the southeastern sector of the Abitibi Greenstone Belt in Québec. The Government of Québec (Ministere des Ressources naturalles) and the mining industry supported this study generously.

Table 2: Turbidity flow classification (from Lowe, 1982; Bouma, 1962). Table organized in idealized depositional sequence.

Short-hand notation	**Flow-type**	**Sedimentation**	**Features**
T_e	Low-density	Suspension	Massive – structureless - laminated
T_d	Low-density	Suspension ± traction	Fine laminations and textural sorting
T_c	Low-density	Suspension + traction	Cross-laminations
T_b	Low-density	Suspension + traction	Laminations
T_a/ S_3	High-density	Suspension	Massive – structureless or normal graded
S_2	High -density	Traction	Inverse grading and basal shear laminations
S_1	High -density	Traction	Plane laminations and cross stratification
R_3	High -density	Suspension	Normal grading
R_2	High -density	Traction	Inverse grading
R_1	High -density	Traction	Stratification and tractional structures

CHAPTER 2

GEOLOGY

The study area is located within the Archean Superior Province, which is composed of numerous fault-bounded, geologically discrete domains or belts that collectively form an extensive craton (Card, 1990; Thurston and Chivers, 1990) extending over 1500 km from northern Québec through Ontario and into northern Minnesota (**Figure 2**). Northern domains, postulated to be older, form a more continental-type magmatic arc setting (Stern et al., 1994), whereas the southern Wabigoon, Wawa, and Abitibi belts represent accreted juvenile volcano-plutonic terranes formed in an oceanic arc environment (Calvert and Ludden, 1999). The 2.7 to 2.67 Ga Abitibi Subprovince, composed of an assemblage of granitic-volcanic-sedimentary rocks, is located in the southeast corner of the Superior Province (**Figure 2**). The prominence of mafic volcanic rocks and characteristic greenschist metamorphic grade defines the Abitibi Subprovince as a greenstone belt, whereby the *Abitibi Greenstone Belt*, measuring 700km x 300km, is the largest coherent Archean greenstone belt in the world.

2.1 Abitibi Geology

The Abitibi Greenstone Belt forms an east-west linear assemblage of metavolcanic and metasedimentary rocks intruded by syn- to post-orogenic granitic plutons (**Figure 3**). This belt is bounded to the east by the Grenville Front, a laterally extensive deformation

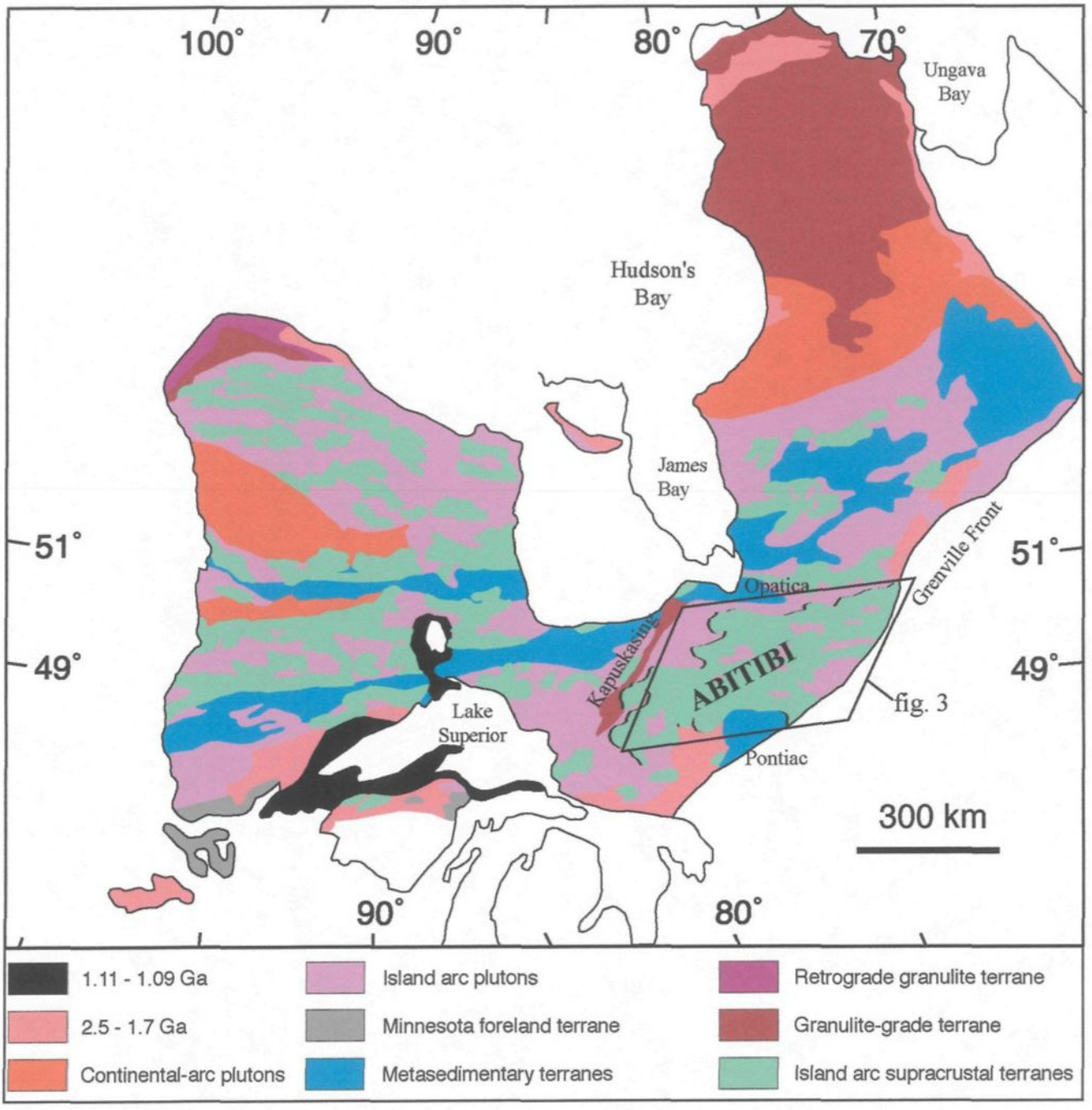

Figure 2: Simplified geology of the Superior Province outlining the various terranes. The study area is outlined (Abitibi Greenstone Belt). Modified from Calvert et al. (1999) and Card (1990).

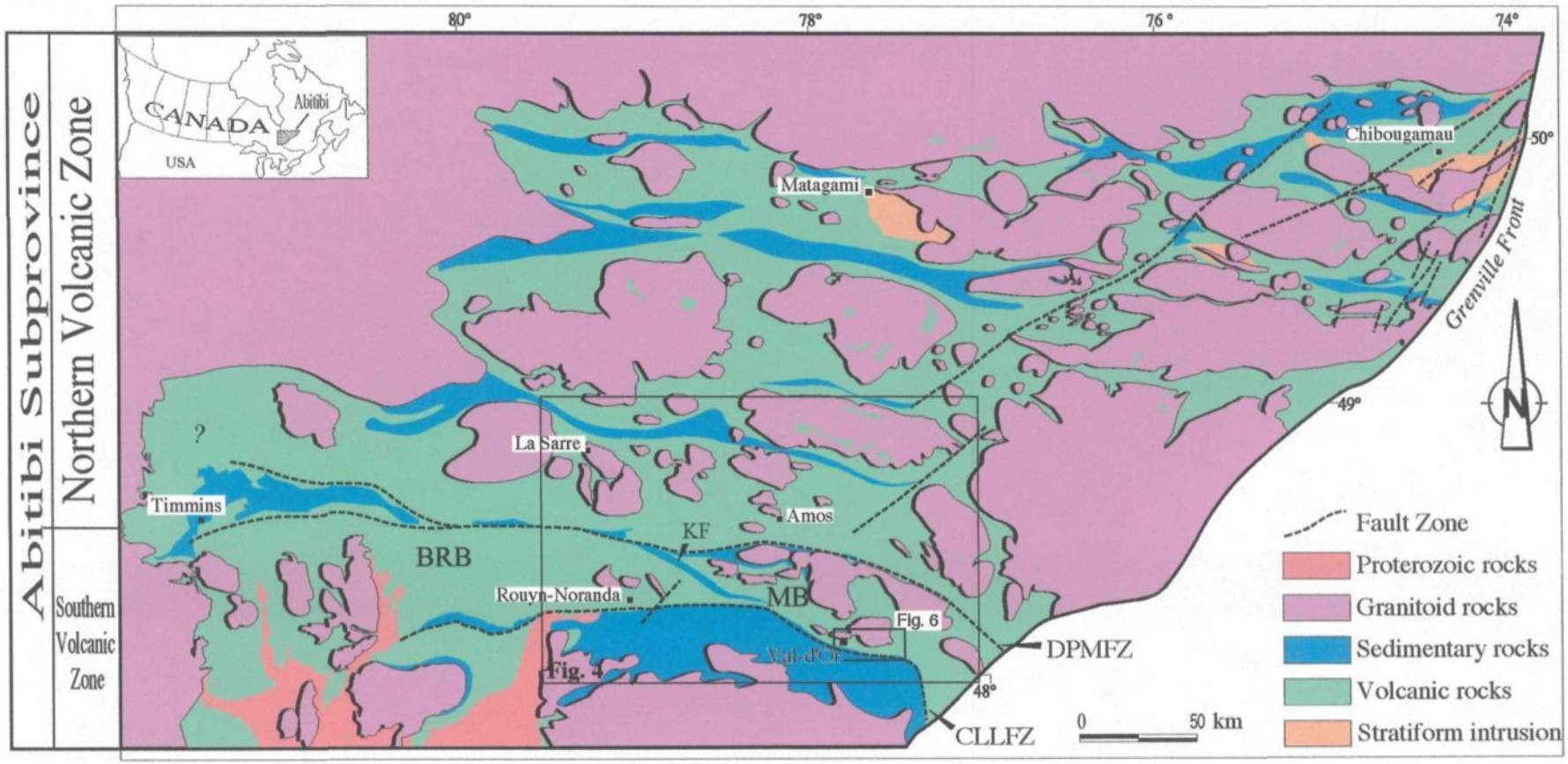

Figure 3: Regional geology of the Abitibi Subprovince, which is subdivided into two volcanic zones based on distinct volcanic and sedimentary cycles. SVZ is subdivided into the Blake River Block (BRB) to the west and the Malartic Block (MB) to the east, separated by the sedimentary Kewagama Formation (KF). The Destor-Porcupine-Manneville (DPMFZ) and Cadiallac-Larder Lake fault zones (CLLFZ) define the northern and southern boundaries of the SVZ, respectively. Study area is outlined. Modified from Chown et al. (1992), Mueller and Donaldson (1992), and Mueller at al. (1996).

zone consisting of a Proterozoic thrust fault that defines the contact between the Superior and Grenville provinces, and to the west by the Kapuskasing Structural Zone, a discontinuous northeast-trending zone of gneissic rocks (**Figure 2**). To the north, the boundary is defined by the para- and orthogneiss of the Opatica Subprovince (Card, 1990), and to the south by the Cadillac Break, which separates the Abitibi Subprovince from metasedimentary rocks of the Pontiac Subprovince.

Early work by Goodwin and Ridler (1970) recognized a division in the Abitibi stratigraphy and defined northern and southern volcanic zones separated by an axial orogenic zone. Further work by Dimroth et al. (1982) defined a northern Internal and a southern External zone based on the large volume of komatiitic volcanism in the south and the greater amount of intrusions, and mafic and ultramafic sills in the north and an overall difference in thickness. Recent work identified two distinct zones based on similar plutonic, volcanic, and deformation histories, as well as age constraints and are referred to as the Northern (NVZ) and Southern Volcanic Zones (SVZ) (**Figure 3**; Chown et al., 1992). The division between the ca. 2730-2710 Ma NVZ and ca. 2705-2695 Ma SVZ (Corfu et al., 1989; Mortensen, 1993a; Mortensen, 1993b) is by a series of east-west faults such as the Destor-Porcupine and Manneville Faults (Chown et al., 1992; Daigneault et al., 1994) as well as by collisional flysch-type sedimentary basins (Mueller et al., 1996). An overall younging direction towards the south from the NVZ to the SVZ suggests a progressive evolution, which is supported by southward evolution of the sedimentary basins (Mueller and Donaldson, 1992).

Defined U-Pb zircon age constraints, detailed volcano-sedimentary terrane analyses and stratigraphy suggest a window of 2730-2640 Ma for initial deposition to final exhumation of the Abitibi belt (Mueller et al., 1996). Through sedimentary and structural work, the Abitibi Greenstone Belt is considered to represent a well-defined arc collage (Chown et al., 1992). Subsequent work recognized four evolutionary phases spanning the 90 My formation of the Abitibi belt from: (1) arc formation and construction (2730-2698 Ma); (2) arc-arc collision (2696-2690 Ma); (3) arc fragmentation (2689-2680 Ma); and (4) arc exhumation (2660-2640 Ma) (Mueller et al., 1996).

The geodynamic setting of the NVZ is considered an extensive subaqueous mafic plain with isolated mafic, mafic-felsic, and felsic volcanic centers that collectively formed a diffuse arc (Chown et al., 1992; Mueller et al., 1996). Flysch- and molasse-type sedimentary basins within the NVZ are associated with arc construction and emergence, respectively (Mueller et al., 1989; Mueller and Donaldson, 1992; Mueller et al., 1996). In contrast, the SVZ is separated into the Blake River Block in the west (Dimroth et al., 1982) and the Malartic Block in the east (Desrochers et al., 1993), each interpreted as an individual lithotectonic domain, separated by sedimentary rocks of the Kewagama Formation (**Figure 2**; Mueller and Donaldson, 1992). The 2703-2698 Ma (after Mortensen, 1993b) Blake River Block is thought to form an oceanic arc, underlain by tholeiitic basalts and evolving up section to more calc-alkaline mafic to felsic volcanic and volcaniclastic deposits (Dimroth et al., 1982). The 2715-2700 Ma Malartic Block has been interpreted in numerous ways: (1) progressive deposition from an ultramafic-mafic oceanic platform to arc-related volcanism (Dimroth et al., 1982); or (2) a collage of accreted oceanic plateaus

composed of ultramafic to mafic lava flows and a post-accretion eruption of arc-related intermediate to felsic lavas and associated volcaniclastic sedimentary rocks (Desrochers et al., 1993).

The inferred north dipping subduction zone(s), as initially suggested by Dimroth et al. (1983b), associated with the construction of the Abitibi Greenstone Belt, has been corroborated by Calvert et al. (1995) and Calvert and Ludden (1999), by seismic refraction. Metamorphism is predominantly greenschist facies, with amphibolite facies rocks around the batholiths (**Figure 4**; Daigneault et al., 2002). Primary volcanic textures are well preserved outside major shear zones and intrusions. For brevity the suffix 'meta' is omitted in describing the lithological facies.

2.2 Malartic Block of the SVZ

The SVZ (**Figure 3**) is divided into the western Blake River and eastern Malartic blocks (Babineau, 1983; Dimroth et al., 1982) and is separated by the Kewagama Formation (Mueller and Donaldson, 1992). The dilemma confronting this and subsequent chapters stems from the use of *block* versus *group* in describing the geologically distinct regions in the SVZ. The term "block" represents a distinct lithotectonic domain. Group is defined as a lithostratigraphic unit composed of several formations (Parker, 1997). Even though group is correct for the region, the term "block" is utilized, such that Malartic Block refers to a distinct lithotectonic domain in the southeastern part of the SVZ.

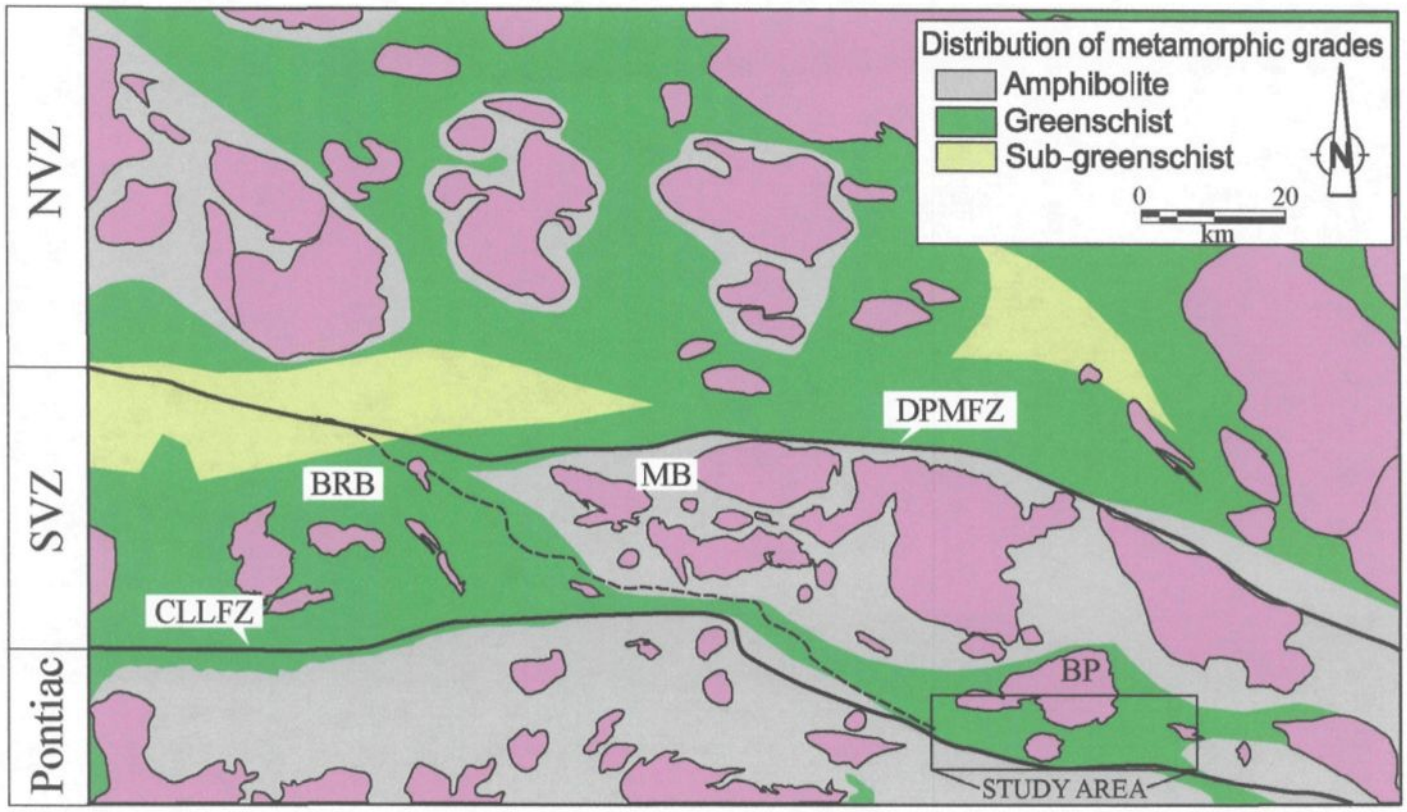

Figure 4. Distribution of metamorphic grade in SE Abitibi Greenstone Belt. Study area outlined (see Figure 6). Destor-Porcupine-Manneville Fault Zone (DPMFZ) and Cadillac-Larder-Lake Fault Zone (CLLFZ) delineate the SVZ, which is subdivided into the Blake River Block (BRB) to the west and the Malartic Block (MB) to the east. Adapted from Daignault et al. (2002).

The extent of the Malartic Block has undergone numerous revisions over the past six decades (**Figure 5A**), starting with regional work by Gunning and Ambrose (1940) for the Geological Survey of Canada. Initial stratigraphic subdivisions proposed by Gunning and Ambrose (1940) were based on their mapping of alternating sequences of volcanic and sedimentary assemblages through the Val d'Or and Malartic areas. They recognized four groups, which from oldest to youngest were: (1) the volcanic Malartic Group, (2) the sedimentary Kewagama Group, (3) the volcanic Blake River Group, and (4) the sedimentary Cadillac Group. Subsequent work in the area redefined the stratigraphy based on top determinations, whereas Norman (1943, 1947a, b) recognized that the volcanic rocks of the Blake River Group were not younger than the sedimentary Kewagama Group.

Latulippe (1966) subdivided the Malartic area into a northern Lower Malartic and southern Upper Malartic subgroups (**Figure 5A**) based on the volcanic stratigraphy. The Lower Malartic was characterized by voluminous ultramafic flows and associated intrusions, whereas the Upper Malartic comprised a series of mafic to felsic lava flows and intercalated volcaniclastic deposits cut by post-eruptive dioritic to granodioritc intrusions (**Figure 5A**). In the 1970's, Imreh identified ultramafic rocks of the Lower Malartic subgroup and recognized pillowed flows and flow top breccias, along with spinifex textures indicative of flows rather than previously mapped intrusions (Imreh 1974a, 1974b, 1974c, 1976, 1985). This work defined numerous formations based on volcano-sedimentary associations and these were grouped into two major lithotectonic assemblages (Imreh 1976, 1985) in the Malartic Block. Imreh's *Malartic Group* was composed of the ultramafic and mafic volcanic lava flows of the La Motte-Vassan and Dubuisson formations interpreted to

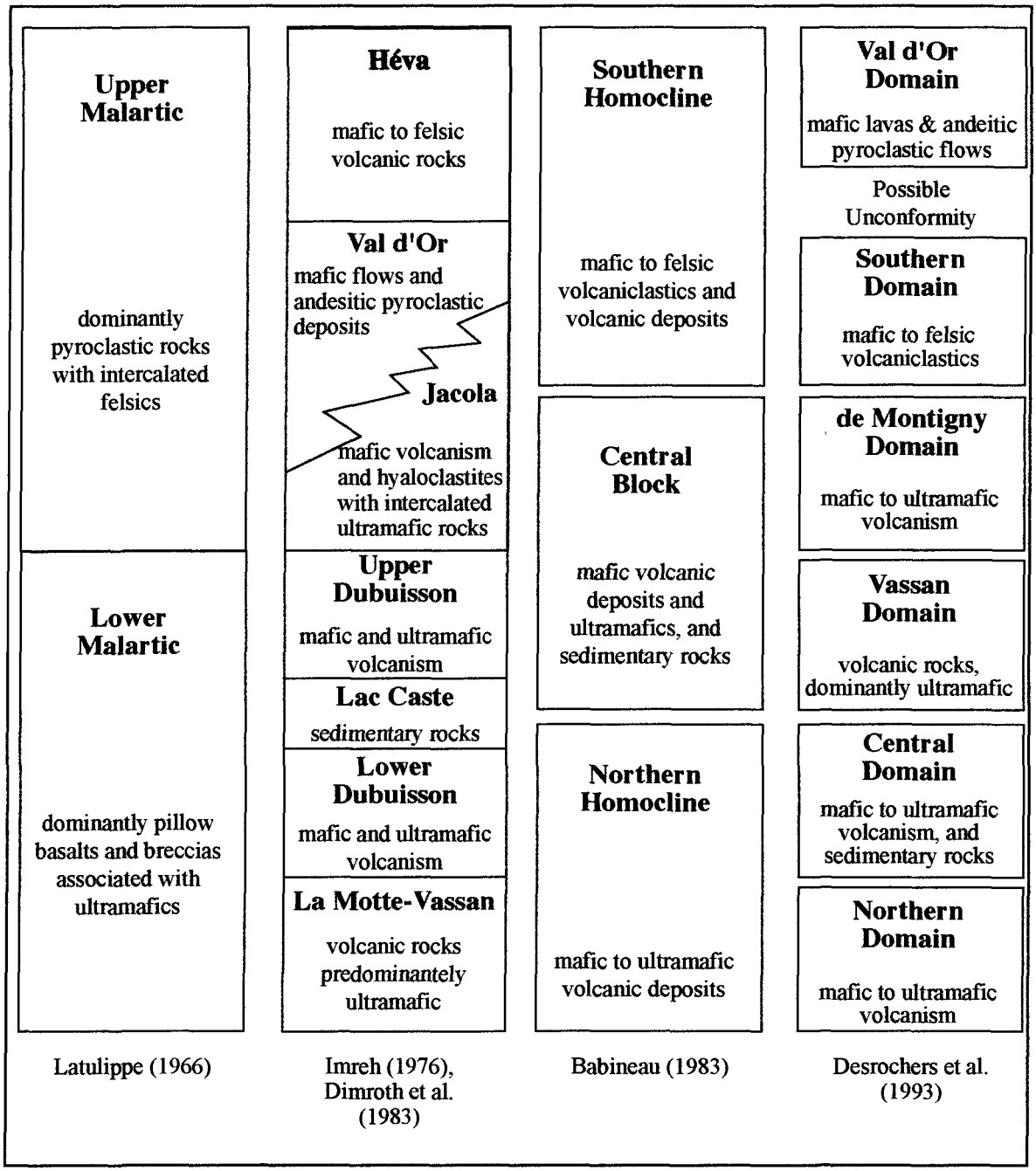

Figure 5A: Stratigraphic interpretations for the Malartic Block (after Desrochers et al., 1996)

form an oceanic lava plain and the *Val d'Or Volcanic Complex* comprised the Jacola, Val d'Or, and Héva formations (**Figure 5A**; Imreh 1976, 1985).

Up until now, the Malartic Block was mapped and interpreted as a single homoclinal stratigraphic succession younging southward to the Cadillac-Larder Lake Fault (**Figure 3**). However, work in the 1980s (Babineau, 1983; Gaudreau et al., 1986; Ludden and Hubert, 1986) and 1990s (Desrochers and Hubert 1996; Desrochers et al. 1993; 1996) challenged this simple stratigraphy by offering a more structural viewpoint on the construction of the Malartic Block. These authors proposed that the Malartic Block was composed of an assemblage of separate lithotectonic domains based on zones of varying strain within the volcano-sedimentary stratigraphy (**Figure 5A**). This hypothesis culminated in Desrochers et al. (1993) renaming the Malartic Block as the **Malartic Composite Block**, which reflects their interpretation of an assemblage of lithotectonic domains for the Val d'Or-Malartic region. The Malartic Composite Block is divided into five mafic to ultramafic domains and one calc-alkaline lithotectonic domain represented by the Northern, Central, Vassan, de Montigny, Southern, and Val d'Or domains (**Figure 5A**), respectively. The mafic-ultramafic domains were interpreted as remnant terranes of Archean oceanic plateaus composed of komatiitic and tholeiitic mafic-felsic lavas and subordinate intercalated volcaniclastic sedimentary rocks. Each of these domains display their own: (1) lithological assemblage; (2) structural fabrics (i.e., S_1, S_2); and (3) geochemical signature. Subsequent accretion formed an allochthonous assemblage of *exotic,* fault-bounded blocks, whereby there are no stratigraphic relationships across their faulted contacts. In contrast, the calc-alkaline volcanism of the Val d'Or Domain represents

extensional processes where mafic to felsic lava and associated fragmental rocks were deposited onto, but rest unconformably on the Central and Southern domains (Desrochers and Hubert, 1996), thus making the Val d'Or Domain the *youngest* within the Malartic Composite Block.

2.2.1 Southern Malartic Block: formations within the study area

The formations studied include, from north to south: (1) the Jacola Formation, (2) Val d'Or Formation, and (3) Héva Formation (**Figures 6 and 7**). Initial interpretation of formations in the Malartic Block placed the Jacola Formation within the interpreted *Val d'Or Volcanic Complex* , a central submarine volcanic complex (Dimroth et al., 1983; Imreh, 1985), in spite of a prevalence of ultramafic and mafic lava flows (Imreh, 1985). This interpretation most likely originated from the inferred lateral transition from the Jacola to the Val d'Or formation, on the south flank of the La Motte-Vassan anticline. Both formations were deposited on the Dubuisson Formation, which formed part of the La Motte submarine lava plain (**Figure 5B**). The volcanic environment evolved from west to east, with the Jacola Formation considered as *transitional* from tholeiitic to calc-alkaline. It is located along the flank of the central volcanic complex (Imreh, 1985). Furthermore, Imreh (1985) documented characteristics akin to both fissural and central volcanic complexes within the Jacola Formation, suggesting a transitional phase between these tectonic environments.

Toward the east, volcanic facies become fragmented and of calc-alkaline affinity, to which Imreh (1985) attributed facies typical of a central volcanic facies and characterized

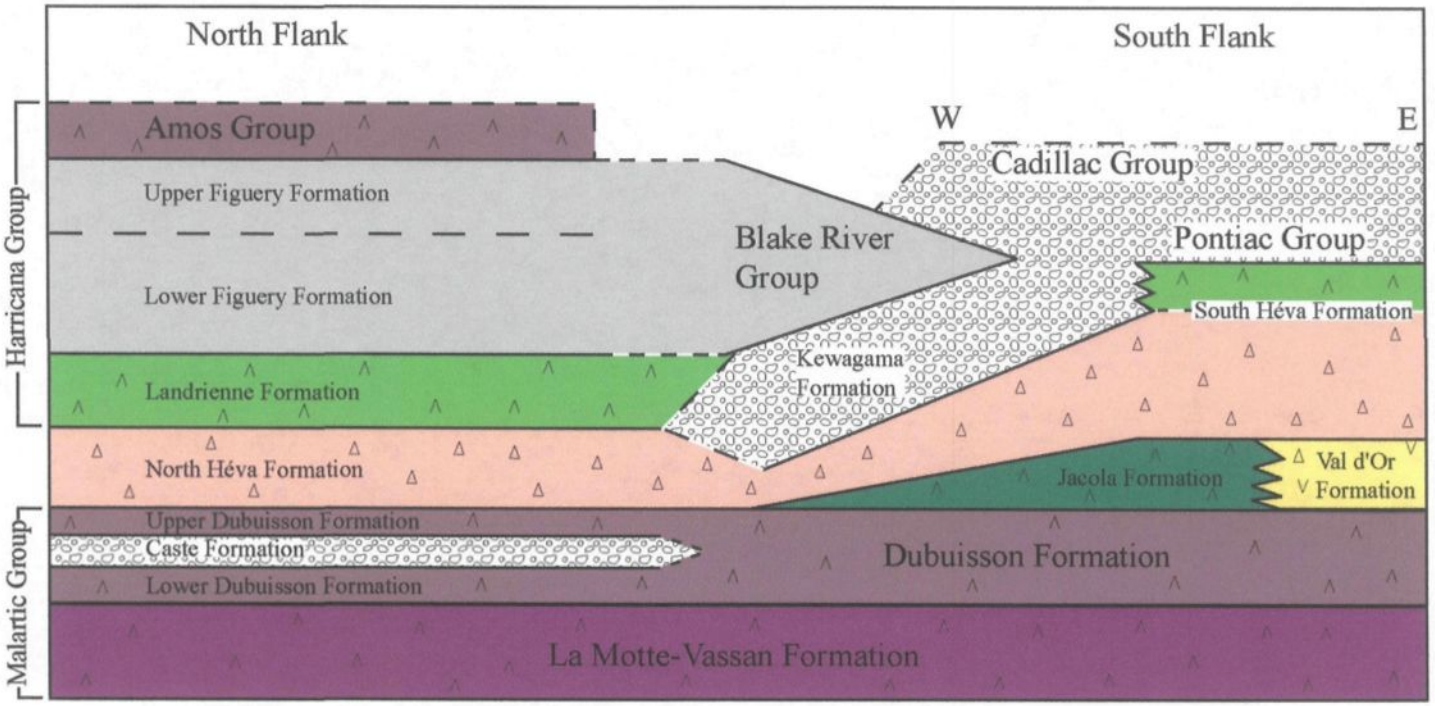

Figure 5B: Stratigraphic correlation across the northern and southern flanks of the La Motte-Vassan anticline. Note that the Jacola, Val d'Or and Héva formations are not included in the Malartic or Harricana groups. Adapted from Imreh (1985).

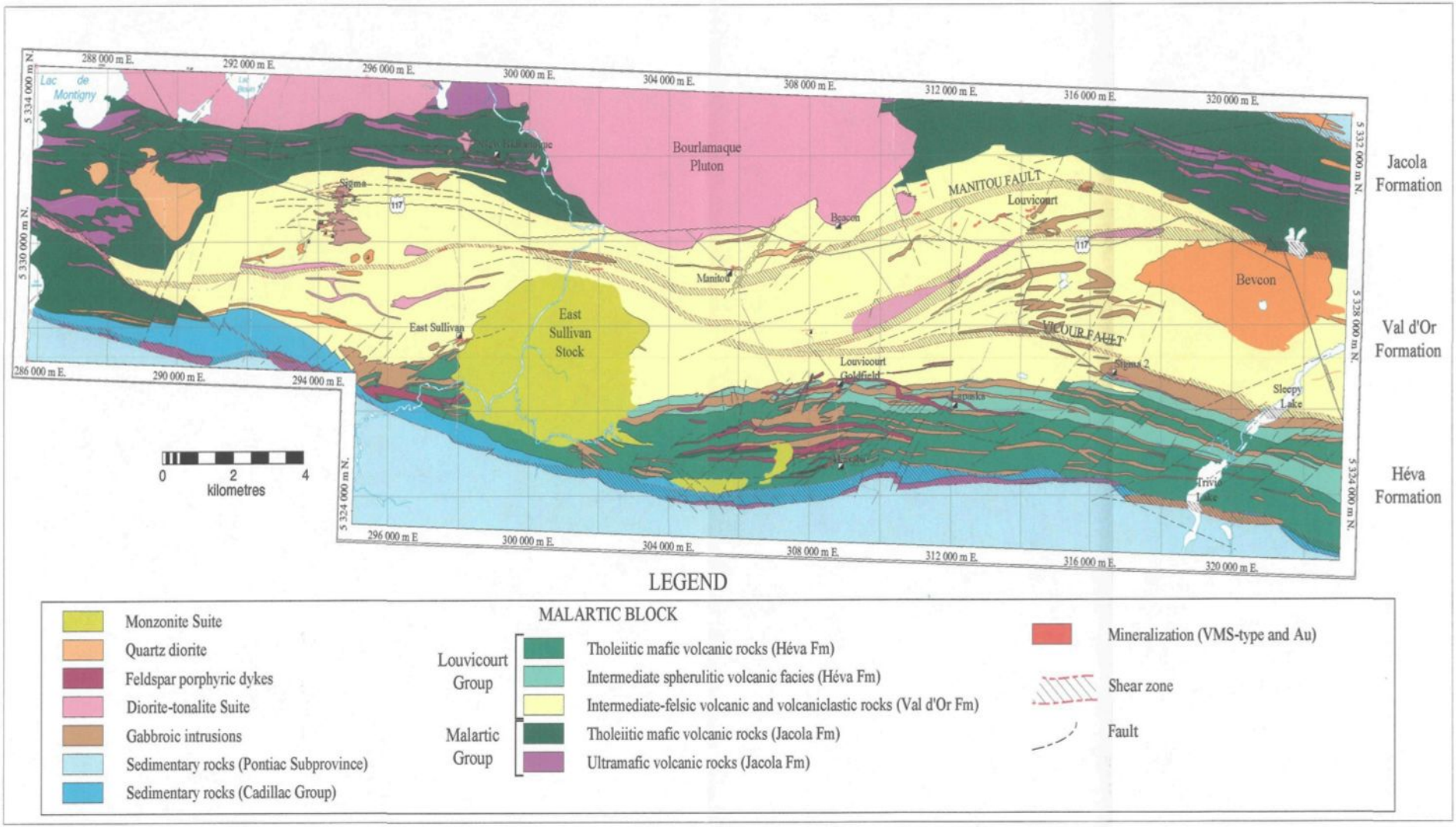

Figure 6: Simplifed regional geology of the Val d'Or region. Geologic compilation after Pilote (MRN), Lavoie, Scott, Riopel, Champagne (UQAC), Beaumont (MRN), and Mueller (UQAC) (2003).

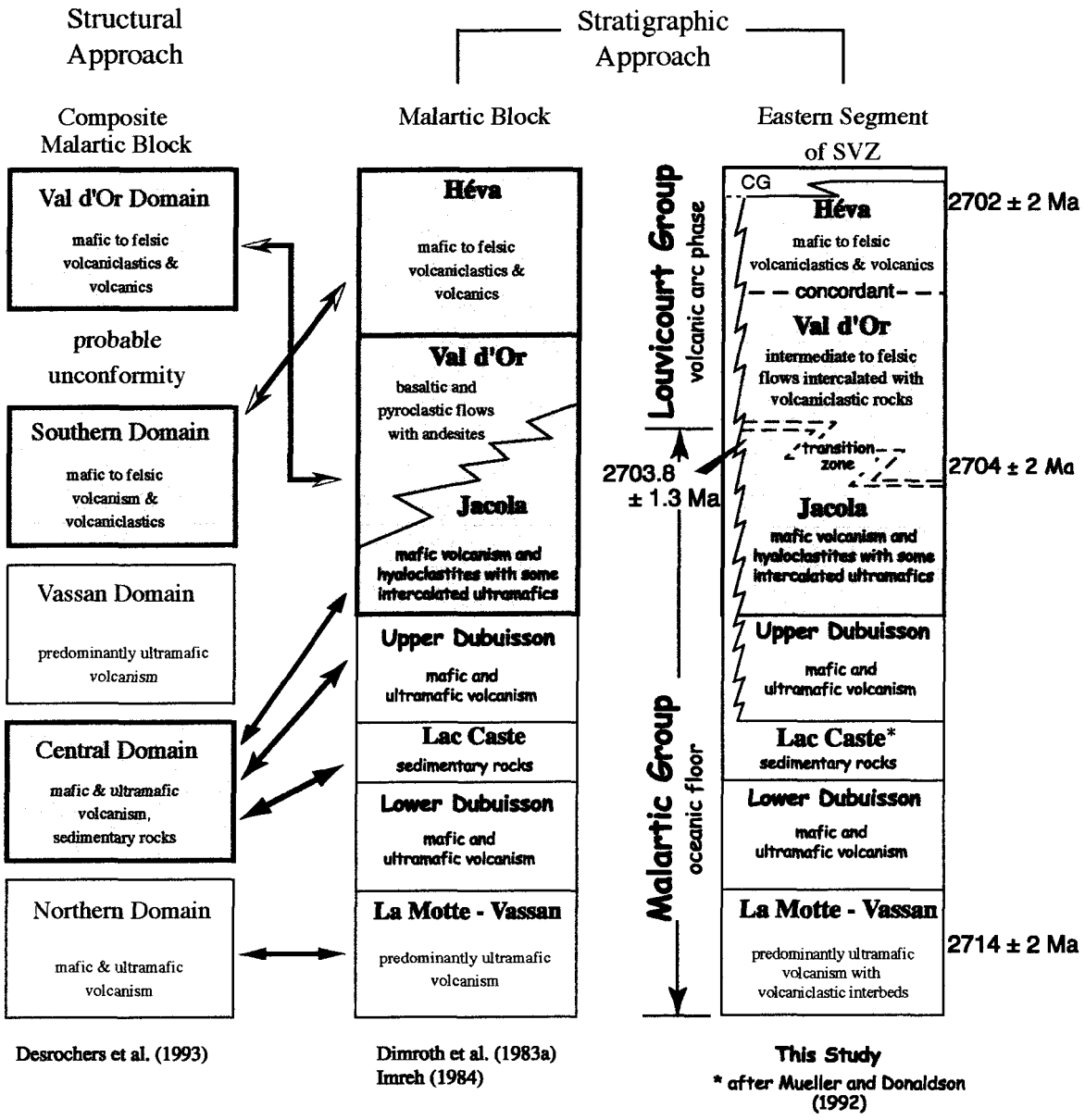

Figure 7. Malartic Block units based on a: (1) structural approach (Desrochers et al. 1993) and (2) stratigraphic approach (Dimroth et al., 1983; Imreh, 1985). The proposed stratigraphy for this work recognizes two new groups based on tectonic affiliation; Malartic Group represents oceanic floor and the Louvicourt Group represents a volcanic arc. The Cadillac Group (CG) forms a forearc sedimentary package of flysch-type deposits that is the lateral equivalent to the Héva Formation along strike to the west (see Figures 5B & 6). This links this region with the Blake River Block indicating a complete allochthonous assemblage (see Discussion - Chapter 7). Equivalent assmeblages are linked by arrows with those studied in gray.

the Val d'Or Formation. Lava composition varied from basalt to rare dacite, with volcaniclastic facies dominantly of andesitic composition. The up-section transition to the Héva Formation is indicated by the predominance of massive basaltic flows (Imreh, 1985). Basalt flows are typically extensive facies mappable for several kilometers along strike, suggesting a change to more effusive volcanism, thereby signifying the end of the central volcanic complex.

2.3 Geodynamic Models for the Malartic Block

Contrasting geodynamic models were proposed as a consequence of different stratigraphic interpretations for the Malartic Block. The basis for these models resides in a structural/tectonic versus stratigraphic approach. The structural approach advocates the concept of exotic blocks forming the Malartic (Composite) Block (cf. Desrochers et al., 1993), whereby the characterization of local stress fields, deformation events, and bedding orientation suggests an allochthonous college (Desrochers et al., 1996). In contrast, the regional stratigraphy, with emphasis on bedding and contact relationships as well as volcanic architecture, supports a homoclinal stratigraphic sequence younging to the south (Dimroth et al., 1982; Imreh, 1976). Both interpretations identify an extensive ultramafic to mafic oceanic base and an upper calc-alkaline Val d'Or Formation/Domain (see **Figure 7**).

The geodynamic model of Desrochers et al. (1993) inferred the accretion of five individual domains to form the Malartic Composite Block. These domains were accreted during a subduction-related shortening that defines their faulted contacts (**Figure 8**). The

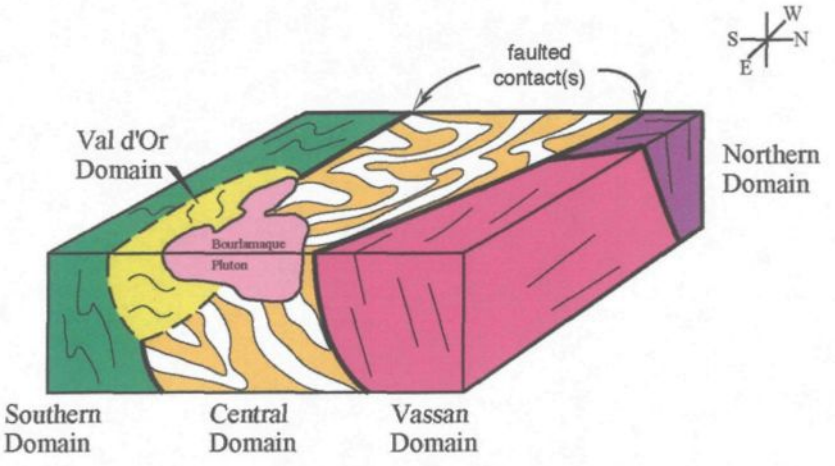

Figure 8A: Block diagram of various domains of the Malartic Composite Block. Solid lines between contacts represent faults and dashed line is an unconformity. The varied patterns within domains represent the individual deformation history of each domain (after Desrochers et al., 1993).

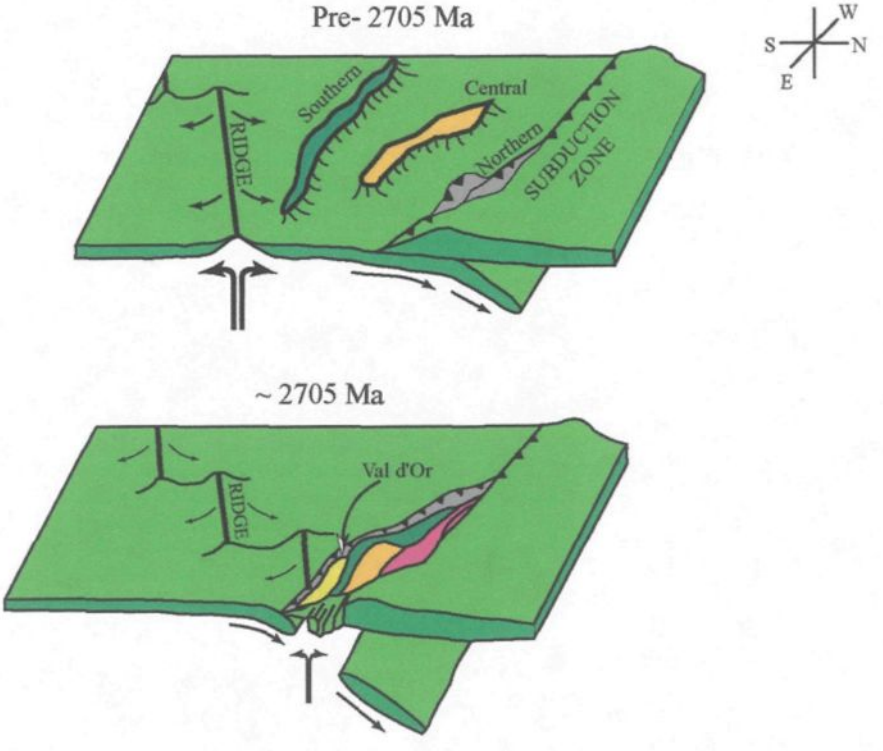

Figure 8B: Proposed tectonic model for Malartic Composite Block. Mafic domains are oceanic plateaus (top) accreted during oblique ridge subduction. Calc-alkaline volcanic rocks (Val d'Or Domain) form on top of accreted plateaus (after Desrochers et al., 1993).

youngest domain, the calc-alkaline Val d'Or Domain, is produced by extension-related volcanism that erupted through the newly accreted and deformed plateau collage, possibly from ridge subduction in a regime of oblique convergence (**Figure 8B**).

The lithostratigraphic evolutionary model of Dimroth et al. (1982; 1983a; 1983b) envisaged five to seven overlapping phases for the construction of their Southern External Zone, which is the equivalent to the SVZ. The external zone was subdivided into two volcanic cycles; namely a Lower and an Upper cycle corresponding to local stratigraphy and change in volcanic style from basaltic flows with intergraded rhyolites and associated sedimentary rocks to overlying ultramafic and tholeiitic sequences. The Upper Cycle or cycle II corresponds to the deposition of the Malartic Block. The ultramafic sequence includes the La Motte-Vassan and Dubuisson formations made up of komatiite and tholeiitic flows, and includes the sedimentary Lac Caste Formation. The sequence is overlain by a prominent tholeiitic basalt sequence ranging from massive to pillowed flows, minor intercalated brecciated felsic flows and pyroclastic rocks that collectively form the Jacola, Val d'Or and Héva formations (**Figure 7**). Ultramafic and mafic flows are interpreted as submarine lava plains composed of laterally extensive lava flows (> 30-km), erupted during effusive fissure-type volcanism. Subsequent felsic volcanism formed *Central Volcanic Complexes*, defined as 30-km wide zones (**Figure 9**). These complexes are dominantly felsic with proximal massive to distal brecciated facies, display variations in vesicularity, indicating volcano-tectonic subsidence, and show lateral changes in thickness and lenticularity of volcanic deposits (Dimroth et al. 1982, 1983a, 1983b).

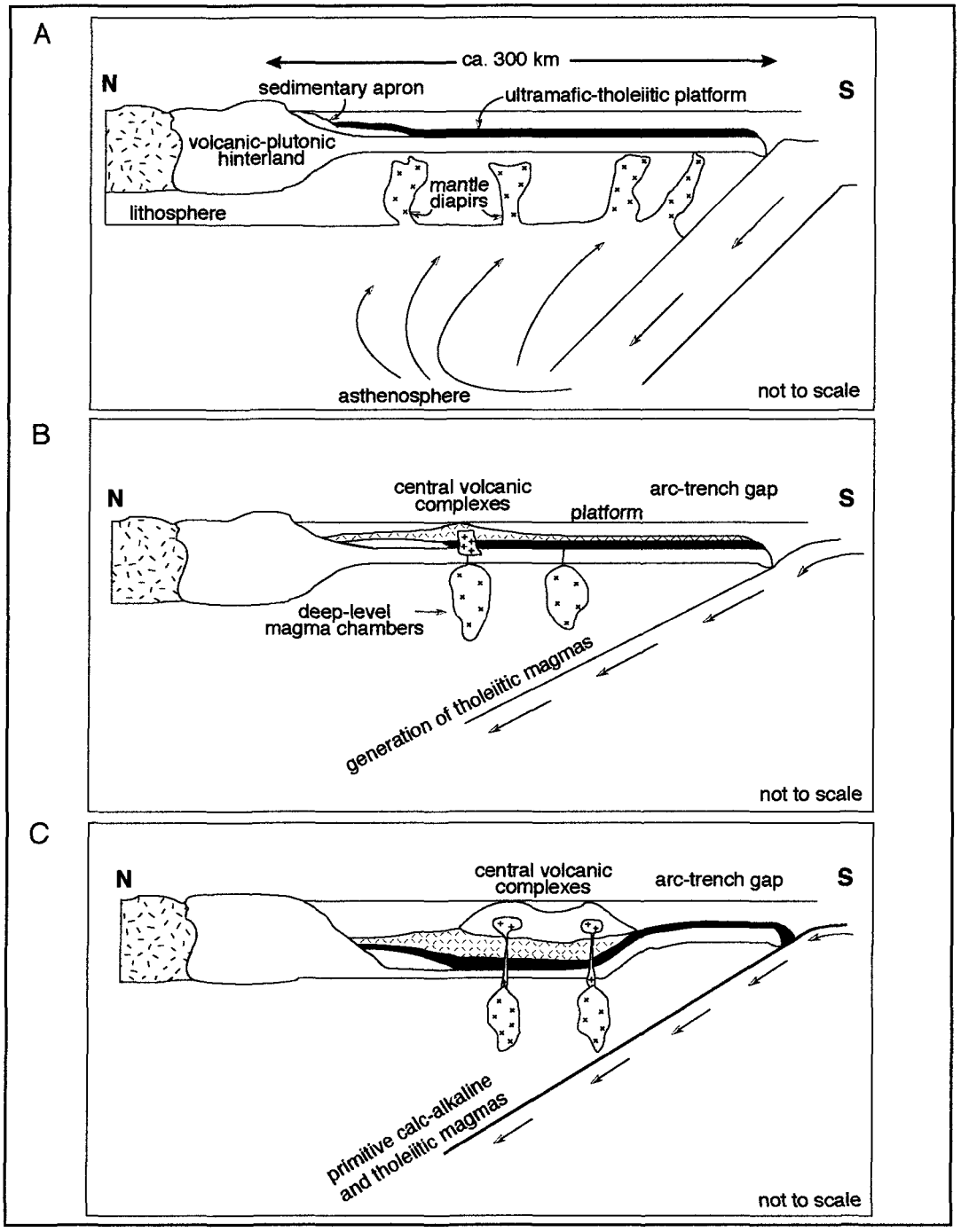

Figure 9: Three phase volcanic arc model for the evolution of southern Malartic Group. A) Formation of extensive submarine mafic-ultramafic lava plain. B) Start of subduction and development of central volcanic complexes. C) Evolution and buildup of central volcanic complexes to calc-alkaline volcanism at shallower levels (modified from Dimroth et al., 1983b).

The stratigraphy and the character of the volcano-sedimentary units of the Malartic Block suggest a continuum of depositional events commencing with the ultramafic-mafic La Motte-Vassan Formation, the felsic volcanic Val d'Or Formation, and terminating with the mafic Héva Formation. The ultramafic-dominated sequences form an extensive, effusive submarine platform (from deep mantle diapirs), referred to as the Roquemaure Plain (**Figure 9A;** Dimroth 1983b). Northward subduction may have been initiated during this period, as indicated by proto-arc related tholeiitic volcanism (**Figure 9B**). Subsequent volcanic evolution is indicated by calc-alkaline arc volcanism. Arc-type volcanism is characterized by numerous central vents that produce abundant fragmental material forming laterally-restricted deposits (Dimroth et al. 1982; 1983a, 1983b).

In summary, both the tectonic and stratigraphic models recognize the importance of mantle-derived (ultramafic) magmas, but differ in the interpretation of the temporal evolution of the volcanic rocks. This study will describe the individual formations in chronological order with their respective characteristics in order to develop a new geodynamic model, based on volcano-sedimentary facies analysis, geochemistry, new U-Pb zircon-age determinations, and recent structural studies by Daigneault et al. (2002).

CHAPTER 3

JACOLA FORMATION : AN OCEANIC PLATFORM

The Jacola Formation (JF) represents the oldest rocks within the Val d'Or region. Imreh (1985) mapped the 3000 m-thick JF as an ultramafic to basaltic sequence composed of lava flows and associated brecciated rocks. Discontinuous basaltic breccias were interpreted as hyaloclastic in origin and represent the construction of a volcanic edifice, hence placing the JF at the base of the Val d'Or Volcanic Complex, (e.g., Dimroth et al., 1982). Their interpretation is supported by an apparent lateral transition from the JF in the west to the Val d'Or Formation in the east (**Figures 5B and 10**), which would suggest a conformable or transitional relationship.

The ultramafic/mafic volcanism of the JF was considered to be the transition from the underlying La Motte mafic plain (Malartic Group; Imreh, 1985) to the overlying central volcanic complex (Val d'Or and Héva formations). Spatially, the JF was envisaged to be deposited along the flank of the Val d'Or Volcanic Complex and influenced by the underlying La Motte submarine mafic plain (Imreh, 1985). A deep submarine environment was inferred based on the absence of vesicles and broken pillows, along with minor hyaloclastites (Dimroth et al., 1982; Imreh, 1985). Up section, hyaloclastites become more abundant and the transition to the Val d'Or Formation is marked by the recognition of pillowed basalt flows and isolated pillow breccia of calc-alkaline affinity (Imreh, 1985), both of which are consistent with a shoaling sequence (e.g., Staudigel and Schminke, 1984).

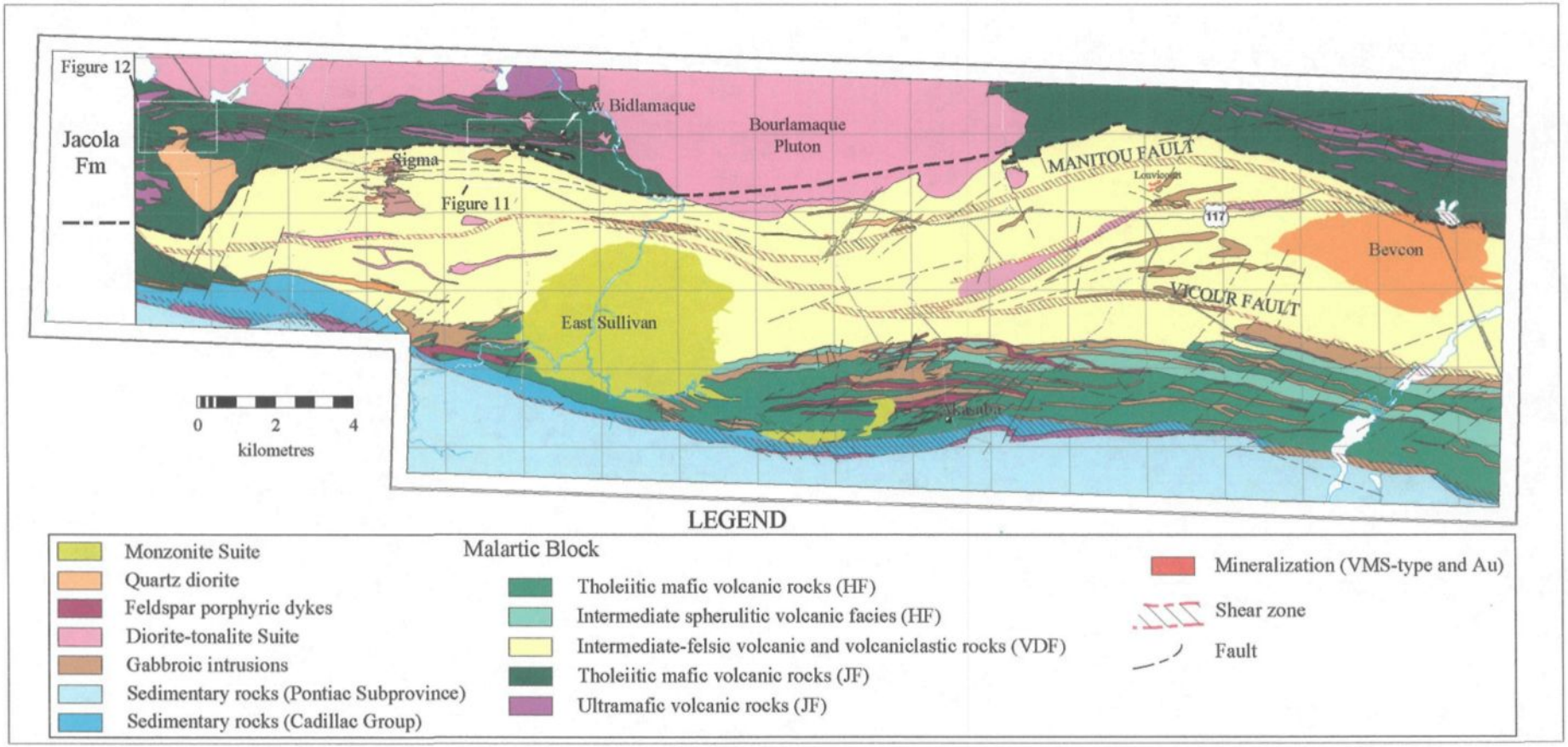

Figure 10 : Simplifed regional geology of the Val d'Or region outlining the Jacola Formation. Several areas of interest studied in detail are indicated. See Figure 6 for more detail.

3.1 Reasoning

Originally, this thesis was restricted to facies mapping of the Val d'Or and Héva formations, however, after the initial field campaign (Summer, 1997), it became apparent that it was necessary to include the JF. The objective was to evaluate the contact between the Jacola and Val d'Or formations, due to its importance with respect to the overall stratigraphy and reconstruction of the geodynamic setting and tectonic model. For the present study, mapping of the JF was limited to exposed outcrops in proximity to the Val d'Or Formation; thus only the upper contact of the JF is discussed (**Figures 10 and 11**), with some supportive geochemistry from an internal report (Champagne et al., 2002). Outcrops east of Sigma mine represent two of only five outcrops (**Figure 11**) in an area covering 627.74 hectares within the New Bidlamaque and Union Gold properties (Prud'Homme, 1996). A third outcrop, known as the New Bidlamaque showing (**Figures 10 and 11**), was mapped by another UQAC Masters student (Riopel, in progress), the significance of which is discussed below. Other outcrop locations were from road cuts and small exposed ridges in and around the town of Val d'Or.

3.2 Characteristics of the Jacola Formation

The studied JF is represented by a 1-2 km-thick sequence of tholeiitic basalts, komatiites, and subordinate mafic volcaniclastic deposits (**Figure 12**). Pillowed, brecciated, and the more dominant massive basalts, are interstratified with 100-200 m-thick massive to

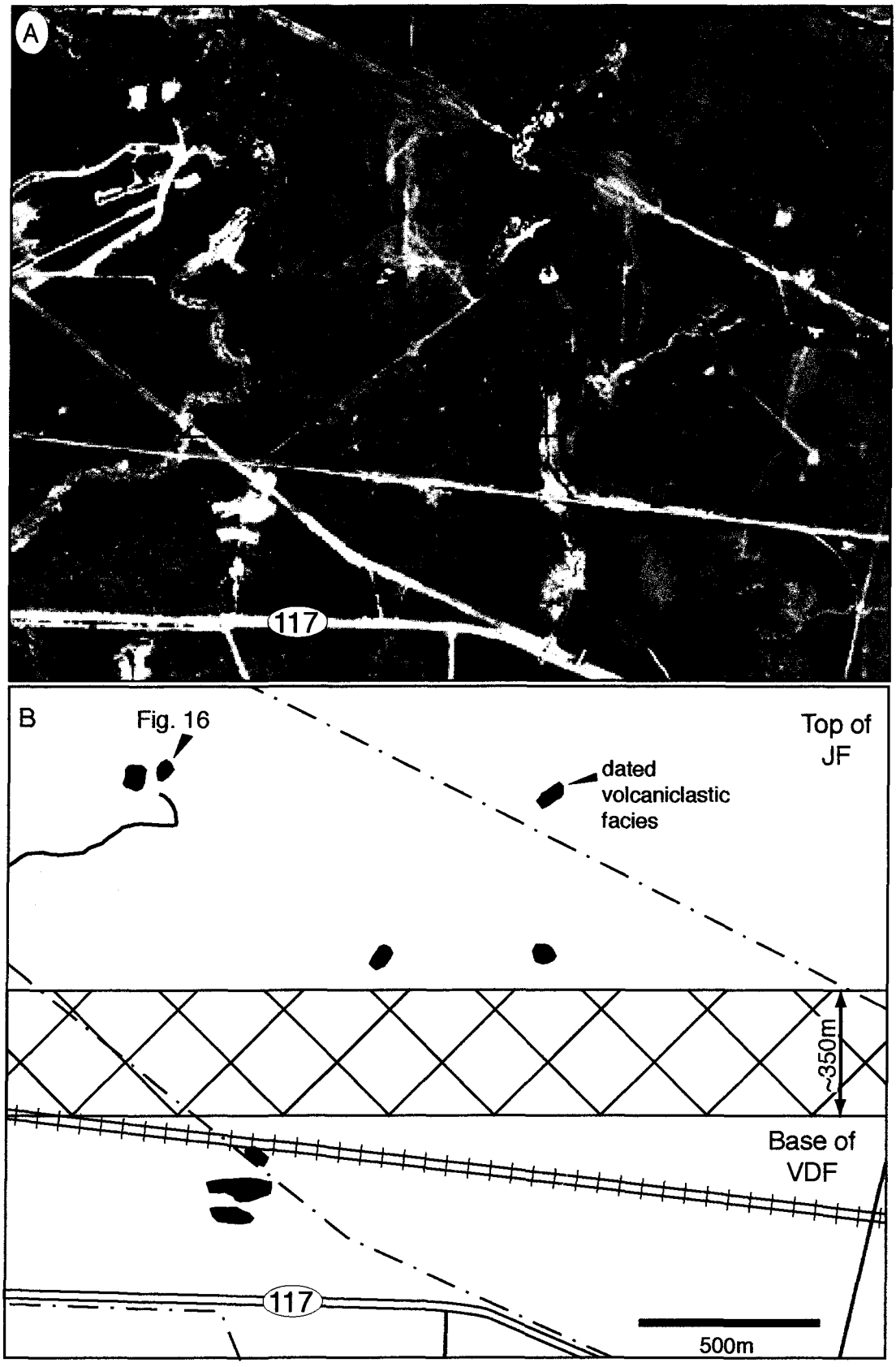

Figure 11. A) Aerial photograph of area just east of Val d'Or depicting outcrops from the Jacola and Val d'Or formations. Cross-hatched zone outlines the probably contact between these formations. B) Sketch of aerial photograph outlining stripped outcrops (shaded) between the formations.

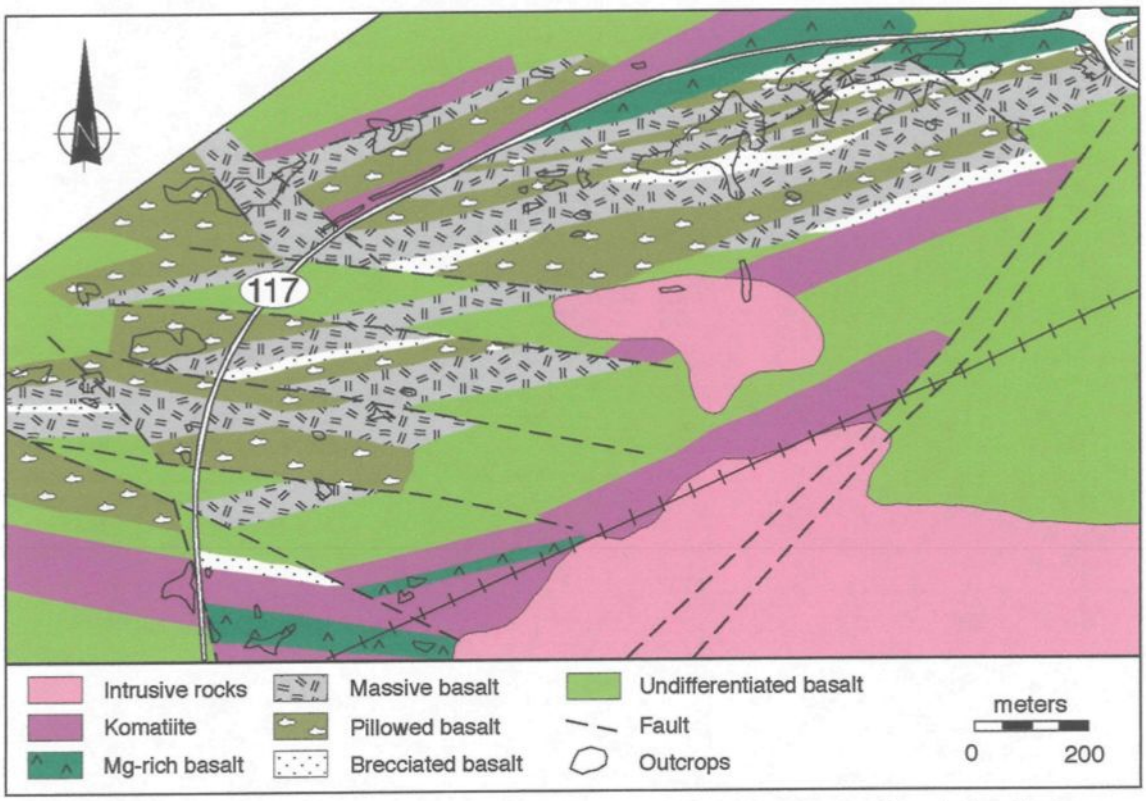

Figure 12. Mapped areas of the Jacola Formation just west of Val d'Or showing the relationship between komatiites and massive, pillowed and brecciated basalt. Modified from Champagne et al. (2002).

pillowed komatiitic lavas that extend laterally at least 14 km (Champagne et al., 2002). Minor intercalated volcaniclastic deposits are only locally observed and are typically discontinuous (**Figure 12**). Intense alteration, such as chloritization and serpentization, destroyed most primary volcanic textures. Nonetheless, relict spinifex texture is observed in cm-sized veins (**Figure 13**) and within flow-top breccias of thicker deposits (**Figure 14**).

Komatiites form 100 m-thick, discontinuous flow units that are commonly truncated by NW-SE or NE-SW trending faults (**Figure 12**). Individual flows range from 4 to 20 m-thick and are overlain by massive-to-brecciated, Mg-rich basalts (Champagne et al., 2002). Primary textures are preserved, but the original mineralogy has been overprinted by an alteration assemblage of chlorite, amphibole, and serpentine. Original olivine spinifex is represented by 0.30 to 0.45 mm-long blades of chlorite and serpentine (Champagne et al., 2002). Massive lavas are composed of an olivine and/or pyroxene cumulate forming 0.7 mm equant crystals now recrystallized to amphibole, serpentine and/or chlorite (**Figure 15A**; **Appendix A-1/2**).

Basalts are typically massive and brecciated and can be subdivided into Fe-rich and rare Mg-rich basalts (Champagne et al., 2002). The Mg-rich variety is distinguished in the field by its pale gray color, fine- to medium-grained character, and its association with komatiitic lavas. Massive flows range from 30 to 70 m-thick and isolated breccias up to 20 m-thick. In thin section, an interstitial texture is defined by 1-mm long plagioclase crystals and pyroxene now altered to amphibole (**Figure 15B**).

Massive to pillowed Fe-rich basalt is altered a green-gray to dark green, aphanitic, non-vesicular and upwards to 25 m-thick. Massive basalts commonly evolve to pillowed

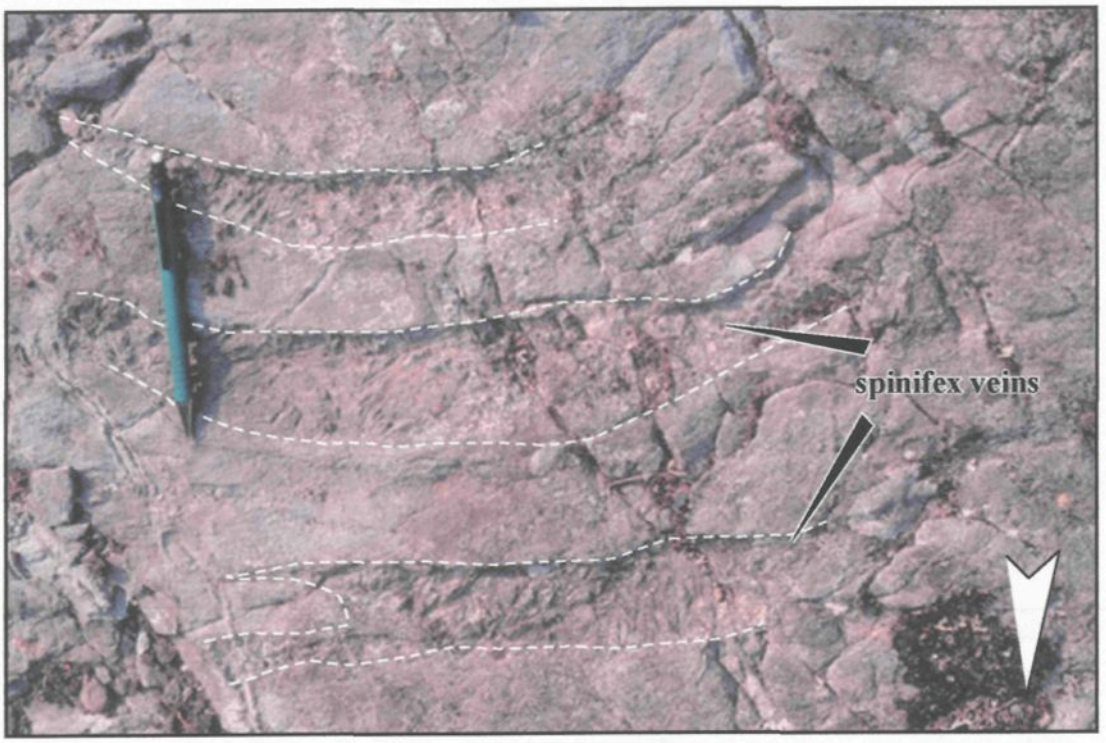

Figure 13. Spinifex texture within bands/veins of variable thickness. Tops indicated by arrow. Pencil is 15 cm-long.

Figure 14. Spinifex crystals randomly oriented with brecciated facies. Lens cap is 5.5 cm, with tops indicated by arrow.

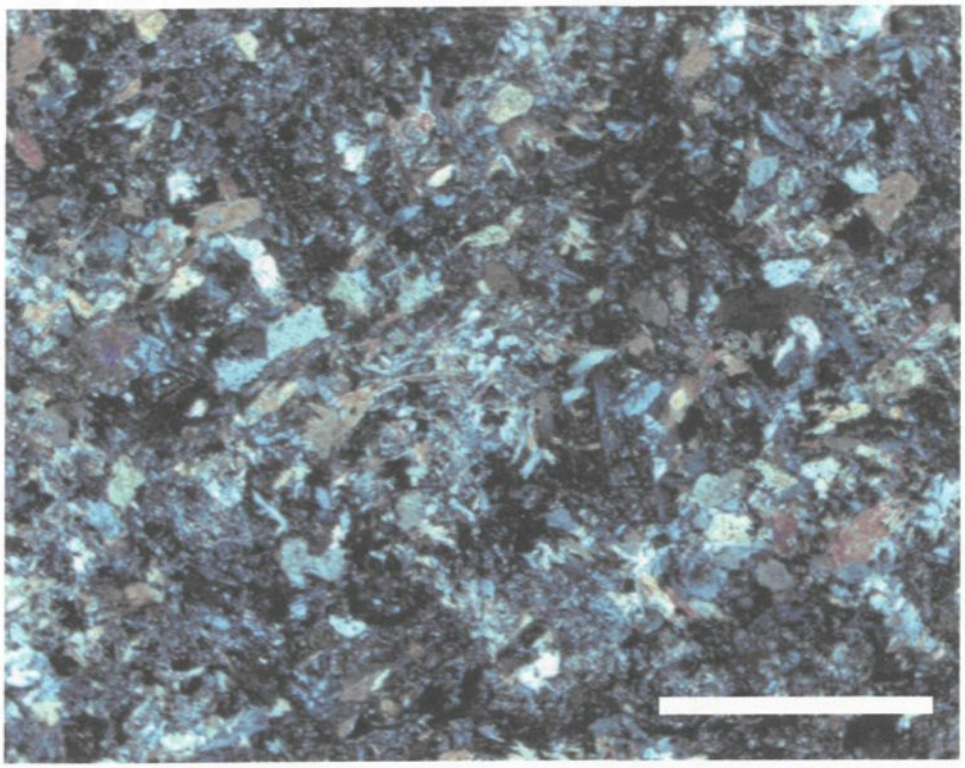

Figure 15A. Crossed nicols photomicrograph of recrystallized texture of massive basaltic komatiite flow from JF. Scale bar is 2mm. See appendix A-2 for in depth description and addition photo.

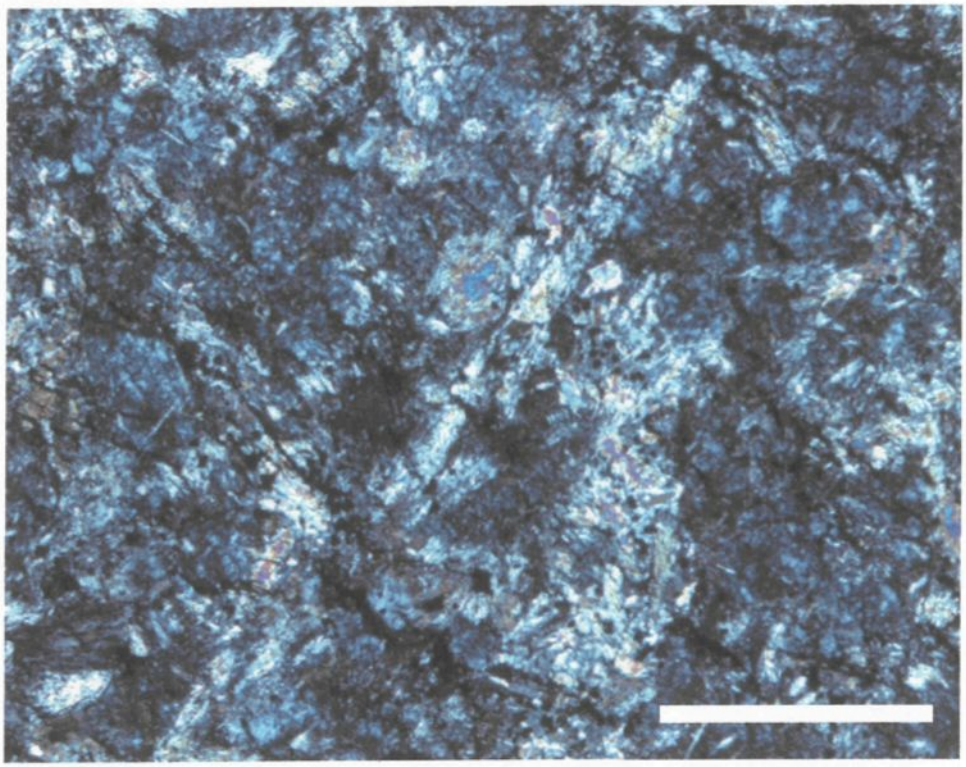

Figure 15B. Cross nicols photomicrograph of relict bladed pyroxene (now amphibole) within massive basaltic komatiite flow from JF (See appendix A-1: thin section CS97-246A). Scale bar is 2mm

facies both laterally and vertically, and in some cases capped by a massive facies that may represent a change in eruptive dynamics (**Figure 16**). Some gabbroic textured lithofacies may in fact be coarse-grained massive basalt as indicated by an apparent transition from mapped massive basalt. Unfortunately, contact relationships are obscured by shear zones (**Figure 16**) or are not exposed. Massive basalts are also characterized by angular lapilli fragments (**Appendix A-3**) that mantled tongue-like terminations of pillowed flows (**Figure 17**), which are characteristic of water-lava interaction forming hyaloclastites (Wohletz, 1983). Similar angular fragments constitute local deposits of stratified m-thick lapilli tuff and tuff breccias.

Pillow morphology ranges from mattress-, bun-, and sausage-shaped and suggest a southward younging direction (**Figures 16 & 18**). Lateral changes from oblong sausage forms to more inflated bun-to-mattress forms are locally observed. Pillows are characterized by well-developed chilled margins, varioles, and *in situ* hyaloclastites at pillow junctions. Intercalated hyaloclastites comprise cm-sized fragments localized between pillows (**Figure 19**) with elongated, cuspate to subrounded morphologies. Chilled margins are several mm-thick, aphyric and altered a blue-green color (**Figure 20**), which are similar to elongated/tabular fragments described previously. Individual, spherical grayish-green varioles, first appear within several mm of pillow margins and become progressively larger toward pillow interiors until they form a homogenous mass of aggregated varioles, giving pillows a grayish-green appearance (**Figure 20**). Measured pillow dimensions (long and short axes) documented from the detailed outcrop (**Figure 16**) have a 3.6:1 ratio indicating a prominent elongation (**Figure 16, Table 3**). In contrast to the

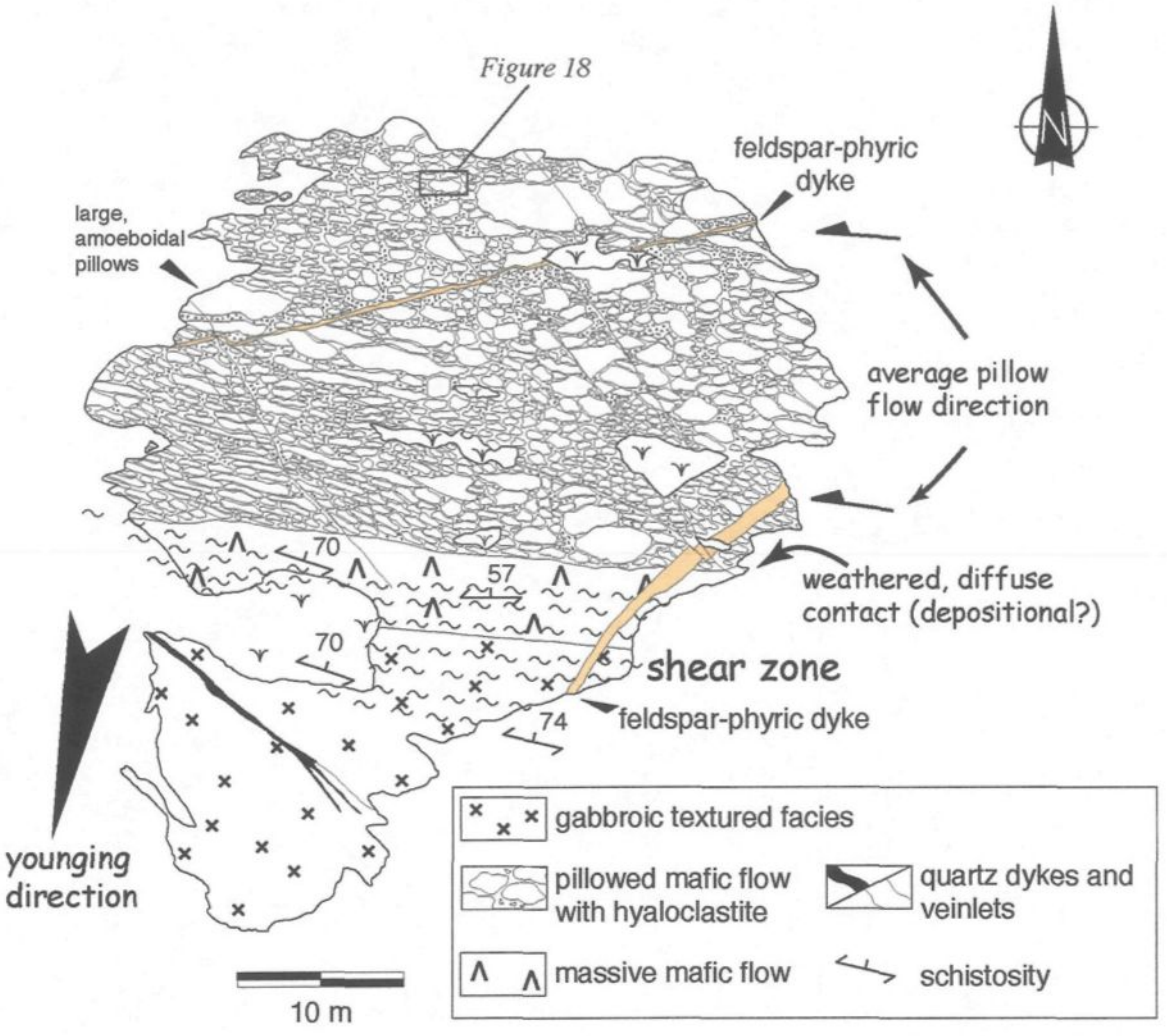

Figure 16. Mapped outcrop within the upper section of the Jacola Formation. Pillow structures indicate an undulatory propagation indicating an approximate E-W (azimuth) flow direction. Pillow morphology indicates a south-younging direction.

Figure 17. Tongue-like pillow termination mantled by pillow fragmental breccia. Pillowed exterior is characterized by polygonal cooling joints. Both lava and fragments are characterized by chilled margins. Pencil is 15 cm-long.

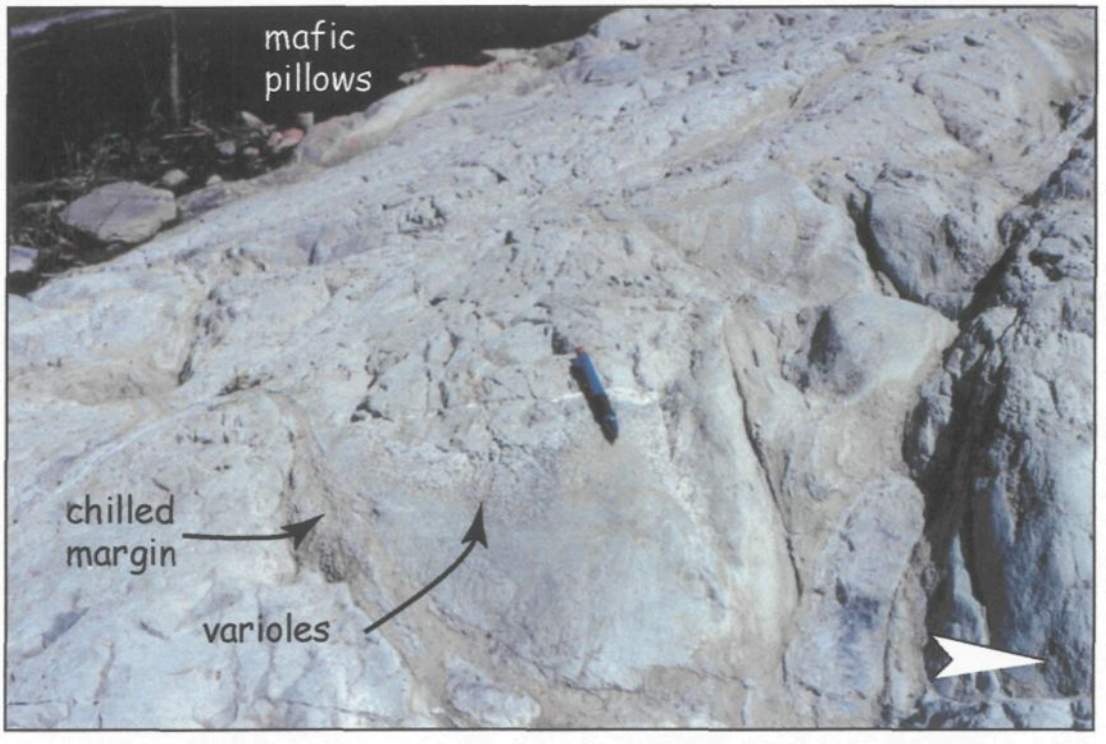

Figure 18. Sausage-shaped pillow looking towards the east. Pillow is plunging towards the viewer. Chilled margin and varioles evident. Arrow points south towards younging direction. Pencil is 15 cm-long.

Figure 19. Subrounded to subangular pillow fragmental breccia fragments (f) located between pillows. Scale bar is 10 cm-long.

Figure 20. Basaltic pillow structure: chilled margin (c), isolated varioles (v), and agglomerated massive interior (I). Scale bar is 10 cm-long.

Placer Dome Inc. report (Prud'Homme, 1996), no vesicles were observed, and it is possible that varioles were mistaken for vesicularity.

Table 3: Pillow sizes

Pillows	Long axis (m)	Short axis (m)	Area (m^2)
	7	2.5	17.5
	7	3	21
	5	2	10
	6	2.2	13.2
	4	1.2	4.8
	3.5	1.2	4.2
	4.7	0.9	4.23
	4	1.1	4.4
	4	1.2	4.8
	2.5	1	2.5
	3.5	0.9	3.15
	4.5	0.5	2.25
	3.5	0.5	1.75
	6.3	0.4	2.52
	3	0.3	0.9
Average	**4.6**	**1.3**	**6.5**

Minor dykes are observed on most outcrops, with two main populations distinguished based on appearance and geochemistry (see below). A deep green dyke phase appears associated with ultramafic lavas and may serve as conduits to overlying ultramafic flows, although no direct field relations supporting this hypothesis were observed. The second phase is a brownish-green aphyric dyke that cuts the local stratigraphy at near right angles, but highly convoluted in cross section. These dykes are also possible feeder dykes, but again no direct observations are present to support this claim.

Upper and lower inter-formational contacts are not exposed and are considered to be transitional over 100s of meters and defined by the abundance and appearance of fragmental material, respectively (Imreh, 1985; **Figure 11**). The nature of the contact relationship between the JF and Bourlamaque Pluton (BP) was examined in order to ascertain their temporal association. In this regard, dykes, emanating from the BP, were observed intruding and crosscutting the JF (**Figure 21**). The upper contact marks a change

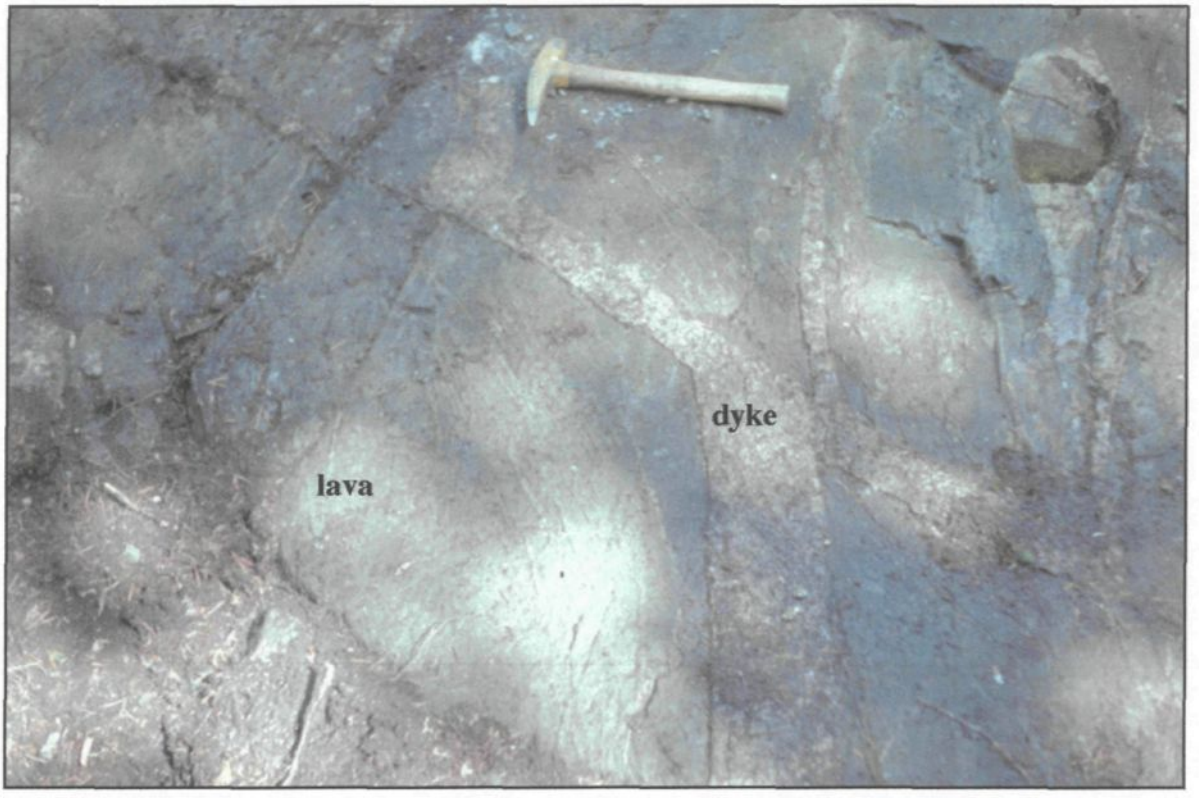

Figure 21. Field photo of dykes from the Bourlamaque Pluton crosscutting massive basaltic lava of the Jacola Formation. Hammer is 35 cm-long.

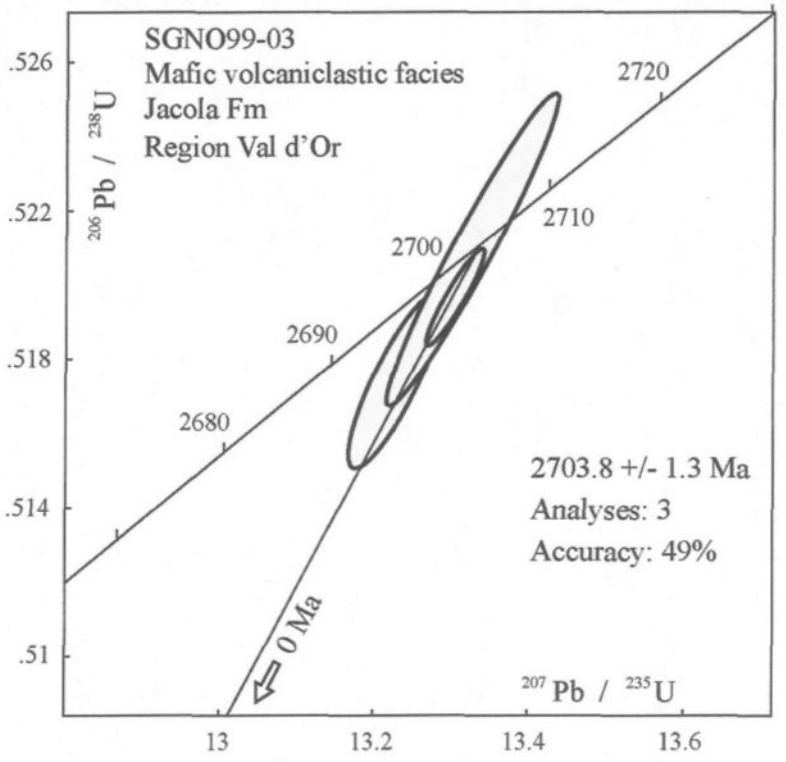

Figure 22: Age date of mafic volcaniclastic at the summit of the Jacola Formation, taken from New Bidlamaque showing. Modified from Pilote et al. (in press).

Table 4: Structural and bedding measurements

Schistosity	Type	Strike	Dip
	S_1	283	74
	S_1	280	75
	S_1	288	70
	S_1	290	77
	S_1	286	70
	S_1	274	58
	S_1	269	57
	S_1	265	80
average		**279**	**70**

Pillow flow tops	Strike	Plunge
	286	41
	284	43
	278	29
	284	41
	278	30
	271	30
	270	18
	282	52
	272	32
	273	35
	273	30
	277	18
	271	39
	285	35
	278	22
	285	34
average	**278**	**33**

from basaltic to komatiitic lavas and local mafic volcaniclastic deposits of the JF to abundant volcaniclastic deposits of transitional, intermediate to felsic composition of the lower Val d'Or Formation. The actual contact is probably located within a 350 m-wide zone, based on field relationships (**Figure 11**). Deformation is weakly to moderately developed in the studied areas with localized cm- to m-sized shear zones. Regional schistosity, the only one recognized, ranges from N270° to N290° with an average dip of 70° (**Table 4**), which is subparallel to bedding, as defined by pillowed facies, of 98°. Bedding is subvertical and commonly overturned with younging direction always to the south (**Figure 16**). Pillow propagation, as suggested by sausage-like structures (**Figures 16**

and 18), averages 278° with a plunge of 33° (**Table 4**). Metamorphic grade is low, ranging from prehnite-pumpellyite to lower greenschist facies.

At present only one age date is available for the upper JF. This recent U-Pb dating gives an age of 2703.8 ± 1.3 Ma (**Figure 22**) and was taken from a mafic volcaniclastic deposit (New Bidlamaque showing, **Figures 10 and 11**) close to the presumed contact with the Val d'Or Formation (Pilote et al., 1999). These volcaniclastic deposits are normal graded tuff breccias to lapilli tuffs with truncated bedding indicating erosive processes. They are capped by massive lava to amoeboidal pillows of mafic composition, similar in appearance to the underlying fragments (Riopel, MSc in progress).

3.3 Interpretation

Massive and pillowed flows (Table 5) are suggestive of effusive volcanism in a subaqueous setting (Dimroth et al., 1978; Cousineau and Dimroth, 1982). Moreover, the low aspect ratio (flow length versus flow thickness, see Table 5) of basaltic and komatiitic flows implies voluminous eruptions consistent with fissural-type. These fissure sources are capable of forming thin, lenticular deposits necessary to construct a submarine lava plain. Finally, the non-vesicular nature of volcanic lithofacies may indicate a deep-water environment of 2000m or more (Gill et al., 1990), whereby hydrostatic pressure inhibited volatile exsolution.

Lateral variations in pillow morphology may indicate changes in viscosity and/or temperature, which may be related to proximity to the source. Dimroth et al. (1978)

suggested that massive lava could change to pillowed and ultimately brecciated facies with increasing distance from the erupting source. As a lava flow advances, it loses heat to the surrounding water, which increases the effective viscosity of the flow. This results in morphological changes from fluidal to more compact pillows forms (e.g., sausage-to-bun shaped). Other parameters to consider are decreases in the eruptive and/or flow rate(s), which will restrict the supply of fluidal lava to the flow front. The sausage-shaped pillow morphology is suggestive of small feeder tubes (Decker and Decker, 1989) and is characterized by an undulatory east-west propagation (**Figures 16 and 18**) indicating a westward flow direction. Such tubes may result from gravitational forces from a paleoslope and/or low viscosity lava (Moore, 1975; Walker, 1992), both of which suggest proximity to the erupting fissure/vent. Additional support for a proximal setting for pillow lavas mapped in the New Bidlamaque region (**Figures 10 and 11**) is the presence of varioles and aphyric nature, which are indicative of high temperature lava. Varioles observed within pillow margins are similar to those described by Gélinas et al. (1976) and are probably composed of spherulites of acicular plagioclase originating from a central point (Fowler et al., 2002). These spherulites are considered the result of crystallization as they are parallel to the cooling contact (Lofgren, 1971; Davis and McPhie, 1996) (**Figure 20**) and become progressively larger towards pillow interiors (Fowler et al., 2002). The typical morphological variation is from a spherulite-rich margin to a microlite-rich core, but Fowler et al. (2002) suggest that some tubes and large pillows can have varioles concentrated toward pillow centers, similar to those observed (**Figure 20**). Moreover, Fowler et al. (1986) suggested that plagioclase spherulites formed because of pronounced

undercooling from a superheated basaltic melt. Therefore, it is proposed that the mafic lavas of New Bidlamaque were proximal, hot, fluidal lava, initially above the liquidus for intratelluric crystallization and were subsequently undercooled, resulting in extensive spherulitic crystallization. A continuous magma supply, together with the insulating effect of lava tubes, keep the lava at elevated temperatures for longer periods of time. This also facilitated the construction of the lava plain (Fornari, 1986).

Local volcaniclastic deposits composed of angular basaltic hyaloclastites are considered lava-fed and comparable to group III density currents (cf. White, 2000), Such fragments are spalled from an advancing subaqueous lava flow and redistributed downslope via gravity-driven turbidity currents (Bergh and Gudmunder, 1991; White, 2000). Fragmentation is most likely a combination of thermal shock granulation and dynamo-thermal spalling along flow margins (White, 2000), as opposed to steam explosions, based on the conspicuous absence of both vesicles and fine tuff-sized deposits. These deposits likely represent the distal equivalent to pillowed flows formed upslope, similar to the transitions observed along young seamounts (Lonsdale and Batiza, 1980). **Figure 23** outlines the lateral variation envisaged for basaltic and komatiitic rocks in the JF and is comparable to studied Archean flows (e.g., (Dimroth et al., 1978; Bergh and Gudmunder, 1991; White, 2000).

Elongated fragments are envisioned to be multiple chilled margin selvages that became detached similar to those described from Oamaru, New Zealand (from Walker, 1992; **Figure 24**). Such fragments represent an initial stage of fragmentation and are classified as pillow breccia (cf. pg. 372; Batiza and White, 2000). Subrounded fragments

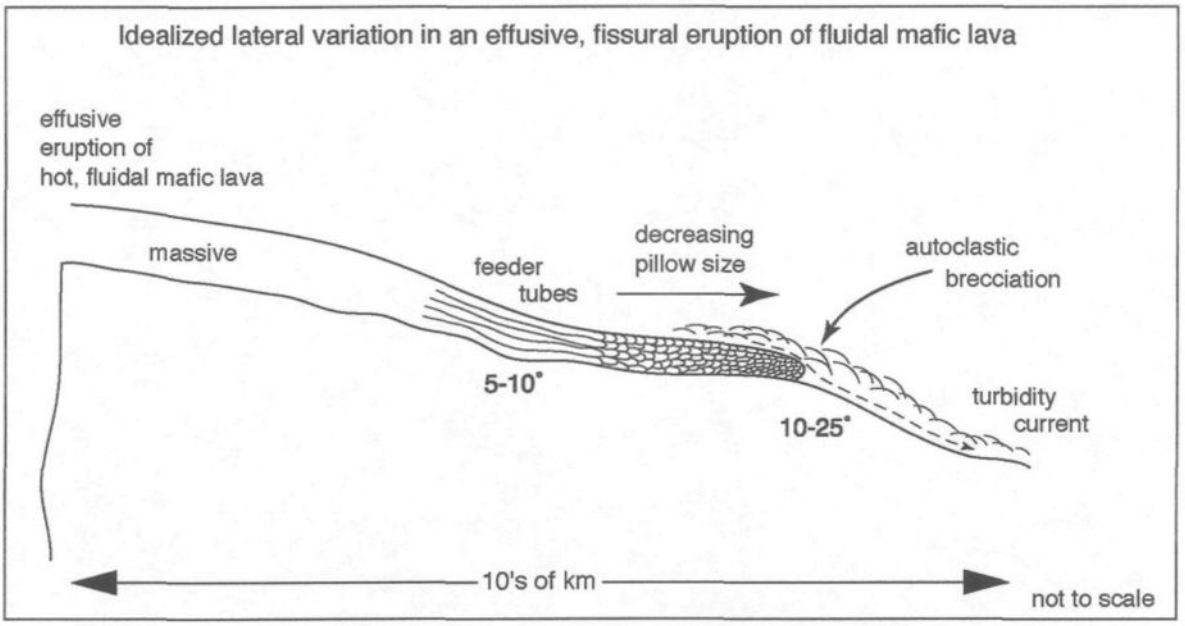

Figure 23. Conceptual sketch of lateral variation of an effusive, fissural eruption of basaltic lava. Modeled from ideas of Dimroth et al. (1978), Bergh and Sigvaldason (1991) and White (2000).

Figure 24. Multiple chilled margins on Omarau pillow basalts from the South Island, New Zealand. Similar characteristics as pillows mapped from the New Bidlamaque property (Figures 16 and 18). Field of view is roughyl 1.5 m.

are probably pseudo-pillows or pillow selvages (Walker, 1992) formed by spalled hot fluid magma that plastically deformed and are supported by cooling fractures outlining some of the larger fragments (**Figure 19**).

In summary, volcanology and petrography of observed massive to pillowed lava flows suggest effusive volcanism in a subaqueous setting (Cousineau and Dimroth, 1982; Dimroth et al., 1978). The inherent low aspect ratio of komatiitic and basaltic flows implies voluminous eruptions consistent with a fissure-type source that potentially could form a subaqueous lava plain. In addition, the non-vesicular character of the basaltic lithofacies may indicate a deep-water environment (> 2000 m; cf. Gill et al., 1990). Erupted komatiites and associated Mg-rich basalts imply a high heat flow probably from a mantle plume source (Campbell et al., 1989). Crosscutting dykes may be associated with overlying lavas of the Val d'Or Formation, suggesting a temporal and spatial relationship between the two formations.

CHAPTER 4

VAL D'OR FORMATION: ARC CONSTRUCTION

The 3-5 km-thick Val d'Or Formation (VDF) represents the arc construction phase and is composed massive, pillowed and lobate lavas and associated volcaniclastic deposits with minor intrusions of diorite and gabbro. In the field, volcano-sedimentary deposits were identified as intermediate or felsic, whereby intermediate is andesitic and felsic includes rhyolitic and dacitic compositions. Compositionally, these volcanic deposits are dominantly composed of 50% andesites, 30% dacites, and 20% rhyolites. Andesites are grouped into 1 km-thick and 9 km-long amalgamated flow units composed of massive to pillowed lava and interstratified monolithic volcaniclastic rocks. Dacitic to rhyolitic lavas are areally restricted, typically measuring between 200-800 m-thick and 1-3 km-long.

The VDF is subdivided into lower and upper sectors for simplicity and weak trends in geochemical affinity (see chapter 6). Moreover, the upper part of the formation is slightly more felsic in composition as compared to the base. This division is arbitrary, but it may identify a possible evolutionary change during arc construction; as such, they will be treated separately in this chapter. Numerous regions of interest (ROI) are recognized, based on location in the stratigraphy and outcrop accessibility (**Figure 26**). Various styles of volcanism (i.e., phreatomagmatic) are documented for the ROI's, which are affected by their paleogeographic setting (i.e., deep marine).

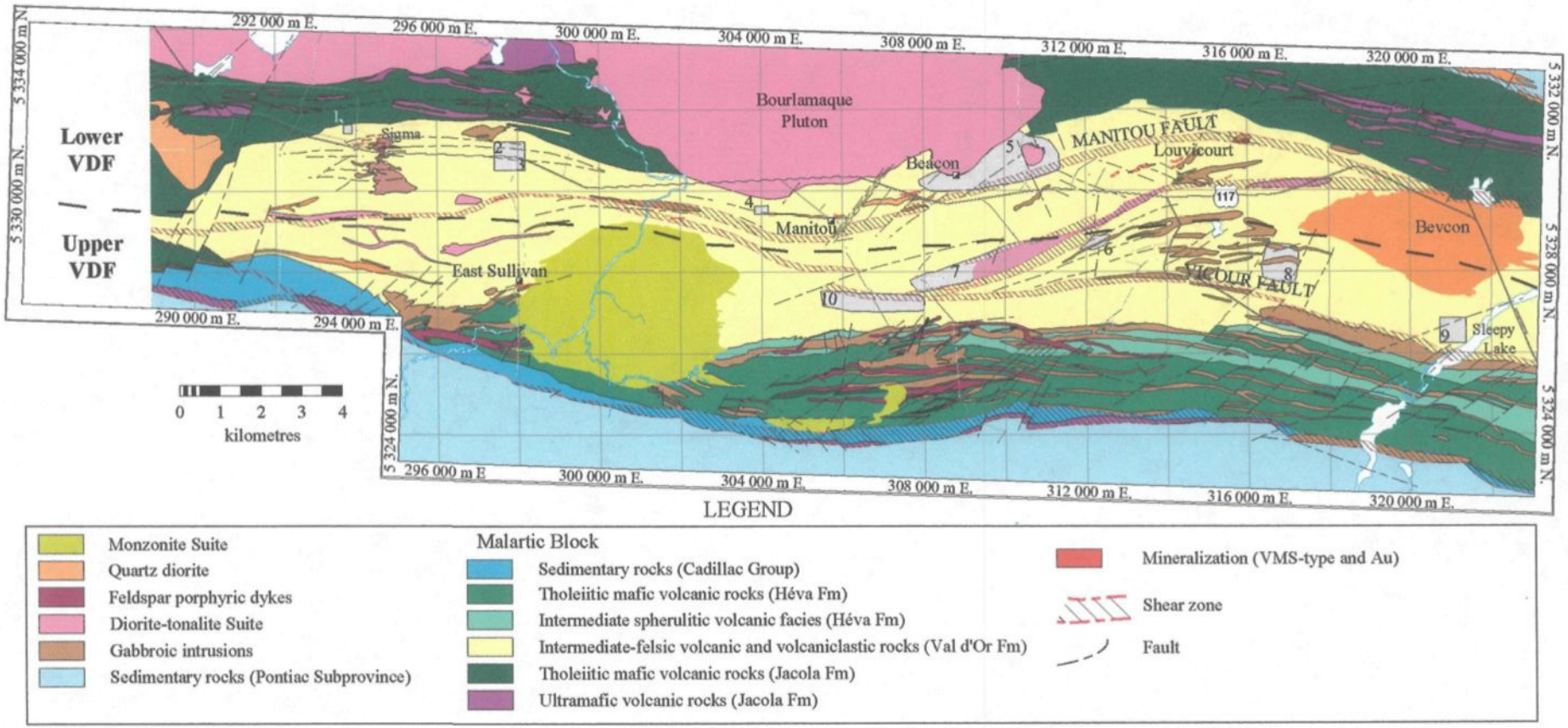

Figure 25: Simplifed regional geology of the Val d'Or region. Arbitrary division of VDF represented by dashed line. Lower VDF regions of interest: 1. Playground area; 2 - Placer Dome North; 3 - East Sullivan outcrops; 4 - Manitou west; 5- Camnet. Upper VDF regions of interest: 6 - Relais; 7 - Dunraine east; 8 - Abitibi Copper; 9 - Sleepy Lake; and 10 - Dunraine west.

4.1 Lower Val d'Or Formation

The lower VDF marks a significant change from the laterally extensive lavas of the underlying Jacola Formation to the restricted volcaniclastic deposits of the VDF. Several stripped outcrops are located fortuitously close to the presumed contact between the Jacola and Val d'Or formations (**see Figure 11**), thereby permitting a comparison between the different styles of volcanism. To the east, where large outcrops are scarce, the stratigraphy is completed by closely spaced traverses within former exploration areas of Camnet and Manitou (**Figure 25**) - the latter a former base metal operation. The following subsections describe the lithology and interpretation of individual regions or outcrops situated within the lower portion of the VDF.

4.1.1 Base of sequence; Val d'Or Playground (ROI 1)

This area is located to the extreme west of the VDF in close proximity to the presumed contact with the underlying Jacola Formation (**ROI 1; Figure 25**). Vertical exposure is good to fair permitting an excellent cross section through a volcaniclastic sequence.

4.1.1.1 Description of Playground stratigraphy

The 45 m-thick sequence at the base of the VDF can be conveniently subdivided based on depositional features (**Table 5; Figure 26**). The younging direction for the

Table 5: Lithofacies of playground area (ROI 1)

Depositional Units	Lithofacies	Characteristics and petrographic features	Interpretation, processes, and setting
Upper Depositional Unit 25 m-thick	Lapilli tuff breccia	Two clast-supported, massive beds composed of subrounded-to-subangular monolithic clasts. Clasts are irregular with 1-2 mm-thick chilled margins that enclose a 5-20 vol% vesicular core. Clasts are aphyric.	Magmatic fragmentation of an energetic fire fountain formed under high hydrostatic conditions. Breccia-sized fragments ejected to form a massive, high-concentration flow that was deposited under laminar flow conditions.
	Lapilli tuff	Matrix-supported, massive to weakly stratified. Fragments are subangular to subrounded with serrated terminations. Matrix is composed of liberated feldspars and elongated chlorite clasts. Chlorite clasts are molded around feldspar phenocrysts.	Hydroclastic fragmentation phase as ambient water invaded the expanding steamy fountain resulting in finer and more angular fragments. Formed low-to-high concentration turbulent flows that formed massive to stratified deposits.
Lower Depositional Unit 22 m-thick	Tuff	0.5-1 m-thick, normal-graded with laminations and scour features (Ta, Tb-d).	Capping sequence from the remobilization of unconsolidated material along the slopes of a subaqueous edifice. Represents the fallout and transport of a fine turbulent cloud which forms high-to-low concentration turbidity flow deposits.
	Lapilli tuff	Matrix-supported, 1-2 m-thick, normal-graded (S3) bed. Localized outsized subrounded breccia clasts.	High-concentration turbidity flow deposit from remobilized volcanic material.
	Lapilli tuff breccia	Matrix-supported, 2-5 m-thick, normal-graded (R3) bed. Subrounded to subangular breccia-clasts form lenses at the base of bed (R1).	High-concentration turbidity flow deposit from remobilized volcanic material. Represents the base of a single depositional event.
	Crystal-rich sill	1 m-thick, stratabound with 30-40% euhedral feldspar phenocrysts.	Late stage injection of crystal-rich magma.

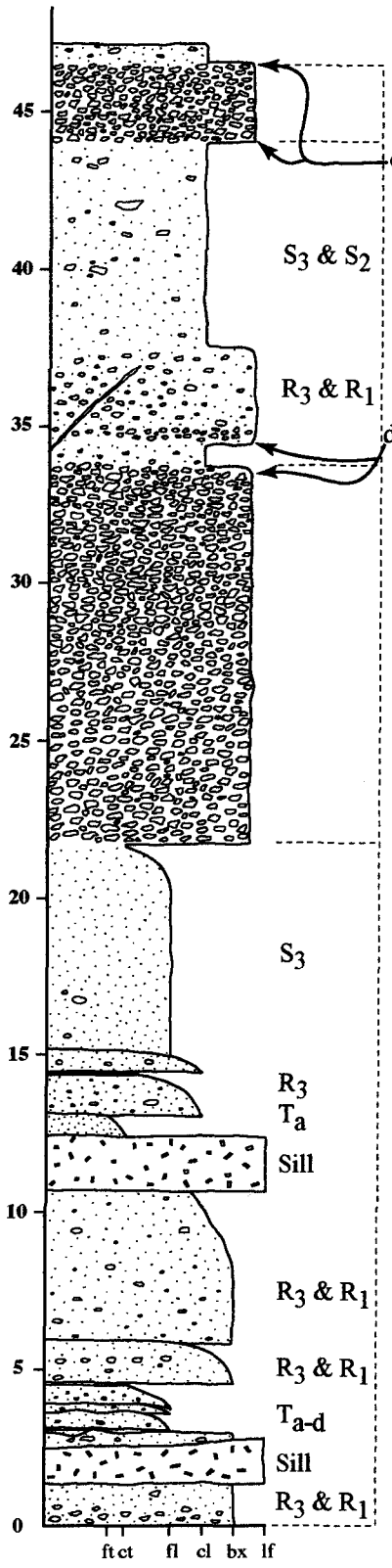

Figure 26: Stratigraphic section from playground region (ROI 1) located in the Lower VDF. Support mechanism and fragment characteristics indicate different fragmentation processes.

sequence is towards the south as suggested by erosive contacts, low-angle scouring (**Figure 27**), and grading (**Figure 26**).

The lower 22 m-thick depositional unit (**Figure 26**) is characterized by matrix-supported lapilli tuff breccia, lapilli tuff, and tuff beds (**Table 5**). The 2-5 m-thick lapilli tuff breccia beds are normal-graded and characterized by subrounded monolithic breccia clasts. These breccia clasts form basal or medial lenses parallel to bedding, which define a weak stratification (**Figure 26**). Lapilli tuff beds are normal-graded and characterized by erosive contacts with bounding beds and local outsized clasts (**Figures 26 and 27**). Subordinate tuff beds are massive to laminated with distinct scour features (**Figure 27**). In addition, two crystal-rich facies, which have diffuse contacts (**Figure 28**) with bounding facies, are considered to be sills as they *cut* the stratigraphy (**Figure 26**). These sills are composed of 30-40-vol%, gray-to-white, 1-2 mm euhedral feldspar phenocrysts that vary from blocky and equant to tabular forms.

The overlying 25 m-thick sequence is characterized by two clast-supported lapilli tuff breccia deposits separated by a matrix-supported, normal-graded coarse lapilli tuff (**Table 5; Figures 26, 29, and 30**). The 10 m-thick, matrix-supported lapilli tuff bed is massive with clast-rich zones that define a crude stratification (**Figure 26**). Fragments are subrounded to subangular, but become compressed adjacent to other fragments (**Figure 30**). More localized deformation is observed where *in situ* fractures within some of the larger fragments are bent when juxtaposed with other fragments (**Figure 30**). Fragments are monolithic with a vesicularity of 5-20-vol% based on a visual estimate of quartz amygdules and voids (**Figure 30 and Appendix A-4**). Breccia-sized fragments have an aphyric, 1-2

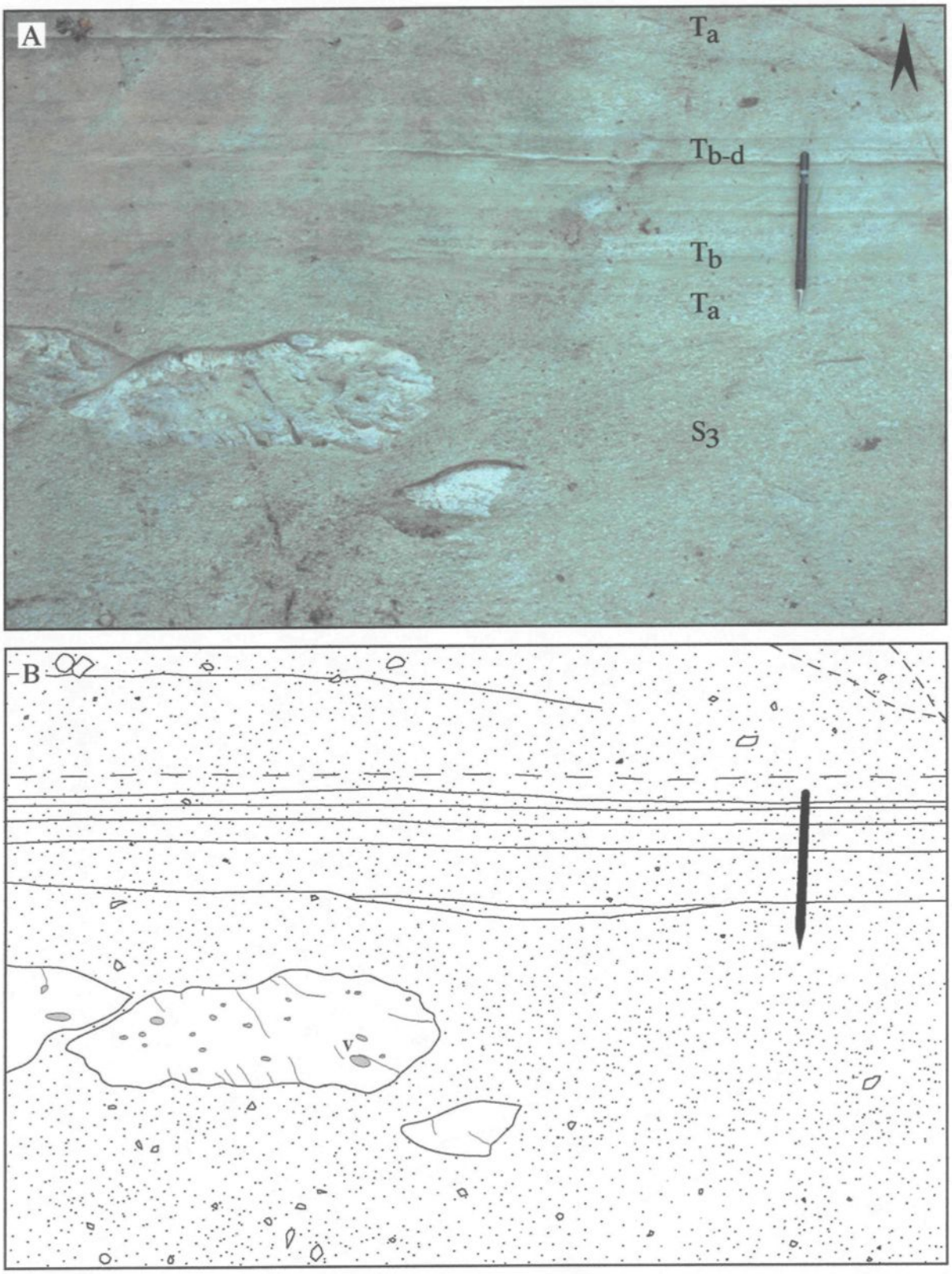

Figure 27. (A) Scour-like features from tuff facies indicating younging direction towards the south (arrow), as well as isolated subrounded weakly vesicular (v), breccia-sized fragments with possible cooling fractures. Pencil is 15 cm long. (B) Sketch of photo in A.

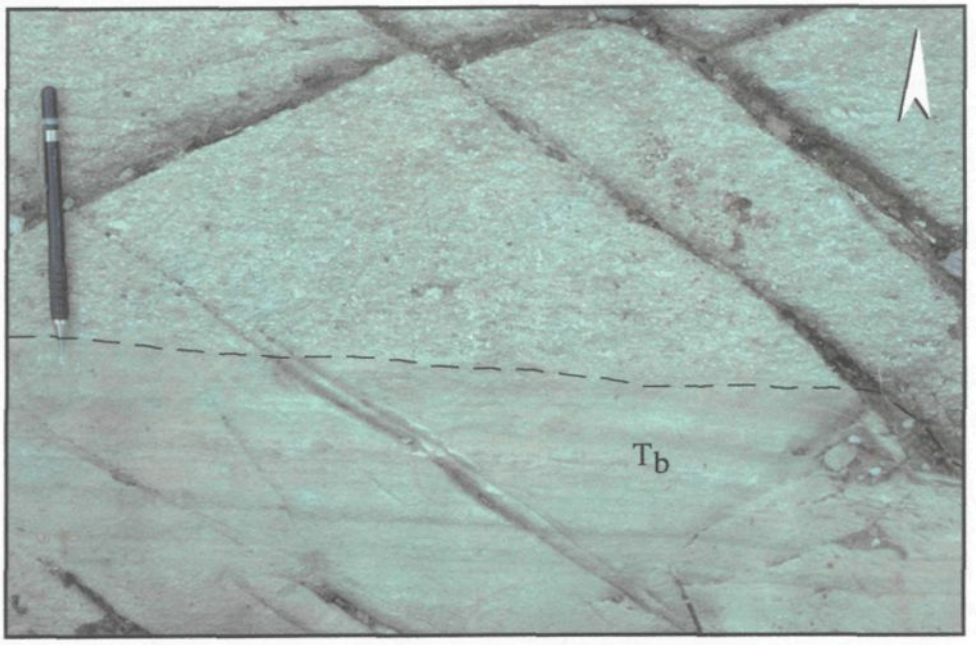

Figure 28: Contact relationship between stratified tuff facies and overlying feldspar-phyric sill. Pencil is 15 cm long and pointing towards the north, arrow points in younging direction.

Figure 29: Diffuse contact with underlying tuff to lapilli tuff and overlying clast-supported tuff breccia (spatter unit). Book is 34 cm-long and arrow points in younging direction.

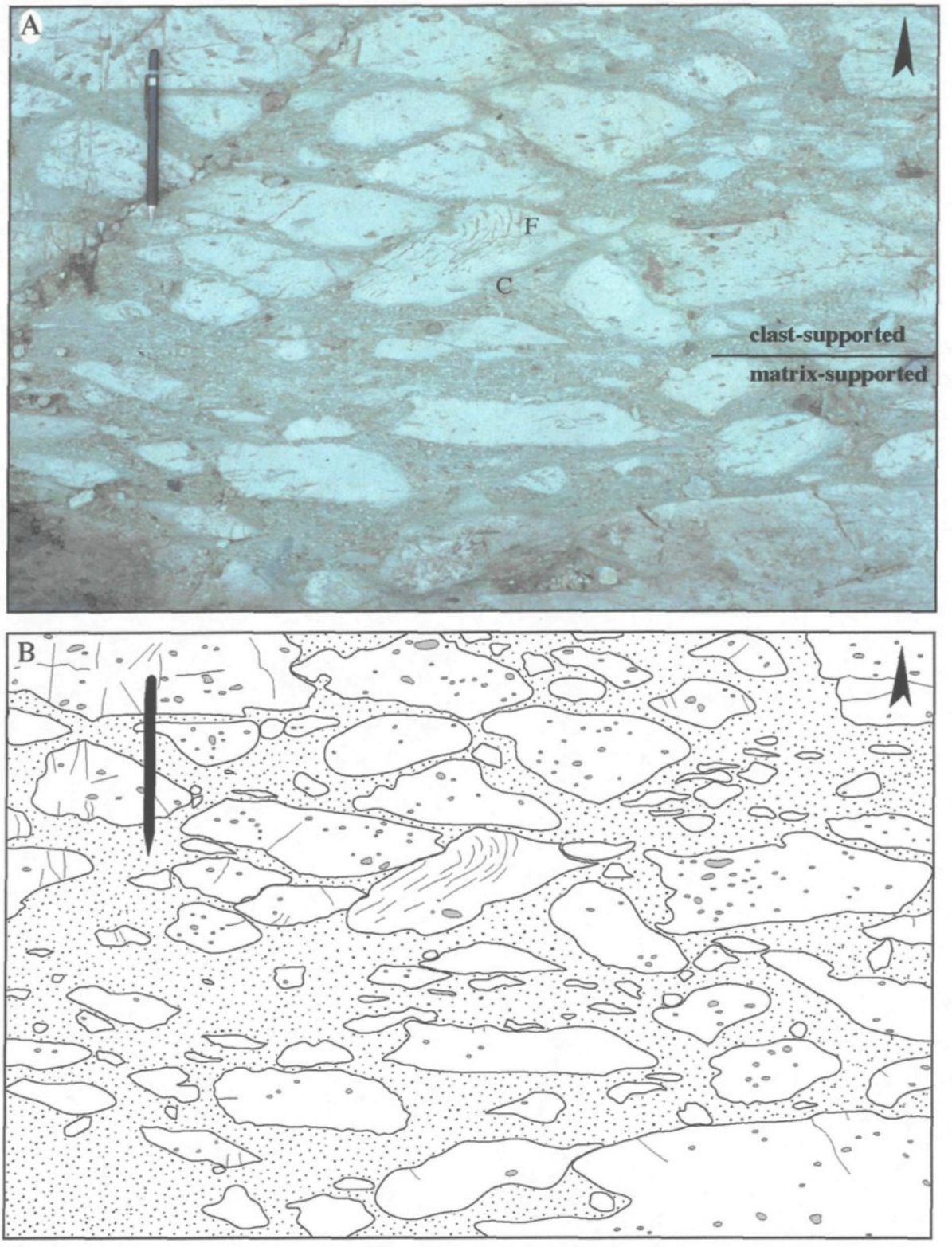

Figure 30: A. Clast-supported nature of lapilli tuff breccia facies, with monolithic population of subrounded, weakly vesicular fragments. Chilled margins (C) and synsedimentary (plastic) deformation of probable cooling fractures (F). B. Sketch emphasizing vesicularity and deformation textures; gray areas are recongizable vesicles. Pencil is 15 cm long and arrow points in younging direction (south).

mm-thick chlorite rim that define a possible chilled margin that separates the white, vesicular core from the matrix. In thin section, chilled margins form a very fine grained, subrounded border on the order of 1-2 mm in thickness around fragments (**Figure 31 and Appendix A-5**). Chloritization of lapilli- to tuff-sized fragments increases as the fragment size decreases.

The two clast-supported lapilli tuff breccia beds are characterized by irregular fragments, such as oval-, amoeboid-, and spindle-shaped (**Figure 29**). These fragments appear exactly the same as those hosted in the sandwiched lapilli tuff bed (**Figure 26**). Lapilli- and tuff-sized fragments comprising the matrix of the clast-supported lapilli tuff breccia beds are characterized by serrated to wispy terminations. Abundant 1-2 mm, blocky and equant, feldspar phenocrysts liberated in the chloritized matrix are randomly oriented.

Petrographically, the matrix is composed of 5-10% equant-to-blocky-to-lath-shaped, sieved, 1-2 mm sized, feldspar phenocrysts in a fine-grained quartz + feldspar + epidote + carbonate matrix and abundant elongated chlorite shreds. A lineation pattern is defined by the deformation and general molding of chlorite around randomly oriented feldspar phenocrysts (**Figures 32 and Appendix A-5**). Such textures are similar to described peritaxitic textures, defined as the coalescence of bubble wall shards that form swirl-like structures around lithics and crystals, which delineate a foliation and where recrystallization to spherulites and other fibrous textures has occurred (Dimroth and Yamagishi, 1987). Breccia-sized fragments are characterized by oval-shaped, mm-sized quartz/carbonate amygdules and randomly oriented, lath-shaped feldspar microphenocrysts (**Figure 33**) with

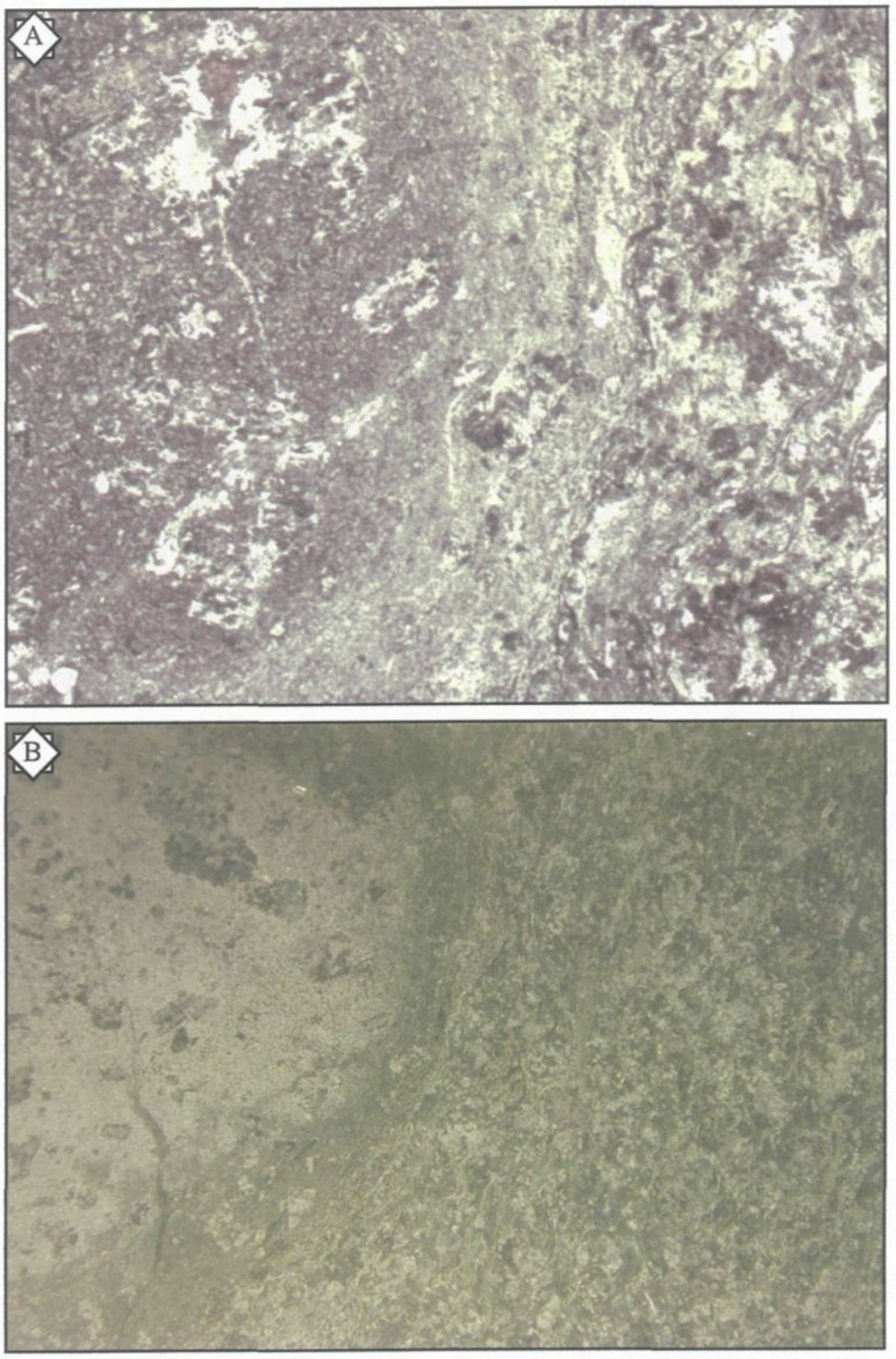

Figure 31: A. Photomicrograph of contact between lapilli fragment and vitrophric-rich matrix. Contact characterized by a mm-thick chloritized zone that may represent a chilled or baked contact between the fragment and matrix. Field of view is 7mm, plane polaried light. Thin section CS99-2466B. See appendix A-5 for detailed description. B. Same thin section, but macroscopic photo detailing the molded nature of contact between fragment and matrix; field of view is approximately 3 cm.

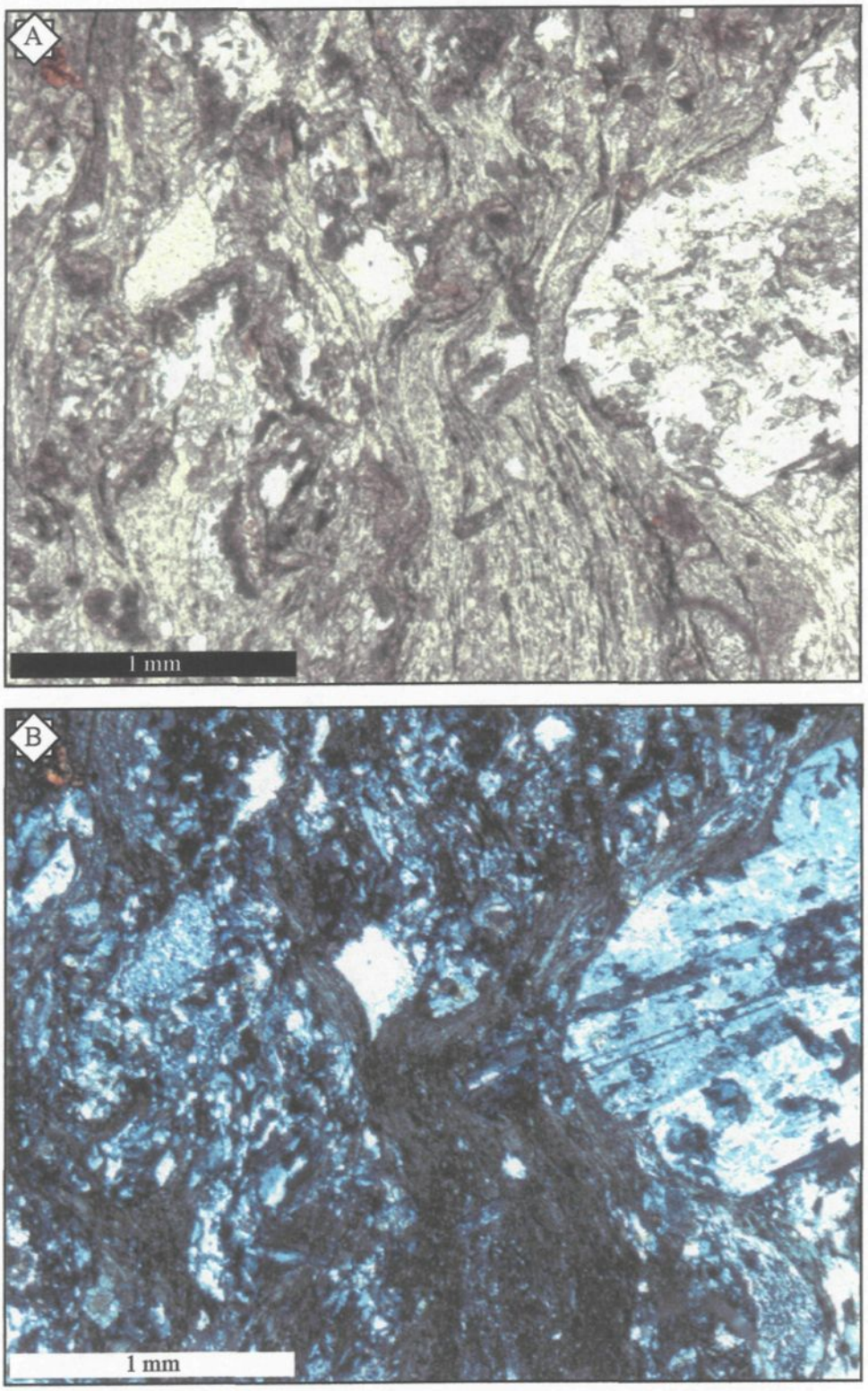

Figure 32: Photomicrographs of lapilli tuff matrix documenting relict vitrophyric shards. Former shards are represented by chlorite bands that are molded around denser, sieved feldspar phenocrysts. Liberated feldspar phenocrysts are not oriented in the same plane as chlorite shards. A. Plane polarized light. B. Crossed-nicols.

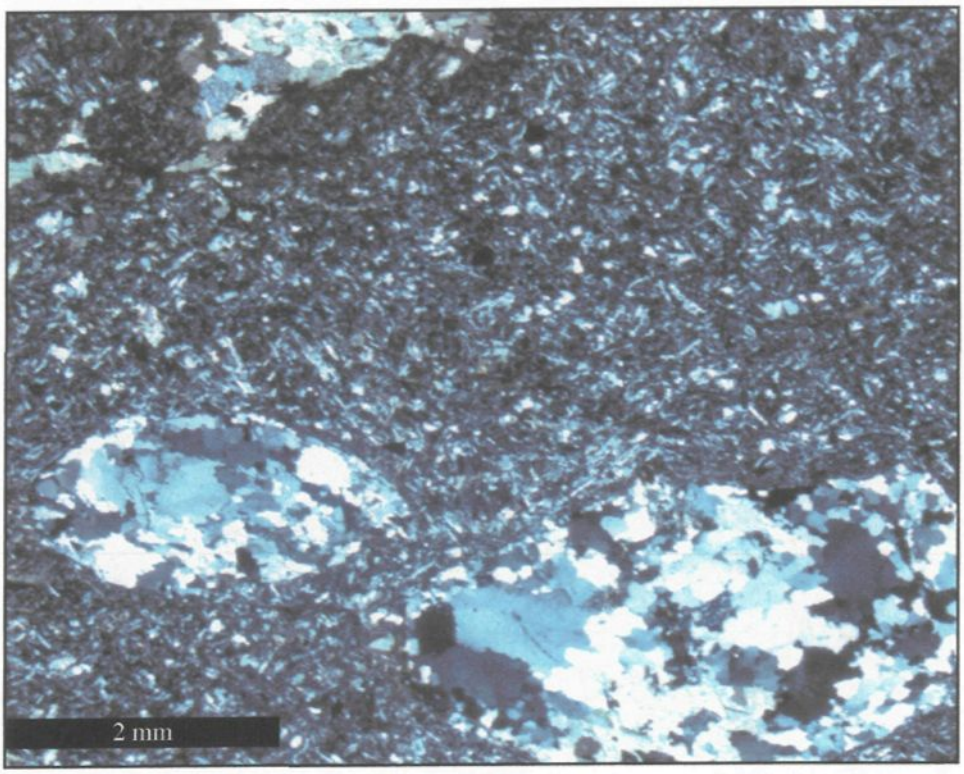

Figure 33: Cross-nicols microphotograph of oval-shaped quartz amygdules in fine-grained feldspar-rich groundmass of breccia-sized fragment.

subordinate (< 1%) lath-shaped, sieved feldspar phenocrysts. The groundmass is composed of fine-grained feldspar and quartz, with minor epidote alteration and no chlorite alteration.

4.1.1.2 Interpretation of Playground stratigraphy

The difference in the support mechanism between the lower and upper parts of the mapped stratigraphic section seems to indicate a possible change in their mode of transport, as well as their origin (**Table 5**). Nevertheless, their monolithic character and absence of background sedimentation would suggest that both are deposited from sedimentary gravity flows, originating from penecontemporaneous disruption of a volcanic edifice and not post-eruptive weathering of consolidated deposits (i.e., epiclastic; cf. Fisher and Schmincke, 1984).

The lower 22 m-thick, matrix-dominated lapilli tuff breccia, lapilli tuff, and tuff beds record deposition from high- and low-concentration turbidity currents ranging from R-, S- and T-types, respectively (cf. Lowe, 1982). The monolithic volcanic fragments comprising this sequence suggest two possible modes of origin: (1) eruption-fed, but water-supported, subaqueous turbidity currents (cf. White, 2000); or (2) remobilization of unconsolidated volcanic material previously fragmented, such as volcanic debris accumulated along a volcanic slope. An absence of doubly graded beds (cf. Fiske and Matsuda, 1964) and textural features, suggestive of hot emplacement of individual fragments or beds, argues against an eruption-fed origin. Therefore deposition by cold turbidity currents originating from the reworking of unconsolidated material, initially emplaced from an earlier eruption on the paleoslopes of a subaqueous volcanic vent is

favored. The lapilli tuff breccia beds represent initial slumping of coarse grained, water-saturated juvenile material. During transport, finer grained material becomes elutriated and lofted into a trailing turbulent cloud. Differential settling resulted in finer grained turbidity flows and deposition of normal-graded beds. The lack of tuff beds indicate the overall instability of the area, as there were probably a rapid succession of remobilized material. Temporal events are impossible to ascertain, but it is envisaged that transport and deposition of these volcano-sedimentary facies were penecontemporaneous with initial fragmentation, whereby final deposition could be days to even months after initial fragmentation. However, breccia-sized fragments are not deformed suggesting they had sufficiently cooled to behave as a rigid solid before remobilization. Such remobilization is common in proximity to an active volcanic vent due the abundance of volcanic material (Carey, 2000), unstable slopes, and seismicity associated with volcanism.

The massive, clast-supported nature of the two overlying lapilli tuff breccia beds suggests deposition from a concentrated cohesive debris flow within the laminar flow regime (Lowe, 1982). The predominance of weakly vesicular and fluidal fragments, vitric tuff matrix, wispy fragments (serrated terminations), and abundance of liberated crystals in the matrix imply a pyroclastic origin (Dimroth and Yamagishi, 1987; Mueller and White, 1992; McPhie et al., 1993). Moreover, the overall thickness of these deposits (> 4m; **Figure 26**) would imply that these volcaniclastic deposits are primary pyroclastic deposits based on considerations by Dimroth and Yamagishi (1987). Explosive subaqueous volcanism occurs via phreatomagmatic or magmatic processes (Kokelaar, 1986; White and Houghton, 2002, White et al., 2003), whereby fragmentation is controlled by external or dissolved

volatiles, respectively. The breccia-size and subrounded nature of fragments precludes a possible (efficient) phreatomagmatic mechanism; as such, explosive fragmentation typically produces fine-grained tephra, which are generally angular in shape (Wohletz, 1983; Morrissey et al., 2000). In addition, the irregular fragment shapes indicate that magma fragmentation occurred in a semi-fluid state (cf. Mueller and White, 1992). Magmatic explosivity is controlled by the acceleration of exsolving magmatic volatiles, thereby providing the initial ejection velocity of magma/lava from the volcanic vent. The inherent problem with subaqueous magmatic eruptions is the ubiquitous effect hydrostatic pressure has on the exsolution of volatiles. As the hydrostatic pressure increases with depth, volatile exsolution is suppressed, which resulted in earlier researchers to infer that explosive subaqueous eruptions were restricted to around 500 m below sea level (see Cas and Wright, 1991; Stix, 1991). Recent work on seamounts, however, has observed fragmented material at depths in excess of 2000 m (Gill et al., 1990; White et al., 2003). Furthermore, some researchers have described fluidal clasts at depths > 1000 m (Batiza et al., 1984; Batiza et al., 1989) with inferred subaqueous fire-fountaining (Smith and Batiza, 1989). These inferences lead Mueller and White (1992) to interpret an Archean volcaniclastic sequence as being deposited from a subaqueous fire-fountain eruption and to the construction of an *idealized* stratigraphic sequence for such an eruption (**Figure 34**).

Although clast support was provided by water, the subrounded nature, chilled margins, and possible plastic deformation between juxtaposed fragments imply that most breccia-sized fragments were transported and emplaced in a hot state. Plastic deformation is considered to be a primary feature as denser material, such as feldspar crystals, are

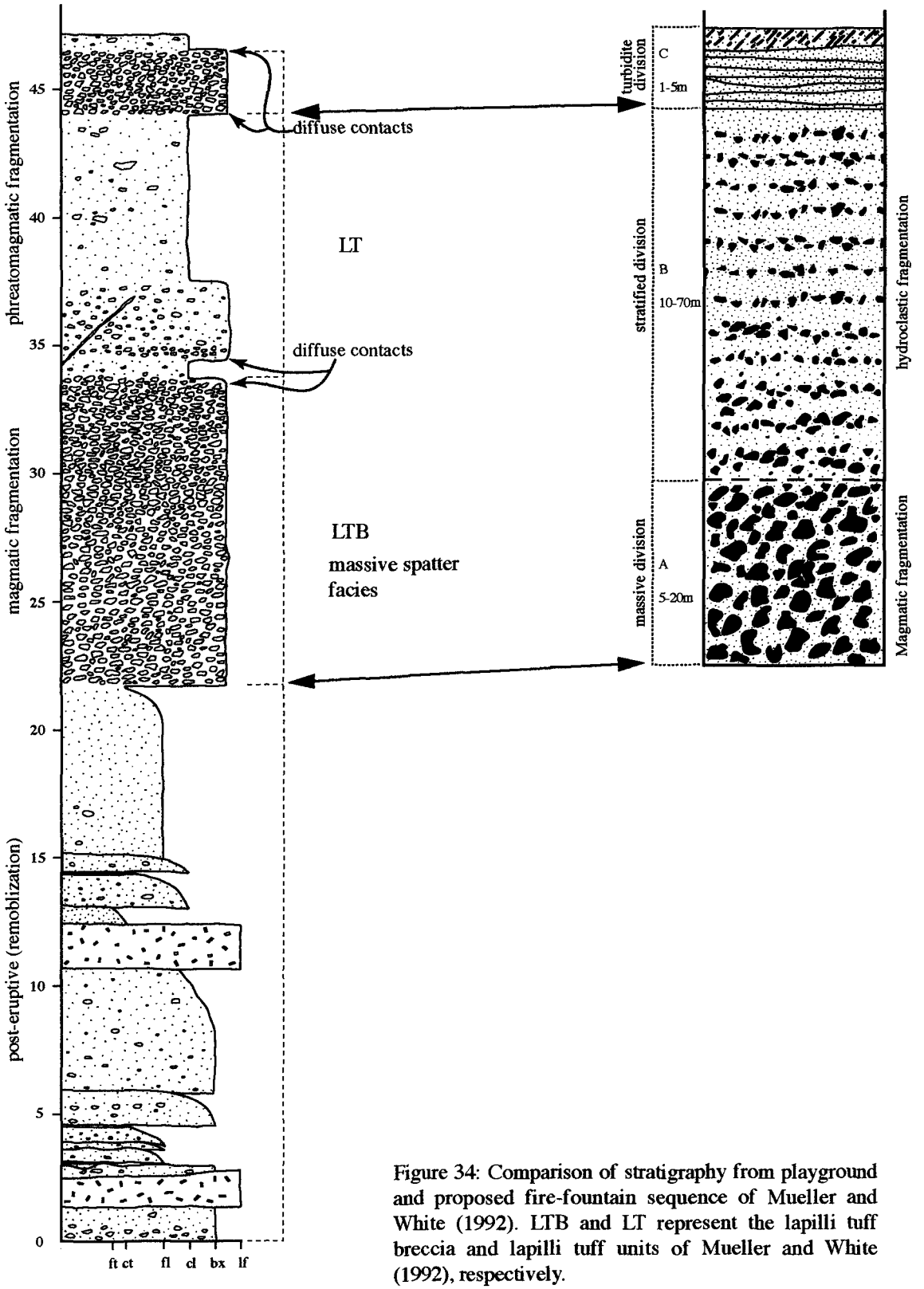

Figure 34: Comparison of stratigraphy from playground and proposed fire-fountain sequence of Mueller and White (1992). LTB and LT represent the lapilli tuff breccia and lapilli tuff units of Mueller and White (1992), respectively.

unaffected, whereas former vesicles are slightly flattened and tuff- to lapilli-sized chlorite fragments (former glass shards?) in the matrix are molded around crystals. Such *in situ* viscous deformation indicates welding (White, written communication 2003; (Smith, 1960) of hot pyroclasts subsequent to deposition. If deformation was a result of tectonic forces or sedimentary compaction, then all constituents of the deposit should be deformed. While the interstitial fluid was water, fragments remained hot due to the possible formation of a protecting steam envelope (Kokelaar, 1983; Kokelaar, 1986), whereby larger fragments are more apt to generate and preserve this envelope for an extended period. Therefore, it is envisioned that these flow units were eruption-fed, but mixed with water (cf. White, 2000), without any repose period. A remobilized scenario is opposed, as chilled margins are likely to crack and post-depositional plastic deformation improbable.

The intervening 10 m-thick, matrix-supported lapilli tuff (**Figures 26 and 34**) facies records a change from magmatic to more phreatomagmatic conditions (cf. Mueller and White, 1992) as the initial gas-thrust of the fire-fountain stage weakens, thereby enabling water to ingest into the steamy eruption column resulting in more efficient fragmentation into finer-grained pyroclasts. As the eruption weakens further, the eruption column wanes and the lofted finer material collapses to form high- to low-density turbidity flows. A capping turbidite division, envisaged by Mueller and White (1992), is absent probably because of a return to a fire-fountain eruption stage due to a possible recharge of fresh volatile-rich magma within the subvolcanic magma chamber, which deposits another clast-supported tuff breccia composed of fluidal fragments (**Figures 26, 29, and 34**).

The interpreted subaqueous fire-fountaining origin is based on the juvenile, breccia-sized, vesiculated fluidal clasts and deposit characteristics. A paleowater depth of > 1000 m is inferred from the breccia-sized yet fluidal and vesiculated fragments that comprise the sequence indicating that the hydrostatic pressure was high enough to suppress efficient fragmentation, but not vesiculation. The underlying matrix-supported deposits may have resulted from slope failure and subsequent remobilization due to associated seismicity as magma inflated the volcanic edifice prior to the fire-fountain eruption.

4.1.2 Placer Dome North (ROI 2)

This sector represents a series of three east-west elongated outcrops and two rectangular zones (**Figures 11 and 35**). These outcrops are located 3km east of Val d'Or, approximately 400m north of highway 117 via an old road located opposite a Hydro-Québec power line (**Figure 25**). All outcrops were part of a former gold exploration program by Placer Dome Inc. and this zone is along strike with the Sigma Mine located 5.5 km to the west. Another probable reason for work at this particular site is possible magnetic anomalies associated with two lamprophyre plugs exposed in the two-stripped rectangular zones (**Figure 35**). Focus was on the largest of the three elongated outcrops with detailed mapping conducted to examine lateral transitions in an effort to understand fragmentation and transportation processes. The northernmost outcrop is composed of volcaniclastic deposits that were deeply weathered, the southernmost outcrop is composed of intermediate pillows capped by in situ breccia, whereas the middle outcrop has a 16-23 m-thick volcaniclastic sequence sandwiched between intermediate pillowed facies. The extensive

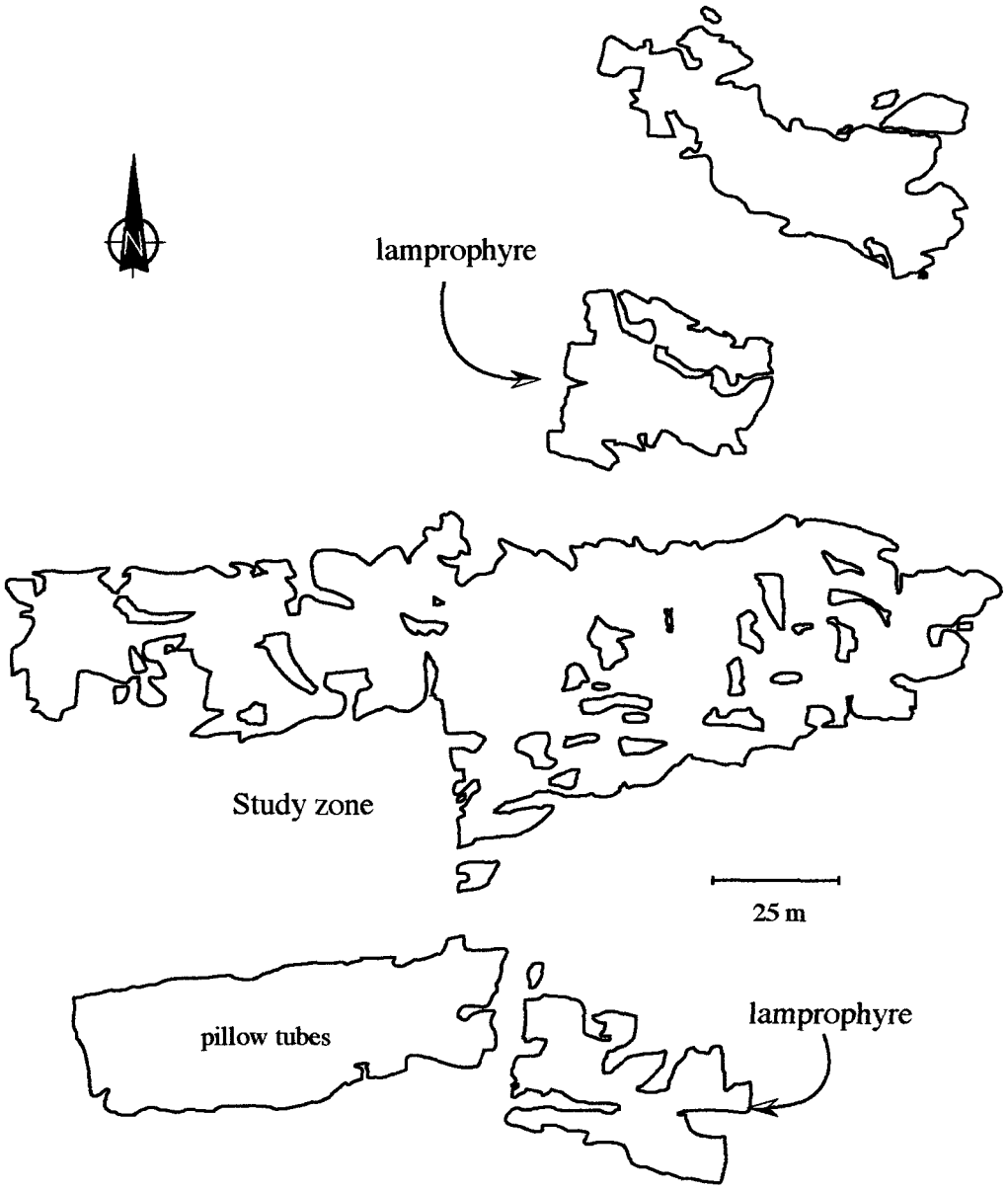

Figure 35: Outline of outcrop zones for Placer Dome North, Val d'Or Formation.

lateral and vertical exposure of this volcaniclastic sequence offers unprecedented observations on lithologic transitions from lava to sediment, as well as flow transformations within individual sedimentary gravity flows.

4.1.2.1 Description of outcrop characteristics

The central outcrop, measuring 185m x 50m, was mapped at scales of 1:200 and 1:5 to outline the general stratigraphy and detail any lateral and vertical transitions, respectively. This particular outcrop offers the best continuous exposure of the lower part of the VDF and is characterized by volcaniclastic deposits that are bounded by intermediate pillowed flow facies (**Figure 36**).

Pillowed Facies

The conspicuous feature of the intermediate pillowed facies is the variability in pillow morphology (**Table 6**). Within the lowermost pillowed unit, pillows range from amoeboidal to bun-shaped both along strike, in an east-west direction, and up section (**Figures 37 and 38A**). Furthermore, amoeboidal pillows may exhibit a continuum of morphological changes from isolated, irregular bulbous masses to more regular amoeboid forms and bun-shaped pillows over 100m along strike in a westerly direction (**Figure 37**). Irregular pillows range from amoeboidal (**Figure 38B**) to more elongated, stretched and folded spatter-like forms (**Figures 38C/D**), but are all characterized by chilled margins (**Figure 38A**). Irregular pillow sizes vary from meters to several centimeters with no correlation to stratigraphy. A minimum thickness of 10m is observed for the lower pillowed

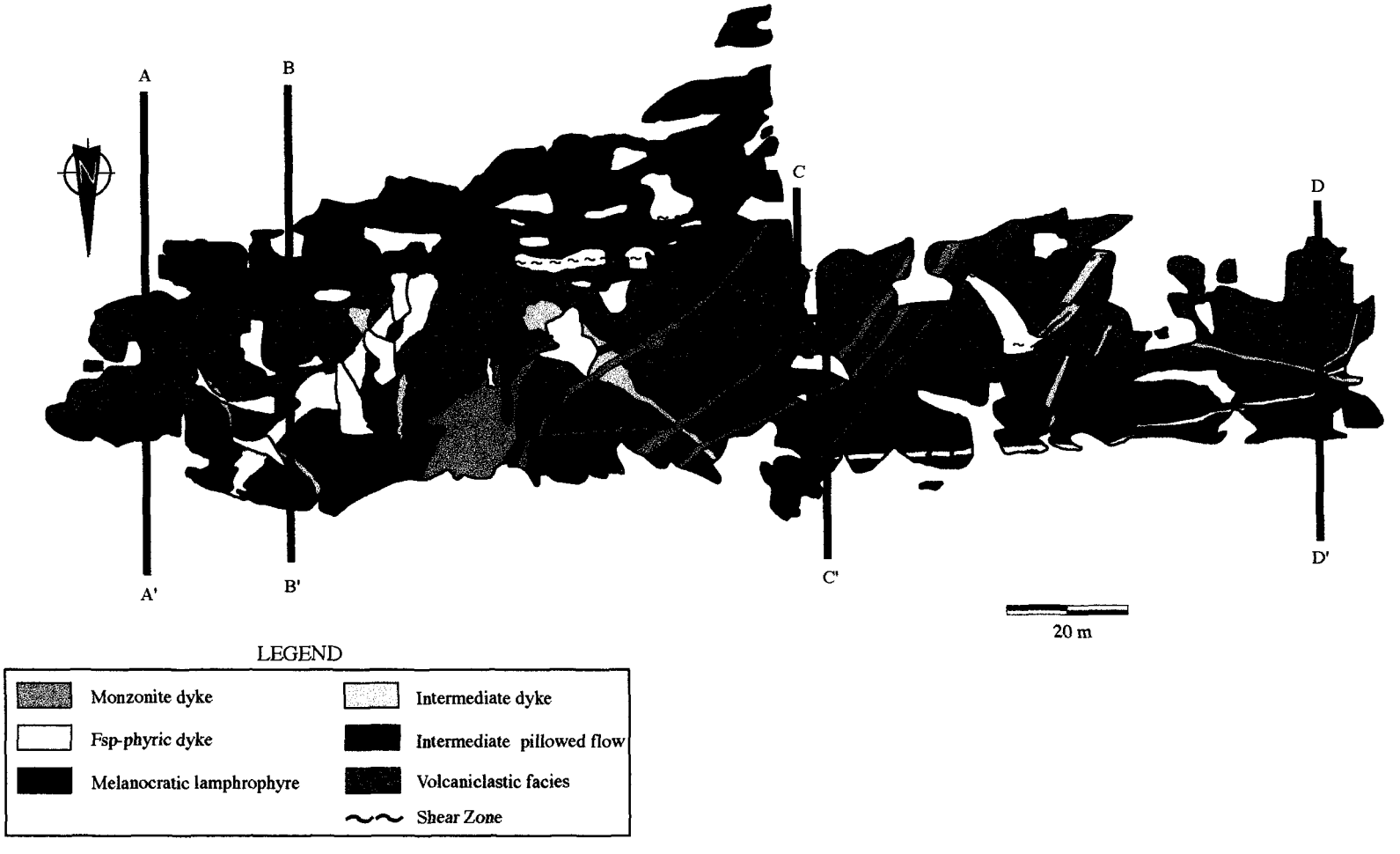

Figure 36: Simplified geology map of stripped outcrop, with volcaniclastic facies situated between two intermediate pillowed facies. Four dyke generations crosscut the stratigraphy at various angles. General thickening of volcaniclastic facies towards the west. Location of stratigraphic sections from figure 37 are shown.

Table 6: Volcano-sedimentary lithofacies of Placer Dome North outcrops

Lithofacies	Facies, structure, characteristics	Origin, process, deposit	Setting, locus
Volcanic Thickness: 10-70 m	Intermediate pillowed and pillow breccia flows; Pillow morphology varies from amoeboidal-, tubular-, or bun-shaped; aphyric and <5% amygdules	Effusive low-volume lava flow(s); aphyric nature and low vesicularity suggest a low-viscosity flow which formed amoeboidal pillows	Near vent setting with an east to west propagation based on amoeboidal- to bun-shaped transition and tube forms; low vesicularity suggests a deep-water environment
Intercalated spatter facies	Highly irregular spatter composed of fluidal, spindle, tightly folded lava ribbons, and agglutinated clasts	Spatter units record boil-over or tearing of low-viscosity lava that was transported only 10s of meters; lava spatter rapidly chilled by ambient water and compressed by subsequent lava flow	Deposition along vent paleoslope caused tearing of low-vesicular, fluidal lava; overriding lava deformed hot clasts
Volcaniclastic a) Tuff turbidite (2-8 m thick)	a) Progressive thickening towards the west; fine planar laminations (T_b), grading and erosive contacts comprise a series of T_{ab} and T_{abd} beds; monolithic subangular to subrounded clasts with slight flattening; aphyric and non-vesicular	a) Fine-grained material produced during subaqueous phreatomagmatic disintegration of intermediate lava Collapse of eruptive column generated a series of low density sedimentary gravity flows (T_{abd})	Subaqueous transport of juvenile material associated with small phreatomagmatic eruptions due to ingestion and rapid vaporization of seawater; proximal deposition below wave base
b) Lapilli tuff breccia (12-14 m thick)	b) Subdivided into three separate depositional units measuring between 1-9 m thick; each unit grades from a 1-3 m thick, massive tuff breccia (R_{1-3}), 1-2 m thick, weakly stratified, lapilli tuff ($S_{1,3}$), to a 0.55-2 m thick, laminated tuff (T_{abd}); monolithic subrounded clasts; aphyric and highly variable amygdule content (0-35 vol%)	b) Autoclastic fragmentation of intermediate lava flow forms a "lava-fed" massive tuff breccia; deposition by water-supported, laminar debris and high density sedimentary gravity flows of pillow breccia Water ingestion produced weak localized phreatomagmatic explosions; deposition by high- to low-density sedimentary gravity flows ($S_{1,3}$ and T_{abd})	Subaqueous fragmentation in proximity to the source vent; deposition below wave base

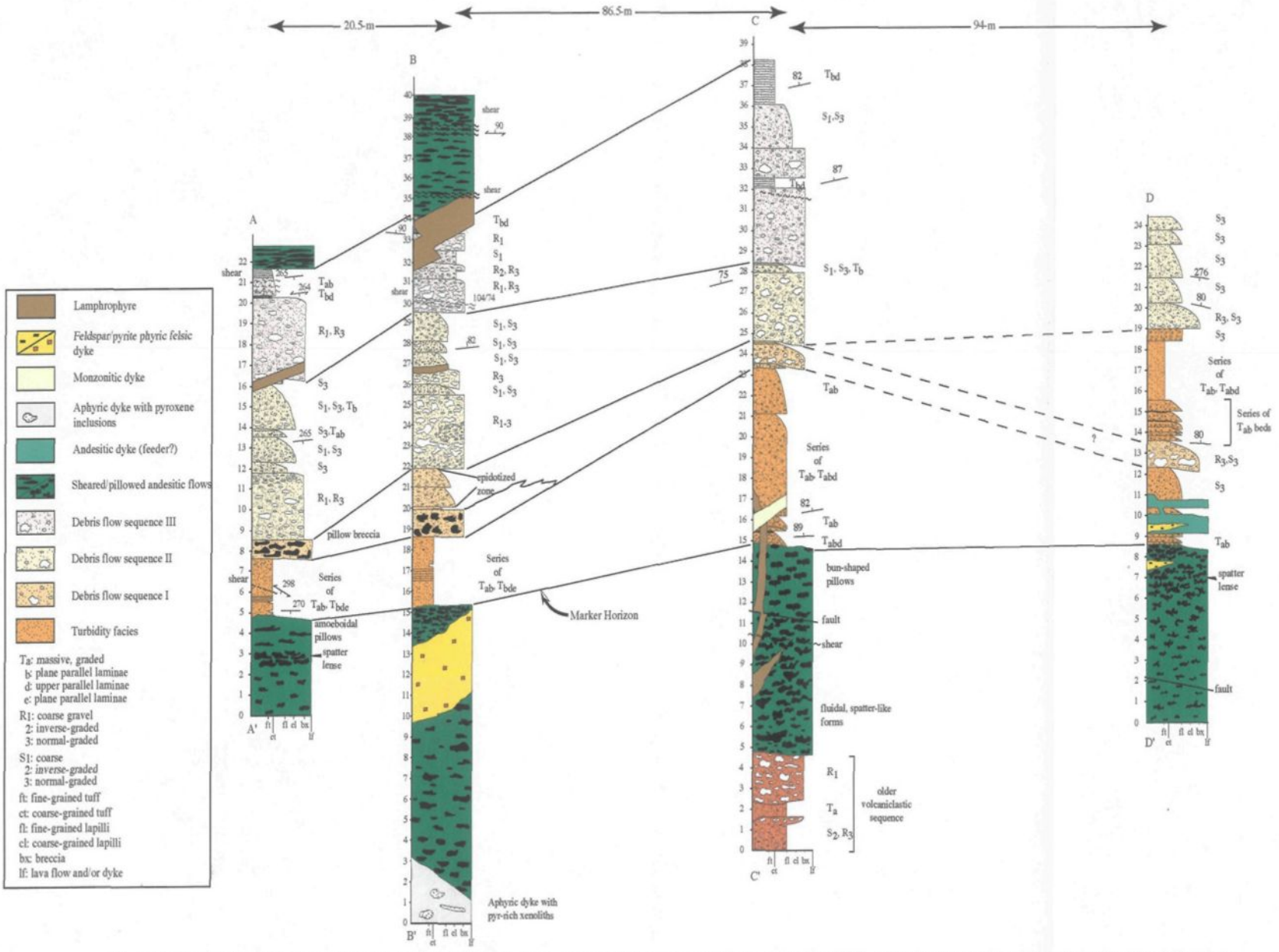

Figure 37: Four stratigraphic columns illustrating the lateral changes in three separate sedimentary gravity flows, ranging from high- to low-density particulate flows. Vertical and lateral changes in lava morphology are also indicated, suggesting changes in intrinsic lava conditions.

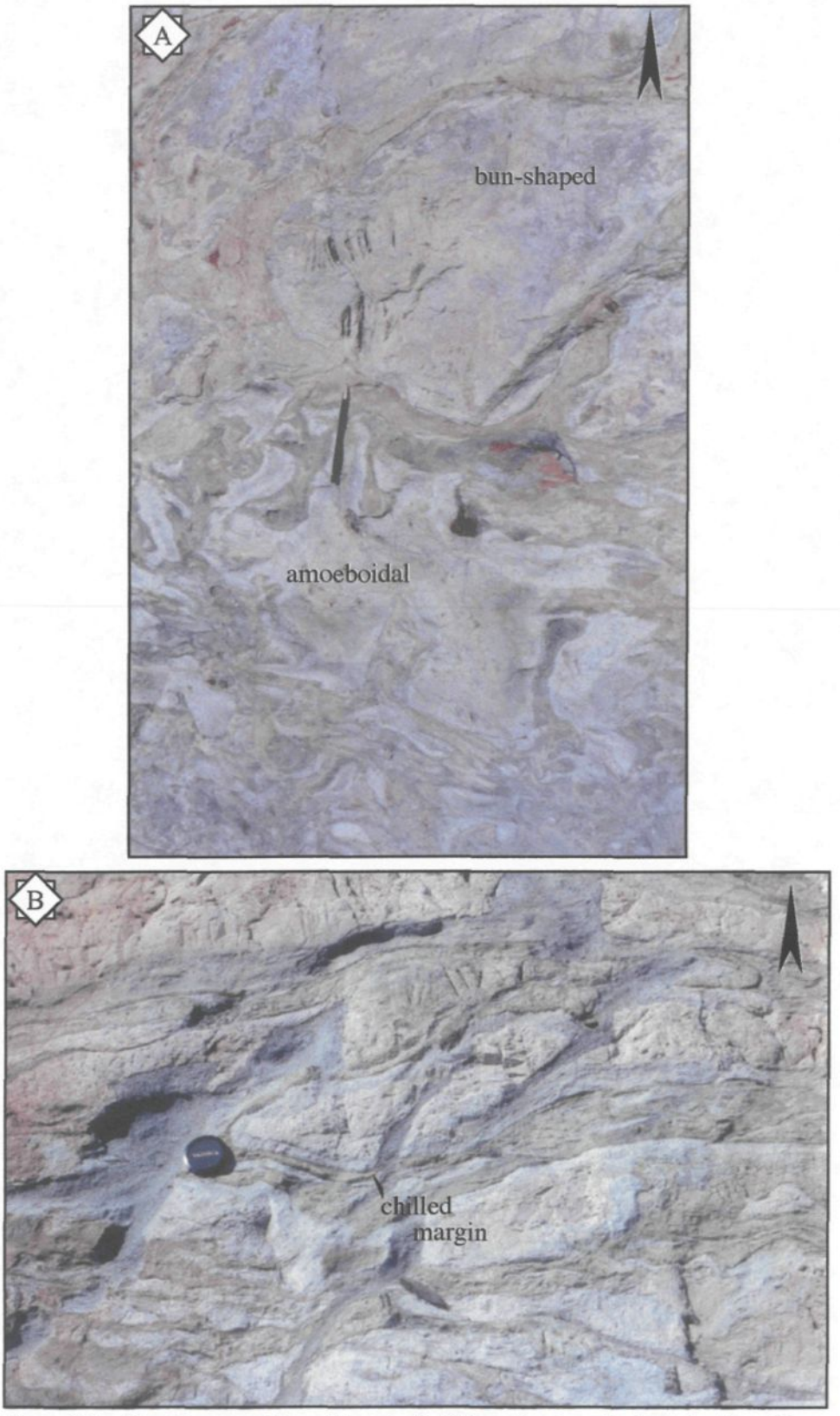

Figure 38: Pillow forms and transitions to fluidal spatter breccia deposits from Placer Dome North outcrop. A. Vertical transition from amoeboidal pillows to more bun-shaped up section; arrow points in younging direction (south). Pencil is 14.5 cm long. B. Irregular, amoeboid pillow forms from base of lava flow. Lens cap is 5.5 cm wide.

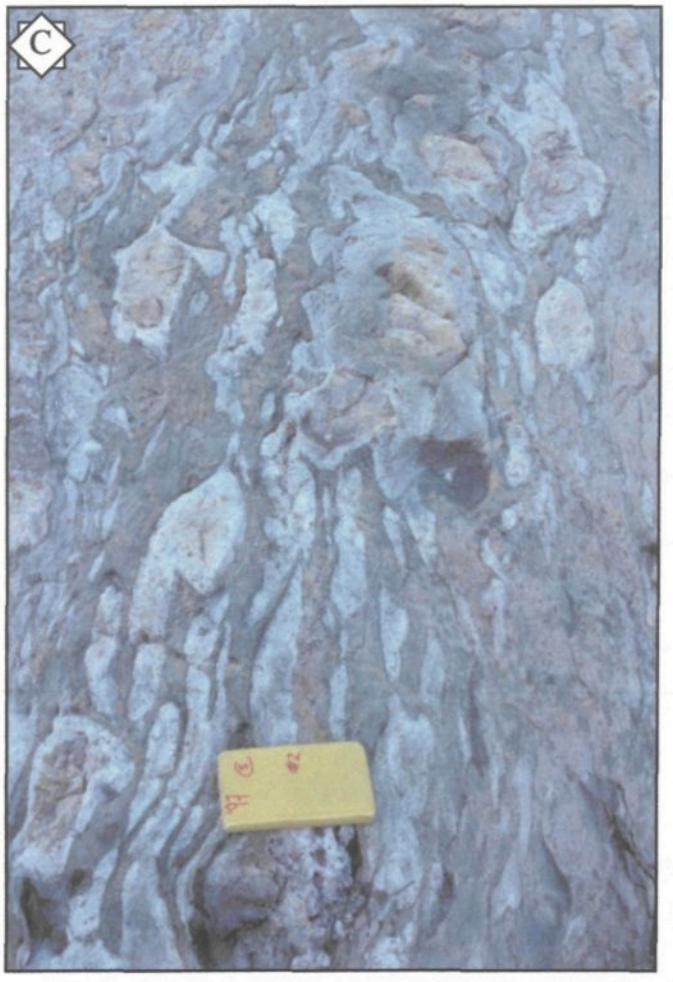

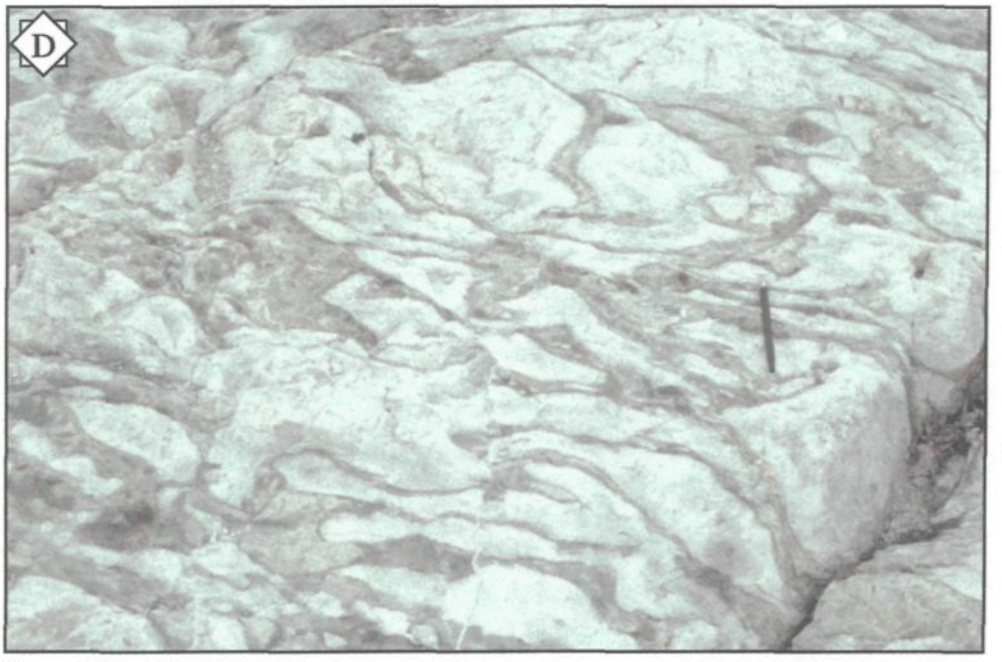

Figure 38 (con't): Fluidal spatter breccia deposits composed of highly irregular lava rags; located to the east of mapped section (see Figure 43), field book for scale (19 cm long). C. Spatter-like character of lava. D. Amoeboid morphology and (plastic) deformation of low viscosity lava. Pencil for scale (14.5 cm long)

facies (**see strat C-C', Figure 37**). The uppermost-pillowed flow extends from the middle outcrop to the southern outcrop with a combined thickness of approximately 70m (**Figure 35**). This pillowed flow grades into a coarse-grained *in situ* breccia in the SW corner of the southern outcrop (**Figures 35 and 39**). Pillows are typically larger with no amoeboidal forms and most are elongated with low aspect ratios, suggestive of feeder tubes (**Figure 39**). A minor shear zone (270°/90°) has disrupted a meter wide zone within this pillowed facies giving it a brecciated appearance. All pillows are aphyric and non-vesicular regardless of pillow morphology with a bleached grayish-white appearance. Interstitial material is ubiquitously altered to a fine-grained matrix of chlorite, sericite, and epidote. Pillows are completely chloritized with some cores having been replaced by epidote.

Petrographically, pillows are composed of a fine-grained matrix of chlorite + epidote + quartz ± albite ± carbonate. Relict crystal forms of hornblende are recognized, along with possible feldspar. Microlites of acicular feldspar comprise upwards to 30-vol% of core regions (**Figure 40**) where epidote alteration is less intense, whereas epidote-rich zones are typically aphyric (**Appendix A-6**). Vesicularity is low and characterized by trace to 5-vol% quartz amygdules.

Volcaniclastic Deposits

The volcaniclastic deposits can be divided into a tuff sequence and a series of tuff breccia to lapilli tuff facies (**Table 6; Figure 41**) based on grading, sharp and erosive contacts, stratification and bed repetition. The tuff unit gradually thickens from 3 m in the east to over 8 m in the west (**Figures 37 and 41**). Contacts are sharp with bounding

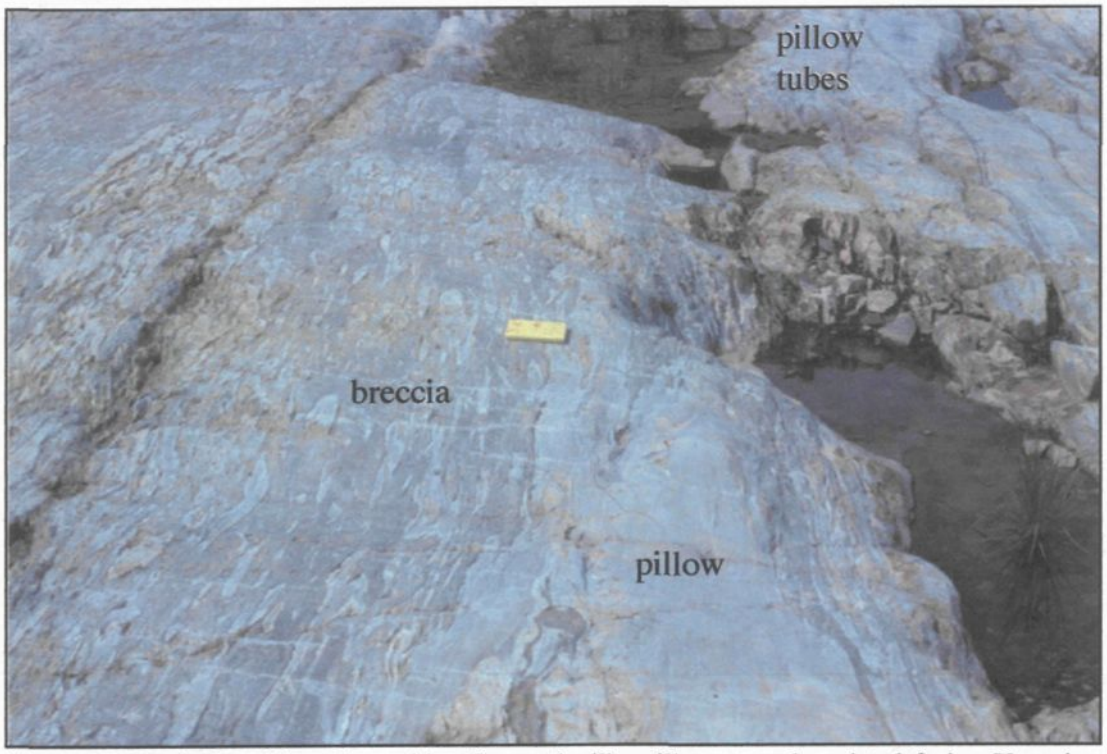

Figure 39: Vertical and lateral transition from tube-like pillows to a brecciated facies. Younging direction is to the south (arrow). Field book (19 cm) for scale.

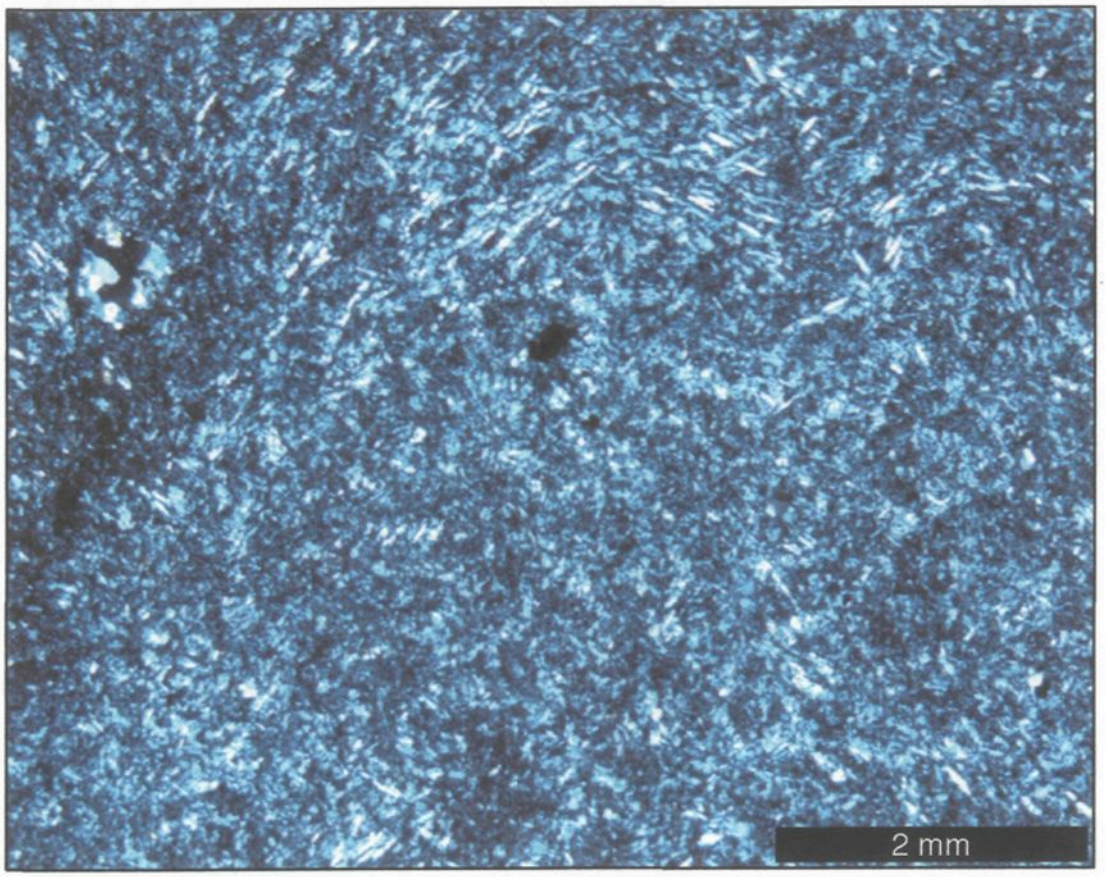

Figure 40: Cross-Nicols photomicrograph of pillow groundmass of fine-grained acicular feldspar microphenocrysts, with one observed quartz amygdule.

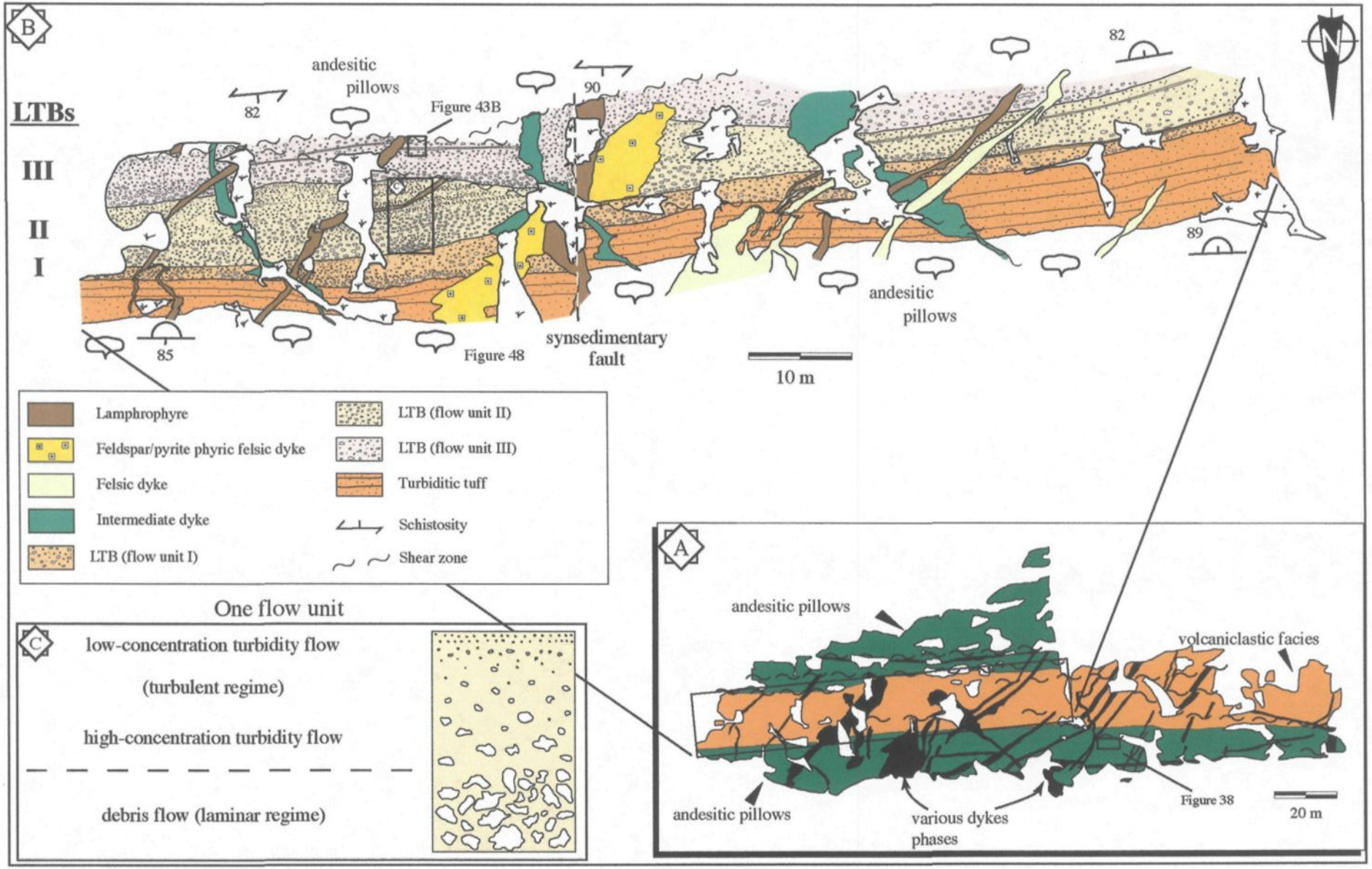

Figure 41: (A) General geology and location of detailed map. (B) Detailed map outlining the various volcaniclastic deposits, from a basal tuff turbidite and three subsequent lapilli tuff breccias (LTB). (C) A depositional unit showing the vertical variation from coarse-grained laminar facies to fine-grained turbulent facies.

lithofacies and erosive with the underlying pillowed facies, which also serves as a marker horizon for this particular outcrop (**Figure 37**). This fine-grained tuff is composed of multiple T_{ab} and T_{abd} Bouma sequences (cf. Lowe, 1982), recognized by grading and erosive contacts (**Figure 42**). Both grading and erosive contacts indicate younging direction to the south. Fragments are altered a grayish-white with a pale grayish-green matrix due to quartz-albite re-crystallization and chloritization, respectively. The monolithic fragment population varies from a subangular to subrounded morphology with a slight elongation parallel to bedding. Vesicularity is not observed on surface. Petrographic work recognized tuff- to lapilli-sized fragments that have been altered to a fine-grained quartz-albite mosaic hosted in an epidote + chlorite + quartz + sericite ± albite matrix. Fragments have a slightly flattened appearance with 1:3 to 1:4 aspect ratio (**Figure 43A**). Vesicles or amygdules are not observed.

Overlying the tuff sequence is a series of lapilli tuff breccia beds that can be subdivided into three depositional units based on grading and contact relationships (**Table 6; Figures 37 and 41**). Each depositional unit is composed of several beds, which from base to top have: (1) a massive to normal graded, 1-3 m-thick basal tuff breccia; (2) several normal- to rare reverse-graded, 1-2 m-thick, coarse- to fine-lapilli tuff beds; and (3) a capping normal graded, 0.5-2 m-thick, coarse- to fine-tuff beds (**Figures 44 and 45**). The overall thickness of each depositional unit varies along strike, whereby the lower two flow units pinch and swell, and the uppermost unit has a general thickening trend towards the west. Stratification is weak or diffuse, but becomes more evident further to the west over a distance of 10s of meters (**Figures 37, 41 and 46**). Furthermore, there is an overall

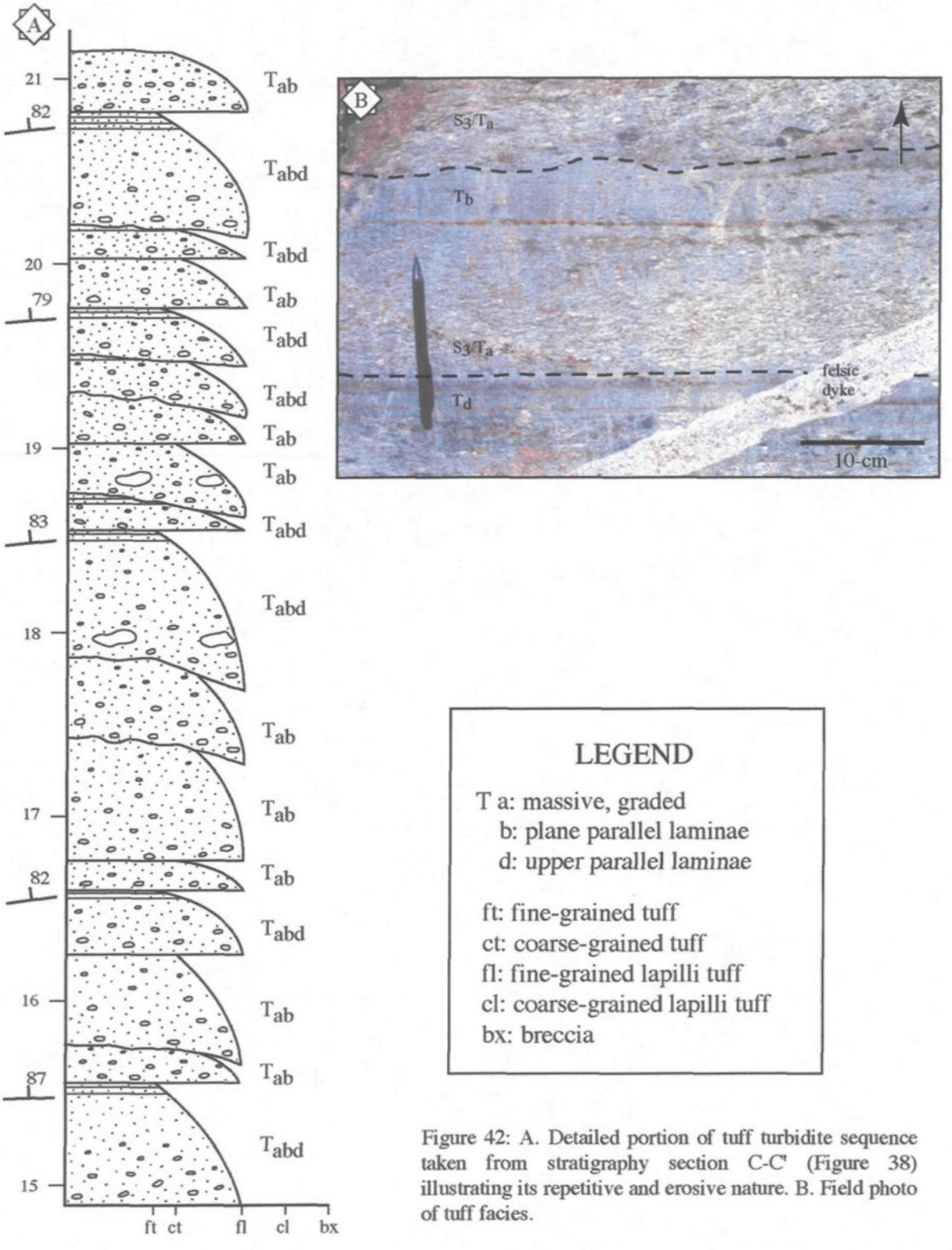

Figure 42: A. Detailed portion of tuff turbidite sequence taken from stratigraphy section C-C' (Figure 38) illustrating its repetitive and erosive nature. B. Field photo of tuff facies.

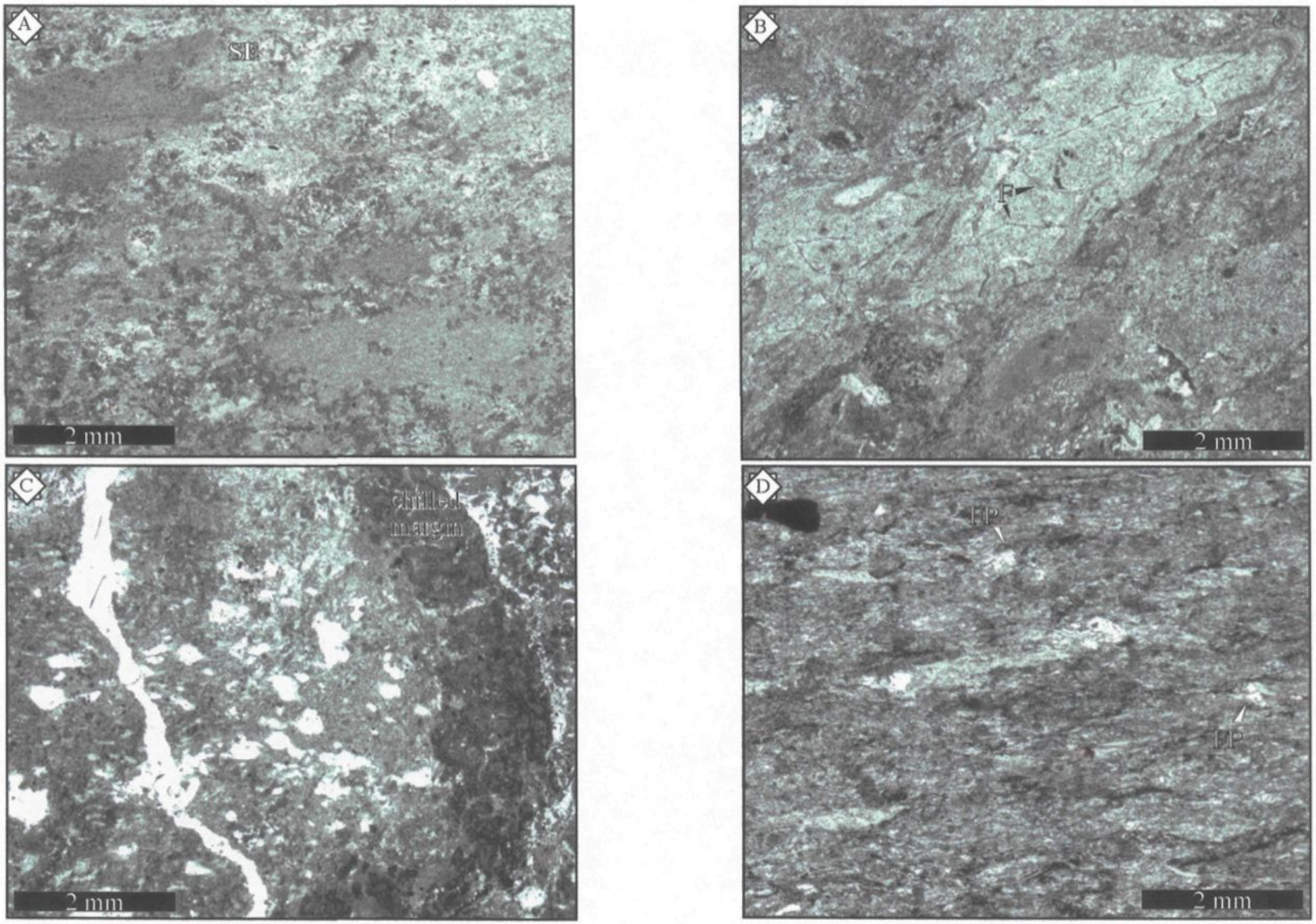

Figure 43: Photomicrographs of various textures of fragments within tuff and lapilli tuff facies from Placer Dome North outcrops. All are taken from the finer grained part of the tuff breccia facies, except for (A), which is from the lower tuffaceous facies. A. Completely re-crystallized fragments that are characterized by serrated edges (SE). B. Chloritized fragment that has possible relict perlitic fractures (F) and chilled margin (C). C. Vesicular fragment with well developed aphyric (chilled?) margin. D. Wispy, flattened chloritized fragments from coarse tuff facies; liberated broken feldspar (FP) microphenocryts are not aligned with these fragments.

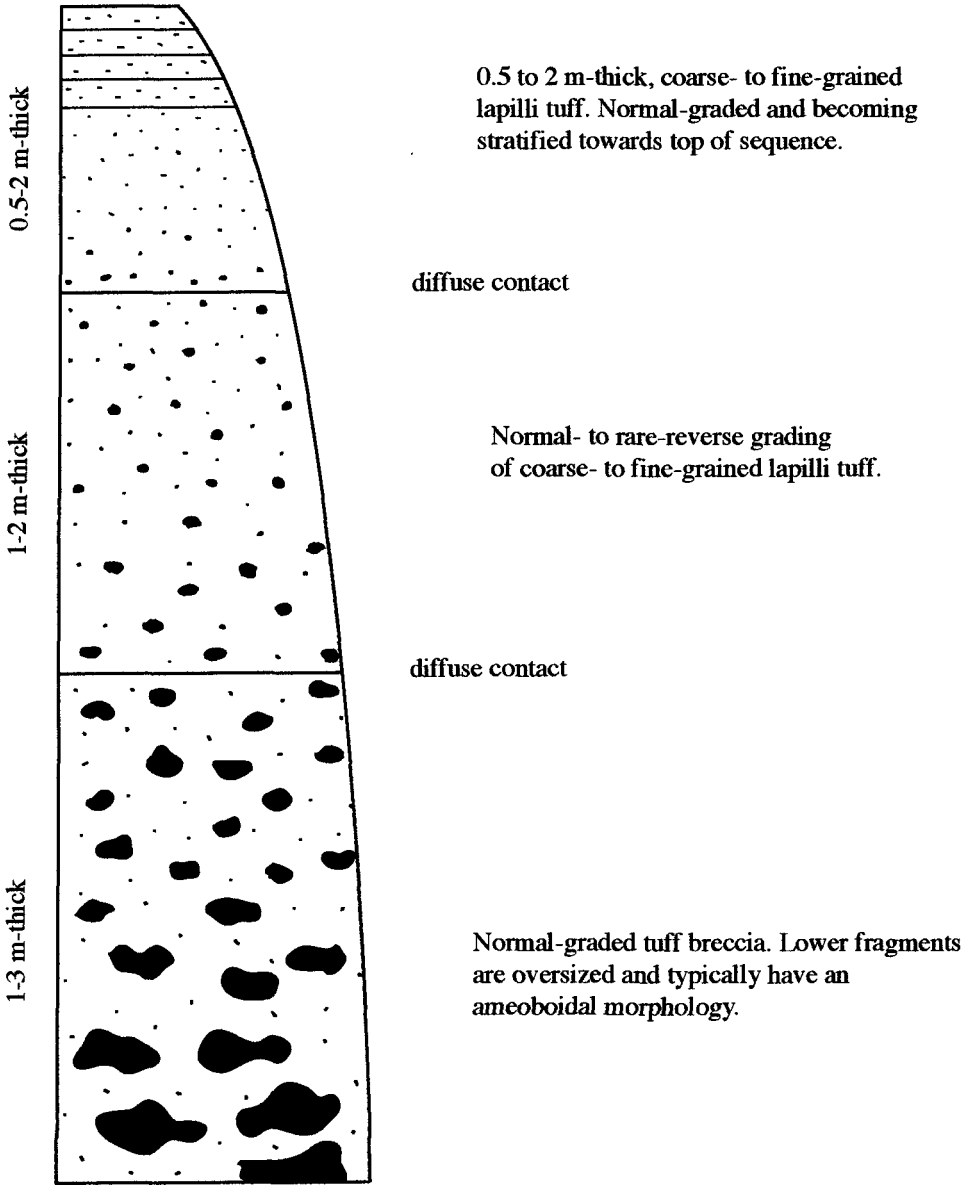

Figure 44: Idealized stratigraphic section of a single volcaniclastic debris flow sequence from Placer Dome North.

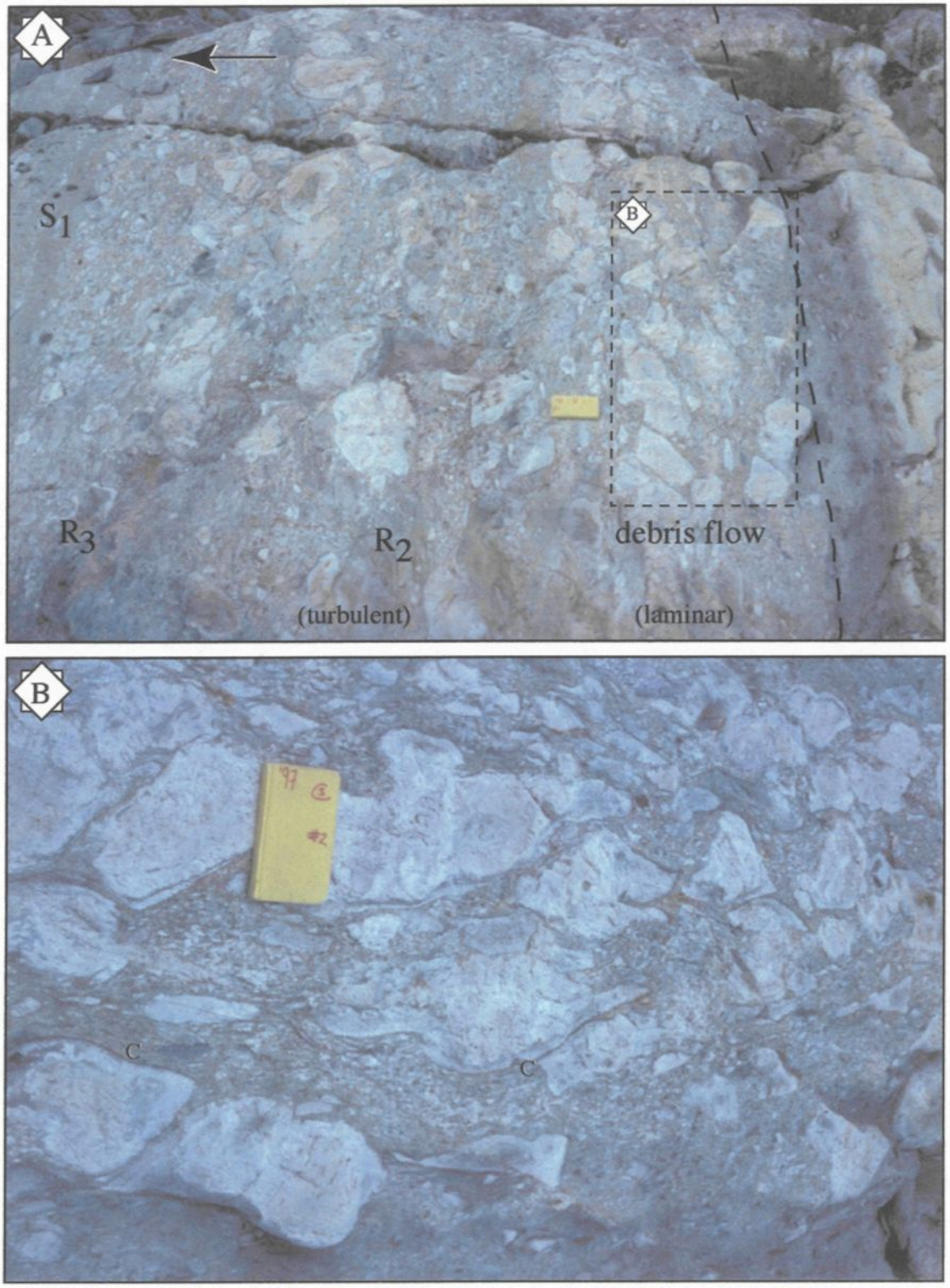

Figure 45: Photos from lower debris flow deposit; fieldbook for scale (19 cm). A. Vertical transition of lower part of one depositional unit from basal debris flow (laminar regime) facies to high- (R-type) and low-concentration (S-type) turbidity flow (turbulent regime) facies. B. Closeup of amoeboidal fragments within basal debris flow facies. Fragments are plastically deformed, pillow-like, and have chilled margins (C).

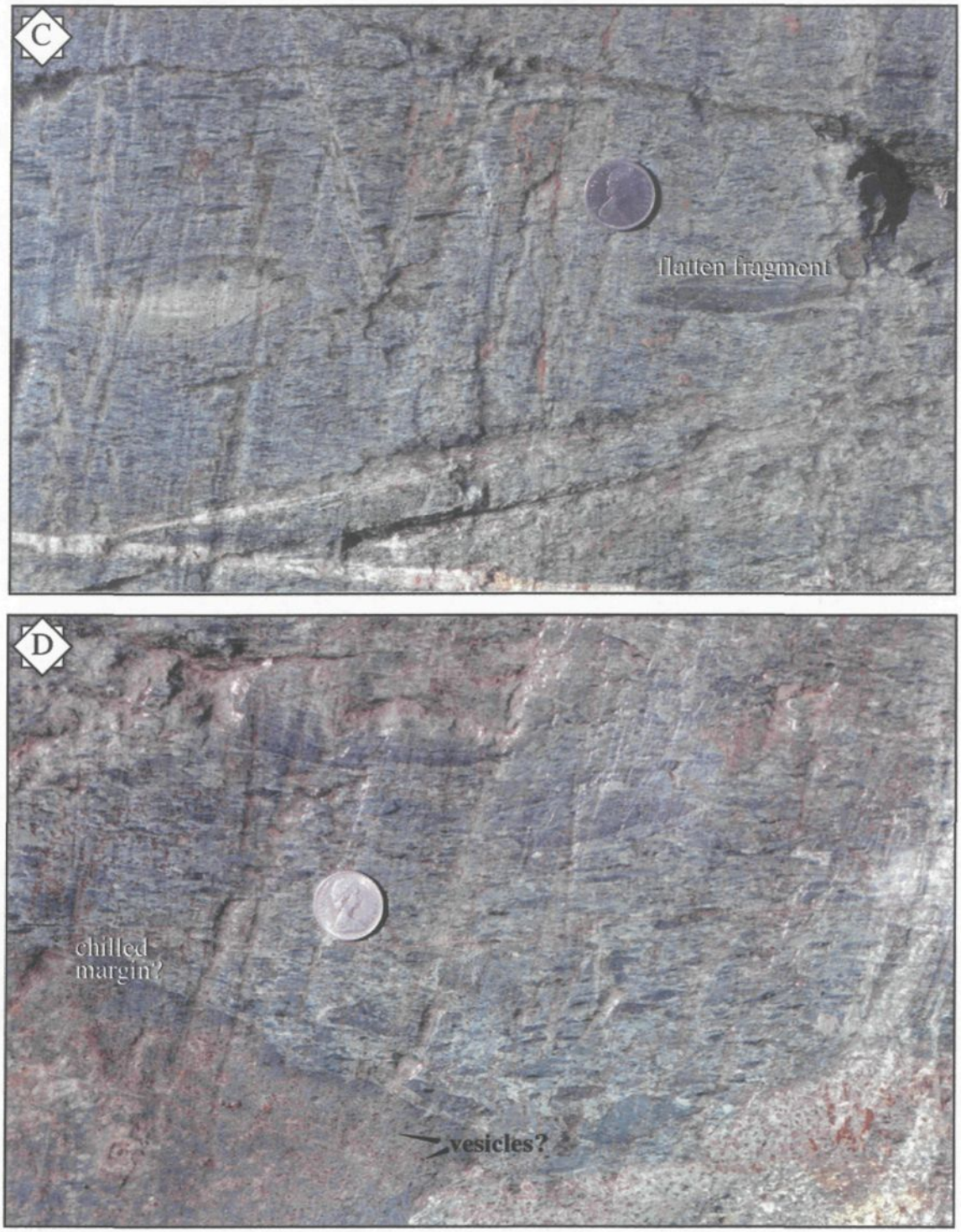

Figure 45 (con't): Fragment morphology within turbulent regime of depositional unit. Coin for scale (23 mm). C. Numerous flattened lapilli fragments, some of the larger fragments are slightly vesicular. D. Similar flattened fragments, with larger vesicular breccia-sized fragment with a chloritized, non-vesicular margin, which may represent a chilled margin.

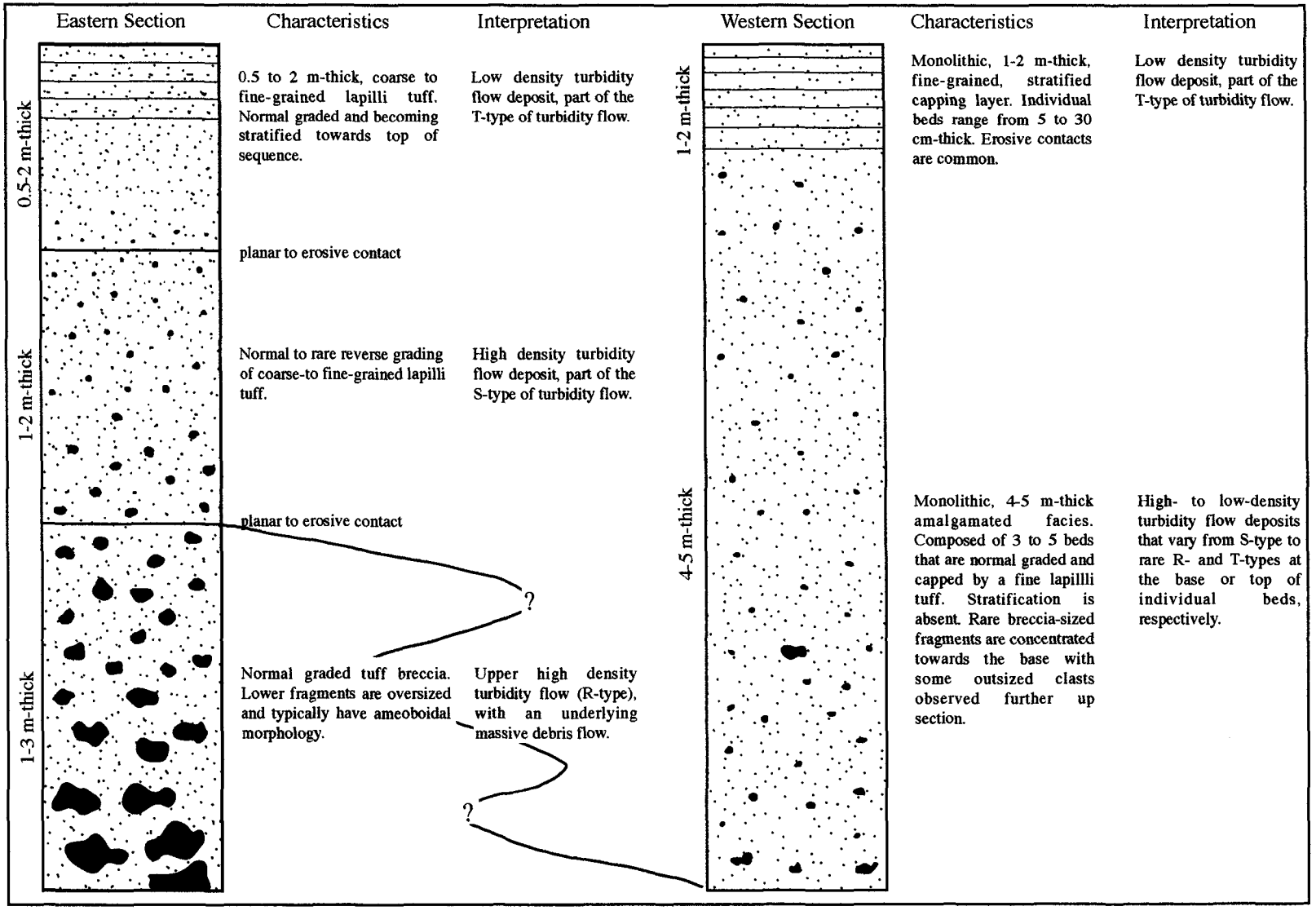

Figure 46: Lateral variations observed within lapilli tuff breccia flow unit from east to west over ~70m.

decrease in fragment size towards the west as large breccia (> 40-cm) fragments become increasingly rare (**Figure 46**). Fragments are aphyric and weakly-to-moderately vesicular (upwards to 35-vol%; visual estimate), with larger breccia-sized fragments typically having a subrounded, amoeboidal form and highly epidotized (**Figures 44 and 45**). Texturally, these fragments are similar to the underlying pillow facies, but no direct transition from the pillowed facies is observed.

Petrographically, two fragment populations are identified based on style of alteration and vesicularity. One fragment type is altered to chlorite with a conspicuous epidote margin (**Figures 43B/C; Appendix A-7**). Such fragments are slightly flattened or elongated (**Figures 45C-D**), with a vesicularity up to a maximum of 35-vol%, as represented by quartz amygdules (**see Figure 43C**). Trace amounts of lath-shaped feldspars are not oriented or flattened in the same plane as the fragments or amygdules (**Figure 43D**). Exterior morphology is angular, flattened, and characterized by cuspate chilled margins (**Figure 43B**). The second fragment population is composed of fine-grained quartz and albite. These quartzo-feldspathic fragments are slightly larger than the chloritic fragments. Vesicles are absent and crystals are rare. Contact with the matrix is not well defined, as the matrix is altered to the same alteration assemblage, with fragments being finer-grained (similar to fragment in **Figure 43A**). The matrix consists of fine-grained epidote + chlorite + carbonate + albite. Subordinate lath-shaped feldspar microphenocrysts are randomly scattered throughout.

Intrusive phases

Another conspicuous feature is the number of different dyke populations that crosscut the stratigraphy (**Figures 36 and 37**). A total of six dyke phases are recognized, which based on cross-cutting relationships are, from oldest to youngest: (1) aphyric intermediate dyke, (2) feldspar-pyrite porphyry dyke, (3) melanocratic lamprophyre, (4) feldspar-phyric dyke, and (5) monzonitic dyke. The sixth dyke is a small greenish intrusion that is pyroxene-rich and does not cut other phases. All dyke phases, with the exception of the feldspar-phyric dyke, crosscut the volcanic sequence. The lamprophyric dyke has subrounded, cm-sized leucocratic, holocrystalline blobs composed of medium- to coarse-grained feldspar, quartz, and biotite. Detailed mapping of a lamprophyric stocks recognized different generations of lamprophyre based on color variations and xenoliths.

Deformation

Deformation is minor outside of the previously described shear zone associated with the pillowed facies. The stratigraphy is near vertical, with an average schistosity of 267° dipping 85° to the north and bedding of 085° dipping 87° to the south. As the younging direction is to the south, beds are 'upright', within only rare cases of beds being overturned or dipping to the north. A conspicuous offset observed within the volcaniclastic beds (**Figure 41B**) records a N-S fault that is obscured by a lamphrophyric dyke. This dyke does not propagate into the overlying pillowed facies (**Figures 36 and 41B**) and may represent a synvolcanic fault.

4.1.2.2 Interpretation of Placer Dome North stratigraphy

These outcrops represent a rare opportunity in Archean rocks to observe lateral and vertical transitions from pillowed facies to associated volcaniclastic deposits. Moreover, internal facies variations record changes as a function of distance from the source (i.e., vent).

Volcanic processes and mechanisms

Lateral variations in pillowed lava morphology records the changing properties of the propagating lava during transport. Its aphyric nature suggests a high-temperature lava, which would imply the lava had a relatively low-viscosity (i.e., fluidal). Amoeboidal pillowed forms support this notion. The intercalated spattered zones represent localized disruption during transport of the fluidal lava. Subaerial lava spatter is associated with the release of dissolved gases during eruption (i.e, Strombolian) as are some interpreted subaqueous vesicular basaltic welded clasts (i.e., Sumisu rift; Gill et al., 1990). However, these deposits are non-vesicular. Two possible modes are envisaged for their formation: (1) gravitational collapse and/or (2) lava overpressure. Downslope movement of pillowed flows could result in tearing/shearing of fluidal lava into hot lava rags that tumble and roll several meters down the flank of the vent (**Figure 47**). The vertical propagation of pillowed flows (i.e., trap door) may be inhibited by high hydrostatic pressures, which could result in lava overpressure. If lava pressure exceeds the overlying hydrostatic pressure it could "pop" or the steam carapace could implode forming lava spatter (**Figure 47**). This pillow spatter would be quickly covered by the advancing lava front, which compressed this hot

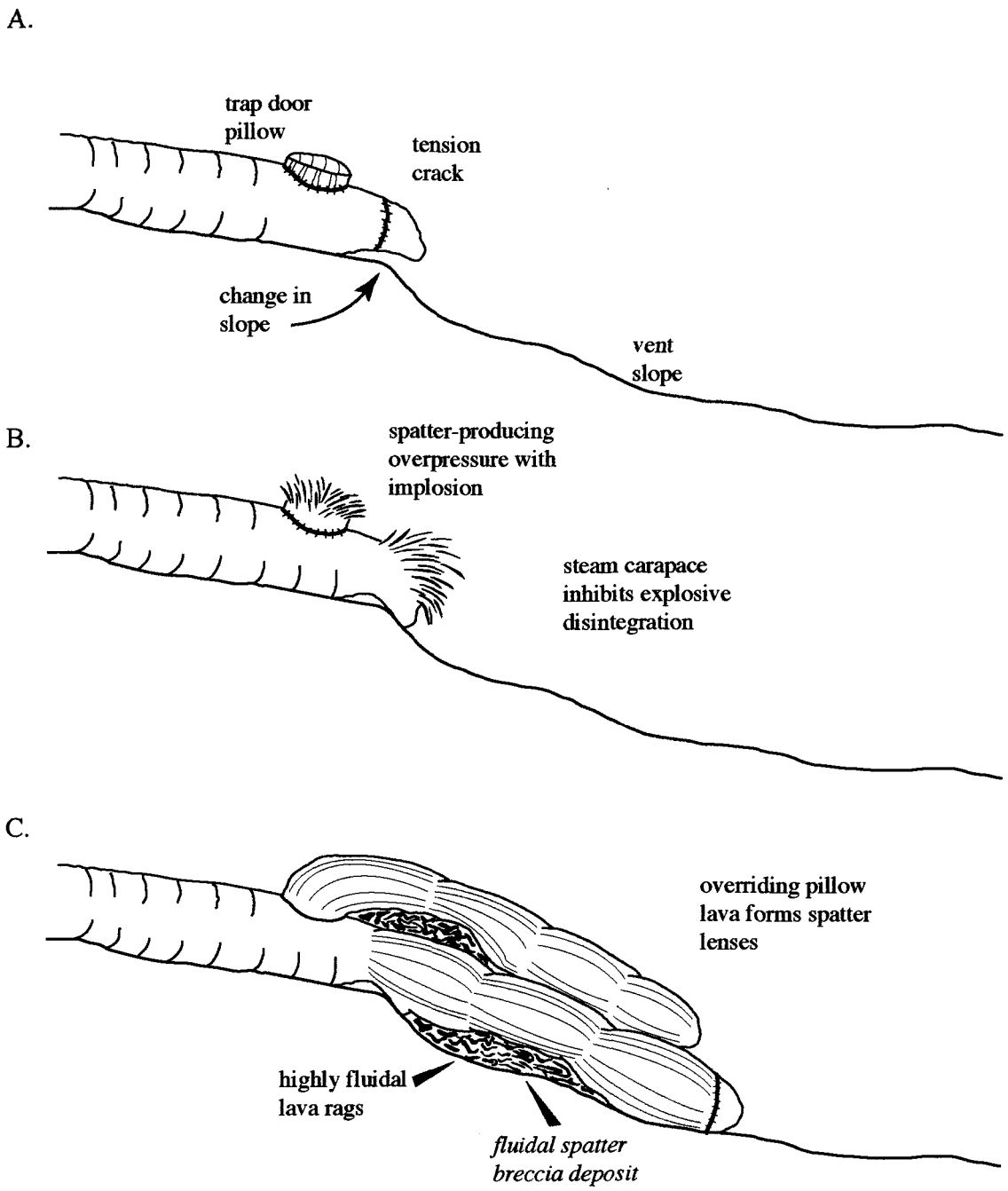

Figure 47. Schematic sketches outlining possible formation of spatter-like lenses during propagation of a low viscosity pillow lava. A. Two possible conditions to produce spatter; formation of trap door pillow or topography variation along vent slope. B. Implosion stage; spatter formation due to over pressure or flow front collapse. C. Continued pillow growth overrides spatter forming spatter lenses composed of fluidal lava rags; "fluidal spatter breccia deposit". Ideas of pillow propagation from Moore (1975) and Batiza and White (2000) and references therein.

debris. This could form the isolated lenses of spatter, defined as *fluidal spatter breccia* deposits, bounded by amoeboidal- to bun-shaped lava (**Figures 37 and 47**).

The variability of amoeboid textures attests to a very fluidal lava that was erupted under low to moderate discharge rates and relatively small volumes. Otherwise, such fluidal lava would probably form deposits that are more massive, and which grade into pillowed varieties further from the erupting vent (cf. Dimroth et al., 1978). Lava spatter is similar to the Playground deposits (**see Figure 29**); however, the association with pillowed lava and predominance of complex, interlocked and folded fragments (**Figures 38C/D**) precludes a fire-fountaining mechanism, as any significant transport would destroy them. Furthermore, the low vesicularity (< 5-vol%) is not consistent with a fire-fountaining mechanism underwater (Gill et al., 1990; White et al., 2002) or on land (Vergniolle and Mangan, 2000). This has a two-fold effect: (1) fragmentation is highly inefficient, thus forming only large lava blobs; and (2) deposition is restricted to within tens of meters of the source.

The tube-like morphology of the overlying 70-thick pillowed sequence suggests a feeder system probably close to the erupting vent. A direct transition from a pillowed to fragmental facies in the southwest corner of the upper outcrop indicates autoclastic fragmentation as the pillowed flow appears disintegrate by non-explosive processes.

Volcaniclastics: explosive processes and mechanisms

The main volcaniclastic sequence (**Figures 37 and 41**) has no direct transition observed between pillowed flows and fragmental units, unlike that observed for the

southern flows where pillows grade into a lapilli breccia (**Figure 39**). Nonetheless, the monolithologic character, mineralogy, pillow breccia forms and spatial relationship to underlying pillowed facies all suggest they are genetically related.

Tuff sequence

The 3-8 m-thick sequence of tuff units represent an amalgamation of up to 27 individual beds, ranging from T_{ab} to T_{abd}, and measuring between 5 and 40 cm-thick (**Figure 42**). Bedding characteristics, such as stratification, grading, and grain-size suggest that these beds were deposited by low-density turbidity flows (Lowe, 1982). Scouring of underlying pillowed facies and interbedded truncations indicate that these flows were erosive during transport.

Their fine-grained nature indicates either a change in eruptive style or efficient weathering and reworking of older, unconsolidated deposits. The latter would describe an epiclastic process (pg. 89; Fisher and Schmincke, 1984) that typically would have an overall larger grain size and a more diverse fragment population. Therefore, it is envisioned that the tuff beds record a change from effusive volcanism to a more fragmental volcanic eruption. The monolithic population of juvenile material suggests efficient fragmentation, and given the subaqueous environment, fragmentation must be a variety of phreatomagmatism: defined by Morrissey et al. (2000) as "Volcanic activity resulting from the interaction between magma/lava and groundwater or surface water including seawater, meteoric water or lake water." Similarly described deposits, thin bedded, weakly vesicular tuffs to lapilli tuffs were interpreted by Németh and White (2003) as being formed during

phreatomagmatic fragmentation and transported by turbulent, low-concentration pyroclastic density currents (cf. Chough and Sohn, 1990). The complete sequence records deposition from successive collapse of tuff-sized material from a subaqueous eruptive column (Fiske and Matsuda, 1964).

Lapilli tuff breccia

The subsequent three lapilli tuff breccia deposits indicate another change in style of volcanism. Individual deposits can be subdivided into two transport regimes corresponding to two or more flow types. The basal lapilli tuff breccia unit is composed of preserved pillowed forms (**Figure 45**) and pillow breccia suggesting contemporaneous transport of hot fragments from disrupted pillowed lava. This unit typically grades from massive to normal-graded (rare reverse-graded) both up section and along strike to the east (**Figures 37 and 46**), which can be described as a transformation from a laminar to a turbulent flow regime, respectively. These flow regime transformations can be attributed to changes in the hydraulic conditions in relation to surface and/or fluidization transformations (cf. Fisher, 1983) due to the ingestion of water or upward movement of fluids within the flow (Fisher, 1983). Their massive nature is similar to described cohesive debris flows (Lowe, 1982), whereby such flows are capable of transporting large blocks in a matrix of lapilli- and ash-sized fragments (Prothero and Schwab, 1996). Subsequent grading from coarse-grained breccia, to a stratified lapilli tuff and/or tuff (**Figures 44 and 46**) indicate deposition from high- to low-density turbidity flows (Lowe, 1982, 1988). This grading probably records

progressive deposition, probably from a single eruptive event (cf. Fiske and Matsuda, 1964) originating from 'lava-fed density currents' (White, 2000).

The predominance of fluidal, pillow-like fragments in the basal lapilli tuff breccia (**Figures 44 and 45**) suggests a non-explosive, dynamo-thermal spalling along a lava flow margin. Finer-grained fragments represent possible weak phreatomagmatic explosions that were localized to the upper lava margins during discrete periods of water-magma mixing within a hyaloclastite carapace. These finer-grained juvenile fragments can be subsequently lofted and mixed with ambient water due to initial ejection or entrained by convecting hot water above flow margins as observed for Hawaiian lava flows (Moore et al., 1973). Together, the laminar and turbulent partitions form a single depositional unit, similar to the 'standard depositional unit' defined by Berg and Gudmunder (1991) for lava-fed hyaloclastite sequences in Iceland.

These lapilli tuff breccia deposits may also be described as a subaqueous equivalent to subaerial block and ash deposits. Notwithstanding the density difference between air and water (cf. Stix, 1991), observed gravitational collapse (Merapi-type) of lava lobe margins at Unzen volcano in Japan typically formed small volume flows that traveled between 1.5 and 5.6 km from the flow front (Ui et al., 1999). Such flows were deposited on gentle slopes (< 20°) with a cumulative thickness up to 5 m of massive to reversely graded, non-vesicular to vesicular blocks in a fine-grained ash matrix (Miyabuchi, 1999). Larger blocks had radial cooling joints, indicating they were emplaced hot (Miyabuchi, 1999), which would be analogous to the amoeboidal forms observed from the lapilli tuff breccias (**Figure 45B**). While more than 9000 block and ash flows were recorded at Unzen volcano, most were

very small volume and formed channel- or finger-like deposits (Ui et al., 1999), similar to those deposited at Soufriere Hills, Montserrat (**Figure 48**). Thus, the deposits mapped here probably do not record the complete eruptive sequence.

Another possible interpretation for these deposits is the accumulation of pillow debris during post-eruptive remobilization to form talus-like deposits downslope (cf. Tanner and Calvari, 1999). However, such talus accumulations typically are clast-supported, non-graded and poorly sorted, lacking juvenile, fine-grained material, and breccia-sized fragments are dominantly subangular (Tanner and Hubert, 1991; Wright and Gamble, 1999), all of which are not observed for these deposits. Furthermore, such talus deposits form wedge-shaped beds that thin in the direction of transport, with complex interfingering of other deposits (Tanner and Calvari, 1999), which is also not evident for the mapped deposits. Such talus accumulations are observed at the base of steep topographic slopes indicating mass wasting of lavas (Lonsdale and Batiza, 1980; Wright and Gamble, 1999).

Intrusive phases

The abundance of dykes that cut the sequence is another possible indication of proximity to the volcanic vent. Only the intermediate dyke phase is observed to cut the uppermost pillowed facies, which, based on its composition and orientation may indicate that it is a feeder dyke for flows to the south (i.e., Pole Line deposits, discussed below). Furthermore, the synvolcanic fault probably formed in response to slumping and faulting in proximity to a tectonically active volcanic vent (cf. Cousineau and Bédard, 2000). The

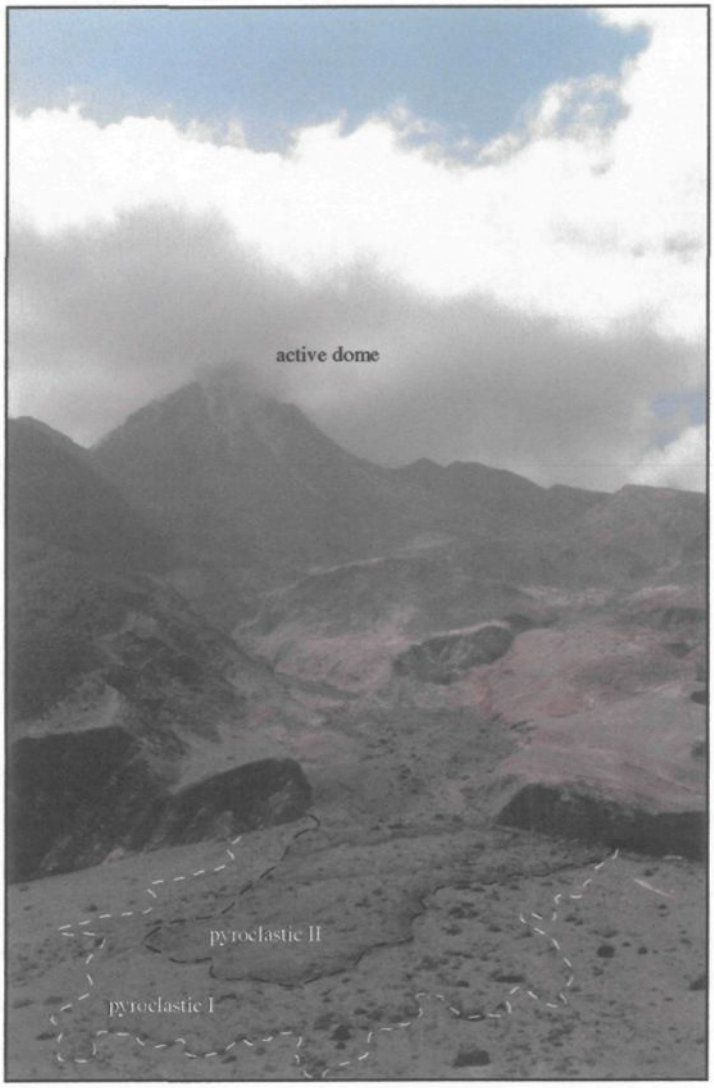

Figure 48: Subaerial examples demonstrating the morphology of pyroclastic flow deposits and how sucessive flows cover prior flows forming a complex assemblage of fragmental deposits. Approximately 2 km to the active Soufriere Hills Volcano, Montserrat (Caribbean).

lamprophyric dykes are younger than the 2700 ± 1 Ma Bourlamaque Pluton (Wong et al., 1991) as rounded xenoliths of the Bourlamaque are entrained in these dykes.

In conclusion, these series of outcrops represent a monogenetic subaqueous volcano of intermediate composition (see Chapter 6 for discussion on composition). Volcanism evolved from effusive volcanism to a period of explosive phreatomagmatic activity and remobilization of non-explosive disintegration of lava, back to effusive pillow formation of an intermediate system.

4.1.3 East Sullivan Outcrops (ROI 3)

The East Sullivan outcrops include two large stripped areas located about 3.5 km east of Val d'Or on either side of the dirt road that leads to the past producing East Sullivan mine site (**Figure 25**). Stripping was conducted for gold exploration; in particular for quartz-tourmaline veins that commonly host gold in the Val d'Or Mining Camp. These outcrops offer continuous exposure of volcaniclastic deposits with intercalated intermediate pillowed lavas and subordinate dykes and veins. Both outcrops were mapped at 1:20 scale to emphasize any lateral and vertical changes in stratigraphy. Together, these outcrops cover approximately 400 m along strike and 75 m in thickness of the local stratigraphy (**Figure 49**).

4.1.3.1 Lithology of outcrops

The stratigraphy can be subdivided into two principal components, namely intermediate pillowed lavas and volcaniclastic deposits (**Table 7**).

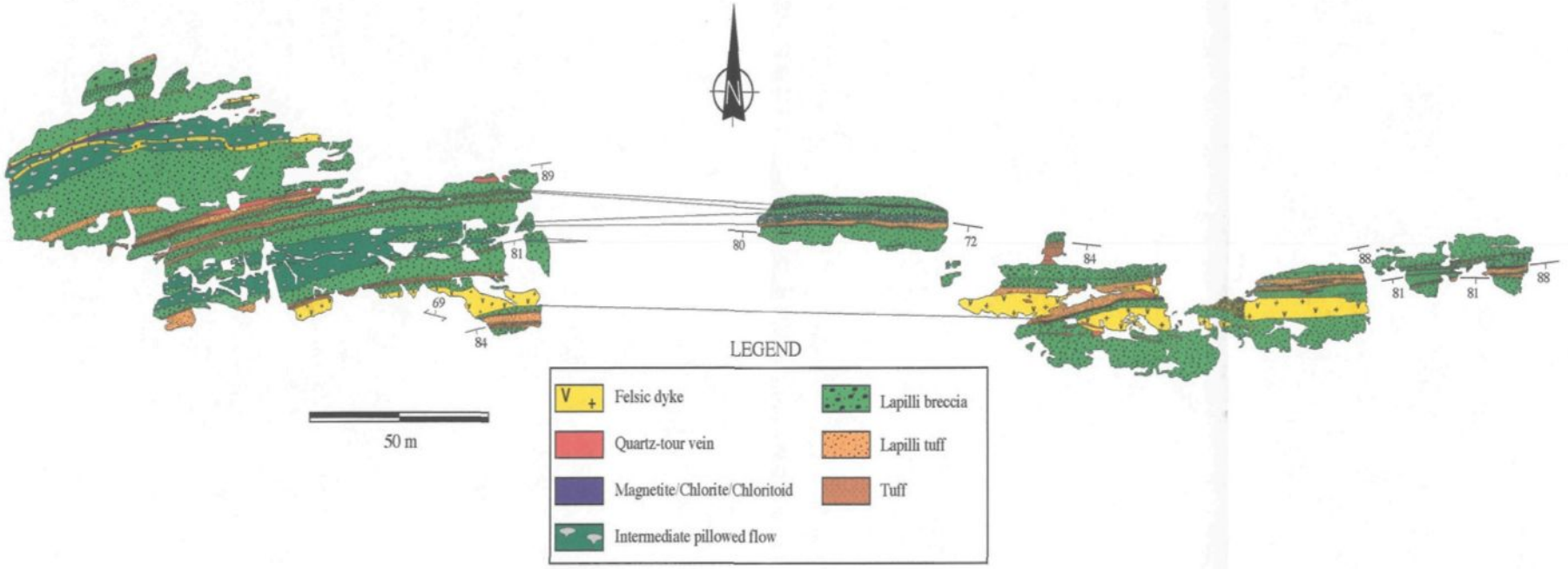

Figure 49: Correlated stripped outcrops of intercalated volcano-sedimentary deposits demonstrating a complex series of density currents and amoeboidal pillow lavas.

Table 7: Characteristics of volcano-sedimentary deposits of East Sullivan areas.

Lithofacies	Thickness & Morphology	Characteristics	Transport/Deposition	Origin/Process/Interpretation
Volcanic				
Pillowed	Tabular units, 5-9 m-thick	Bun- to mattress shaped; vesicular (5-40 vol%); 15-20 vol% plagioclase	Lava flow	Effusive subaqueous volcanism
Amoeboid clast dominated lava	Discontinuous lenses, 1-2 m-thick	Monomictic; vesicular; subrounded/amoeboidal; vesicular; plastic deformation; localized lenses	Laminar flow regime; limited transport; cohesive debris flow deposit	Effusive volcanism to possible boil-over eruption; also possible spatter along flow front; subaqueous clastogenic flow
Volcaniclastic				
Tuff	Discontinuous beds; 0.1-1 m-thick	Monomictic; diffuse to well-developed bedding; erosive; liberated, broken, euhedral crystals	Fallout; low concentration turbidity currents; turbulent flow regime	Hydrovolcanic fragmentation
Lapilli tuff	Tabular units, 0.5-4 m-thick	Monomictic; crude to diffuse bedding; erosive; liberated, broken, euhedral crystals; subrounded to subangular clasts; vesicularity 5-30%	Fallout/ballistic; low- to high-concentration flows; turbulent flow regime; traction carpets	Hydrovolcanic fragmentation; fire-fountaining
Tuff breccia	Tabular, 1-12 m-thick	Monomictic; massive or normal- to reverse-graded (R_3 and R_2); upward fining; subrounded/fluidal/spindal; plastic deformation; epidotized cores; cooling fractures; vesicularity 5-40%	Ballistic/boil-over; cohesive debris flow (subaqueous clastogenic flow?) to high concentration flow (R-type); laminar to turbulent flow regime	Fire-fountaining to boil-over subaqueous eruption

Volcanic lithofacies

Two separate pillowed flow deposits are mapped, with the uppermost deposit extending across the complete mapped section (**Figures 49, 50, and 51**). The lower deposit (only exposed in the west; **Figure 49**) is composed of bun-shaped pillows that form a somewhat lenticular unit with a nearly consistent thickness of 5 m. The upper lava flow consists of bun- to mattress-shaped pillows (**Figure 52A**) that are separated by an interstratified tuff breccia (**Figure 50**), for a combined thickness of 9 m. The eastern section is characterized by amoeboidal and/or highly irregular to massive pillowed forms (**Figures 49, 51B and 52B**). Amoeboidal pillowed forms are highly irregular, contorted, and rounded cm-to-m sized blobs that are eroded by the overlying lapilli tuff facies (**Figures 52B and 53**). This intermediate lava has a vesicularity index of 30-40-vol% (visual estimate) represented by quartz- and carbonate-filled amygdules.

In thin section, pillows are characterized by approximately 15-20-vol%, subhedral to euhedral, 3-4 mm, tabular plagioclase phenocrysts that are altered or completely replaced by sericite, chlorite, and/or epidote. The groundmass is composed of μm-sized acicular feldspar and a mosaic of quartz, chlorite, sericite, and epidote, with 5-10-vol% carbonate and quartz amygdules.

Volcaniclastic lithofacies

The volcaniclastic deposits are composed of 20-30 m-thick amalgamated beds of tuff breccia, lapilli tuff, and tuff (**Table 7; Figures 54 and 55**). Tuff breccias form 1-12 m-

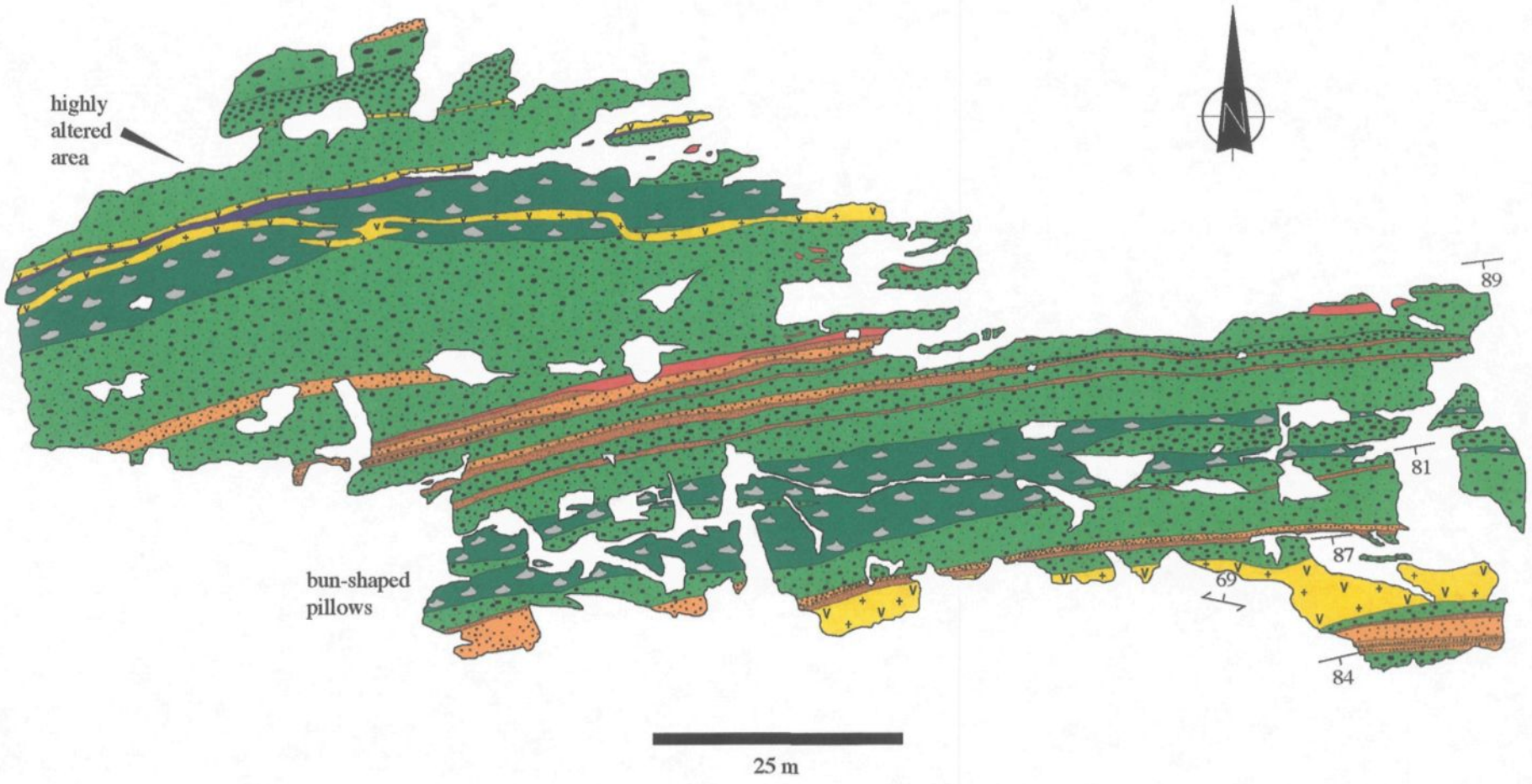

Figure 50: Closeup of western outcrop documenting the complex stratigraphy between the various volcaniclastic deposits and associated intermediate bun-shaped pillow lavas. Southern pillowed unit can be correlated to eastern section. See Figure 49 for legend.

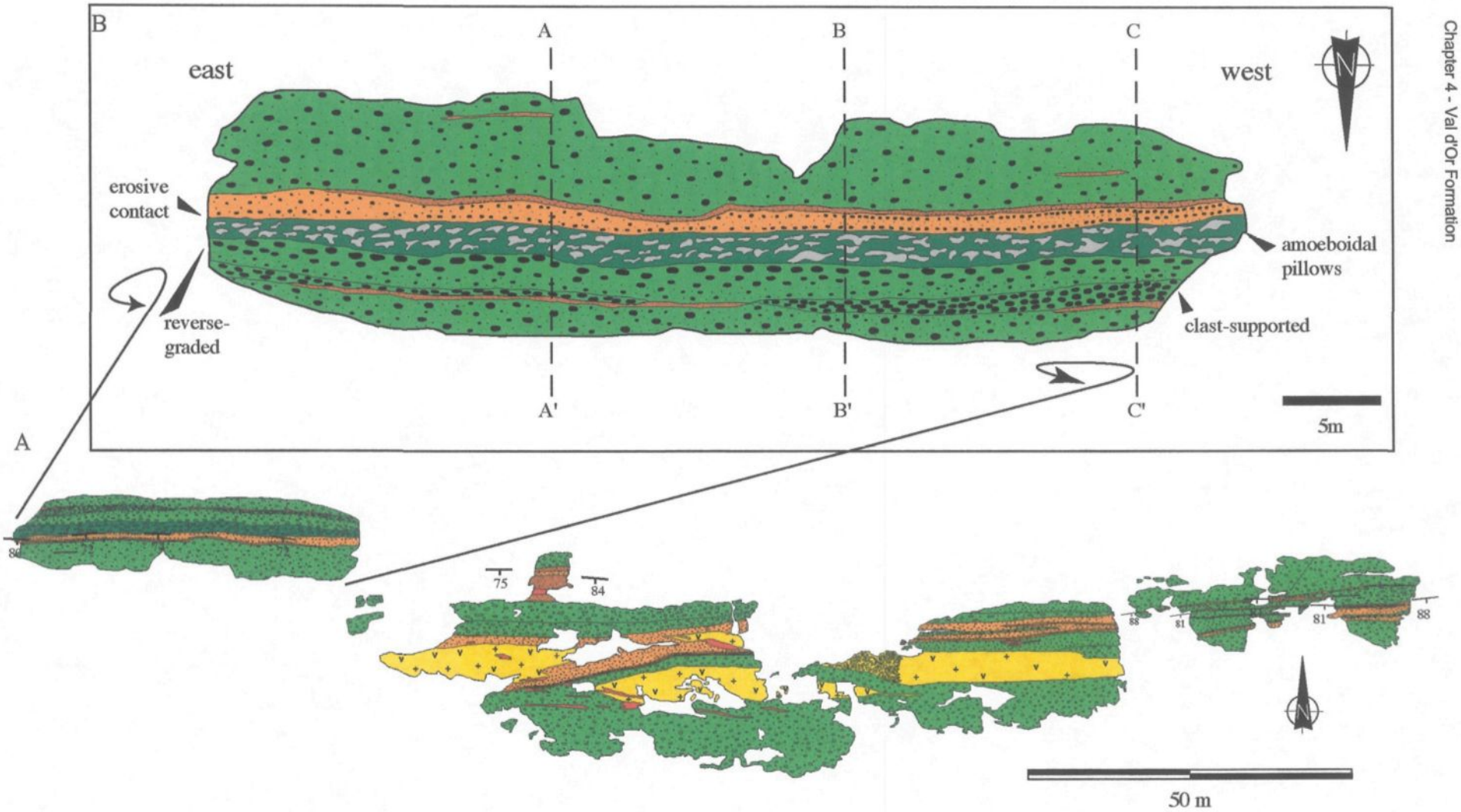

Figure 51: Eastern section of East Sullivan outcrops. A. Complete mapped outcrop. B. Blowup of one segment that is oriented with the younging direction towards the top. See Figure 49 for legend. Location of stratigraphic sections (Figure 56) indicated by dashed lines.

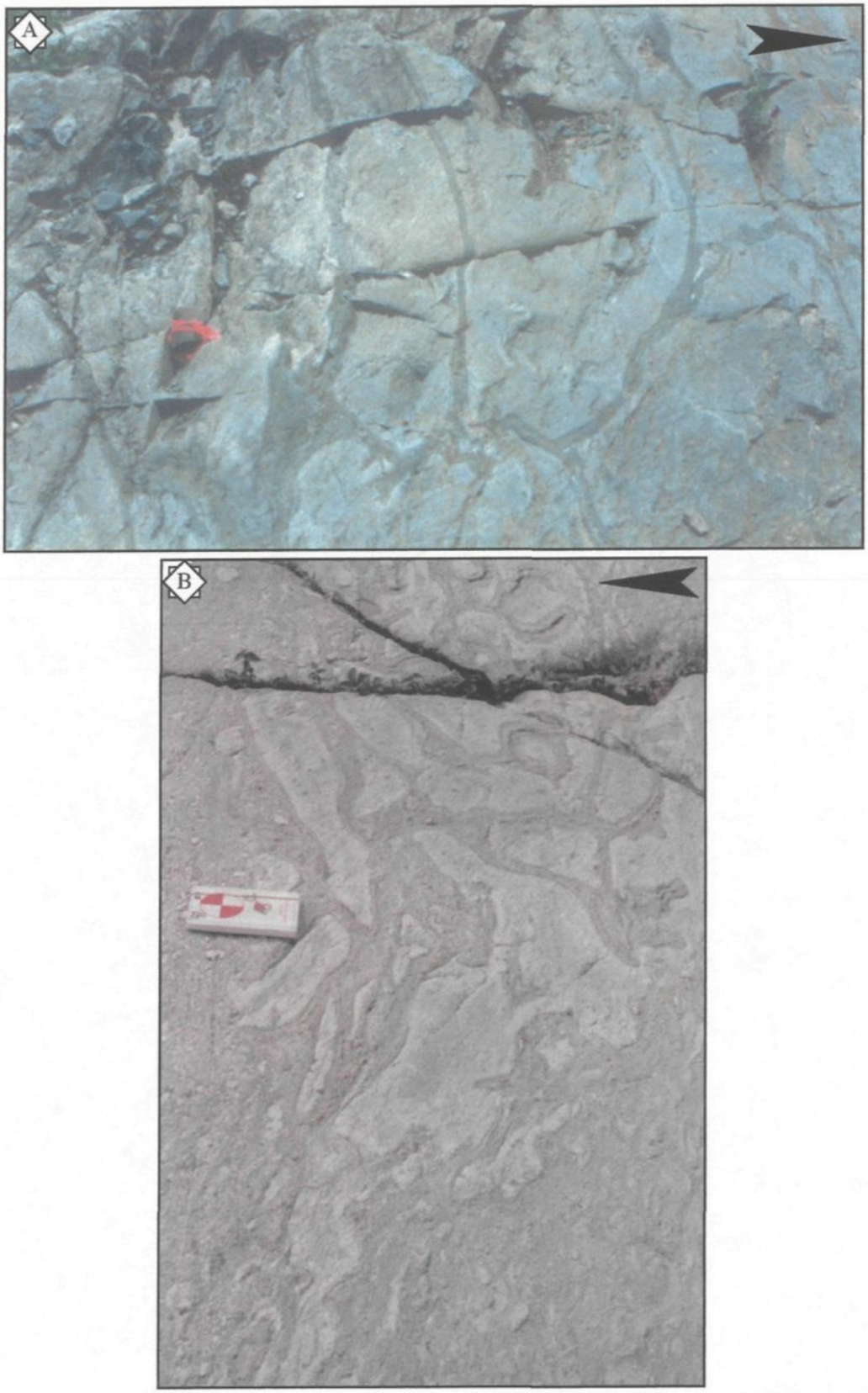

Figure 52: Variations in pillow morphology from East Sullivan outcrops (ROI 3). A. Bun- to mattress-shaped pillows from western outcrop. B. Irregular, fluidal pillow-forms from eastern outcrop. Field book (19 cm long) for scale. Arrow points in younging direction.

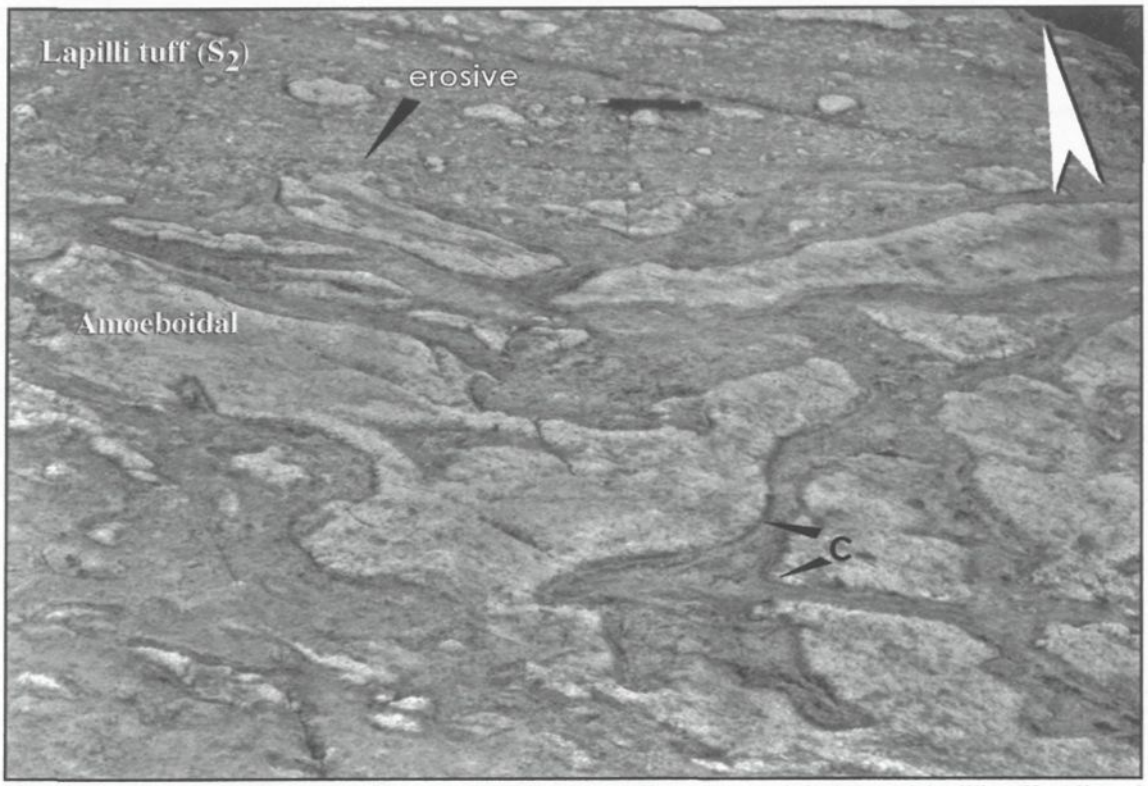

Figure 53: Erosive contact between amoeboidal intermediate pillowed facies and lapilli tuff. Aligned fragments suggest traction carpet processes within this high-concentration turbidity flow deposit (S_2). Chilled margins (C) of lava 'rags' indicate undercooling with external water. Pencil (15 cm long) lies in plane of lapilli tuff; arrow points in younging direction.

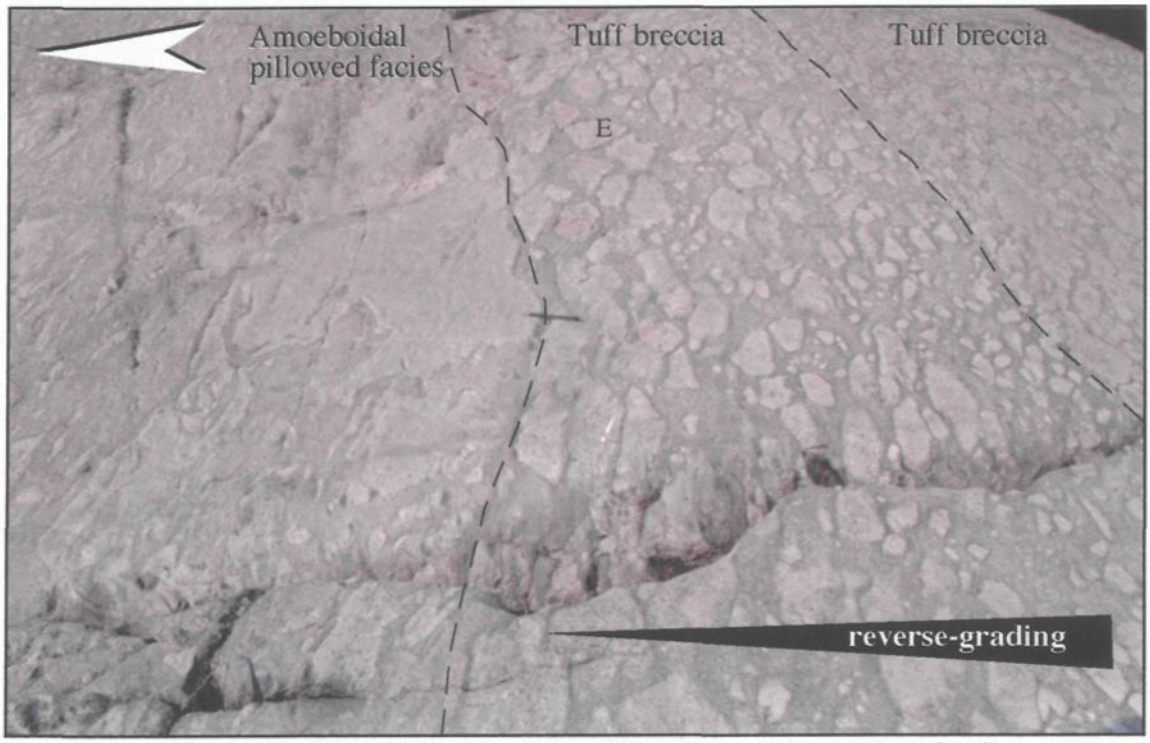

Figure 54: Stratigraphy of East Sullivan outcrops illustrating characteristics of tuff breccia and amoeboidal lava facies. Underlying tuff breccia is reverse-graded with subrounded breccia-sized fragments aligned with bedding plane. Note the common epidotized (E) nature of breccia fragments. Dashed lines are contacts between different depositional units. Plastic deformation is common where fragments are in contact. Pencil (15 cm-long) is at contact betweeen the facies; arrow points in younging direction (south).

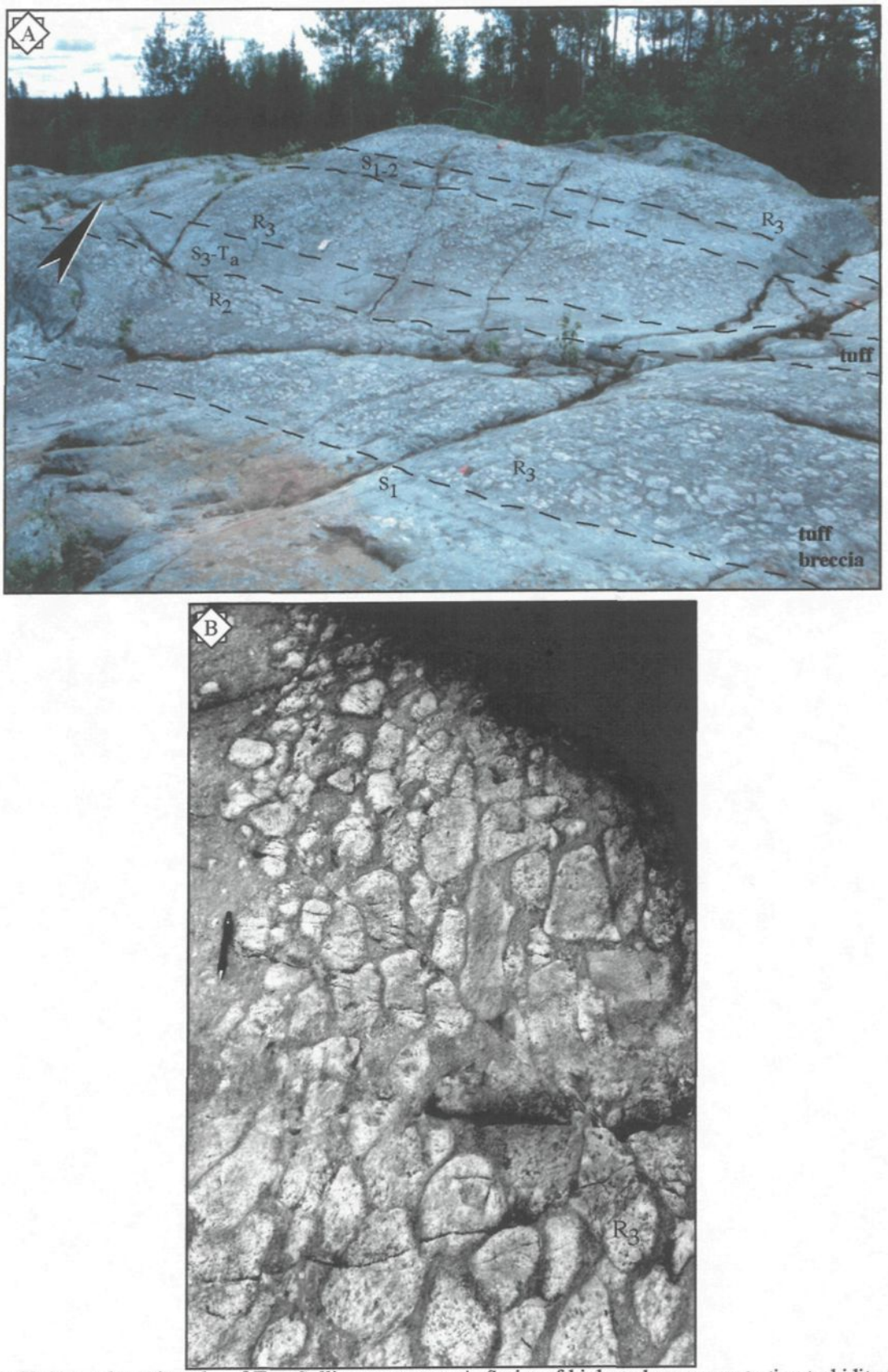

Figure 55: General stratigraphy of East Sullivan outcrops. A. Series of high- to low-concentration turbidity flow deposits composed of vesicular breccia- to tuff-sized intemediate fragments. Fieldbook for scale. B. Normally graded, clast-supported, high-concetration turbidity flow deposit (R_3). Highly vesicular fragments have chilled margins and are plastically deformed when in contact with other fragments. Pencil (14.5 cm-long) for scale.

thick beds that vary from normal- to reverse-graded and from matrix- to clast-supported (**Figure 54**), but have an overall decrease in maximum fragment size up section (**Figure 55**). All fragments are aligned such that their long axis is parallel to the bedding surface (**Figure 54**). These beds are laterally continuous over 100s of meters without any noticeable change in thickness (**Figure 49**). Interbedded contacts are sharp and typically erosive.

The lapilli tuff beds range from 0.5-4 m-thick and are comprised of normal-graded, typically stratified beds. Stratification is commonly developed in the finer grained upper portion of each bed, but is also recognized in the alignment of lapilli-sized fragments at its base (**Figure 53**). Contacts are sharp to gradational, whereby the former is commonly erosive.

Subordinate 0.1-1 m-thick, coarse- to fine-grained tuff beds typically overlie lapilli tuff facies, or more rarely, as discontinuous lenses within tuff breccia beds (**Figures 53 and 56**). All tuff beds are stratified with gradational to sharp contacts with underlying beds. Outsized subrounded breccia-sized fragments are commonly present within thicker coarse-tuff beds.

Fragments can be classified based on their size, which has a direct correlation to their morphology. All fragments larger than tuff-size are grayish-white, feldspar- and/or hornblende-phyric, and vesicular, which form a distinct monolithic population (**Figure 56**). The phenocryst assemblage and vesicularity (**Table 8**) varies up section from feldspar-phyric fragments with high vesicularity (20-40-vol %; **Figure 57; Appendix A-8**) at the base to hornblende- and feldspar-phyric with low vesicularity (<5-vol%; **Figure 58**) at the

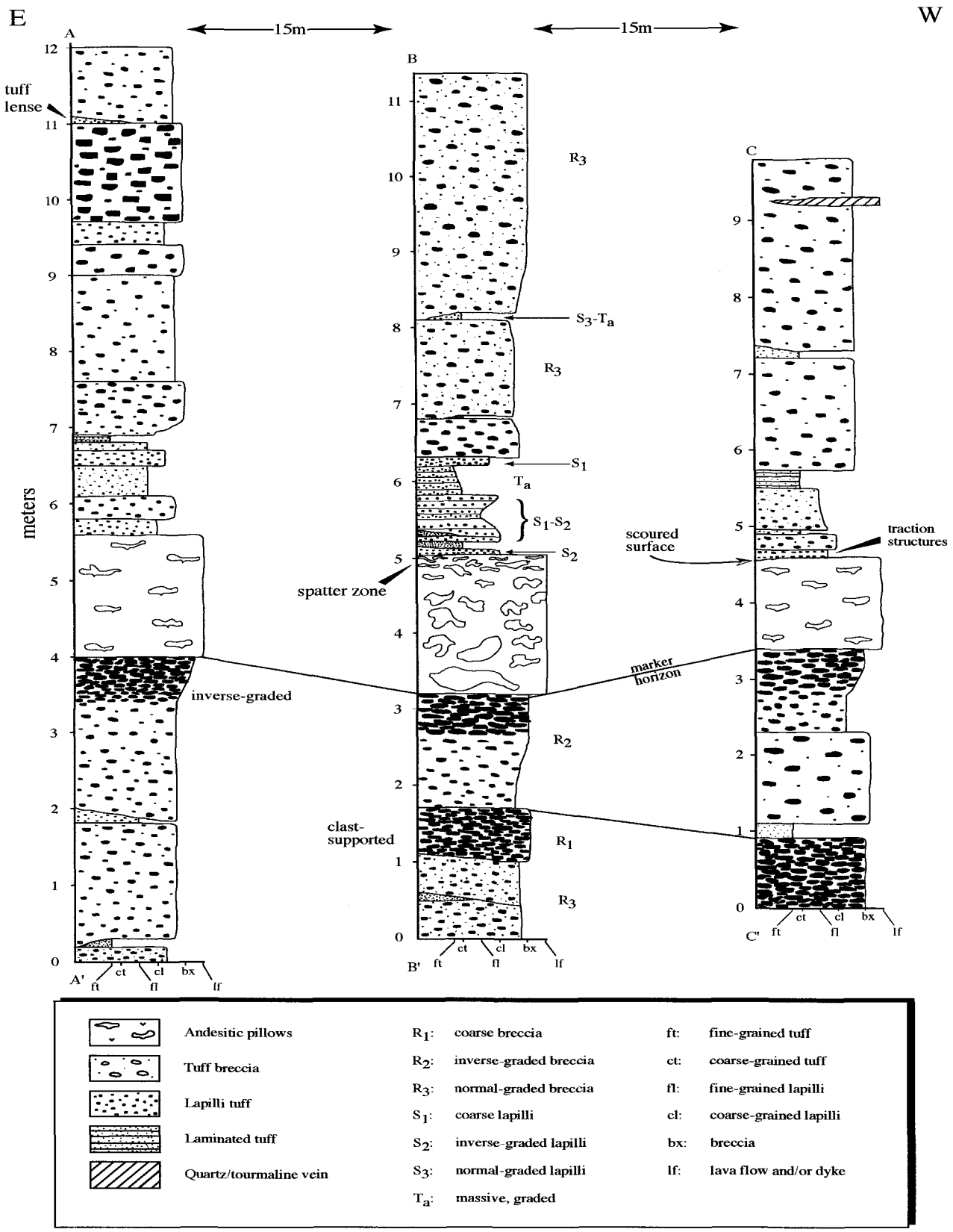

Figure 56: Stratigraphic sections from eastern outcrops (see Figure 51 for locations) documenting thickness and lateral variations of individual volcaniclastic facies. Nomenclature for high- to low-concentration density flow deposits after Lowe (1982). Intermediate pillowed facies serves as a maker horizon for region. Sections are 15 m apart.

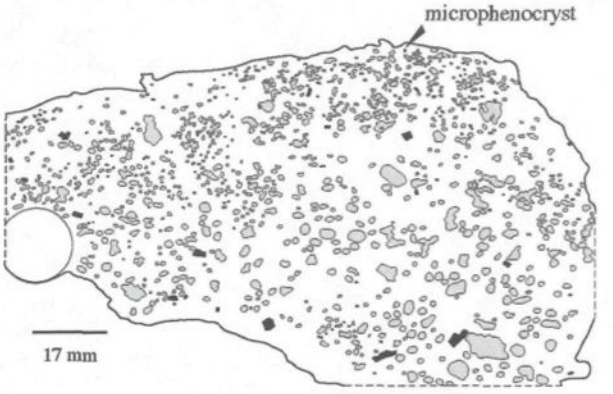

altered glass	51.58 +/- 3.83%
microphenocryts	9.08 +/- 0.44%
amygules	39.33 +/- 4.28%

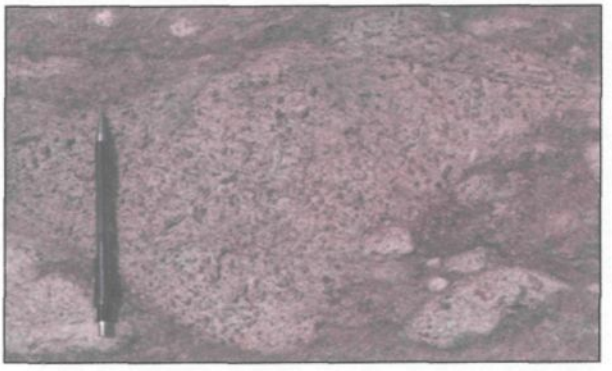

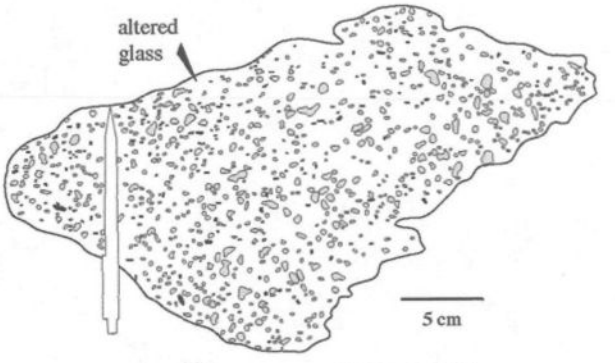

altered glass	69.08 +/- 3.85%
microphenocryts	8.49 +/- 1.49%
amygules	22.43 +/- 2.52%

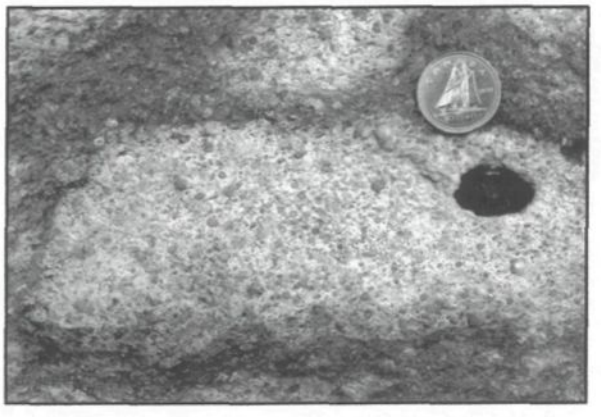

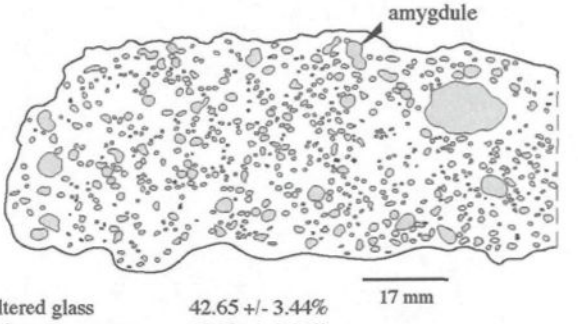

altered glass	42.65 +/- 3.44%
microphenocryts	12.29 +/- 2.25%
amygules	45.06 +/- 1.19%

Figure 57: Subrounded, breccia-sized, vesicular fragments. Point counting to calculate the vesicularity index (see Table 8). Left side are field photos and right side are cartoons illustrating vesicularity.

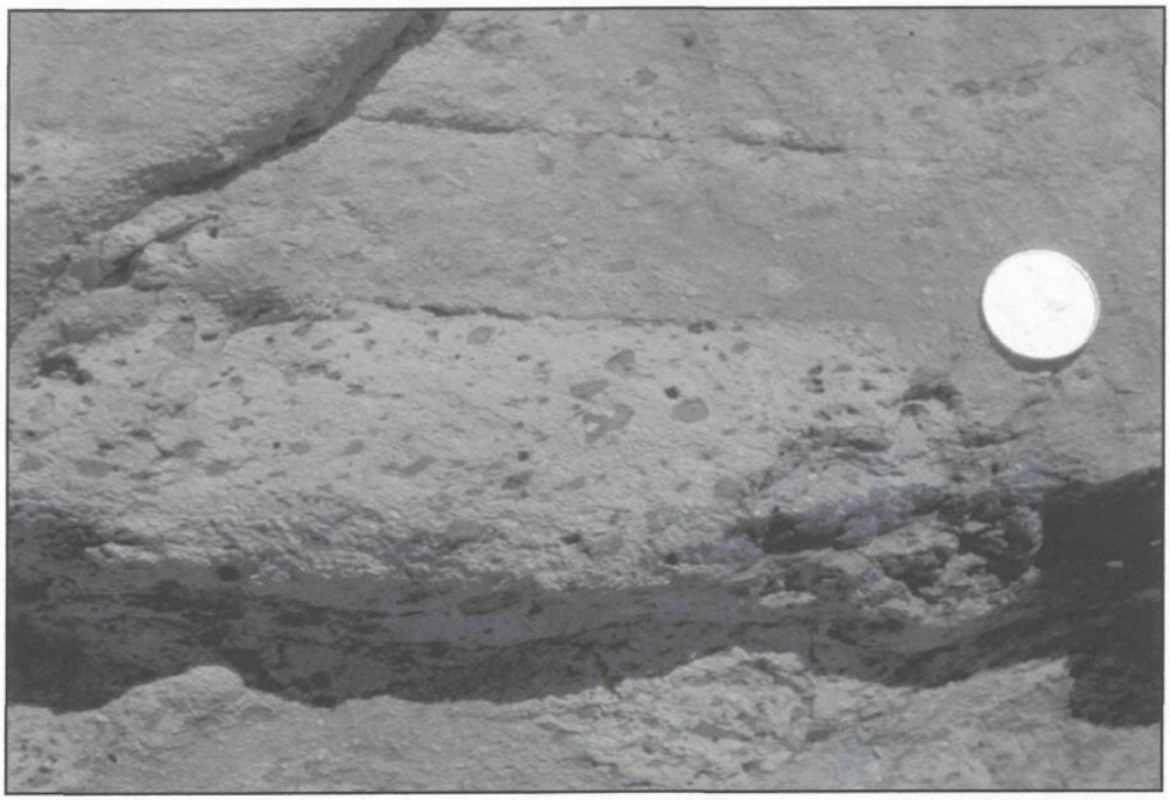

Figure 58: Hornblende-rich, non-vesicular, breccia-sized fragment from the upper (southern) part of East Sullivan sequence. Scale 2.5 cm in diameter.

Table 8: Point counting from hand samples and thin sections of amoeboidal fragments.

Sample	Counts	Altered Glass	Microphenocrysts	Amygdules
East Sullivan				
Hand Sample	1328	42.65 ± 3.44	12.29 ± 2.25	45.06 ± 1.19
Hand Sample	1889	51.58 ± 3.83	9.08 ± 0.44	39.33 ± 4.28
Hand Sample	3005	63.18 ± 2.73	8.12 ± 0.31	28.70 ± 2.43
Hand Sample	3186	59.98 ± 3.25	9.55 ± 1.72	30.47 ± 1.75
Hand Sample	6011	65.69 ± 0.23	7.48 ± 0.98	26.83 ± 0.86
Hand Sample	1393	73.00 ± 2.03	8.08 ± 1.29	18.92 ± 1.00
Hand Sample	1624	69.08 ± 3.85	8.49 ± 1.49	22.43 ± 2.52
Average		60.74 ± 2.77	9.01 ± 1.21	30.25 ± 2.00
Thin Section	400	67.73 ± 4.21	12.47 ± 1.78	19.9 ± 4.41
Thin Section	400	63.95 ± 1.77	23.1 ± 1.98	10.35 ± 3.32
Thin Section	400	53.95 ± 1.77	40.45 ± 1.77	5.5 ± 0.0
Thin Section	400	66.6 ± 2.69	13 ± 0.71	20.35 ± 3.32
Thin Section	400	77.75	5.75	16.5
Thin Section	400	63.88 ± 3.36	12.25 ± 6.01	23.88 ± 2.65
Thin Section	400	80	4.25	15.75
Average		67.69 ± 1.97	15.90 ± 1.75	16.03 ± 1.97
Dunraine				
Thin Section	400	48.25	24.5	27.25
Thin Section	400	55.25	11.5	33.25
Average		51.75	18	30.25

top. Fragments within lower sequences, particularly clast-supported beds, have a subrounded morphology (**Figure 56 and 59**) with a change to subangular, corresponding to a decrease to fine lapilli, some of which have serrated margins (**Appendix A-8**). Juxtaposed, breccia-sized fragments are characterized by flattened or molded features

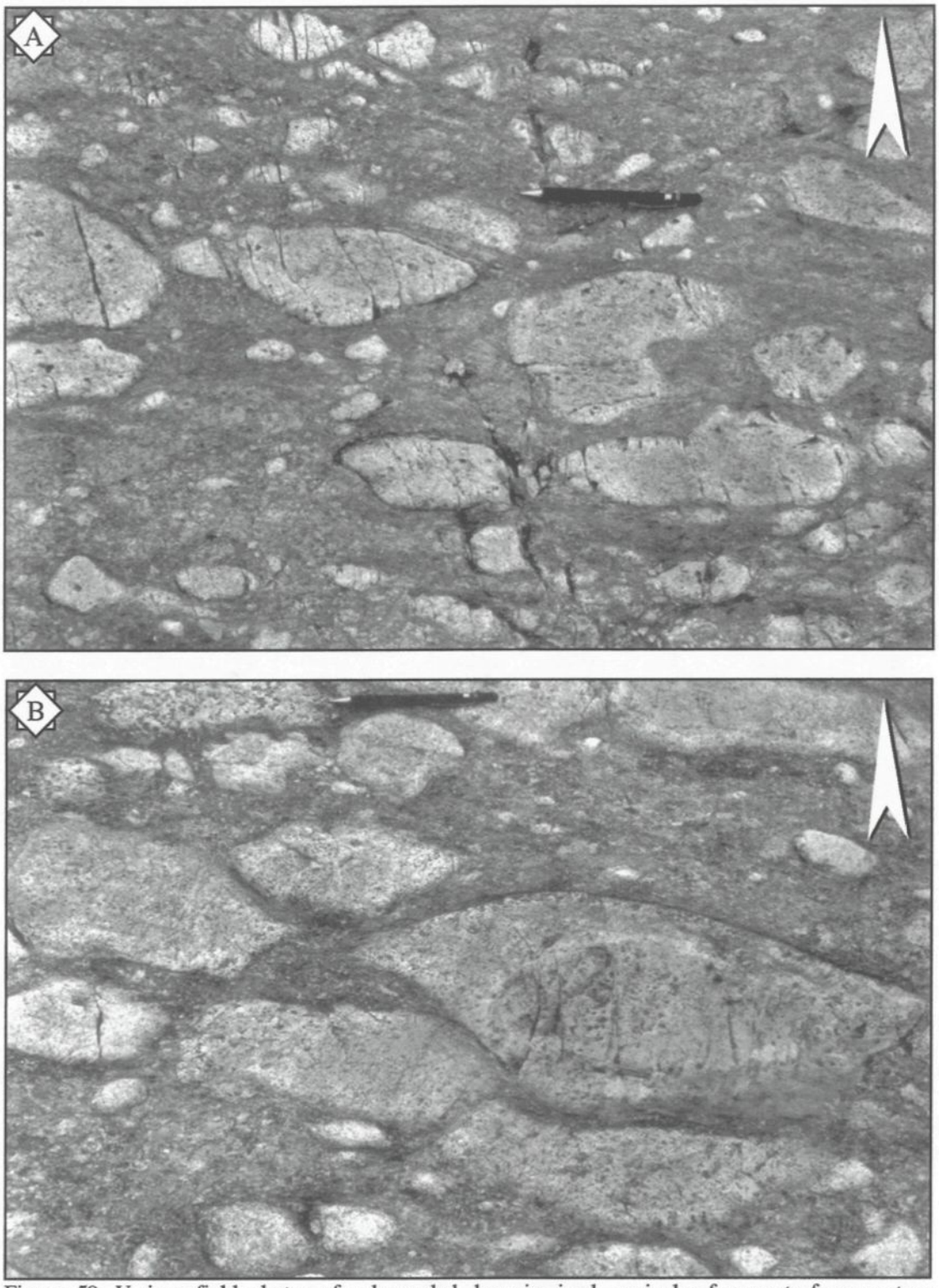

Figure 59: Various field photos of subrounded, breccia-sized, vesicular fragments from eastern outcrops. Pencil (15 cm-long) is aligned with bedding. Arrow indicates younging direction. A. Irregular vesicular fragments. B. Oblong morphology of vesicular fragments. Plastic deformaion is evident where fragments are in contact within deposit.

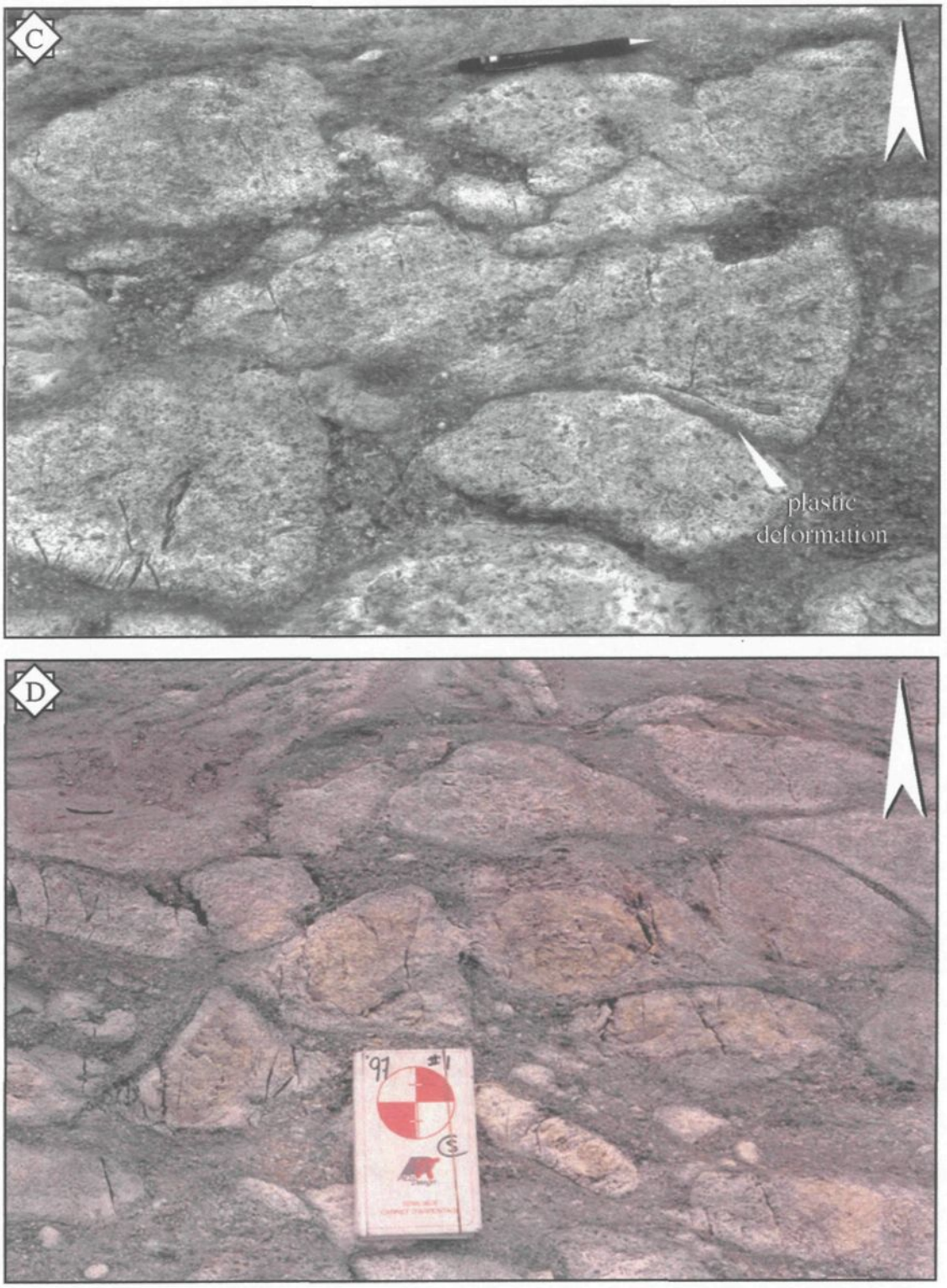

Figure 59 (con't): C. High degree of plastic deformation illustrating welding of hot fragments. D. Welding and epidotization of hot fragments. Irregular, erosive contact with overlying facies. Prominent fractures are restricted to fragments suggesting cooling control. Fieldbook (19 cm-long) and pencil (15.5 cm-long) for scales.

(**Figure 59**), as well as jigsaw patterns (**Figure 60**). These particular fragments typically have chilled margins, which mark a general trend in decreasing vesicularity, and sometimes epidotized cores (**Figure 59D**) and/or fractures that propagate from the margin towards the interior (**Figure 59**). Tuff-sized constituents comprise smaller aggregates of previously described fragments and feldspar phenocrysts. These fragments are more angular and are distinguished from the recrystallized matrix of quartz + feldspar + chlorite + epidote + sericite + carbonate by acicular feldspar. Feldspar phenocrysts liberated within the matrix have an euhedral to subhedral habit and are typically fractured or broken. One particular (crystal) tuff facies located on the western outcrop is composed exclusively of feldspar phenocrysts with an interspersed matrix recrystallized to quartz and albite (**Figure 61**).

Late-stage facies

Other facies of note are a feldspar-phyric intrusion, a magnetite-chlorite-chloritoid unit, and quartz-tourmaline veins. A large feldspar-phyric dyke/sill cuts the stratigraphy at a shallow angle and extends across both outcrops (**Figure 49**). The dyke is not completely continuous on surface, as it pinches out on the eastern outcrop (**Figure 49**), only to reappear about 10 m along strike. Another conspicuous feature is a 10 m zone of *in situ* brecciation (**Figure 51**). The magnetite-chlorite-chloritoid unit forms a 1 m-thick, stratabound unit between an overlying intermediate pillowed facies and lower highly altered tuff breccia facies (**Figure 50**). *Climbing* fractures of chloritoid crystals are observed extending upwards towards the contact with the pillowed facies. Quartz-

Figure 60: Vesicular, breccia-sized fragments that appear to fit together suggesting *in situ* fragmentation (jigsaw fit). Lense cap (5.5 cm) for scale.

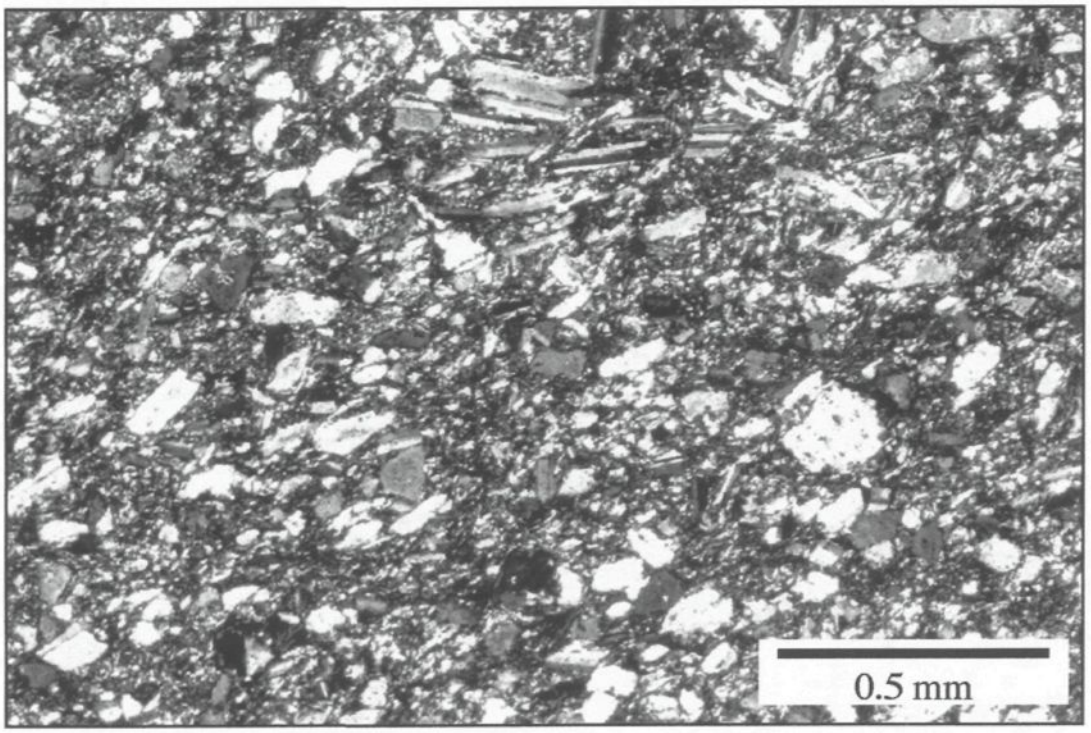

Figure 61: Photomicrograph of a crystal tuff. The abundance of broken, euhedral plagioclase microphenocrysts suggests an explosive origin.

tourmaline veins form cm- to m-thick intrusions that are semi-parallel to bedding and the original focus of Au-exploration in the region.

Deformation

Deformation is weakly developed with only minor shear zones observed on either outcrop. Structural and bedding measurements average 280°/77° and 273°/84°, respectively. Both pillow morphology and bedding relationships indicate a southward younging direction.

4.1.3.2 Pole Line Deposits

Located approximately 85 m to the west of the East Sullivan outcrops are a series of ridges exposed along an existing hydroelectric line. Due to their proximity and similar features, they are described and interpreted with the East Sullivan lithologies. Moreover, not only are these outcrops along strike with East Sullivan, but they are also directly up section from the PDN outcrops (**Figure 62**).

These ridges can be subdivided into two facies: intermediate pillowed to massive lavas and amalgamated volcaniclastic deposits (**Table 9**). Intermediate pillowed lavas vary from bun- to amoeboidal-shaped (**Figure 63A**), which can sometimes be traced laterally and vertically into a brecciated facies (**Figure 63B**). Massive lavas become more dominant further up section and are mineralogically identical to pillowed facies, although no direct transition is observed. These lavas are feldspar-phyric, with subordinate hornblende, and have a vesicularity of 2-20-vol%, as represented by quartz and carbonate amygdules.

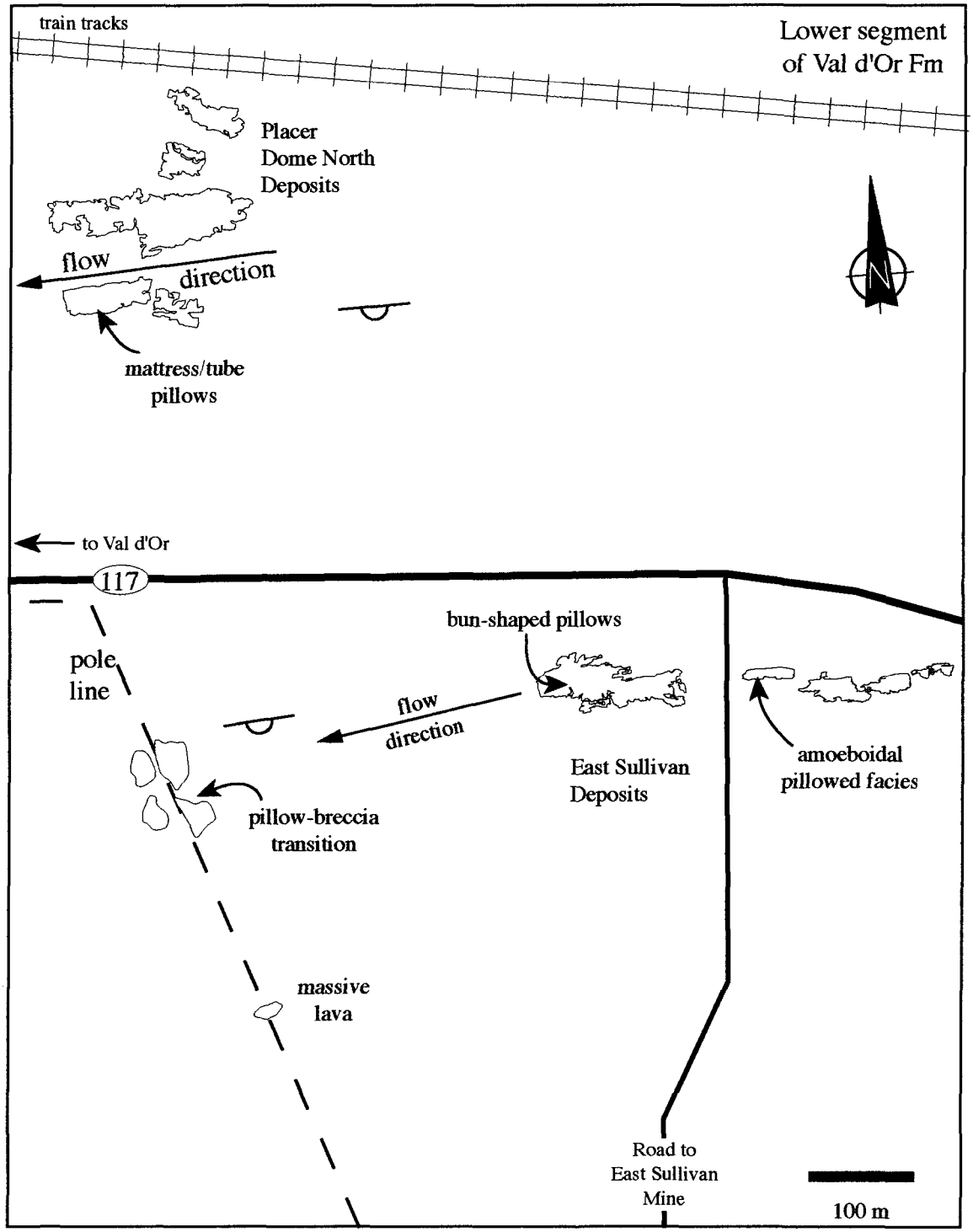

Figure 62: Sketch drawing (from aerial photo) of the outcrops described in detail from the western part of the lower VDF. Sketches outline the relationships between the outcrops and documents lateral and vertical facies transtions. Both East Sullivan and Placer Dome North outcrops are drawn to scale, pole line outcrops are roughly drawn from photo. Changes in lava facies are highlighted to illustrate possible flow direction (to the west).

Table 9: Characteristics of Pole Line deposits

Lithofacies	Thickness & morphology	Characteristics	Transport/deposition	Origin
Volcanic				
Pillowed flow	Tabular	Bun- to amoeboidal-shaped; 2-20 vol% amygdules; chilled contacts; feldspar-phyric; lateral transition to pillow breccia	Low-angle slope; lava flow	Effusive subaqueous lava flow
Massive flow	Tabular	2-20 vol% amygdules; chilled contacts; feldspar-phyric	Proximal location; high-discharge; lava flow	Effusive subaqueous lava flow
Volcaniclastic				
Lapilli Tuff	Tabular?	Matrix-supported; monolithic, subrounded to subangular fragments; 5-20 vol% amygdules; feldspar- and hornblende-phyric; liberated, broken, euhedral feldspar in matrix	High concentration turbidity flow (S-type);	Fire-fountain
Tuff breccia	Tabular	Matrix-supported; monolithic, subrounded to subangular fragments; 5-20 vol% amygdules; feldspar- and hornblende-phyric; jigsaw patterns; liberated, broken, euhedral feldspar in matrix	High concentration turbidity flow (R-type); fragments were emplaced hot	Fire-fountain

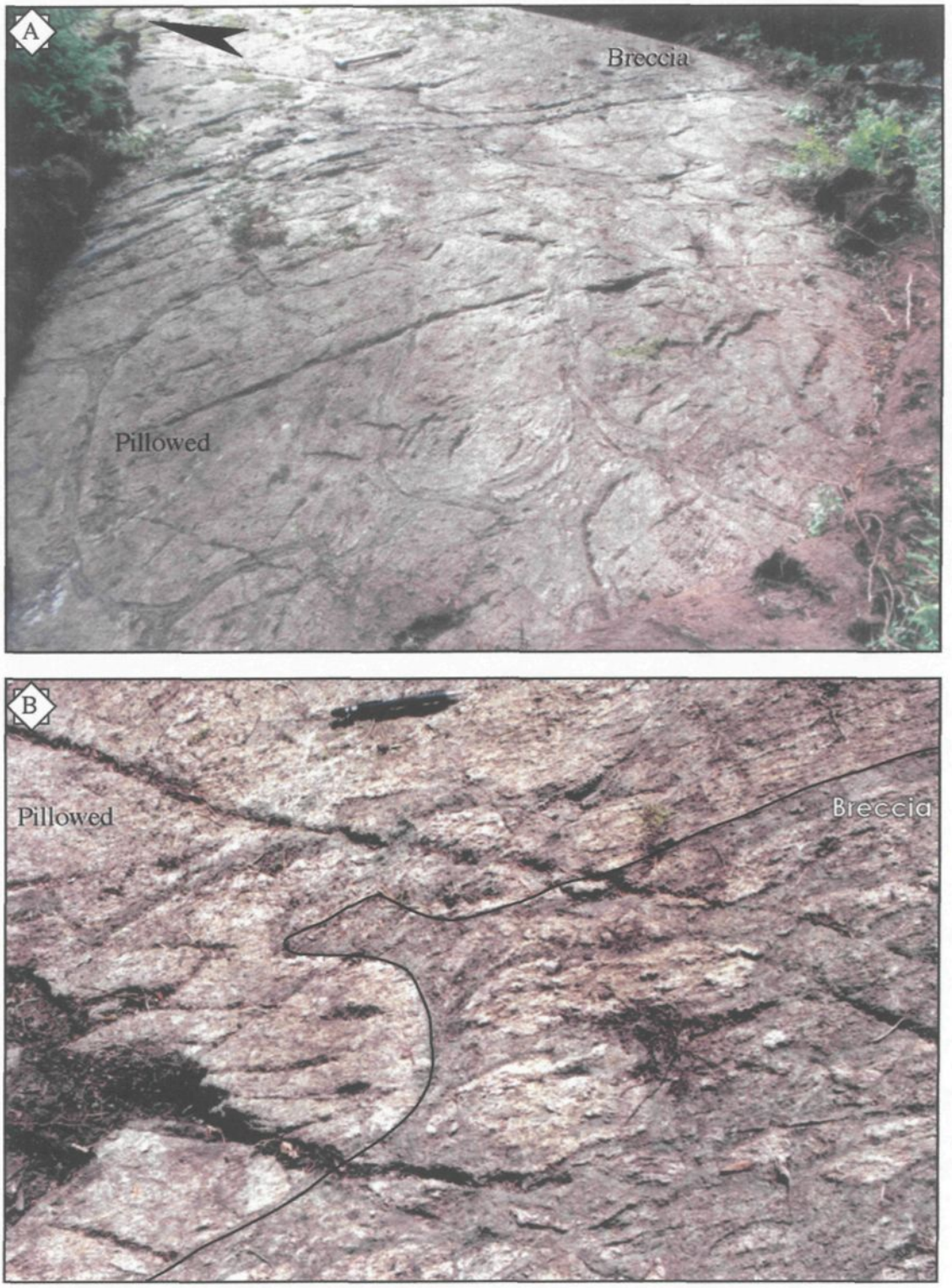

Figure 63: Field photographs along pole line, west of East Sullivan outcrops. A. Well-developed pillow morphology, indicating younging direction to the south (arrow), grades into an in situ breccia. Hammer for scale (37 cm). B. Closeup of grading from pillowed to brecciated facies. Pencil for scale (14.5 cm).

Chilled margins are commonly developed between lavas and associated tuff breccia facies (**Figure 63B**). Lavas are altered to a green to greenish-brown.

Amalgamated volcaniclastic deposits are dominantly tuff breccias with subordinate lapilli tuff beds. However, exposure limits a detailed stratigraphic analysis, which probably explains the absence of recognizable tuff beds. Several outcrops appear to have two or more flow units based only on grading characteristics, as contacts are gradational. All beds are matrix-supported and composed of a monolithic population of subrounded to subangular, grayish-white, vesicular, feldspar- and hornblende-phyric fragments (**Figure 64A**). The vesicularity of 5-20-vol%, represented by quartz- and carbonate-filled amygdules, is characterized by a negative correlation with the abundance of hornblende that varies from 1-10-vol%. Fragments have a distinct positive relief with larger fragments commonly in groups of five or more clasts that are broken in situ or form a jigsaw-like pattern with juxtaposed fragments (**Figure 65**). The matrix is highly chloritized and hosts liberated euhedral and broken phenocrysts of feldspar (**See Appendix A-10; Figure 64B**).

Other mapped features include minor quartz tourmaline veins and green aphyric dykes. Quartz tourmaline veins typically measure 10s of cm in width and are discontinuous. The green aphyric dykes have an anastomosing form, but typically propagate upwards, cutting the stratigraphy. These dykes, while subordinate in volume, are significant due to their similarity with likewise observed dykes from the PDN outcrops, which are directly below this outcrops in the stratigraphy (**Figure 62**).

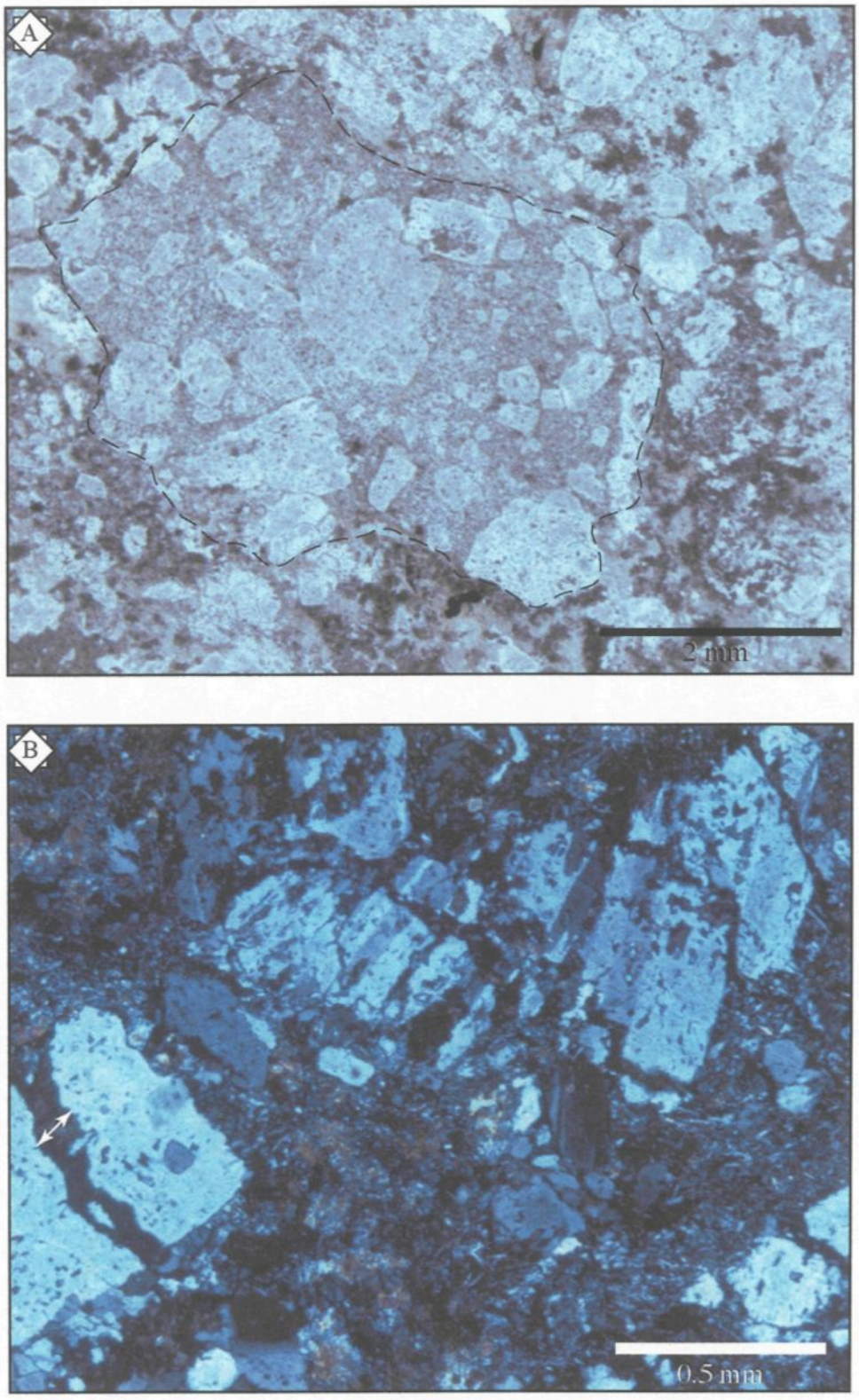

Figure 64: Microphotographs of tuff breccia matrix. A. Lapilli-sized, feldspar-phyric fragment hosted in feldspar-phyric matrix; plane polarized light. B. Abundant broken, euhedral feldspar microphenocrysts liberated in the matrix, cross-nicols.

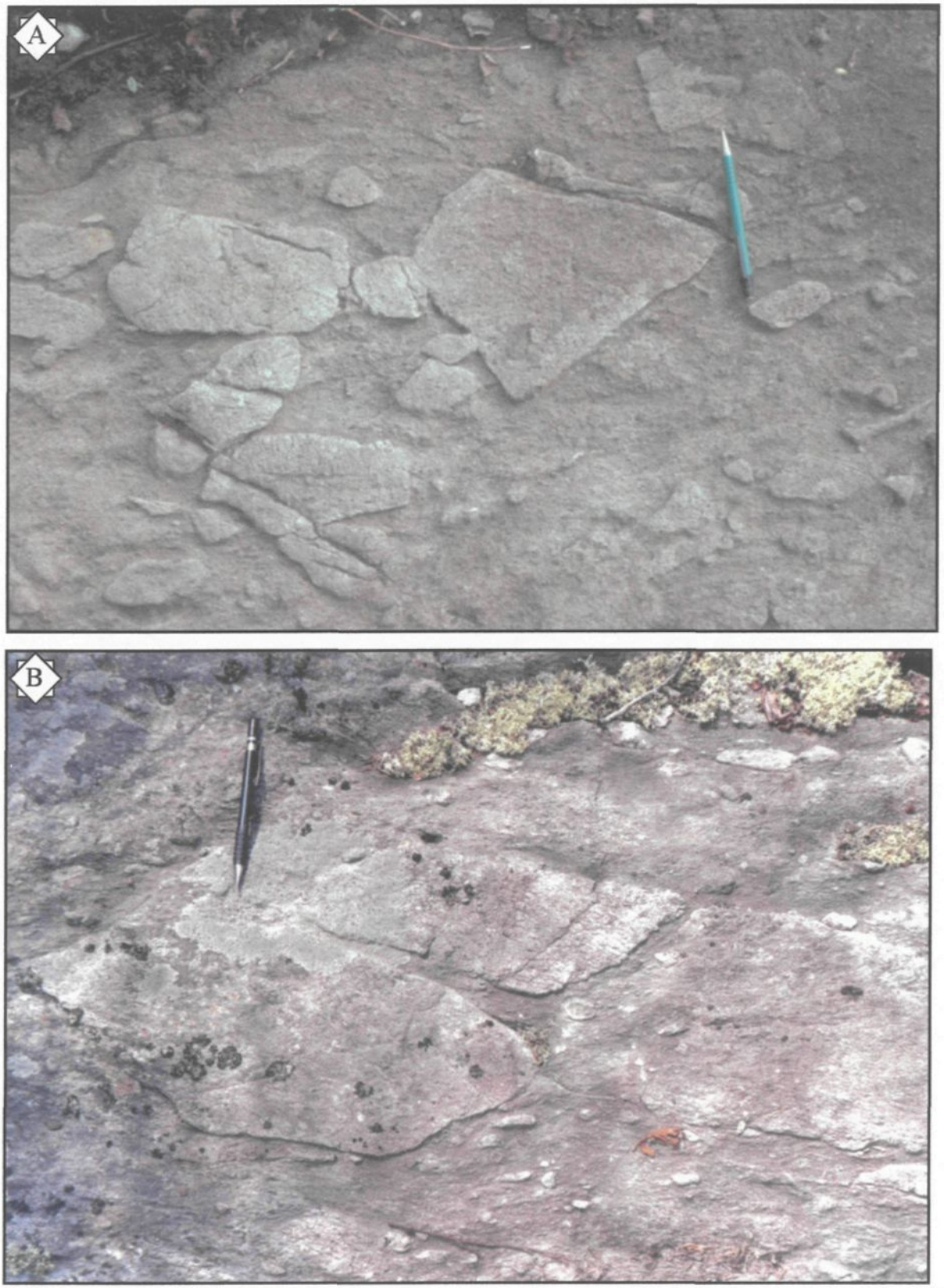

Figure 65: Field photos of tuff breccia facies. A. *In situ* brecciated nature of subangular, breccia-sized fragments. B. Subangular breccia fragments form a jigsaw-texture, as the blocks can be fit together. Pencil for scale (14.5 cm).

4.1.3.3 Interpretation of lithofacies

Overall, the pillowed facies and grading of the volcaniclastic deposits attest to a subaqueous environment of deposition for the complete sequence. Eruptive processes, emplacement, transportation, and deposition of these lithofacies can be inferred from described characteristics and variations in lava morphology and interbedded volcaniclastic deposits (**Table 7**).

Pillowed lava processes and origin

Lava morphology, particularly pillow-forms, can suggest conditions of emplacement (Walker, 1992) and proximity to the eruptive vent (Cousineau and Dimroth, 1982). The westward change from amoeboidal- to bun-shaped pillows possibly records an increase in viscosity and/or evidence of a paleoslope (Walker, 1992). Nevertheless, the lack of any apparent hydraulic jump recorded in the volcaniclastic deposits and constant thickness of correlated pillowed facies from east to west sides negates the probable existence of any significant paleoslope. Furthermore, Walker (1992) suggested that close-packed pillows with interstratified sediments, similar to those observed from the western outcrop (**Figure 52A**), are probably formed on low angled slopes; however, an increase in viscosity could explain the change from amoeboidal forms to bun-shaped pillows. The premise is that amoeboidal forms (**Figure 52B**) are low viscosity pillows/lava that have probably undergone some plastic deformation and/or shearing contemporaneous to its emplacement, which subsequently grades into small, more viscous, bun-shaped pillows away from the erupting vent. Further west, along strike, these pillowed flows are observed

to disintegrate into breccia-sized fragments (**Figures 62 and 63**). This lateral propagation is analogous to the hypothesized progression outlined by Cousineau and Dimroth (1982) for an erupting submarine vent (see **Figure 24**). The amoeboidal facies might represent a transitional phase between a massive and pillowed lava, whereby the latter is unobserved. Massive lavas mapped further to the south (**Figure 62**) are probably related to a new eruptive phase and/or different vent. These lavas are capped by pillowed deposits similar to the idealized sequence of Cousineau and Dimroth (1982). Localized lava rags probably represent localized spattering of low viscosity lava.

Volcano-sedimentary processes and origin

The amalgamated volcaniclastic sequence records a change in the mode of transportation and deposition, with fragment analysis facilitating the recognition of mode of fragmentation. The graded nature of all the volcaniclastic deposits indicates transport by water-supported sedimentary gravity flows (Stix, 1991). Graded beds indicate internal organization probably related to a more turbulent flow regime, rather than a laminar or plug-type flow (Prothero and Schwab, 1996). Thus, these deposits were transported by some variety of turbidity current. Tuff breccias form coarse-grained high concentration turbidity deposits (Lowe, 1982), whereby normal- to reverse-graded beds describe R_3 to R_2 gravel beds, respectively (cf. Lowe, 1982, Whitham and Sparks, 1986). Basal lapillus stratification within lapilli tuff beds is suggestive of traction carpet transport and sedimentation similar to S_2 beds of Lowe (1982). Basal shear forces associated with these high-concentration turbidity currents are capable of eroding the underlying facies - in this

case, the amoeboidal pillowed facies (**Figure 53**). This erosion is facilitated if deposition was penecontemporaneous with the extrusion of the pillowed facies (i.e., Simpson and McPhie 2000), as the amoeboidal pillows would still be hot and plastically deformable. Normal-graded lapilli tuff beds are suspension deposits of sand-sized particles from high- to low-concentration turbidity flows representing S_3 beds (Lowe, 1982). Massive to graded, fine- to coarse-grained tuffs form high- (S_3 or T_a) to low-concentration (T_{bc}) turbidity deposits (**Figure 56**). These deposits form during suspension sedimentation after passage of a turbulent flow, except for T_b, which typifies deposition by traction sedimentation that forms laminated bedforms (Lowe, 1982).

The conspicuous subrounded, vesicular breccia fragments of the tuff breccia facies (**Figures 55, 57, and 59**) may represent an inefficient fragmentation mechanism. Or, do they? The first concern is to ascertain whether these fragments are primary in origin or secondary reworking of either some former debris or lava flow. Abrasion during secondary mass transport can create the observed subrounded forms. Nonetheless, preservation of delicate textures such as chilled margins, *in situ* plastic deformation, as well as the monolithic fragment population all point to a primary origin, whereby deposition is syneruptive (Cousineau and Bedard, 2000). Not all fragments have chilled margins, in fact chilled margins are limited to only larger breccia-sized vesicular fragments, which suggest a greater thermal insulation of larger fragments interacting with water (Kokelaar, 1986; Mueller and White, 1992; Simpson and McPhie, 2001), probably due to the development of a localized steam carapace (Kokelaar, 1986). Furthermore, epidote alteration of the core is a possible artifact of thermal insulation, whereby the cores of larger fragments remained hot

and were subjected to low-temperature hydrothermal alteration if any fracture propagated into this hot interior. The fractures probably represent thermal contraction features originating from undercooled crust and propagation towards the interior of the fragment (Kano et al., 1993). These fractures do not extend into the matrix of the deposit (**Figure 59**), suggesting they are a primary feature and not related to post-depositional deformation. Finally, observations of *in situ* fragmentation, forming conspicuous jigsaw patterns (**Figure 60**), indicate that little to no remobilization has occurred; therefore, it can be concluded that these tuff breccias are *primary* deposits. A primary origin is with respect to being deposited ***directly*** from the collapse of an eruption column (White, 2000), regardless of the support mechanism of the transporting gravity flow (cf. Stix, 1991). It is envisaged that these breccia-sized (bombs) fragments were *ballistically** propelled through the *water* column during an energetic fire fountaining eruption. Mueller et al. (2000) envisaged steam-envelopment of the fragments, either self-generating (Kokelaar, 1986) or within a steam zone developed during continuous explosions (Moore, 1985), which could protect and permit ballistic emplacement in a subaqueous environment. The rounded/fluidal morphology of these fragments reflect their initial transport through water, but fragment orientation parallel to bedding (**Figures 54 and 55B**) suggests that these tuff breccias are not fall deposits, but have undergone some subsequent flow transport, albeit probably restricted to a proximal vent location (Kokelaar and Durant, 1983; Kokelaar, 1986; Simpson and McPhie, 2001). In addition, the observed reverse-grading may record the possible buoyancy of fragments, rather than being purely due to dispersive forces (Bagnold Effect) (Bagnold, 1954) in a moving flow; however, such buoyancy is apt to be time-

restricted as hot vesicular fragments will efficiently absorb water (Whitham and Sparks, 1986).

The feldspar-rich tuff beds (**Figure 61**) support a more vigorous fragmentation process in comparison to the tuff breccia beds. The concentration of tuff-sized (< 2mm), angular and broken feldspar, of otherwise euhedral crystals, forming laminated (T_b) to massive (T_{ae}) beds suggest deposition by low concentration turbidity currents originating from explosive fragmentation. The fine-grained quartz-albite matrix is the possible re-crystallization or alteration of former vitrophyric clasts. Thin (cm-thick) massive discontinuous tuff beds, intercalated with tuff breccias (**Figures 51, 52, and 56**), probably represent elutriation of fine-grained material during transport of high concentration turbidity flows (i.e., tuff breccia) and subsequent suspension sedimentation. Their discontinuous character probably reflects the successive and eroding nature of overlying flows. Bedded crystal tuffs may form through the formation of a low concentration turbidity flow, composed of elutriated material and/or *primary* fragmented material either from a waning eruption column (cf. Fiske and Matsuda, 1964) or vertical collapse of an eruption column.

4.1.4 Manitou Area (ROI 4)

The Manitou area includes Manitou Mine and outcrops in and around the mine workings, including a small-stripped outcrop to the west (**ROI 4; Figure 26**). The open pit was not accessible due to flooding. The mine sequence is associated with felsic volcanic

rocks, both fragmental and lava flow deposits (**Table 10**). Shearing and sericite alteration, with rusty iron staining, characterize all felsic lithofacies within the mine sequence.

Further from the mine sequence, the volcanics become *intermediate* in appearance as chloritization becomes dominant at the expense of silicification and sericitization type alteration, as well as quartz becoming less abundant as feldspar increases. Furthermore, *in situ* brecciation, typically observed with felsic facies, is absent in the described intermediate facies. Both north and south of the mine sequence, the stratigraphy is composed of intercalated intermediate lavas and volcaniclastic deposits, whereby individual facies are commonly meters-thick. Intermediate lavas range from massive to pillowed and 20-vol% feldspar phenocrysts (visual estimate) and upwards to 5-vol% quartz amygdules (**Table 10**).

Volcaniclastic deposits are characterized by chlorite alteration, upwards to 20-vol% euhedral feldspar phenocrysts, and 5-7-vol% (maximum) vesicularity (represented by quartz amygdules). Fragments are subrounded to subangular with a similar mineralogy to lavas, and matrices are re-crystallized to a fine-grained mosaic of quartz + carbonate + chlorite ± albite with 10-15-vol% liberated, euhedral (sometimes broken) feldspar phenocrysts (**Figure 66**).

The local stratigraphy and bedding relationships are examined (**Figure 26**) in a 27 m by 20 m outcrop (**Table 10**). This outcrop outlines two separate volcaniclastic sequences, two dyke phases, minor quartz-tourmaline veins, and several discontinuous faults (**Figure 67A**). Non-volcanic interbeds are not observed. The volcaniclastic sequences are composed of individual beds based on inter- and intra-bedding relationships, such as erosive contacts

Table 10: Lithofacies of the Manitou area.

Lithofacies	Thickness & morphology	Characteristics	Transport/deposition	Origin
Volcanic				
Felsic lava	10s m; tabular?	Massive to *in situ* (sheared) brecciation; sericite alteration; rusty weathering due to mineralization in proximity to mine sequence; aphyric?	Lava flow; viscous shearing and autobrecciation	Effusive? Local felsic lavas associated with hydrothermal venting (mineralization)
Intermediate lava	1-5 m; tabular?	Massive to pillowed; < 5-vol% feldspar phenocrysts	Lava flow	Effusive subaqueous eruption
Volcaniclastic				
Tuff	10-30 cm, discontinuous	Faint planar laminations (T_b) capping individual deposits	Low concentration turbidity flow to fallout	Finer grained lofted pyroclasts that settled from waning eruptive column from phreatomagmatic eruption.
Lapilli Tuff	2-4 m	Monolithic; normal-graded (S_3), faint stratification (S_1); non-vesicular; 10 vol% feldspar	High concentration turbidity flow	Phreatomagmatic mechanism due to ingestion of ambient water
Tuff breccia	6-8 m	Monolithic; subrounded to subangular; normal-graded (R_3); non-vesicular; 10 vol% feldspar	Cohesive debris to high concentration turbidity flow; *en mass* freezing	Inefficient explosive fragmentation

Figure 66: Character of lapilli tuff facies, with subrounded lapilli; larger fragments (under pencil; 14. 5 cm long) are vesicular.

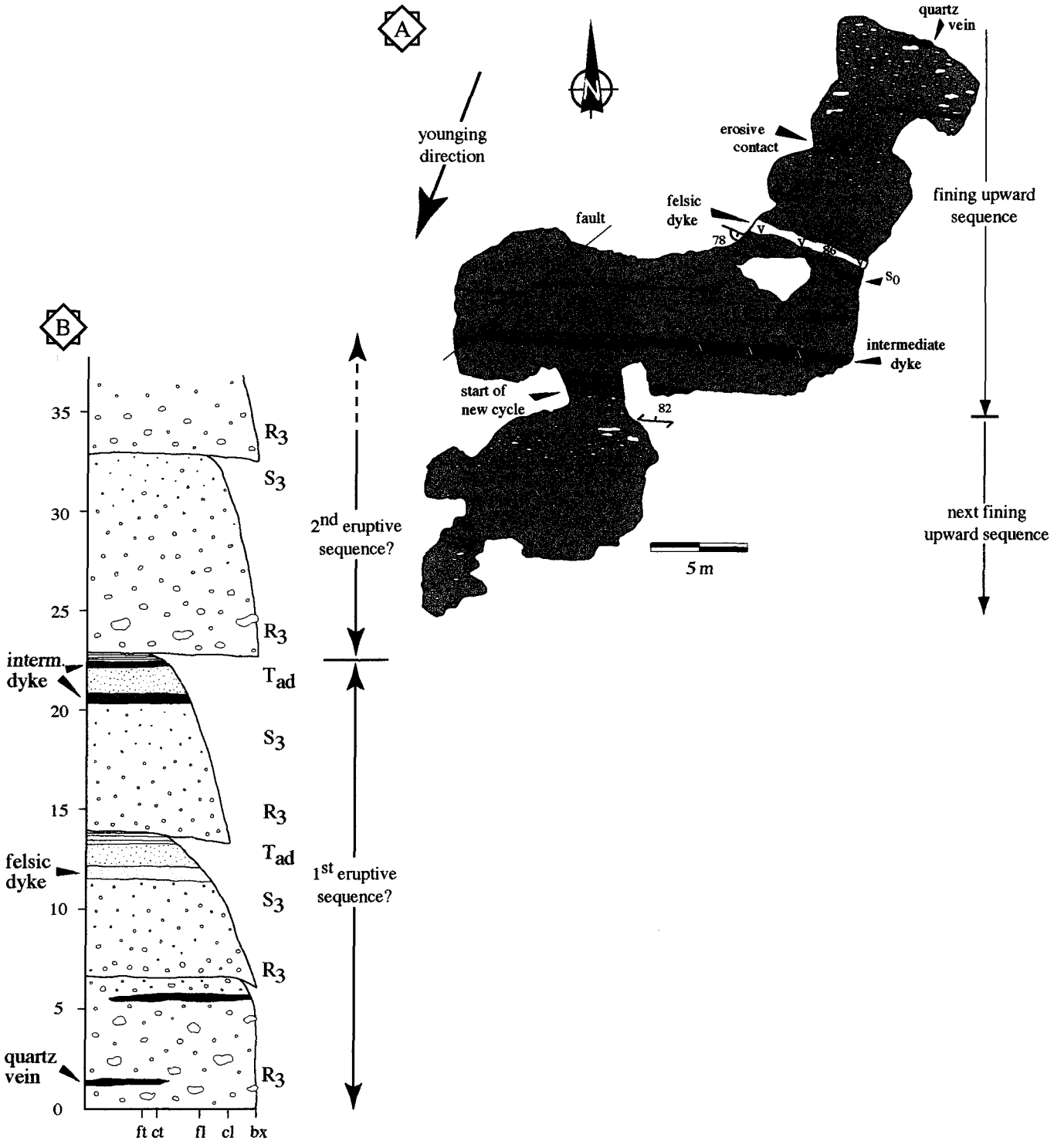

Figure 67: Detailed mapping west of Manitou Mine. A. Mapping of stripped zone illustrating relationships between different facies and two potential eruptive sequences. B. Stratigraphic section showing the relative fining up section within each possible eruptive sequence. R-S-T turbidity flow types after Lowe (1982).

and grading, respectively; both of which suggest a southward younging direction. Faint planar bedding features (S_0) indicate the strike direction of the sequence (**Figure 67A**). Each sequence is defined by an overall fining upward trend between individual beds, varying from breccia to coarse lapilli at the base, to dominantly lapilli to tuff sized at the top (**Figure 67B**). The next volcaniclastic sequence reverts to coarse-grained breccia fragments at its base and lapilli towards the top. This style of grading may be considered a doubly graded, coarse-grained equivalent to the fine-grained sequence described by Fiske and Matsuda (1964). All volcaniclastic beds have a monolithic fragment population of whitish green, feldspar-phyric (10-vol%), non-vesicular clasts that are subrounded to subangular in appearance.

4.1.4.1 Interpretation of Manitou area

The mine sequence is associated with felsic volcanism, which is typical for VMS-type mineralization (Gibson et al., 1999). The combination of higher viscosity lavas and propagation of high-temperature hydrothermal fluids resulted in *in situ* brecciation and intense alteration, such as silicification, sericitization, and Fe-staining (or mineralization).

Intercalated intermediate volcano-sedimentary facies represents changes from effusive to fragmental processes forming small volume composite cones (**Table 10**). Fragmental facies probably indicate episodes of increased discharge rates due to possible increases in volatile (vesicularity) contents. Higher discharge rates increase the surface area of lava interacting with external water, thereby promoting fragmentation (Wohletz, 1983). The efficiency of fragmentation is reflected in the overall fragment size, as crystal tuffs

represent a more explosive event as evidenced by the abundance of liberated, broken euhedral feldspar phenocrysts in the matrix. Subrounded breccia fragments may have been transported and deposited at elevated temperatures, thus permitting plastic deformation after emplacement.

The doubly graded volcaniclastic sequence and lack of background sedimentation (i.e., non-volcanic) is consistent with direct deposition from one subaqueous eruptive event (Fiske and Matsuda, 1964; Cousineau, 1994). The coarse grain size is possibly due to inefficient fragmentation as compared to the classic Tokiwa tuffs described by Fiske and Matsuda (1964). The apparent stacking of coarse-grained deposits within the eruptive sequence may record deposition from subflows that develop in response to trailing turbulent flows overtaking the decelerating flow front (Busby-Spera, 1986; Cousineau, 1994). As fallout rates and particle concentration decreases, it is possible to form layering at the top of a subflow (Cousineau, 1994), which could explain the diffuse laminations. The subsequent tuff breccia deposit indicates renewed activity, such that finer tuff deposits were either not deposited or were eroded by the passage of the next high concentration turbidity flow.

4.1.5 Camnet Area (ROI 5)

The Camnet area is a region along the southeast portion of the Bourlamaque Pluton and extends east towards the Louvicourt Mine (**ROI 5; Figure 68**). Also included in this area is the Cornel Plug, a small diorite-tonalite intrusion. The area is lithologically diverse, which is further complicated by moderate to high deformation that probably results from

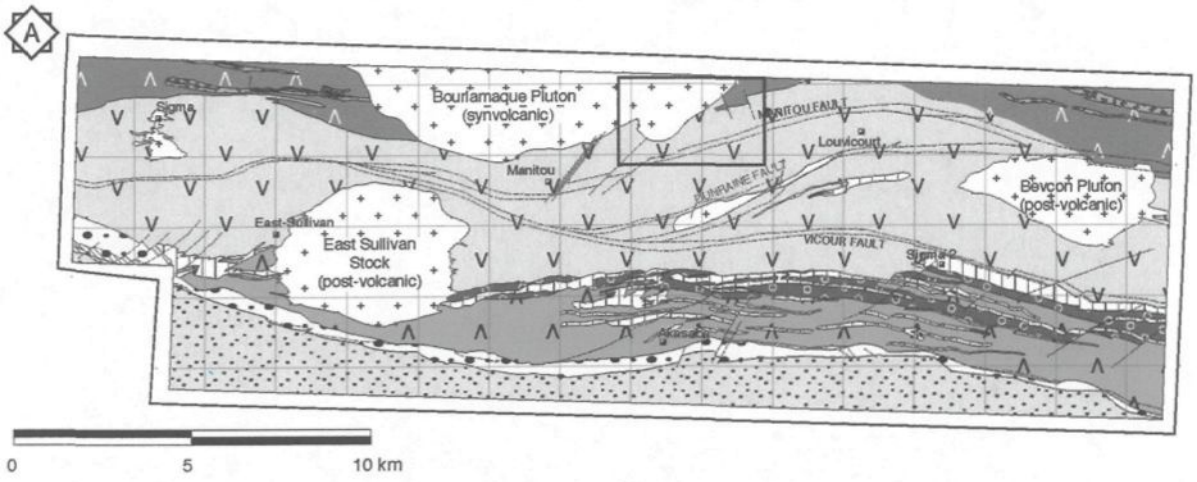

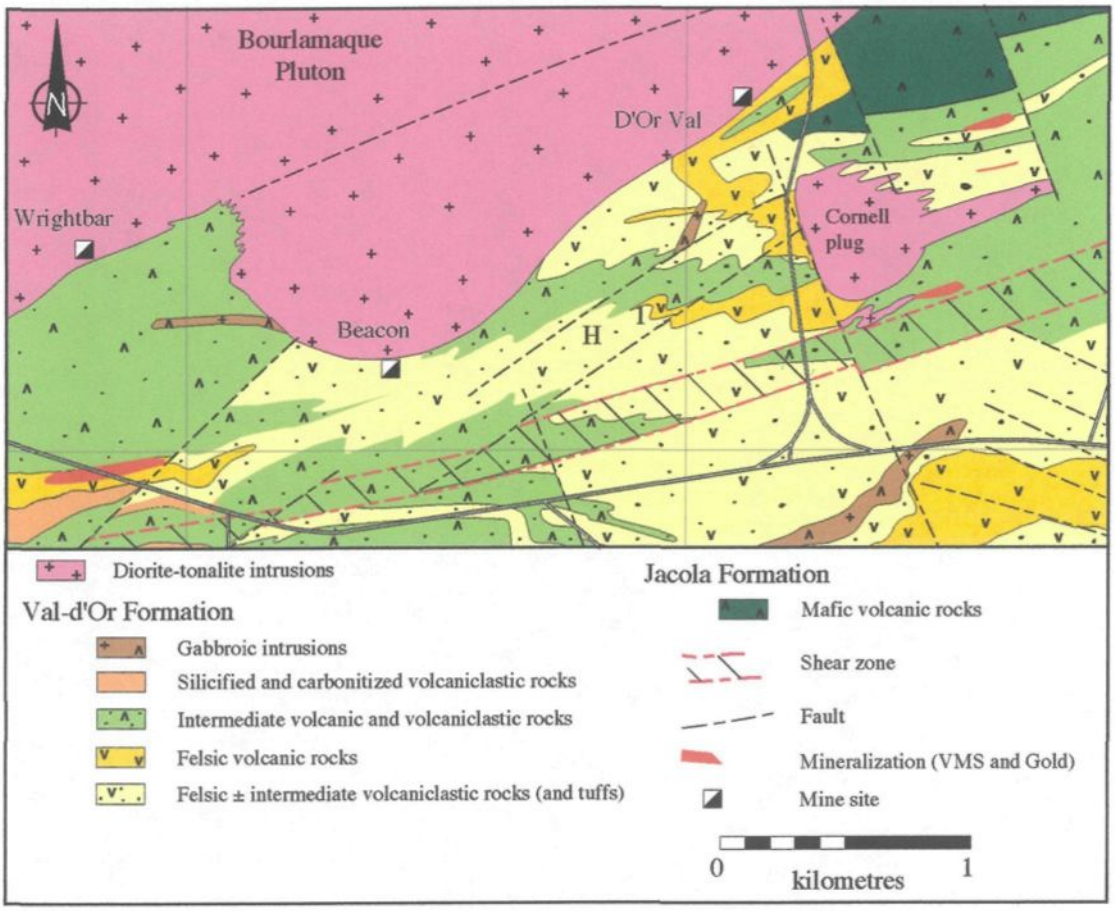

Figure 68: Closeup of Camnet field area taken from Figure 26. Mapping on a regional scale, except for previously stripped outcrop (1) and Hollow showing (H); approximate locations.

proximity to the Bourlamaque Pluton. Intermediate volcanism is dominant in the form of lavas and associated volcaniclastic deposits with local areas of felsic lavas and associated volcaniclastic facies (**Figure 68**). As the area represents the eastern sector within the lower part of the VDF, fieldwork was focused on outlining any lateral variations in order to complete the regional stratigraphy. Mapping entailed closely spaced traverses and the examination of several previously stripped outcrops.

4.1.5.1 Lithology and Stratigraphy of Camnet Area

Deformation and silicification are locally intense in proximity to the Bourlamaque and Cornell intrusions. Nevertheless, it is possible to identify and map certain volcano-sedimentary sequences. Lavas and associated volcaniclastic facies vary from felsic to intermediate, with the latter being dominant (**Table 11**). Overall, fragment size of volcaniclastic deposits is smaller than previously described deposits, with the typical facies being a lapilli tuff.

Volcanic lithofacies

Lavas range from felsic to intermediate in composition and typically form either massive or pillowed facies, respectively (**Table 11**). Felsic lavas are recognized based on field characteristics, as felsic lavas are typically more sheared and fractured *in situ* with intense sericitization (**Figure 69**). Two discontinuous bands of felsic rocks are recognized in the area, each forming 200-300 m-thick amalgamated sequences of massive to brecciated rocks. The northern segment is cut by the Bourlamaque Pluton to the west and a fault zone

Table 11: Volcano-sedimentary lithofacies of the Camnet area.

Lithofacies	Thickness & morphology	Characteristics	Transport/deposition	Origin
Volcanic				
Felsic lava	200-300 m tabular sheets and/or lobate masses	Massive to *in situ* brecciation; flow banded; white- to cream-alteration; Fine-grained with feldspar (2-10-vol%) and quartz (2-4-vol%); up to 10-vol% quartz amygdules	Subaqueous lava flow; effusive extrusive to intrusive emplacement	Endogeneous lobes and exogeneous lava flows; *in situ* brecciation in contact with water
Intermediate lava	10s of meters pillowed to massive, minor exposure	Fine-grained with 10-vol% feldspar; *in situ* brecciation to form pillow breccia (?); intercalated with volcaniclastic deposits	Subaqueous effusive eruptions	Effusive eruptions with autoclastic spalling to form pillow breccia
Mafic lava	Few meters; massive to pillowed	Fine-grained with tabular hornblende (after pyroxene?); *in situ* brecciation with interstitial magnetite	Effusive lava flow	Subaqueous lava flow
Feldspar-phyric lava	Few meters	Stratabound to crosscutting; 15-20-vol% tabular, euhedral feldspar; chilled margins; *in situ* brecciation; jigsaw pattern	Injection through volcaniclastic sediments	Hypabassal feeder dykes/sills
Volcaniclastic				
Lapilli tuff (breccia)	Meters thick	Clast- to matrix-supported; normal-graded; subrounded to subangular clasts; greenish alteration; moderate sorting; gradational contacts, with minor erosive; 5-40-vol% euhedral, tabular feldspar; 1-8-vol% acicular hornblende; 2-20-vol% quartz amygdules	Water-supported, high concentration turbidity flow	Non-explosive granulation and weakly phreatomagmatic
Tuff breccia	Meters thick	Clast- to matrix-supported; massive; non-sorted; flow banded subangular to angular clasts; cream- to white-alteration; 10-vol% feldspar and 2-5-vol% quartz; 0-30-vol% quartz amygdules	Water-supported, high concentration turbidity to cohesive debris flow	Lava fed autoclastic to hydroclastic fragmentation

Figure 69: Massive rhyolitic lava that is moderately sheared and brecciated *in situ*, with fractures filled by sericite. Trace of regional schistosity (S_1) indicated by dashed line. Pencil for scale (14.5 cm).

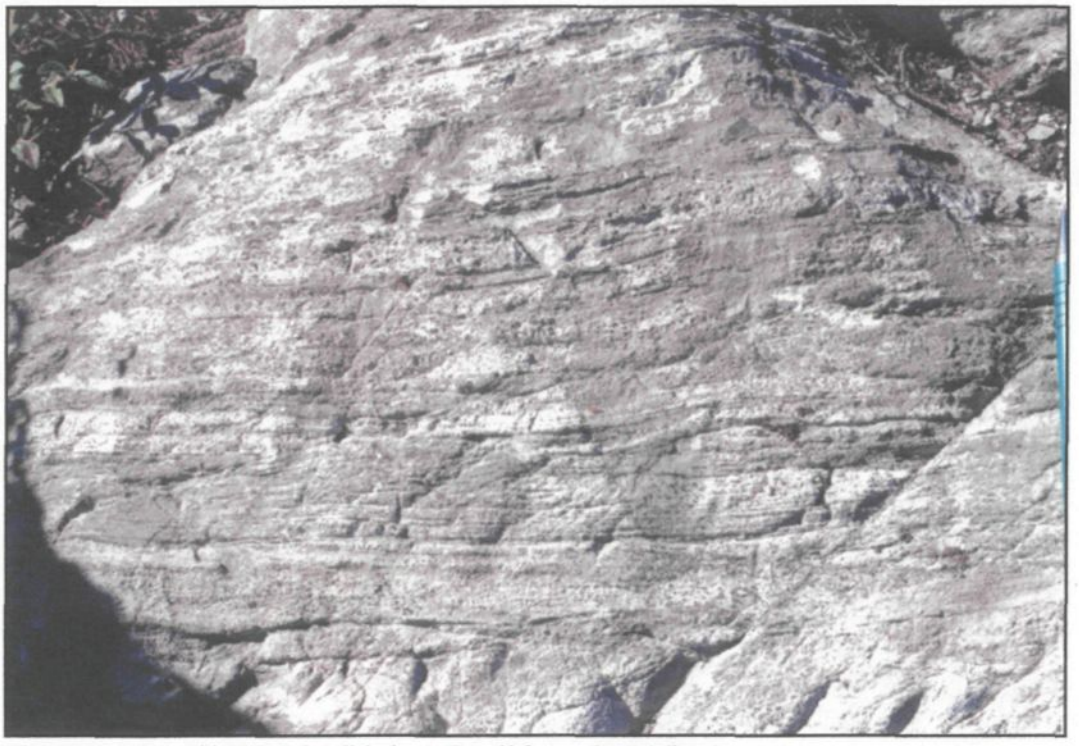

Figure 70: Flowed banded rhyolitic lava. Pencil for scale (14.5 cm).

to the east, whereas the southern segment pinches out to the west and terminates within intermediate volcaniclastic deposits to the east (**Figure 68**). Lavas appear to form tabular sheets to lobe-like masses that intruded fragmental facies. Typically, these lavas are massive, but are fragmented *in situ* with sericite filling the interstitial space between fragments (**Figure 69**) and are flow banded (**Figure 70**). Surface weathering varies from white to cream. Felsic lavas are fine grained with feldspar and quartz phenocrysts comprising about 2-10 and 2-4-vol%, respectively. Vesicularity is low, as represented by quartz amygdules up to a maximum of 10-vol% (visual estimate).

Intermediate lavas are represented by minor pillowed sequences intercalated with volcaniclastic deposits. An association with volcaniclastic facies is probable due to along strike transitions from pillowed to amoeboidal tuff breccias (**Figure 71**). These transitions do not form a continuous exposure, but are observed to occur over 10s of meters,. Furthermore, *in situ* brecciation is evident along pillow flow margins. The observed volume of intact intermediate lava flow deposits are subordinate in comparison to associated volcaniclastic deposits. These lavas are fine grained with about 10-vol% feldspar phenocrysts.

Massive to pillowed mafic lava flows deposits are locally observed in the northeast sector of the region. Pillow-forms are relict in character and associated with brecciated facies. Typically, they are fine grained, but have rare phenocrysts of former tabular pyroxene (**Appendix A-11**). Mafic fragmental facies are subangular to angular (**Figure 72**), with a dark green to pale green weathered surface similar to pillows (**Figure 73**) and have

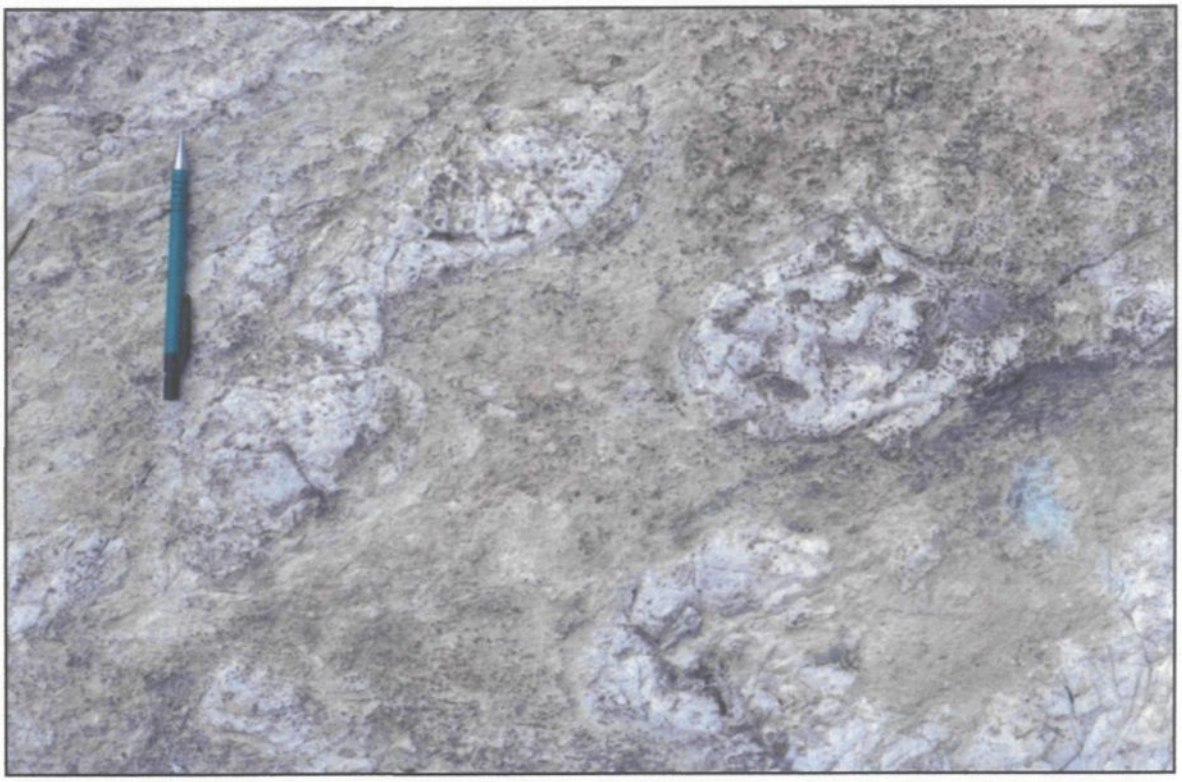

Figure 71: Amoeboidal, breccia-sized fragments in proximity to intermediate pillowed facies. Pencil for scale (14.5 cm).

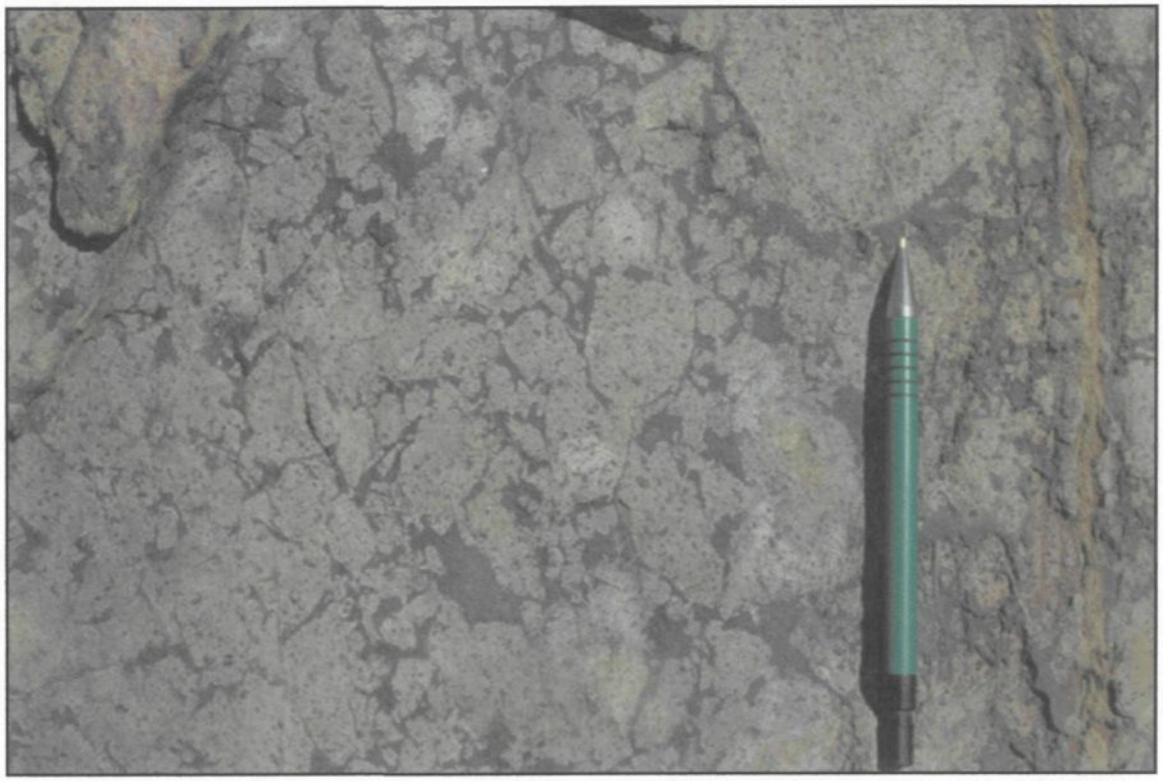

Figure 72: Angular to subangular mafic hyaloclastites. Pencil for scale (14.5 cm).

Figure 73: Tube-like mafic pillows. Pencil for scale (14.5 cm).

10-vol% pyroxene phenocrysts. Magnetite is commonly observed in the matrix of fragmental facies.

Volcaniclastic deposits

Volcaniclastic deposits are the predominant lithofacies in this sector and are interspersed throughout felsic and intermediate lava flow deposits (**Table 11; Figures 74 &75**). Deposits are commonly normal-graded and vary from clast- to matrix-supported. Interbedded contacts are typically gradational with rare examples of erosive behavior, which indicate a southward younging direction (**Figure 76**). Lapilli tuff breccia facies are composed of subangular to subrounded fragments. Tuff breccia facies are characterized by a monolithic population of flow-banded, subangular to angular fragments (**Figure 77**). Graded and sorted beds are absent in these course grained beds.

Fragment morphology, mineralogy, and texture are varied as a function of composition. Subrounded fragments are normally lapilli-sized and greenish in color (**Figure 78**). Vesicularity is variable as represented by 2-20-vol% quartz amygdules (**Figure 79**). These clasts are characterized by 5-40-vol% tabular, euhedral feldspar and 1-8-vol% acicular hornblende (**Appendix A-12**). Subangular to angular fragments are more apt to be cream- to off-white and flow banded (**Figure 77**). Crystallinity varies from feldspar (up to 10-vol%) and quartz (2-5-vol%) or aphyric. Vesicularity is generally low (< 5-vol%), but some breccia-sized clasts have quartz amygdules up to 30-vol% (**Figure 79**). Both fragment types occur together in volcaniclastic deposits that are matrix-supported, whereby the matrix is chloritized with abundant liberated euhedral feldspar phenocrysts (5-

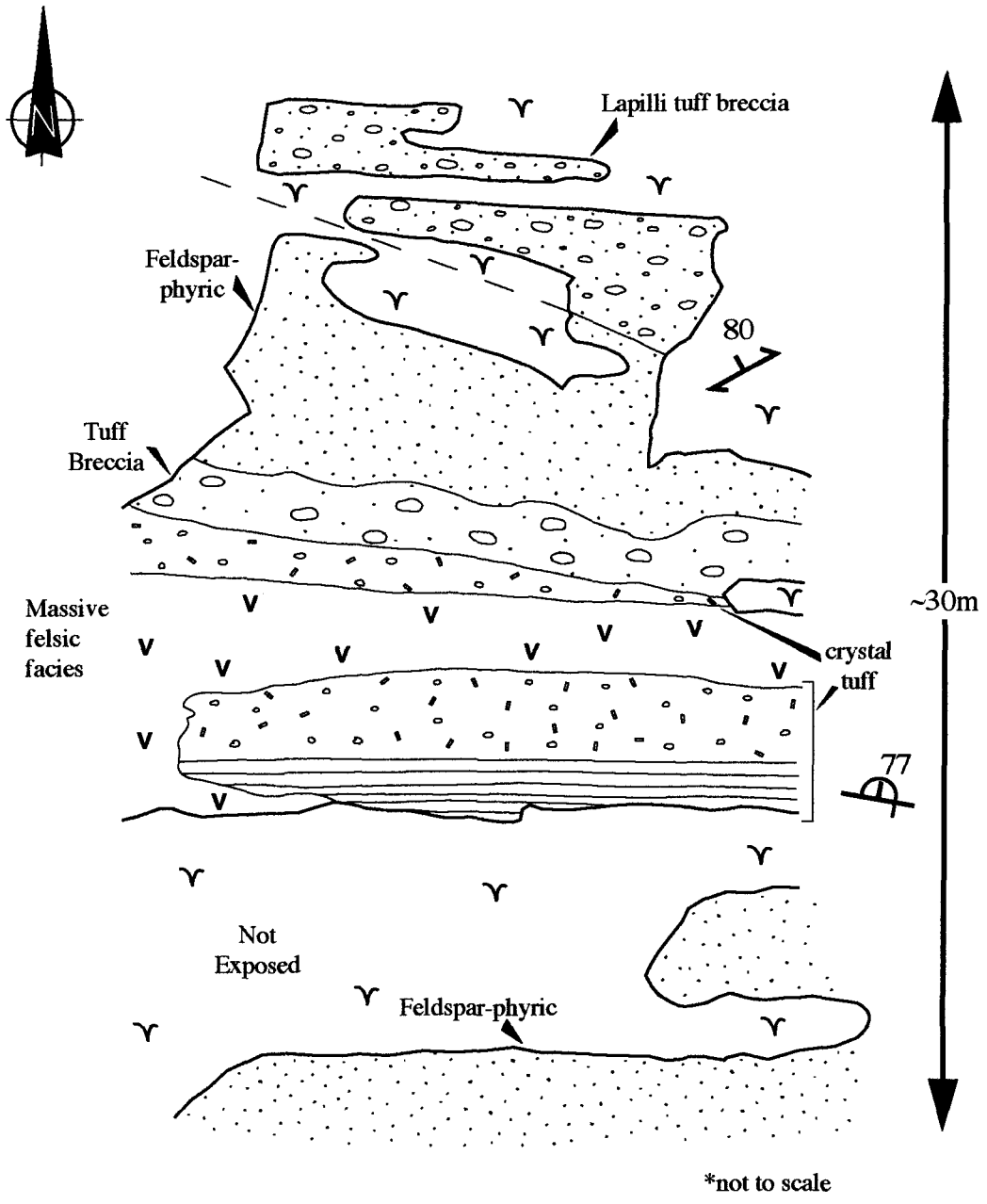

Figure 74: Field sketch of small stripped outcrop depicting the contact relationships in the region. Feldspar-phyric facies appears to crosscut the stratigraphy.

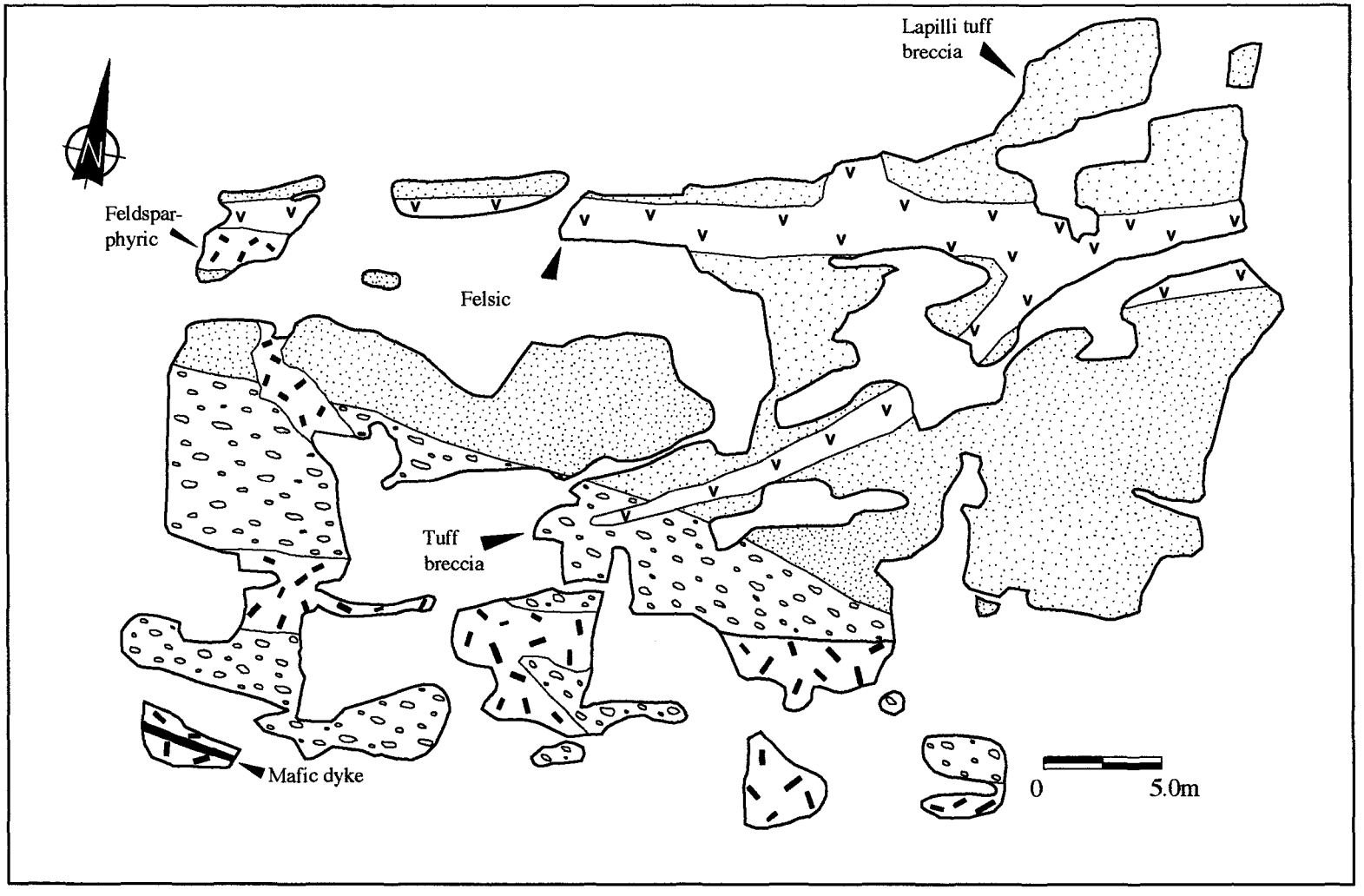

Figure 75: Geology of the Hollow showing illustrating the facies relationships between the volcaniclastics and felsic and feldspar-phyric (FP) facies.

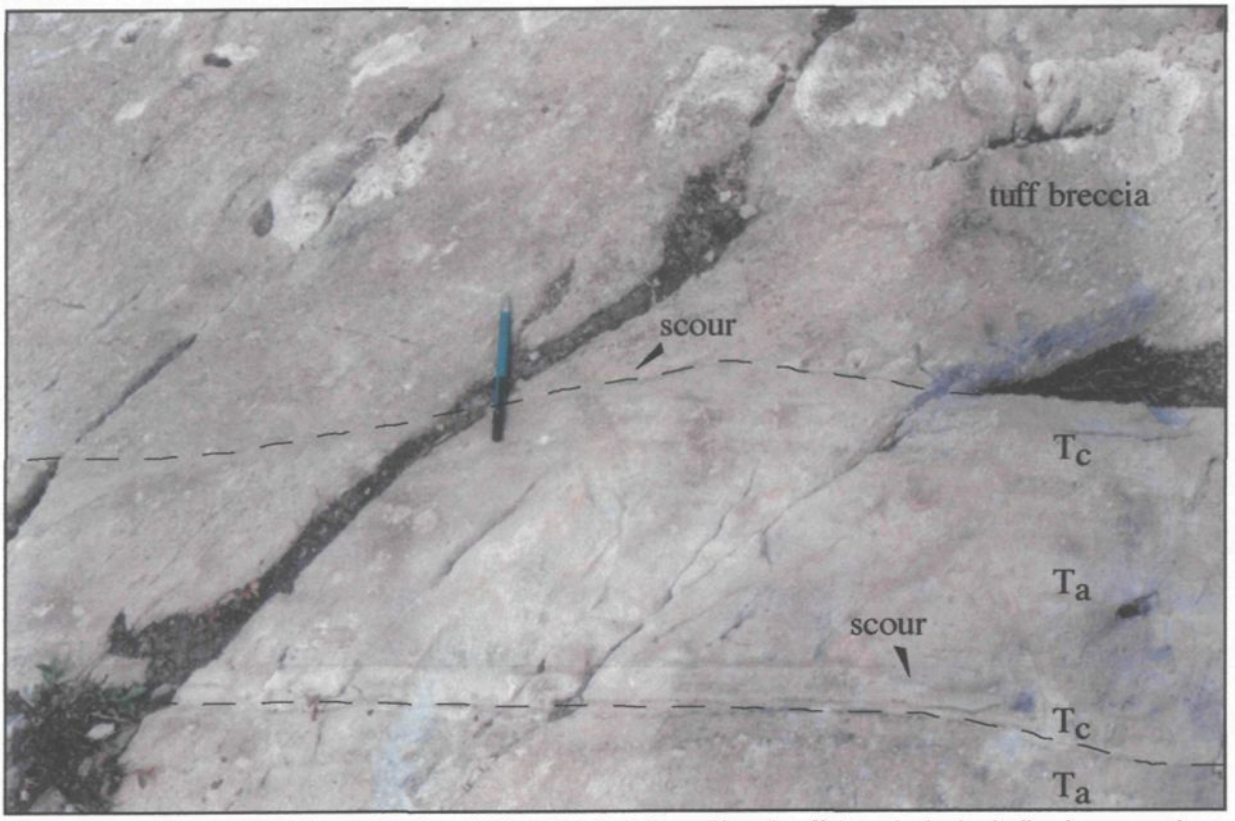

Figure 76: Truncated bedding of tuff turbidite (T_c) bed by tuff and tuff breccia beds, indicating younging direction towards the south (pencil; 14.5 cm-long).

Figure 77: Flow-banded, subangular felsic fragment. Pencil for scale (14.5 cm).

Figure 78: Subrounded, lapilli-sized fragments with epidotized cores and quartz-amygdules hosted in a feldspar-rich matrix. Pencil for scale (14.5 cm).

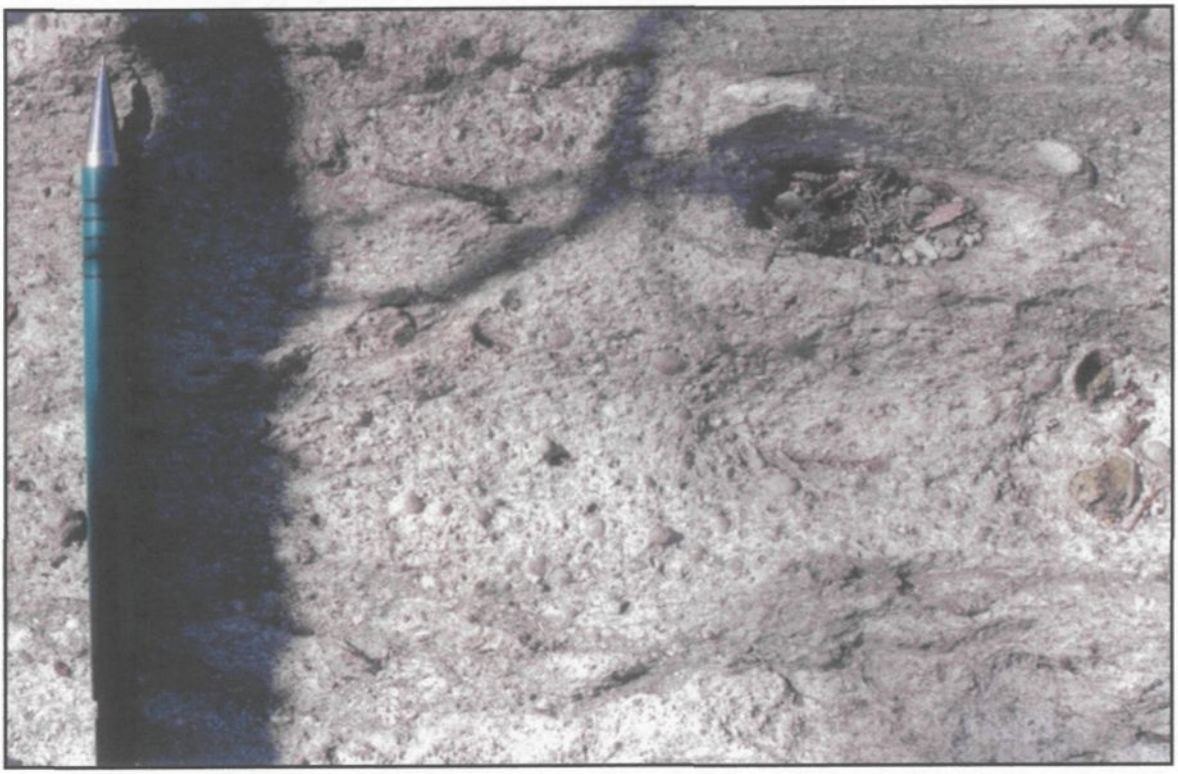

Figure 79: Slightly flattened, vesicular-rich (quartz-epidote amygdules) intermediate fragment. Pencil for scale (14.5 cm).

15-vol%; **Figure 80**; **Appendices 13/14**). Further to the south and just north of Highway 117, a small ridge comprised of a highly sheared (**Figure 81**) lapilli tuff breccia is characterized by sulfides fragments, along with fragments that are subrounded and amygdaloidal or flow-banded.

Petrographically, the matrix is dominantly composed of a fine crystalline mosaic of equigranular quartz and feldspar and 6-8-vol% feldspar microphenocrysts. Feldspars form euhedral to subhedral tabular crystals that are < 2 mm in length, characterized by albite twinning, and are commonly fractured or broken into smaller pieces. Replacement of zeolites by prehnite-pumpellyite (Dimroth and Lichtblau, 1979) within vesicles indicates a low-grade metamorphism for some of this deposits (**Appendix A-12**).

Feldspar-phyric (FP) lava facies

A feldspar-phyric (FP) lava facies is conspicuous as it is both stratabound and cuts the stratigraphy (**Table 11**). This facies is defined by 15-20% mm sized, tabular, euhedral feldspar phenocrysts within the groundmass. An intrusive nature is suggested by irregular and crosscutting contact relationships (**Figure 74**) evident in several outcrops, whereby the FP facies cuts volcaniclastic and lava flow facies and has a weakly developed chill margin (**Figure 82**). The FP facies is commonly fragmented *in situ* forming subangular to subrounded lapilli- to breccia-sized clasts with jigsaw patterns (**Figure 83**). Such fragmented zones are characterized by abundant quartz amygdules hosted in the matrix (**Figure 84**).

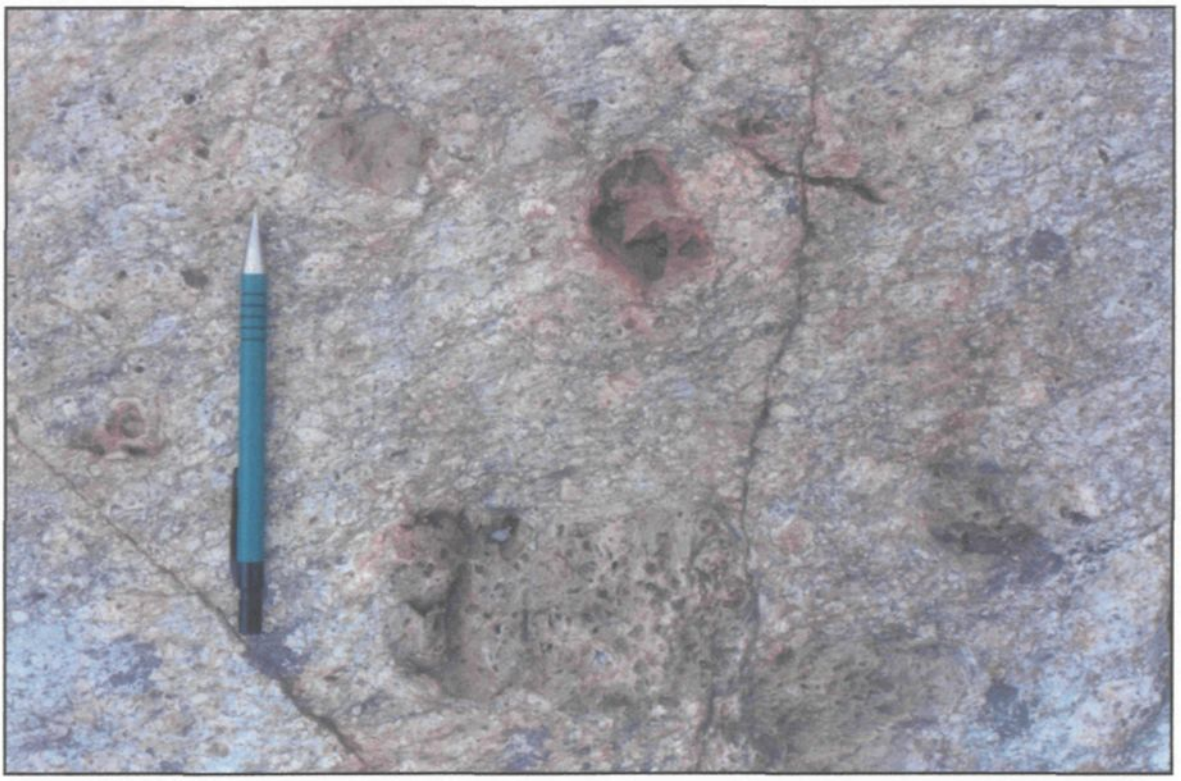

Figure 80: Nature of lapilli tuff facies from Hollow showing; with vesicular lapilli fragments and abundant feldspar phenocrysts liberated in the matrix. Pencil for scale (14.5 cm long).

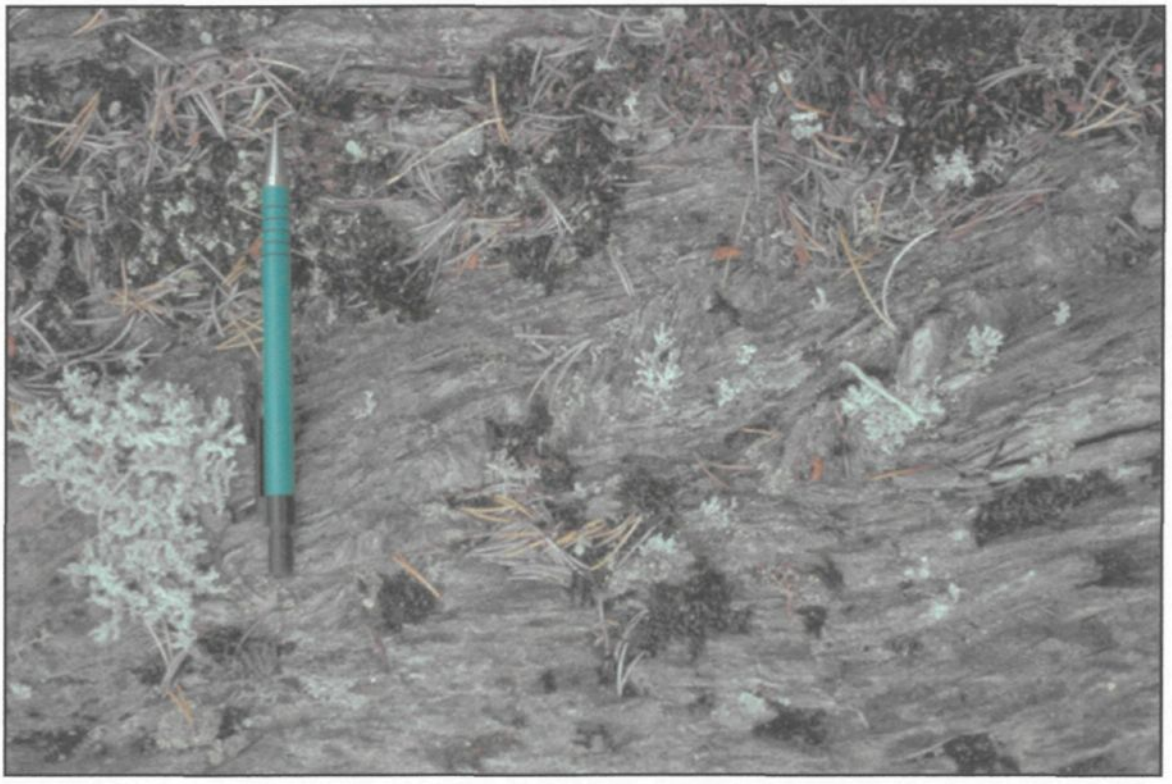

Figure 81: Kink banding in shear zone within lapilli tuff. Pencil for scale (14.5 cm).

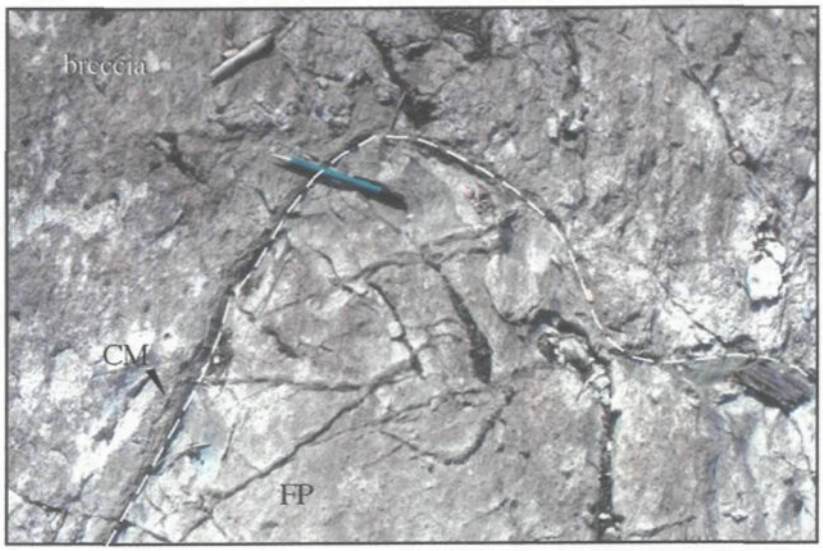

Figure 82: Intrusive contact relationships between feldspar-phyric (FP) facies and brecciated facies outlined by a possible chilled margin (CM). Pencil (14.5 cm long) points towards the north.

Figure 83: In situ brecciated appearance of feldspar-phyric facies with many of the fragments forming jigsaw-patterns. Pencil (14.5 cm long) points towards the north.

Figure 84: Vesicular nature (quartz amygdules) of feldspar-phyric facies. Pencil for scale (14.5 cm long).

Deformation and structural features

The structural complexity of the region is affected by localized deformation, such as the Manitou Shear Zone to the south and several major north-northwest and east-northeast faults (**Figure 68**). Field evidence includes observed chevron folds and areas of high shear (**Figure 81**). Deformation and alteration are common in proximity to the Bourlamaque Pluton and Cornell Plug, which deform normal stratigraphic successions and destroyed primary textures and original contact relationships.

4.1.5.2 Interpretation of Camnet area

The predominance of felsic-related volcano-sedimentary facies separates this region from other regions of interest discussed in previous sections. In addition, proximity to the synvolcanic Bourlamaque Pluton (and Cornell Plug) and Manitou Shear Zone significantly altered primary volcanic textures due to silicification and deformation. However, careful documentation of the various facies, particularly petrographic analyses, permits some conclusions to be made regarding fragmentation and transportation, as well as evolution within monogenetic volcanic complexes.

Mapping outlines several felsic lava sequences, measuring 200-300 m-thick and 1-3 km-wide (minimum dimensions). These sequences are composed of a complex intercalation of massive felsic lavas and felsic volcaniclastic facies. These fine-grained, quartz- and feldspar-phyric lavas exhibit stratiform and crosscutting relationships that suggest a probably a continuum from intrusive to extrusive emplacement. The FP facies emulate these contact relationships. The hyalocrystalline character of these felsic facies

indicates incomplete crystallization, which may be due to moderate degrees of undercooling; therefore these facies probably range from hypabyssal to extrusive. Observed vesicularity (**Figure 84**) is probably a function of decompression as they approach the surface. Prominent jigsaw patterns attest to interaction with external water. The water source may originate from unconsolidated volcaniclastic sediments, thereby making these brecciated intrusions peperitic sills/dykes (Branney and Suthren, 1988), which are commonly associated with viscous magmas (Kokelaar, 1982). However, it is impossible to ascertain whether the sediments are deformed (cf. Duffield et al., 1986), although fluidization can inhibit significant deformation induced by direct stress during magma intrusion (Kokelaar, 1982). Finally, when characterized by broken, euhedral phenocrysts, they probably have interacted explosively with external water and are completely extrusive and are thus termed crystal tuffs. Observed lateral transitions from massive to fragmental facies further support a hypabassal to extrusive setting.

These feldspar-phyric facies probably represent a continuum of phases of a synvolcanic feeder system that supplied magma to the edifice and any satellite vents. Such sequences probably represent isolated felsic vents from small volume felsic eruptions that are mantled by a brecciated carapace of felsic fragments. Vesicularity is low, but numerous thin bedded lapilli tuff facies are probably pyroclastic in origin based on the abundance of liberated, broken feldspar crystals in the matrix (**Figure 80; Appendices 13/14**). Furthermore, interbedded feldspar-phyric facies, interpreted as crystal tuffs, form during periods of efficient fragmentation (i.e., pyroclastic). Explosive ejection of these facies into the water column results in water ingestion and subsequent vertical collapse of a water-

fragment mixture. These collapsing, tephra-charged columns may become deposited along the flanks of the edifice or flow downslope, either immediately or after some period of repose.

Intermediate lava facies are intercalated with and overlie felsic volcanics, which suggest a possible genetic relationship. Moreover, intermediate flows have a similar feldspar population and modal percentage to underlying felsic deposits. Lateral (along strike) variations from massive lava to brecciated facies imply non-explosive granulation due to spalling of lava flow margins (Type III; White, 2000).

Mafic deposits are restricted to the east of the area and are likely associated with another volcanic system, as no other mafic volcanics are observed to the west (**Figure 68**).

Volcaniclastic formation

Massive coarse-grained facies composed of flow-banded, angular fragments represent non-explosive hydroclastic to autoclastic processes (brittle fragmentation; Alidibirov and Dingwell, 2000) fed by thermal quenching and mechanical failure (i.e., spalling) of felsic flow margins (Type III; White, 2000). The non-sorted nature indicates that turbulence was limited and that they were probably transported as a cold, water-supported, cohesive debris or plug flow (Lowe, 1982; Cousineau, 1994). Deposition was due to *en masse* frictional freezing (Lowe, 1982).

Intermediate volcaniclastic facies are either autoclastic to pyroclastic in nature based on association with massive lava and/or matrix constituents. Deposits correlated to massive lavas are considered lava fed by autoclastic processes (White, 2000). Other

deposits characterized by abundant broken, euhedral feldspar crystals in their matrix were probably formed via a more explosive event. Grading, interbedded relationships, and erosive properties all suggest deposition via water-supported, high- to low-concentration turbidity currents (Lowe, 1982). Heat retention textures are absent; therefore, these currents were probably deposited in a cold state, but eruption-fed (Type II; White, 2000).

Sulfidic fragments hosted in intermediate volcaniclastic deposits probably originate from the vent area in a region of active hydrothermal venting. As they are along strike to known VMS deposits to the east (**Figures 26 & 68**), these deposits probably represent turbidity flows that picked up these sulfide fragments as they passed over a mineralized zone; therefore, the paleo-flow direction was from east to west.

4.2 Upper Val d'Or Formation

Five regions of interest (ROI) are identified within the upper Val d'Or Formation (**Figure 85**), which include: Relais, Dunraine east, Dunraine west, Abitibi Copper, and Sleepy Lake. Unfortunately, only one localized area had previously been mapped in detail for mineral exploration, therefore large exposed outcrops are lacking in the upper VDF and mapping is done by closely spaced traverses.

4.2.1 Study of Relais area (ROI 6)

The Relais region represents a transition from volcanics associated with the lower VDF to those of the upper VDF, which is reflected in its geochemical affinity (see **Figure**

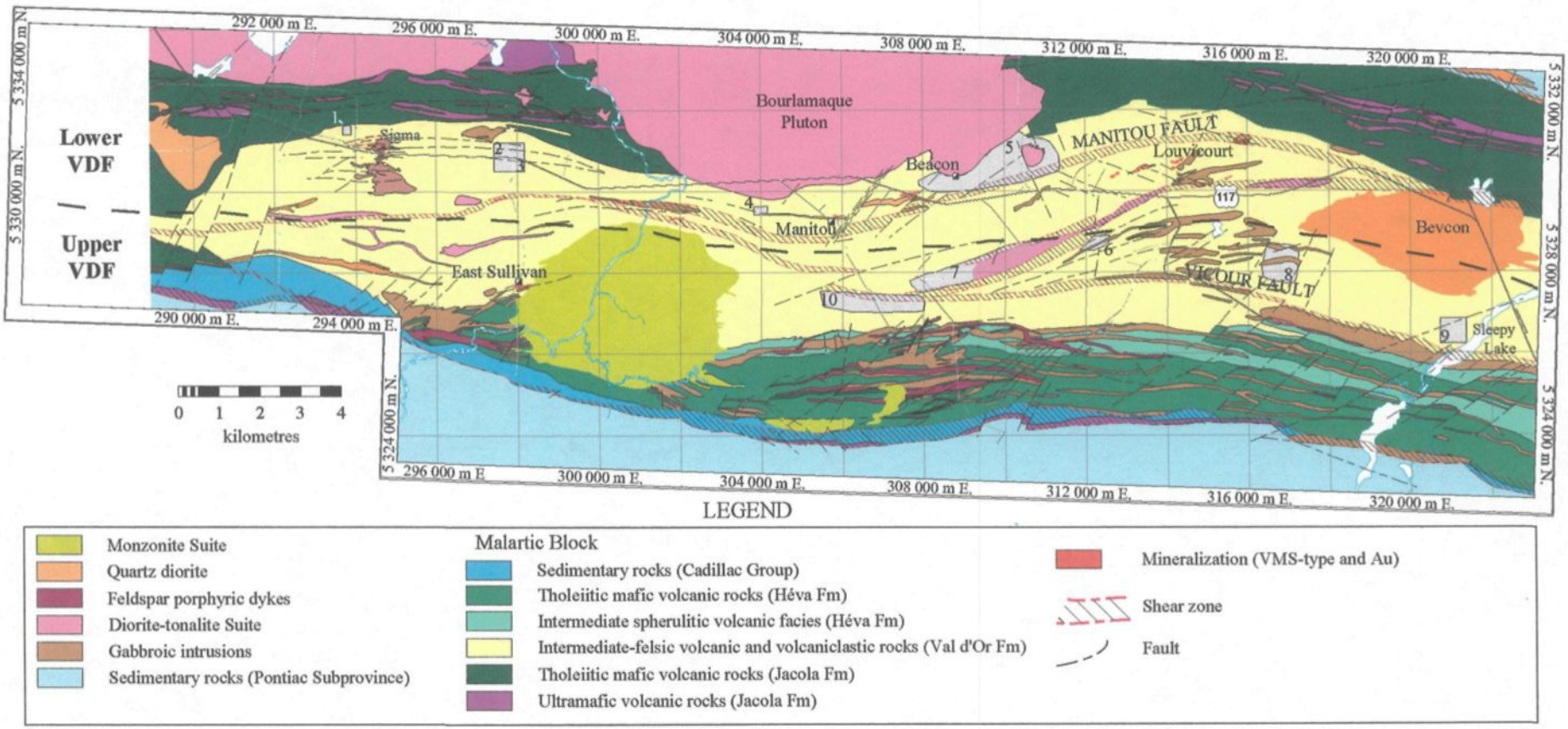

Figure 85: Simplifed regional geology of the Val d'Or region. Arbitrary division of VDF represented by dashed line. Lower VDF regions of interest: 1. Playground area; 2 - Placer Dome North; 3 - East Sullivan outcrops; 4 - Manitou west; 5- Camnet. Upper VDF regions of interest: 6 - Relais; 7 - Dunraine east; 8 - Abitibi Copper; 9 - Sleepy Lake; and 10 - Dunraine west.

85) to more calc-alkaline values as the arc matures (Wilson, 1989). The Relais property is ideally located between the Dunraine and Vicour shear zones (**ROI 6, Figure 85**), thus providing a deformation-free window on the local stratigraphy. This mapped sector spans a 1.8 km x 1.6 km area within a series of felsic-dominated volcano-sedimentary deposits (**Figure 86**).

4.2.1.1 Lithology and stratigraphy of Relais area

Facies mapping identified several different felsic lavas and associated volcaniclastic deposits, along with an andesitic massive to pillowed lava based on morphology and mineralogy (**Table 12; Figure 86**). The mapped sequence represents a slice through several felsic lava flows and hyaloclastite facies. Two felsic flow types are recognized based on the relationship between lavas and hyaloclastites. An intervening andesitic lava flow and tuff turbidite illustrate the continuum of events as opposed to a structure overlap.

Volcanic lithofacies

Felsic facies are characterized by gray alteration on fresh surfaces and variable amounts of primary quartz. These 100-250 m-thick units are typically massive deposits and are feldspar and/or quartz phyric, the variations of which permit the identification of individual flow facies (**Table 12; Figure 86**). The lower felsic lava facies forms part of a complex alternating sequence of massive and lobate lava with felsic breccia. The distinctive lobes form m-sized bulbous masses that are internal to the lava and extend into the enclosing breccia (**Figures 87A/B**). Lobe closures are oriented to the west and east in

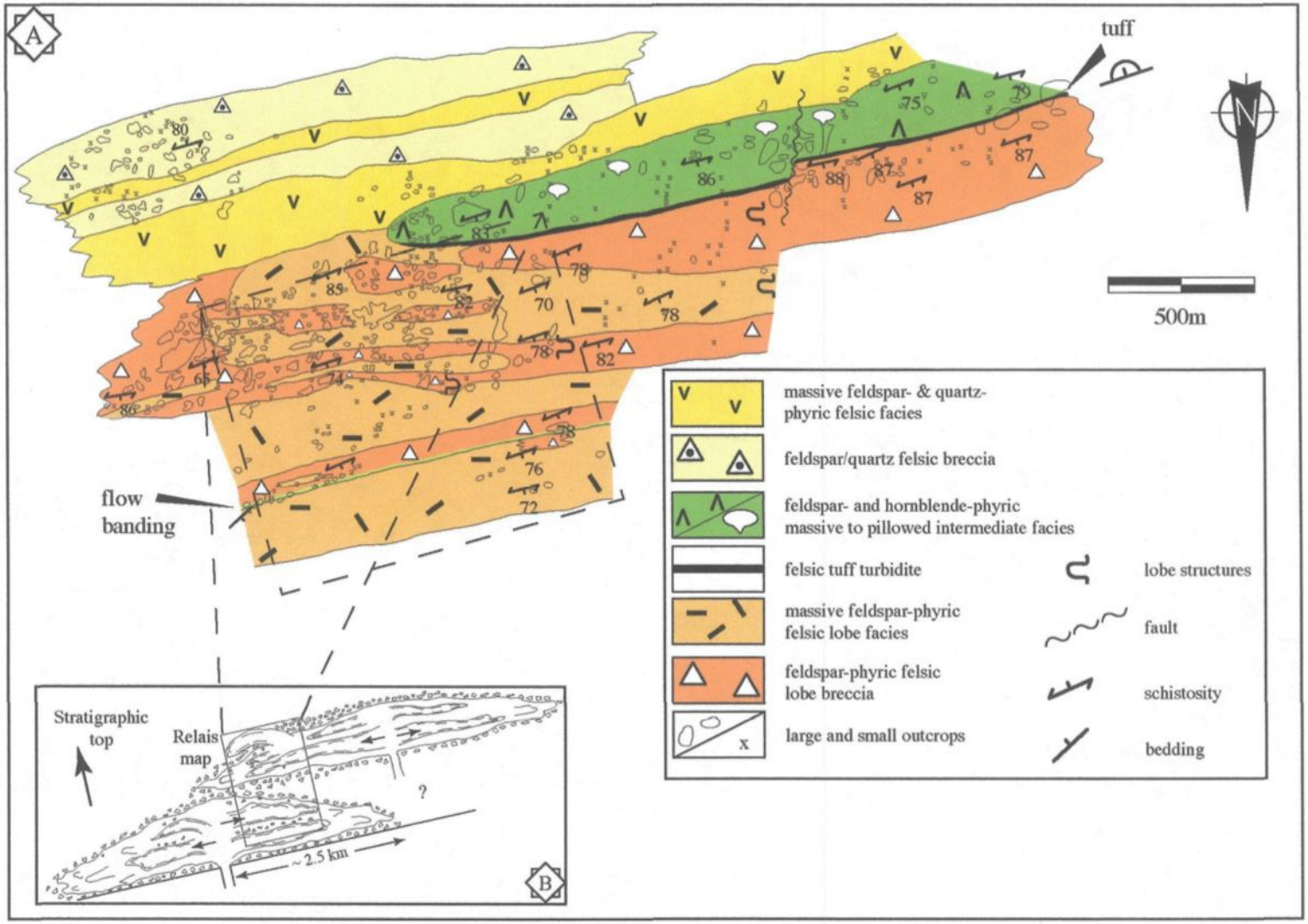

Figure 86: General geology of the Relais region (ROI 6). A. Facies mapping illustrating the complex intercalation of felsic lavas and brecciated facies. B. Possible model of two overlapping felsic lobes, based on intercalated facies and lobe structures.

Table 12: Volcano-sedimentary lithofacies of the Relais area (ROI 6).

Lithofacies	Thickness & morphology	Characteristics	Transport/deposition	Origin
Volcanic				
Lobate felsic lava	100-250 m; tabular to lobate (m-sized lobes)	Massive and columnar jointed; lobate; intercalated with fragmental facies; flow banded; 15-20-vol% euhedral/subhedral feldspar; trace anhedral quartz; 0-15-vol% quartz amygdules	Highly viscous lava; effusive emplacement;	Subaqueous felsic lava dome; lobe inflation into hyaloclastite carapace
Massive felsic lava	100-250 m; tabular	Sheet-like massive flow; 15-20-vol% tabular, euhedral/subhedral feldspar; 10-vol% quartz; basal flow breccia	Effusive flow	Subaqueous lava with possible inflation into a protected breccia carapace
Andesitic lava	250 m; massive to pillowed	20-vol% feldspar; hornblende-phyric	Vertical transition from massive to pillowed flow	Subaqueous effusive eruption
Volcaniclastic				
Lapilli tuff breccia	50-250 m; irregular	Subangular, angular and blocky fragments; sharp contacts with enclosing felsic lava; 15-20-vol% tabular, euhedral/subhedral feldspar; 0-15-vol% quartz amygdules; perlitic fractures	*In situ* brecciation of upper and lower parts of felsic lava flow	Lobe-hyaloclastite; interaction with water
Tuff	1 m; tabular	Graded bedding; finely laminated; syndepositional features; local marker horizon	Low concentration turbidity flow (T_{abd})	Possible fallout of fine material erupted outside of area

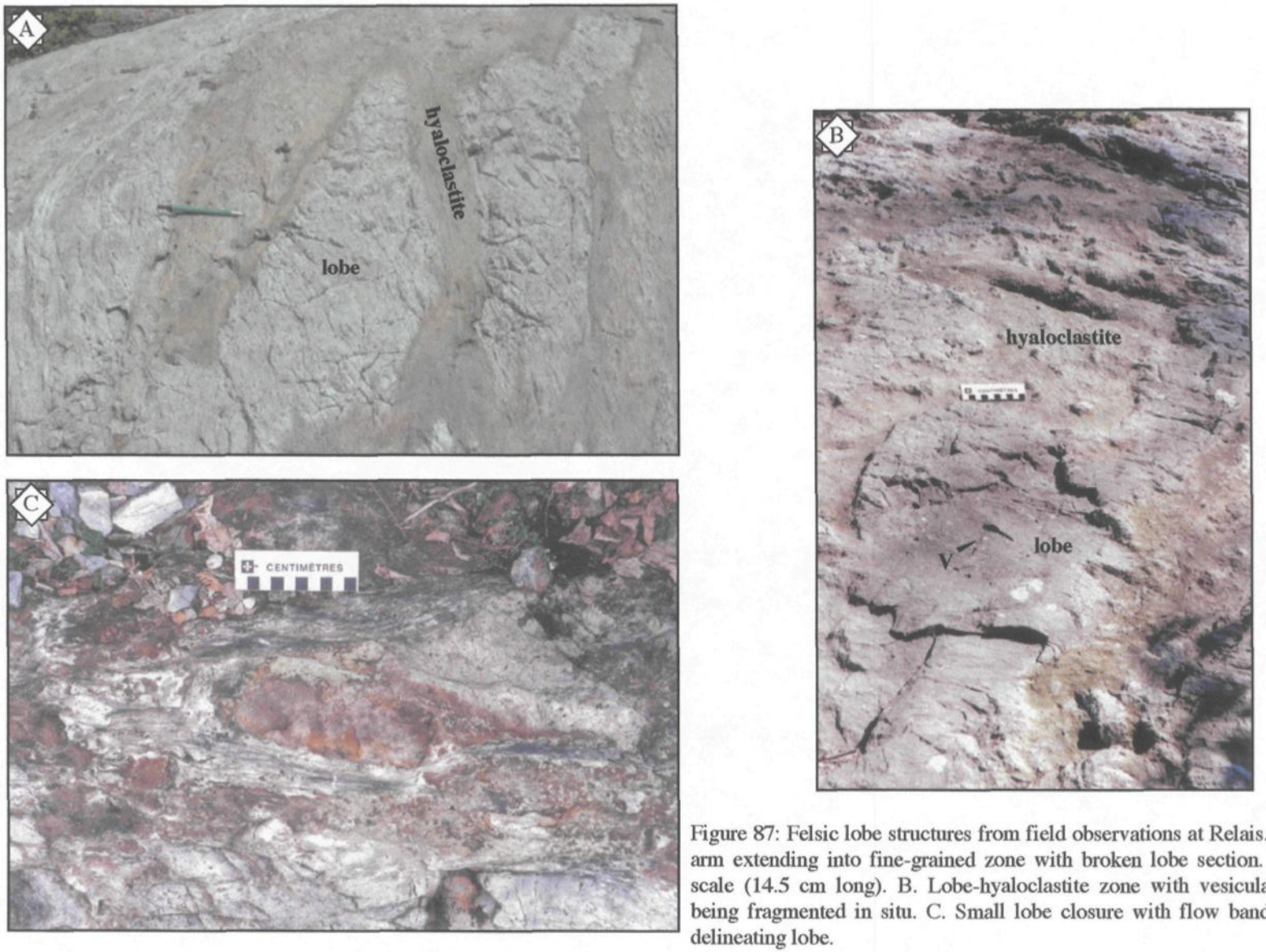

Figure 87: Felsic lobe structures from field observations at Relais. A. Lobate arm extending into fine-grained zone with broken lobe section. Pencil for scale (14.5 cm long). B. Lobe-hyaloclastite zone with vesicular (v) lobe being fragmented in situ. C. Small lobe closure with flow banded margin delineating lobe.

different lava flows (e.g., **Figure 87C**), such that they are facing each other (see **Figure 86**). In addition, thicker units are characterized by polygonal fracture patterns (i.e., columnar jointed; **Figures 88A/B**). Vesicularity varies from 0-15-vol%, as represented by quartz amygdules, and commonly increases towards flow margins, particularly in proximity to brecciated facies (**Figure 87B**). Subordinate flow banding (**Figure 89**) is observed at one stratigraphic level at the summit of a thick massive dacite facies and extends over 1000 m along strike, indicating that it is probably a primary feature and not structurally controlled (**Figure 86**). The southern felsic lava facies are linear and uniform in cross-section with no complex intercalation and an absence of lobe structures (**Figure 86**). Both felsic lava flows are composed of 15-25-vol%, tabular, euhedral/subhedral, feldspar phenocrysts (**Figure 90A**). Quartz is minor in the northern lobate lava, but is upwards to 10-vol% in the southern lavas (**Figure 86**). In thin section, feldspar glomerocrysts are common with acicular feldspar microphenocrysts comprising the groundmass, with subordinate anhedral quartz (**Figure 90B; Appendix A-15**). Alteration is weak to moderate as evident by sericite, carbonate, and minor chlorite.

The 250 m-thick feldspar- and hornblende-phyric facies extends for a minimum of 2.1 km east along strike and is located stratigraphically between the two felsic units, although it terminates abruptly before propagating through the complete sequence (**Figure 86**). Massive and pillowed facies (**Figure 91**) are observed, with pillows generally located along the southern margins, which is also the top of the flow unit as pillow morphology indicates a southward younging direction. In thin section, feldspar phenocrysts comprise upwards to 20-vol%, whereas hornblende is absent or completely altered.

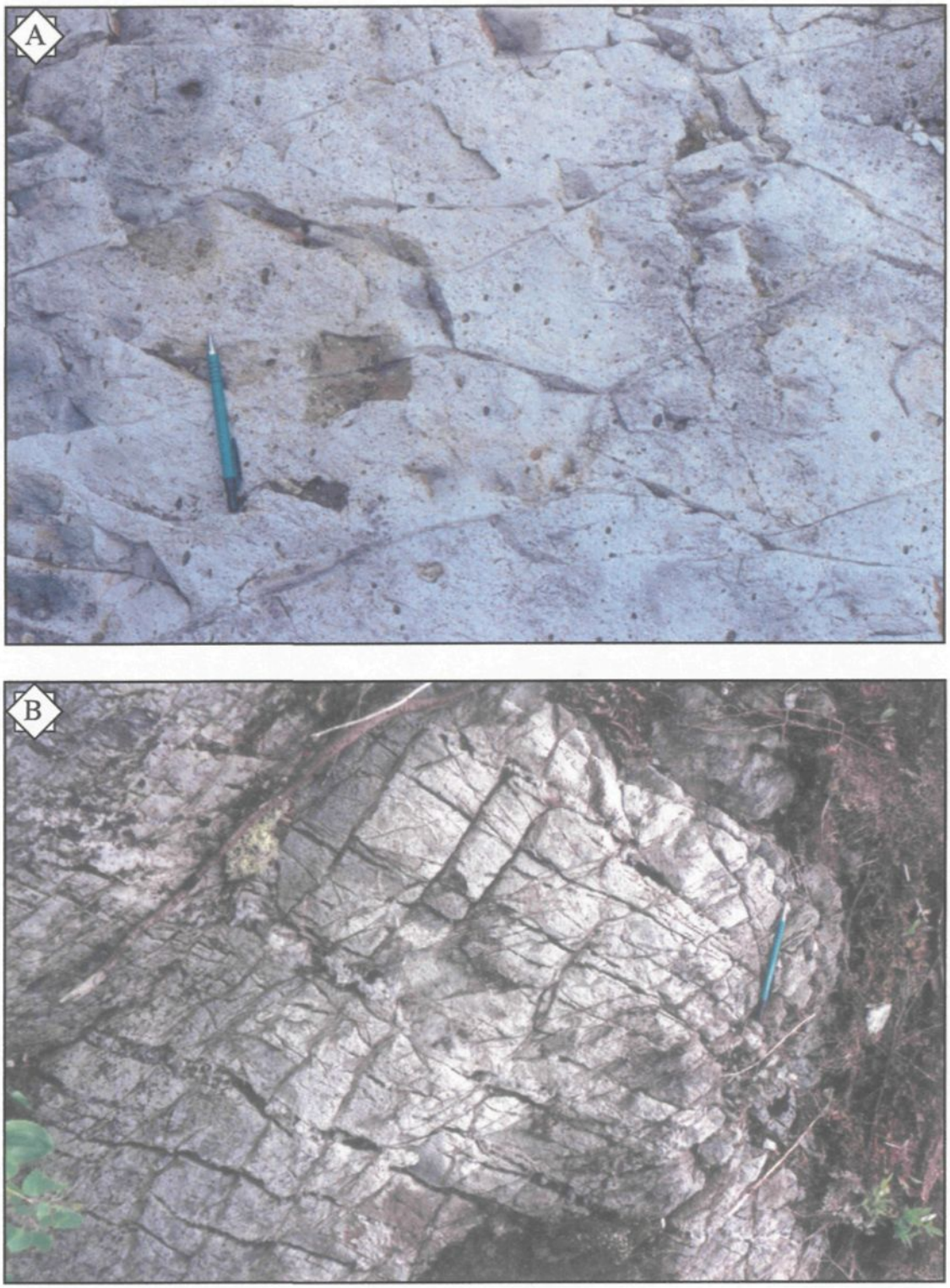

Figure 88: Columnar joints developed in massive felsic lava. A. In vesicular felsic lava. B. *In situ* brecciation and columnar joints (parallel to pencil; 14.5 cm long).

Figure 89: Flow banding in felsic lava. Fieldbook for scale (17 cm-long).

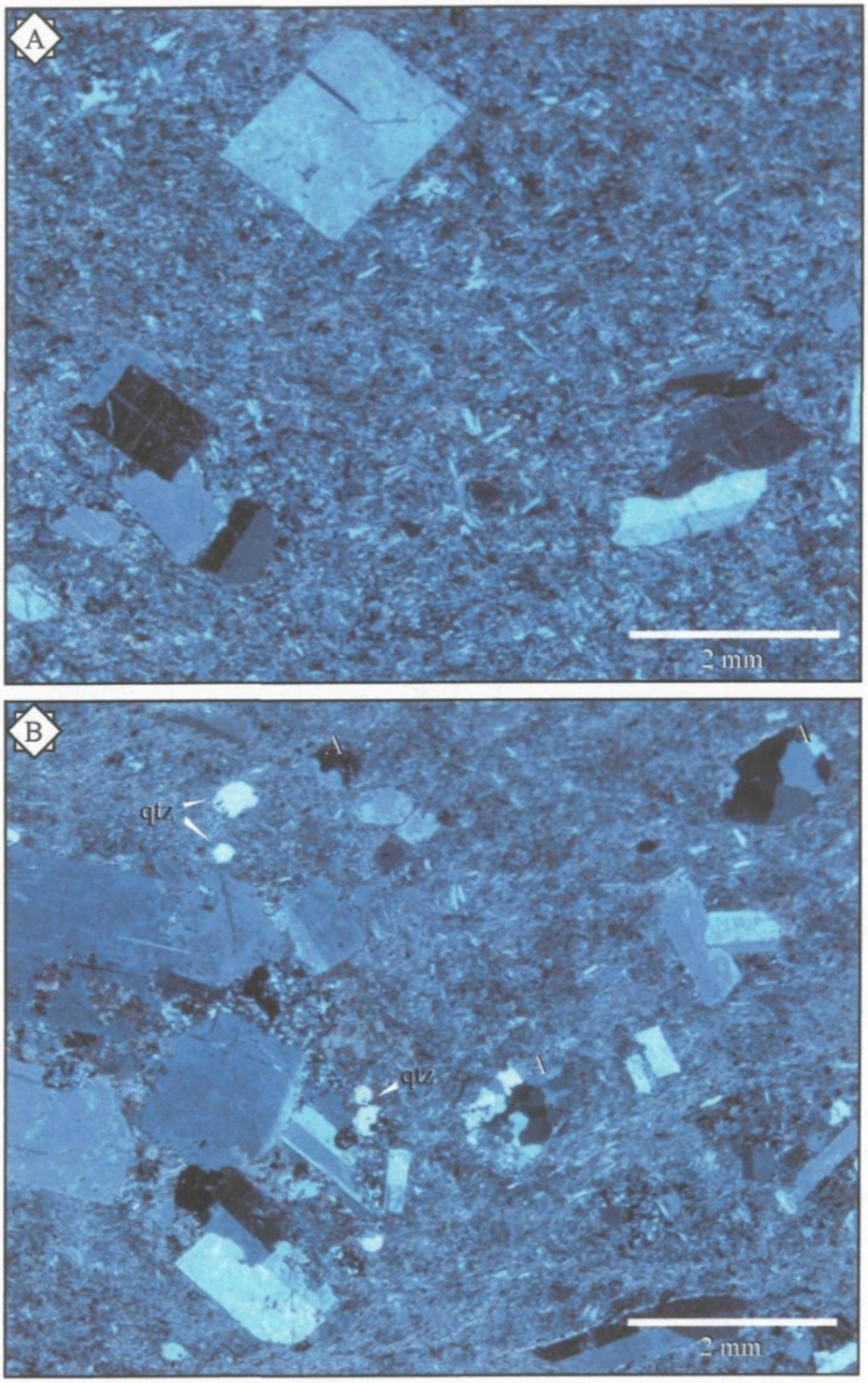

Figure 90: Cross-nicols microphotographs of felsic facies from Relais region. A. Blocky, euhedral feldspar phenocrysts hosted in groundmass of acicular feldspar and re-crystallized quartz (CS99-2017). B. Tabular euhedral feldspar phenocrysts, quartz amygdules (A), and anhedral quartz (qtz) microphenocrysts hosted in groundmass of acicular feldspar (CS98-053).

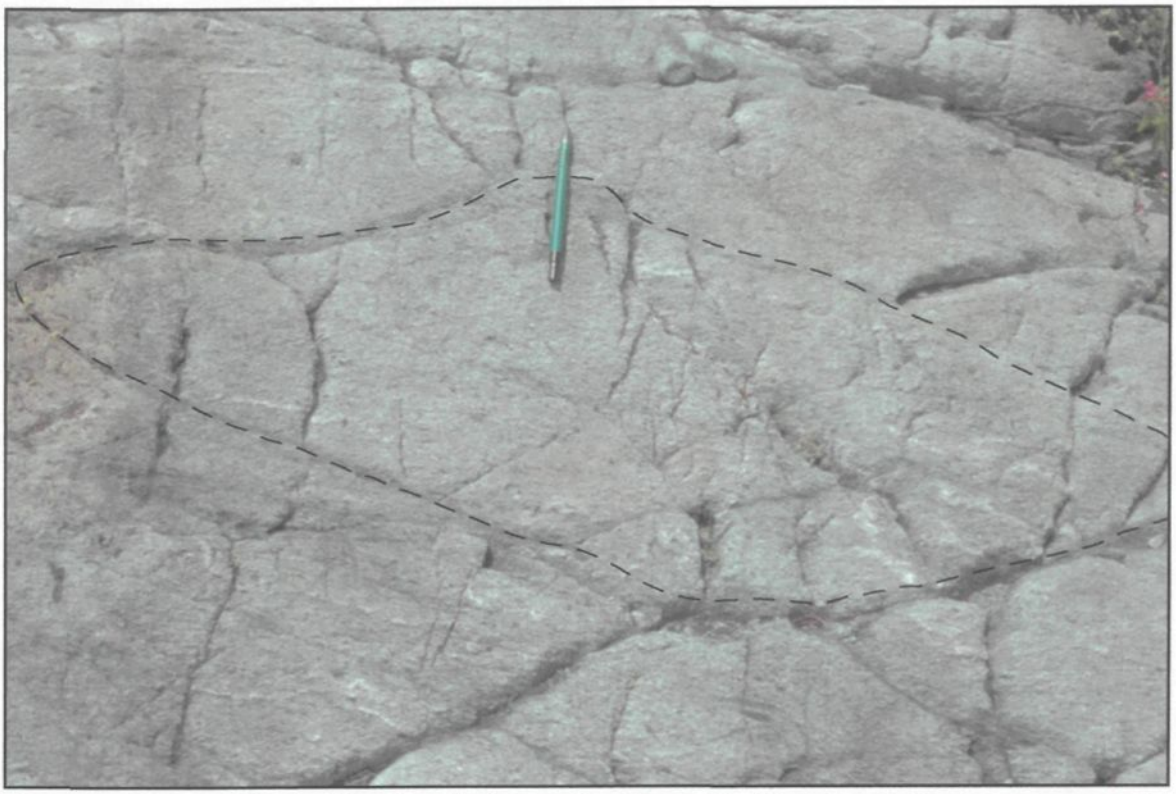

Figure 91: Weakly defined pillow form in intermediate lava with pillow form indicating tops are to the south; pencil points towards the north (14.5 cm long).

Figure 92: Finely laminated tuff turbidite facies with small scale ripples (r), pinching (p), and loading (l) structures indicating younging direction to the south (arrow).

Volcaniclastic lithofacies

A conspicuous feature of the brecciated facies is that they are always located stratigraphically above a felsic lava facies (**Figure 86**). In addition, brecciated facies are texturally and mineralogically similar to enclosing lavas, in that vesicular, feldspar-phyric, lobate breccias overlie vesicular, feldspar-phyric lobate felsic lavas (**Table 12**). Contacts between lavas and brecciated facies are always sharp, with observed transitions from massive felsic lava into a zone of *in situ* breccia, followed by a brecciated facies (**Figures 87A/B**). Sericite alteration is more intense as feldspar phenocrysts are commonly replaced leaving relict tabular outlines. Some of the lapilli fragments are probably former vitroclasts as they are characterized by curvilinear cracks interpreted as perlitic fractures.

The mapped 1 m-thick tuff turbidite facies, while subordinate to the sequence, is significant as it serves as a marker horizon, facilitating correlation of the northern felsic lavas and the recognition of a minor fault (**Figure 86**). Furthermore, erosive contacts, syndepositional structures, and Bouma divisions all indicate a southward younging direction (**Figure 92**).

4.2.1.2 Interpretation of Relais area (ROI 6)

The complex intercalation between massive and brecciated facies and an apparent genetic relationship in regard to mineralogy and textures suggest that the brecciated facies is hyaloclastites. Hyaloclastites form during hydrovolcanic fragmentation along the margins of the felsic flow, whereby thermal stresses between the lava and external water

results in disintegration (Fisher and Schmincke, 1984). Polygonal fractures probably form along the flow margin (Stewart and McPhie, 2003) during formation and propagation of first-order fractures (Davis and McPhie, 1996). Subsequent infiltration of water into the now fractured lava and sustained lava movement will increase fragmentation and form a thick mantling deposit of brecciated lava. Furthermore, the northern felsic facies can be called a *lobe hyaloclastite* based on observed lobe structures (**Figure 87**). Such mantling hyaloclastites are characteristic of a subaqueous felsic lobe hyaloclastite dome/flow complex (Yamagishi and Dimroth, 1985; Gibson et al., 1997, De Rosen-Spence et al., 1980; Furnes et al., 1980). Gibson et al. (1997) envisaged lobate massive felsic facies to form during endogenous growth, whereby lobes were emplaced similar to large balloons within the interior of the flow, thereby insulated from ambient water (**Figure 93**). These lobes invaded the hyaloclastite carapace/pile as a highly viscous lava that inflates to form lobe-like appendages. This genesis is different from described cryptodomes as inflation is self-contained within a growing subaqueous lava dome as opposed to a shallow level intrusion that results in the disturbance of overlying sediments (Minakami et al., 1951). Moreover, there is no evidence of bounding strata being crosscut or deformed, common for cryptodomes (Stewart and McPhie, 2003), but there are genetically associated felsic clasts intercalated with lobes that suggest interaction with copious amounts of water (Fisher and Schmincke, 1984) and re-sedimentation, which are associated with subaqueously extruded lava domes (Gibson, 1999).

Opposing lobe directions (see **Figure 86**) imply overlapping flows from different vents (**Figures 86B and 93**), but not necessarily separate lava sources. It is envisioned that

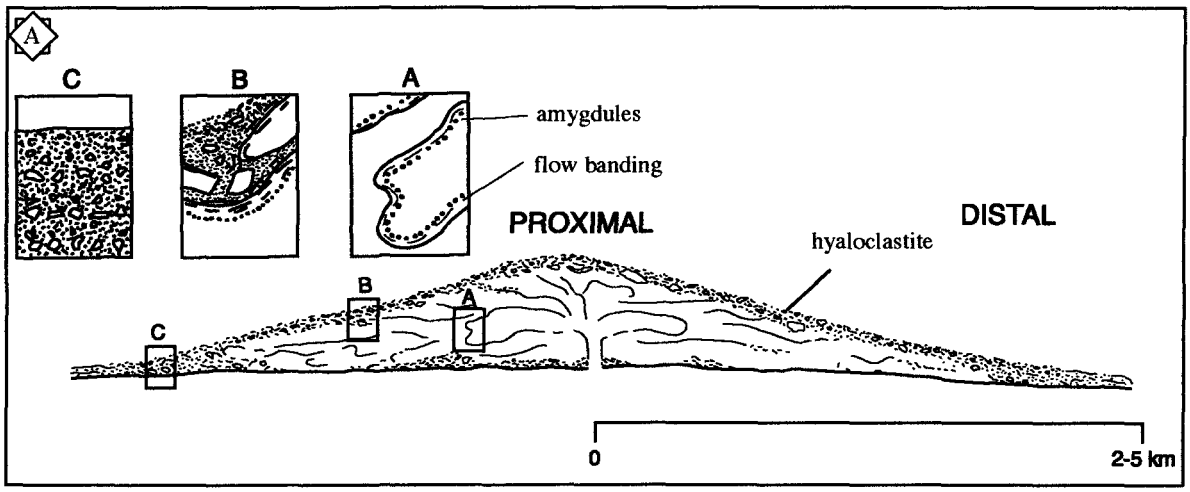

Figure 93: Typical cross-section through a felsic lobe-hyaloclastite flow demonstrating flow morphology and structures common of proximal and distal facies. Modified from Gibson et al. (1997). Compare to Relais dome complex Figure 86B.

there were two eruptions that were coeval with each other and may even have tapped the same subvolcanic chamber based on mineralogical and textural similarities. The thin tuff turbidite facies probably represents a brief period of repose during which time finer grained material became remobilized along the flanks for the western dome. Effusive eruption of intermediate lavas may signal renewed activity from this vent. The transition from massive to pillowed morphology suggests initial volcanic activity had higher temperatures, and/or higher discharge rates forming massive flows, but changed to lower temperatures and/or lower discharge rates forming pillowed flows. The complete sequence was then covered by series of feldspar-quartz phyric felsic lavas. The tabular nature of these felsic lavas indicates a flow morphology rather than a dome. Bounding felsic breccias are probably the insulating carapace and foot breccias produced during emplacement (De Rosen-Spence et al., 1980; Yamagishi and Dimroth, 1985; Scutter et al., 1998).

The identification of a km-scale felsic dome complex represents a potential exploration target for a volcanogenic massive sulfide deposit (cf. Gibson et al., 1997). Field mapping did not identify any significant surface mineralization, but similar economic deposits have been discovered in similar facies associations (i.e., Millenbach-D68; cf. Gibson et al., 1997).

4.2.2 Dunraine east area (ROI 7)

This area covers a zone west of the Relais sector (**ROI 7; Figure 85**) and is characterized by two prominent ridges that extend along strike, which facilitates the identification of any lateral relationships. The Dunraine area owes its name to a previous

exploration project conducted by Cambior that covers an approximate 6.6 km x 1.7 km area (**Figure 94**) Regional mapping utilized former company maps in an effort to outline the general stratigraphy. In this regard, 71 stations were noted in order to document any contact relationships within and between facies.

4.2.2.1 Lithology and stratigraphy of Dunraine east area

The general stratigraphy of the region can be divided into four main geologic units, based on mineralogical, textural, and contact relationships. Felsic and intermediate lavas are recognized by their massive nature and a felsic intrusion on its massive, crystalline nature, with the remainder composed of an extensive amalgamated volcaniclastic unit (**Table 13; Figure 94**).

Volcanic lithofacies

Three separate felsic facies are identified in the field based on stratigraphy, and in one case, lack of lateral continuity, which are the: (1) northern; (2) western; and (3) eastern lava facies (**Table 13**). All felsic facies are massive and typically sheared, giving an *in situ* brecciated appearance, the fractures of which are filled by omnipresent sericite alteration. Surface weathering gives each felsic facies a white to cream appearance. The northern felsic facies measures upwards to 200 m-thick and may be correlated up to 3000 m along strike. Shearing is intense in places (**Figure 95A**), but in the western part of the facies, it is possible to identify the intermingling of two different felsic units based on vesicularity and intensity of brecciation. The contact is irregular and oriented in a rough north-south

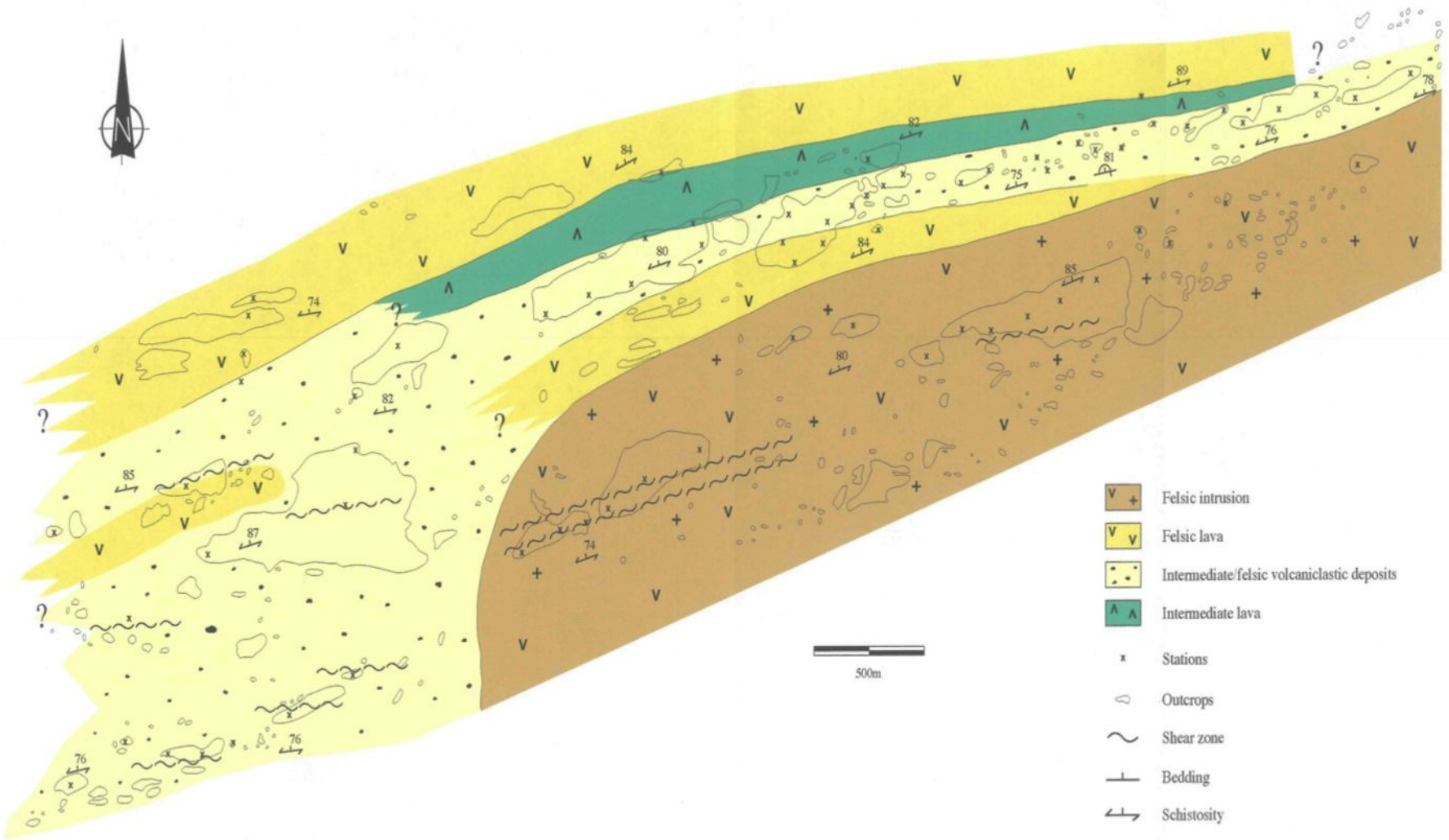

Figure 94: Simplified geology of Dunraine east sector (ROI 7).

Table 13: Volcano-sedimentary lithofacies of the Dunraine East area (ROI 7).

Lithofacies	Thickness & morphology	Characteristics	Transport/deposition	Origin
Volcanic				
Felsic	massive	*In situ* brecciation, white- to cream-weathering	Subaqueous lava flow or inflation into brecciated unit as a viscous lava	Effusive or hypabassal emplacement
- northern unit	200 m-thick, 3000 m-long	Two felsic lavas based on vesicularity and brecciation; irregular contact; (i) massive with mm-sized amygdules and (ii) brecciated and flow-banded; 3-vol% feldspar; 1-vol% quartz		
- western unit	50 m-thick; discontinuous	Caps mineralized zone; 10-vol% feldspar; 8 –vol% quartz		
- eastern unit	20-50 m-thick	8-vol% feldspar		
Intermediate	30-50 m-thick; massive	20 vol% tabular, euhedral feldspar; no contact relationships observed	Subaqueous lava flow	Effusive subaqueous eruption
Volcaniclastic				
Lapilli tuff to tuff breccia	Individual beds between 4- and 17 m-thick	Massive to graded clast- to matrix-supported beds; normal-graded ($R\text{-}S_3$), erosive ($R\text{-}S_1$), rare stratified beds (S_1 and T_b); matrix has 10-vol% feldspar	Water-supported, laminar, cohesive debris flows to high- and low-concentration turbidity currents; *en masse* frictional freezing to bed-by-bed deposition	Explosive to boil-over volcanism?
	Fragments types:	Angular: lapilli- to tuff-sized; flow-banded; 3-vol% feldspar; 2-vol% quartz		
		Subrounded: breccia-sized; *in situ* fractures and jigsaw fit; up to 33-vol% quartz amygdules; 10-25-vol% tabular, euhedral feldspar		

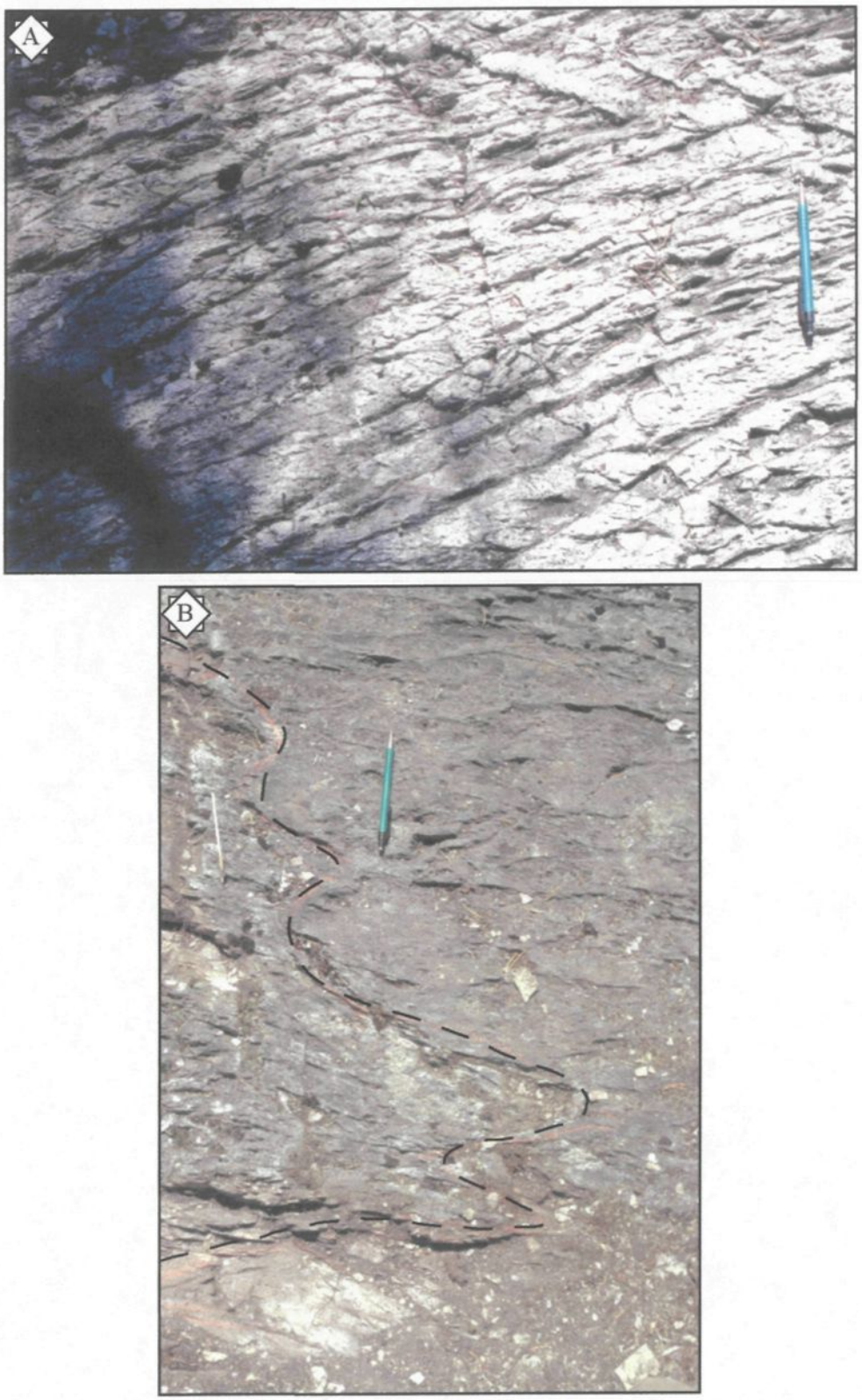

Figure 95: Felsic facies from Dunraine region. A. Sheared nature of felsic facies with sericite along fractures. B. Contact between two felsic facies (dashed line), where the massive facies on the right appears lobate and less sheared. Pencil for scale (14.5 cm long).

direction (**Figure 95B**). Both units are mineralogically similar, each composed of 3-vol% feldspar and 1-vol% quartz phenocrysts. However, one phase is more massive and characterized by rounded, mm-sized quartz-amygdules, whereas the other phase is more brecciated and typically flow-banded.

In thin section, the massive phase has mm-sized oval quartz-amygdules with trace amounts of tabular to blocky euhedral feldspar microphenocrysts, all within a slightly developed fabric that defines weak *in situ* brecciation in some places (**Figure 96**). The groundmass is a fine-grained mosaic of quartz + albite + sericite + carbonate ± chlorite, whereby chlorite is restricted to infilling brecciated areas (**Figure 96**).

The western and eastern felsic facies are at the same stratigraphic level, but are not laterally continuous (**Figure 94**). The western felsic facies is characterized by a well-developed foliation with *in situ* fragmentation, whereby the fractures are filled by sericite. This facies is composed of 10-vol% feldspar and 8-vol% quartz phenocrysts and measures upwards to 50 m-thick. Immediately to the north of this facies is an extensive mineralized zone hosted in a volcaniclastic deposit (discussed below), but the felsic facies is not mineralized.

Petrographically, this facies is dominated by anhedral, blobby quartz phenocrysts that make up to 30-vol%, whereas feldspars are rare and form relict tabular forms now completely altered to sericite (**Appendix A-16**). The groundmass is composed of sericite + chlorite with rare muscovite blades. The eastern facies has a similar morphology, but has no observed quartz and 8% feldspar. No mineralization is associated with this eastern felsic facies.

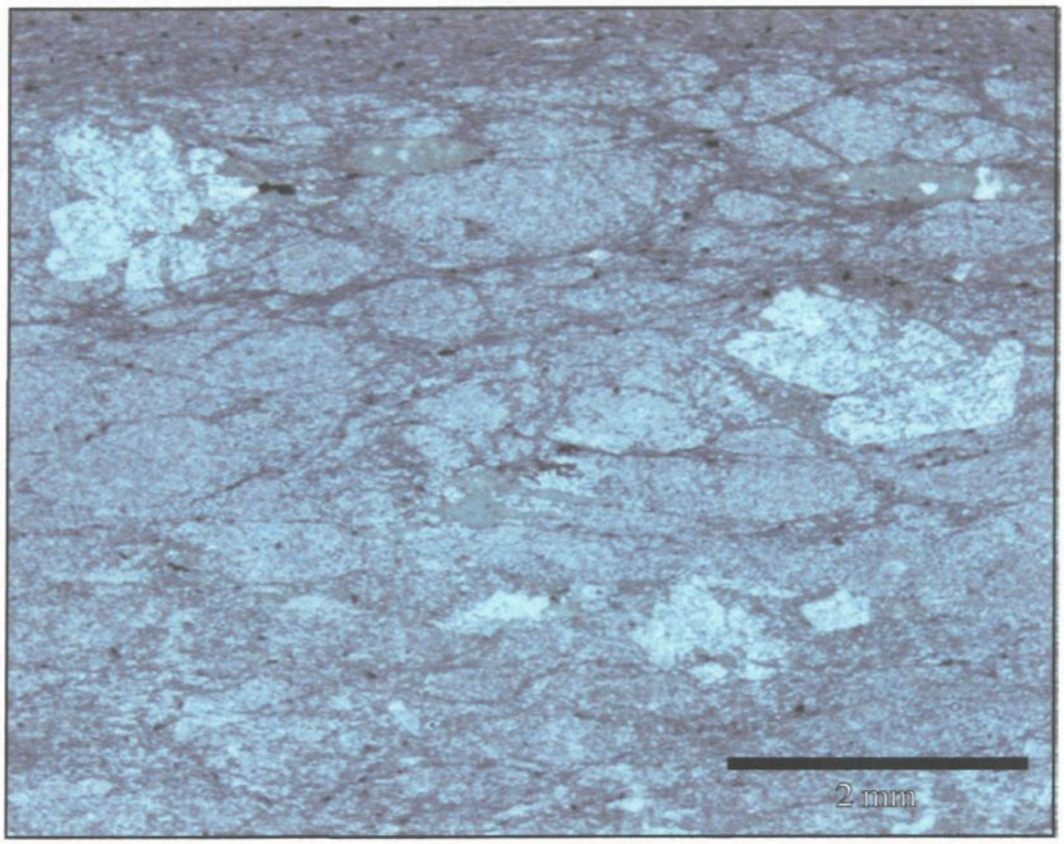

Figure 96: Plane polarized microphotograph of *in situ* brecciation of felsic facies with feldspar glomerocrysts.

The intermediate facies forms a limited sequence that only outcrops in several areas and has no identified contact relationship with bounding lithofacies. This facies is massive and feldspar phyric, with tabular, euhedral phenocrysts comprising upwards to 20-vol%. In thin section, feldspar phenocrysts are strongly altered to sericite leaving only relict mm-sized tabular outlines in a groundmass of quartz + albite + sericite + chlorite + carbonate.

Volcaniclastic lithofacies

Volcaniclastic deposits are composed of numerous 2-4 m-thick lapilli tuff and 2-14 m-thick tuff breccia beds with fine-grained tuff beds conspicuously absent (**Table 13; Figure 97**). Surficial weathering gives this facies a cream to orange hue, but on fresh surfaces, they are more a dull gray. On weathered outcrops, where contacts are not exposed, numerous transitions from clast- to matrix-supported facies imply bedding, but when observed, grading (**Figure 97**) and erosive features (**Figure 98**) suggest a southward younging direction.

Two distinct fragment types are recognizable based on morphology, grain size and texture. Angular fragments are lapilli- to tuff-sized with rare breccia-sized clasts. Occasional flow-banded (**Figure 99**) and chert-like varieties are also included in this group. Mineralogically, these fragments are composed of 3-vol% feldspar and 2-vol% quartz phenocrysts. Subrounded fragments are typically breccia-sized and are characterized by quartz-amygdules up to 33-vol% (**Figure 100 and Table 8**) and 10-25-vol% tabular, euhedral feldspar phenocrysts that are altered to sericite. Other features include jigsaw patterns (**Figure 101**) in clast-supported beds and *in situ* fractures (**Appendix A-17**).

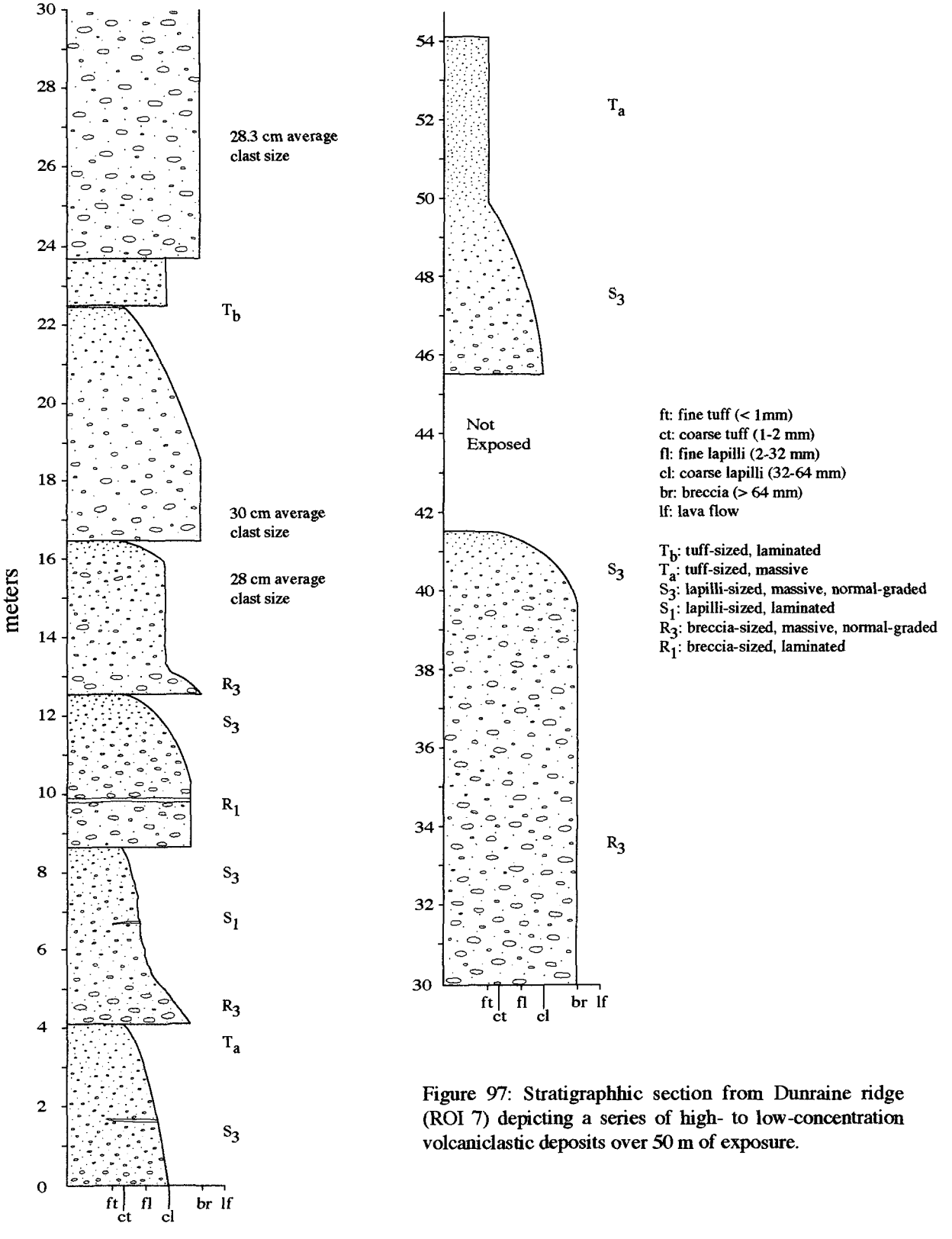

Figure 97: Stratigraphhic section from Dunraine ridge (ROI 7) depicting a series of high- to low-concentration volcaniclastic deposits over 50 m of exposure.

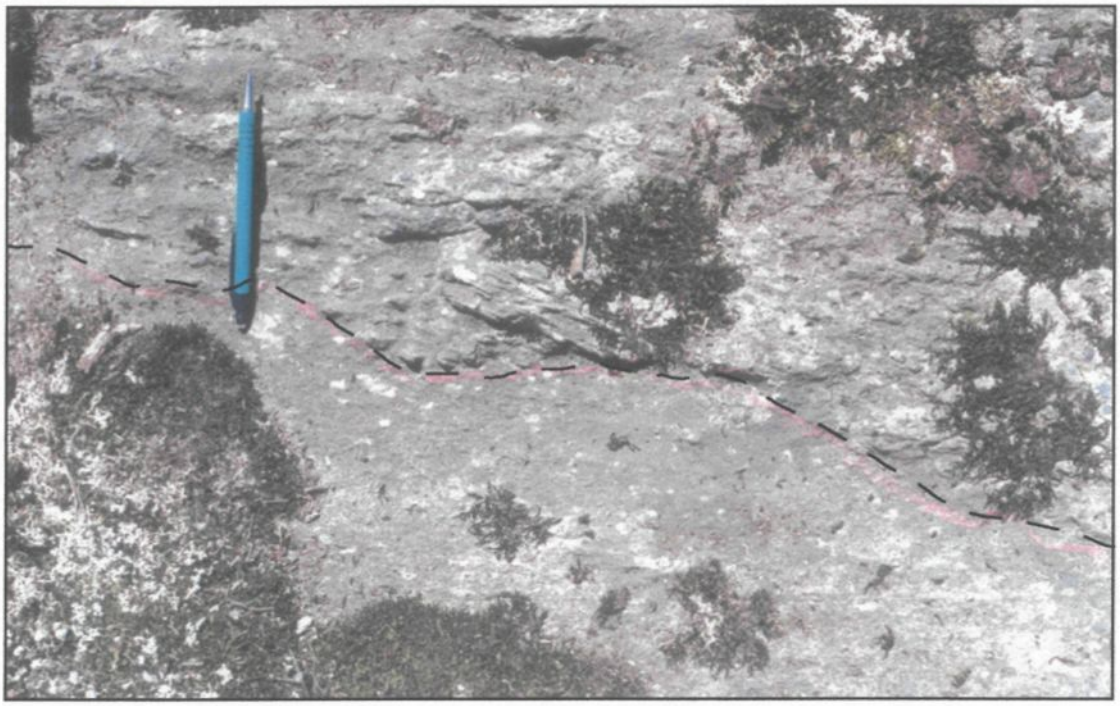

Figure 98: Erosive contact between underlying tuff breccia and lapilli tuff (dashed line) indicating tops to the south (pencil points to the north; 14.5 cm long).

Figure 99: Subrounded, flow-banded (thin, dashed lines), breccia-sized fragment (outlined). Pencil for scale (14.5 cm long).

Figure 100: Subrounded, vesicular, breccia-sized fragment from tuff breccia bed. Pencil for scale (14.5 cm long).

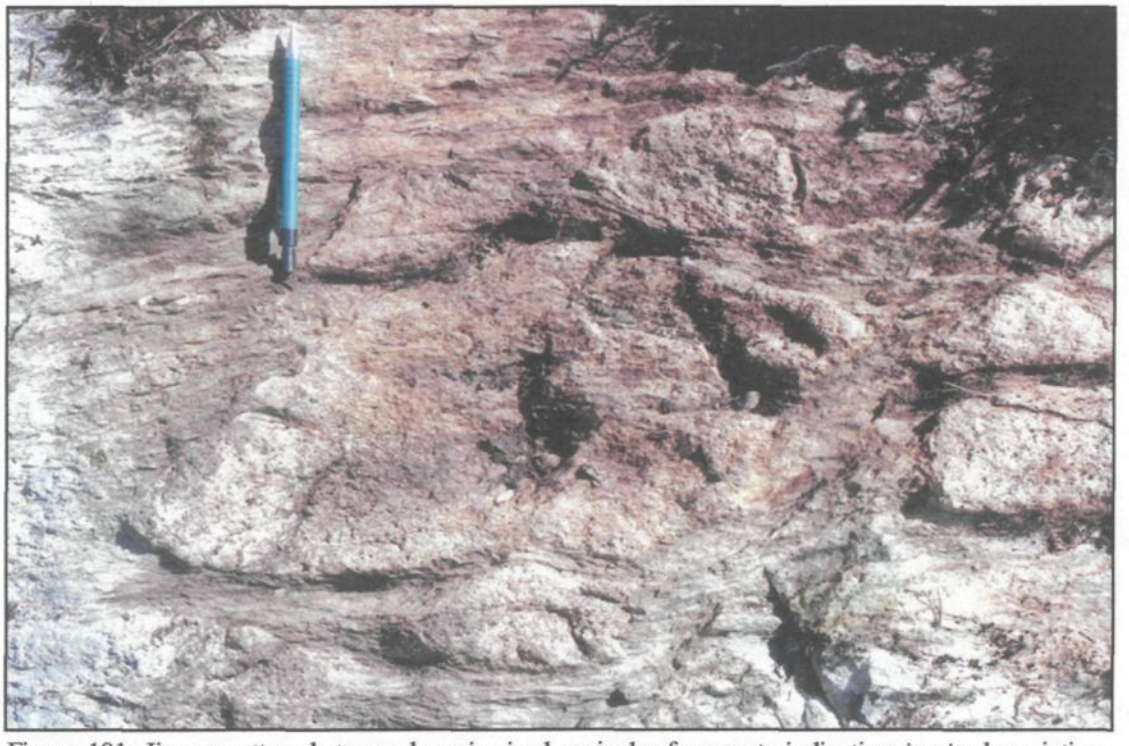

Figure 101: Jigsaw-pattern between breccia-sized vesicular fragments indicating *in situ* brecciation. Pencil for scale (14.5 cm long).

Fragment contacts are commonly sharp, but irregular, having a wispy, serrated appearance (**Appendix A-18; Figure 102**). Rare lapilli-sized sulfidic fragments are observed more to the west associated with a wider gossan zone (**Figure 103**). The matrix is altered to a fine-grained mosaic of chlorite + sericite ± quartz ± albite ± carbonate with upwards to 10-vol% tabular feldspar phenocrysts.

Intrusive phase

The felsic intrusion is restricted to the southeast part of the area with a curved termination towards the west (**Figure 94**). Weathering masks its crystalline nature on surface as it has an uniform cream to off white coloration, and is strongly foliated. On fresh surfaces, it varies from very fine grained to medium grained, composed of 30-60-vol% feldspar, 2-5-vol% quartz, and 5-20-vol% hornblende, with the remaining groundmass being altered to chlorite. No contact relationships between other facies are observed.

Deformation

Deformation is weak to strong in the region depending on proximity to the Dunraine shear zone. The felsic intrusion (Dunraine Sill) is highly sheared as it is bordered to the south by the shear zone. Other localized areas showing varying degrees of deformation are probably associated with smaller shear zones (**Figure 85**).

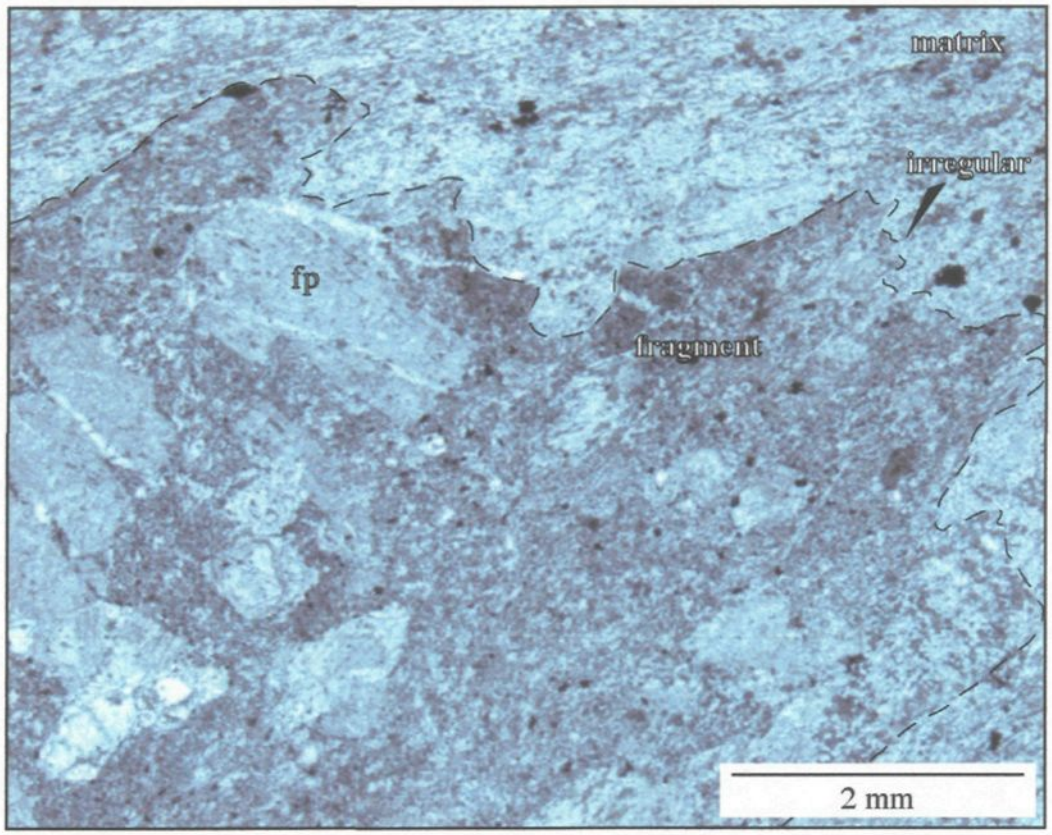

Figure 102: Plane polarized microphotograph of irregular feldspar-phyric (fp) lapilli fragment in recrystallized matrix.

Figure 103: Field photo of mineralized zone hosted in volcaniclastic facies. Hammer for scale (35 cm-long)

4.2.2.2 Interpretation of Dunraine East

The ubiquitous sheared or fractured morphology of the extrusive felsic facies may be a primary feature of these high viscosity of lava flows (Gibson, 1999a). One can argue such shearing is an artifact of regional deformation, particularly as there are various identified shear zones within the field area; however, observed flow bands support at least some synchronous deformation during viscous flow (Yamagishi and Dimroth, 1985). Furthermore, the *in situ* brecciation observed between the contact of the two felsic phases (**Figure 95B**) probably resulted during penecontemporaneous eruption of the more massive felsic phase as it intruded into the earlier felsic lava. Such interactions are associated with cryptodomes or small felsic domes as fresh lava intrudes into previously erupted lava (Gibson et al., 1997). In actuality, the vesicular, but massive nature of second felsic lava, was probably intruded rather than extruded onto the ocean floor, as vesicular felsic lavas are more apt to be fragmented due to violent disintegration. In the southwestern felsic facies, the felsic lava acts as an impermeable layer that seals a minor hydrothermal system resulting in the observed gossan within the permeable volcaniclastic sequence (**Figure 103**).

The intermediate facies, while not volumetrically significant, has a similar mineralogy to the principal fragment population of the volcaniclastic sequence, minus the vesicularity. Nonetheless, this underlying lava may represent the massive part *before* volatiles exsolved in the melt. Once volatiles began to exsolve, a more energetic eruptive phase is possible, probably through a series of "fragmental" events that could result in the deposition of these amalgamated volcaniclastic rocks.

The amalgamated volcaniclastic facies records a succession of events that can be attributed to, in this case, either primary or secondary (e.g., epiclastic) transport of volcanic fragments. The different morphological and textural characteristics (e.g., subrounded versus angular) associated with a varying size range probably indicate different fragmentation controls. Angular lapilli- to tuff-sized fragments are interpreted to be more 'felsic' in composition, which would imply a more viscous lava that is more apt to disintegrate more violently. The flow-banded nature of some angular fragments supports such viscous conditions (Yamagishi and Dimroth, 1985; Gibson et al., 1999). In contrast, subrounded, vesiculated, breccia-sized fragments may characterize a fire fountain or boil-over type eruption involving lower viscosity lava. Evidence of hot emplacement is absent (i.e., chilled margins), but their subrounded morphology could imply either plastic deformation (i.e., "warm" emplacement), or attrition. However, *in situ* fractures and jigsaw fit suggest limited transport favoring *in situ* plastic deformation. In addition, the low volume of fine-grained tuffaceous beds (**Figure 97**) further supports an inefficient fragmentation process, which is typically related to suppressed volcanic eruptions. In the subaqueous environment, this suppression is in the form of elevated hydrostatic pressures that restricts both the rapid expansion of volatiles and efficient mixing between lava and water.

Transport and deposition of these volcaniclastic deposits was from water-supported sedimentary gravity flows. The massive basal beds probably represent deposition from cohesive debris flows within the laminar flow regime (Lowe, 1982). As the grain-size decreases, grading and weak stratification is developed indicating a transformation to more turbulent conditions, whereby deposition was from high- to low-concentration turbidity

flows (Lowe 1982). Grading and stratification in lapilli tuff beds was from high-concentration S_3- to S_1-type turbidity flows, respectively. Likewise, grading and scouring in tuff breccia beds was from high-concentration R_3- to R_1-type turbidity flows, respectively. Deposition was by suspension (S-R_3) and traction (S-R_1; Lowe 1982).

4.2.3 Abitibi Copper area (ROI 8)

The Abitibi Copper region is named for a small base metal showing located south of highway 117 along old back roads (**Figure 85; ROI 8**). This area forms part of the central pyroclastic belt, outlined by Sharpe (1968), and mapped as being composed of mafic to felsic volcanic rocks of effusive and explosive origin. Mapping by Aur Resources recognized three volcanic units across the property (cf. Chartrand and Moorhead, local field guide). Only one unit was examined in detail based on exposure and access (**Figure 104A**). This volcanic unit measures over 500 m in thickness with a southward younging direction (discussed below) that evolves from a massive intermediate lava and capped by a cherty tuff facies (**Figure 104A**).

4.2.3.1 Lithology and stratigraphy of Abitibi Copper

The examined volcano-sedimentary unit includes intermediate and felsic lavas, volcaniclastic facies, and a possible sedimentary facies (**Table 14**). The volcaniclastic facies are composed of numerous beds of lapilli tuff and tuff breccia that form several separate depositional packages.

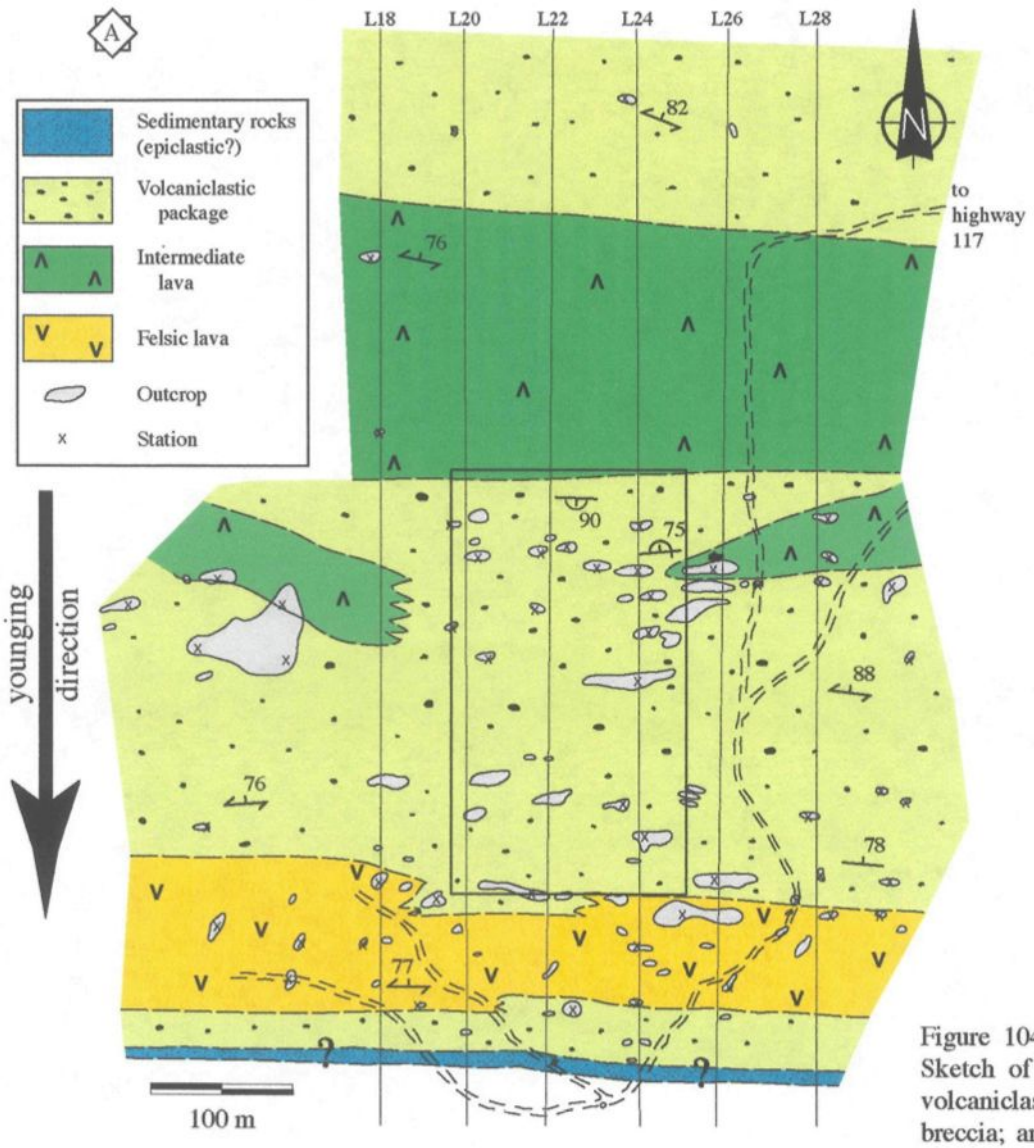

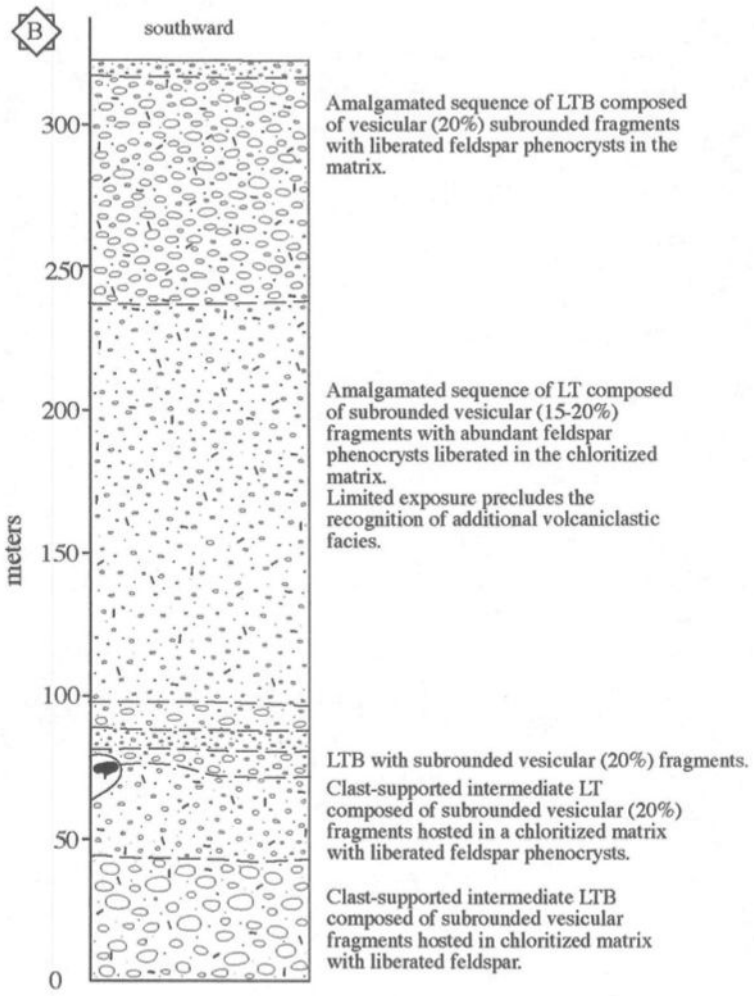

Figure 104: Simplified geology of the Abitibi Copper region. A. Sketch of contacts between major lithofacies and grain-size of volcaniclastic facies; where lb - lapilli breccia; ltb - lapilli tuff breccia; and l - lapilli. B. Outline of different volcaniclastic beds based on field observataions.

Table 14: Volcano-sedimentary lithofacies of the Abitibi Copper area (ROI 8).

Lithofacies	Thickness & morphology	Characteristics	Transport/deposition	Origin
Volcanic				
Felsic	60-100 m; lenticular sheet	Massive to *in situ* brecciation; irregular contacts; 10-vol%, fine-grained euhedral, lath-shaped feldspar; minor mineralization (magnetite + pyrite + chalcopyrite); intense Fe-carbonate alteration	Lava flow with brecciation due to internal shearing or contact with external water	Small volume effusive to hypabassal felsic lava
Intermediate	30-140 m-thick; sheet-like	Northern flow is massive and continuous; porphyric with 10-vol% feldspar and hornblende Two discontinuous lenses are massive to pillowed; 2-5-vol% feldspar; 5-10-vol% quartz amygdules	Lava flows with possible changes in viscosity and temperature forming pillows	Small volume, subaqueous effusive eruption
Volcaniclastic				
Lapilli tuff to tuff breccia (rare tuff)	300 m-thick	Three depositional packages; clast- to matrix-supported; normal-graded (S-R_3) and erosive (S-R_1) Fragments: subrounded; chilled margins; 5-10-vol% feldspar; up to 40-vol% quartz amygdules; perlitic fractures Matrix: 20-vol% feldspar	Eruption-fed, water-supported, high-concentration turbidity to cohesive debris flows; fragments were emplaced hot	Gas-rich, fire-fountaining eruption that generated large fragments; limited hydrovolcanic fragmentation

Volcanic lithofacies

The felsic facies forms a 60-100 m-thick lenticular deposit. Contacts, while not observed, are irregular with lower and upper facies based on vertical and lateral facies changes over several meters (**Figure 104A**). Commonly massive, but locally fragmented, possibly due to *in situ* brecciation (**Figure 105; Appendix A-19**). Only 10-vol% fine-grained, euhedral, lath-shaped feldspar is observed (**Figure 105B**) with some mineralization along the southern contact in the form of magnetite, pyrite and rare chalcopyrite. On fresh surface, this facies has a dull gray color (**Figure 105A**), but it is dominated by iron carbonate alteration on weathered surfaces and within fractures.

Several intermediate lava facies are recognized, with only the northern facies being continuous, whereas two other intermediate lavas have limited exposure and irregular contacts with bounding facies (**Table 14; Figure 104A**). The northern unit is massive and porphyric, composed of 10-vol% of both feldspar and hornblende in a chloritized groundmass, and appears to be continuous and approximately 140 m-thick. The two discontinuous units are stratigraphically on the same level, but define individual lenses to the east and west of a thick volcaniclastic package. The western lens has an undefined shape, but does have a sharp contact with an overlying (south) lapilli tuff volcaniclastic deposit. It has a massive nature with 2-vol% feldspar microphenocrysts and 10-vol% quartz amygdules. The eastern lens is characterized by a transition from massive to pillowed from east to west. Pillows have 5-vol% quartz amygdules and 2-5-vol% feldspar microphenocrysts. Pillow morphology indicates a south younging direction (**Figure 106**).

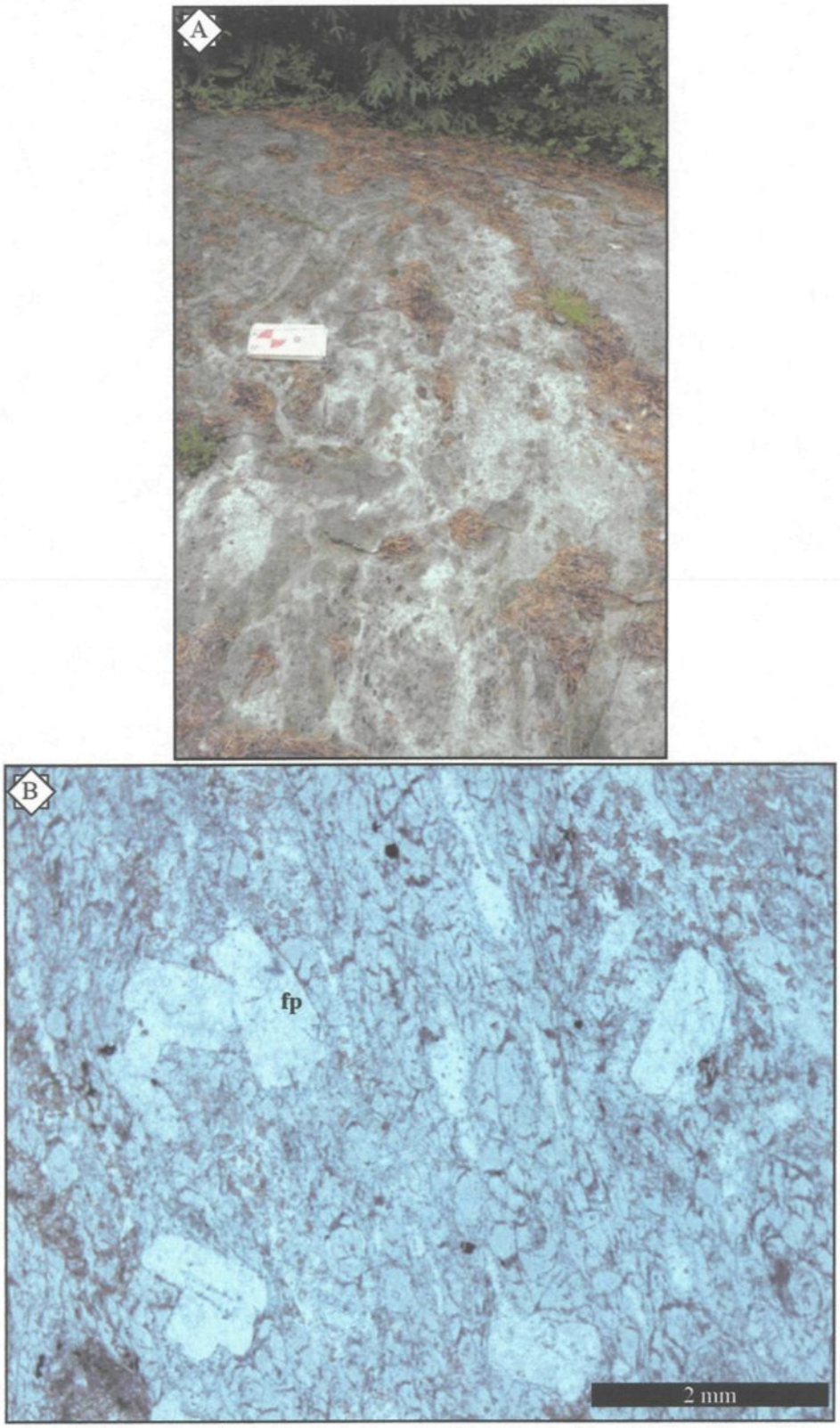

Figure 105: Images of felsic lava facies. A. *In situ* brecciation of felsic lava, fieldbook for scale (17 cm long). B. Plane polarized light photomicrograph of *in situ* brecciation and tabular, euhedral feldspar (fp) phenocrysts.

Figure 106: Meter-sized, bun-shaped, intermediate pillow indicating tops to the south (arrow). Fieldbook for scale (17 cm long).

Figure 107: Series of bedded tuff turbidites ranging from fine tuff (Tc) to fine lapilli (Ta) beds. Pencil for scale (14.5 cm long).

Volcaniclastic lithofacies

Three volcaniclastic depositional packages are recognized in the mapped section (**Figure 104A**). The northern sequence has limited exposure, but is dominantly a lapilli tuff with isolated breccia-sized fragments. Beds are locally clast-supported and normal-graded. Individual beds are not recognized, but grain-size variations between outcrops suggest a multiple depositional history. Fragments are monolithic and subrounded, with upwards to 20-vol% quartz amygdules. The matrix is chloritized with 5-10-vol% feldspar phenocrysts.

The southern sequence is only observed in one outcrop, stratigraphically above the felsic lava facies (**Figure 104A**). This facies is fine-grained with rare breccia-sized fragments and characterized by a strongly carbonized matrix.

The middle 300 m-thick volcaniclastic deposit is composed of an amalgamation of lapilli tuff to tuff breccia and rare tuff beds (**Figures 104B and 107**). Beds are typically clast-supported, normal-graded with possible truncated and erosive features (**Figures 107 and 108**). Clasts are typically subrounded and have jigsaw fitting textures (**Figure 109**). Vesicularity is represented by up to 40-vol% quartz amygdules, with one point count in thin section having 35.25-vol% quartz + carbonate amygdules. Vesicles are also sometimes oriented perpendicular to chilled margins (**Figure 110**). Feldspar crystals are between 5-10-vol%. Fragments have sharp, but irregular contacts with the matrix, some being highly irregular to elongated in nature (**Figure 111**). Smaller angular and curvilinear fragments are probably former glass shards, which are sometimes molded around liberated feldspar phenocrysts and characterized by perlitic fractures (**Appendix A-20**). The matrix is chloritized with abundant feldspar phenocrysts (**Appendix A-20**; max. 20-vol%).

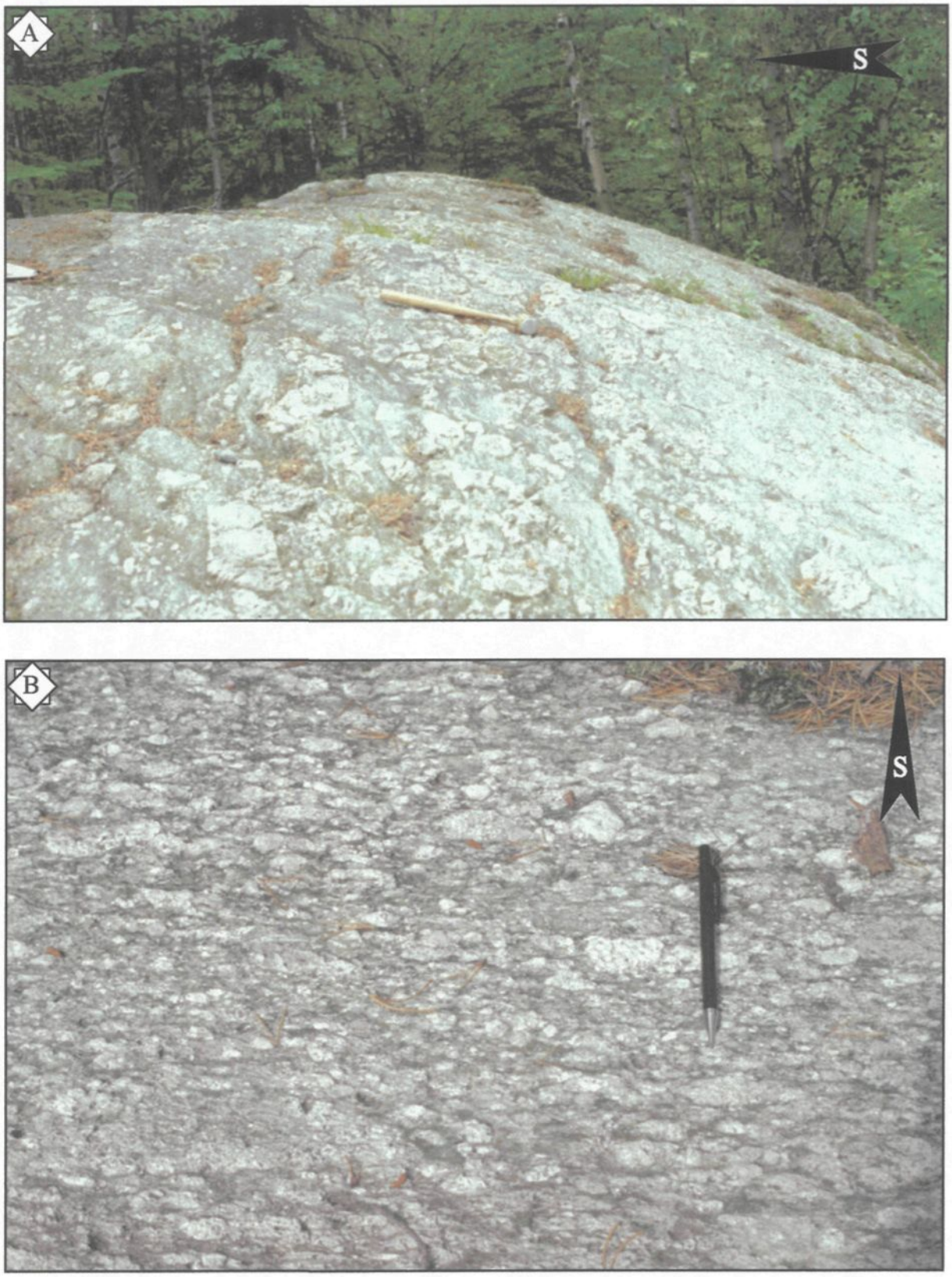

Figure 108: Outcrop photos of clast-supported beds; A. tuff breccia and B. lapilli tuff beds. Hammer (37 cm long) and pencil for scales (14.5 cm long). Tops to the south (arrows)

Figure 109: Closeup of clast-supported, vesicular breccia fragments having jigsaw-fitting texture. Fieldbook for scale (17 cm long).

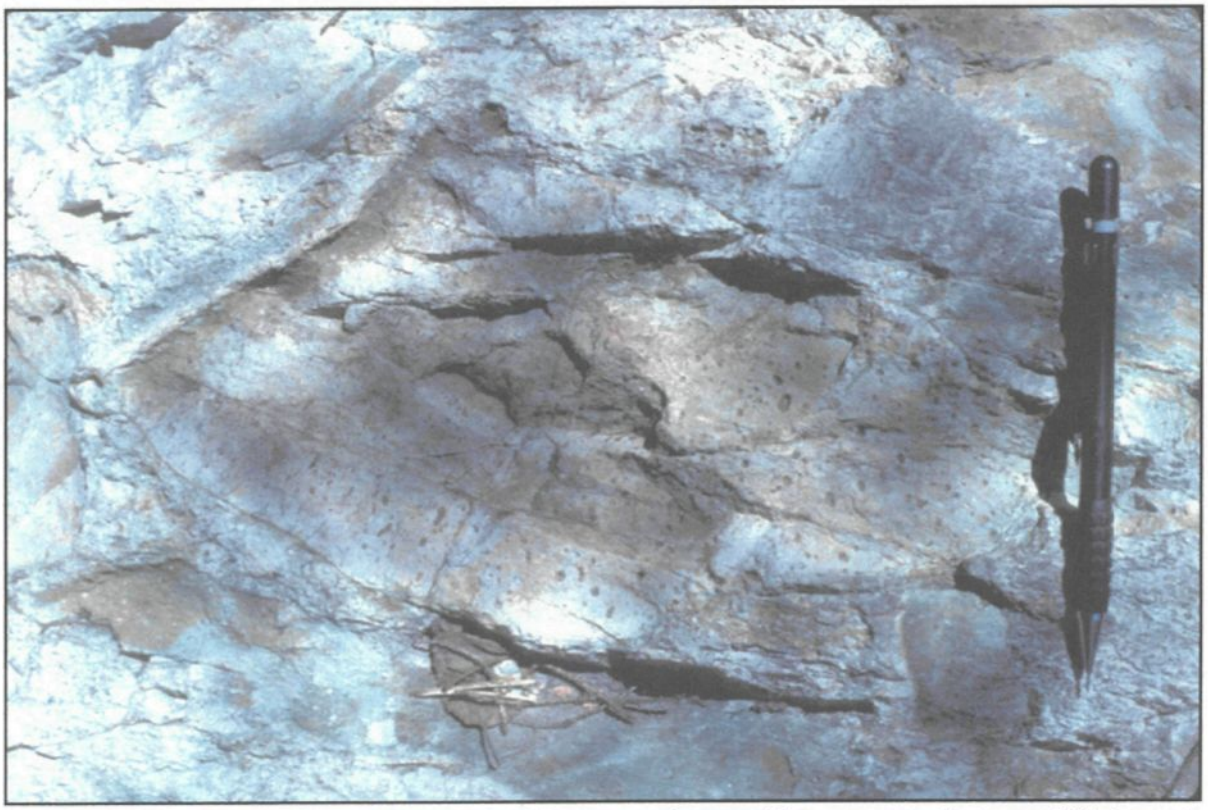

Figure 110: Subrounded, vesicular, breccia-sized fragment, where vesicles are perpendicular to chilled margin. Pencil for scale (14.5 cm long).

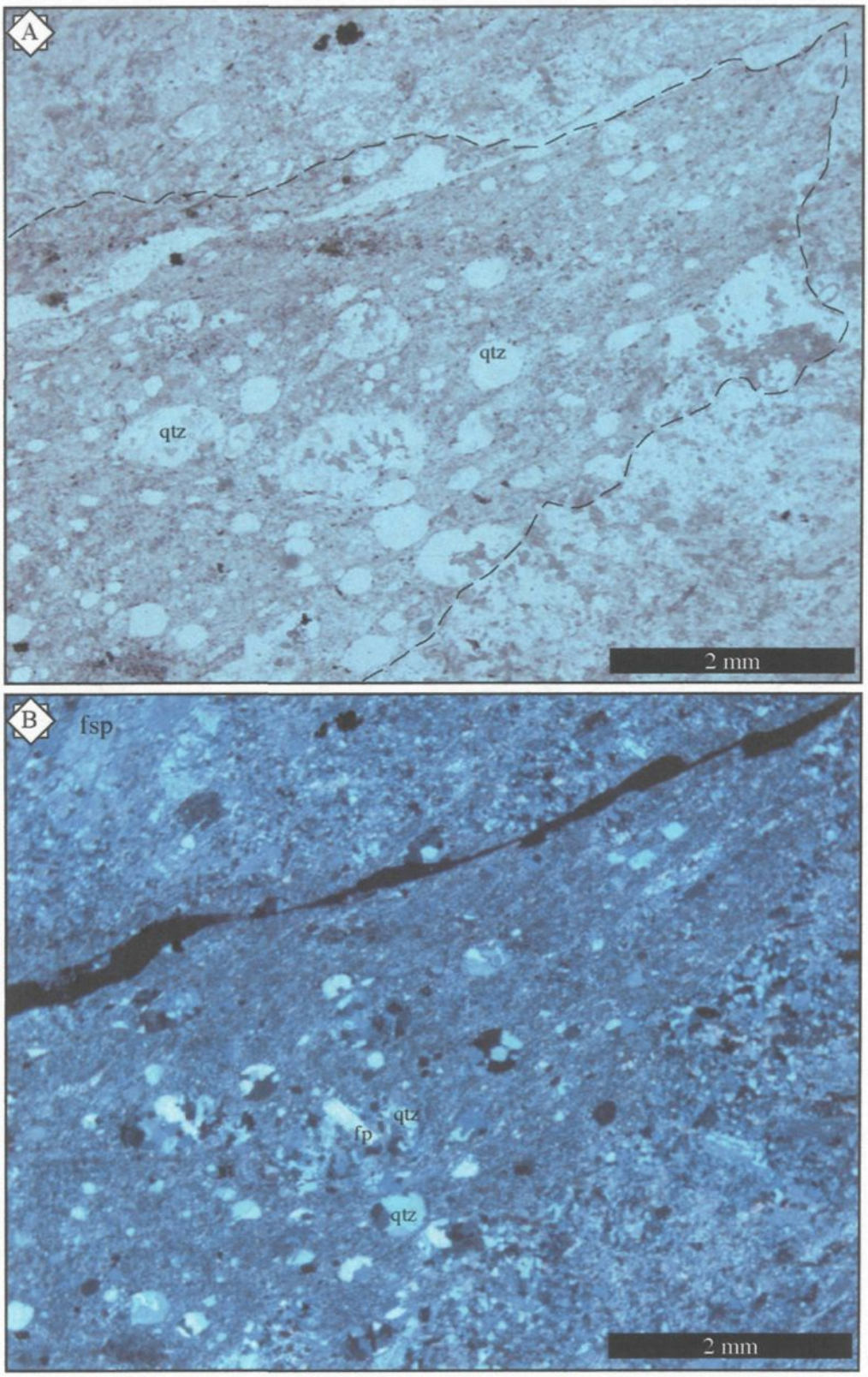

Figure 111. Photomicrographs of vesicular fragment in: A. Plane polarized light and B. Crossed nicols. Fragment has a distinct serrated to wedged shape, with oval quartz amygdules (qtz) and tabular feldspar (fp) phenocrysts. Feldspar (fsp) phenocrysts are also observed in the matrix.

4.2.3.2 Interpretation of Abitibi Copper stratigraphy

The morphology and thickness of the felsic facies suggests that it is either a lava flow, or hypabassal intrusion (sill). *In situ* brecciation implies shearing or interaction with external water, but does not preclude a deformation origin.

The intermediate lava and thick volcaniclastic facies probably represents a near compete eruptive cycle. The massive, non-vesicular intermediate lava may record initial expulsion onto the seafloor at elevated temperatures and pressures. High temperatures and pressures impart a lower viscosity, which in turn inhibits pillow formation, as well as suppresses the exsolution of any volatiles in the melt (which also allows the crystallization of hydrous hornblende). The lavas porphyric nature is a possible result of its thickness, which insulted the flow, permitting low degrees of undercooling and promoted crystallization; a similar mechanism was theorized by Manley and Fink (1987) for spherulitic zones in thick felsic lavas. Overlying intermediate lavas are possible appendages. Both these lavas are vesiculated, with lower crystallization, which can attest to decompression higher in the stratigraphy allowing volatiles to exsolve. This could also increase the viscosity, which when coupled with their thin nature, resulted in the formation of pillows, as is the case for the eastern section.

The thick amalgamated volcaniclastic unit chronicles the explosive disruption of the intermediate lava. Crystallinity and monolithic character suggest that these volcaniclastic deposits are genetically related to the intermediate lavas. Vesicularity of fragments increases upwards to 40-vol% as a function of decompression as volatiles exsolved and expanded. Exsolution of volatiles would provide the driving force for a magmatic eruption.

The variations from lapilli- to breccia-dominant beds may record changes in eruptive style. Subrounded, clast-supported, breccia-dominant beds imply inefficient fragmentation. These beds are probably produced during fire-fountaining episodes. Fire-fountaining eruptions typically form coarser-grained ejecta that is ballistically emplaced in proximity to the vent (ref). These eruption-fed fragments are subsequently transported as a water-supported, cohesive to high-concentration turbidity flow(s) (Lowe, 1982; White, 2000). Transport and deposition was coincident with fragmentation, as plastic deformation, chilled margins and perlitic fractures attest to hot emplacement. In addition, the 90° orientation of vesicles with chilled margins suggest they exsolved after fragmentation, therefore the fragment was hot for an extended period of time. At this stage, water was inhibited from direct contact with fragments owing to the generation of an insulating steam jacket (Kokelaar, 1986). Lapilli- to tuff-sized fragments suggest a more efficient fragmentation mechanism. This may occur due to water ingestion and instantaneous vaporization as steam jackets collapse, resulting in phreatomagmatic explosions (ref). Collapse and transport by water-supported, high- to low-concentration S- and T-type turbidity flows resulted in graded and erosive beds (Lowe 1982). The abundance of liberated euhedral feldspar phenocrysts in the matrix suggests that they were removed from the melt *during* fragmentation, not during weathering/erosion processes.

4.2.4. Sleepy Lake area (ROI 9)

The Sleepy Lake region (**Figure 85, ROI 9**) is subdivided into eastern and western sectors and forms part of a past exploration project by Placer Dome Inc. Work was

concentrated in the easternmost sector as previously stripped outcrops provide exposure in an area covered by extensive glacial till. This area is located approximately 2100 m south of the Bevcon Pluton and 1800 m west of the town of Louvicourt, along the NW shores of Sleepy Lake (**Figure 85**).

4.2.4.1. Lithology and stratigraphy of Sleepy Lake area

The main feature of the Sleepy Lake area is a series of three stripped outcrops, exposed as part of a past exploration project. These stripped areas, together with other outcrops in and around these zones, permit construction of the general stratigraphy of the area. This construction reveals a felsic-rich region; including massive felsic lavas, and numerous felsic volcaniclastic deposits (**Table 15; Figure 112**).

Volcanic lithofacies

Felsic facies are exposed at five different stratigraphic levels, although only two are continuous. The three discontinuous felsic facies are characterized by a lobate morphology and distinct flow banding, pipe vesicles, or columnar joints (**Figure 113**). All felsic facies are massive and vary from homogeneous (**Figure 113**) to a more classic *in situ* breccia (**Figure 115**) façade. Most are aphyric, although 5-vol% quartz is locally present. Columnar joints are observed in m-sized lobes and have elongated vesicles oriented semi-perpendicular to their edges (**Figure 113**). This and other felsic lobes are outlined by distorted bedding planes in juxtaposed tuff deposits (**Figures 112 and 114**) or have curvilinear flow bands within its leading edges (**Figure 116**). Orange surface weathering is

Table 15: Volcano-sedimentary lithofacies of the Sleepy Lake area (ROI 9).

Lithofacies	Thickness & morphology	Characteristics	Transport/deposition	Origin
Volcanic				
Felsic	10-30 m; tabular to lobate	Massive to *in situ* breccia; columnar jointed; flow banded; elongated to pipe 0-25-vol% vesicles; aphyric with local 5-vol% quartz; minor mineralization (disseminated pyrite + Fe-staining)	Effusive lava flows and endogeneous lobes into unconsolidated sediments; sediments insulated lava to developed columnar joints	High temperature eruptions of lava flows and hypabassal intrusions (dome complex)
Volcaniclastic				
Tuff turbidite	70 m; finely bedded	Series of m- to cm-thick beds; normal-graded; synsedimentary features include load clasts; faulting; flame structures, and ball and pillow structures; ripples; laminations; convoluted bedded; cherty and vesicular (> 25-vol%) fragments	Rapid emplacement of a series of low- to high-concentration turbidity flows; fallout and/or remobilization; load pressure causes dewatering and synsedimentary features	Phreatomagmatic eruption related to felsic lavas or distal pyroclastic event.
Lapilli tuff	15-50 m	Subangular to subrounded fragments; massive to weakly stratified; 10-50-vol% quartz amygdules; < 5-vol% feldspar	Water-supported cohesive to high-concentration turbidity flows	Phreatomagmatic eruption of volatile-rich lava
Tuff breccia	80 m	Massive; subrounded to subangular flow banded fragments; *in situ* brecciation; jigsaw patterns; non-vesicular; large m-sized rafts	Massive debris flows; *en masse* frictional freezing	Autobrecciation of felsic lava; remobilization of felsic carapace

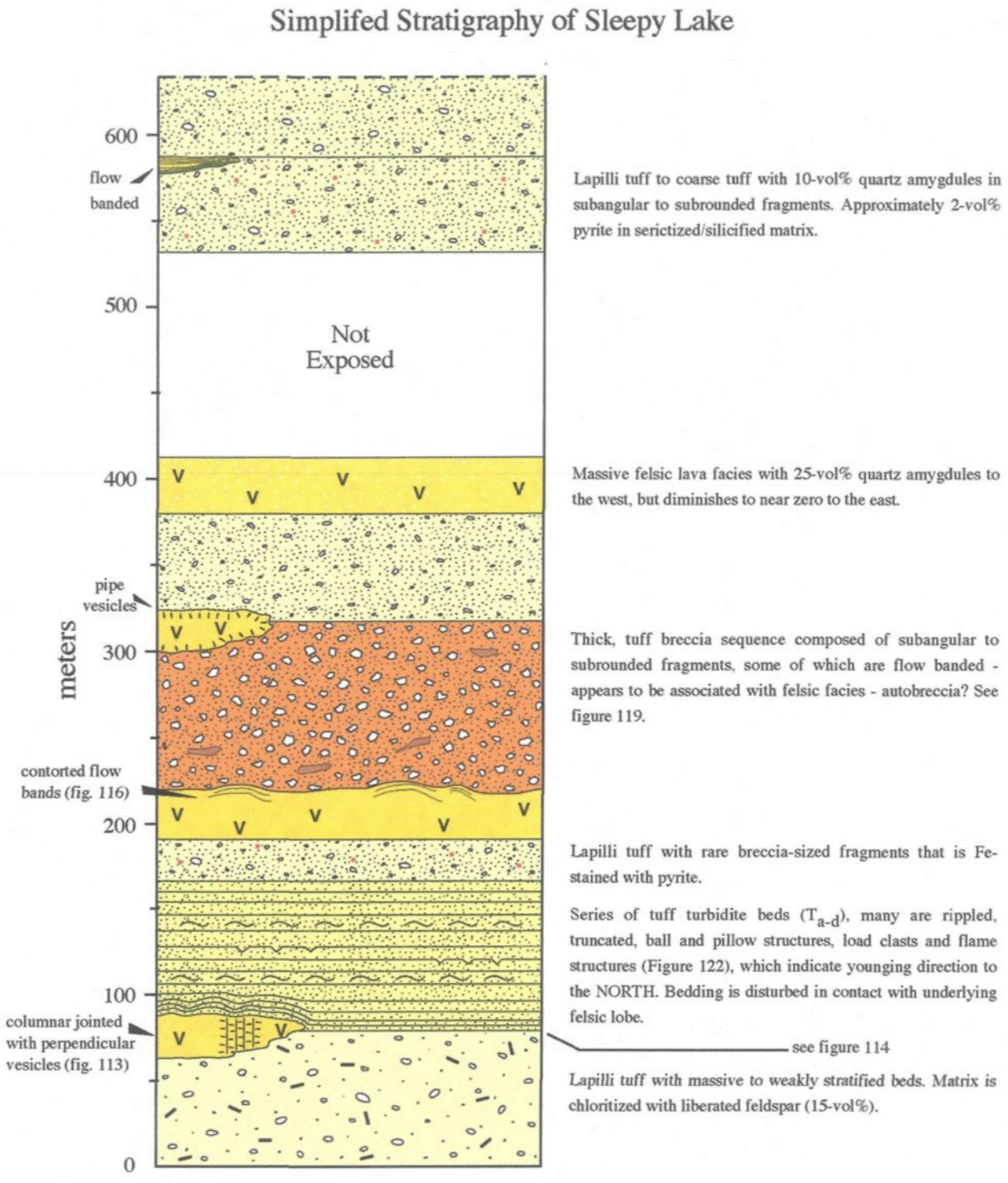

Figure 112: Simplified stratigraphy of the Sleepy Lake area, which includes the three stripped outcrops.

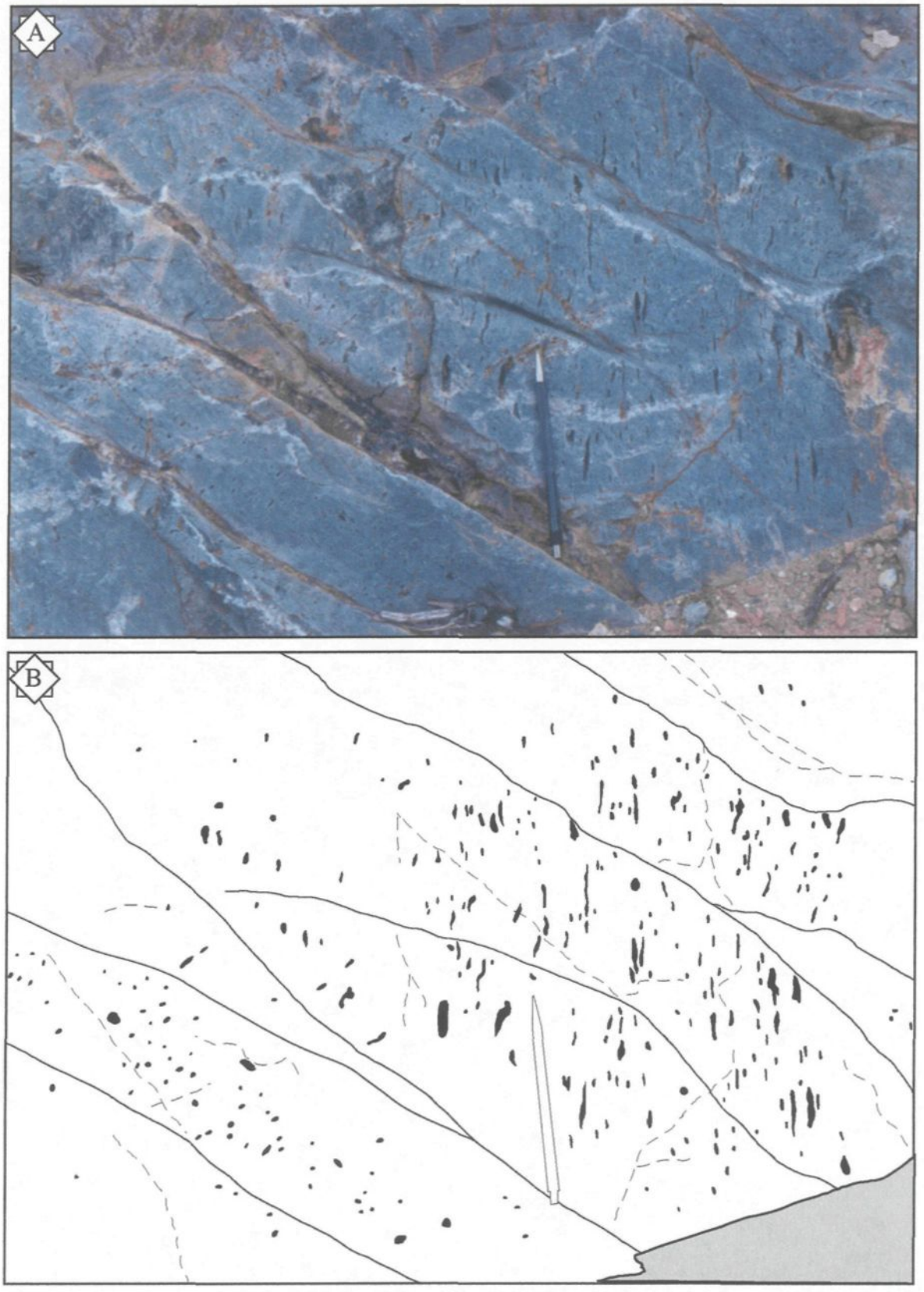

Figure 113: A. Massive, vesicular felsic lava lobe with well developed columnar joints and vesicles oriented perpendicular to cooling surfaces. B. Cartoon illustrating the relationship between columnar joints and vesicles. Dashed lines are fractures, solid lines differeniate individual joints and solid forms outline vesicles. Pencil for scale (14.5 cm long).

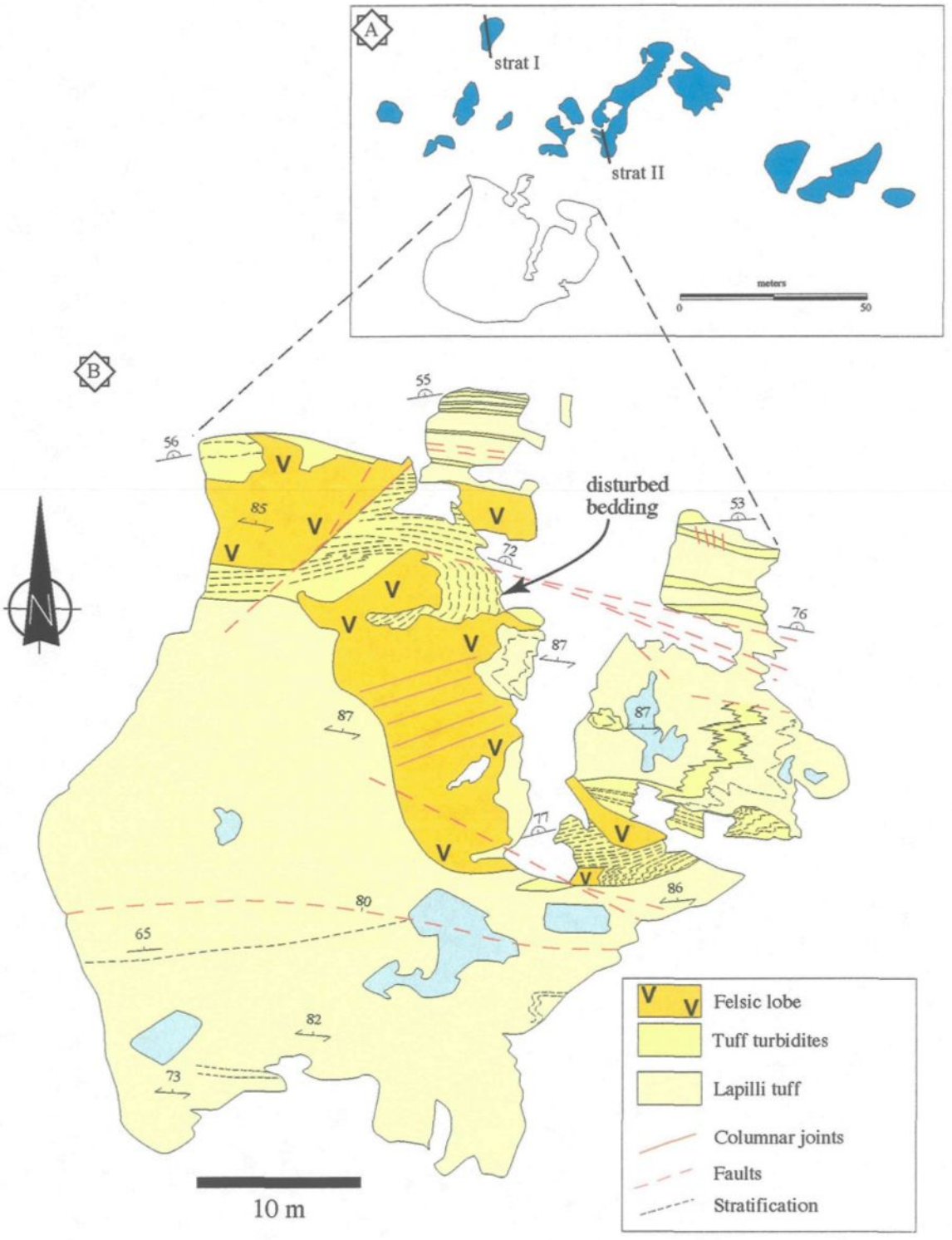

Figure 114: A. Outline of outcrops from stripped zone three in Sleepy Lake region (ROI 9). Location of stratigraphic sections (See Figure 122) are indicated. B. Detailed map illustrating contact relationships between felsic lobe and tuffaceous and intermediate volcaniclastic facies. Mapping done by Mueller and Pilote (1996).

Figure 115: Flow banded felsic lava that is brecciated in situ. Pencil for scale (14.5 cm long).

Figure 116: Irregular contact between flow banded felsic lava and felsic breccia. Flow bands are contorted in contact with breccia. Pencil for scale (14.5 cm long).

common due to minor mineralization, in the form of disseminated pyrite or basic iron staining. Vesiculation is upwards to 25-vol%, but can change radically along strike (**Figure 112**).

Volcaniclastic lithofacies

Felsic volcaniclastic deposits typically underlie and/or overlie felsic lavas (**Figure 112**). Three different depositional facies are recognized based on grain-size; (1) tuff breccia; (2) lapilli tuff; and (3) tuff turbidite facies (**Table 15**). The 80 m-thick tuff breccia forms a massive, clast-supported bed. Fragments range from subrounded to subangular flow banded (**Figure 117**) and chloritized varieties (**Figure 118**). Jigsaw fitting textures are common for both fragment types, but flow banded fragments are typically larger, some forming meter-sized rafts (**Figures 119 and 120**). Disseminated pyrite and chalcopyrite is localized along numerous faults that cut the brecciated sequence (**Figure 119**). No vesicles/amygdules are associated with this particular sequence.

The lapilli tuff facies measures between 15-50 m-thick at five different stratigraphic levels (**Figure 112**). In general, individual facies are matrix-supported and are highly altered by sericitization, silicification, or chloritization. Typically structureless and massive, but locally has weak stratification. Fragments are subrounded to subangular and have between 10-50-vol% quartz amygdules (**Figure 121**). Only 5-vol% tabular to blocky euhedral feldspar crystals observed. The matrix is altered to a fine-grained mosaic of quartz + chlorite + sericite + carbonate ± albite with 20-vol% liberated tabular/blocky, euhedral feldspar phenocrysts, some of which appear broken.

Figure 117: Subrounded, flow banded felsic breccia fragments in clast-supported felsic tuff breccia (see Figure 119). Pencil for scale (14.5 cm long).

Figure 118: Subrounded to subangular, chloritized, lapilli-sized fragments, part of *in situ* felsic tuff breccia (see Figure 119). Pencil for scale (14.5 cm long).

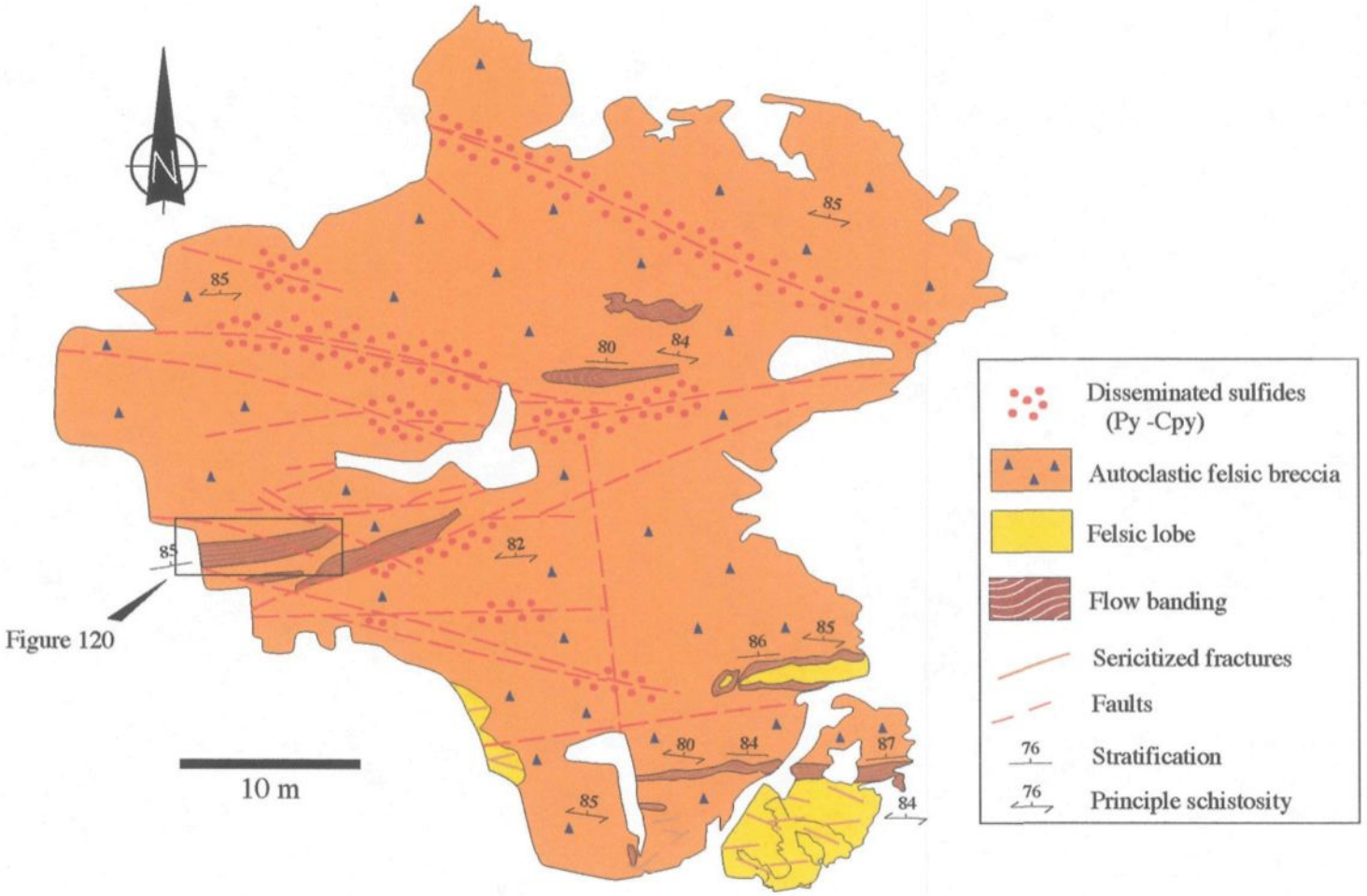

Figure 119: Detailed mapping of autoclastic felsic breccia capping lobate felsic facies. Mapping done by Mueller and Pilote (1996).

Figure 120: Large raft of flow banded felsic lava within autoclastic felsic tuff breccia (see Figure 119 for location). Pencil (outlined by black line) for scale (14.5 cm long).

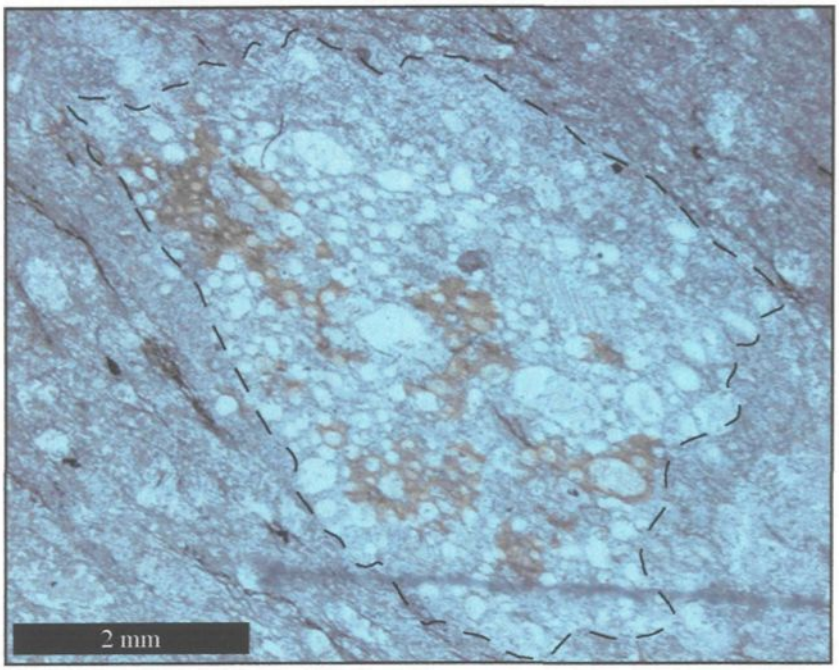

Figure 121: Photomicrograph in plane polarized light of subrounded, vesicular, coarse-lapilli fragment with 51.5-vol% quartz/carbonate amygdules, 4.25-vol% feldspar microphenocrysts and 44.25-vol% groundmass. Sampled from lapilli tuff facies.

The 70 m-thick tuff facies is an amalgamation of numerous m- to cm-thick, fine tuff to coarse lapilli tuff beds (**Figures 112 and 122**). This series forms a normal-graded and finely bedded tuff turbidite that has several fining upward sequences (**Figure 122**). Individual beds are characterized by synsedimentary features such as load clasts, faulting, flame structures, and ball and pillow patterns (**Figures 122C-E**), as well as erosive and truncated contacts (**Figures 122A-B**); all of which indicate a northward younging direction. Grading and sedimentary structures (i.e., ripples, laminations, etc) can be related to T_{a-e} Bouma beds (cf. Lowe, 1982). Surficial weathering varies with grain size, as fine tuff beds are typically reddish and chert-like in appearance (**Figures 122C-E**), whereas lapilli beds are more whitish-yellow or cream. Lapilli fragments are strongly altered and are either vesicular and aphyric or non-vesicular and porporphyric. Vesicular fragments are characterized by irregularly shaped, carbonate-filled vesicles (> 25-vol%) and chloritized rims (**Appendix A-21**), whereas non-vesicular fragments have approximately 5-vol% tabular, euhedral feldspar phenocrysts and sharp angular contacts with the sericite + carbonate + quartz + chlorite matrix.

4.2.4.2. Interpretation of Sleepy Lake area

The general stratigraphy of the Sleepy Lake area outlines a sequence of felsic lavas and intercalated volcaniclastic deposits. The tabular and lobate lava morphology may be controlled by their respective eruptive processes. The massive, aphyric nature of tabular lavas suggest transport via a high temperature flow extruded onto the seafloor. This interaction with water is supported by the overlying massive tuff breccia facies (**Figure**

STRATIGRAPHIC SECTION I

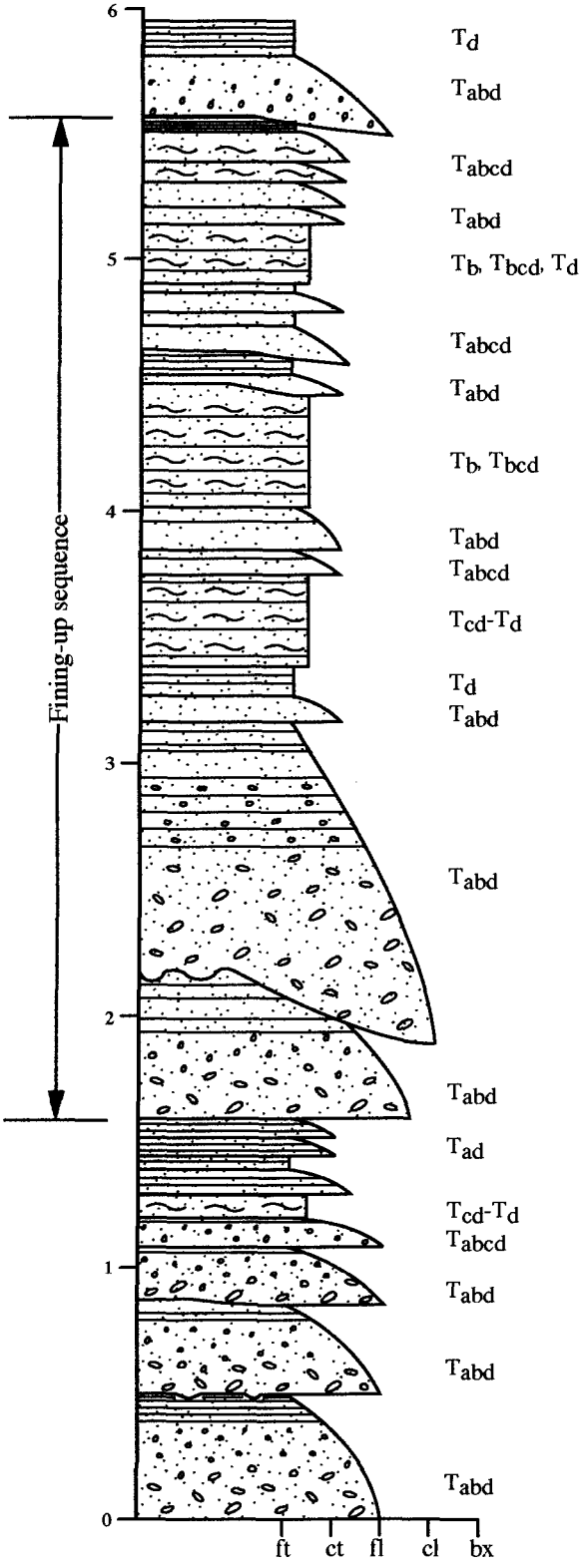

LEGEND

T a: massive, graded
b: plane parallel laminae
c: ripples, wavy laminae
d: upper parallel laminae

ft: fine-grained tuff
ct: coarse-grained tuff
fl: fine-grained lapilli tuff
cl: coarse-grained lapilli tuff
bx: breccia

ripple

load cast

Figure 122A: Stratigraphic section I from Sleepy Lake region (ROI 9) in a tuff turbidite sequence. Location shown in Figure 114. Mapping done by Mueller (1996).

STRATIGRAPHIC SECTION II

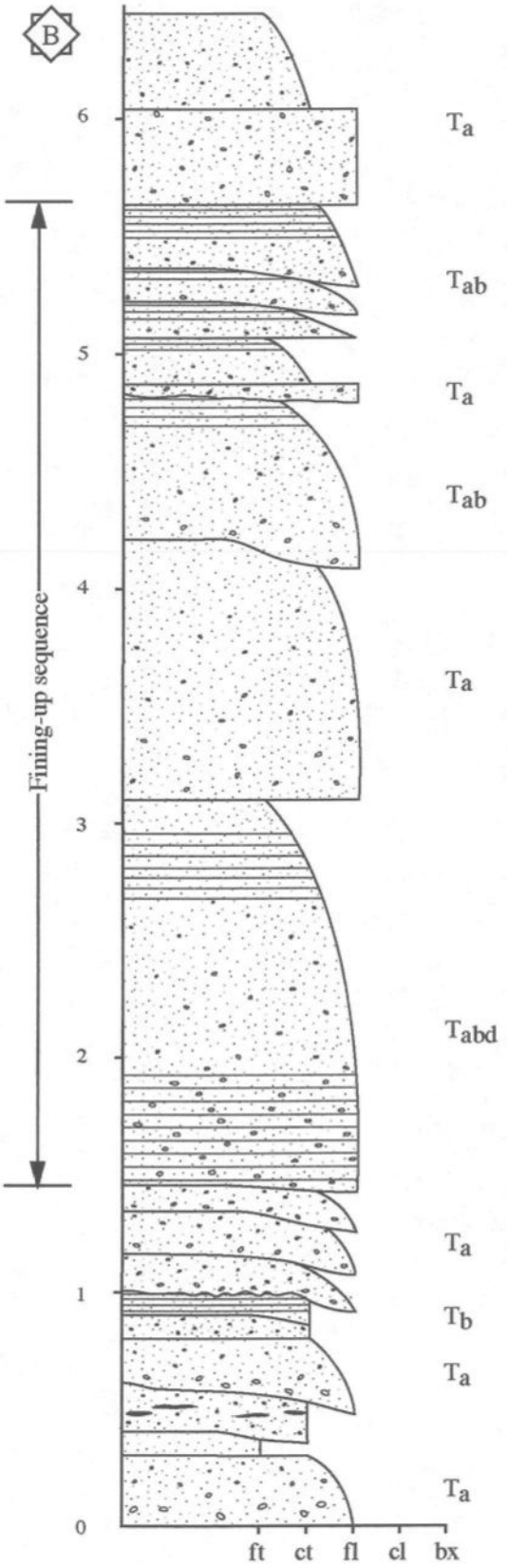

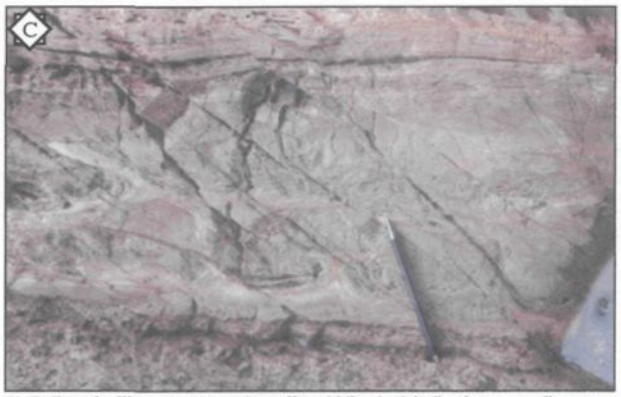

C. Ball and pillow structures in tuff turbidite bed indicating synsedimentary deformation and younging direction (north). Pen for scale (14.5 cm).

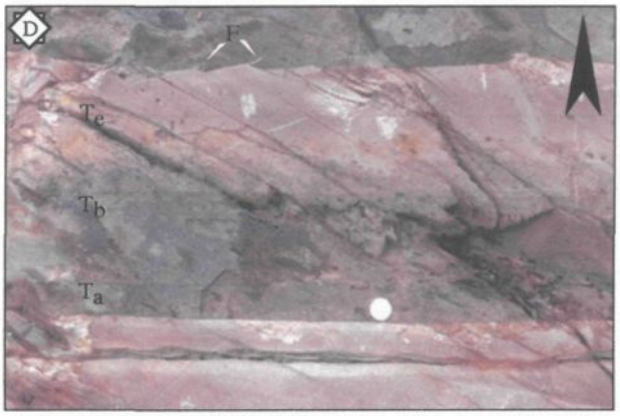

D. Flame structures (F) of tuff extending into overlying coarse tuff bed (T_a). Arrow points in younging direction (north). Quarter for scale (2.3 cm).

E. Numerous synsedimentary faults within tuff sequence along with ripples (R). Pen for scale (14.5 cm).

Figure 122B-E: B. Stratigraphic section II from Sleepy Lake region (ROI 9) in a tuff turbidite sequence. See Figure 122A for legend. C-E. Series of field photos showing the characteristics of the tuff beds.

112). Flow banded fragments, particularly large rafts, probably represent shedding of fragmented flow margins or remnants of disintegrated lobes due to autobrecciation and/or quench fragmentation (Kano et al., 1991; Scutter et al., 1998). Autobrecciation describes a non-explosive mechanism occurring after the lava has formed a cool rigid crust, which is subsequently disintegrated when the tensional stress exceeds the lavas tensile strength (Manley and Fink, 1987), via plastic or brittle means, due to continued movement of the lava, which typically produces *coarse* grained material (Cas, 1992). Quench fragmentation is also non-explosive, occurring when lava is rapidly chilled, resulting in fracturing due to thermal stresses producing *fine* grained material called *hyaloclastites* (Fisher and Schmincke, 1984). Furthermore, distorted flow bands in contact with the tuff breccia record plastic deformation, indicating a temporal relationship between the two facies.

Lobate felsic lavas are more consistent with synvolcanic inflation of lava (Duffield, 1990) into unconsolidated material (Kano et al., 1991; Gibson, 1999). Bedded tuffs are deformed in contact with the intruded lava (**Figure 114**), however, the absence of felsic hyaloclastites imply that the sediments, while unconsolidated, were dry. Flow bands also suggest that the lava was viscous during emplacement (Yamagishi and Dimroth, 1985; Gibson et al., 1999). The development of columnar joints in a m-sized lobe is facilitated by the insulating effect of the enclosing tuffs. Gas exsolved after initiation of columnar joints as suggested by the perpendicular orientation of vesicle to joint cooling surfaces (**Figure 113**).

The various felsic volcaniclastic lithofacies are associated with different felsic lavas. The tuff breccia facies represents a carapace breccia to a massive, flow banded felsic lava

flow (**Figure 119**). The predominance of coarse grain sizes implies that autobrecciation was the dominant fragmentation mechanism (Cas, 1992), although synchronous quench fragmentation was probably important. The clast-supported and jigsaw texture along with the angular to subrounded flow banded fragments (**Figures 117 and 118**) is testament to brittle and plastic *in situ* autobrecciation, respectively (Cas, 1992). The absence of stratification suggests that these deposits were transported as massive debris flows within the laminar flow regime (Lowe, 1982).

The massive to weakly stratified nature of the lapilli tuff lithofacies imply transport by water-supported, cohesive to high-concentration turbidity flows that ranged from laminar to turbulent, respectively (cf. Lowe, 1982). The relationship between the various facies is ambiguous, but the abundance of liberated, broken feldspar phenocrysts in the matrix, and pumiceous lapilli- to tuff-sized fragments suggest a violent beginning. Disturbed stratification and interbedded nature suggest a temporal relationship to overlying felsic lavas and tuffs (**Figures 112 and 114**). The subrounded and weakly flattened nature of pumiceous fragments hint at very weak compaction, but other features suggestive of hot emplacement, such as columnar jointing (Scott et al., 2003), are absent.

The 70 m-thick tuff turbidite sequence has an uncertain origin, but was probably emplaced by a series of water-supported, low concentration turbidity currents based on observed sedimentary structures (cf. Lowe, 1982). The various synsedimentary features (i.e., flame structures, etc) indicate soft sediment deformation that typically follows the rapid deposition of water-saturated sediments (Prothero and Schwab, 1996). Rapid deposition is common along submarine slopes (cf. Prothero and Schwab, 1996), in this case

probably originating from a submarine volcanic slope composed of fine-grained pyroclasts (Fisher and Smith, 1991). Notwithstanding alteration, field and petrographic observations indicate a monolithologic sequence, whereby the recrystallized fine-grained matrix may have originally been composed of abundant aphyric, ash-sized, glassy (obsidian) shards with pumiceous lapilli-sized fragments (**Figure 121**). The composition, morphology, and constituents are similar to described hyalotuffs of de Rosen-Spence et al. (1980), which capped certain subaqueous felsic flows. The ubiquitous fine-grained nature implies an efficient fragmentation mechanism, whereas the pumiceous fragments indicate that volatile exsolution was the potential driving force; therefore, these tuffs probably formed during a phreatomagmatic explosion that may or may not be related to the juxtaposed felsic lavas. Another possibility is that these deposits may record some other distal pyroclastic event. Nevertheless, these tuffs were deposited contemporaneous to the intrusion of the felsic lavas based on synsedimentary deformation of bedding in contact with the lobate felsic facies (**Figure 114**), which can occur only if the sediments were unconsolidated at the time of the felsic intrusion (Duffield, 1990).

The repetitive nature from massive and lobate lavas to fragmental lithofacies (**Figure 112**) outlines a possible cross section through a subaqueous lava dome complex. Therefore, this section is analogous to a dome complex, where the different felsic facies record individual bulbous masses or lobes (Yamagishi and Dimroth, 1985; Kano et al., 1991) rather than a more voluminous subaqueous lava flow.

4.2.5. Dunraine west area (ROI 10)

The Dunraine west area represents the continuation of the Dunraine east region that extends further to the west behind the former Manitou Mine (**Figure 85, ROI 10**). This region is located close to the presumed contact with the Héva Formation, with the first confirmed outcrop of the Héva Formation being approximately 300 m to the south. Mapping was done on a regional scale, along former cut lines where possible, examining previously identified outcrops in an effort to recognize any vertical and/or lateral changes in the stratigraphy (**Figure 123**).

4.2.5.1. Lithology and stratigraphy of Dunraine west

Three general lithofacies fill the stratigraphy in this region. Lavas include both felsic and intermediate compositions, along with intercalated volcaniclastics deposits. Morphological variations permit subdivisions in lavas (i.e., pillows), whereas grain-size variations and fragment composition identify different volcaniclastic facies.

Volcanic lithofacies

The felsic facies has limited exposure, measuring approximately 200 m along strike and only 20-30 m-thick. This facies is massive, but is commonly brecciated or sheared. The sericitized groundmass hosts euhedral to subhedral feldspar phenocrysts and subhedral quartz, however an estimate of modal percentage is not possible due to alteration. In addition, this facies is enclosed by felsic volcaniclastic deposits.

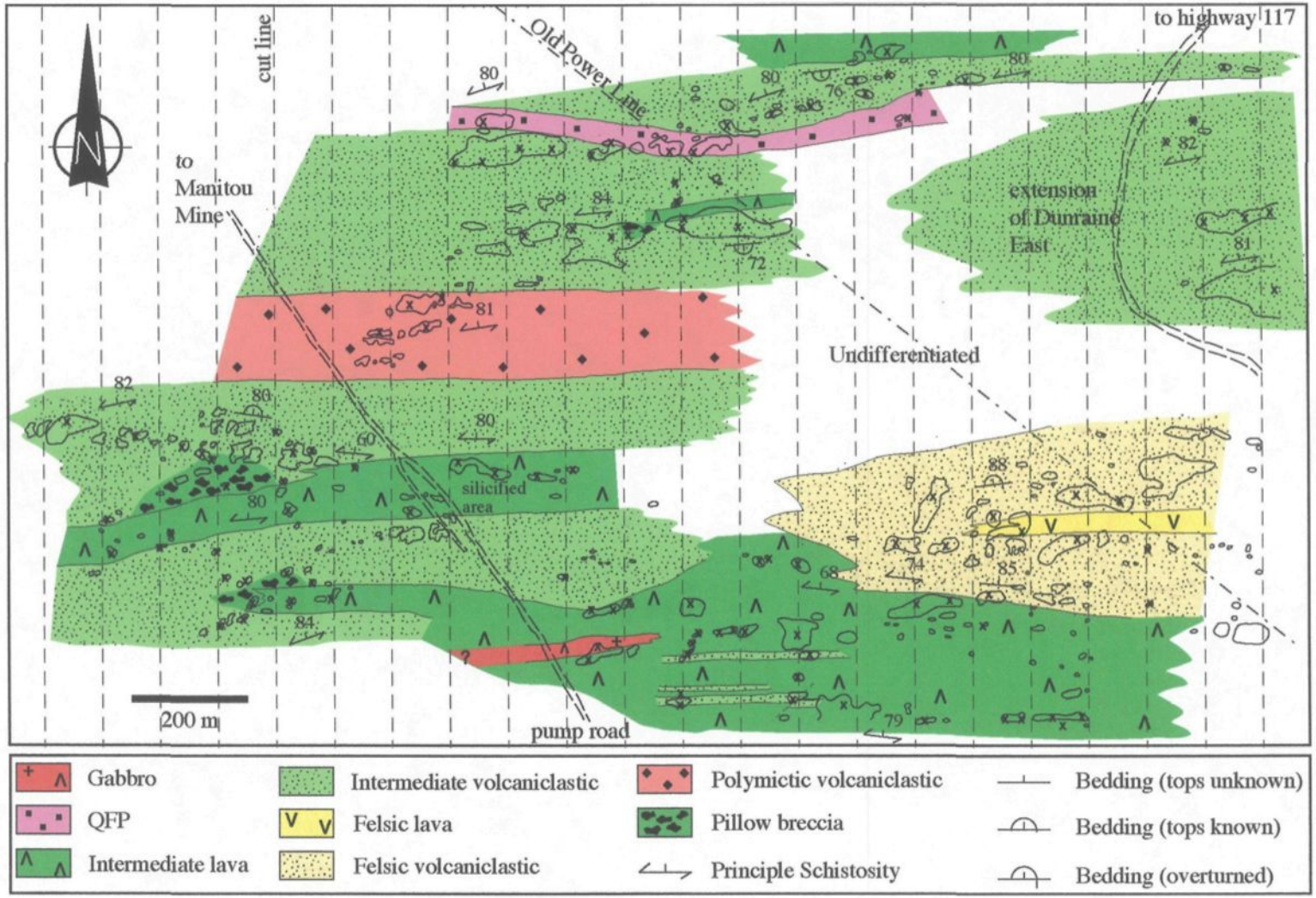

Figure 123: Simplified geology of the Dunraine west region (ROI 10).

Several different intermediate lavas are recognized throughout this area (**Figure 123**). Individual lavas measure between 20-300 m-thick and are dominantly massive with localized pillowed flows (**Figure 123**). Pervasive silicification and deformation (**Appendix A-22**) obscured initial identification as these lavas appear felsic, but recognizable bun-shaped pillows suggested a more intermediate composition. Pillowed flows contain ~ 8-vol% euhedral to subhedral feldspar and 8-vol% quartz amygdules. Pillow morphology indicates a south younging direction. Crystallinity of massive flows vary between 5-30-vol% euhedral/subhedral feldspar (**Figure 124**), as well as having 10-vol% hornblende locally. Vesicularity, represented by quartz amygdules, is upwards to 20-vol% (visual estimate; **Figure 125**), but can be absent.

Volcaniclastic lithofacies

Volcaniclastic deposits are subdivided based on composition and grain-size. A 300 m-thick felsic volcaniclastic package is composed of amalgamated tuff turbidites, lapilli tuffs, and tuff breccias that encloses a thin felsic lava (**Figure 123**). Tuff turbidities are composed of cm- to mm-thick graded beds characterized by erosive contacts and flame structures, which indicate a southward younging direction (**Figure 126**). Beds are commonly orange-weathered due to minor mineralization (**Figure 127**) in the form of pyrite and sphalerite. Otherwise, they are chloritized with upwards to 20-vol% euhedral broken feldspar crystals (**Figure 128**). Lapilli tuff and tuff breccia beds are normal-graded and composed of monolithic sericitized subangular fragments, some of which are flow banded.

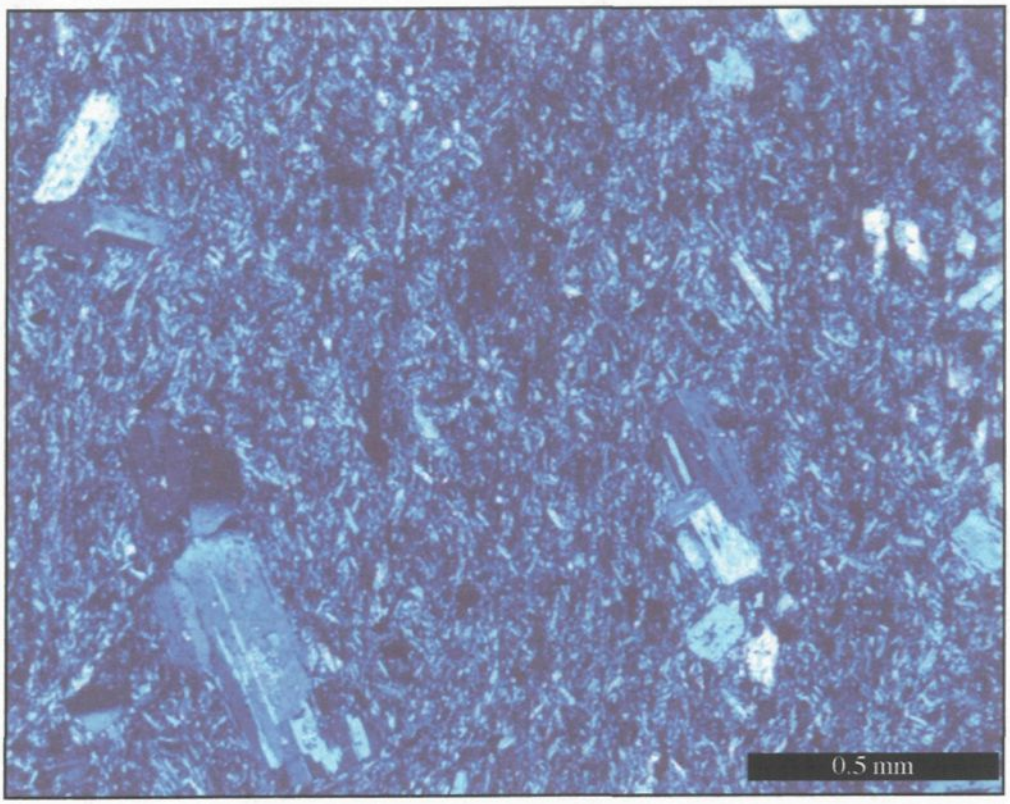

Figure 124: Plane polarized light photomicrograph of groundmass from massive intermediate lava, with tabular, euhedral feldspar phenocrysts hosted in fine-grained mosaic of feldspar microlites and recrystallized quartz + chlorite +/- sericite +/- carbonate.

Figure 125: Vesicular, intermediate bun-shaped pillows. Pencil for scale (14.5 cm long).

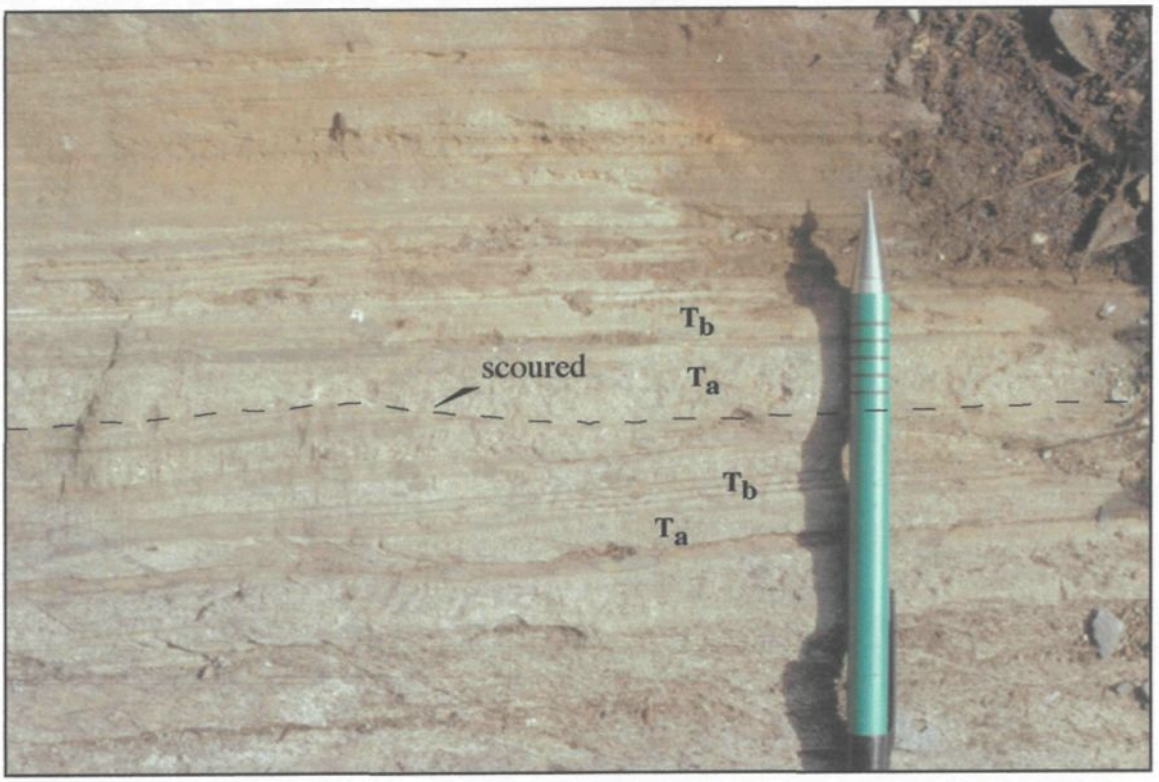

Figure 126: Series of fine tuff turbidite deposits; scouring of laminated (T_b) bed by overlying massive (T_a) bed indicates tops are to the south, in the direction of the pencil (14.5 cm long).

Figure 127: Mineralized units within tuff turbidite sequence. Backpack for scale.

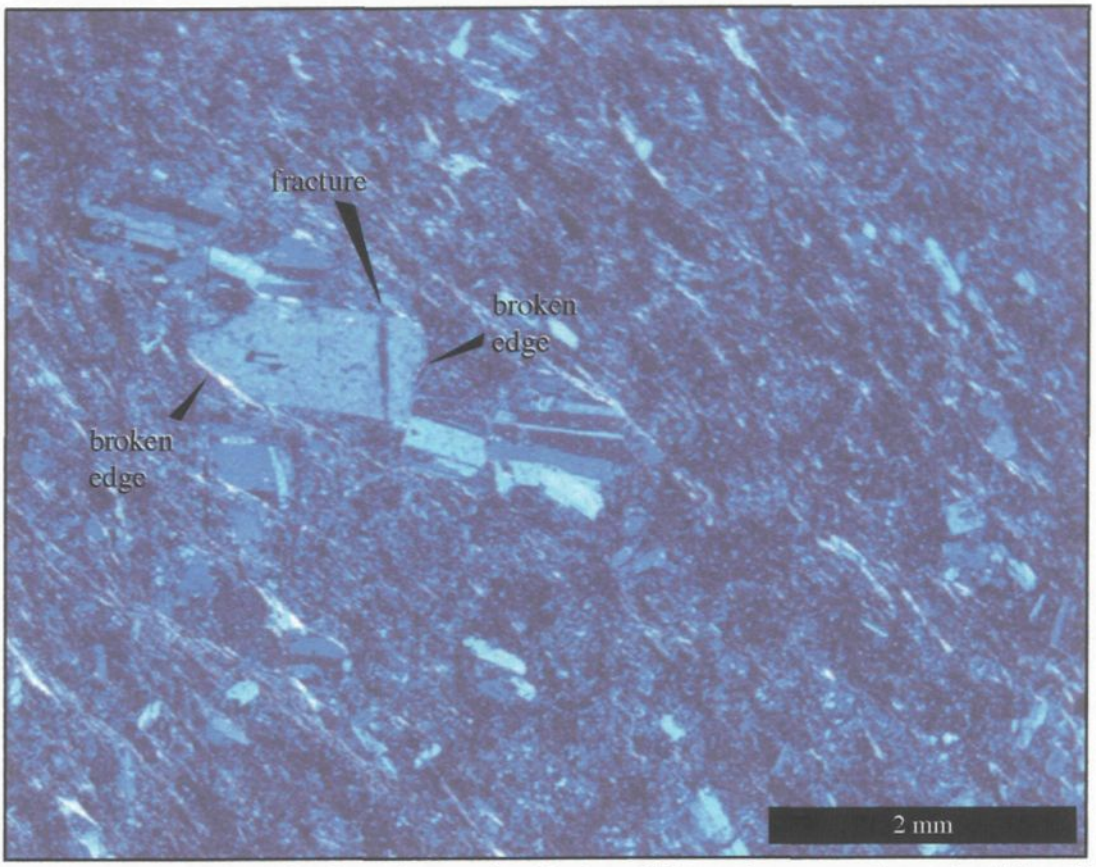

Figure 128: Crossed-nicols photomicrograph of broken feldspar phenocryst observed within tuff sequence.

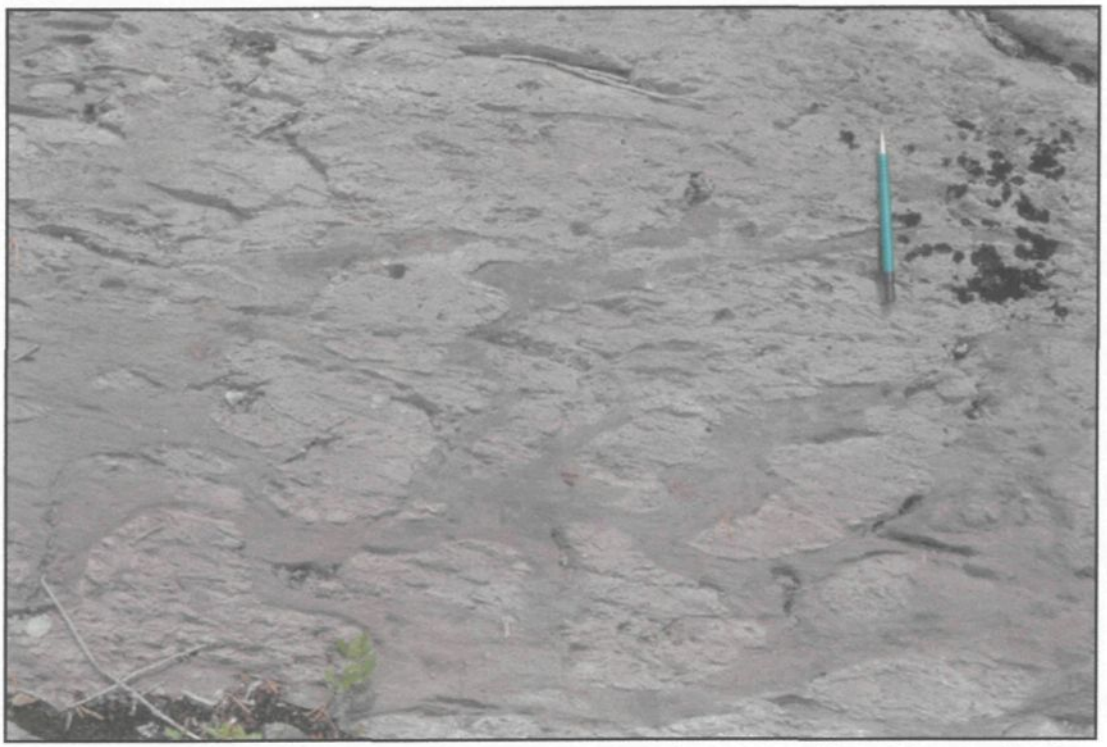

Figure 129: Plastic autoclastic fragmentation along the edge of massive to pillowed intermediate lava forming pillow breccia. Pencil for scale (14.5 cm long).

Intermediate volcaniclastic deposits are dominantly composed of 100-300 m-thick amalgamated lapilli tuff and tuff breccia beds interbedded with intermediate lavas (**Figure 123**). Lapilli tuff beds are weakly stratified whereas tuff breccias are massive and vary from clast- to matrix-supported. Typically, clast-supported tuff breccias are laterally continuous with pillowed lavas (**Figure 129**). Breccia-sized fragments are subrounded and appear plastically deformed (**Figure 130**), as well as having relict pillow forms in cross section or possible pillow margins/rims. The larger of such fragments are characterized by epidotized cores (**Figure 131**), similar to those described from the East Sullivan outcrops (ROI 2). Fragments are composed of 5-15-vol% quartz amygdules (**Figure 130**) and 6-12-vol% feldspar microphenocrysts (**Figure 132A & Appendix A-23**). The matrix is chloritized with 5-20-vol% of liberated, euhedral, tabular feldspar phenocrysts (**Figure 132B & Appendix A-24**).

A 150 m-thick polymictic tuff breccia facies forms an isolated unit correlated for approximately 300 m (**Figure 123**). This facies is characterized by a fragment population that includes: (1) sulfide; (2) sericitized; (3) silicified vesicular; and (4) laminated tuffaceous fragments.

Intrusive lithofacies?

The 30 m-thick feldspar- to quartz-feldspar phyric (QFP) facies is restricted to the northern part of the stratigraphy, but is correlated over 800 m along strike (**Figure 123**). The lack of contact relationships preclude an interpretation as an intrusive or extrusive facies. This facies is characterized by abundant (upwards to 30-vol%) euhedral to

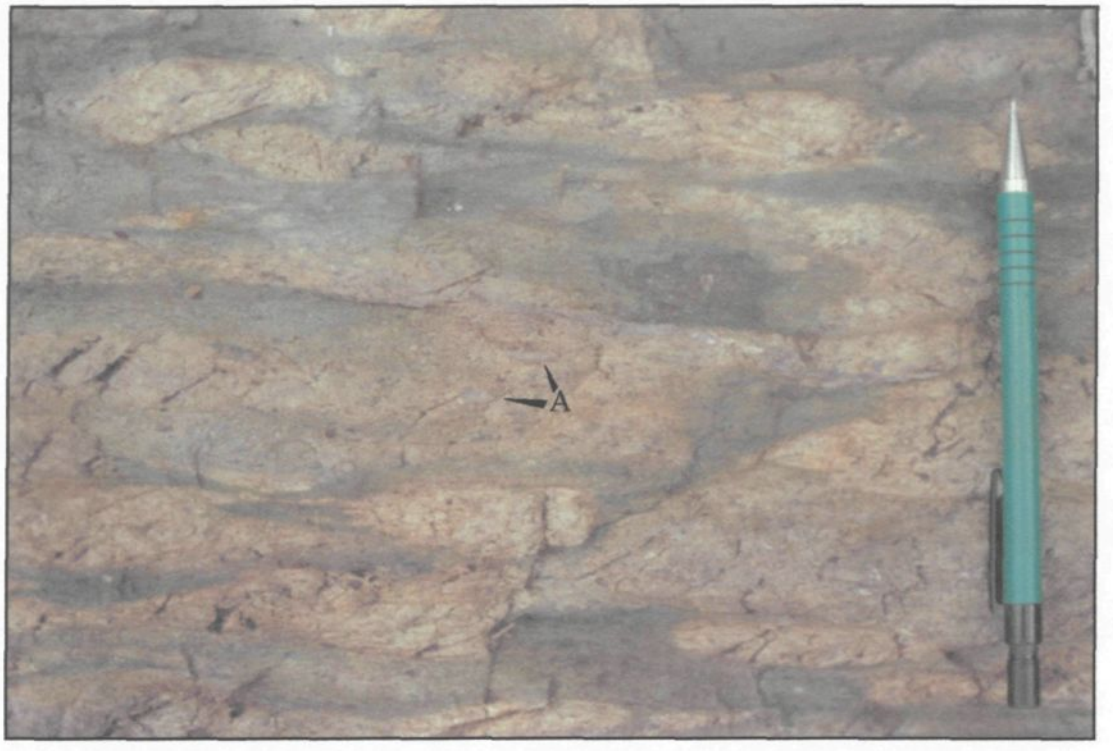

Figure 130: Subrounded, plastically deformed, breccia-sized fragments from a clast-supported tuff breccia. Fragments are characterized by cm-sized, elongated to oval quartz amygdules (A). Pencil for scale (14.5 cm long).

Figure 131: Subrounded, breccia-sized fragment with epidotized core. Pencil for scale (14.5 cm long).

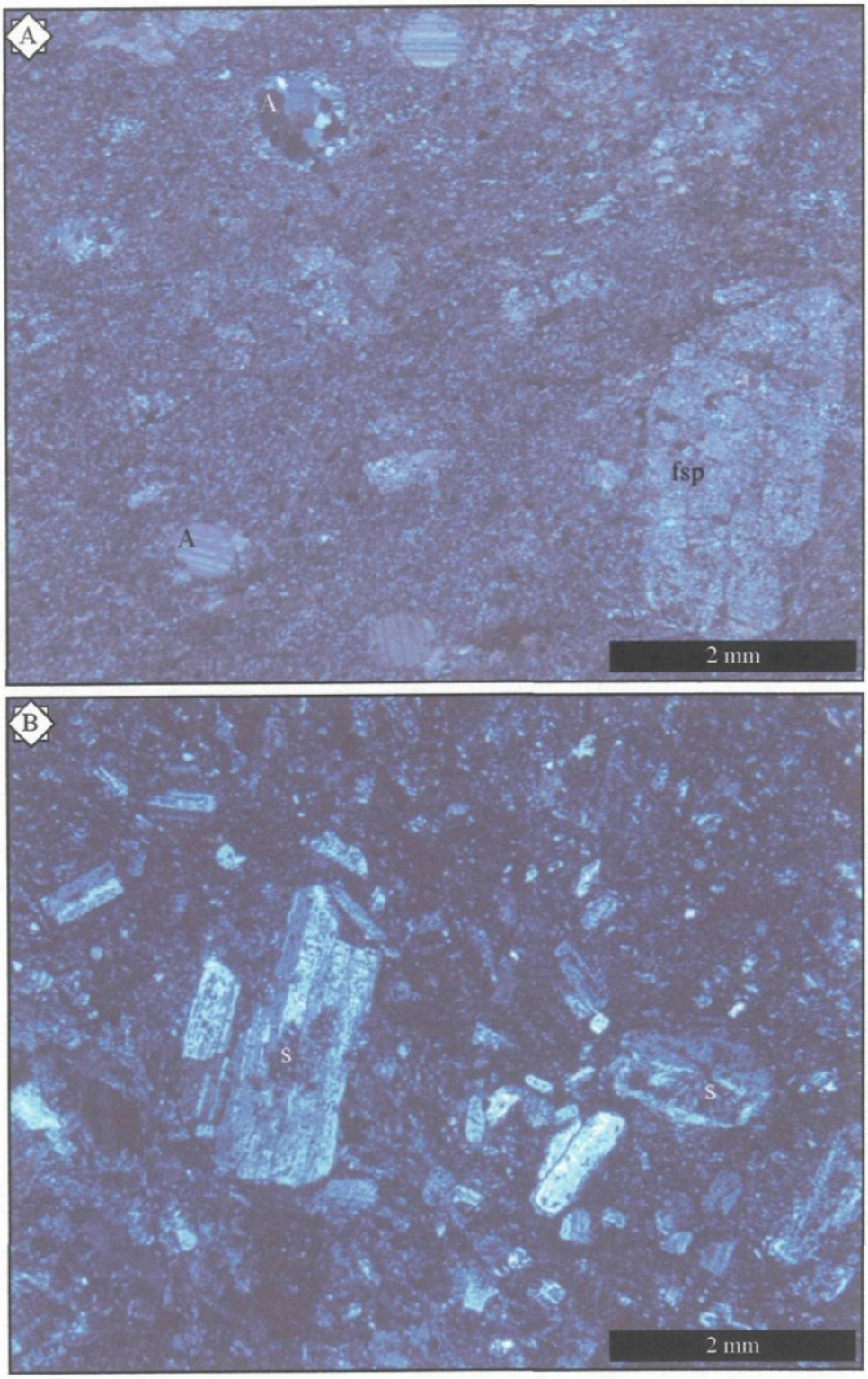

Figure 132: Cross-nicols photomicrographs of tuff turbidite deposit. A. Image of fragment with relict feldspar (fsp) phenocryst, as well as quartz and carbonate amygdules (A) in fine-grained groundmass. B. Image of matrix composed of abundant feldspar phenocrysts, some of which have sieved (s) cores.

subhedral, tabular feldspar phenocrysts (**Figure 133**), and 2-8-vol% quartz, along with local quartz amygdules (5-vol%). The groundmass is chloritized with local orange weathering due to carbonate alteration. Possible pillow-like forms suggest an extrusive origin, but they are not conclusive.

4.2.5.2. Interpretation of Dunraine west area

The limited exposure of the felsic lavas is probably related to their viscous nature. *In situ* brecciation records shearing due to viscosity and possible interaction with water. In addition, the enclosing tuff breccias and tuff turbidites record autobrecciation and phreatomagmatic activity, respectively.

Intermediate lavas represent more effusive processes that change laterally from massive to pillowed lava flows (Dimroth et al., 1978). Other changes from pillowed flows to amoeboidal (**Figure 126**) and subangular fragments indicate autobrecciation in hot and cold states, respectively.

Felsic volcaniclastic lithofacies illustrate changing explosively due to interaction with water. Tuff turbidites represent energetic disintegration of felsic lava, probably from phreatomagmatic processes. These fine-grained fragments are then deposited along the flanks of the subaqueous dome/edifice, either without significant repose or due to slumping by oversteepening. Deposition was by a rapid succession of low-concentration turbidity flows, which resulted in scouring (T_b-beds; **Figure 126**) of underlying beds and formation of soft sediment deformation structures (i.e., flame structures; Prothero and Schwab, 1996). Broken feldspar fragments are similar to type 2 crystal fragments described by Allen and

Figure 133: Field photo illustrating the feldspar-phyric nature of the QFP facies. Pencil for scale (14.5 cm long).

McPhie (2003) that represent fracturing due to explosive eruptions due to decompression or shearing during laminar flow. Coarser-grained lapilli- and breccia-sized fragments are more angular and probably formed during autobrecciation processes along flow margins. Their massive nature suggests deposition from debris flows under laminar flow conditions (Lowe, 1982).

The massive to stratified nature of intermediate volcaniclastics deposits suggest deposition from debris to high-concentration turbidity flows, respectively. They most likely record slumping along the leading edge of an active flow or remobilization of unconsolidated debris from a gravitationally unstable volcanic edifice. Other clast-supported tuff breccias adjacent to pillowed flows represent *in situ* brecciation and a transport. This association represents a depositional continuum and the tuff breccias are termed pillow breccia (**Figure 129**).

The polymictic tuff breccia may represent an epiclastic sequence that formed during a hiatus in volcanic activity. The fragment population is similar to the various mapped facies from Dunraine east, thus they could have originated from weathering of this particular region.

4.3 Stratigraphic Top: South or North?

Throughout the study area, examination of graded bedding and pillow morphology has demonstrated a southward younging direction. Moreover, even if unequivocal evidence

for determination of the stratigraphic top were absent, the relationship between regional schistosity and bedding could be employed. This relationship is such that the measured schistosity trends at a higher azimuth than the bedding (i.e., 290° versus 270°; **Table 16**). This younging direction and relationship holds everywhere except to the Sleepy Lake area, which has a demonstrated northward younging direction preserved in tuff turbidites. This conundrum may represent an overturned packaged or a separate lithotectonic domain. However, mapping and geophysical data within the region do not recognize any fault bounded structure that would suggest a separate domain, so the package is envisaged to have been overturned. A possible mechanism to produce this relationship is a folding relationship whereby one limb is overturned, or part of a recumbent fold.

4.4 Subaqueous Volcanism – A synthesis of explosive and non-explosive behavior

As the Val d'Or and Jacola formations (and the Héva Formation; see Chapter 5) have been shown to have a completely subaqueous depositional history, it is necessary to review subaqueous volcanic processes. Recent and ongoing work has focused on the kinetics involved with generating submarine eruptions (Cas and Wright, 1991; Stix, 1991; Mueller et al., 2000; White et al., 2003) and whether they are explosive and non-explosive in nature. This section examines two eruptive modes of fragmentation that are feasible underwater, as demonstrated through experimentation (Wohletz and McQueen, 1984; Zimanowski et al., 1997; Wohletz, 2002) and field observations (Wohletz, 1986; Mueller and White, 1992; Scott et al., 2002), and relating them to described deposits. The

Table 16: Comparison between principal schistosity and bedding.

Location	Lithology	Schistosity	Bedding	Younging direction	Cartoon
PDN	tuff	264/82	265/85	south	
Pole Line	lapilli tuff	261/71	280/72		
Dunraine	tuff	260/85	090/80	south	
	tuff	255/75	269/82	south	
	lapilli tuff	254/78	260/81	south	
	lapilli tuff	255/80	263/63		
Camnet	tuff	241/80	280/77	south	
	tuff breccia	252/79	261/77		
Relais	lapilli tuff breccia	250/80	260/77	south	
Sleepy Lake	Rhyolite + tuff	273/85	265/86	north	
	Rhyolite + tuff	278/80	272/84	north	

fragmentation mechanisms considered include phreatomagmatic and magmatic eruptions. Phreatomagmatic eruptions involve the interaction between water and lava and magmatic eruptions only involve the lava, where the principal driving force is the thermal contrast and exsolution of volatiles, respectively.

4.4.1 Subaqueous phreatomagmatic eruptions

In this case, the term subaqueous phreatomagmatic eruptions describes volcanic eruptions that occur exclusively underwater, such that there is an excess of water available for mixing with lava. Such an interaction is sometimes considered to be a type of fuel-coolant interaction (FCI; (Buchanan and Dullforce, 1973) between a hot liquid (fuel) above the vaporization temperature of a cold liquid (coolant) (Wohletz, 2002).

In this scenario, an excess amount of seawater, at depths greater than 200m, or below wave base, interacted with hot extruding lava. Initial interaction was non-explosive due to the *Leidenfrost Effect* (cf. White, 1996), which describes the formation of an insulating vapor film. This vapor film retards the transfer of thermal energy between the lava and water, resulting in the formation of pillowed forms during lava propagation on the seafloor, as observed along the coast of Hawaii (Moore and Tepley, 1974). The effusive pillowed to explosive fragmental transformation occurs when this vapor film collapses, resulting in the sudden transfer of heat from the lava to the water, which causes the instantaneous vaporization of surrounding water. As this steam rapidly expands outward, it generates a rarefraction wave in the opposite direction that can disrupt the lava surface (Morrissey et al., 2000). Typically, the eruption of lava on the seafloor is non-explosive, as

indicated by the abundance of pillowed lava, but there have been numerous observations of fragmental material from recent dives on seamounts (Clague et al., 2000; Maicher et al., 2000; Maicher, 2002). Most of these are related to quenching or thermal stress (i.e., Clague et al., 2000), as cooling and contraction of the outer lava surface can result in eventual granulation (pg 54; Cas and Wright, 1987).

The importance of magmatic volatiles during FCI interaction needs further consideration. So it is necessary to ponder whether an initial driving force is required to eject the lava into the water column in order to promote efficient mixing between lava and water. This idea is concerned with the ratios involved during the mixing process. Experiments have shown that the ideal water:lava mass ratio for fragmentation is 0.3 (Sheridan and Wohletz, 1983; Wohletz and Sheridan, 1983), with values above and below this becoming less efficient. Highly explosive phreatomagmatic eruptions are not possible in a subaqueous environment, particularly above the critical pressure for water (cf. Morrissey et al., 2000). Experimentally, the opposite has been shown, with highly efficient FCI explosions occurring at confining pressures greater than 35 MPa (Wohletz and McQueen, 1984), which is at pressures too great to permit volatile exsolution (McBirney, 1963). Nevertheless, Wohletz (1983, 1986) envisaged two possible scenarios for vesicle-free (gas-free) fragmentation: (1) quench granulation (thermal shock); and (2) explosions resulting from sudden expansion of an *external* fluid (e.g., steam), which is controlled by the efficiency of energy transfer and confining hydrostatic pressure. Moreover, Zimanowski (1991) interpreted observed angular, silt-sized glass splinters and slivers as the

products of explosive magma-water interactions, with fragmentation due to the instantaneous transfer of heat from magma to *external* water.

4.4.2 Archean subaqueous phreatomagmatic examples

One potential example of an explosive subaqueous phreatomagmatic eruption can be related to the described volcaniclastic sequence from Placer Dome North (ROI 2). It is envisaged that the eruptive phase postdates a probable low volume stage of the former effusive, pillow-forming eruption, whereby non-explosive quench fragmentation or fracturing of the chilled lava became pervasive. Magma may have moved laterally in tubes or ponded in and around the source to form a shield-like (i.e., low-aspect) dome (**Figure 134A**). Fracturing permitted penetration and percolation of ambient water (cf. Cas and Wright, 1987) into the edifice/dome and subsequent mixing with the newly formed juvenile *sediment* (**Figure 134A**). This coarse mixing resulted in two important effects; (a) increased the surface area of the lava, and (b) effectively increased the viscosity of the coolant (water + sediment). This increase in surface area exposed more lava to ambient water, thereby reducing the water-to-lava mass ratio, which is important as an excess of water commonly precludes efficient explosive interaction (Sheridan and Wohletz, 1983; Wohletz, 1983; Wohletz, 2002). The second effect is concerned with the *purity* of the coolant. White (1996) envisioned an impure coolant, that is, a mixture of water and sediment, interacting with hot lava. This mixture would have a higher viscosity than pure water, which is important as more effective mixing is expected between two immiscible liquids of similar viscosities (Zimanowski and Buttner, 2002). Furthermore, the pillowed

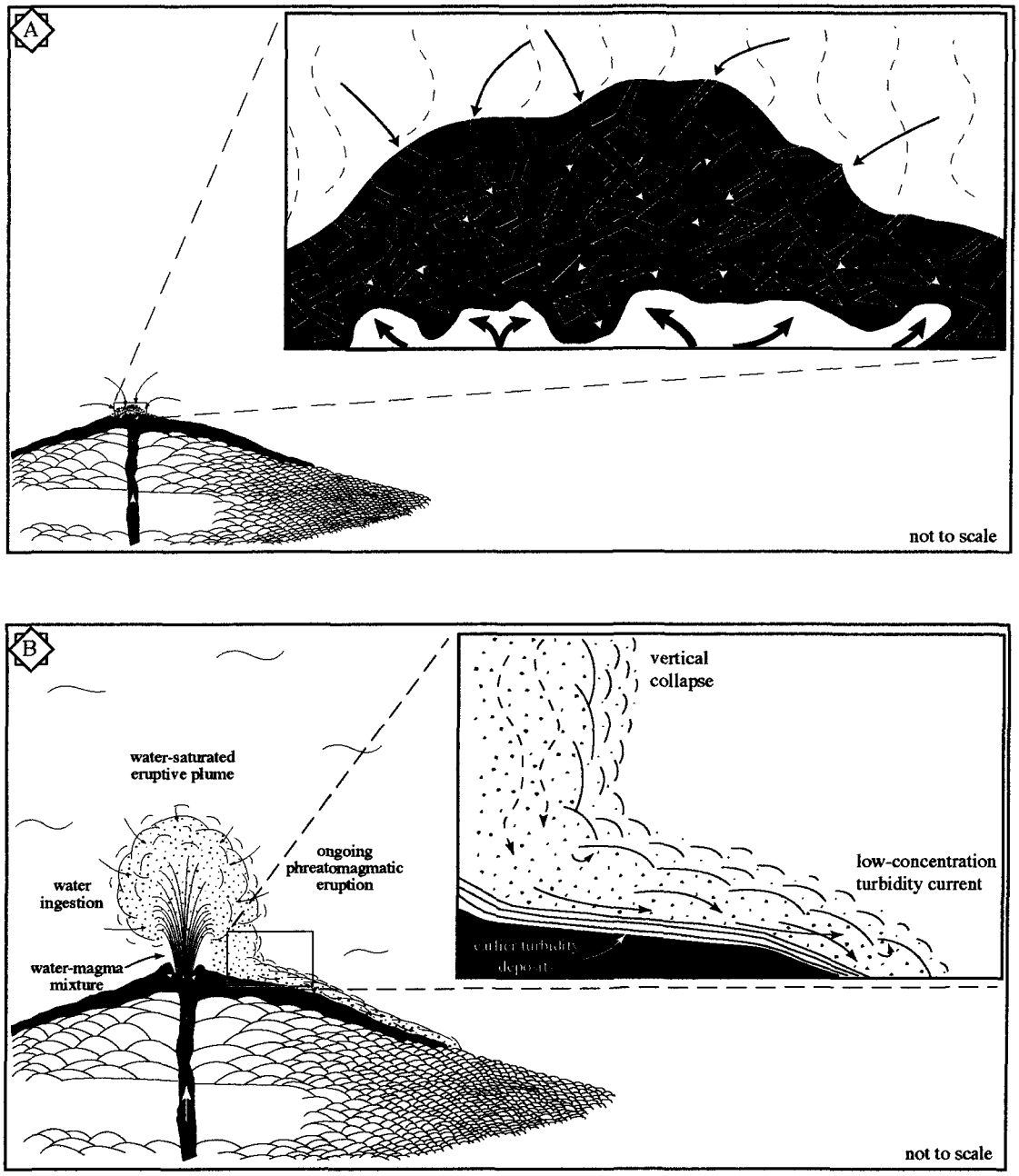

Figure 134: Evolution of the eruptive sequence for Placer Dome North (ROI 2). A. Injection of fresh lava into brecciated pile in and around the vent; whereby ambient water is drawn into the porous sediments and gets heated by fresh lava. The water/sediment mixture serves as a coolant, which has a lower viscosity difference with the lava (fuel). B. Vapor film collapse resulted in a phreatomagmatic eruption, whereby finely fragmented material is lofted into the water column and collapsed to form a water-saturated, low-concentration turbidity current. Additional lava injection could generate subsequent turbidity flows.

morphologies observed, such as amoeboidal shapes are consistent with formation from low-viscosity magma, which further enhances the similarity between the impure coolant and melt. Mixing enables the transfer of thermal energy over a large effective surface area (Morrissey et al. 2000), with the rate of this transfer controlling the explosivity.

The duration of this mixing stage is unknown. At this point, the water probably becomes a superheated fluid as the water pressure increases due to heat transfer to the water over a large area (Morrissey et al., 2000). This increasing water pressure may cause localized condensation and collapse of the vapor film, which can produce water jets that disrupt and penetrate the magma's surface (Morrissey et al., 2000). Such injections can further disintegrate the melt into smaller particles, which further increases the surface area of the melt available to transfer heat.

Another possibility is the inverse situation, whereby a new pulse of fresh magma could jet into the coolant mixture, which would also increase the surface area and provide additional heat. Each pulse may correlate to a depositional sequence (i.e., bed), given the repetitive nature of the deposits (pg. 242, Fisher and Schmincke, 1984). Ideally, a combination of both is probably working. However, an injection of fresh magma into the water-sediment mixture could also be the trigger that causes wide spread collapse of the vapor film leading to explosive fragmentation and ejection of fine fragmented material (**Figures 134A/B**) This eruptive material would include initially quenched fragments, as well as newly disrupted lava originating from the magma injection. Since initial quenching and magma injection were probably confined to the original pillowed edifice, the incorporation of wall rock was probably limited, as the conduit was composed of solidified

lava. In addition, White (1996) considered *wet* eruptions, those with excess water, to have fewer wall rock and/or sediment fragments. Thus, individual beds record discrete volcanic pulses (cf. Doucet et al., 1994), which ejected a water-saturated column of fine-grained pyroclasts into the marine environment (**Figure 134B**). Such columns are probably suppressed due to hydrostatic pressure and the initial high density of the melt-water column mixture. Moreover, these columns probably ingest additional water, the end result being column collapse that generated energetic, water-supported, low density turbidity flows (**Figure 134B**) similar to those envisioned by Fiske and Matsuda (1964). Thus, the efficiency of water-magma mixing will also control subsequent transporting flows and its depositional characteristics (Sheridan and Wohletz, 1983; Wohletz, 1983).

4.4.3 Subaqueous magmatic eruptions

In this situation, volatile exsolution drives the eruption in a similar fashion to the infamous "curtain of fire" eruptions in Hawaii. This type of eruption can be termed a *subaqueous fire-fountain.* A proposed archetype for this type of eruption is from the East Sullivan outcrops (ROI 3), where the inter- and intra-bedding relationships of the volcano-sedimentary sequence records the probable evolution of a single eruptive cycle. The deposits originate from a central volcanic vent, based on mineralogy, sedimentology, and stratigraphy. The proposed single eruptive cycle for this volcano-sedimentary sequence is based on an apparent outcrop scale compositional zoning pattern and degassed state for overlying beds. In this case, zoning is based on a mineralogical change from dominantly feldspar-rich at the base (**Figure 61**) to a more 'mafic', bimodal hornblende-feldspar

assemblage (**Figure 58**) on top. Moreover, this zonation is complemented by a marked decrease in vesicularity from a maximum of 35-40-vol% (**Figure 57**) to < 5-vol% (**Figure 58**). Such a succession is probably the result of the progressive tapping of a zoned magma chamber, whereby the depositional sequence represents the inverse zonation of the source (Blake, 1981). The underlying vesicular facies was produced during the onset of an energetic fire-fountaining phase driven by the release of a gas-charged layer in the sub-volcanic magma chamber (**Figure 135**). This gas-rich layer may have formed through an accumulation process, whereby bubbles formed during finite volatile exsolution rise and collect into a foam layer (Head and Wilson, 2002). Only small amounts of exsolution are needed to more than double the volume of an otherwise volatile-free magma (Orton, 1996), thereby creating magma overpressure that will fracture overlying crust, resulting in an eruption. The integration of these processes could overcome hydrostatic pressures inherent in a subaqueous environment that would otherwise suppress any energetic volcanic eruption. Vesiculated lavas within a deep marine setting has been documented from seamounts at depths greater than 4000 m (Clague et al., 2000). Moreover, the low phenocryst content, bed-thickness, and amoeboidal morphology all suggest a hot and fluid magma, which would enhance the initial vent velocity of the erupting lava facilitating the formation of a fire-fountain eruption. Thus, the first magma tapped during the first phase of the eruption would be a vesicular, feldspar-phyric intermediate magma (**Figure 135**). As the eruption continued, vesicularity decreased and the magma became more *primary*, with a hornblende-feldspar phyric intermediate magma tapped.

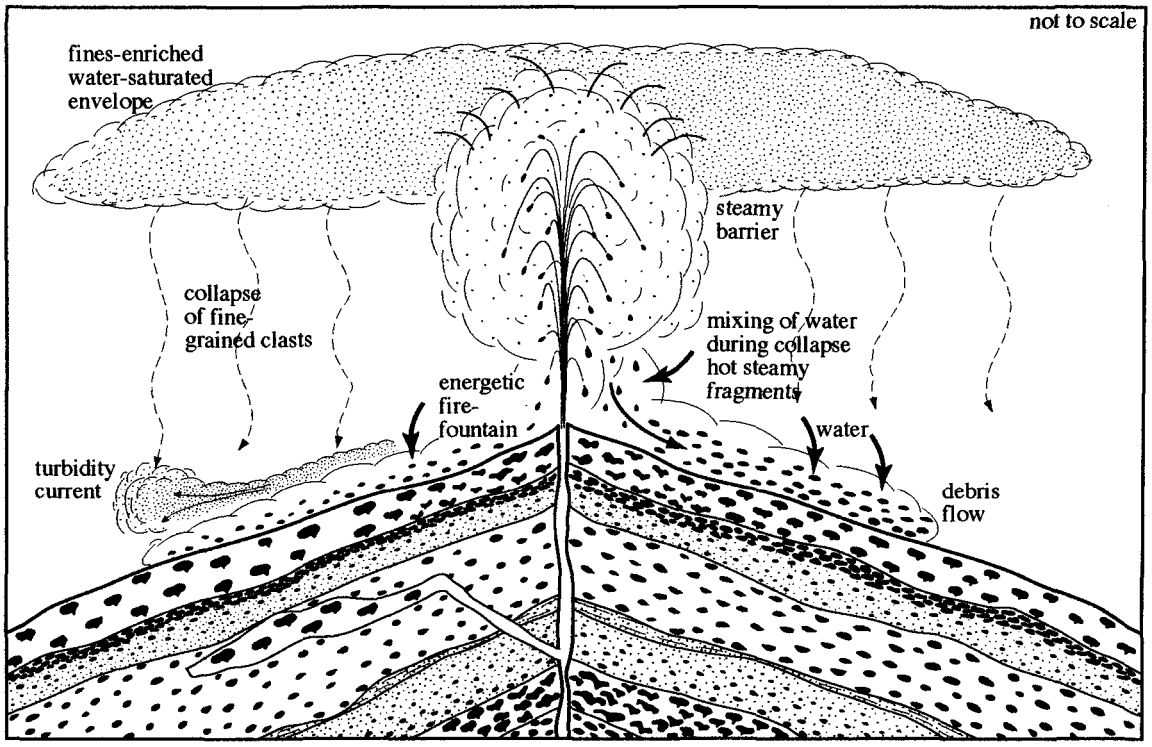

Figure 135: Model of possible subaqueous fire fountain eruption from East Sullivan outcrops (ROI 3). Hot, vesicular, breccia-sized fragments are enveloped in steam as they are ejected through the water column and collapse to form a massive debris to high-concentration turbidity flow. Most finer-grained fragments are lofted above the vent in convecting plumes of hot water before settling to form low-concentration turbidity flows. Actually height of the fountain is restricted to 10's of meters due to hydrostatic pressure. Modified from Doucet et al., (1994) and Cousineau (1994).

The buildup of volatiles controls the height of the lava fountain as is the case for fire fountaining in Hawaii; gas-charged magma results in a 'curtain of fire', whereas gas-depleted magma forms sheet or tube flows. In contrast to Hawaii, the marine environment dictates the height of the fountain and influences the fragmentation processes. The fountain height is simply a function of the hydrostatic pressure and its effects on volatile exsolution. Fragmentation is a two-stage process: (i) magmatic and (ii) phreatomagmatic fragmentation. Magmatic fragmentation is controlled by the exsolution of magmatic volatiles, whereas phreatomagmatic fragmentation is controlled by seawater vaporization at the magma-water interface.

Magmatic fragmentation at elevated hydrostatic pressures is envisaged to be a relatively inefficient mechanism, such that fragments generated are typically coarse-grained and form oblong or amoeboidal shapes (Kokelaar, 1986). This fragment morphology is produced during ballistic ejection of hot, plastic clasts through ambient water, whereby clasts are protected from quenching by a self-generating steam cupola (**Figure 135**; Kokelaar, 1986).

Phreatomagmatic fragmentation was probably delayed due to the initial coarse mixing between large spatter-like hot fragments and water, such that fluid-fluid instabilities were not generated (White, 2000) in the bulk of the eruptive (gas-thrust?) column (**Figure 135**). As water was ingested into the steamy eruptive column, vapor-film collapse of smaller juvenile fragments may have occurred, producing spontaneous vaporization that disintegrated the melt. The resulting shock wave could produce a cascading effect throughout the column inducing further vapor-film collapse. Such pulses of

phreatomagmatic activity form a population of finer-grained tephra (cf. Wohletz, 1986) that collapsed along the edges of the column to form high- to low-concentration turbidity currents (**Figure 135**).

Absent in these deposits is the formation of a hyaloclastite sheet deposit, indicating that these volcaniclastic deposits did not form during thermal fragmentation of a sheet-like lava flow, as envisioned by Maicher et al. (2000).

CHAPTER 5

HÉVA FORMATION: ARC RIFTING

The 2.5 km-thick Héva Formation (HF) is composed of numerous laterally extensive, massive to pillowed mafic flows, interdigitating gabbroic sills and dykes, as well as subordinate and generally localized felsic to mafic volcaniclastic deposits (**Figures 136**). The basal contact of the HF, while not exposed, is gradational over several 100 meters and defined by an abrupt change from calc-alkaline facies of the Val d'Or Formation to tholeiitic volcanism, which is recognized in the field by the appearance of a prominent, voluminous felsic spherulitic flow. In addition, a localized polymictic volcaniclastic sequence appears to be composed of fragments eroded from the Val d'Or Formation, which would suggest a depositional continuum between the formations (**Figure 136**). The upper contact is defined by the Cadillac Fault Zone, which forms the break between the Abitibi and Pontiac subprovinces (**Figure 136**).

Glacial till and swampy conditions restrict comprehensive regional study, but outcrops concentrated along a several kilometer wide north-south corridor (**Figure 137**), accessible via Columbiere road, together with geophysical data (e.g., aeromagnetic) permits the reconstruction of the formation. Four regions of interest are outlined, which from base to summit are: (1) felsic spherulitic unit, (2) Tex-Sol volcaniclastic sequence, (3) Akasaba North, and (3) Akasaba South.

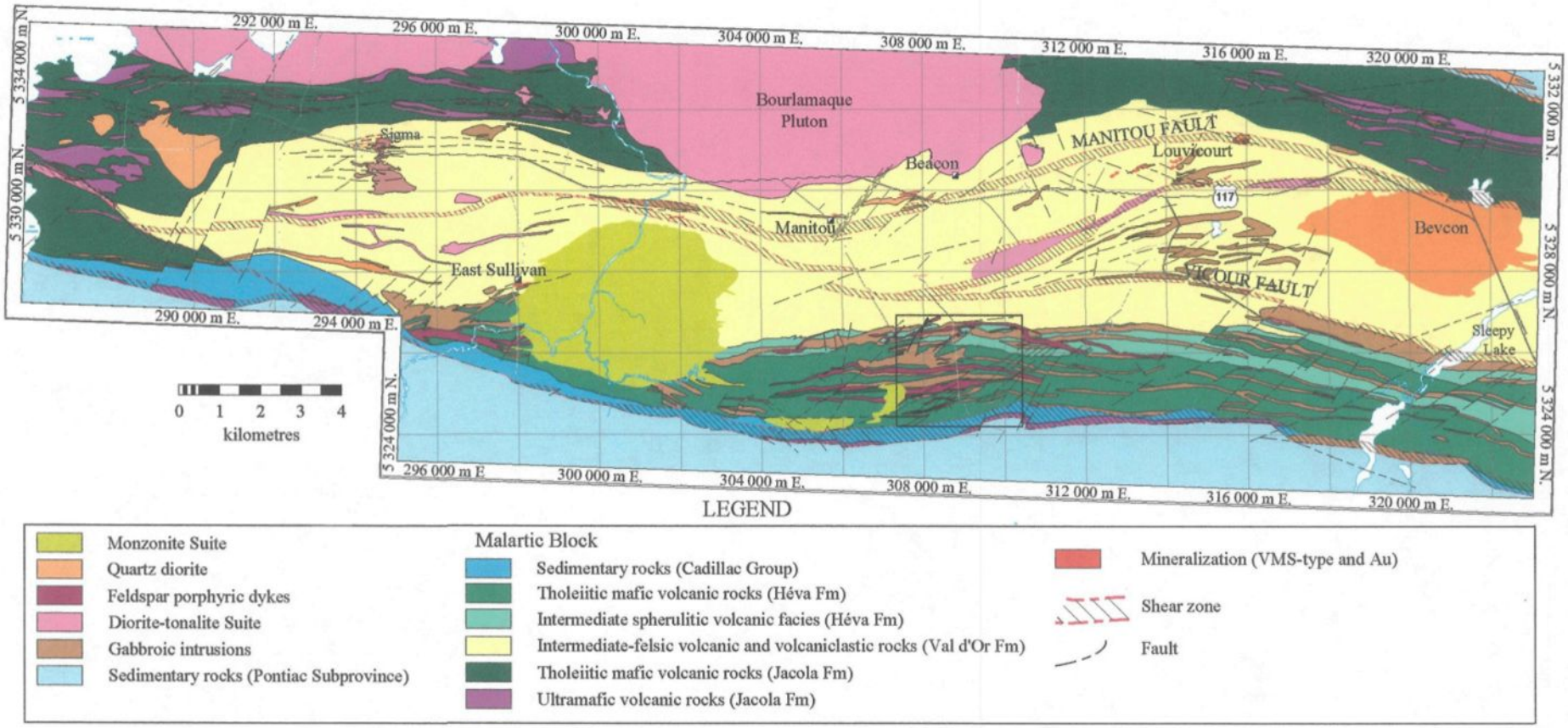

Figure 136: Simplifed regional geology of the Val d'Or region. Corridor of interest outlined (see Figure 137). Geologic compliation after Pilote, Lavoie, Scott, Riopel, Champagne, Beaumont, and Mueller (2003).

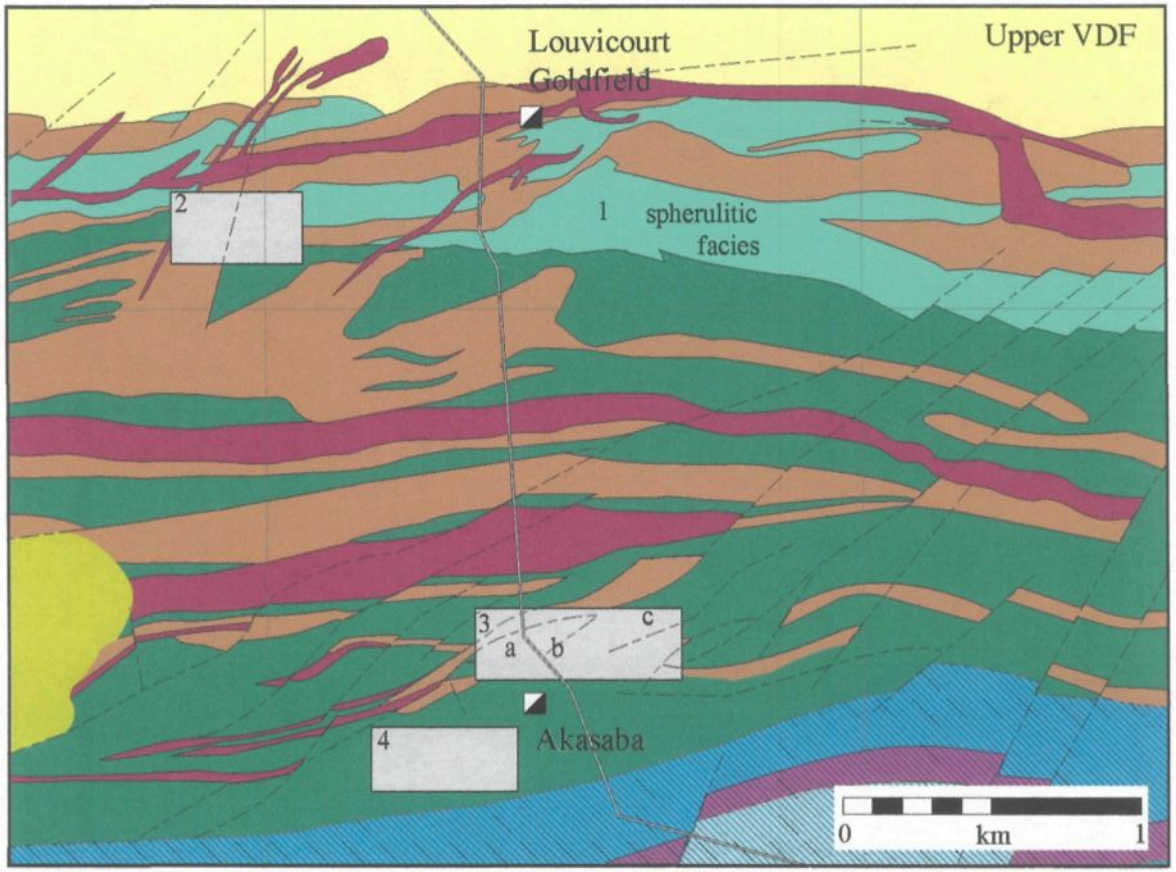

Figure 137. Geology corridor mapped in detailed through the Héva Formation. Areas studied in detailed are: (1) spherulitic facies, (2) Tex-Sol, (3) Akasaba north (a,b, and c), and (4) Akasaba south. See Figure 136 for legend.

5.1 Felsic Spherulitic Unit: Malartic Group marker horizon

Initial work by Norman (1943 and 1947) mapped and described this unit as a laterally extensive spherulitic and variolitic mafic to intermediate lava. Subsequent work did not quell disputes about the different compositions, which varied from mafic (Gaudreau et al., 1986) and felsic (Sharpe, 1968; Sauvé, 1995). Work by Sharpe (1968) and Imreh (1984) correlated this felsic lava for more than 25 km, covering Bourlamaque, Louvicourt, and Vauquelin townships. The physical appearance and length of the flow argued that it was a mafic flow, with high silica values dismissed as being due to silicification (Gaudreau et al., 1986). Recent aeromagnetic data outlined this felsic unit over a minimum 25 km strike length, with an average thickness of 400-m (**Figure 138A**). Current mapping identified this unit at 14 different localities over a strike length of 18 km (**Figure 138B**). Moreover, a spherulitic unit was recognized within drill core taken from the East Sullivan mine (Pilote, pers. com. 1999), suggesting that it extends beyond the East Sullivan Stock (**Figure 136**). This extensive exposure, together with its recognizable spherulitic texture permits this unit to be used as important marker horizon within an otherwise heterogeneous and complex region, similar to a spherulitic rhyolite from the Blake River Group (Péloquin et al., 1996). Overall, this unit is aphyric and non-vesicular, with only rare microphenocrysts and vesicles serving as nucleation points for spherulitic growth.

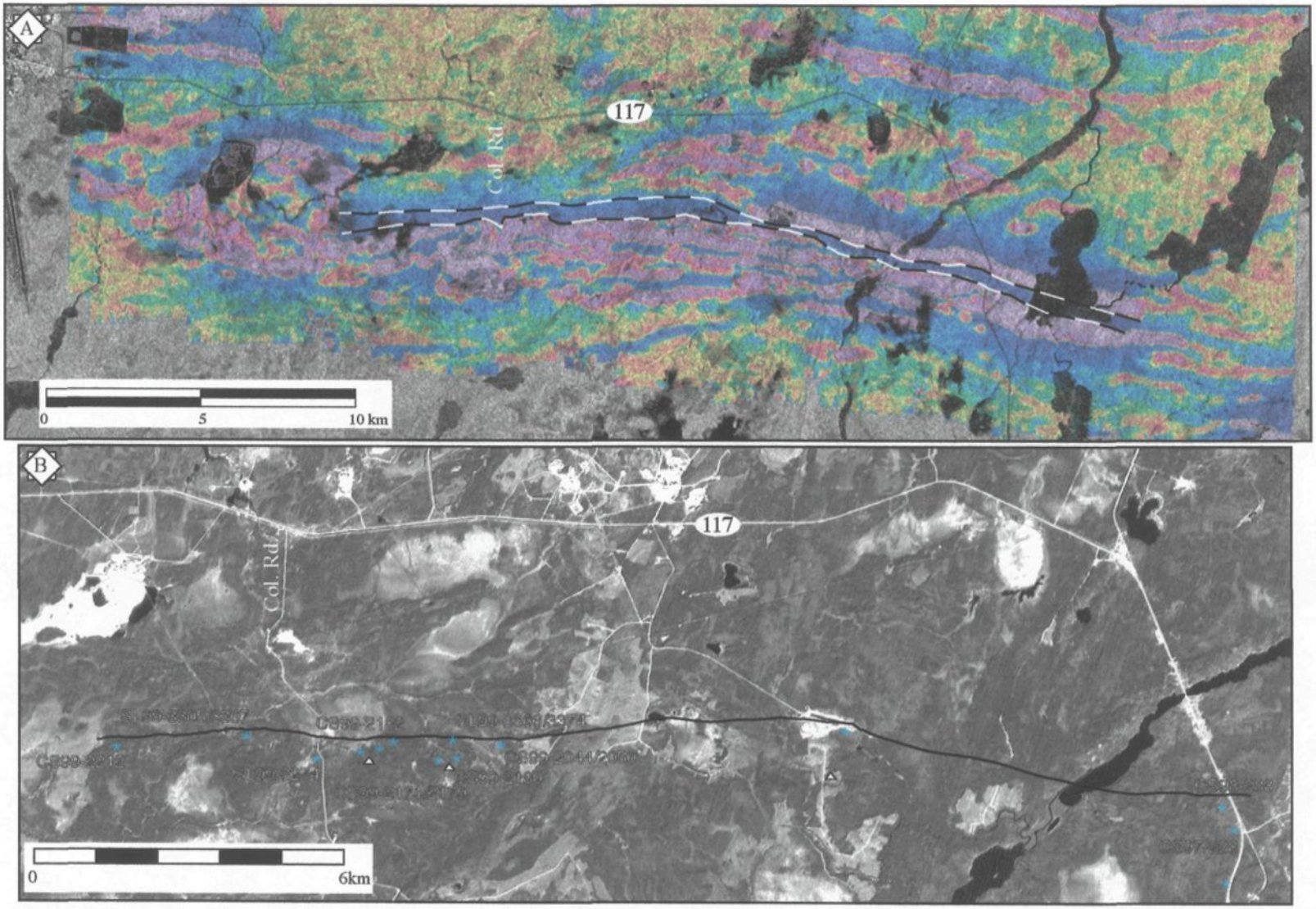

Figure 138. Lateral extent of felsic spherulitic unit. Location of highway 117 and Columbiere Road (Col. Rd.) are indicated. A. Aeromagnetic data superimposed over radar image showing the low aspect of the spheurlitc unit (dashed lines), modified from MRNQ data. B. Aerial photo showing locations of the recognized spherulitic unit mapped in the field.

5.1.1 Lithology of felsic spherulitic unit

Its tabular morphology and undeformed character facilitates the recognition of three distinct facies, which from base to top are; (1) massive; (2) lobe-hyaloclastite; and (3) hyaloclastite (**Table 17; Figure 139**).

Basal massive facies

The 325 m-thick (maximum thickness) basal massive facies is defined by the abundance of spherulites that give a coherent (massive) appearance when completely composed of spherulites (**Figure 140A**) or having zones of isolated spherulites that commonly have a banded appearance (**Figures 140B & 141; Appendix A-25**). Massive zones are sometimes brecciated *in situ* with little to no movement between fragments (**Figure 140A**). In addition, areas with large cm-sized spherulites are interspersed within a *dark* chloritized groundmass (**Figure 142**), which is probably the reason this facies was considered to originally be of mafic composition. A possible basal breccia facies is associated with the base of the massive facies, but is only observed in one locality (**Figure 143**). Contact with underlying facies is not observed, but irregular contacts with gabbroic intrusions are characterized by cm-thick chilled margins within the gabbro (**Figure 144**). Within massive zones, the groundmass consists of a mass of coalescing, oval-shaped, cm- to mm-sized spherical-like (cf. Lofgren, 1974) spherulites composed of finely acicular feldspar that may or may not originate from a central micron-sized microlite or vesicle, with little to no interstitial material (**Figures 145A/B**). In fact, spherulitic growth becomes so intergrown that individual spherulites are no longer recognizable, forming a finely

Table 17: Stratigraphy of the felsic spherulitic unit.

Lithofacies	Thickness & morphology	Characteristics	Transport/deposition	Origin
Basal Massive Facies	325 m; tabular	Aphyric; non-vesicular; acicular feldspar spherulites	Low viscosity, subaqueous felsic lava flow; limited to no interaction with water due to insulation by hyaloclastite carapace, which also thermally insulated the lava; internal shearing formed flow bands and hyaloclastites within the massive flow	High temperature and high volume subaqueous felsic eruption
massive spherulites		Coalesced cm- to mm-sized spherulites; finely crystalline texture; finely developed acicular feldspar		
banded spherulites		Trains of cm-sized, coarse spherulites; 1 or 2 spherulites thick bands; intercalated hyaloclastite		
Medial lobe-hyaloclastite Facies	20 m; tabular	M-sized lobes outlined by spherulitic flow bands; intercalated with lapilli- to tuff-sized, angular, aphyric hyaloclastites; jigsaw/box-like *in situ* breccia; perlitic fractures	Inflation and outbreaks of fresh lava into hyaloclastite carapace; shearing along margins formed flow bands	Lobe growth into hyaloclastite
Capping hyaloclastite	50 m	Clast-supported; lapilli- to tuff-sized, angular, aphyric hyaloclastites; jigsaw/box-like *in situ* breccia; perlitic fractures	*In situ* brecciation with little no transport; intense interaction with water along flow margin; quench fragmentation resulting non-explosive granulation of felsic lava into fine-grained hyaloclastites	Quench fragmentation along flow margins

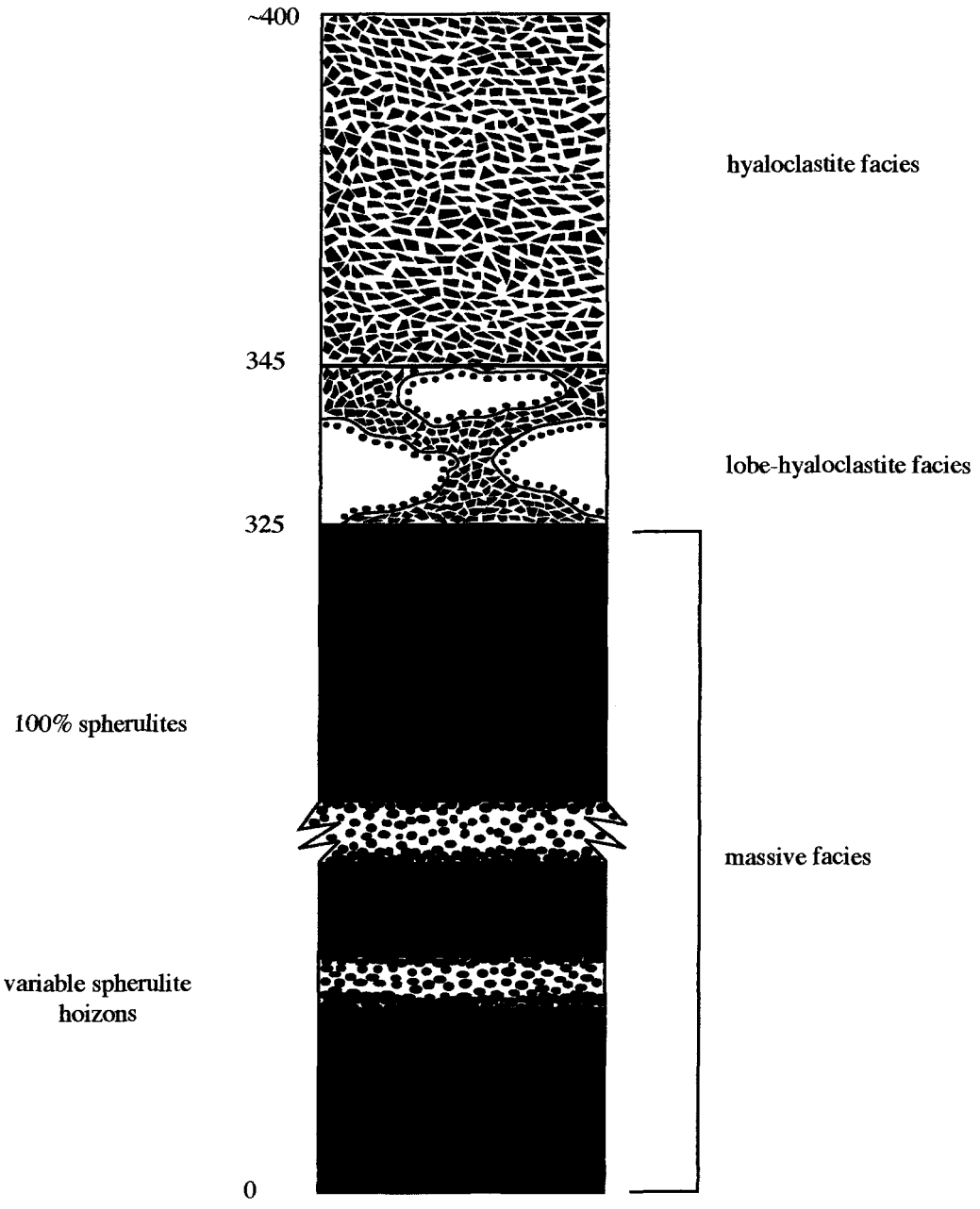

Figure 139. Simplified stratigraphy of felsic spherulitic unit that is subdivided into a basal massive facies, medial lobe-hyaloclastite, and hyaloclastite facies.

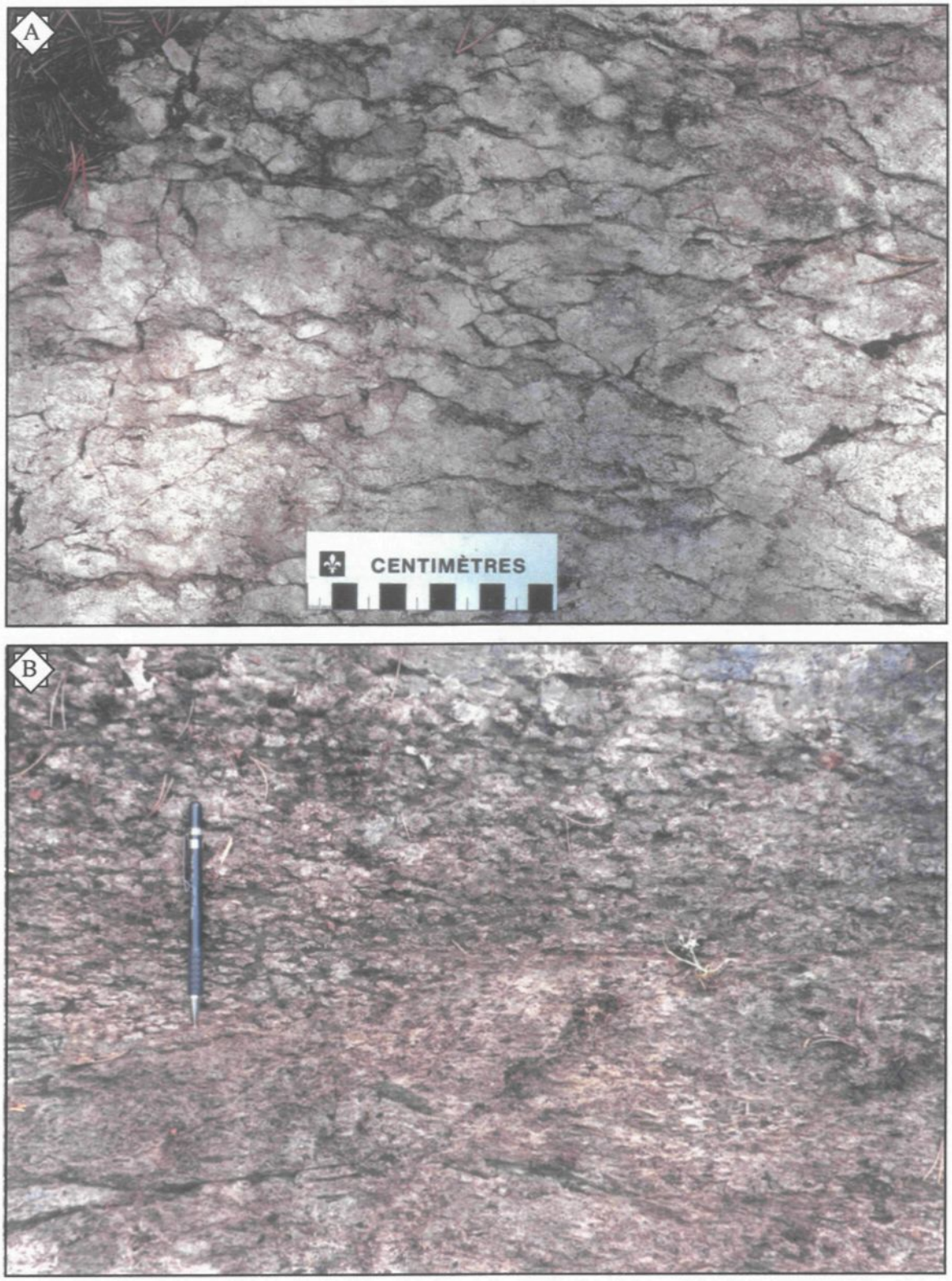

Figure 140. Different parts of the basal massive facies. A. Coherent massive facies composed of 100% spherulites. B. Internal zone within massive facies showing variable amounts of spherulites bounded by massive, coherent zones. Pencil for scale (14.5 cm long).

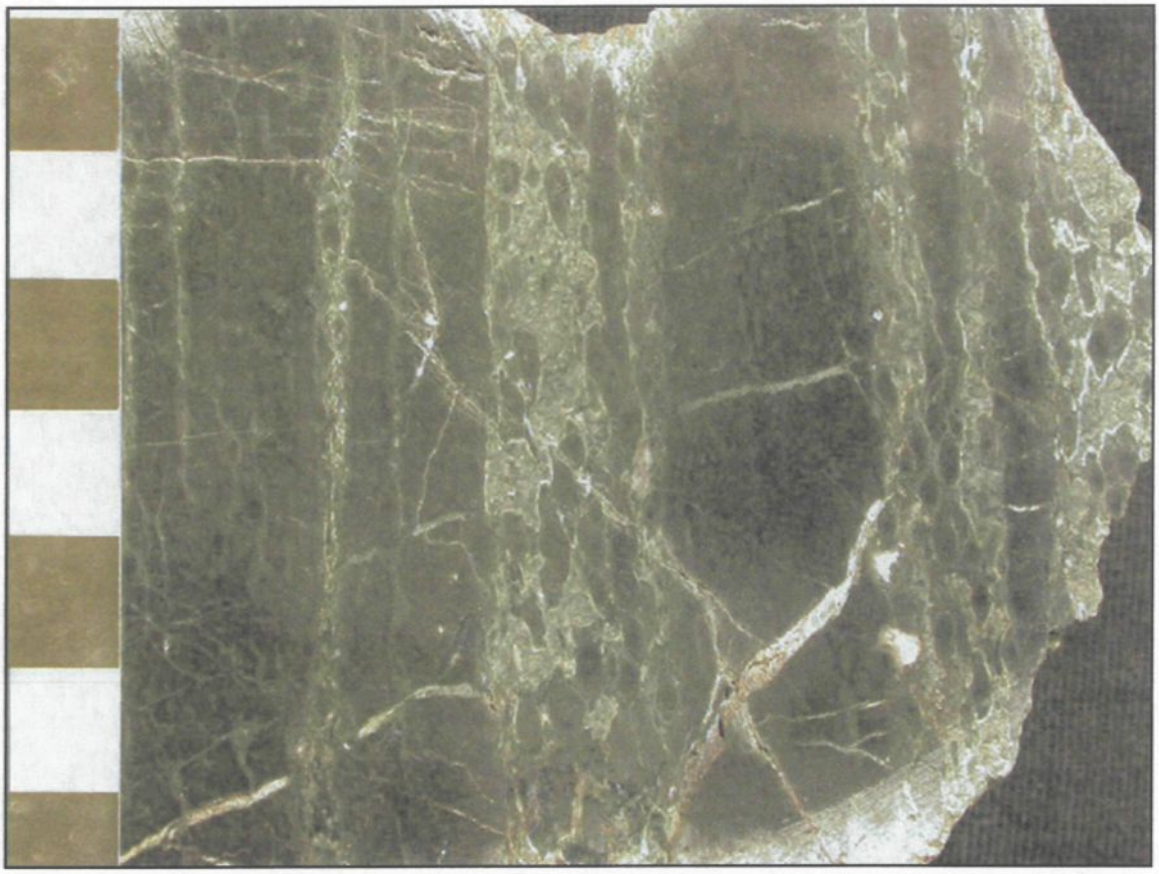

Figure 141. Slab of massive felsic spherulitic facies with flow banding defined by amalgamated spherulites. See Appendix A-25 for thin section description.

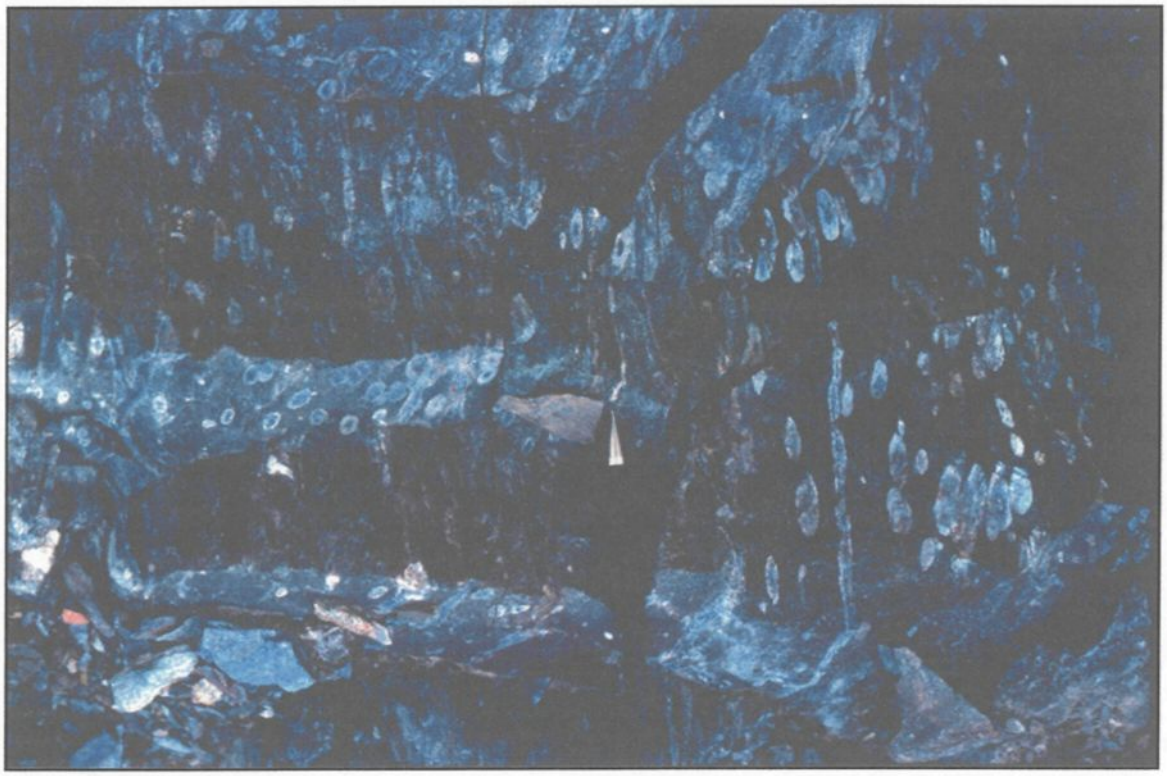

Figure 142. Large, cm-sized, isolated spherulites in dark groundmass. Some rare trains of spherulites also observed. Pencil for scale (14.5 cm long).

Figure 143. Possible *in situ* jigsaw fitting flow-foot breccia composed of massive felsic blocks underlying massive spherulitic felsic facies.

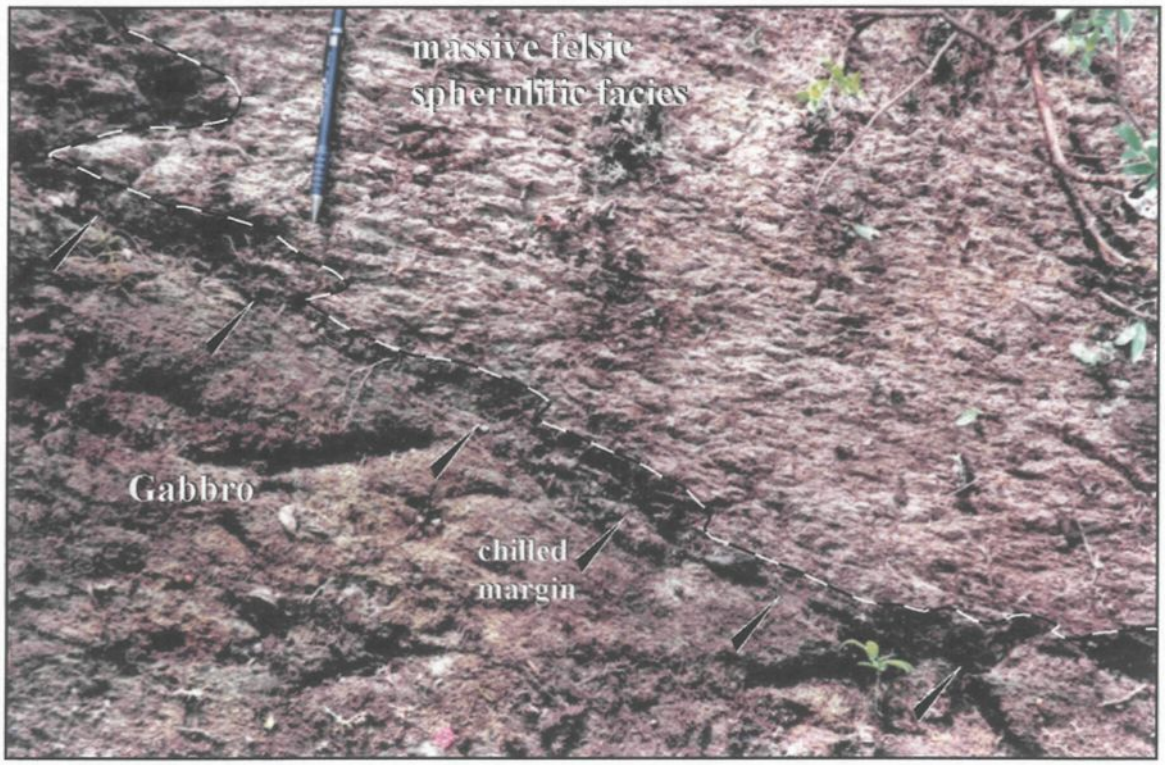

Figure 144. Irregular intrusive contact relationship between massive spherulitic felsic facies and gabbro. Chilled margin in gabbro suggests that the gabbro has intruded and crosscuts the felsic facies. Pencil for scale (14.5 cm long).

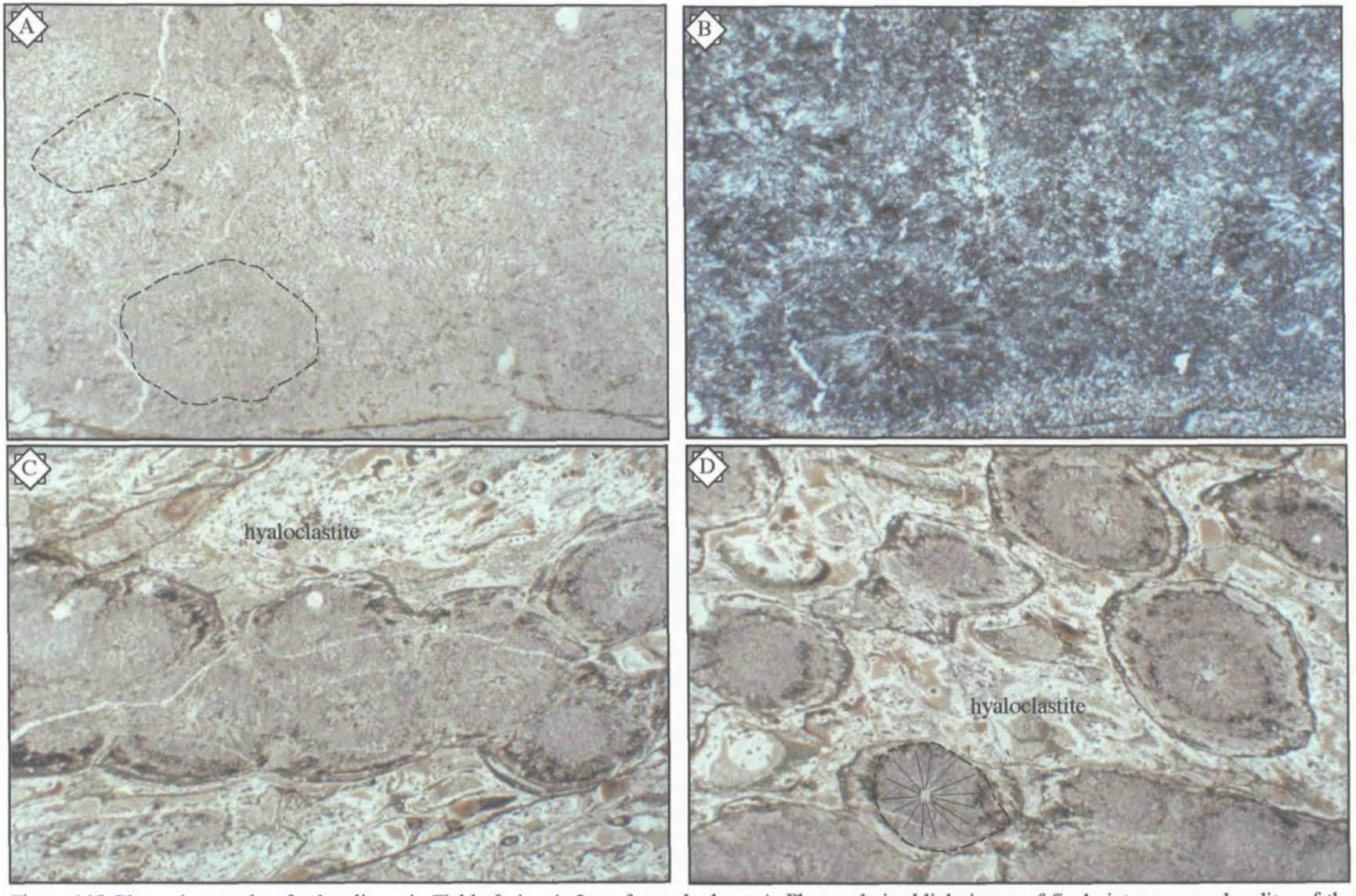

Figure 145. Photomicrographs of spherulite unit. Field of view is 2mm for each photo. A. Plane polarized light image of finely intergrown spherulites of the massive facies. B. Cross-nicols of same field of view as (A). C. Flow-banded spherulites hosted in a groundmass of incipent hyaloclastites and arrested spherulite developement. D. Isolated spherulites within groundmass of incipent hyaloclastite.

crystalline felsic facies (**Appendix A-25**); similar to that described by Swanson et al. (1989) for the central part of a subaerial rhyolitic dome. In contrast, banded zones are defined by trains of large spherulites that can be only one or two spherulites wide (**Figure 145C**), with isolated spherulites situated between bands (**Figure 145D**). Interstitial material is composed of arrested spherulite growth, incipient hyaloclastite and a fine-grained mosaic of quartz + albite (**Figure 145D; Appendices A-25/A-26**).

Medial lobe-hyaloclastite facies

The 20 m-thick medial lobe-hyaloclastite facies is characterized by meter-sized lobes of spherulitic felsic lava mantled by fine-grained, cm-sized, angular aphyric fragments (**Figure 139**). The type section for this facies documents several m-thick lobes, lined by spherulitic flow bands, which are intercalated by hyaloclastite (**Figure 146**), whereby the lobes seem to extend into the hyaloclastite from underlying massive lava (**Figure 147**). Intercalated hyaloclastite material, which is weathered slightly darker than the massive spherulitic lobes (**Figure 146**), is composed of lapilli- to tuff-sized curvilinear fragments. These fragments form clast-supported carapaces that are jigsaw fitting, probably due to *in situ* fragmentation.

In thin section, lobes comprise both banded spherulites along their margins, as well as a finely crystalline core made up of an amalgamated mass of spherulites (**Figure 148**), similar to underlying massive lava. Feldspar spherulites become progressively coarser textured within thin flow bands and isolated spherical spherulites. Hyaloclastites are angular and vary from strongly jigsaw fitting, with little to no interstitial matrix (**Figure**

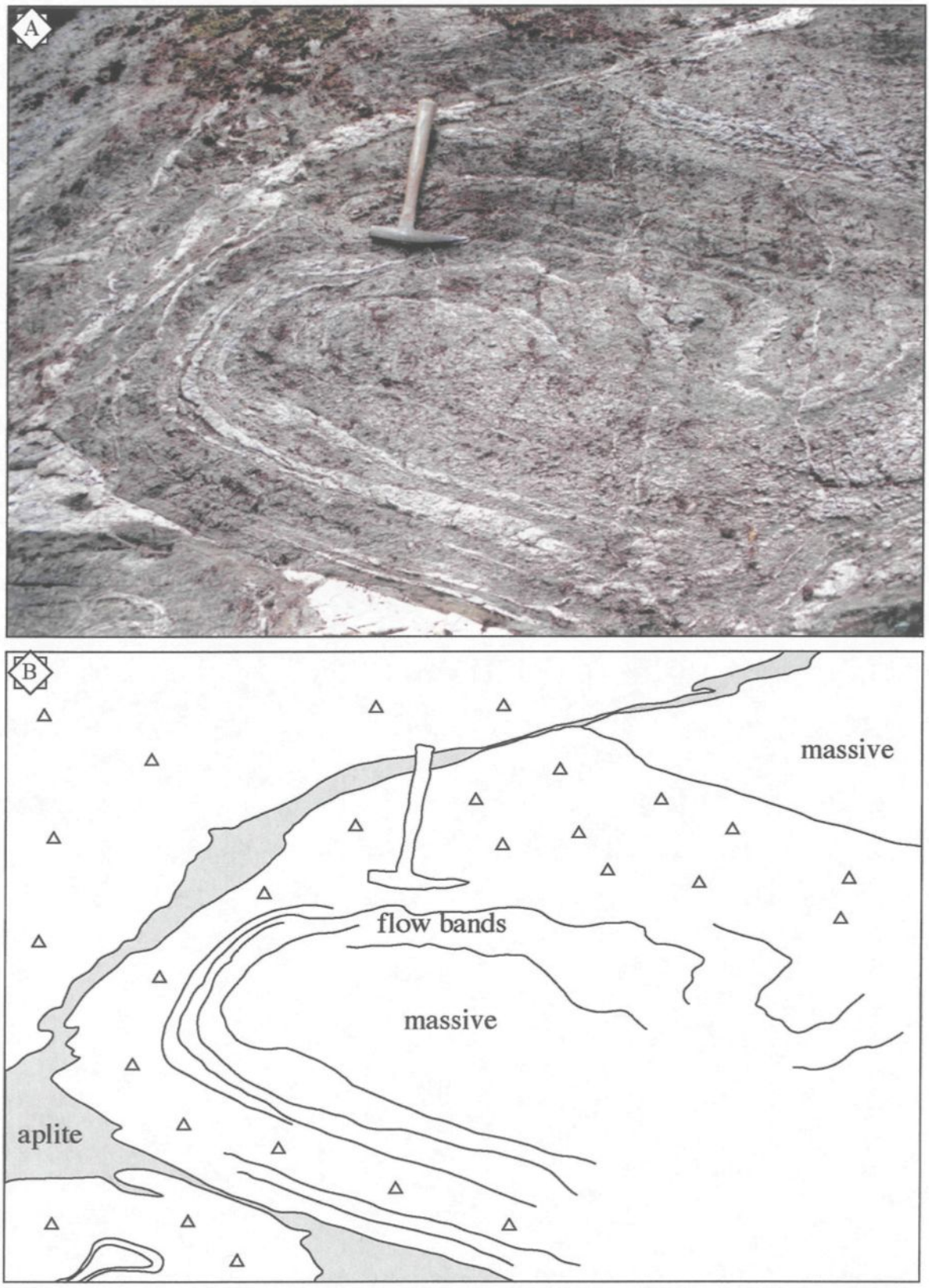

Figure 146. Images depicting relationship between lobes and hyaloclastite. A. Field photo showing intricate flow banding mantling a massive lobe, which is enclosed by a hyaloclasite carapace. B. Cartoon sketch of (A) illustrating the relationship between the lobe and hyaloclastite. Hammer for scale (37 cm long).

Figure 147. Detailed map of lobe-hyaloclastite facies depicted the complex intercalation of lobes and hyaloclastite. Possible to recognize the branching nature of the lava, as smaller lobes bifurcate from large lobes.

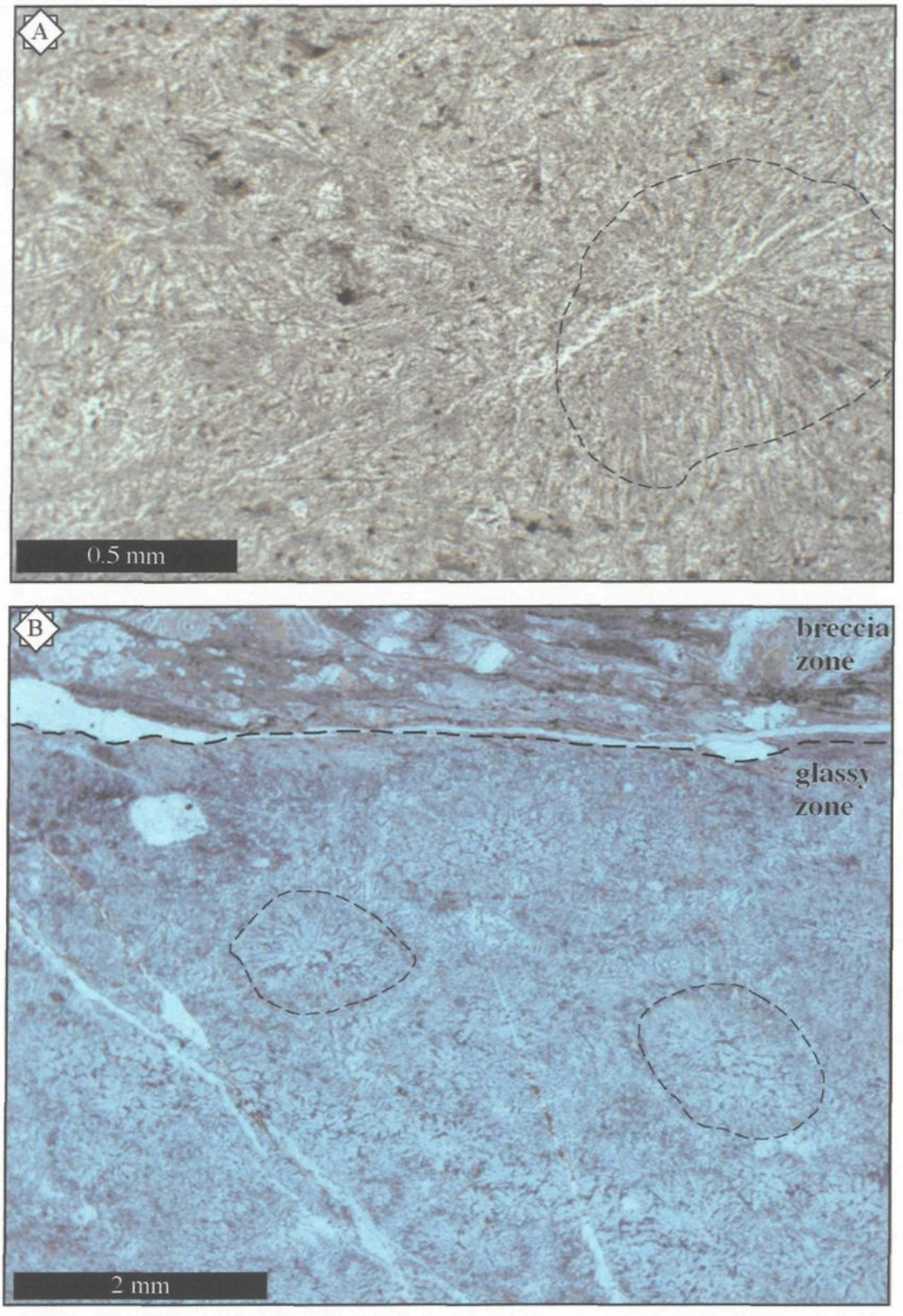

Figure 148. Photomicrographs in plane polarized light of internal parts of spherulitic lobes. A. Close up of amalgamated spherical spherulites that have impinged on each other. B. Margin of lobe with several spherical spherulites identifiable.

149A; Appendix A-27), to separated wedges and plates hosted in a fine-grained quartz + albite + sericite + chlorite matrix (**Figures 149B/C**). Fragment alteration is varied, with three dominant types recognized: (1) chloritic; (2) a high birefringence mosaic; and (3) feldspar + quartz. The former two are typically aphyric and have a wedge- and/or plate-like morphology; whereas feldspar and quartz altered fragments are characterized by curvilinear fracture patterns (**Figure 149D**). Moreover, core-rim boundaries of non-jigsaw fitting fragments are commonly outlined by concentric banding of oxidized material (**Figures 149B/C**), which does not affect internal fractures (e.g. perlitic). Other granules have rims and cores partially replaced by coarse fibro-radial feldspar (**Figure 150; Appendix A-28**), similar to described chessboard albite of Yamagishi and Dimroth (1985), suggesting that they have replaced some fibro-radial mineral (e.g., zeolite).

Capping hyaloclastite facies

The capping 50 m-thick hyaloclastite facies (**Figure 139**) is composed of the same fragment types observed intercalated with the underlying lobe-hyaloclastite facies. This facies has a distinctive black appearance that is characterized by a clast-supported, box-like texture. This facies is massive as no discernable grading or stratification was observed. In thin section, lapilli to tuff sized fragments form jigsaw fitting masses, with curvilinear fracture patterns associated with feldspar + quartz altered fragments (**Figure 151**).

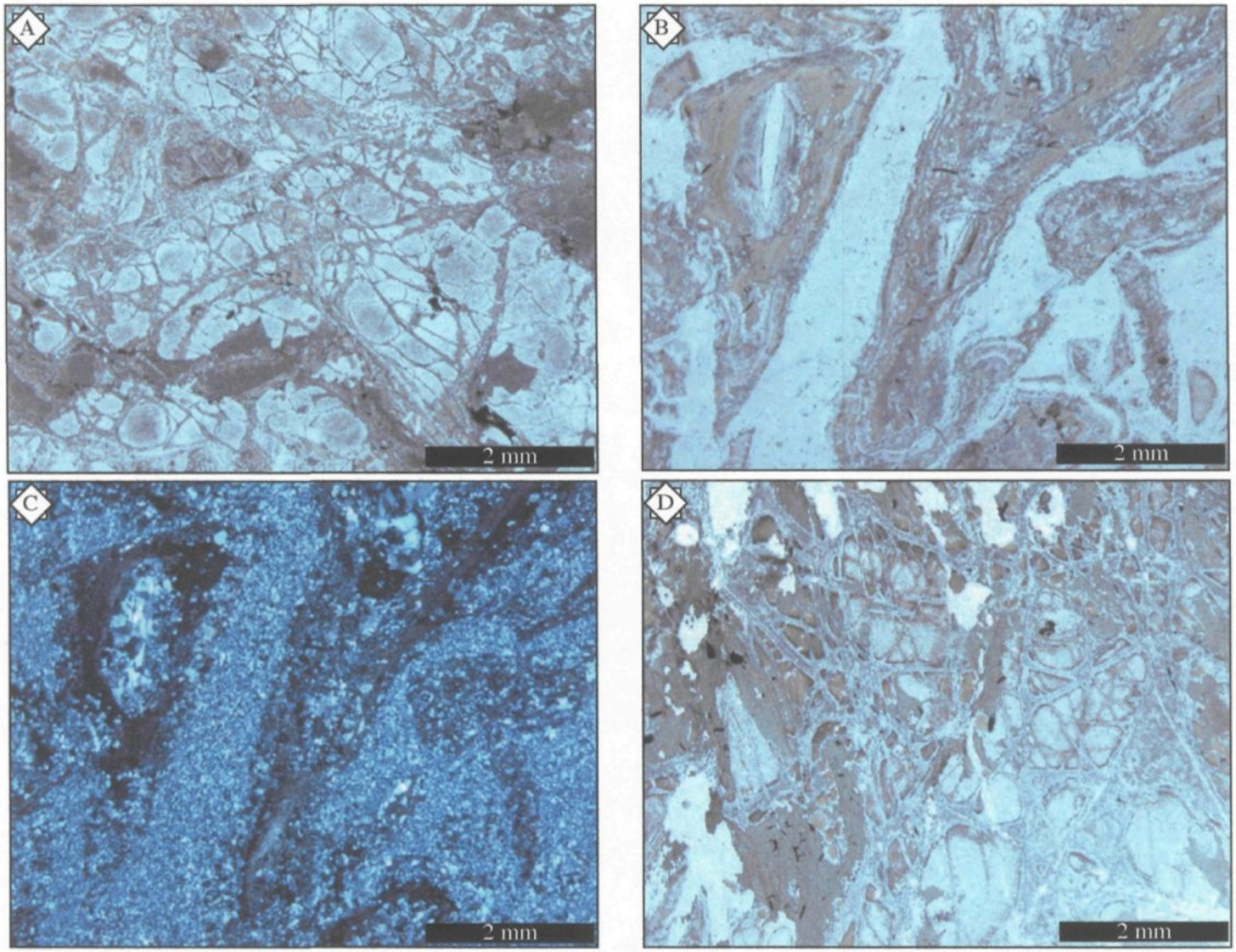

Figure 149. Plane polarized (PPL) and cross-nicols (XN) light microphotographs of hyaloclastite intercalated with lobes. A. PPL image of *in situ* brecciation and jigsaw texture of hyaloclastite. B. PPL image of *in situ* brecciation minus the jigsaw texture, triangle shaped shard also has a mm-sized spherulite in its center. Outer margin of fragments are oxidized. C. XM image of same field of view as (B), note the finely equant, granular mosaic of quartz + albite in the matrix. D. PPL image of perlitic texture of oxidized fragments.

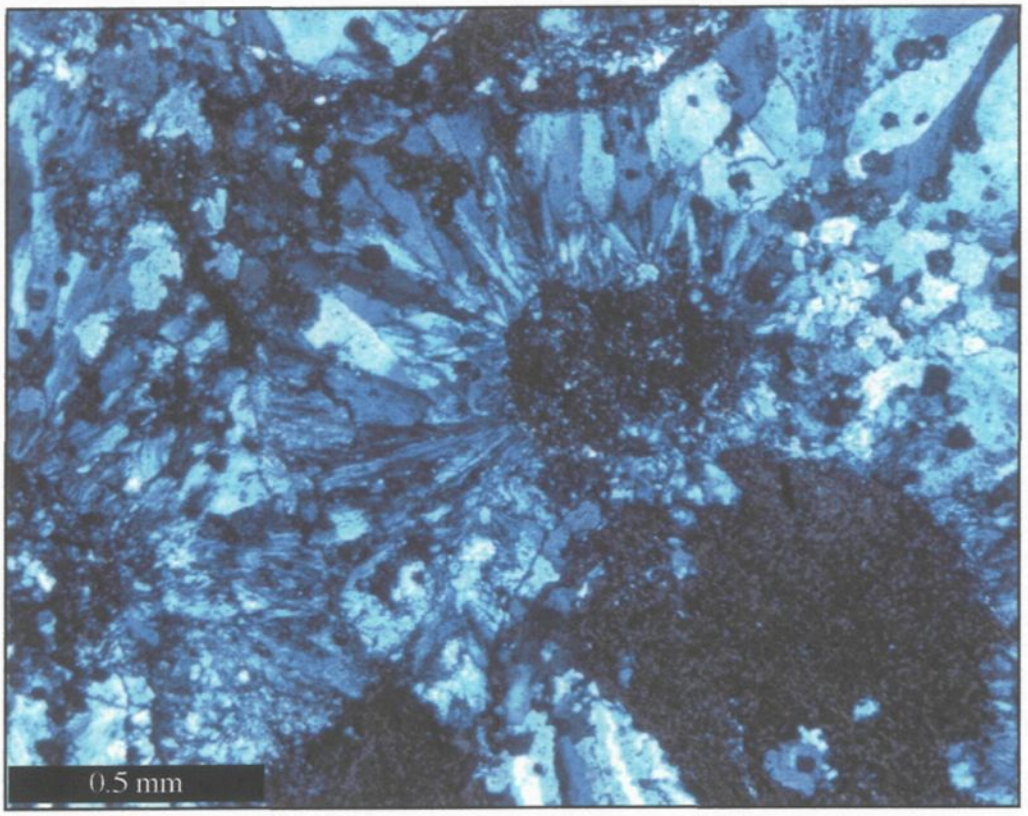

Figure 150. Cross-nicols microphotograph of coarse, fan-like form of albite that probably replaced some fibro-radial mineral (e.g., zeolite).

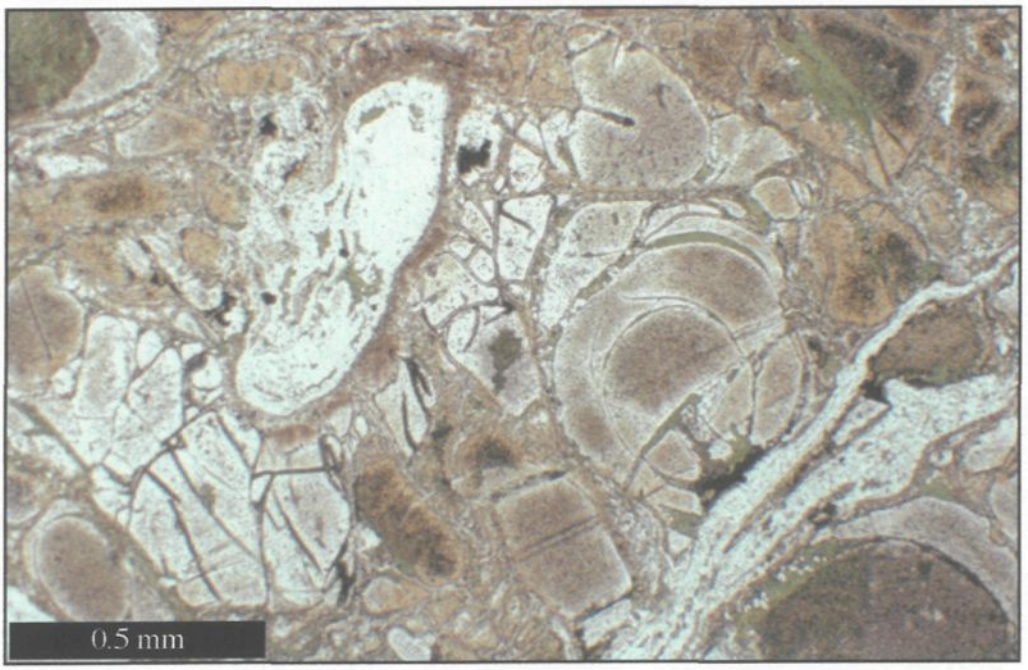

Figure 151. Plane polarized light microphotograph of tuff-sized in situ brecciated hyaloclastite from the capping hyaloclastite facies of the spherulitic dacite lava flows. Evidence of elevated temperatures of hyaloclastite suggested by perlitic texture.

5.1.2 Interpretation of felsic spherulitic unit

The fact that the felsic spherulitic unit serves as a major marker horizon within the Héva Formation is significant as it implies that there is no depositional or structural break between the Val d'Or and Héva formations. This has major ramifications for the region, because if there is a depositional continuum (see section 5.2) between the Val d'Or and Héva formations then it is possible to hypothesize that there are no breaks in the complete group; which has important temporal and spatial implications for any stratigraphic interpretation (see Chapter 7).

The massive nature of the basal facies suggests that it was transported and deposited as a coherent unit without any interaction external to itself. The aphyric nature indicates that this facies was emplaced at elevated temperatures above the crystallization point for felsic minerals (i.e., alkali feldspar and quartz). Spherulites and flow bands are related to the cooling history and laminar shearing within the facies, respectively. The ubiquitous spherulitic texture represents glass devitrification due to sub-solidus crystallization at elevated temperatures (Lofgren, 1971), or above the glass transition temperature; defined as the lowest temperature at which the rate of diffusion can still nucleate spherulites (Manley, 1992). The massive interior of this facies was insulated, thus experienced only limited undercooling. Lofgren (1971) and Swanson et al. (1989) noted that with small degrees of undercooling (ΔT = 50-150°C) spherulites formed large, coarse framework clusters. The lava will undergo compete devitrification forming a finely crystalline core of coalesced spherulites (Garner and McPhie, 1999), sometimes described as a polyhedral mosaic (cf. Shelly, 1992; pg. 182). Flow bands defined by spherulites suggest spherulitic

nucleation on pre-existing inhomogeneities developed in the glass during laminar shearing of viscous felsic lava (Davis and McPhie, 1996). The horizontal orientation of flow bands with regional stratigraphy are indicative of a flow or sill as opposed to a dyke or dome (Scutter et al., 1998). The observed *in situ* clast-supported breccia (**Figure 143**) at the base of this facies probably represents a flow-foot breccia. Flow-foot breccias are associated with felsic lava flows (Bonnichsen and Kauffman, 1987; Manley and Fink, 1987; Scutter et al., 1998) as cooling along the lower contact results in *in situ* brecciation as the flow continues to move.

The medial lobe-hyaloclastite represents an association between fluid lava and fragmental material. The *in situ*, jigsaw fitting, clast-supported nature and lapilli- to tuff-sized, angular monolithic population suggest quench fragmentation processes. This non-explosive process is a result of lava being rapidly chilled by extrusion into water or wet sediment (McPhie et al., 1993) that produced fine-grained hyaloclastites (Fisher and Schminke, 1984). Perlitic fractures indicate that these fragments were hot and glassy (Bevins and Roach, 1978; Cas, 1978; De Rosen-Spence et al., 1980). In addition, the oxide bands that coat hyaloclastites do not affect these internal fractures; therefore, they were probably precipitated from a heated fluid (i.e., seawater) forming Liesegang rings (cf. Dimroth and Lichtblau, 1979). Furthermore, these delicate textures would not survive transport, therefore they were formed in place. These textures indicate that abundant water was available to chill the outer flow margin. Continued propagation of fractures formed due to thermal stress can penetrate and tap the underlying, still molten, felsic lava. Felsic lava would expand and branch into the wet hyaloclastite pile to form lobate structures

(Yamagishi and Dimroth, 1985; Kano et al., 1991). Chilled contacts result in a preferential viscosity contrast that form flow bands (**Figures 146 and 147**) which serve as sites of spherulitic crystallization. Hyaloclastites and arrested spherulitic crystallization observed interstitial to spherulitic flow bands (**Figures 145C/D**) indicate rapid cooling, probably induced by conductive cooling to the surrounding hyaloclastite.

The capping hyaloclastite facies represents the outer margin of the felsic unit that experience rapid cooling from water to form a rigid crust. Quench fragmentation progressed through a series of fractures (Yamagishi and Dimroth, 1985) that formed this thick, massive, clast-supported facies. Perlitic fractures attest to its hot glassy origin and that it was not subsequently transported.

5.1.3 Model of emplacement

Major element geochemistry illustrates that this unit is felsic in composition, specifically a dacite (see chapter 6), so the problem is; how is it possible to emplace a > 20 km long felsic unit? Rheology of felsic magma includes viscosity on the order to 10^7-10^9 poise (for 2 to 1 vol% H_20; pg 124, Best & Christiansen, 2001), which typically precludes the eruption and emplacement of long extrusive felsic lava flows (Manley and Fink, 1987; Manley, 1992; Scutter et al., 1998). In addition, the subaqueous environment interpreted for the Val d'Or Formation and the notion that the Héva Formation is a depositional continuum would imply that the environment remained subaqueous, which would emplace further restrictions (Gibson, 1999) on an (subaqueous) extrusive origin. Three possible scenarios

for this felsic unit include; (1) an intrusive sill, (2) a subaqueous extrusive lava flow, or (3) a subaerial extrusive lava flow.

An entirely intrusive emplacement would be characterized by baked and chilled margins or even a metamorphic aureole (Cas, 1978), both of which are not observed. Moreover, the described stratigraphy from massive to brecciated facies, with a foot breccia (**Figure 143**) implies an extrusive origin. Nonetheless, we cannot completely rule out the intrusion scenario (see below). The chilled margins within gabbros indicate that the felsic spherulitic unit predates their emplacement.

The extrusive hypothesis is limited to an extensive lava flow, rather than the more common felsic dome complex (aspect ratio ≈ 1; pg. 243, Best and Christiansen, 2001), based on its low aspect ratio of ~ 0.2 (thickness/length; 400m/20000m). First let's review the intrinsic and extrinsic conditions that favor an extensive lava flow (cf. Scutter et al. 1998), which include: (1) high eruptive temperatures; (2) low water content of magma; (3) anomalously low viscosity; (4) elevated eruption rates; (5) low cooling rates; and (6) steep local topography. In turn, these conditions need to modify the magma's rheology, which is controlled by the composition, temperature, volatile content, crystallinity, and bubble content (McBirney and Murase, 1984). Such changes have been documented within subaerial (Fink, 1983; Dadd, 1992; Manley, 1992), subglacial (Furnes et al., 1980), and subaqueous (Cas, 1978; De Rosen-Spence et al., 1980; Kano et al., 1991) environments to produce laterally extensive felsic lava flows.

The composition of this felsic magma does not vary from being a dacite (see chapter 6), therefore a change in composition does not control emplacement. The temperature,

while unknown, can be indirectly assumed to be close to or above the liquidus based on the lava's aphanitic nature (< 1 vol% phenocrysts) (Yamagishi and Dimroth, 1985; Eichelberger et al., 1986). The original volatile content is also unknown, however bubbles or vesicles, which indicate volatile exsolution, are observed in only trace amounts. Therefore, this may be a function of the original volatile content or extrinsic forces (e.g., pressure) limited volatile exsolution. Shaw (1974) experimentally showed that there is a positive correlation between H_2O solubility and pressure. Either way, the absence of vesicles/bubbles will decrease a lava's viscosity (Cas, 1978; Yamagishi and Dimroth, 1985; Orton, 1996), even more so if volatiles are kept in solution (Hess and Dingwell, 1996).

In summary, the aphanitic, non-vesicular nature of this unit suggests that this lava was erupted at high temperatures and was either *dry* or volatile exsolution was suppressed. A possible mechanism for volatile suppression could be elevated hydrostatic pressures within a subaqueous environment (Wallace and Anderson, 2000). Thus, the absence of crystals, an assumed high temperature, and lack of volatile exsolution combine to greatly ***reduce*** the viscosity of otherwise high viscosity lava (Cas, 1978; Yamagishi and Dimroth, 1985; Orton, 1996). Elevated discharge rates and paleotopography are difficult to ascertain in ancient volcanic systems. Nevertheless, the general planar nature of the felsic unit in cross-section would seem to suggest that there was no significant topography change that might have played a role during deposition. This is further implied by the absence of any stratified fragmental facies, which would suggest remobilization due to slumping. Therefore, a possible source is a fissure-fed eruption, where flows would form broad,

gentle-sloped shields or plateaus, similar to those envisaged for mafic eruption (Gibson, 1999).

Fissural-fed lavas are typically high-volume, high-temperature events (Duffield, 1990) that form sheet flows (Bonatti and Harrison, 1988), which favor the lateral propagation of (felsic) lava. Bonnichsen and Kauffmann (1987) suggested that subaerial felsic lava flows originate from high-discharge, fissural eruptions at temperatures upwards to 1000°C. Thick flows, whether they are felsic or mafic, form tabular sheets (**see Figure 138**), which would facilitate heat retention that further increases exponentially with thickness (Fink, 1983); thereby inhibiting any increase in viscosity and keeping the flow mobile (Manley, 1992). However, how is heat retention maintained in the subaqueous environment? Interaction between cold ambient seawater and hot, fluidal felsic lava would result in either explosive disintegration or rapid cooling of the lava's exterior. Evidence of a possible explosive phreatomagmatic-type eruption, such as vesiculated, finely comminuted tuff, forming density graded or stratified deposits, is absent (Wohletz and Sheridan, 1983). What is observed is a monomictic, massive, clast-supported, jigsaw-fitting upper facies composed of lapilli- to tuff-sized glassy hyaloclastite fragments; which indicates subaqueous emplacement or intrusion into wet sediment (McPhie et al., 1993).

Therefore, it is envisaged that a rigid crust quickly formed, which may have effectively sealed the erupting fissure and the propagating flow front from the persistent cooling effects of water. As the eruption continued to feed the distal extremities, it inflated (see Cashman et al., 1998) the complete sequence as the outer margin continued to cool. The glassy rigid margin proceeded to undergo quench fragmentation through a series of 1st

to 3rd order cracks perpendicular to cooling surfaces, resulting in *in situ* disintegration (Yamagishi and Dimroth, 1985), forming a capping microbreccia (cf. De Rosen-Spence et al., 1980). Busby et al. (2003) suggest that very efficient quench granulation may be a feature of high volume flows emplaced at high temperatures. Distally located flow breccia deposits commonly associated with felsic lava flows (Pichler, 1965; De Rosen-Spence et al., 1980; Furnes et al., 1980) are not observed in contact with the massive facies, but might be present but not observed due to lack of exposure or restricted high laminar shear movement of cooler, more viscous lava. Continued propagation of 1st order fractures may eventually tap the underlying molten interior of the flow resulting in branching lobes that extruded onto or into the hyaloclastite pile (Yamagishi and Dimroth, 1985; Kano et al., 1991).

The underlying massive interior of the felsic lava remained at elevated temperatures for an extended period of time, which facilitated the lateral propagation. This also kept temperatures above the glass transition temperature, thereby promoting spherulitic crystallization.

To conclude, this spherulitic dacite unit is interpreted as a subaqueous felsic lava flow that is subdivided into three facies; a basal massive lava, medial lobe-hyaloclastite, and capping hyaloclastite, which is similar to the subaqueous lobe-hyaloclastite felsic flow of Gibson (1999). Finally, it is conceivable that portions of this unit may be a hypabassal sill complex, whereby felsic magma intruded into unconsolidated sediment (Batiza and White, 2000); and in general the injection of lava into the hyaloclastite pile behaves in a similar manner.

5.2 Tex-Sol area (volcaniclastic facies)

The Tex-Sol region (ROI 2) represents a small volume sequence of polymictic volcaniclastic tuff breccias and interstratified gabbros, located approximately 500 m from the presumed contact with the underlying calc-alkaline volcano-sedimentary rocks of the Val d'Or Formation (**Figure 137**). Their polymictic nature and proximity to the Val d'Or Formation is important in unraveling the depositional history of the region. The contact with the Val d'Or Formation is approximate at best and based on aeromagnetic data (**Figure 138**), rather than field-based observations, which is a function of outcrop exposure. Nevertheless, there is a change over several hundred meters from dominantly intermediate volcanism of the Val d'Or Formation to mafic volcanism, or the appearance of the spherulitic dacite unit (**Figure 136**). Moreover, this change in composition is accompanied by a change in geochemical series from calc-alkaline to tholeiite (see chapter 6); whereas the spherulitic dacite unit is a marker horizon, the Tex-Sol outcrops preserve evidence that there was a depositional continuum between the Val d'Or and Héva formations.

5.2.1 Lithology of Tex-Sol area

The Tex-Sol area is represented by a several stripped outcrops oriented roughly north-south; the most westerly outcrop is mapped in detailed. This particular outcrop is composed of several tuff breccia beds, a fine-grained tuff, an aphyric mafic and felsic intrusion (?) and several gabbroic intrusions.

Four volcaniclastic tuff breccias are recognized, based on grading and internal erosive contacts (**Figure 152**). The lowermost (northern) tuff breccia is characterized by a 5 m-thick clast-supported base that grades into a matrix-supported lapilli tuff (**Figure 152**). The next three tuff breccias are normal-graded, matrix-supported, and range between 7- to 15 m-thick, separated by sharp, irregular contacts (**Figure 152**). All tuff breccias are massive and characterized by a bimodal fragment population (**Table 18**).

Population one consists of angular to subangular, yellowish brown fragments that range from breccia- to tuff-sized. Their vesicularity is upwards to 5-vol%, represented by quartz amygdules (**Figure 153A**). In thin section, they are feldspar-rich (~ 20 vol%), with phenocrystic and microphenocrystic populations. Feldspars commonly form 3-mm tabular phenocrysts that vary from euhedral to subhedral habits (**Figure 153B**). Microphenocrystic feldspars have a tabular to acicular morphology and an euhedral habit that make up to 35-vol% of the groundmass (**Figure 153B**). Quartz amygdules comprise < 1-vol%.

Fragment population two is rounded and altered a grayish-blue, with 20-vol% quartz amygdules (**Figure 154B**). Petrographically, euhedral, tabular feldspars compose about 5-vol%, with an average size of 1-mm (**Figure 154B**). Alteration is minor, with < 1 vol% chlorite + epidote + carbonate. Vesicularity is upwards to 20-vol% in the form of quartz amygdules, with some amalgamation occurring between juxtaposed vesicles (**Figure 154B**). Amygdules larger than 5-mm become progressively elongated, whereas those greater than 1-cm appear tube-like in cross-section (**Appendix A-29**).

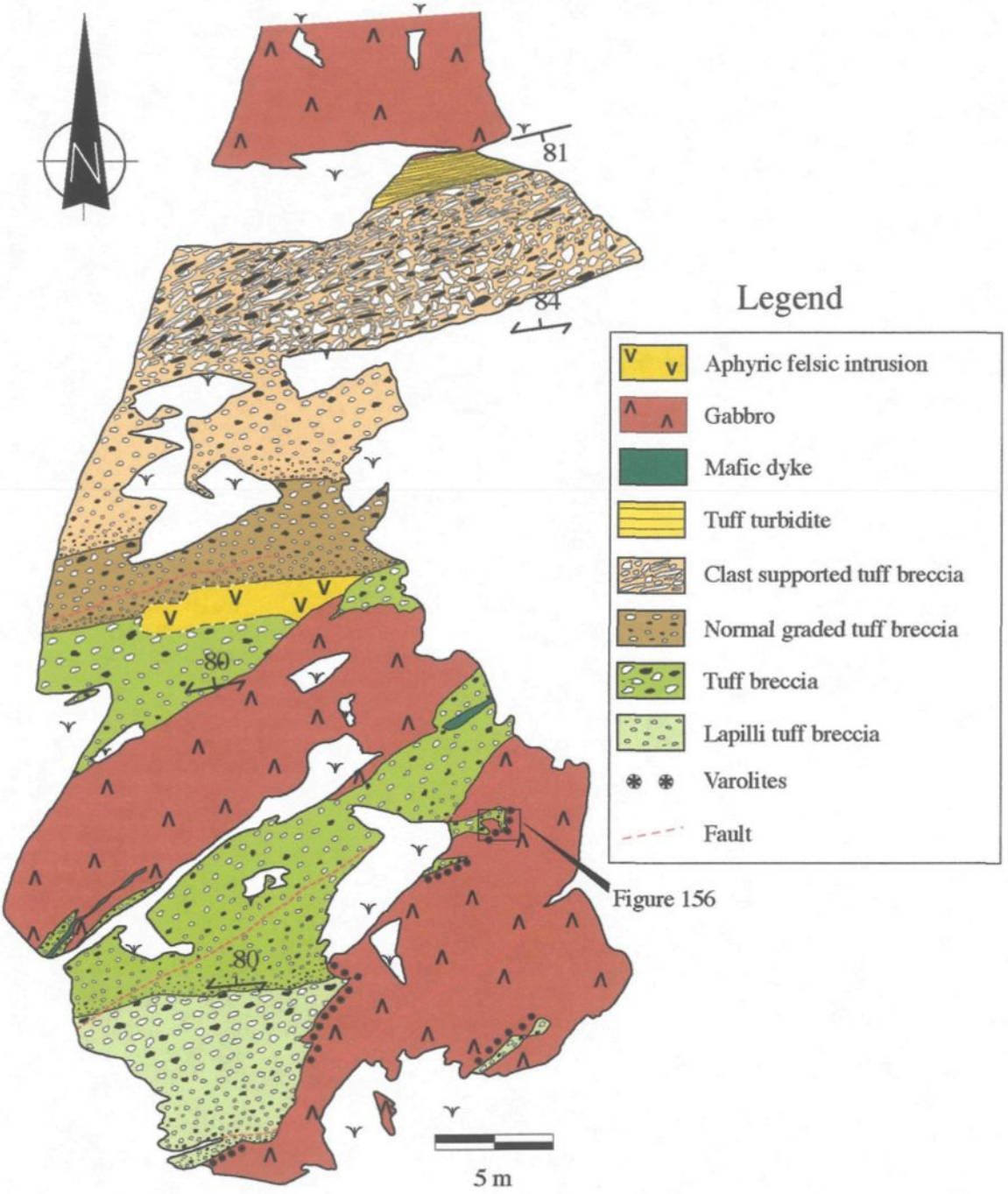

Figure 152. Detailed mapping of Tex-Sol outcrop illustrating the interbedded relationships between the various volcaniclastic beds and contacts with the felsic, mafic and gabbroic intrusions.

Table 18: Lithofacies of Tex-Sol area (ROI 2).

Lithofacies	Thickness & morphology	Characteristics	Transport/deposition	Origin
Volcaniclastic				
Tuff	2-3 m-thick; planar beds	Laminated, normal-graded beds; orange weathered; sharp contacts	Series of low-concentration turbidity flows	Resedimented tuff-sized material possibly originating from more explosive volcanism from underlying Val d'Or Formation
Tuff breccia to lapilli tuff breccia	7-15 m-thick; planar to irregular beds	Clast- to matrix-supported; massive; normal graded; sharp planar to irregular, erosive contacts; two fragment populations:	Cohesive debris and high- to low-concentration turbidity flows	Epiclastic deposit composed of eroded clasts from Val d'Or Formation
		Angular fragments : Breccia- to tuff-sized; yellowish-brown; < 5-vol% quartz amygdules; 20-vol% feldspar	Limited transportation	
		Rounded fragments: Breccia- to tuff-sized; grayish-blue; 20-vol% quartz amygdules; 5-vol% feldspar	Abraded due to transportation	

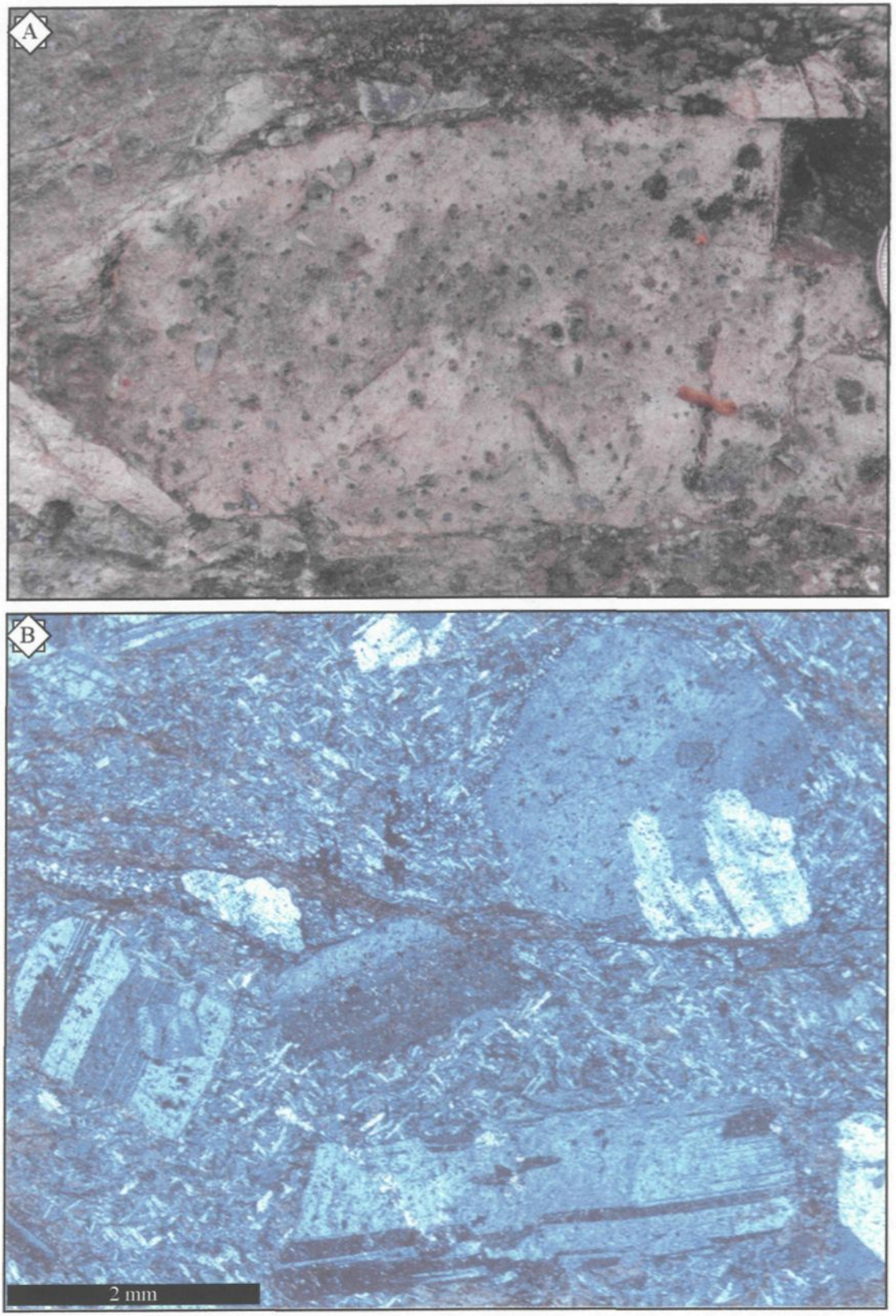

Figure 153. Photos of mafic fragment. A. Outcrop shot showing vesicular nature of angular fragment. Edge of quarter for scale. B. Crossed-nicols photomicrograph illustrating feldspar-phyric nature.

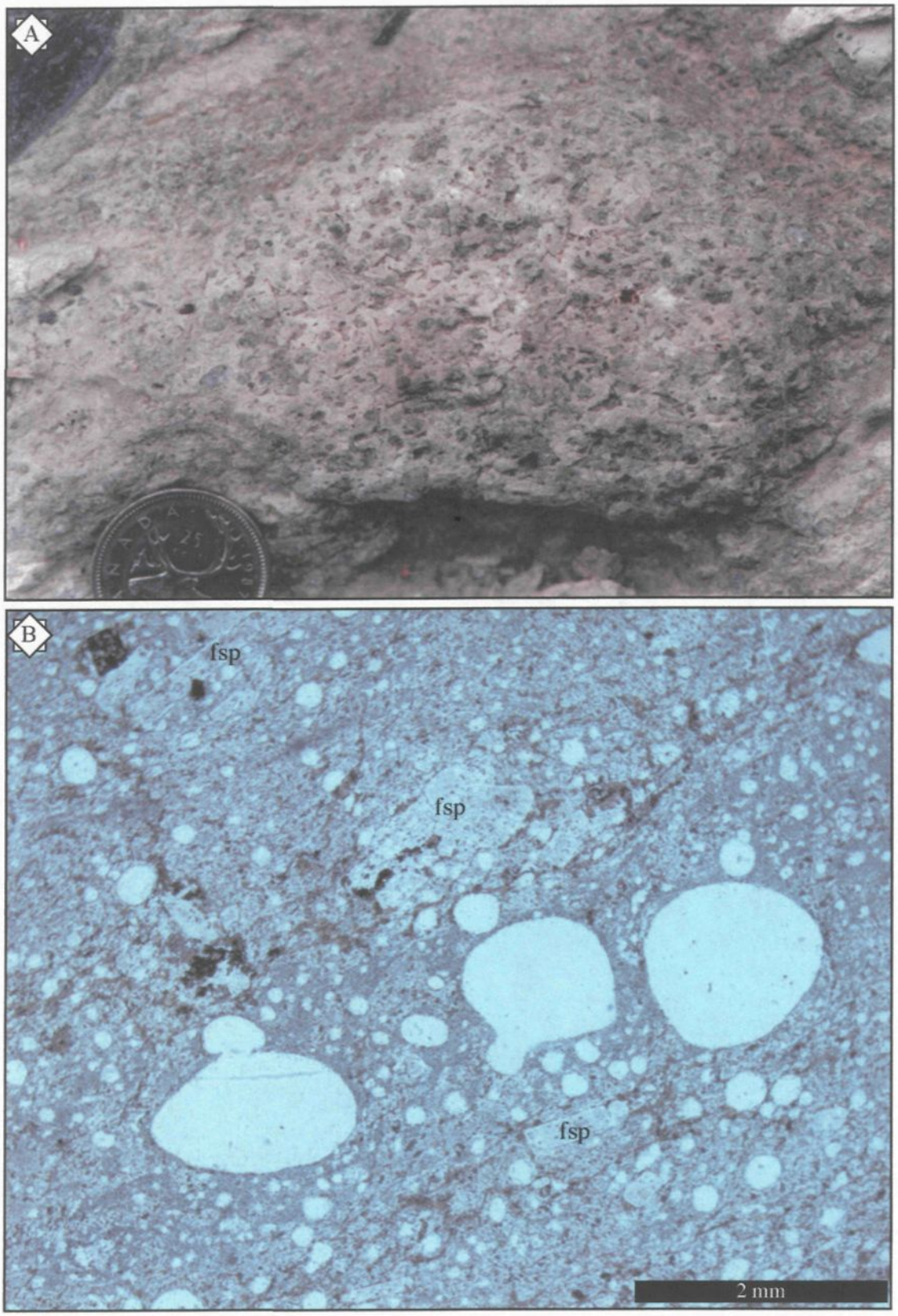

Figure 154. Images of rounded fragments. A. Image of rounded morphology and vesicular nature of pumice fragment; quarter for scale. B. PPL microphotography showing vesicular nature and tabular feldspar (fsp) phenocrysts in groundmass. Note the rounded nature of quartz-filled vesicles.

The subordinate 2-3 m-thick tuff turbidite sequence is highly weathered and altered to an orange hue, thereby precluding any useful sedimentological analyses. However, it appears to be truncated by the overlying (southern) tuff breccia (**Figure 152**).

The aphyric felsic and mafic intrusions are discontinuous, but cut the volcaniclastic stratigraphy. The felsic intrusion appears to be a sill as it is parallel to bedding, but its contact relationship with the gabbro is ambiguous, thus making a temporal interpretation impossible. In contrast, the mafic intrusion cuts both the sediments and gabbros, thus making it younger (**Figure 152**).

Gabbroic intrusions are composed of fine-grained feldspar and hornblende, with the latter being pervasively altered to chlorite. Contacts with the volcaniclastic lithofacies are characterized by conspicuous soft sediment deformation, variolitic (**Figure 155**), and peperitic textures (**Figure 156**). Varioles are restricted to within 30-50 cm of the volcaniclastic contact (**Figure 152**) and are composed of fibrous feldspar microlites that form isolated, cm-sized, sub-spherical forms (**Figure 157**) or amalgamated mats composed of fans of acicular feldspar (**TS104; Appendix A-30**).

5.2.2 Interpretation of Tex-Sol area

The bimodal character of these volcaniclastic tuff breccia beds suggests a resedimented origin, whereby the rounded and angular fragments were mixed during transport via high- to low-density sedimentary gravity flows (**Table 18**). The rounded nature and grayish weathered appearance suggest that these fragments are felsic in composition, whereas the more angular, yellowish fragments are more mafic in

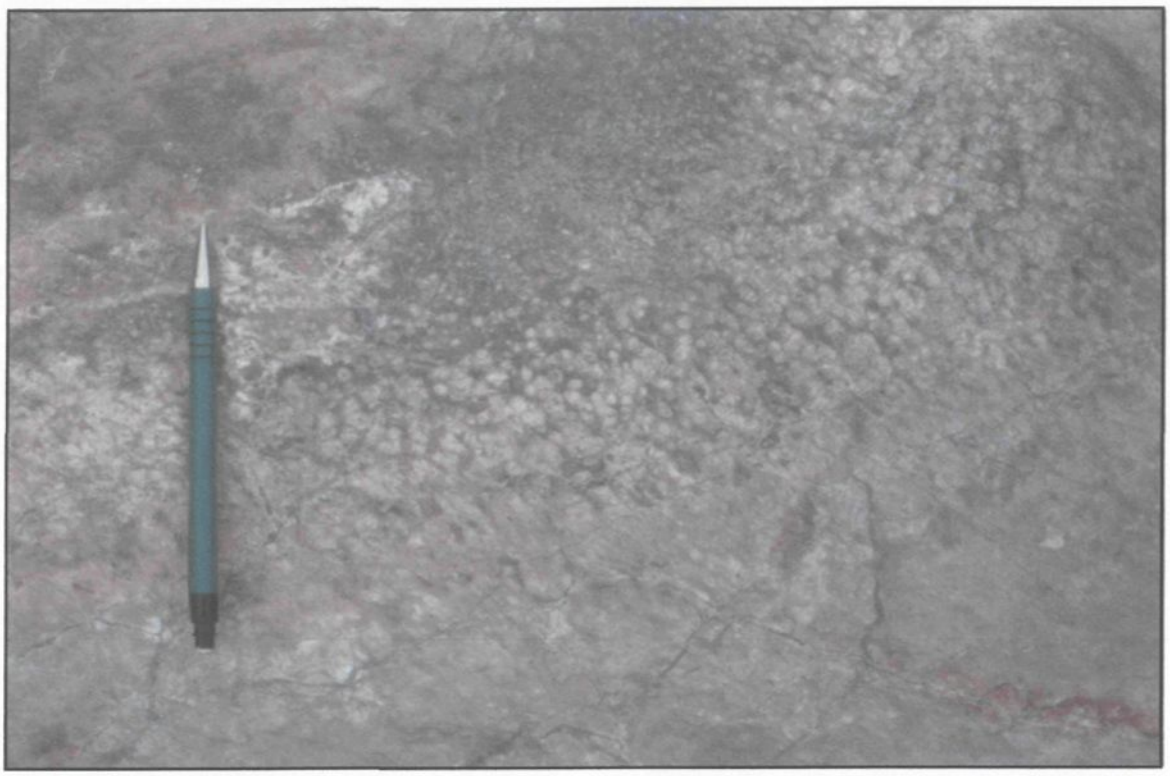

Figure 155. Variolitic margin of gabbroic intrusion in contact with volcaniclastic sedimentary rock. Pencil for scale (14.5 cm long).

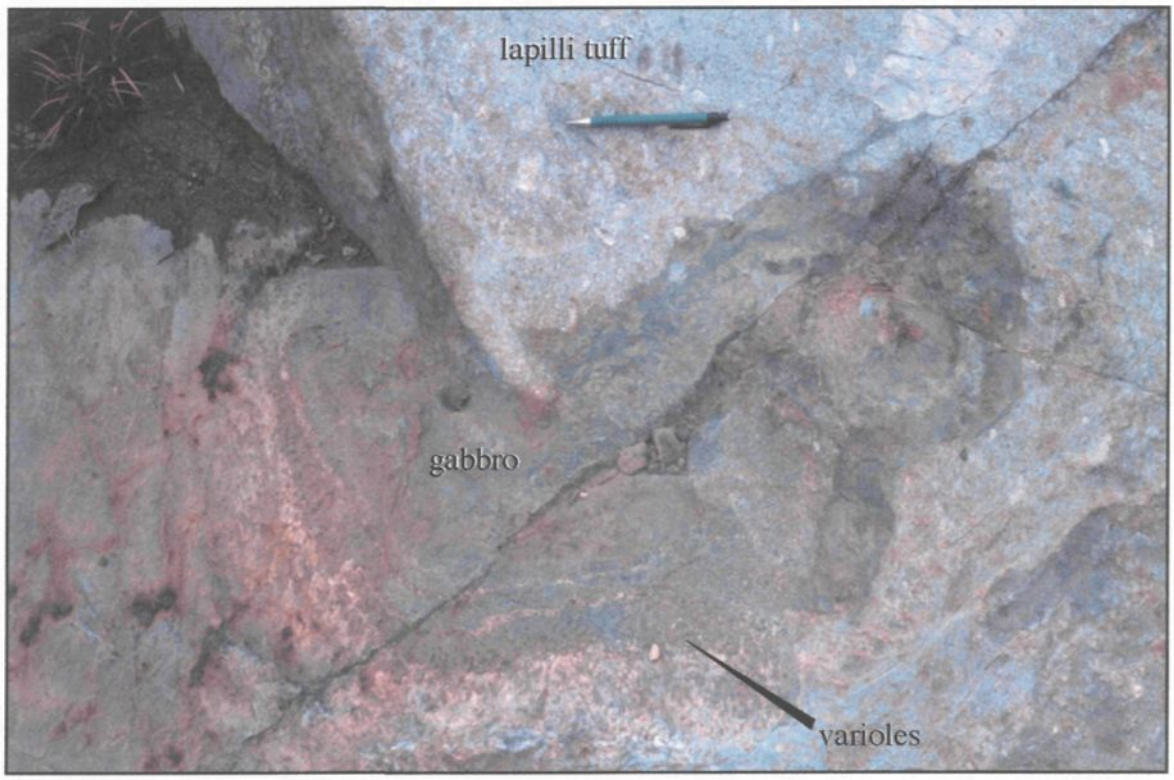

Figure 156. Irregular mixing of gabbro and volcaniclastic sediment forming a peperite. Contact is also defined by varioles within gabbro. See Figure 152 for location. Pencil for scale (14.5 cm long).

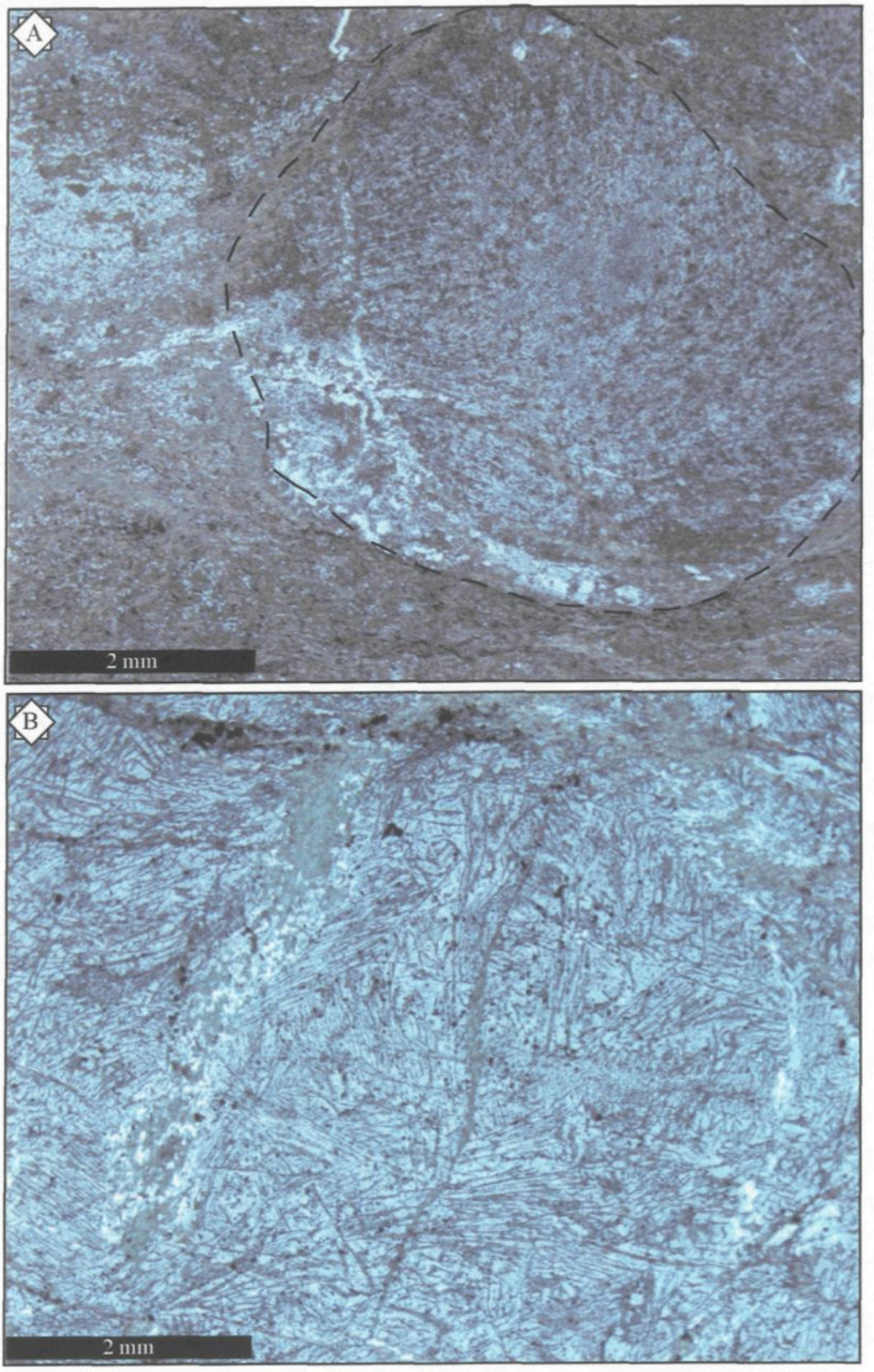

Figure 157: Photomicrographs of varioles observed along gabbroic margin. A. Crossed-nicols image of isolated, fibrous microlites of feldspar forming a sub-spherical spherulite. B. PPL image of amalgamated mat of acicular feldspar.

composition. Their morphology also implies that the rounded felsic fragments were abraded during transport, but the angular mafic fragments have undergone limited abrasion (i.e., short residence time). Therefore, these volcaniclastic deposits are considered epiclastic in origin (Fisher and Schmincke, 1984). In addition, the calc-alkaline to transitional nature of these fragments (see chapter 6) suggests that they probably originated from the underlying Val d'Or Formation.

This provenance has important ramifications for the geologic history of the area as this suggests a **depositional continuum**, whereby the contact between the Val d'Or and Héva formations is conformable. Moreover, this supports the hypothesis that the Héva Formation is **younger** than the Val d'Or Formation. In addition, these deposits support the notion of rifting, since with rifting there is an increased potential of erosion of the arc, which may explain the polymictic population of fragments located close to the presumed contact with the Val d'Or Formation (cf. Carey, 2000). The erosive and graded nature of these deposits indicates a southward younging direction, which is accordance with a transition from the Val d'Or to Héva formation.

Soft sediment deformation, peperites, and varioles all indicate contemporaneous injection. Soft sediment deformation records the internal disruption of structures within the sediments, which is only possible if they are still wet and unconsolidated. Furthermore, peperite development indicates the fluidization of wet sediments by the generation of water vapor along the magma-sediment interface. Fluidization results in the destruction of sedimentary structures, as the sediment is mixed and sometimes even transported. In such cases, magma replaces the sediment, while the remaining sediment is undisturbed, retaining

its original bedding (Kokelaar, 1982). Moreover, the peperites are subrounded, not blocky (**Figure 156**), thus magma-sediment interaction was non-explosive, indicating that steam was not generated (Busby-Spera and White, 1987). A lack of steam suggests that available water was either limited, or the combined lithostatic and hydrostatic pressures inhibited vaporization of pore water. The former maybe be viable since evidence of synvolcanic emplacement is limited to the southernmost gabbro, suggesting the underlying sediments had already become too dehydrated and/or consolidated to provide substantial water. In addition, while elevated pressures do suppress vapor generation, experiments have demonstrated phreatomagmatic fragmentation at depths equal to greater than 3000m (Morrissey et al., 2000); thus it would seem that the quantity of water was the controlling factor. The formation of varioles provides further support for contemporaneous emplacement. The cooling effect of water along the contact facilitates the growth of varioles or they may represent immiscible mixing between the sediment and magma (Fowler et al., 2002).

5.3 Akasaba North region (ROI 3)

The Akasaba North region encompasses four separated outcrops previously stripped for exploration in proximity to the former Akasaba Mine, which is located approximately 100 m to the south (**Figure 137**). These four outcrops cover three sections of the local stratigraphy that spans approximately 200-250 m of the vertical sequence (a-c, **Figure 137**), with each outcrop zone measuring between 40 m x 45 m and 75 m x 40 m. Akasaba

one and two are about 50 m apart and roughly on strike with each other. Akasaba three is located about 120 m northeast of Akasaba two and represents the lower part of the local stratigraphy (see below).

The region is composed of three principle lithofacies: (1) volcaniclastic tuff to lapilli tuff; (2) pyroclastic lapilli tuff; and (3) gabbroic intrusions (**Table 19**). Also of note are minor zones of mineralization that have replaced some of the volcaniclastic deposits, and prominent peperitic textures developed between gabbroic intrusions and volcaniclastic rocks.

5.3.1 Lithology of Akasaba region

The volcaniclastic and pyroclastic lithofacies are recognized based on contact relationships and fragment populations. Gabbros are typically fine-grained and cross-cut all both these lithofacies. Contact between gabbros and volcaniclastic tuff is characterized by fluidal and blocky peperite textures and disruption or destruction of bedding.

Volcaniclastic lithofacies (tuff and lapilli tuff)

The lower part of the sequence is characterized by an approximate 30 m-thick continuous succession of intercalated volcaniclastic tuff to lapilli tuff beds (**Figures 158 and 159**); the only such location of voluminous deposits of fine-grained volcano-sedimentary rocks recorded within the Héva Formation. Stratified tuffs form thin repetitive beds on the order of several cm's to a maximum of 2 m that cap m-thick, massive non-sorted lapilli tuff beds (**Figure 159**). Fine-scale truncation of individual lamina (**Figure**

Table 19: Lithofacies of the Akasaba area (ROI 3).

Lithofacies	Thickness & morphology	Characteristics	Transport/deposition	Origin
Volcaniclastic				
Tuff	cm- to m-thick; tabular	Finely laminated (T_{bd}) to massive (T_a); normal graded; sharp to truncated contacts; rip up clasts; flame structures; localized disturbance of bedding and featureless in proximity to gabbro; 10-40-vol% broken, euhedral feldspar	Low-concentration turbidity flow(s); series of temporal flows with soft sediment deformation and erosion	Explosive fragmentation followed by periodic slumping or eruptive pulses
Lapilli tuff	m-thick; tabular	Massive (T_a); unsorted; 10-40-vol% broken, euhedral feldspar	Low- to high-concentration turbidity flow; deposition probably by suspension/fallout	Explosive fragmentation and fallout
Pyroclastic				
Lapilli tuff	5-15 m-thick; irregular to tabular	Massive to localized weakly developed stratification; clast- to matrix-supported; subrounded, vesicular (40%), aphyric fragments; flattened, aphyric fragments; armoured lapilli fragments; chilled lapilli; bedded tuff fragments, some up to several m-long; broken crystals in matrix	Laminar plug flow; erosive flow that ripped up clasts from underlying bedded tuff; *en masse* freezing	High temperature, gas-charged pyroclastic (magmatic) eruption; limited water-interaction; primary facies
Intrusive				
Gabbro	5-20 m-thick; sill- to dyke-like	Irregular contacts with tuff; fine-grained, plagioclase- and hornblende-phyric; xenolithics of featureless tuff; fluidal and blocky peperitic margins in contact with tuff	Injection into volcaniclastic and pyroclastic lithofacies	Syn-volcanic intrusion into wet, unconsolidated tuffs

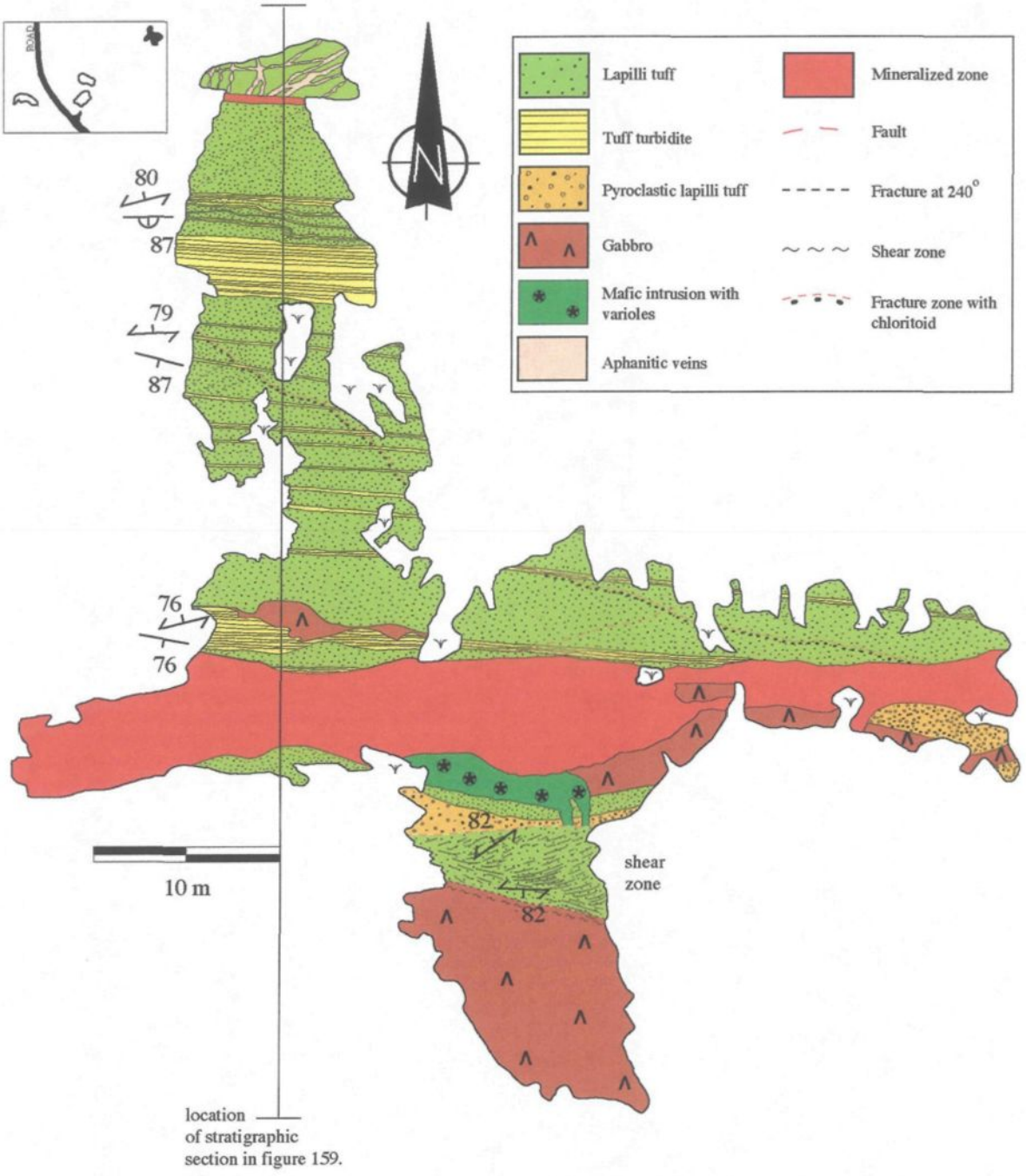

Figure 158. Detailed map of easternmost outcrop within Akasaba North region. Area is characterized by abundant fine-grained material and a mineralized zone that has replaced the lapilli tuff facies. Small cartoon of general location of outcrop in relation to other zones shown in upper left.

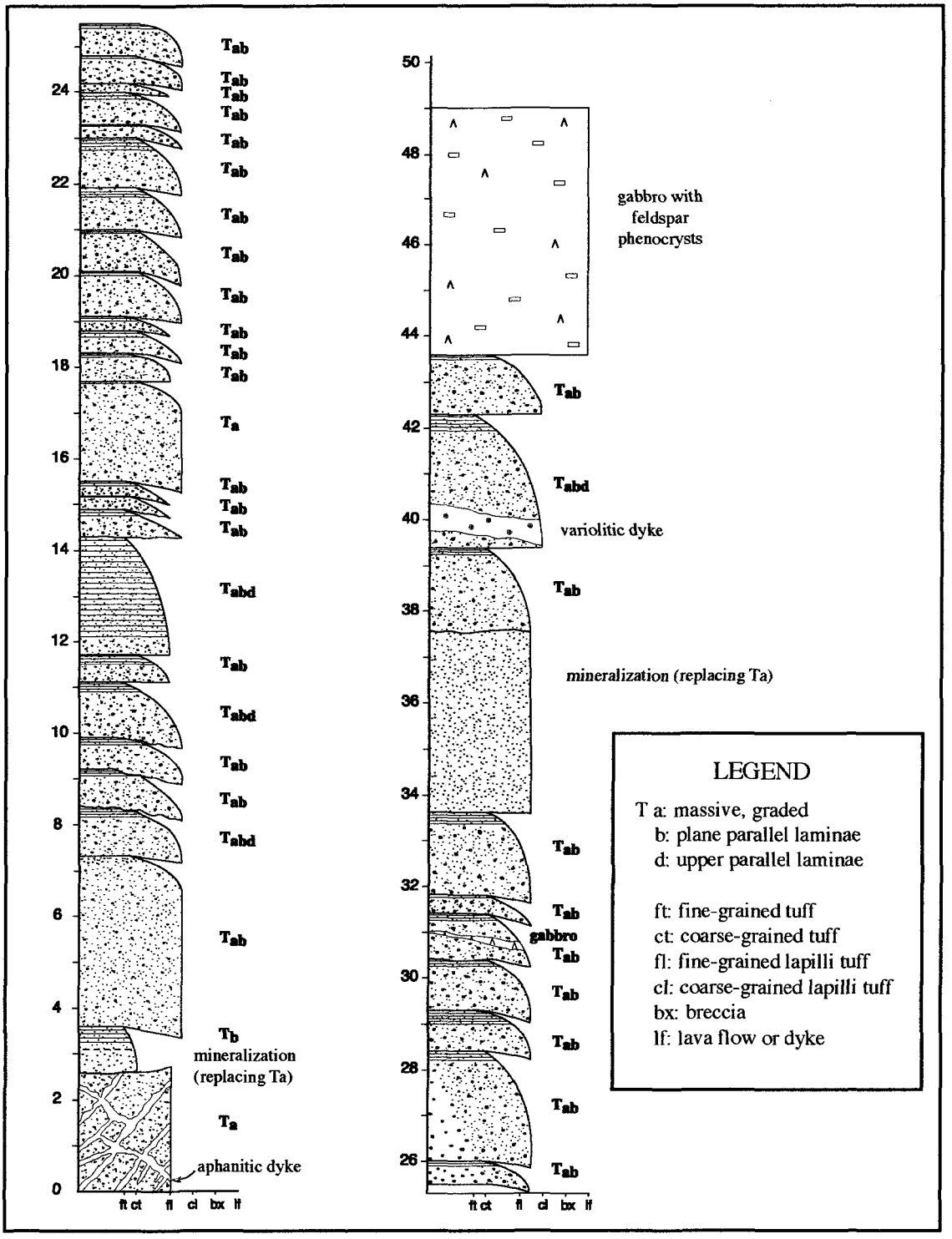

Figure 159. Stratigraphic column of easternmost outcrop from Akasaba North area. Note the thickness of the tuff - lapilli tuff facies.

160A), rip-up clasts (**Figure 160B**), flame structures (**Figure 160C**), and grading (**Figure 160D**), indicate a southward younging direction. Lapilli tuff beds are absent further up section and tuffs become discontinuous (**Figures 161 and 162**). These discontinuous zones appear as m-sized rafts of tuff intercalated with gabbro and pyroclastic lapilli tuff (**Figures 161 and 162**). Bedding of tuff rafts is preserved when hosted in pyroclastic lapilli tuff, but typically disturbed (**Figure 163A**), folded, or destroyed adjacent to gabbro. When destroyed the tuff appears homogeneous and featureless (**Figure 163B**). Contact with the pyroclastic lapilli tuff facies is sharp and typically planar. In contrast, contacts with gabbro are sharp to gradational, but especially irregular ranging from; (1) extensions of gabbro intruding between bedding planes and even incorporating pieces of tuff (**Figure 163C**); (2) gabbro being brecciated in proximity to the sediments (**Figure 163D**); or (3) sediments being brecciated by penetrating fingers of gabbro (**Figure 163E**). Elsewhere, gabbro has intruded into and pooled to form rounded, amoeboidal forms (**Figures 163F/G**) within sediments. In such cases, sediments are bleached (silicified?) and are featureless within several cm's of the gabbro (**Figures 163G/H**). In proximity to the mapped mineralized facies (**Figure 158**), the lapilli tuff facies contains stringers of sphalerite with pyrite (**Appendix A-31**).

In thin section, the tuff and lapilli tuff beds are composed of 10-40-vol%, tabular to blocky, euhedral to subhedral, broken feldspar microphenocrysts (**Figure 164A**; **Appendix A-31**). Finely bedded tuff is composed of a fine-grained mosaic of quartz and albite. Mixed zones of sediment and gabbro are highly altered, but it is possible to recognize patches of fine-grained quartz and albite with tabular broken phenocrysts of feldspar adjacent to

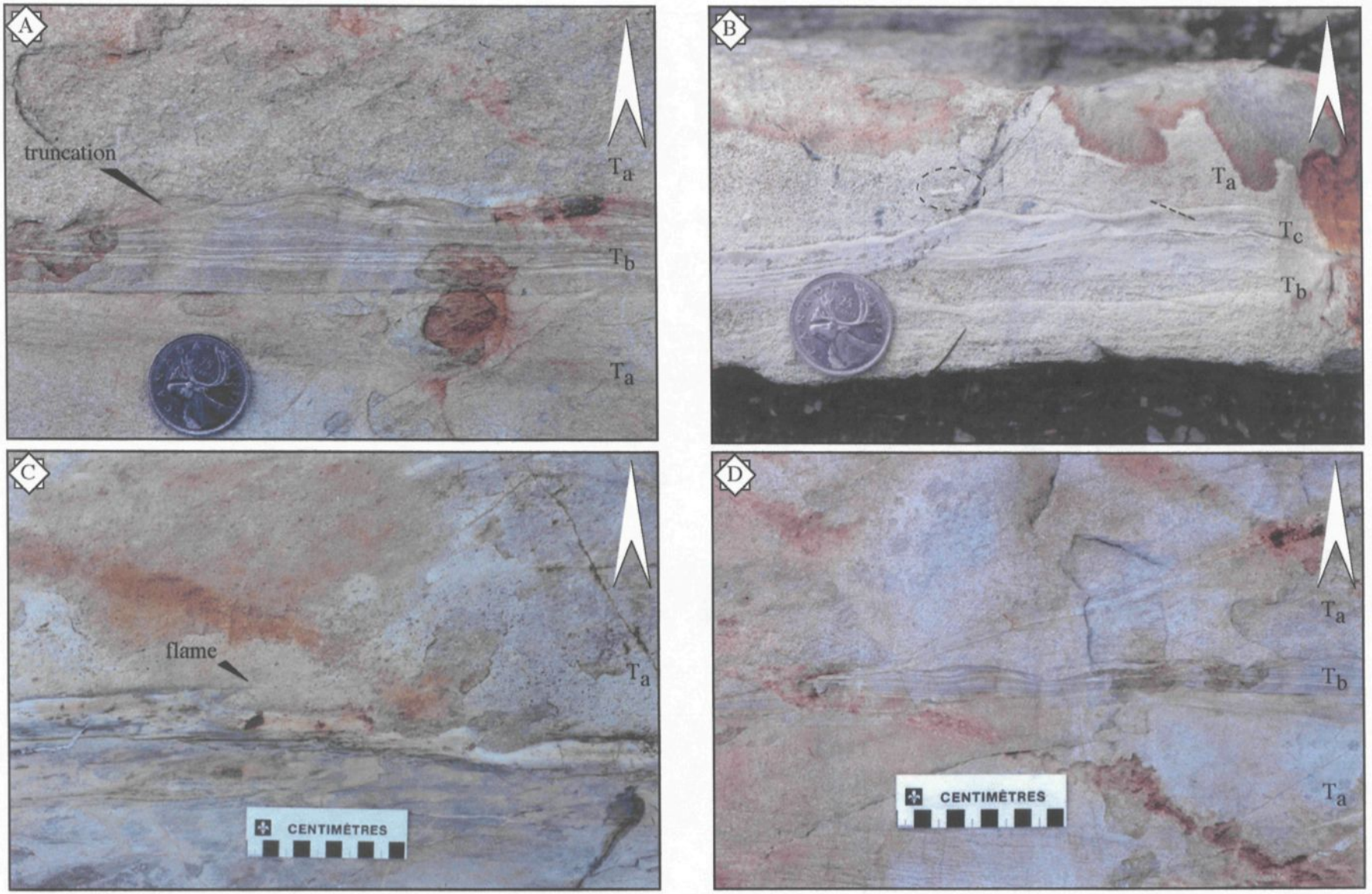

Figure 160. Series of field photos showing the contact relationships and sedimentary features of tuff and lapilli tuff beds. A. Finely laminated tuff with individual laminae being truncated by overlying lapilli tuff (Ta). Tuff also has a convoluted top. B. Bedded Tc bed being eroded by overlying Ta, with rip-up clasts (circled) of tuff hosted in lapilli tuff (Ta). Small synsedimentary faults (dashed line) also evident in tuff. C. Flame structure, as tuff extends into overlying lapilli tuff (Ta). D. Grading of felsic sediments from lapilli tuff (Ta) to fine-bedded tuff (Tc), back to a lapilli tuff (Ta). Arrow points in younging direction (south), quarter for scale.

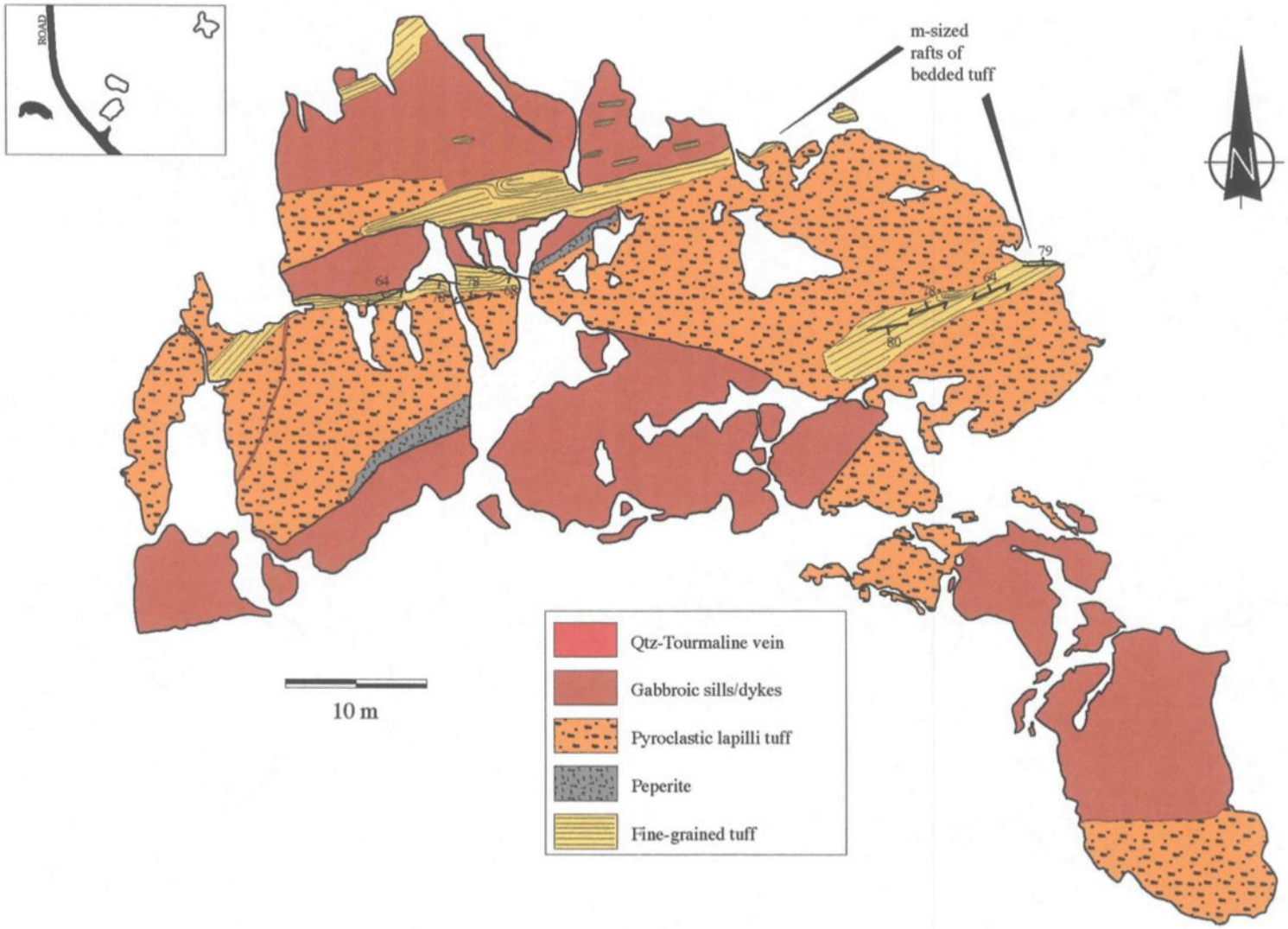

Figure 161: Simplified geology of western outcrop, Akasaba region.

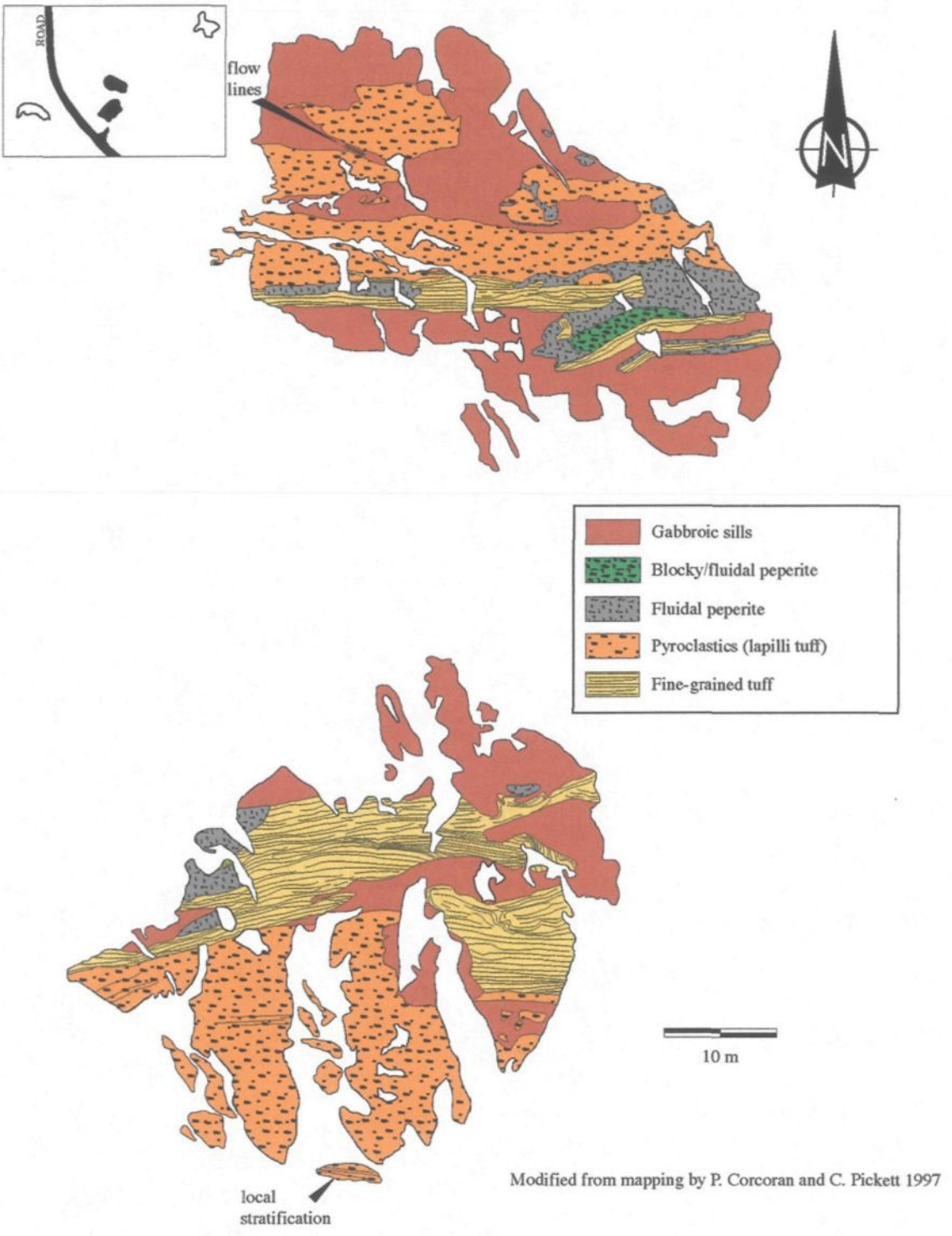

Figure 162. Simplified geology of eastern outcrops, Akasaba region.

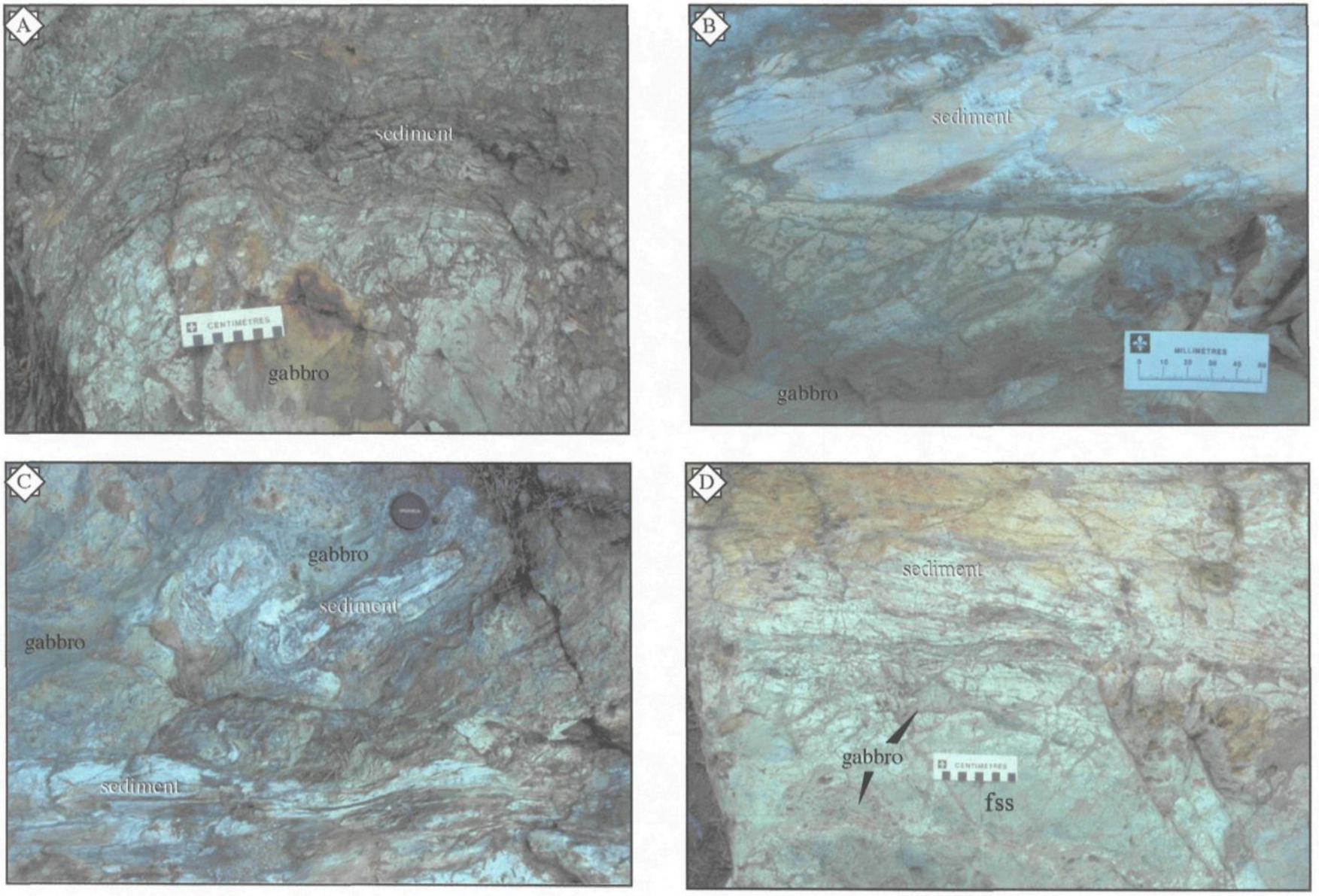

Figure 163. Contact relationships between volcaniclastic tuff and gabbro. A. Highly disturbed bedding of tuff facies. B. Homogeneous, featureless tuff in contact with gabbro. C. Laminated tuff fragment hosted in gabbro, lens cap for scale. D. Blobs and veins of gabbro that have brecciated featureless, silicified sediment (fss).

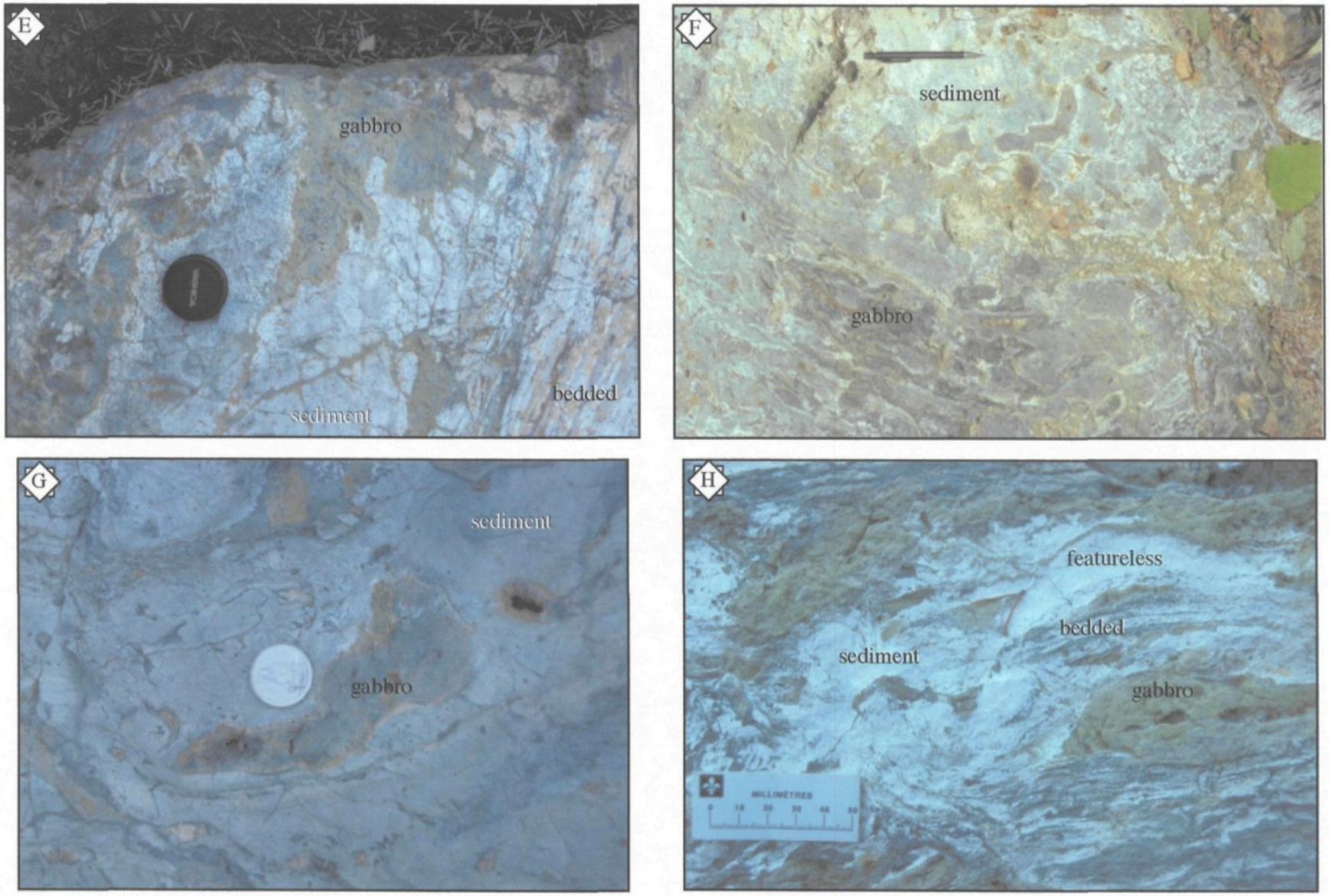

Figure 163 (con't). Peperitic textures. E. Penetrating fingers of gabbro into homogeneous tuff, lens cap for scale. F. Amoeboidal forms of gabbro in featureless tuff, dime for scale. G. Closeup of amoeboidal form of gabbro, pencil for scale (14.5 cm long). H. Bleached, featureless tuff adjacent to epditozed gabbro.

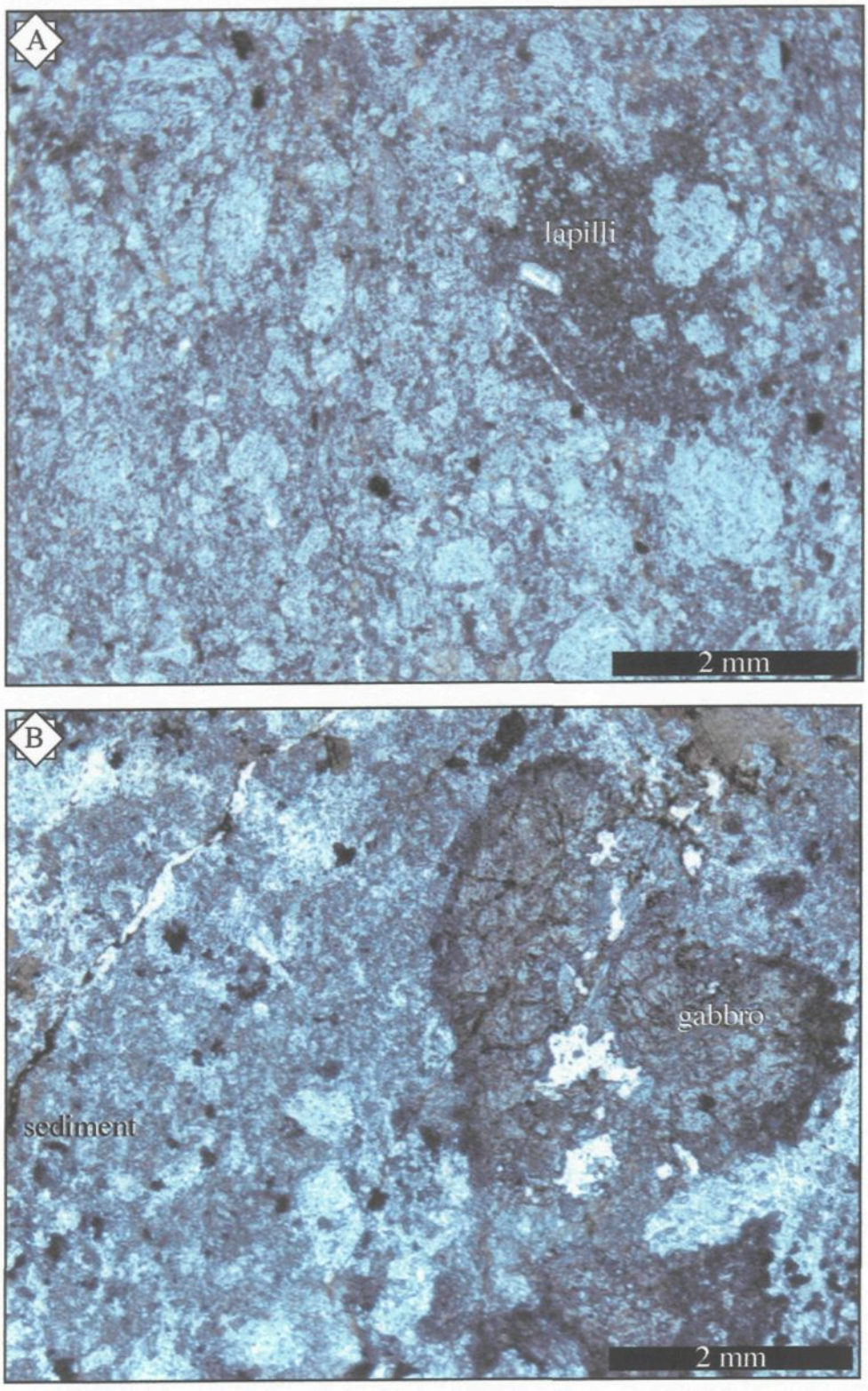

Figure 164. Thin section images of tuff. A. PPL microphotography of lapilli tuff bed characterized by ~30-vol%, blocky to tabular, euhedral to subhedral, broken feldspar phenocrysts, with a subrounded feldspar-phyric lapilli fragment. B. PPL microphotography of tuff and gabbro. Tuff has feldspar phenocrysts, whereas gabbro has cm-sized hornblende.

globular areas of cm-sized euhedral plagioclase and tabular hornblende phenocrysts (after pyroxene; **Figure 164B; Appendix A-32**).

Pyroclastic lapilli tuff

The pyroclastic lapilli tuff lithofacies is massive, with only localized, weakly developed, stratification (see **Figure 161**), and stratigraphically overlies the volcaniclastic tuff-lapilli tuff lithofacies (**Figures 158, 161 & 162**). Discontinuous exposure and the ubiquitous intrusion(s) of gabbro make estimates on its original thickness ambiguous. Nonetheless, this facies is observed over 500 m along strike, from its first appearance at the base of the Akasaba section (**Figure 158**) to outcrops southwest of the old Akasaba mine site (**Figure 137**). This facies has a clast- to matrix-supported character, whereby the former is conspicuous due to deformation between juxtaposed fragments. This facies has a mixed population of subangular to subrounded fragments, consisting of fine-grained, bedded tuffs (**Figure 165A**), vesicular (**Figure 165B**) and flattened clasts (**Figure 165C**), broken crystals (**Figures 165 B-E**), and armored (**Figure 165D**) and chilled margin lapilli. Notwithstanding tuff fragments, all fragment types are lapilli-sized. Bedded tuff fragments are angular and vary from cm-sized blocks to megablocks over 10 m in length (**Figure 160**), some of which are stained orange due to minor mineralization (**Figure 165F**). Vesicular fragments are subrounded and aphyric, as well as recessively weathered (**Figure 165B**). Pervasive epidote alteration gives them a greenish yellow honeycombed appearance (**Figure 165B**). Vesicularity is difficult to assess due to alteration and surficial weathering, but is probably greater than 40-vol% in some instances. Flattened fragments are oblong,

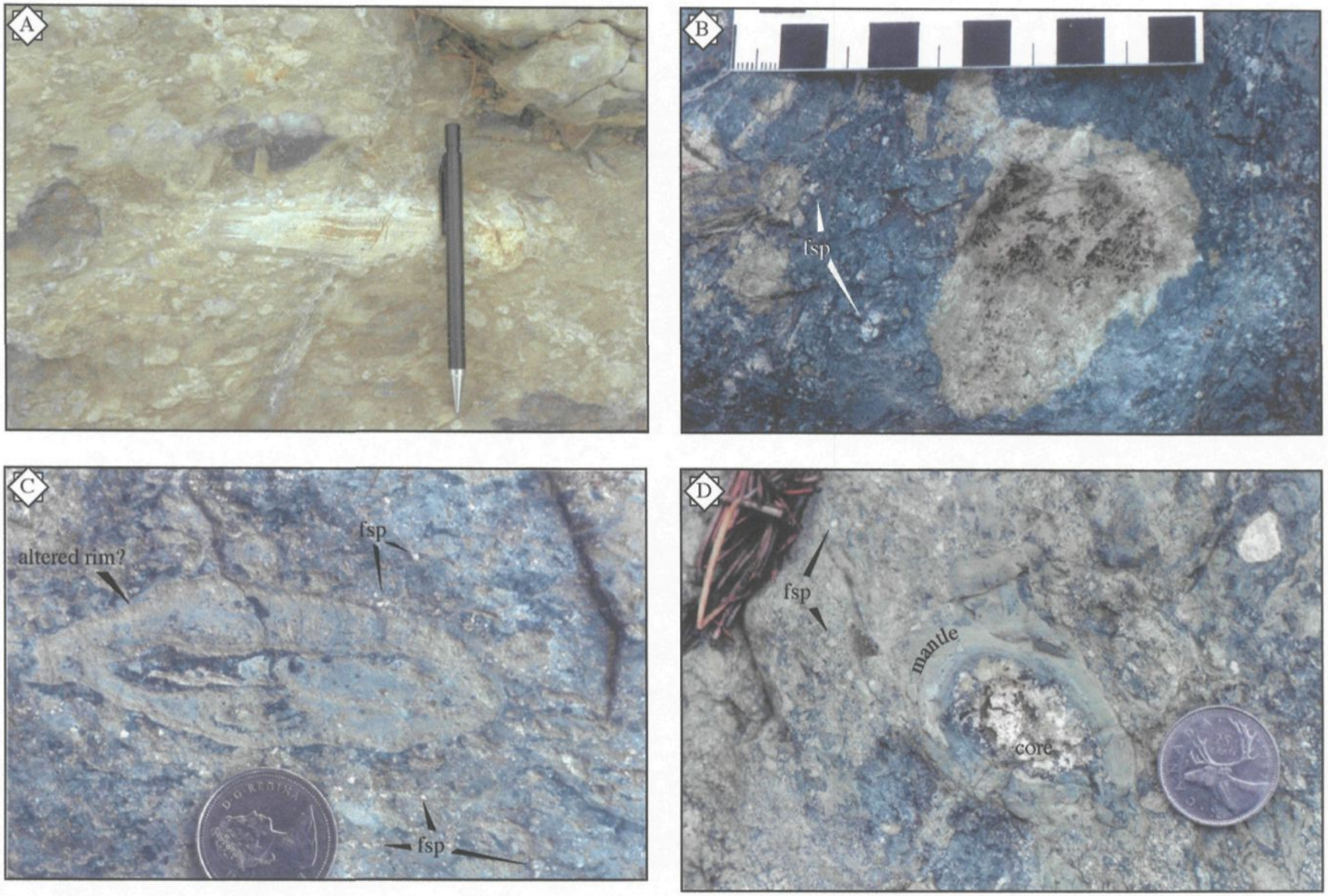

Figure 165. Field photos of pyroclastic lapilli tuff. A. Angular, bedded tuff fragment hosted in pyroclastic facies, pencil for scale (14.5 cm long). B. Subrounded, vesicular, recessively weathered fragment with feldspar (fsp) in matrix. C. Flattened fragment with liberated feldspar crystals in matrix, quarter for scale. D. Armored lapilli fragment and feldspar (fsp) crystals in matrix, quarter for scale.

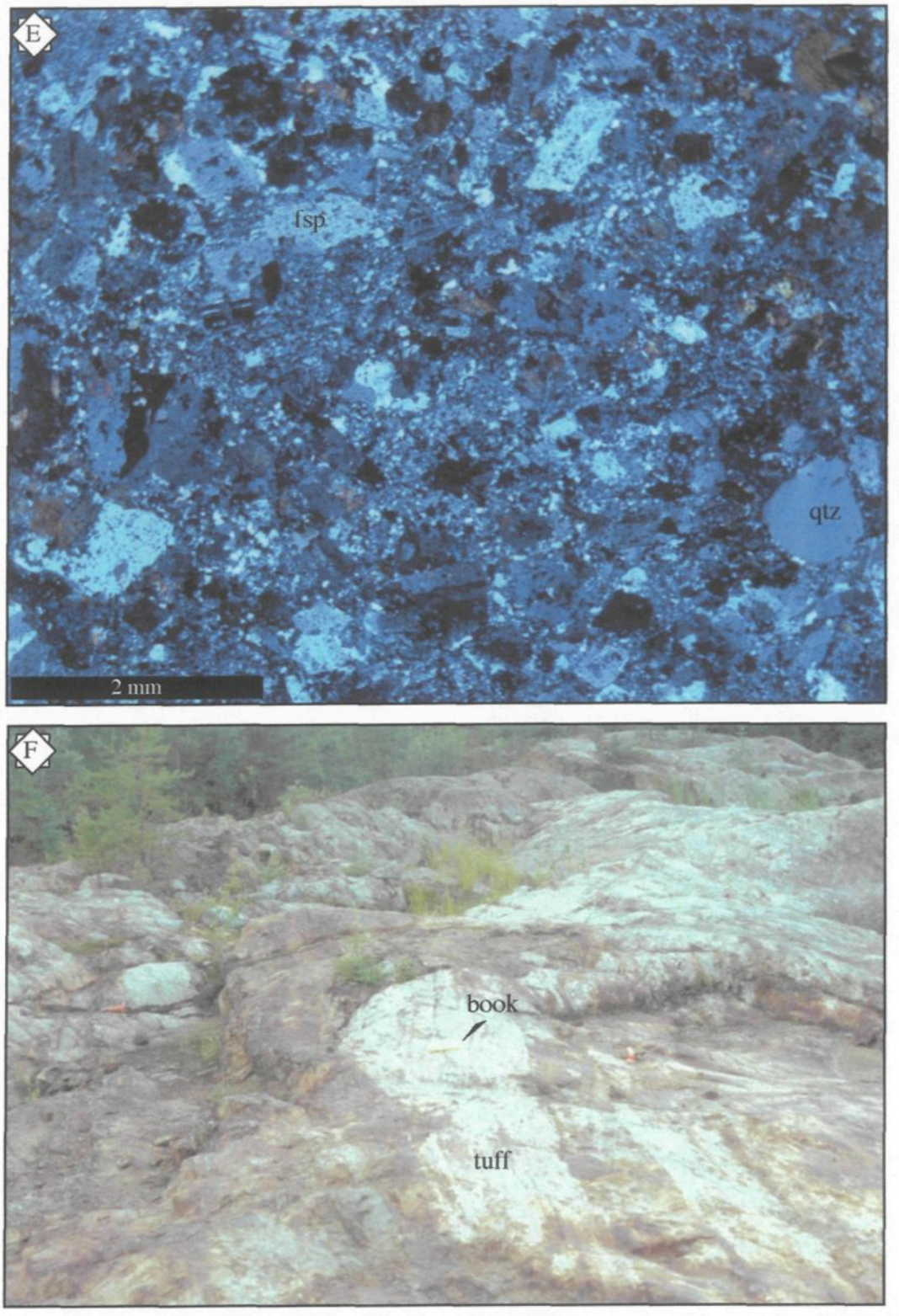

Figure 165 (con't). E. Cross-nicols microphotography of pyroclastic lapilli tuff composed of abundant broken euhedral feldspar (fsp) phenocrysts and rare anhedral quartz (qtz). F. Megablock of orange-stained tuff hosted in pyroclastic lapilli tuff; fieldbook for scale (34 cm).

grayish green with rare mm-sized tabular hornblende, as well as fine-grained, tabular white feldspar microphenocrysts (**Figure 165C**). Cores are darker colored and if not completely compressed, appear to have trapped fine-grained material that is similar to the matrix (**Figure 165C**). In addition, rims are altered a slightly different color (**Figure 165C**). Armored lapillus describes elliptical fragments with a mm-thick, finely laminated tuff that mantles a core that is epidotized and/or composed of material similar to the matrix (**Figure 165D**). White tabular feldspar microphenocrysts liberated in the matrix are similar in appearance to previously described feldspar hosted in the flattened fragments (**Figure 165C**).

In thin section, feldspars are mm-sized, blocky, euhedral to subhedral, broken phenocrysts, which are commonly sieved, and make up approximately 20-vol% of the matrix (**Figure 165E; Appendix A-33**). Rare anhedral quartz is observed, along with a highly birefringent altered phase that has irregular outlines. The remainder of the matrix is composed of a fine-grained mosaic of quartz and albite with subordinate tabular chlorite (**Appendix A-33**).

Gabbroic Intrusions

Gabbroic intrusions crosscut the stratigraphy at all levels, but become more intimately *mixed* when adjacent to the volcaniclastic tuff (**Figure 161; Appendix A-32**). This is epitomized by the aforementioned contact relationship described above between tuffs and gabbro (**Figures 163 E-G**). Such *mixing* in rarely observed between gabbro and the pyroclastic lapilli tuff facies (**see Figure 160**), but a small neck of gabbro penetrating

this facies displays a series of linear ripples (**Figure 166A**). Crystal grain size is variable and appears to be related to proximity to tuff beds. Only a few outcrops have visible crystals of plagioclase and hornblende, but one sequence lower in the stratigraphy has conspicuous cm-sized glomerocrysts of plagioclase.

Under the microscope, plagioclase and hornblende/chlorite (?) are intergrown, giving a fine- to medium-grained crystalline texture (**Appendix A-34**). One particular fine-grained gabbro has conspicuous mm-sized, sub-spherical blebs that are cored by tabular, euhedral (?) feldspar and mantled by an irregular pattern of chlorite laths (**Figure 167; Appendix CS97-232**). A localized homogeneous silicified phase is host to distinct amoeboidal and generally irregular blebs of gabbro that are aphyric and altered a deep green, forming a clast-rich area (**Figures 166B-C**). Contact with the light green chilled phase is characterized by a mm-thick whitish band that is fractured perpendicular to the bleb surface (**Figures 166B-C**).

Mineralization

Mineralization is associated with the volcaniclastic tuff and lapilli tuff lithofacies. The main 2-6 m-thick layer at the base of the local stratigraphy is oriented semi-parallel to bedding and caps the volcaniclastic sequence (**Figures 158, 159 & 167**). The deep orange-red appearance and whitish streaks (**Figure 168**) characterize this zone and are probably due to weathering of iron and sphalerite, respectively.

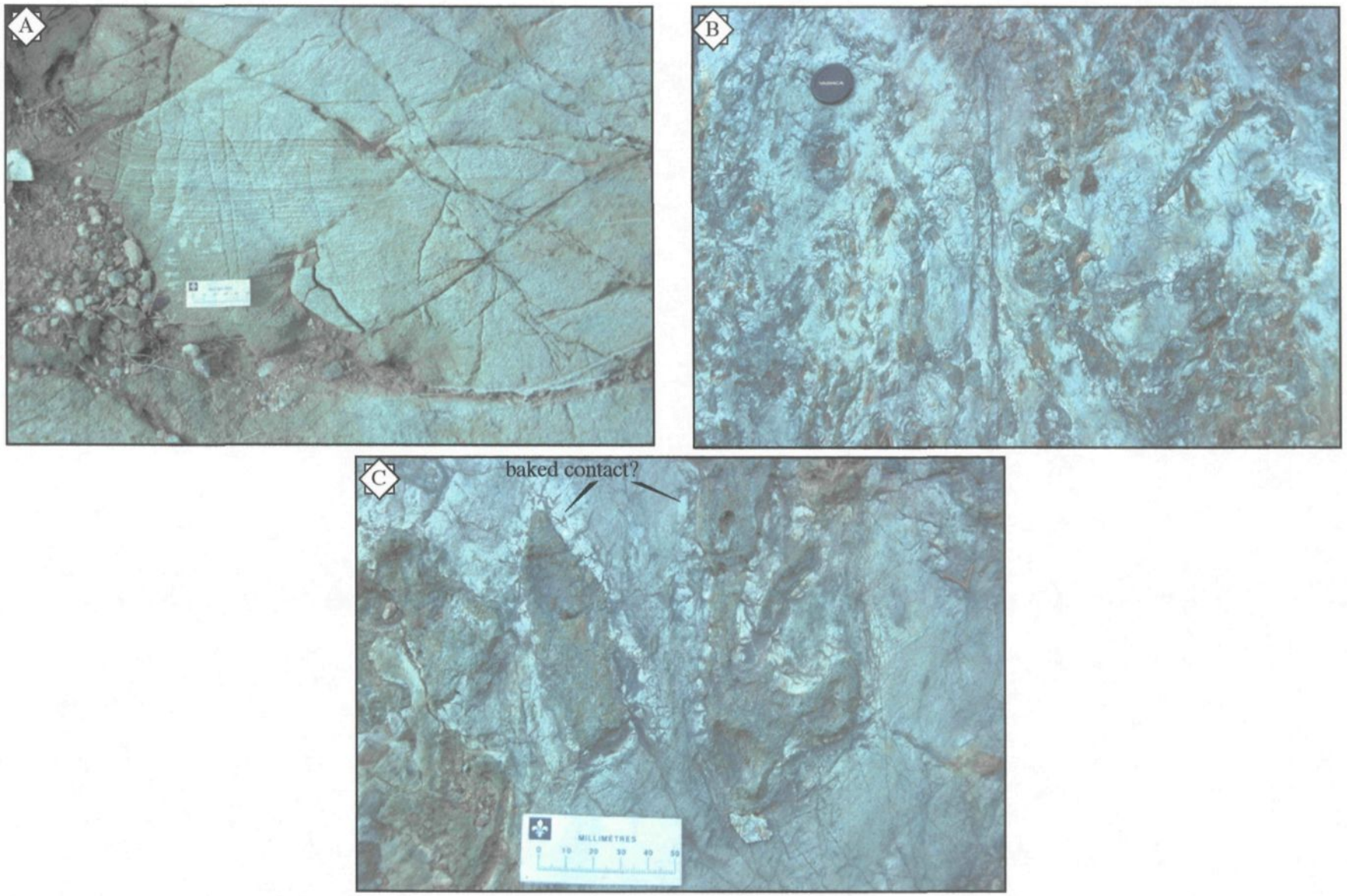

Figure 166. Field photographs of gabbro intrusion. A. Fine laminations in gabbro in proximity to pyroclastic lapilli tuff facies. B. Collection of irregular dark green blobs scattered through featureless silicified tuff. Lens cap for scale. C. Closeup of amoeboidal blobs with whitish contact hosted in featureless silicified tuff, with fractures extending out, perpendicular to blob contact.

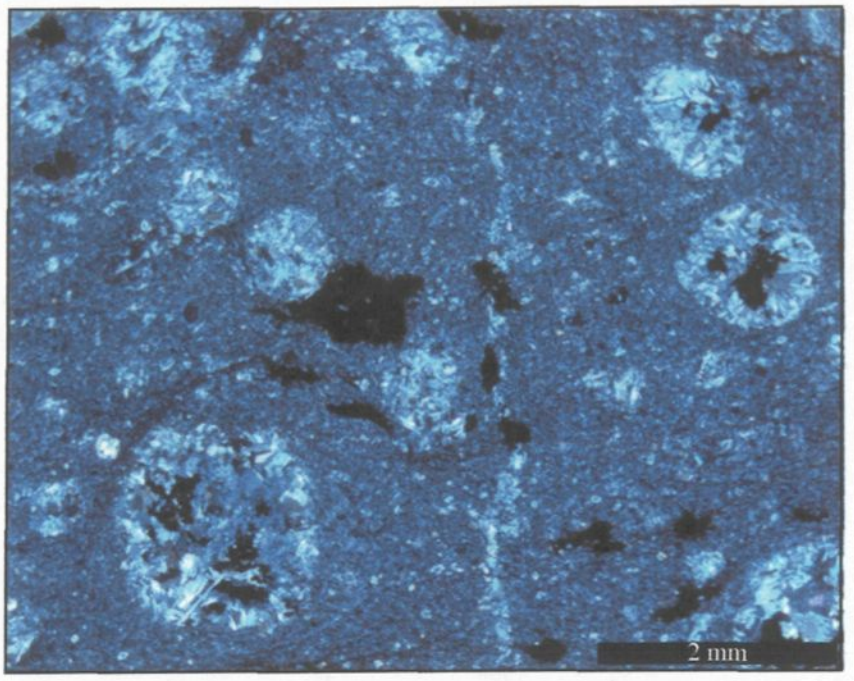

Figure 167. Cross polarized microphotograph of fine-grained gabbro with sub-spherical forms that are cored by feldspar and mantled by non-oriented laths.

Figure 168. Contact relationship between underlying lapilli tuff - tuff facies and orange-red stained zone. The lowermost part of mineralized zone has relict bedding indicating that hydrothermal fluids have probably replaced the sediments. Pyrite and sphalerite (white powder) are the dominant mineral phases. Hammer for scale (37 cm-long).

5.3.2 Interpretation

The complete stratigraphy exposed within this region represents roughly contemporaneous deposition of two different subaqueous volcanic eruptions; namely a felsic calc-alkaline sequence (volcaniclastic lithofacies) and a tholeiitic sequence (pyroclastic lithofacies) (see chapter 6).

Volcaniclastic lithofacies origin

The finely bedded and repetitive nature of the volcaniclastic sequence (**Figures 158 and 159**) indicates these beds originated from a series of water-supported, low-concentration turbidity currents (cf. Lowe, 1982), deposited below wave base (White and McPhie, 1996). The abundance of broken, euhedral feldspar microphenocrysts liberated in the matrix, together with the absence of non-volcanic debris, suggests deposition during or immediately after an explosive (pyroclastic?) eruption (Cole and Stanley, 1994). These deposits most likely record fine-grained pyroclastic material accumulated from a waning eruption column, which periodically slumped from unstable slopes of a subaqueous edifice (Fiske and Matsuda, 1964), or by pulses of jetted volcanic material (White, 1996). In addition, the unabraded, sharp angular morphology of feldspar 'fragments' implies a relatively short transport distance, thus these deposits are envisaged to be near the eruptive vent (McPhie, 1995). Subaerial ejection and subsequent particle settling is dismissed, as such deposits are well sorted and extensive (McPhie et al., 1993; Fiske et al., 1998). Each lapilli tuff – tuff set probably records a single depositional event (Cole and Stanley, 1994), with the thickness of the tuff beds possibly reflecting a positive relationship with the

volume and/or magnitude of the volcanic eruptions. Overall, the composition and volume of these fine-grained deposits is inconsistent with normal deposition within the Héva Formation, suggesting it is probably a local phenomenon.

Pyroclastic lithofacies origin

The pyroclastic lapilli tuff facies massive, clast- to matrix-supported nature, together with abundance of juvenile fragments, including vesiculated (scoria?) and crystal fragments, and accidental tuff suggest a primary pyroclastic origin (pg. 90; Fisher and Schmincke 1984). Moreover, some fragments appear to have been deposited hot, as evident by their flattened morphology (**Figure 165C**) that is suggestive of *in situ* plastic deformation. In addition, lapilli fragments appear to be agglutinated and/or flattened in clast-rich areas, indicating welding between hot plastic fragments (White, personal communication). The lack of grading and stratification implies that this deposit was probably dry during transport and deposition, whereby the supporting mechanism could have been gas (?). Direct evidence of gas-support is absent and only based on indirect evidence, such as the lack of sedimentary structures. A curious observation is the absence of peperite in association with intruding gabbro, particularly when you consider that the pyroclastic lapilli tuff was deposited penecontemporaneous with the peperite-rich felsic tuff lithofacies, based on tuff fragments within the former (**Figures 161 and 163C**). Several possible theories for this absence are: (1) there was no water available to form peperites; (2) the hot pyroclastic deposit was insulated from the gabbro by its own vapor barrier (gas-supported?); or (3) density contrast precluded mixing (Kokelaar, 1982; McPhie, 1993;

Donaire et al., 2002). Evidence supporting at least the present of gas is by the amount of vesiculated fragments (**Figure 165B**). Armored lapilli (**Figure 165D**) offer possible support of at least a water-poor eruption, as their formation is considered impossible after 25-wt% water due to bed liquidification (Schumacher and Schmicke, 1995). However, considering a subaqueous environment is a paradox, as subaqueous formation of armored lapilli has never been demonstrated. Nonetheless, White (1996) envisaged the formation of a water-exclusion zone within a vent, due to the formation of a steam cupola (cf. Kokelaar, 1983), whereby a fragment could be repeatedly circulated to form a mantle of fine ash.

Peperites

The complex and highly irregular contact relationship between the felsic tuffs and gabbro suggests mixing between an unconsolidated sediment and hot magma, forming a peperite (Busby-Spera and White, 1987; Skilling et al., 2002). Peperite formation is supported by (cf. Hunns and McPhie, 1999): (1) normally bedded sediment is homogeneous and featureless in contact with gabbro (**Figures 163F-H**) (Kokelaar, 1982; Hanson and Hargrove, 1999); (2) silicification of sediment adjacent to gabbro (**Figure 163B**), which suggests thermal metamorphism; and (3) highly irregular blebs of gabbro (**Figures 163F-G, 166B-C**), indicating plastic, fluidal behavior of hot magma. Therefore, the intrusion of gabbro was contemporaneous with felsic sediment deposition. Some of the forms gabbroic clasts have are; irregular, pod-like, amoeboidal, hook-like, and teardrop shaped (see **Figure 163**), which are classified as fluidal peperites (Busby-Spera and White, 1987; Skilling et al., 2002); observed hook-forms are probably equivalent to described

platy/elongate fluidal clasts of Skilling et al. (2002). These fluidal gabbro clasts are hosted in narrow zones of featureless, silicified tuff adjacent to bedded, fine-grained felsic tuffs (**Figure 162**). These zones probably represent intense fluidization due to heating of interstitial pore fluids (Kokelaar, 1982; Kano, 1989, 1991; McPhie, 1993; Hanson and Hargrove, 1999; Dadd and Van Wagoner, 2002) during the initial injection of hot mafic magma (**Figure 169**). Subsequent passive mingling was possible due to fluid instabilities (Wohletz, 1983) together with contrasting densities (Kokelaar, 1982; McPhie, 1993; Donaire et al., 2002), whereby oscillations along the magma – host sediment interface may generate globules of fluidal magma (Busby-Spera and White, 1987). The resulting globules mingle only when vapor films are maintained as this effectively insulates the segregated fluidal clasts from quenching by its cold, wet sediment host, which is facilitated by the density contrast between felsic sediment and mafic magma. Furthermore, such mingling seems to be favored when the host is a fine-grained sediment (Busby-Spera and White, 1987; Hanson and Hargrove, 1999; Donaire et al., 2002), as larger grains will destabilize vapor films (Busby-Spera and White, 1987) and/or be too permeable to trap heated pore fluids (Hanson and Hargrove, 1999). Mingling is further enhanced if the intruding magma is of low viscosity (Dadd and Van Wagoner, 2002). These conditions are analogous to the Akasaba section. The observed sub-spherical blebs represent possible microscopic evidence of immiscible mixing between felsic sediment (fluidized) and mafic magma (Busby-Spera and White 1987), which can be termed varioles (cf. Fowler et al., 2002). A filled amygdule or devitrification origin is rejected, as the fibrous array is not geometrically arranged (i.e., no geopetal form; cf. Busby-Spera and White, 1987) and there are no other vesicles orfilled

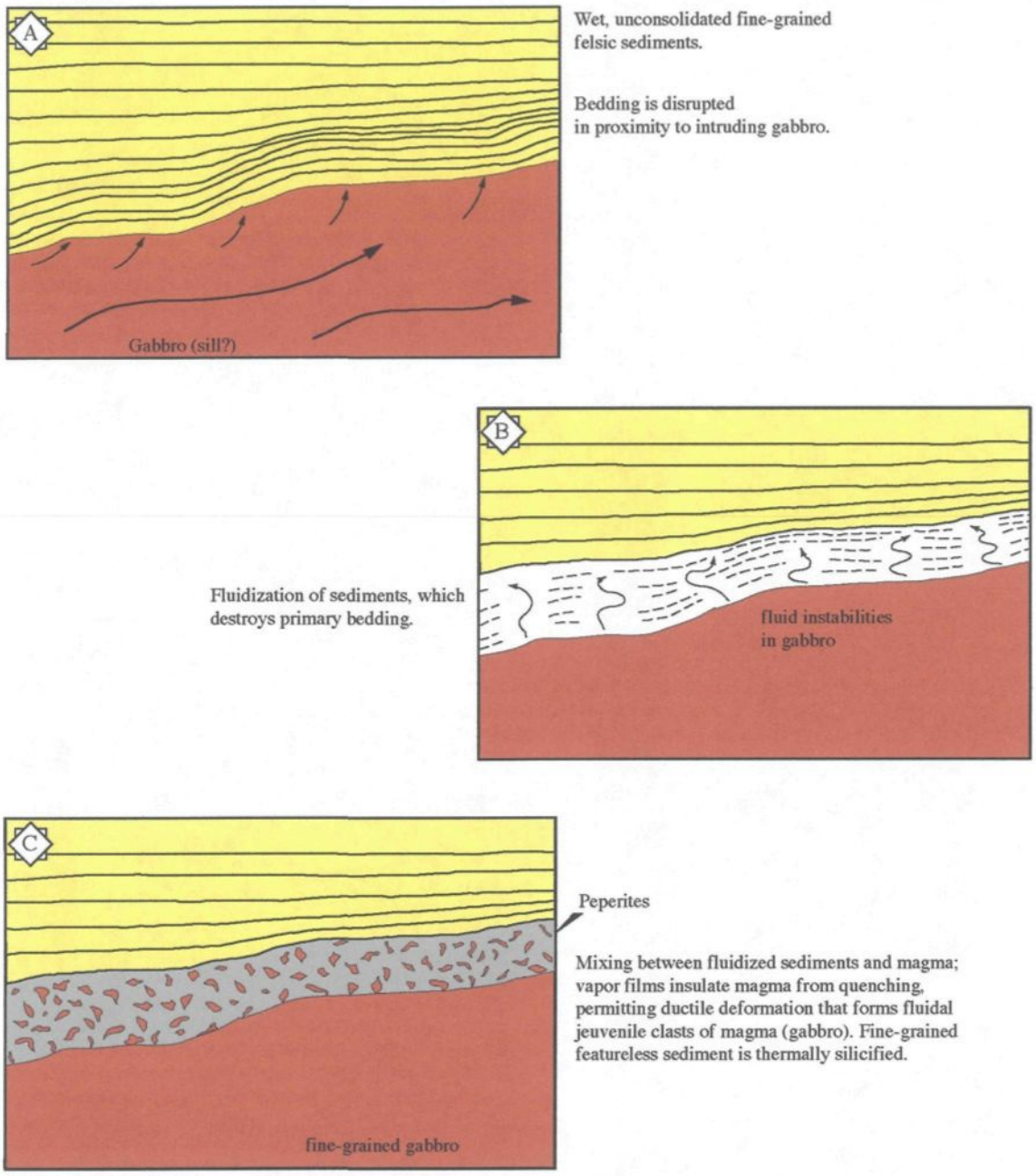

Figure 169. Cartoon of possible series of events that result in peperite formation. A. Initial injection of gabbro into wet, unconsolidated, bedded, fine-grained felsic tuff; bedding was probably disturbed adjacent to intrusion. B. Heating of pore fluids resulted in fluidization of sediments, which destroyed the original bedding. Fluid instabilities at the magma-sediment interface resulted in segregation of hot, fluidal clasts of magma that mixed with the now featureless sediment. C. Abundant mixing occurred in a narrow zone between bedded sediments and gabbro; which formed a fluidal, clast-rich peperite. The homogeneous felsic sediment becomes silicified due to thermal alteration in proximity to the gabbro.

vesicles observed in the gabbro. In addition, the feldspar core is similar to observed feldspar liberated in felsic tuffs, which argues against sediment infilling a vesicle (Dadd and Van Wagoner, 2002). Therefore, it is envisaged that felsic sediment became fluidized; such that a feldspar crystal was entrained as it mixed with the intruding gabbro, whereby the spherical form is just the simplest geometric form (as per gas; vesicles). In contrast, zones of *in situ* brecciated tuff (**Figures 163D-E**) probably record localized areas that have either dewatered and/or consolidated enough to inhibit fluidization and promote brecciation.

Alternate interpretation of fluidal textures

Another possible scenario advocated for this sequence is for complete alteration due to metasomatic fluids propagating along NE-SW oriented faults originating from a small igneous intrusion located approximately 1.6 km to the west (**Figures 136 and 137**), to form a skarn-type deposit (Chartrand, per. comm. 1997). Meinert (1998) surmised that high-grade skarns (5-15 g/t Au) are typically associated with granodiorite-diorite plutons and dyke/sill complexes, with skarns being hosted in clastic-rich protoliths, including volcaniclastics. However, skarn-type minerals (i.e., garnet) are absent in the general area and the theory that contact metamorphism by metasomatic fluids from a distant intrusion producing peperite-like textures is difficult to resolve. Furthermore, the associated mineralized zone located at the top of the felsic tuffs is composed of massive sulfides (pyrite and sphalerite) and considered to be a replacement deposit due to hydrothermal fluids circulating through the porous volcanic pile that replaced the coarser felsic lapilli tuff

bed and became stratabound as it pooled beneath the impermeable gabbro (**Figure 158**). The amount of hydrothermal fluids and the type of mineralization are analogous to deposits associated with VMS-type deposits (Gibson et al., 1999).

Temporal considerations

Timing of deposition and intrusion(s) within this complex stratigraphy is revealed in crosscutting and inclusion relationships. Large blocks of undisturbed tuff represent rafts of felsic tuffs that became entrained during intrusion of gabbro (see Hanson and Hargrove, 1999) and deposition of the pyroclastic lapilli tuff (**Figure 161 and 162**), suggesting that the felsic sediments were deposited first with contemporaneous emplacement of the pyroclastic lapilli tuff and gabbro (**Figure 170**). The amount of sedimentation in this particular area probably explains the absence of pillowed facies, as feeder dykes form hypabassal intrusions as opposed to being extruded on surface. Such hypabassal complexes are recognized as an important component of ancient island arcs and young spreading centers (Batiza and White, 2000).

5.4 Akasaba South (ROI 4)

The Akasaba South region (**Figure 137; ROI 4**) represents the upper extension of Akasaba North, as well as the most southern exposed part of the Héva Formation before the Cadillac Fault Zone; thus defining the capping sequence to the study area. The focus of this

not to scale

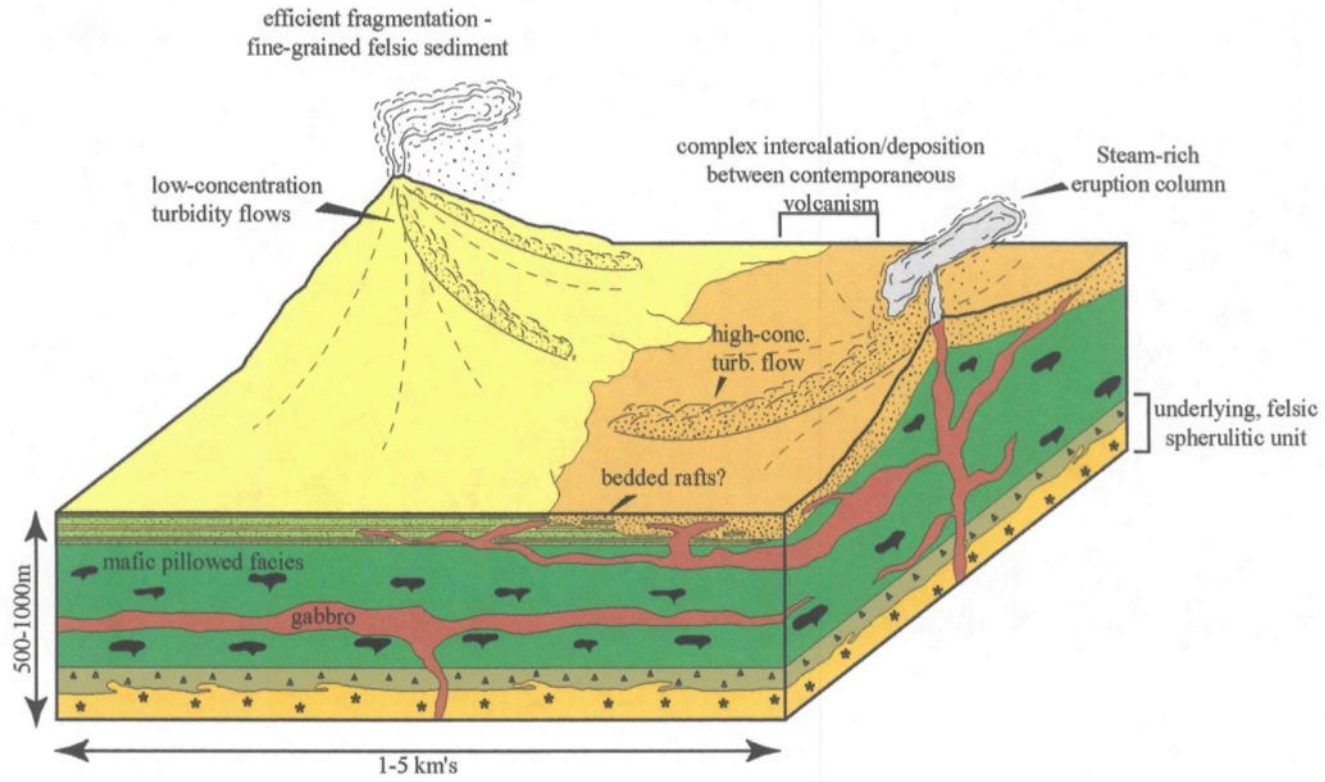

Figure 170. Cartoon illustrating temporal and spatical relationships between felsic and mafic deposits and gabbro intrusions.

area is a series of stripped outcrops located approximately 500 m to the southwest of Akasaba North and about 350 m west southwest of the former Akasaba Mine (**Figure 137**).

5.4.1 Lithology of Akasaba South

The area mapped in detail covers an approximate 90 m x 40 m area of discontinuous exposure highlighted by four stripped outcrops (**Figure 171**). Mafic-related volcanism dominants the sequence, with subordinate intercalations of felsic tuffs, mineralized hyaloclastites and a small intrusive granodiorite (**Table 20**).

Mafic Volcanism

Mafic volcanism can be subdivided, based on texture, into massive and pillowed facies (**Table 20**). Massive facies are between 15-20 m-thick and pillowed facies up to 5 m-thick. These facies are typically separated by thin intercalated tuff turbidites (**Figure 171**) or irregular, but sharp contacts (**Figure 171**). Both facies are aphyric, however, they also commonly have conspicuous cm-sized plagioclase glomerocrysts (**Figure 171 and 172A-B**).

Pillowed facies form close-packed, dm-sized, bun-shaped pillows indicating a southward younging direction (**Figure 172B**), with magnetite commonly interstitial between pillows (**Figure 172B**). Contact relationships define at least two pillowed flows, which are correlated over 60 m, but appear to pinch out over 30 m to the west due to the lateral appearance of a massive facies (**Figure 171**).

Figure 171. Deatiled mapping of a series of outcrops located in the Akasaba South region (ROI 4).

Table 20: Lithofacies of the Akasaba South area (ROI 4).

Lithofacies	Thickness & morphology	Characteristics	Transport/deposition	Origin
Mafic volcanism				
Massive	15-20 m-thick, tabular to irregular	Massive; sharp, but non-planar contacts; aphyric with cm-sized plagioclase glomerocrysts	High temperature, low viscosity lava/magma; extrusive to intrusive properties	Effusive lava to hypabassal sill/dyke
Pillowed	5 m-thick, tabular	Dm-sized close-packed pillows; aphyric with rare plagioclase glomerocrysts; interstitial magnetite and hyaloclastites	High temperature lava; water-lava interaction forming hyaloclastites; low-temperature hydrothermal alteration	Effusive, subaqueous eruption
Volcaniclastics				
Tuff turbidite	~1 m-thick; tabular	Massive fine lapilli (T_a) to bedded tuff (T_b); disturbed bedding; isolated blocks or discontinuous bedded tuff	Low-concentration turbidity flow; low-volume	Distal extension of fragmental material from localized explosive eruption
Hyaloclastites	1.5-2.5 m-thick; semi-tabular	Massive; angular to subangular, lapilli-sized fragments; jigsaw fitted; matrix of magnetite + pyrite ± sphalerite	*In situ* brecciation	Water interaction and low hydrothermal alteration between pillowed facies

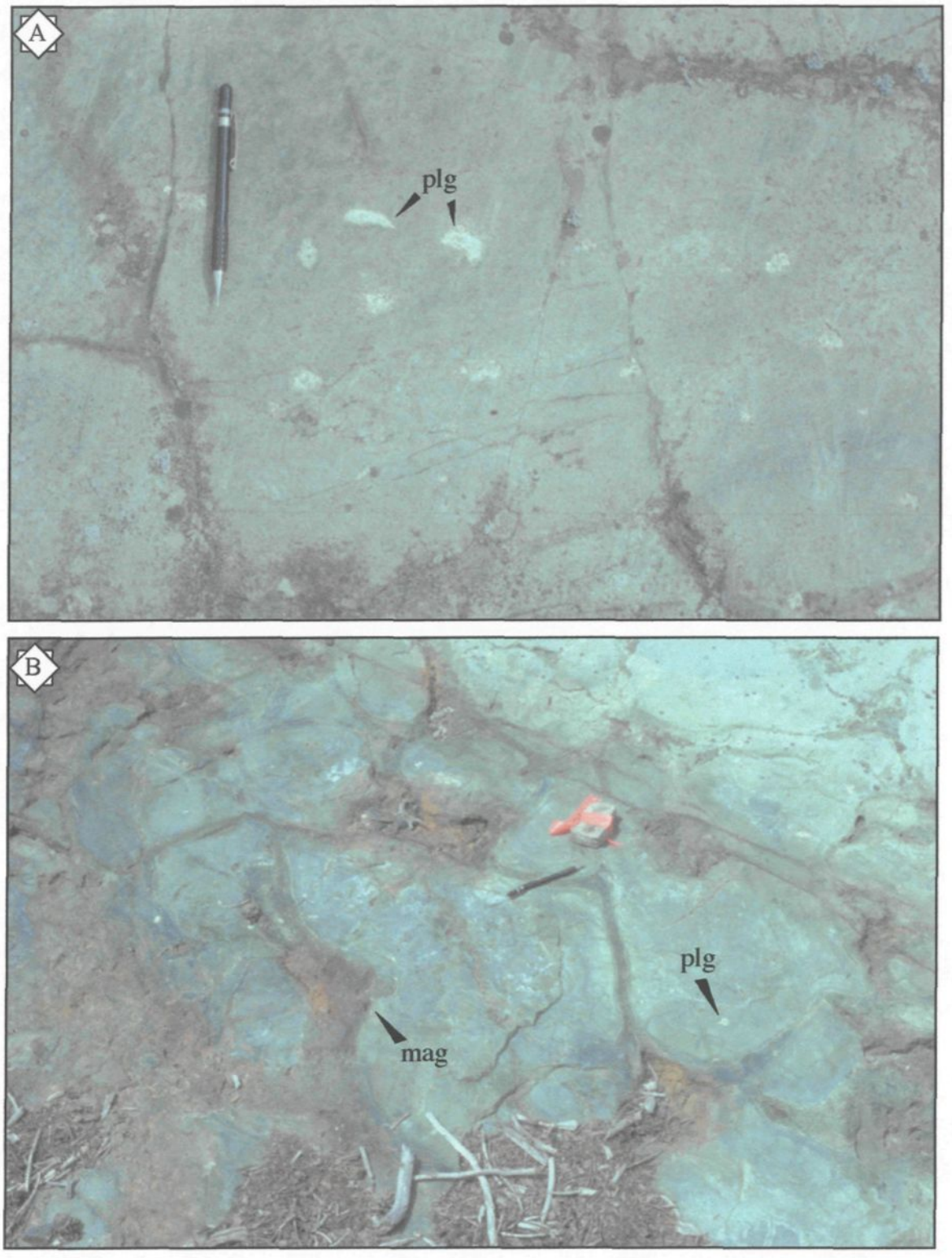

Figure 172. Field photos of mafic facies from Akasaba South. Pencil (14.5 cm-long) points towards the north. A. Massive facies with plagioclase (plg) glomerocrysts. B. Bun-shaped mafic pillow with plagioclase (plg) glomerocrysts and intersitital magnetite (mag).

Different massive units are identified based on contact relationships and by the presence of plagioclase glomerocrysts. The westernmost outcrop has a contact between these different massive facies, which is sharp and defined by the sudden absence of plagioclase glomerocrysts (**Figure 171**). Another apparent difference is the contact between the glomerocryst-free facies and tuff turbidites, which is characterized by a thin zone of *in situ* brecciation immediately underlying the tuffs (i.e., to the north; **Figure 171**). The western example has perpendicular fractures (**Figures 171 and 172C**) that extend a meter from the tuffs into the massive facies, ending in a zone of jigsaw-patterned breccia. Another example, from the southernmost outcrop, has a zone of angular and rounded mafic breccia fragments hosted in fine- to coarse-grained volcaniclastic rocks (**Figure 172D**). A similar interaction is recorded within the southernmost glomerocrystic massive facies, whereby adjacent to a discontinuous laminated sedimentary unit there are fluidal peperites hosted in a homogeneous facies (**Figures 171 and 172E**).

Volcaniclastic tuff turbidites

The tuff turbidites are subordinate, but serve as important local marker horizons in correlating individual outcrops (**Figure 171**). At least three individual units are recognizable, which relate to at least three depositional events. Beds are relatively thin, with the thickest only 1.2 m. The typical succession is graded from massive fine-lapilli to laminated tuff, with only one sequence having a repeated tuff layer; such grading indicates a southward younging direction. Several beds are slightly offset or disturbed and epidote

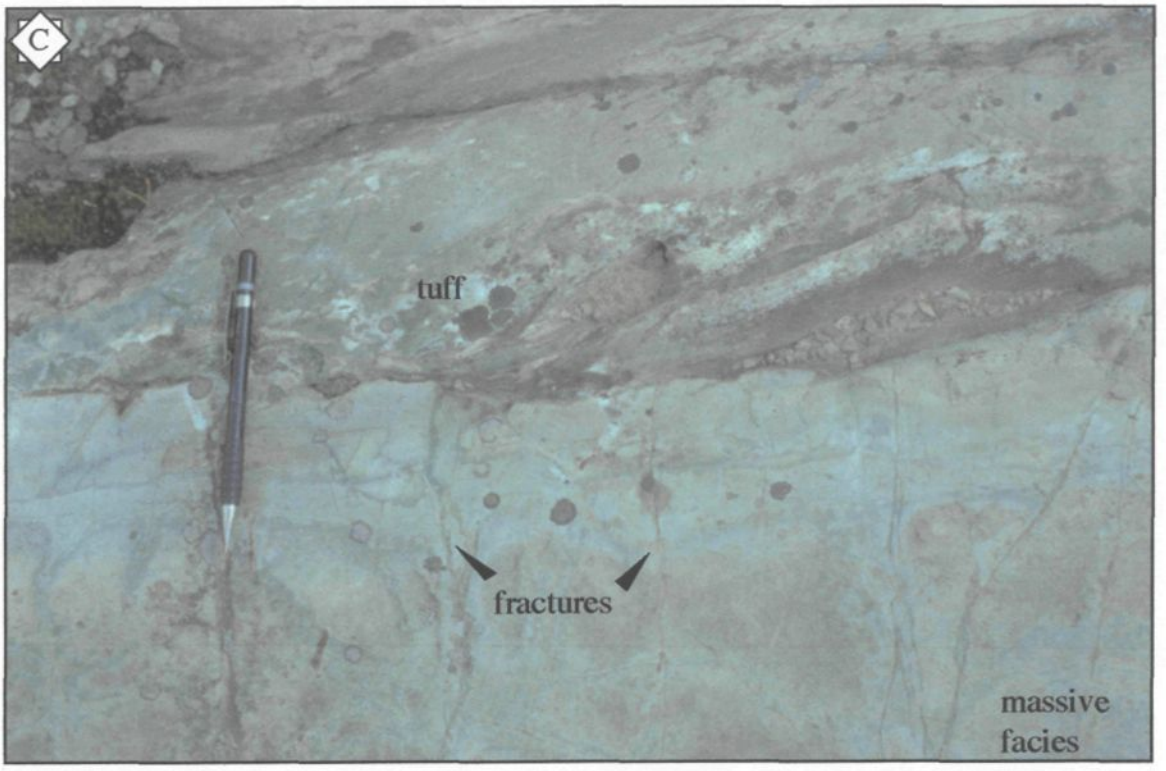

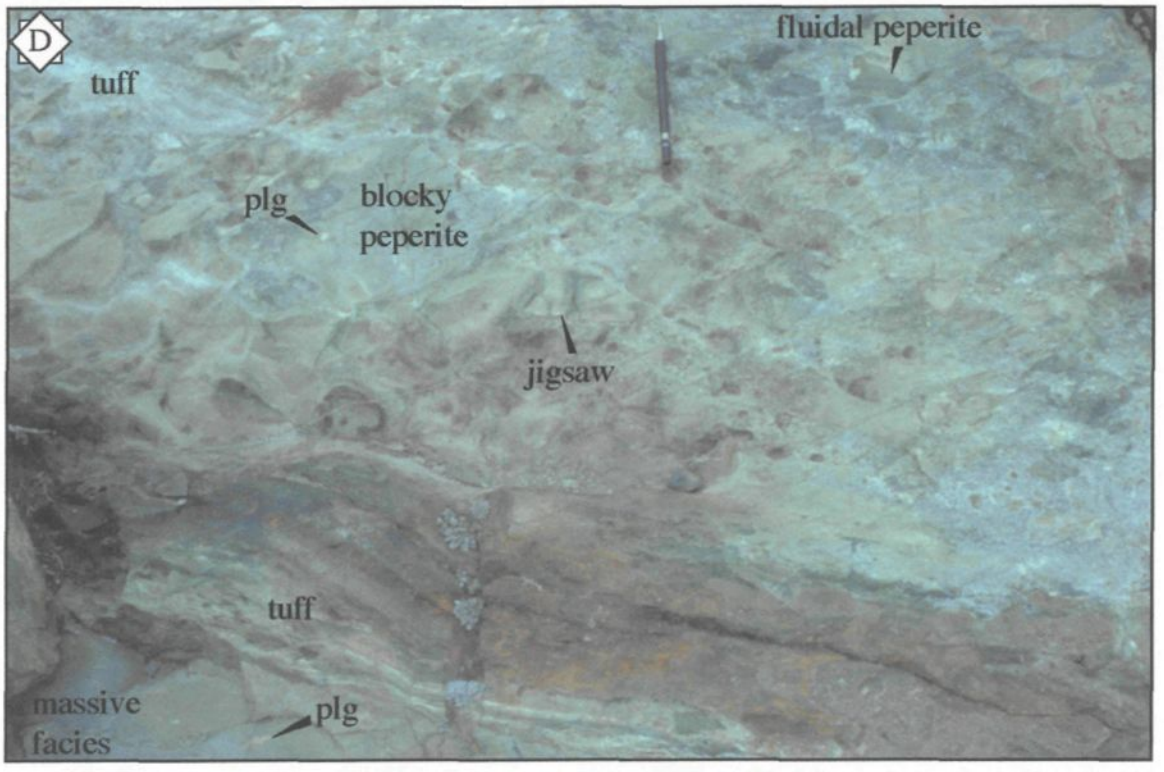

Figure 172 con't. C. Contact between tuff and massive facies characterized by perpendicular fractures propagating into the massive facies and ending in an *in situ* breccia (see Figure 171). D. Fluidal and blocky peperite underlying tuff; blocky peperite typically form jigsaw textures. Plagioclase (plg) glomercrysts observed in mafic facies above and below tuff.

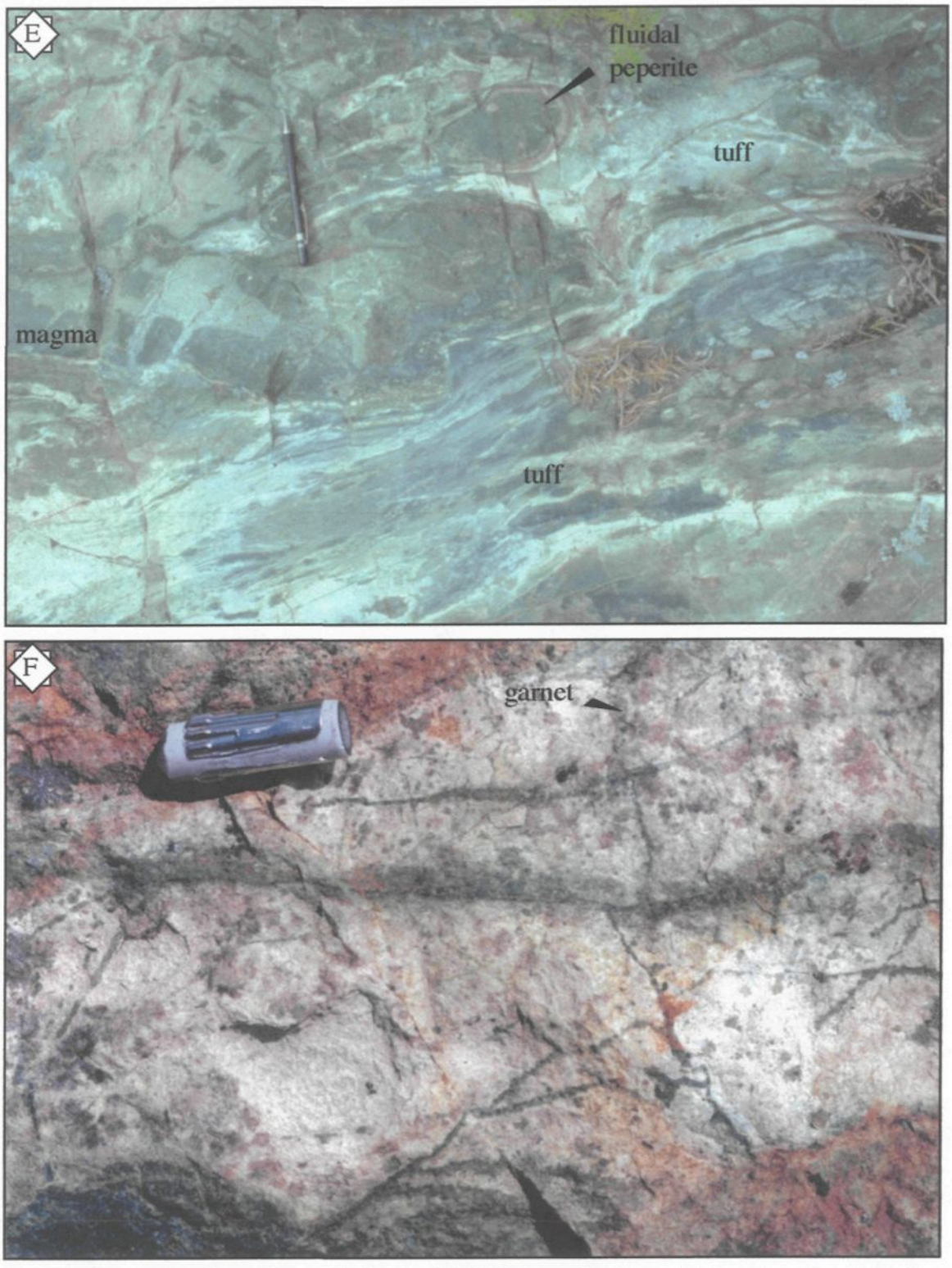

Figure 172 con't. E. Thin, laminated tuff facies with fluidal peperite. Located in southermost outcrop (see Figure 171). Garnet microphenocrysts associated with granodioritic intrusion (see Figure 171). Eraser (1 cm) for scale.

and sericite alteration is intense, along with orange-red iron staining and magnetite precipitation (**Figure 172D**).

Hyaloclastites

The 1.5 to 2.5 m-thick mineralized hyaloclastite unit is correlateable across the entire sequence (**Figure 171**). This brecciated zone appears to be associated with the mafic-pillowed facies, although it is not in direct contact with it to the west. Fragments are composed of angular to subangular, lapilli-sized mafic clasts, with a supporting matrix of magnetite and minor pyrite and sphalerite(?). A conspicuous, unaltered lobe of granodiorite penetrates this zone within the central part of the area (**Figure 171**). In proximity to this intrusion are localized, mm-sized garnet crystals (**Figure 172F**).

5.4.2 Interpretation of Akasaba South

The predominance of mafic-related rocks is possibly related to proximity to the eruptive source. The aphyric nature of massive mafic rocks suggest they cooled rapidly and irregular, non-planar contacts imply that at least several of these units cut the stratigraphy at low angles. These units are probably stratabound sills that represent shallow hypabassal intrusions. Plagioclase glomerocrysts genetically link some of these massive facies to pillowed flows, whereby the former may have fed the extrusive lavas from a common subvolcanic magma chamber that hosted these intratelluric crystals. A temporal relationship is further supported developed peperitic margins in contact with tuff turbidites, suggesting a

sill-origin (Skilling et al., 2002). However, the lowermost (northern) massive facies does not have a peperitic margin and may in fact be extrusive (**Figure 171**).

The thin, fine-grained volcaniclastic tuff turbidites probably represent a distal or extrabasinal deposit that was transported via a low-concentration turbidity flow. These tuffs may be the distal equivalent to the underlying tuff turbidites observed at Akasaba North. Thus they probably originate from localized explosive processes. The presence of peperites, however, suggest a temporal relationship with mafic volcanism.

Variations in peperite morphology, from angular to rounded, are analogous to blocky and fluidal peperites identified by Busby-Spera and White (1987). The development of fluidal peperites was discussed in section 4.3.2. Blocky peperite is consider to form in response to sediment grain size (Busby-Spera and White, 1987; Hanson and Hargrove, 1999) or due to changes in magma viscosity (Squire and McPhie, 2002; Goto and McPhie, 1996; Dadd and Van Wagoner, 2002). Of these examples, only Squire and McPhie (2002) describe intermixed blocky and fluidal peperite populations originating from the interaction between the same magma and sediment, which is similar to the mixed population observed (**Figure 172D**). Viscosity may play a role, but the limiting factor may be the availability of water, as the adjacent tuffs are only 20-25 cm-thick (**Figure 171**). Fluidal peperites are probably formed during the initial interaction (cf. Squire and McPhie, 2002), when more water was available to sustain a vapor film necessary to insulate the magma from thermal effects (Kokelaar, 1982), as well as to fluidize the sediment. Once water levels drop below some critical level, vapor films probably become unstable, thus causing rapid heat transfer that can result in quenching and hydromagmatic explosions (Skilling et al., 2002). For this

example, the observed blocky peperites form jigsaw textures (**Figure 172D**), hence are consider to form during *in situ* quench fragmentation (Kokelaar, 1982; Brooks, 1995; Hanson and Hargrove, 1999), as opposed to hydromagmatic processes that would widely distribute juvenile clasts (Skilling et al., 2002). The *in situ* brecciated/hyaloclastite zone observed several cm's below the tuff turbidites to the west (**Figure 171**) possibly represent fluids leaching from the overlying sediments due to the orientation of fractures that extend from the tuffs and end in the brecciated zone (**Figure 172C**). These tuffs were probably consolidated to a point that inhibited fluidization, but permitted circulation of pore fluids.

The mineralized hyaloclastite zone is a possible passageway for hydrothermal fluids related to the erupting edifice. However, the presence of unaltered granodiorite and associated garnet (**Figure 172F**) has caused some workers envisaged metasomatism related to high-grade skarns (Meinert, 1998). These skarn related indicator minerals (i.e., garnet) are limited to within several cm's of the intrusion itself, which suggest that if metasomatic fluids did circulate they were spatially restricted.

CHAPTER 6

GEOCHEMISTRY & GEOCHRONOLOGY

Geochemical and geochronological data provide important information concerning the temporal evolution of supracrustal sequences. The geochemistry facilitates: (1) volcanic rock classification; (2) characterization of the geochemical affinity; and (3) identification of a geotectonic environment, whereas the geochronology constrains individual formational ages.

A total of 223 samples were analyzed for major, minor, and some trace elements (Zr, Y, Cu, and Zn) at the Centre de Recherche Minérale (Sainte-Foy, Québec) using X-ray fluorescence (XRF), except for Zn and Cu (ICP-AES). Major elements SiO_2, Al_2O_3, Fe_2O_3, MgO, and Na_2O have a detection limit of 0.10%; K_2O, TiO_2, MnO, P_2O_5, and Cr_2O_3 have a detection limit of 0.01%; and CaO a detection limit of 0.02%. Zirconium and Y have detection limits of 3 ppm, whereas Cu and Zn have a detection limit of 1 ppm. In addition, a total of 50 samples were selected for analysis of a wide range of trace and rare earth elements (REE) by instrument neutron activation analysis (INAA) collected at the Université du Québec à Chicoutimi (UQAC) following the procedure of Bédard and Barnes (1990). A standard was analyzed in every run of 25 samples to verify precision. Results for this sample indicate a standard error of less than 5% for Rb, Ba, Th, Ta, La, Ce, Nd, Sm, and Yb, with anomalous errors of 35 and 104% for Zr, and K, respectively. Analyses with loss on ignition (LOI) values greater than 6-wt% where discarded, except for those associated with ultramafic rocks. Other discarded analyses included those with totals

greater than 101 and less than 98-wt%. Table 21 gives a representative suite of the geochemistry for the three formations with a more complete data set in appendix B.

6.1 Geochemical Characteristics

The geochemistry of the Jacola, Val d'Or and Héva Formations displays distinct magmatic signatures. The major and trace elements, as well as REE geochemistry, coupled field observations help unravel the evolution of the Val d'Or mining camp. The Jacola and Héva formations are tholeiitic, whereas the Val d'Or Formation varies from a basal tholeiitic sequence through to a transitional and finally to an upper calc-alkaline sequence

Majors elements SiO_2 and TiO_2 coupled with Zr in a Winchester and Floyd diagram (1977; **Figure 173A**) show distinct inter- and intra-formational trends that are consistent with an early ocean floor or plateau (Jacola Fm) evolving into an arc (Val d'Or Fm) that was subsequently rifted (Héva Fm). A similar overall trend is evident in the major element Jensen and Pyke (1982; **Figure 173B**) ternary diagram, but this plot accentuates convincingly the distinct break between JF komatiites and VDF and HF tholeiitic-calc-alkaline rocks.

Trace elements and REE abundances and ratios support formational divisions and major element trends, but in addition permit identification of intraformational variations. The average Th/Yb and $(La/Yb)_n$ ratios of the Jacola Formation rocks are 0.06 and 0.60, respectively, whereas the mafic rocks of the Héva Formation are higher with Th/Yb of 0.23 and $(La/Yb)_n$ of 1.42. The tholeiitic to calc-alkaline trend of the Val d'Or Formation is

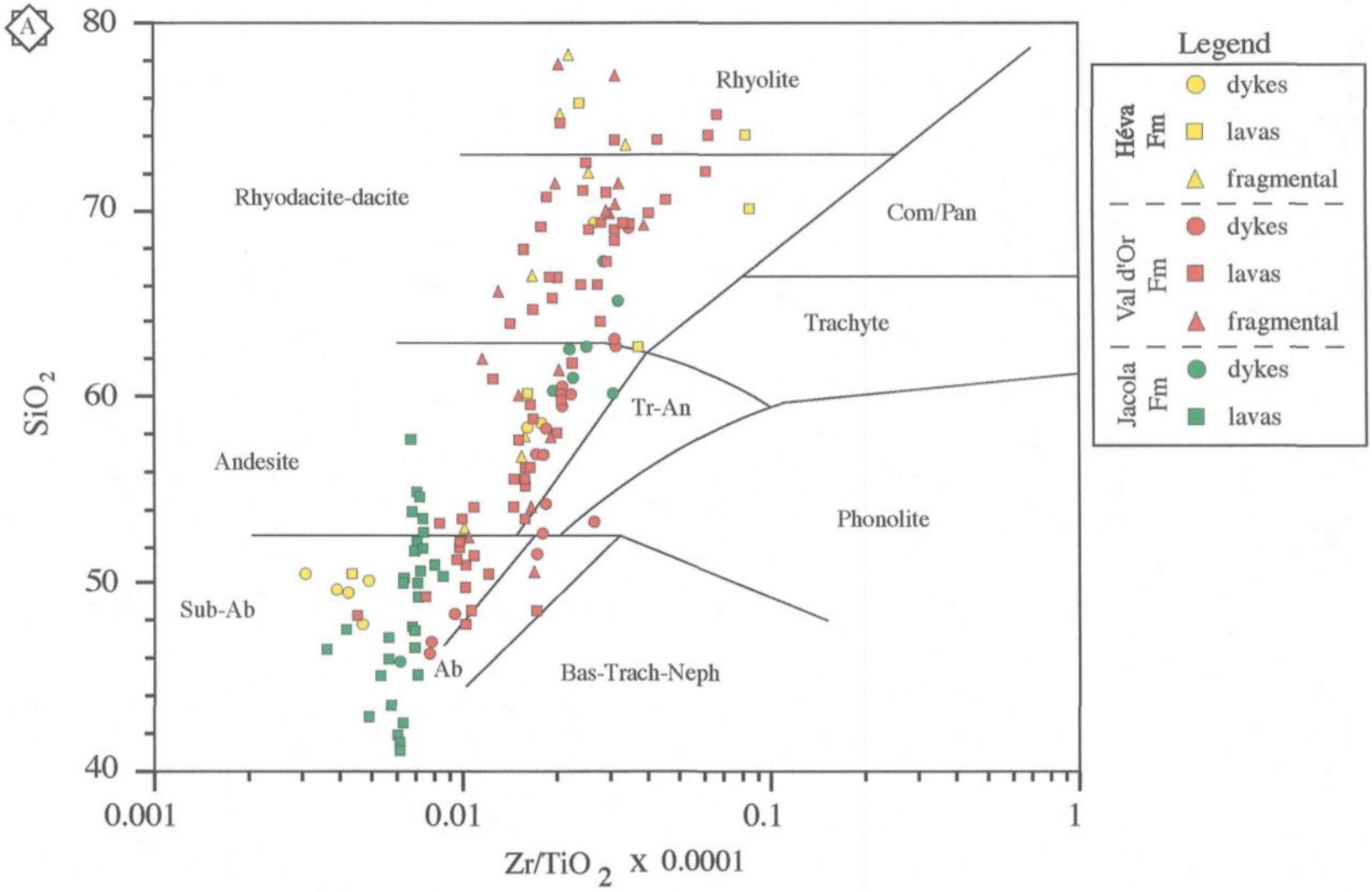

Figure 173. Classification of the different volcano-sedimentary facies within the study area. Yellow (23 points), red (96 points), and green (41 points) symbols represent the Héva, Val d'Or, and Jacola formations, respectively. Circles, squares, and triangles represent dykes, lavas, and volcaniclastic lithologies, respectively. A. SiO_2 vs. Zr/TiO_2 diagram outlining the various compositions for the three formations (after Winchester and Floyd, 1977) and B. Jensen cation ternary diagram for rock composition (after Jensen and Pyke, 1982).

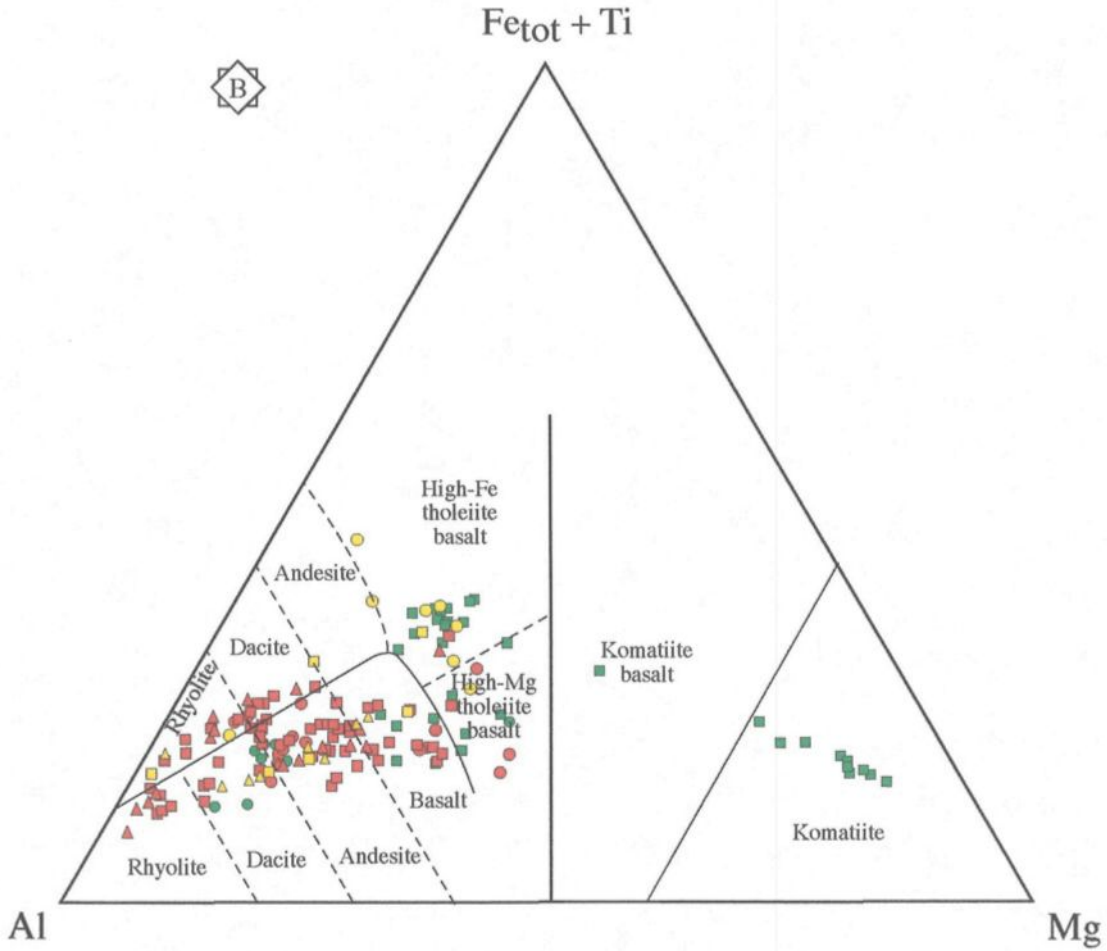
Fetot + Ti
B
High-Fe
tholeiite
basalt
Andesite
Dacite
Rhyolite
High-Mg
tholeiite
basalt
Komatiite
basalt
Basalt
Komatiite
Rhyolite
Dacite
Andesite
Al
Mg

evident with lower Th/Yb and $(La/Yb)_n$ ratios of 0.52 and 2.79 in the lower and elevated Th/Yb and $(La/Yb)_n$ ratios of 0.92 and 4.76 in the upper VDF, respectively (**Table 21**). Higher trace element and REE-ratios for the upper VDF compare favourably with the tuff turbidites and fragments in the Tex-Sol tuff breccia (see 5.2) of the HF, that have average Th/Yb and $(La/Yb)_n$ ratios of 0.93 and 4.23, respectively. Their geochemical similarity implies a genetic relationship between the two formations, which has important ramifications for the overall depositional (and stratigraphy) history of the region (see below).

6.2 Major Element geochemistry

Major element geochemistry of the Jacola, Val d'Or, and Héva formations (**Table 21**) displays wide compositional range, and is correlative with a distinct tectonic environment. Because of the mobility of $Na_2O + K_2O$ in ancient rocks, the Winchester and Floyd (1977) diagram is preferred for identification of magma types, where immobile elements of Zr and Ti are plotted against $Si0_2$ (**Figures 173A**). An alternative that is especially useful for ultramafic volcanic rocks, is the Jensen cation plot (**Figure 173B**; (Jensen and Pyke, 1982). This classification method is restricted to volcanic rocks that have undergone weak metasomatism, as the elements Fe^{2+}, Fe^{3+}, Ti, Al, and Mg are stable under low grades of metamorphism (Rollinson, 1993).

The chemistry of the Jacola Formation lava flows is characterized by primitive compositions as reflected in the predominance of high-Mg basalts, and komatiites (SiO_2 <

Table 21: Representative geochemistry of study area.

	Jacola Formation									
Sample number	CS97-246A	CS97-246C	CS99-2496	CS99-2497B	CS99-2482A	CS99-2487A	CS99-2193A	CS99-2193B	CS98-001	CS97-240
General Location	HW 117	HW 117	Val d'Or	Val d'Or town	Val d'Or town	Val d'Or town	N.Bidlamaque	N.Bidlamaque	PDN	PDN
Description	Ultramafic Lava	Ultramafic Lava	Mafic Lava	Mafic Lava	Mafic Lava	Ultramafic Lava	Mafic Lava	Dyke	Massive Interm. lava	Pillowed Interm. lava
SiO_2(wt%)	42.80	46.50	40.9	45.3	51.9	40.1	48.4	55.8	54.00	50.50
TiO2	0.38	1.06	0.34	0.36	0.79	0.26	0.45	0.73	0.6	0.85
Al_2O_3	5.47	15.70	4.89	21.1	13.5	3.81	14.6	16.9	19	16.60
Fe_2O_3	10.90	11.40	11.5	9.49	15	10.8	11	7	6.15	7.81
MnO	0.20	0.18	0.16	0.16	0.24	0.19	0.15	0.1	0.09	0.22
MgO	27.60	9.64	29.3	8.89	6.16	25.5	10.5	4.89	4.93	5.62
CaO	5.16	9.65	3.55	7.35	7.85	7.38	9.9	8.93	6.57	11.60
Na_2O	0.17	2.11	0.16	2.04	1.95	0.13	2.31	3.56	1.18	3.16
K_2O	0.01	0.62	0.01	0.33	0.24	0.02	0.05	0.07	2.8	0.64
P_2O_5	0.03	0.24	0.01	0.01	0.06	0.01	0.03	0.12	0.16	0.16
Cr_2O_3	N.D.	N.D.	0.35	0.01	0.02	0.27	0.08	0.02	0.03	N.D.
LOI	7.30	2.62	8.62	4.61	2.03	10.4	2.74	1.75	3.86	2.98
TOTAL	100.02	99.72	99.79	99.65	99.74	98.87	100.21	99.87	99.37	100.14
Zr(ppm)	19	75	21	23	59	19	35	114	90	104
Y	8	21	7	13	38	8	20	20	20	21
Cu	22	43	63	3	100	35	11	85	1	49
Zn	62	92	55	87	87	43	30	17	34	92
Ba	3	99	N.D.	N.D.	N.D.	N.D.	N.D.	N.D.	630	223
Co	107	47	110	53	51	90	46	21	N.D.	46
Cr	2300	377	2300	75	96	1800	500	84	82	670
Ni	1600	225	1600	130	80	1300	220	40	163	319
Rb	4	23	3	18	7	3	3	3	80	19
Sr	10	182	3	86	108	22	77	144	161	293
Sc	22	40	22	51	82	21	50	33	38	40
La						0.62	1.49		10.76	16.63
Ce						2.46	5.27		23.56	38.49
Nd						1.85	3.10		14.79	21.06
Sm						0.71	1.09		3.48	4.51
Eu						0.24	0.55		1.07	1.37
Ho						0.46	0.62		0.46	0.54
Tb						0.18	0.34		0.48	0.61
Yb						0.58	2.48		2.27	1.99
Lu						0.10	0.41		0.40	0.33
Cs						1.58	N.D.		1.90	0.37
Hf						0.48	0.98		1.99	2.76
Ta						0.04	0.07		0.20	0.16
Th						N.D.	0.14		1.29	2.87
Zr/Y	2.38	3.57	3.00	1.77	1.55	2.38	1.75	5.70	4.50	4.95
Th/Yb						N.D.	0.06		0.57	1.44
$(La/Yb)_n$						0.77	0.43		3.39	6.01
$(La/Sm)_n$						0.57	0.88		2.00	2.38
$(Sm/Yb)_n$						1.36	0.49		1.70	2.52

N.D. = not detected; REEs and Cs, Hf, Ta, and Th determined by INAA

Lower Val d'Or Formation												
CS99-2397B Val d'Or town Pillowed Interm. lava	CS97-054 East Sullivan Pillow Interm. lava	CS97-064 East Sullivan Pillowed Interm. lava	CS99-2453A Pole Line Pillowed Interm. lava	CS98-260A Pole Line Pillowed Interm. Lava	CS98-165b Camnet Massive Felsic lava	CS98-203 Cambior Massive Felsic lava	CS98-149 Camnet Massive Felsic lava	CS98-290 Playground Crystal tuff	CS97-245 PDN Lapilli Tuff	CS97-040 East Sullivan Lapilli Breccia	CS98-080 East Sullivan Tuff Turbidite	CS98-202A Cambior Fragment
64.1	51.90	51.00	53.4	55.6	68.90	73.7	75.00	44.1	55.40	52.50	51.20	65.5
0.85	0.85	0.84	0.89	0.7	1.04	0.65	0.28	0.83	0.66	0.85	0.87	1.14
14.5	19.80	19.50	18.7	18.3	13.4	14.2	13.1	17.3	16.40	18.80	19.2	15.1
7.3	7.82	7.85	8.79	7.35	4.73	1.01	2.19	9.82	7.27	8.01	9.54	2.11
0.14	0.14	0.14	0.15	0.12	0.12	0.03	0.04	0.14	0.10	0.13	0.15	0.08
3.93	4.62	5.08	4.64	4.11	1.65	0.06	0.62	3.98	4.83	5.01	5.3	0.49
2.14	4.03	5.92	4.84	6.11	3.09	1.54	1.5	12.4	4.95	5.41	4.46	5.41
3.75	6.65	5.25	5.01	4.38	4.48	4.63	5.55	2.82	3.85	4.87	4.46	3.19
0.57	0.01	0.06	0.02	0.2	0.04	1.88	0.2	0.06	0.38	0.13	0.11	2.36
0.14	0.08	0.09	0.1	0.12	0.29	0.15	0.05	0.08	0.12	0.09	0.11	0.28
0.01	N.D.	N.D.	0.01	0.02	0.01	0.01	0.01	0.02	N.D.	N.D.	0.02	0.04
2.93	4.27	4.32	3.59	2.45	1.88	2.03	1.28	7.98	5.94	4.15	4.35	3.68
100.36	100.17	100.05	100.14	99.46	99.63	99.89	99.82	99.53	99.90	99.95	99.77	99.38
85	85	87	93	104	272	284	193	70	107	91	91	152
19	26	26	30	23	36	47	46	24	20	27	28	36
62	54	74	51	28	1	15	1	15	11	42	56	49
94	71	75	84	N.D.	82	N.D.	19	N.D.	72	76	67	N.D.
N.D.	18	24	N.D.	76	50	410	65	52	126	93	65	470
25	28	24	26	N.D.	N.D.	N.D.	N.D.	N.D.	21	23	N.D.	N.D.
20	29	49	35	89	20	20	20	73	103	44	43	200
15	45	45	31	N.D.	20	N.D.	39	N.D.	57	60	65	N.D.
16	3	5	3	5	3	39	3	4	10	5	5	68
109	188	197	156	132	193	130	137	72	152	215	215	210
40	43	42	50	N.D.	23	N.D.	9.5	N.D.	20	43	49	N.D.
8.02	5.24	5.31	4.99	7.25	22.20	21.27	24.02	3.65	7.25	5.55	5.52	23.16
22.25	12.38	15.55	16.04	18.92	58.52	61.85	65.23	10.74	17.45	15.54	15.66	56.18
14.78	8.35	10.33	10.27	10.16	29.43	30.03	31.05	7.17	11.47	10.06	8.07	26.57
3.09	2.77	2.76	2.86	2.89	6.97	6.91	7.15	2.21	2.62	2.68	2.86	6.00
0.69	1.03	1.17	1.03	1.04	1.53	1.63	1.24	0.96	0.97	1.03	1.24	2.12
0.68	0.99	0.71	1.08	0.79	1.03	1.52	1.27	0.72	0.74	1.03	0.59	1.19
0.44	0.64	0.67	0.68	0.56	0.94	1.26	1.07	0.52	0.54	0.55	0.63	0.94
2.28	3.48	3.55	3.57	2.59	3.77	3.75	4.29	2.80	2.13	3.35	3.51	2.45
0.38	0.57	0.60	0.60	0.43	0.58	0.56	0.64	0.44	0.34	0.57	0.57	0.37
0.92	N.D.	N.D.	N.D.	N.D.	N.D.	2.23	N.D.	N.D.	0.69	0.48	N.D.	3.28
2.06	2.42	2.27	2.41	2.76	7.79	8.35	6.44	1.86	2.88	2.26	2.45	3.75
0.28	0.20	0.25	0.25	0.24	0.56	0.73	0.66	0.10	0.32	0.19	0.22	0.44
1.10	0.52	0.58	0.54	0.76	3.61	3.50	5.41	0.26	0.83	0.56	0.64	1.56
4.47	3.27	3.35	3.10	4.52	7.56	6.04	4.20	2.92	5.35	3.37	3.25	4.22
0.48	0.15	0.16	0.15	0.30	0.96	0.93	1.26	0.09	0.39	0.17	0.18	0.64
2.52	1.08	1.07	1.00	2.01	4.22	4.06	4.02	0.94	2.44	1.19	1.13	6.79
1.67	1.22	1.24	1.12	1.62	2.05	1.99	2.17	1.07	1.78	1.34	1.25	2.49
1.51	0.88	0.86	0.89	1.24	2.05	2.04	1.85	0.88	1.37	0.89	0.90	2.72

N.D. = not detected; REEs and Cs, Hf, Ta, and Th determined by INAA

						Upper Val d'Or Formation						
CS99-2017 Relais Feldpsar-phyric lobe	CS99-2013 Relais Pillowed Interm. lava	CS98-045 Dunraine Pillowed Interm. lava	CS98-235 Dunraine Massive Felsic lava	CS99-2326 Dunraine Massive Felsic lava	CS99-2385B Dunraine Massive Felsic lava	CS98-040 Dunraine Massive Interm. lava	CS98-041 Dunraine Massive Interm. lava	CS97-092 Abitibi-Cu Massive Interm. lava	CS99-2250 Abitibi-Cu Massive Felsic lava	CS97-216A1 Sleepy Lake Massive Felsic lava	CS97-078 Sleepy Lake Massive Felsic lava	CS97-127 Sleepy Lake Massive Felsic lava
65.2	59.1	51.50	65.9	65.4	72.9	54	51.2	53.50	66.4	69.00	67.80	69.30
1.06	0.88	1.01	1.05	0.79	0.9	0.77	0.8	0.69	0.81	1.24	1.28	0.53
14.2	15	21	12.7	15.4	11.8	17.4	16.7	16.50	14	13.90	15.00	11.60
6.09	6.78	6.08	5.9	5.57	0.84	7.48	7.9	6.59	4.82	6.18	3.52	4.73
0.09	0.1	0.1	0.09	0.09	0.06	0.12	0.16	0.16	0.06	0.11	0.08	0.10
1.38	5.06	2.97	1.41	5.35	0.1	5.44	7.75	5.34	0.69	3.15	0.38	1.25
1.62	3.13	6.92	3.95	0.35	3.77	8.46	8.8	4.84	2.06	0.44	2.37	3.80
6.22	5.33	3.82	2.85	0.28	5.58	1.8	2.52	6.46	6.27	0.29	4.99	3.40
0.84	0.07	1.19	1.25	2.2	0.57	0.07	0.2	0.18	0.81	2.28	1.36	1.03
0.29	0.2	0.14	0.24	0.37	0.27	0.11	0.09	0.17	0.17	0.32	0.29	0.11
0.01	0.03	0.03	0.02	0.02	0.01	0.02	0.13	N.D.	0.01	N.D.	N.D.	N.D.
2.95	4.67	4.53	4.83	4.13	2.91	4.51	3.65	5.56	3.18	3.07	3.28	4.23
99.95	100.35	99.29	100.19	99.95	99.71	100.18	99.9	99.99	99.28	99.98	100.35	100.08
211	150	112	260	234	170	85	78	113	248	230	209	179
34	27	34	42	31	30	23	18	21	36	34	33	29
21	47	71	92	14	68	40	6	5	170	55	130	92
110	55	64	N.D.	230	7	N.D.	N.D.	84	110	492	17	72
N.D.	N.D.	390	250	N.D.	N.D.	50	130	98	N.D.	781	215	187
8	22	N.D.	N.D.	5	5	N.D.	N.D.	28	8	7	19	3
20	160	76	20	90	20	98	760	140	20	20	20	20
1	68	43	N.D.	26	4	N.D.	N.D.	135	1	1	21	2
22	3	32	41	40	15	3	8	6	20	41	34	27
92	241	176	107	223	117	212	163	155	68	165	106	42
33	30	34	N.D.	24	13			26	21	34	22	19
25.66	16.2189	6.9137	21.78	26.18	16.8405	8.9066	6.7299	17.1058	32.08	25.64	22.81	14.5534
67.54	41.9175	21.4734	57.82	72.10	44.7753	22.732	17.5202	43.3147	84.98	68.76	63.67	38.4978
34.83	21.2049	12.8915	31.03	41.44	23.7627	14.5074	11.9626	25.745	47.01	38.16	31.93	19.7324
8.08	5.5241	4.1406	6.96	8.36	5.7986	3.4027	2.8719	5.8461	9.40	8.61	7.43	5.353
2.24	1.6068	1.5554	1.81	1.91	1.5089	1.2228	1.0344	1.7139	2.47	2.17	2.30	1.4443
0.50	0.7715	1.2239	1.62	1.38	1.0183	0.8662	0.856	0.8006	1.06	1.49	0.87	0.9367
1.09	0.7639	0.8188	1.08	1.03	0.907	0.5517	0.5078	0.7173	1.11	1.16	1.01	0.9076
3.33	2.6633	3.3053	4.16	3.00	2.4802	2.1837	1.968	1.9563	3.57	3.51	3.18	3.7443
0.51	0.4153	0.5196	0.63	0.49	0.3774	0.3688	0.3156	0.3105	0.57	0.58	0.49	0.5963
1.85	N.D.	1.8811	1.53	1.56	0.66	N.D.	1.1247	1.8867	1.52	1.90	2.26	1.0453
6.12	4.0795	3.1289	7.38	6.13	4.5556	1.8876	2.0374	3.1767	7.02	6.55	5.93	5.2667
0.45	2.2774	0.3146	0.64	0.52	0.4182	0.1935	0.2261	0.2779	0.57	0.62	0.45	2.4215
3.61	0.3603	1.0461	3.28	3.74	2.1114	1.1154	0.7842	2.2929	5.10	4.97	3.14	2.4215
6.21	5.56	3.29	6.19	7.55	5.67	3.70	4.33	5.38	6.89	6.76	6.33	6.17
1.08	0.14	0.32	0.79	1.25	0.85	0.51	0.40	1.17	1.43	1.42	0.99	0.65
5.53	4.37	1.50	3.75	6.27	4.87	2.93	2.45	6.27	6.45	5.24	5.15	2.79
2.05	1.90	1.08	2.02	2.02	1.87	1.69	1.51	1.89	2.20	1.92	1.98	1.76
2.70	2.30	1.39	1.86	3.10	2.60	1.73	1.62	3.32	2.93	2.72	2.60	1.59

N.D. = not detected; REEs and Cs, Hf, Ta, and Th determined by INAA

		Spherulitic Unit - Héva Formation				Mafic Extrusive to Intrusive - Héva Formation				
CS98-020c Dunraine Tuff Turbidite	CS98-115 Dunraine Intermediate Fragment	CS98-288A HW 117 Spherulitic Facies	CS99-2055A Lapaska Spherulitic Facies	CS99-2212A Anamaque Spherulitic Facies	CS99-2180E sph facies Spherulitic Facies	CS98-270 Akasaba w Mafic pillowed lava	CS99-2164A Goldfields Mafic pillowed lava	CS99-2158A Tex-Sol Massive Mafic lava	CS97-218 Akasaba 2 Gabbro	CS98-266A Akasaba 3 Gabbro
69.10	62.00	73.9	62.6	69.7	65.7	50.5	48.7	49.9	49.50	47.8
0.81	1.62	0.45	0.83	0.49	0.74	1.74	1.29	1.24	1.56	0.93
17.3	14	11.6	12	11.9	15.6	13.9	13.9	13.6	13.40	15.2
2.56	5.93	4.17	8.14	6.31	4.09	13.1	15.8	14.8	15.40	12.3
0.06	0.1	0.06	0.1	0.05	0.06	0.19	0.24	0.2	0.19	0.17
0.44	1.24	2.36	1.86	1.76	1.33	5	6.37	6.23	5.25	7.85
1.31	4.94	1.18	4.55	1.63	2.24	11.2	8.97	9.13	10.70	11.6
2.75	3.23	3.69	3.38	4.61	7.58	2.97	1.6	1.76	2.01	0.83
2.09	0.67	0.07	0.64	0.4	0.06	0.25	0.11	0.08	0.53	0.15
0.39	0.24	0.06	0.21	0.07	0.14	0.1	0.07	0.1	0.09	0.04
0.02	0.02	0.01	0.05	0.01	0.03	0.02	0.02	0.02		0.06
2.83	5.1	1.91	5.25	2.07	1.96	1.07	3.19	2.58	1.48	3.19
99.66	99.09	99.46	99.61	99	99.53	100.04	100.26	99.64	100.11	100.12
321	190	383	314	387	101	78	53	82	68	45
40	29	143	114	118	21	28	22	33	26	17
88	160	3	12	62	140	2	140	160	111	130
30	96	N.D.	81	63	52	0.5	150	94	78	0.5
350	670	50	N.D.	N.D.		50	N.D.	N.D.	40	50
N.D.	N.D.	N.D.	9	7	46	N.D.	53	53	55	N.D.
20	20	20	320	20	150	31	93	88	27	300
35	44	N.D.	6	6	98	28	78	66	61	120
68	33	3	17	17	3	5	5	3	18	6
301	251	73	134	57	105	98	93	81	119	106
14	35	N.D.	23	11	28	420	53	50	49	260
40.11	15.265	22.48	19.93	17.94	9.1247	3.94				
106.57	42.1165	90.77	76.30	61.45	25.0576	11.51				
66.04	23.6573	38.79	31.73	32.84	9.8946	8.67				
12.32	5.4228	13.98	13.17	10.33	3.4993	2.96				
2.37	1.4887	5.57	4.31	3.07	2.0361	1.32				
0.83	0.9215	4.61	4.03	4.51	0.7092	1.37				
1.25	0.8435	3.47	3.06	2.63	0.6346	0.71				
2.95	2.7216	14.76	12.21	14.58	2.1844	2.88				
0.46	0.4344	2.22	1.85	2.24	0.3264	0.46				
2.85	1.8299	N.D.	0.76	0.54 nd		N.D.				
8.66	5.0938	11.95	9.68	12.45	3.0477	2.15				
0.85	0.4363	1.07	0.79	1.10	0.2235	0.22				
5.72	2.2487	2.09	1.72	2.21	1.3382	0.37				
8.03	6.55	2.68	2.75	3.28	4.81	2.79	2.41	2.48	2.62	2.65
1.94	0.83	0.14	0.14	0.15	0.61	0.13				
9.75	4.02	1.09	1.17	0.88	3.00	0.98				
2.10	1.82	1.04	0.98	1.12	1.68	0.86				
4.64	2.21 W	1.05	1.20	0.79	1.78	1.14				

N.D. = not detected; REEs and Cs, Hf, Ta, and Th determined by INAA

Extra-formational lithofacies within Héva Formation				
CS98-263C Tex-Sol Felsic Fragment	CS98-263B Tex-Sol Mafic Fragment	CS99-2153B Val-doria Tuff	CS97-220 Akasaba 2 Tuff	CS98-263J Tex-Sol Tuff
75	56.8	55.5	78.30	71.9
0.82	0.77	0.89	0.59	0.77
11.4	16.8	17.9	9.93	13.6
2.36	9.25	9.48	2.57	3.85
0.02	0.06	0.08	0.05	0.02
1.18	4.8	3.04	1.45	0.29
2.11	0.8	6.32	1.90	0.8
4.93	5.59	3.94	4.22	4.55
0.8	2.45	0.47	0.03	2.02
0.21	0.2	0.14	0.13	0.16
0.01	0.07	0.01	N.D.	0.01
0.92	1.89	2.36	0.84	1.44
99.76	99.48	100.13	100.01	99.41
177	122	182	135	202
30	23	48	17	32
2	1	1	26	1
N.D.	1.4	36	64	N.D.
210	660	N.D.	6	750
N.D.	N.D.	21	11	N.D.
20	380	34	40	20
N.D.	120	12	42	N.D.
25	86	15	3	50
92	119	199	35	80
N.D.	170	27	16	N.D.
15.59	16.84	14.34	12.55	
49.99	36.27	35.71	32.36	
20.74	20.33	18.48	14.70	
6.30	5.57	5.65	3.60	
1.84	1.67	1.78	0.79	
0.98	0.74	1.56	0.67	
0.99	0.78	1.28	0.52	
3.11	1.96	5.26	1.80	
0.47	0.32	0.81	0.28	
2.30	12.17	0.94	N.D.	
4.94	3.38	5.33	3.69	
0.38	0.29	0.52	0.34	
2.75	2.88	2.03	1.91	
5.90	5.30	3.79	7.94	6.31
0.89	1.47	0.39	1.06	
3.59	6.17	1.96	5.01	
1.60	1.95	1.64	2.25	
2.25	3.16	1.19	2.23	

N.D. = not detected; REEs and Cs, Hf, Ta, and Th determined by INAA

42 wt%; MgO > 25 wt%; **Table 21**) in comparison to the Val d'Or and Héva formations (**Table 21**). Dykes intruding the Jacola Formation have an intermediate composition, and are similar to lavas from the overlying Val d'Or Formation (**Figure 173A/B**). Volcano-sedimentary rocks from both the Val d'Or and Héva Formations display a wide compositional range (**Figure 173A/B**), but detailed facies mapping of each formation (e.g., **Figure 174**) permit distinction. The spherulitic HF lava unit has both a dacitic and rhyodacitic composition (**Figure 174**), suggesting magmatic differentiation and numerous flow units. In addition, fragments from the Tex-Sol tuff breccia unit (see **Figure 152**) have andesite and rhyolite clasts (**Figure 174**). Moreover, the tuff turbidite facies in the Akasaba region, near the top of the HF, are felsic (rhyolite to rhyodacite), in contrast to the typical pillowed to massive basalt lava flows and gabbro sills/dykes (**Figure 174**).

6.3 Geochemical Trends

The geochemical trends between the Archean formations is complex but if formations are plotted separately (**Figures 175A, B, C**) striking characteristics can be observed if there is a distinction between lava flow, dyke-sill, or volcaniclastic deposit. The diagram of Barrett and MacLean (1997), using trace elements Y and Zr, defines tholeiitic, transitional and calc-alkaline fields, and is particularly well-suited for identifying geochemical affinities in Archean volcanic rocks. Ratios of Zr/Y < 4 are considered tholeiitic, and > 7 are calc-alkaline, with those in between being transitional. The ultramafic to mafic volcanic rocks from the JF have low abundances of Zr and Y and plot within the

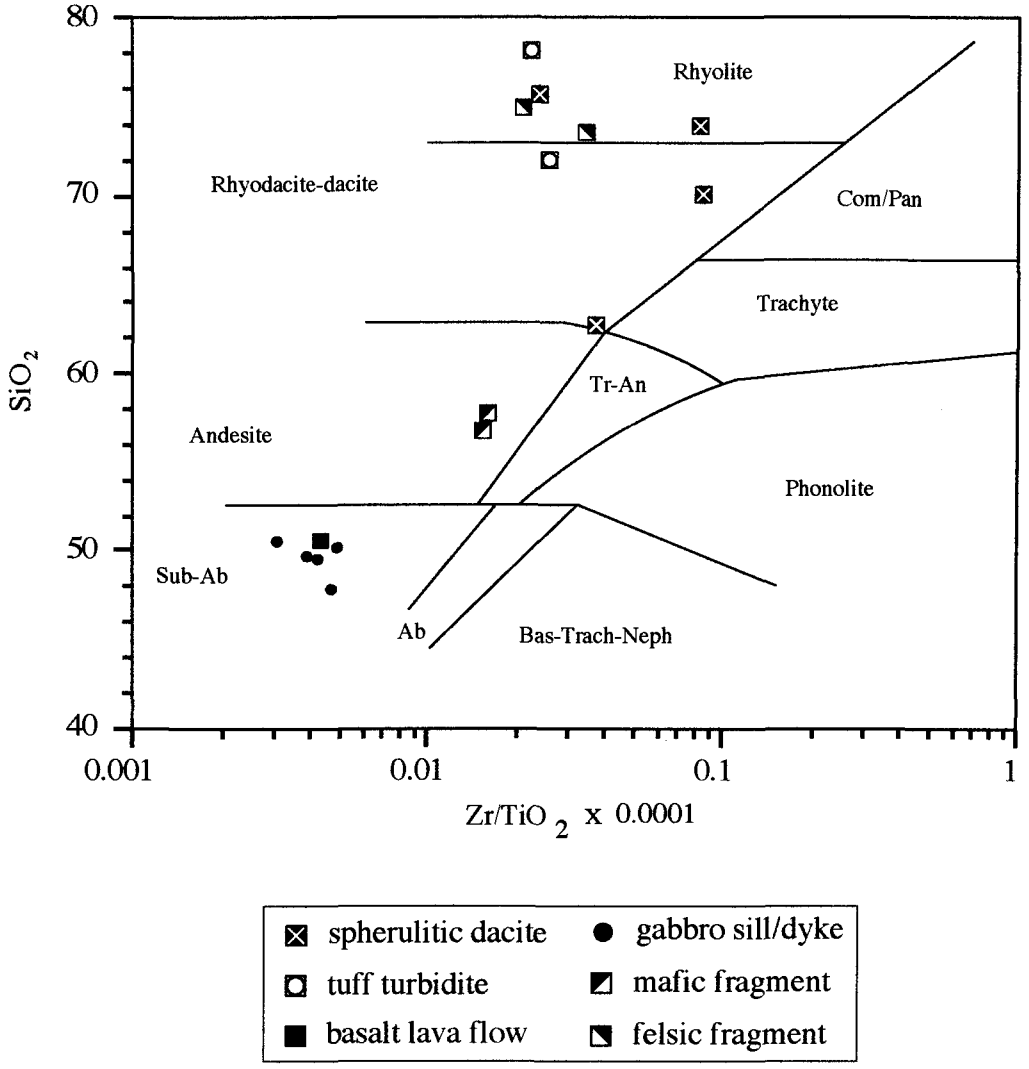

Figure 174. Major element geochemistry of the Héva Formation. Compositional ranges of lavas from the Héva Formation (after Winchester and Floyd, 1977).

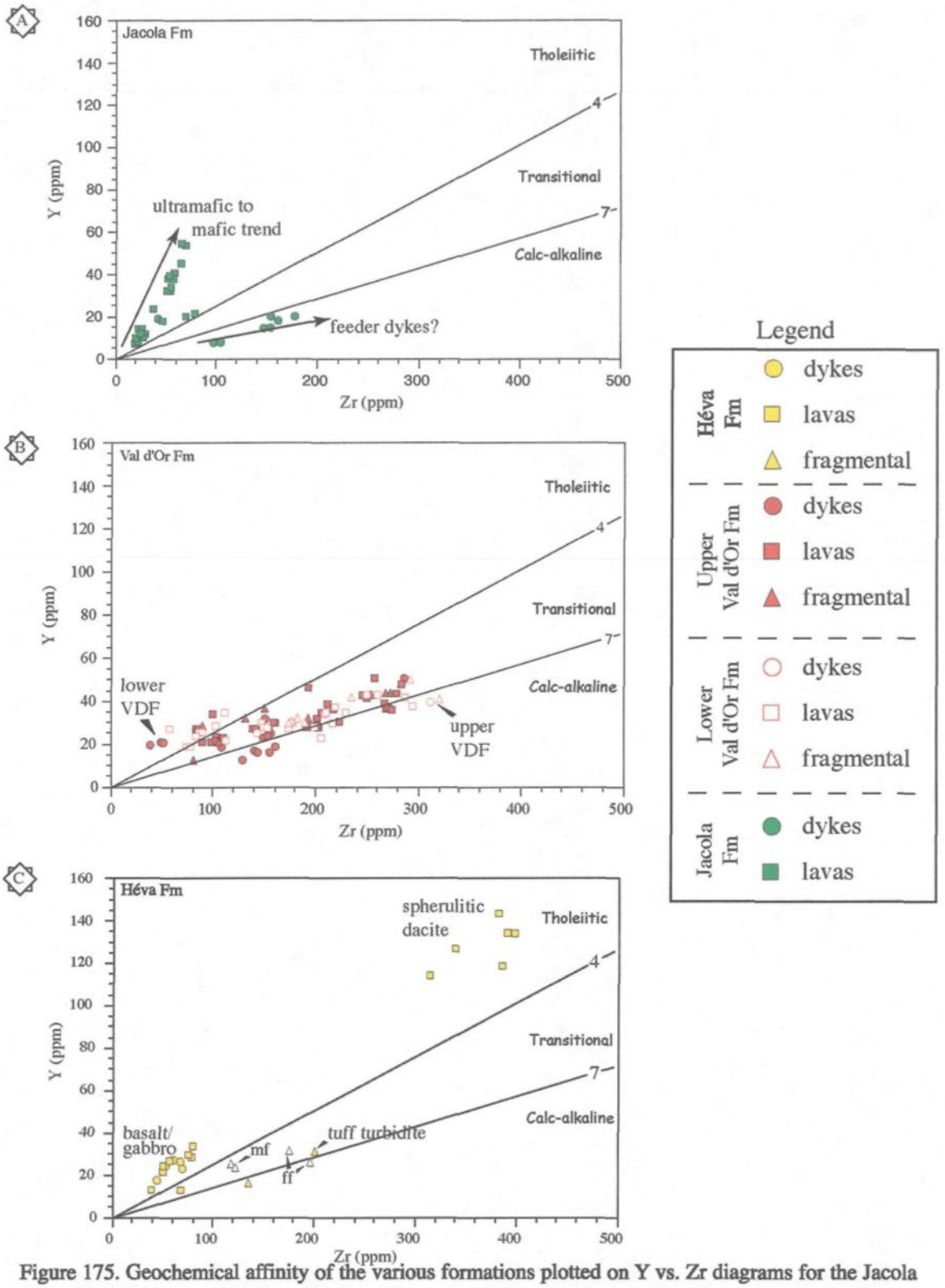

Figure 175. Geochemical affinity of the various formations plotted on Y vs. Zr diagrams for the Jacola (A), Val d'Or (B), and Héva (C) formations. Symbols after figure 177. Two possible trends are recognized within the Jacola Formation; ultramafic to mafic evolution; and possible feeder dykes to the VDF. Filled and opened symbols, in B, for the lower and upper VDF, respectively. Fields after Barret and MacLean (1997).

tholeiitic field displaying a positive linear relationship delineating an ultramafic-mafic trend with a near constant Zr/Y ratio of 1.5 (**Figure 175A**). The calc-alkaline dykes in the JF are geochemically similar to the lower VDF lava flows (see **Figure 175B**), and therefore considered feeders to the VDF. VDF volcanic rocks define an overall tholeiitic to calc-alkaline trend up-section (**Figure 175B**). As seen in **Figure 175B,** Zr increases with near constant Y values. This observed evolutionary sequence supports the subdivision of the VDF into lower and upper segments. The variation in the HF, however, is not attributed to a simple evolutionary trend, but erosion of the arc edifices. The mafic volcanic rocks and intrusions plot within the tholeiitic field with a Zr/Y ratio of ~2.4 (**Figure 175C**), whereas volcaniclastic tuff turbidites and tuff breccias (**Figure 175C**) are of a different origin. For example, the felsic and mafic fragments from the Tex-Sol tuff breccia (see section 5.2), from the base of the HF, are transitional and calc-alkaline, respectively (**Figure 175C**), but underlying these volcaniclastic deposits are the *tholeiitic* spherulitic dacite unit (**Figure 175C**), the proposed base of the Héva Formation. In addition, tuff turbidite facies further up section are calc-alkaline (**Figure 175C**) and interbedded with tholeiitic basalts (**Figure 175C**). This geochemical complexity in conjunction with the regional stratigraphy is best explained by contemporaneous erosion of the Val d'Or and arc rifting arc as represented by the HF. The tuff breccias and tuff turbidite deposits were derived from the arc and deposited down-slope in areas of rift-related volcanism.

6.4 Rare Earth and Trace Elements

Rare earth elements and certain trace elements are considered immobile during low-grade metamorphism, weathering, seafloor alteration, and low-temperature hydrothermal activity (Rollinson, 1993). Therefore, these elements are well suited to assess ancient volcano-sedimentary successions and enable a comparison with modern environments. Furthermore, the geochemical behavior of REE and trace elements can emphasize petrogenetic processes which are related to a specific tectonic setting or source (Pearce and Cann, 1973; Rollinson, 1993; Pearce and Peate, 1995; Kerrich and Wyman, 1996).

The mafic and ultramafic rocks of the JF display an overall decrease in abundance in REE (**Figure 176A**), with an average of $(La/Yb)_n$ of 0.60 (see **Table 21**). The basalt sample has an enrichment trend for heavy REE (HREE) with a $(Sm/Yb)_n$ ratio of 0.49, whereas the komatiite sample is slightly depleted with a $(Sm/Yb)_n$ ratio of 1.49 (**Table 21**).

The VDF has a complex volcanology and the geochemistry supports this notion as various geochemical patterns, depending on locality and stratigraphic position, are recorded. The REE patterns of the volcanic rocks display light REE (LREE) enrichment with an average $(La/Yb)_n$ of 2.79 (**Figures 177A-D; Table 21**). However, numerous sampled areas have MORB-type flat REE patterns (**Figures 177A-B; Table 21**). As to be expected, the upper VDF is more evolved and has a more pronounced LREE enrichment (**Figure 177D**), averaging $(La/Yb)_n$ 4.76.

The various units of the HF also have distinct REE patterns (**Figure 178**). For example, the spherulitic dacite unit, the base of the HF, has enriched REE values (up to

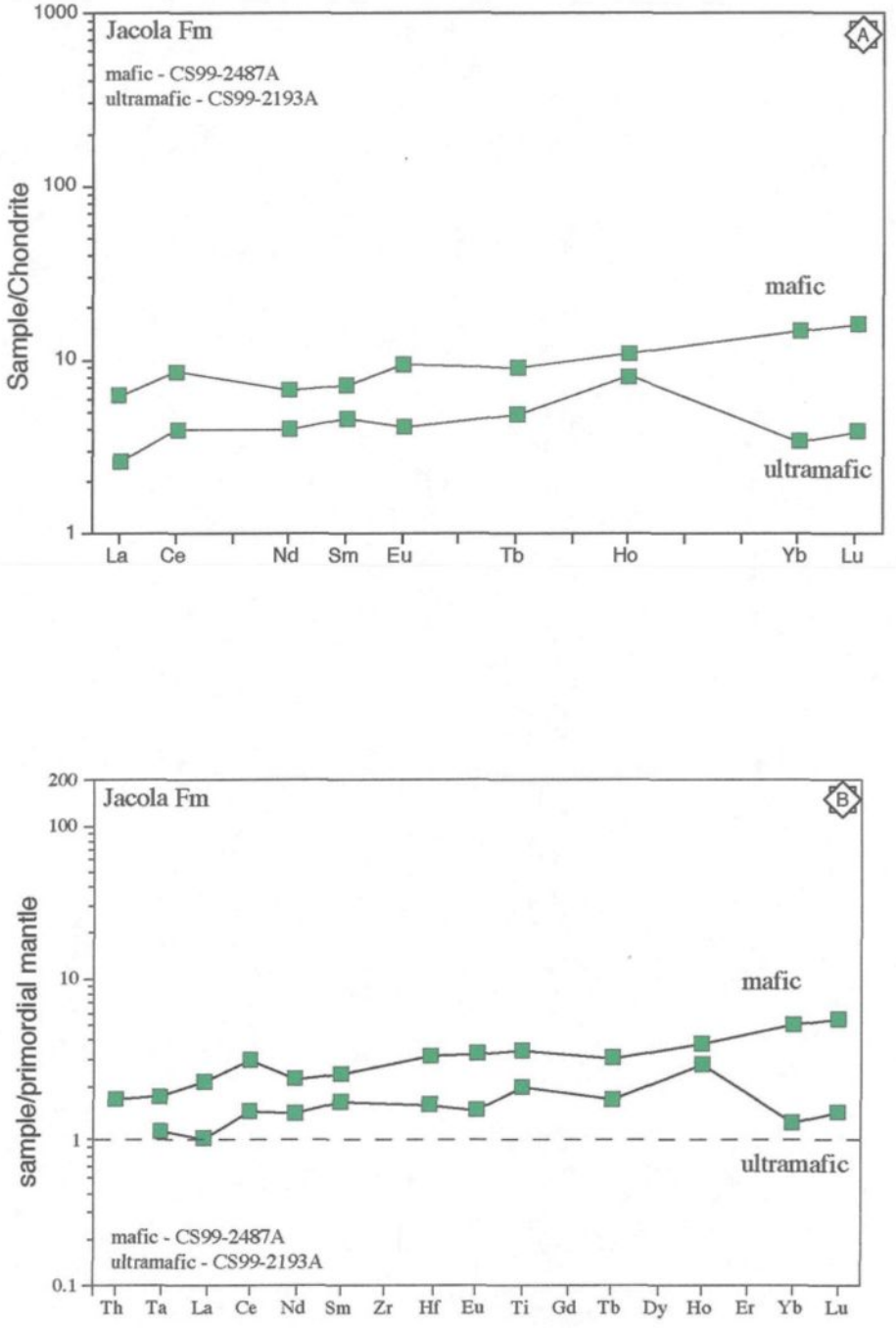

Figure 176. Rare earth element (A) and multi-element (B) diagrams for the Jacola Formation. REE are chondrite normalized and trace elements are primordial mantle normalized. Normalization values taken from McDonough and Sun (1995).

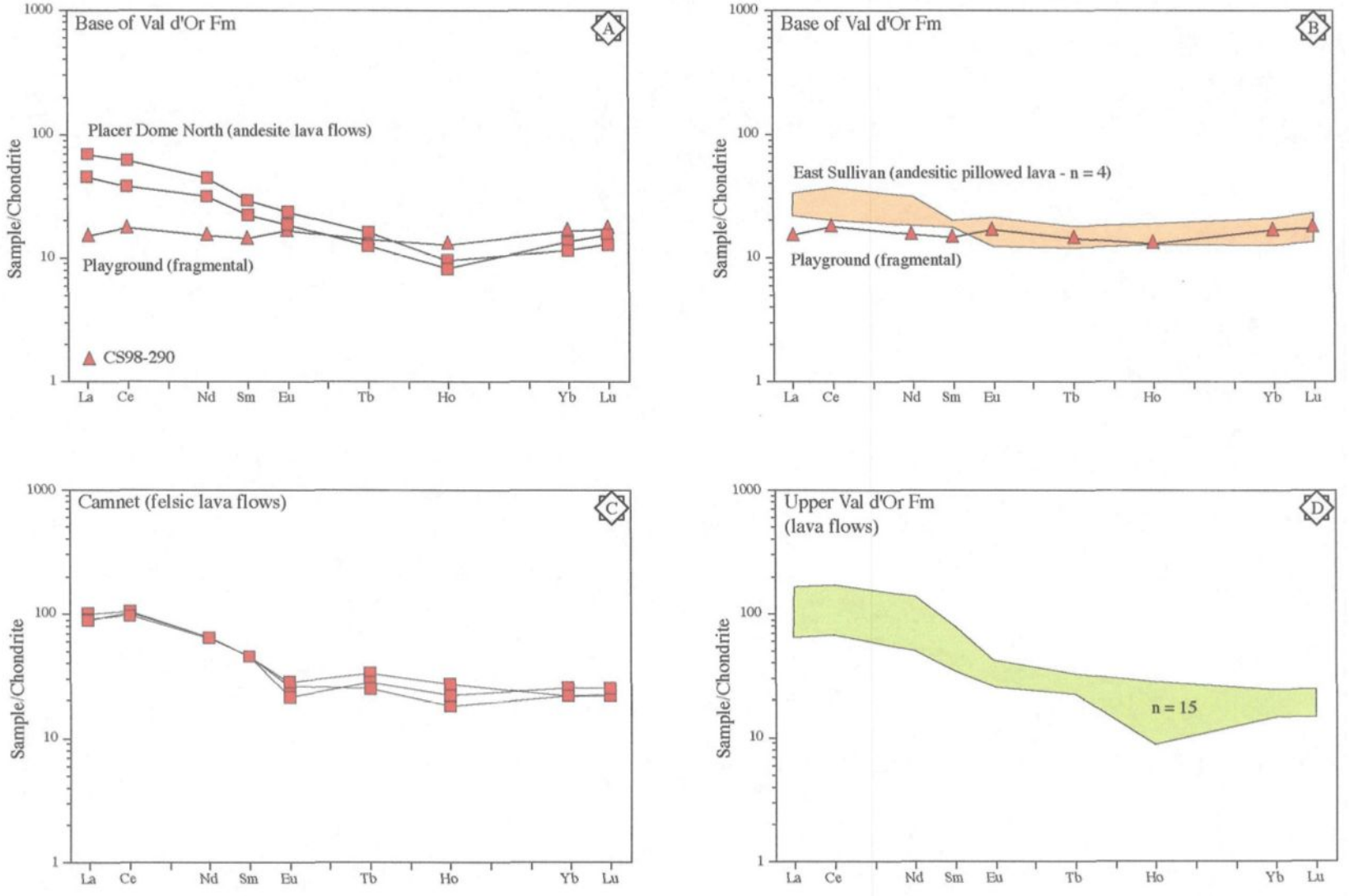

Figure 177. Chondrite-normalized rare earth element (REE) plots for different regions within the Val d'Or Formation. Normalization values taken from McDonough and Sun (1995). Comparison between (A) basal outcrops; playground and Placer Dome North; (B) East Sullivan and playground; (C) Camnet (Lower VDF); and (D) upper VDF.

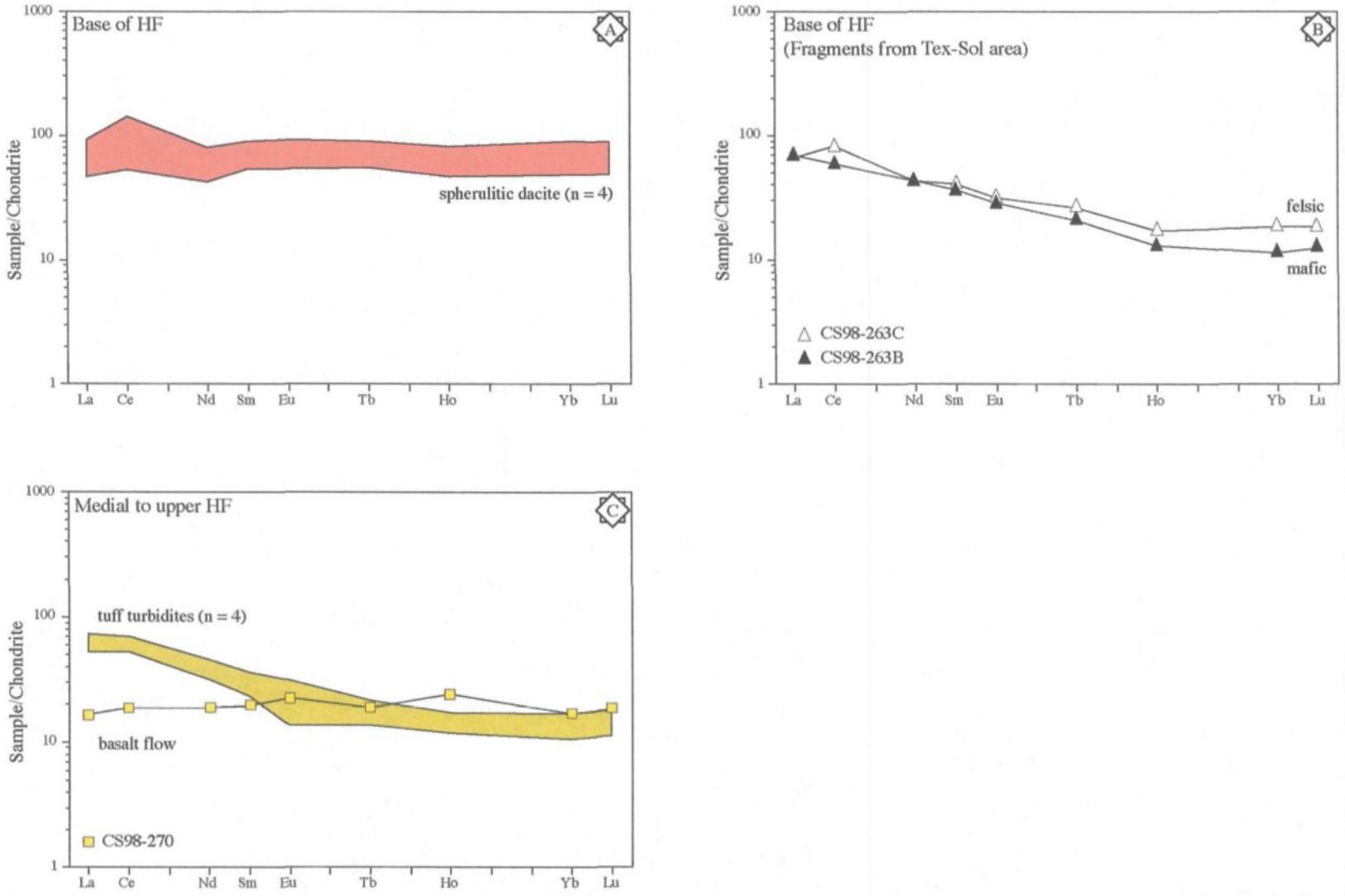

Figure 178. Chondrite-normalized rare earth element (REE) plots for different regions within the Héva Formation. Normalization values taken from McDonough and Sun (1995). A. Spherulitic dacite facies; B. Felsic (open triangle) and mafic (closed triangle) fragments from Tex-Sol area; and C. Tuff turbidites (yellow) facies and basalt lava flow (square).

100X chondrite), but a flat REE profile (**Figure 178A**) with an average $(La/Yb)_n$ of 1 (Table 21) that is typical of tholeiitic rhyolites fractionated from mafic tholeiitic magmas (Hollings et al., 1999). The HF mafic volcanic rocks have a flat REE profile (**Figure 178C**) with an average $(La/Yb)_n$ of 0.94 (Table 21), that is comparable to N-MORB (see pg. 139, Wilson, 1989). In contrast, the mafic and felsic fragments sampled from the Tex-Sol volcaniclastic deposits have strongly fractionated REE profiles (**Figure 178B**) with $(La/Yb)_n$ values of 6.17 and 3.59, respectively (Table 21), and similar REE patterns for HF tuff turbidites are recorded (**Figure 178C**). Such trends are analogous to those from the upper VDF (**Figures 177D and 178B**). These beds have fractionated REE profiles (**Figure 178C**) with an average $(La/Yb)_n$ of 3.5 (Table 21).

Trace elements displayed in multi-element diagrams represent another efficient method in identifying magma lineage and principal characteristics. Lavas of the JF are characterized by a flat profile when normalized to primordial mantle, whereby ultramafic lavas are slightly depleted in comparison to Mg-rich lavas (**Figure 176B**). The VDF volcanic rocks exhibit a negative Ta anomaly (**Figure 179**), with the base geochemically less evolved (**Figures 179A/B**) as compared to the felsic lavas of the Camnet area and those from the upper VDF (**Figure 179C/D**). They are also characterized by slight to strong negative Ti anomalies. (**Figures 179C/D**).

The multi-element diagrams of HF units, which cap the VDF, display numerous trends. The spherulitic dacite unit has a relatively flat profile at 4-30X primordial mantle and a conspicuous negative Ti anomaly (**Figure 180A**). Similarly, mafic lava flows and gabbroic sills/dykes have relatively flat profiles, but are not as enriched, with values of only

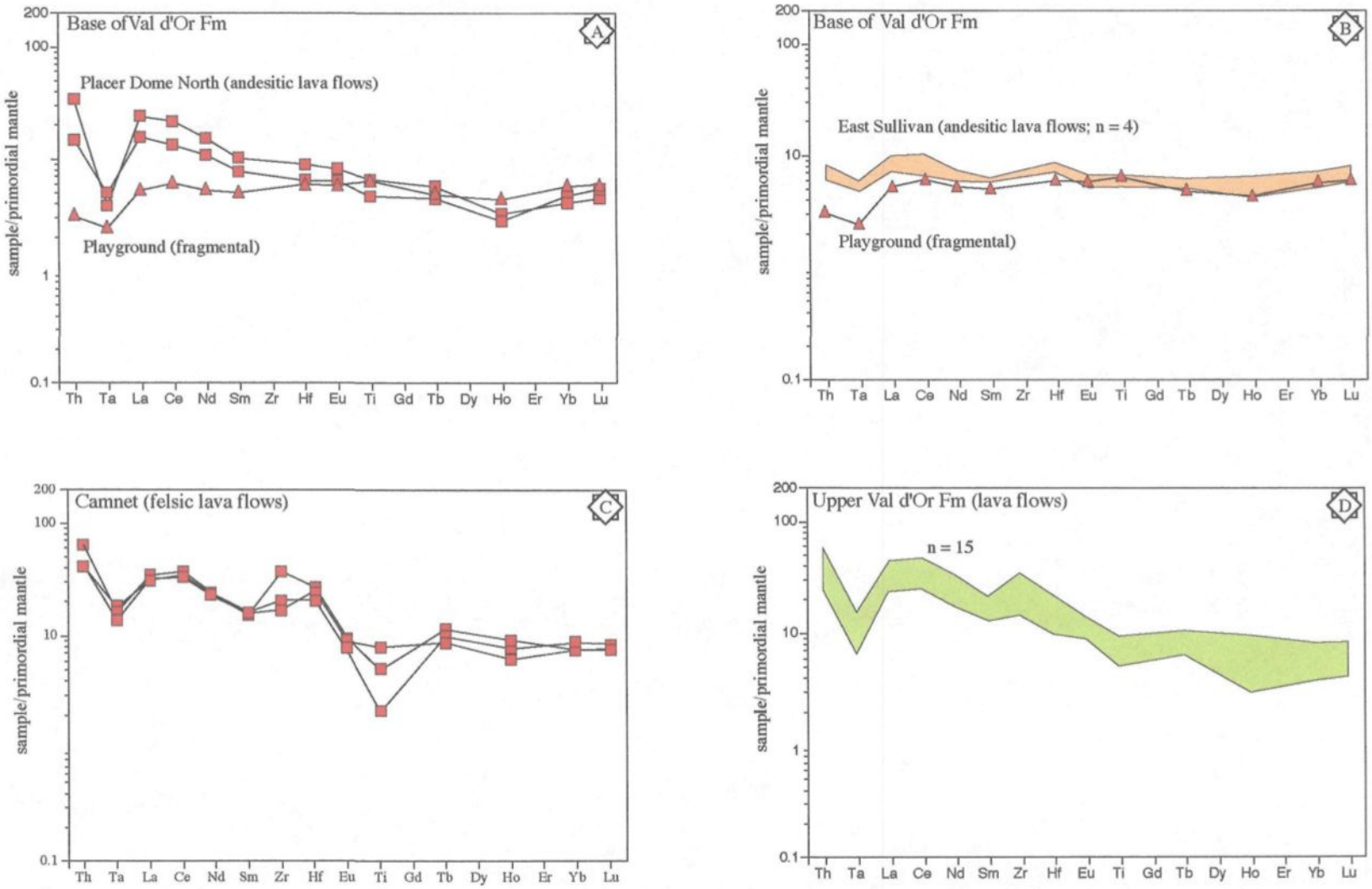

Figure 179. Multi-element diagrams of selected trace elements from the VDF normalized to primordial mantle. Normalization values taken from McDonough and Sun (1995). Comparison between (A) playground and Placer Dome North; (B) East Sullivan and playground; (C) Camnet (lower VDF); and (D) upper VDF.

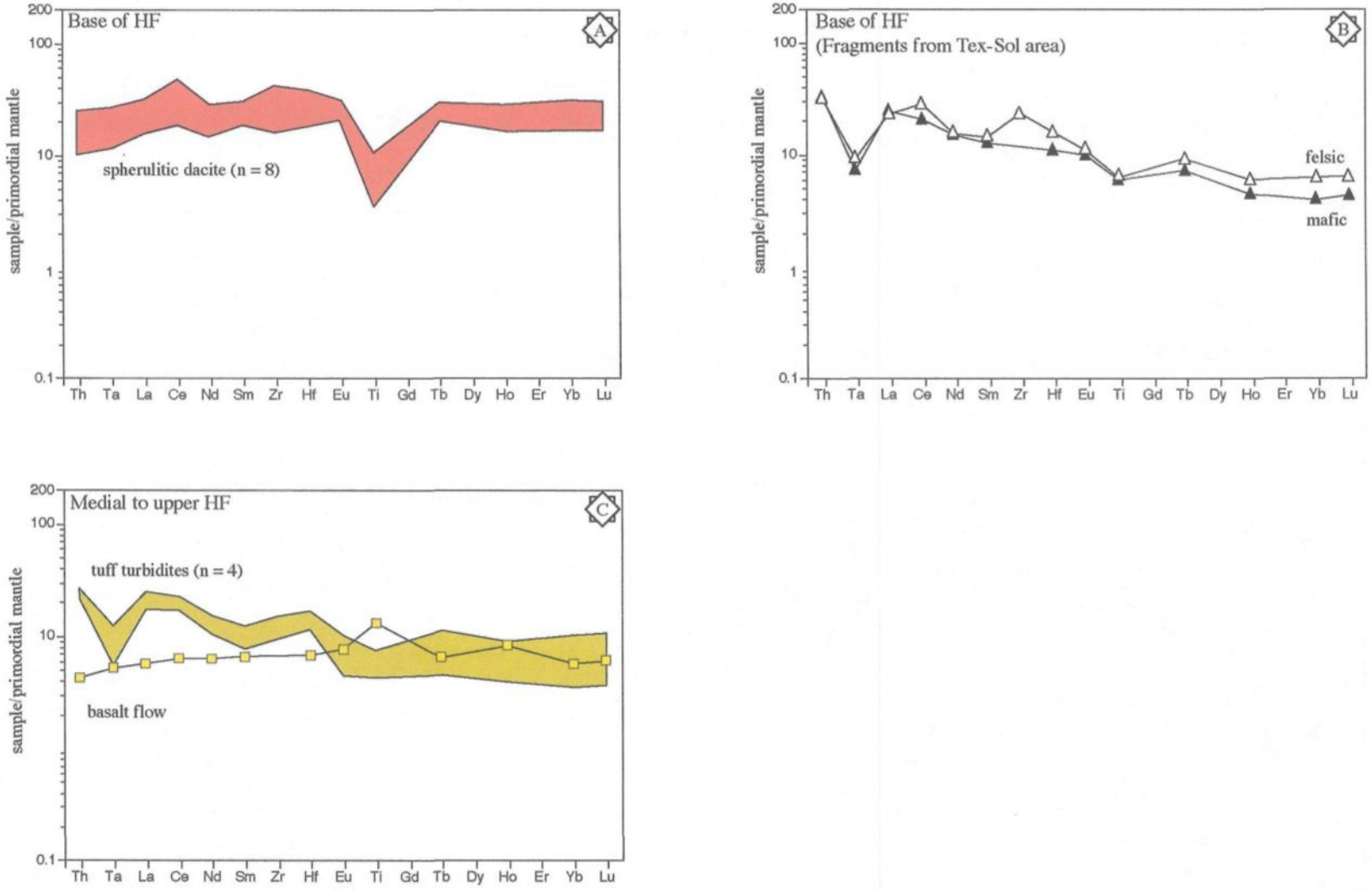

Figure 180. Multi-element plots of selected trace elements for different regions within the Héva Formation. Normalization values taken from McDonough and Sun (1995). A. Spherulitic dacite facies; B. Felsic and mafic fragments from Tex-Sol area; and C. Tuff turbidite (yellow) facies and basalt lava flow (square).

4-10X primordial mantle (**Figure 180C**). In contrast, fragments from Tex-Sol tuff breccia are characterized by prominent negative Ta anomalies and slight enrichment of the more incompatible elements (i.e., Th, La, and Ce; **Figure 180B**), favoring a direct comparison with VDF units (see **Figure 179D**), as do the tuff turbidite deposits (**Figure 180C**).

6.4.1 *Discussion of REE and Multi-element diagrams*

Multi-element and REE diagrams for the JF have relatively flat profiles that are probably related to the primitive nature of Mg-rich basaltic and komatiitic lavas (**Figure 176**). In addition, the near unity profiles for trace elements normalized (**Figure 176B**) to primordial mantle points to a possible mantle plume source. Overall, the basaltic rocks are similar to N-MORB, whereas the ultramafic rocks are considered depleted komatiites based on Al_2O_3/TiO_2 ratios of around 14 (Table 21; Champagne et al., 2002). Their REE and multi-element profiles are also very similar to the depleted Tisdale komatiites described by Fan and Kerrich (1997), with slight convex-up REE pattern (**Figure 176A**) and relatively flat multi-element trend (**Figure 176**). The low CaO/Al_2O_3 (avg. (n=13) = 1.25) ratio is similar to their values, which they suggested was due to secondary depletion of Ca (Fan and Kerrich, 1997). Fan and Kerrich (1997) interpreted these patterns and ratios as either garnet retention or fractionation within a mantle plume.

Rare earth and trace element data from the lower VDF have two distinct trends: (1) relatively flat; and (2) LREE/incompatible element enriched (**Figures 177 and 179**). The playground and East Sullivan regions have relatively flat trends comparable to the underlying Mg-rich basalts of the JF, which suggests a possible influence of a mantle

plume source. Nevertheless, these same rocks have a weak negative Ta anomaly (**Figure 179**) suggestive of an arc signature (Pearce and Peate, 1995; Pearce, 1996). Therefore this "influence" may be an artifact or partial contamination due to their temporal and spatial evolution within the overall stratigraphy as the lower VDF is contemporaneous with the JF. The complexity of the plumbing system of this proto-arc is demonstrated by the enriched LREE rocks from Placer Dome North (PDN), which are interstratified between these former regions (**Figures 177A/B and 179A/B**), thus these deposits probably originated from different source vents/magma chambers. The PDN volcanic rocks have a strong Ta anomaly (**Figure 179A**) characteristic of arc-related volcanism (Pearce and Peate, 1995; Pearce, 1996). Further to the east, the felsic volcanics within the Camnet area have similar enriched LREE profiles and strong negative Ta anomalies (**Figures 177C and 179C**), which may be a function of the distance from the complex western contact between the Jacola and Val d'Or formations (see **Figure 136**) The upper VDF is characterized by LREE/incompatible element enriched trends and prominent negative Ta anomalies (**Figures 177D and 179D**). This up section evolution probably records the maturation of the arc system (Wilson, 1989). As the arc sequence gets thicker, the possible influence of the underlying mantle-related JF becomes less and less. It is also possible that the mantle plume is beginning to breakup or destabilize (Daigneault, unpublished data).

The HF has various trends on both REE and multi-element diagrams that can be divided based on mapped lithofacies (**Figures 177 and 179**). The flat enriched REE and multi-element profiles of the tholeiitic spherulitic dacite unit defines the base of the HF (**Figures 176A and 178A**). The enriched profiles imply an enriched mantle source rather

than a plume source (**Figure 178A**), as compared to the near unity profiles of the JF (**Figure 176A**). The negative Ti-anomaly for these felsic lavas might indicate a Ti-rich phase, such as titanite, remained in the source during low degrees of partial melting. Mafic rocks have similar relatively flat REE and multi-element profiles, but not as enriched therefore suggesting a similar enriched mantle source. Mafic rocks, however, have a positive Ti-anomaly (**Figure 180C**) suggestive of higher degrees of partial melting that incorporated a Ti-rich phase (i.e., titanite). A possible environment for these volcanic rocks could be a rift zone. In contrast, fragments from the Tex-Sol tuff breccia deposits that immediately overlie the spherulitic dacite unit, as well as other voluminous tuff turbidite deposits further up in the stratigraphy, have similar profiles as the upper VDF (**Figure 181**). REE profiles are LREE enriched with $(La/Yb)_n$ values between 6.17 to 3.5 as compared to an average of 4.76 for the upper VDF (**Figure 181A**). Even more conspicuous is the prominent negative Ta-anomaly for the volcaniclastic deposits within the HF (**Figure 181B**), which is suggestive of arc-related volcanism. The bimodal fragment population that forms the Tex-Sol tuff breccias probably originated from the upper VDF during secondary transport (i.e., weathering) and subsequent transport into the rifting environment. The finer-grained tuff turbidites could represent a similar process or localized explosive volcanism that tapped arc magmas.

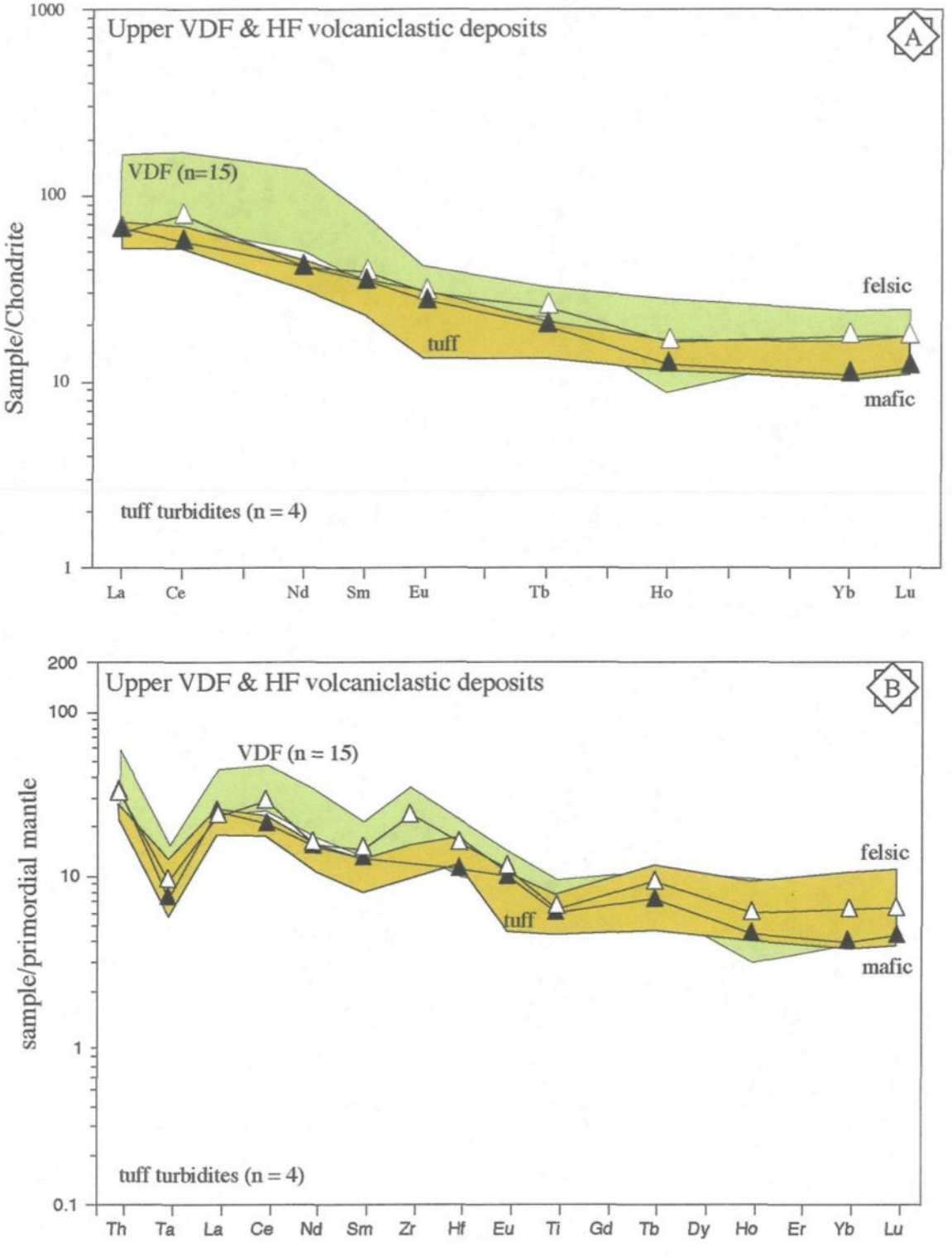

Figure 181. Comparison between upper VDF volcanic rocks and volcaniclastic deposits from the HF. A. REE profiles. B. Multi-elements profiles.

6.5 Discrimination Diagrams

The trace element geochemistry used to delineate tectonic settings is based on the concept that element variability may be controlled by its tectonic setting (Rollison, 1993). However, such discrimination diagrams should not be used as unequivocal proof of a tectonic environment, but rather as an affiliation (Rollinson, 1993). Most discrimination diagrams for igneous rocks are only useful for basaltic compositions, but the Th-Hf-Ta ternary diagram proposed by Wood (1980) can also be applied to intermediate and silicic volcanic rocks. The application of immobile high field strength elements precludes most alteration processes, including hydrothermal, seafloor alteration and low to medium metamorphic grades (cf. Rollison, 1993). This diagram identifies different MORB types, as well as making a distinction between tholeiitic and calc-alkaline volcanic arcs by a Hf/Ta tie line, whereby ratios greater than 3 are considered tholeiitic (**Figure 182**).

The singular Jacola Formation analysis plots along the edge of the N-MORB field, indicating its primitive nature (**Figure 182A**). Analyses from the VDF all plot within the volcanic arc field, but on both sides of the Hf/Ta tie line (**Figure 182A**), indicating possible tholeiitic and calc-alkaline magmatic series. Both the playground and East Sullivan samples have Hf/Ta values > 3, suggesting a tholeiitic affinity, whereas those from PDN, Camnet and upper VDF are possibly calc-alkaline rocks (**Figure 182A**). Samples from the overlying HF range from N-MORB to calc-alkaline volcanics. Both the spherulitic dacite unit and mafic rocks plot as N-MORB, with the latter stretching into the tholeiitic volcanic arc field (**Figure 182B**). However, the Tex-Sol fragments and tuff turbidite deposits all plot

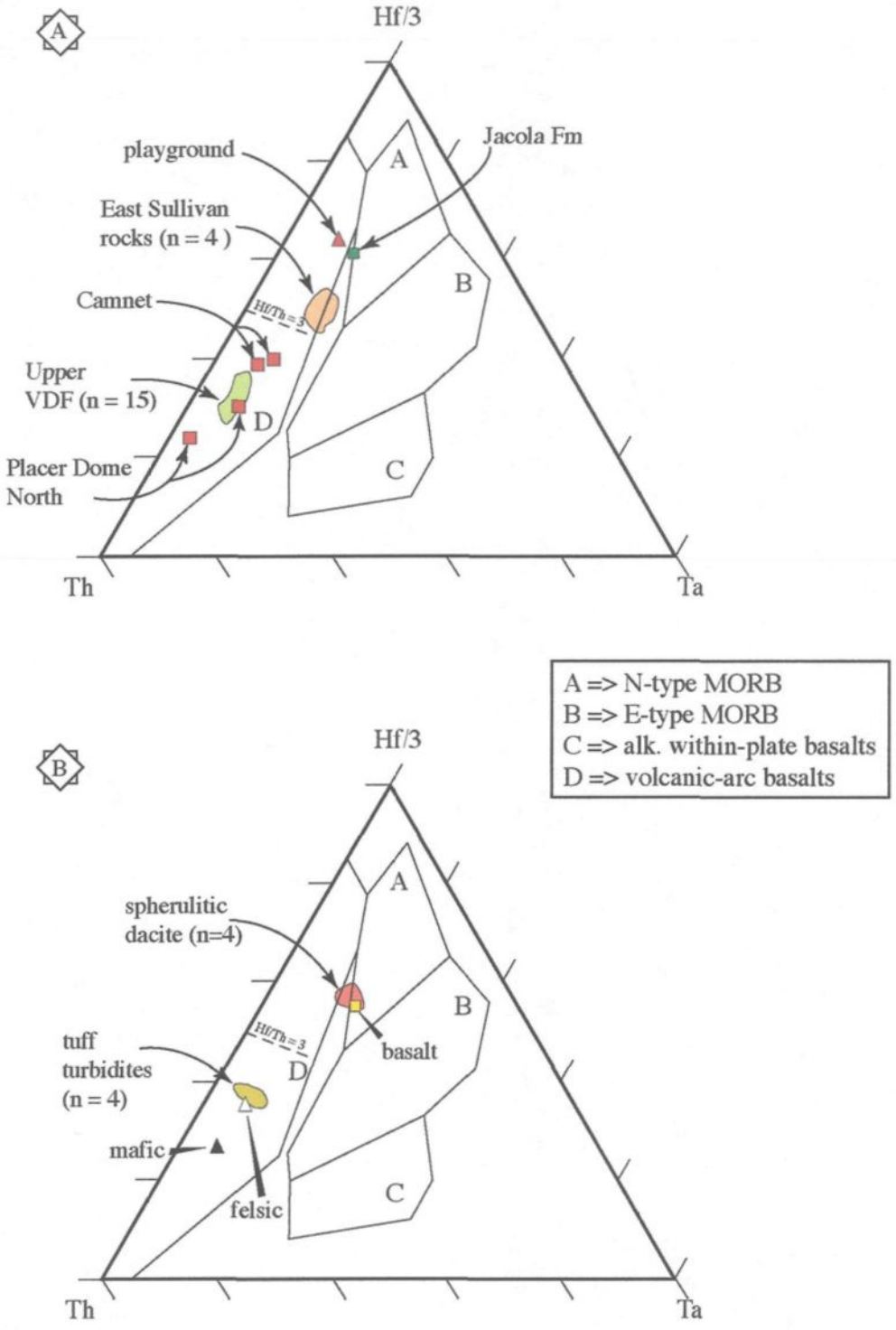

Figure 182. Th-Hf-Ta tectonomagmatic discrimination diagrams (after Wood, 1980). The Hf/Th = 3 divides the volcanic arc field into tholeiitic (Hf/Th< 3; upper) and calc-alkaline (Hf/Th > 3; lower) fields. A. Discrimination diagrams for the Jacola and Val d'Or formations. B. Discrimination diagrams for the Héva Formation.

within the calc-alkaline volcanic arc field (**Figure 182B**), which is the same as deposits from the underlying VDF (**Figure 182A**).

6.4 Geochronology

Geochronological support was provided by past U-Pb dating and an ongoing age dating program by the Québec government. The Jacola Formation was recently dated at 2703.8 ± 1.3 Ma (Pilote et al., 1999), which overlaps with the base of the Val d'Or formation, dated at 2704 ± 2 Ma (Scott et al., 2002). The overlying Héva Formation has an age of 2702 ± 2 Ma. Other age relationships in the region include an age of 2699.8 ± 1.0 Ma (Wong et al., 1991) for the Bourlamaque Pluton, suggesting that it may serve as the main sub-volcanic magma chamber for the Val d'Or Formation.

CHAPTER 7

DISCUSSION

The underlying theme of this work is the paleogeographic reconstruction of the Val d'Or Mining Camp based on facies mapping, which utilized aspects of physical volcanology, sedimentology, stratigraphy, and supplemented by geochemistry. A derivative benefit in modeling the geodynamic environment within an Archean greenstone belt is the assessment of whether evolution is through autochthonous (Dimroth et al., 1983; Chown et al., 1992), or allochthonous (Ludden and Hubert, 1986; Desrochers et al., 1993) tectonic processes, or a combination of both. Geotectonic modeling within the Archean is complicated by numerous assumptions of plate behavior due to the assumed higher heat flow of the early Earth. This higher heat flow raises the issue as to whether Archean plate tectonics is exactly analogous to modern concepts (e.g., Condie, 1994; Hamilton, 1993) and fuels the old debate of moblist versus stablist ideas (cf. Hamilton, 1988). Nevertheless, abundant geochemical (Capdevila et al., 1982; Wyman et al., 1999), stratigraphical (Dimroth et al., 1982), and structural (Chown et al., 1992; Daigneault et al., 2002) evidence, supported by geochronology (Mortensen, 1993), all indicate secular evolution from divergent to convergent environments for individual greenstone belts that comprise the Superior Province.

Such an evolutionary sequence was documented by Dimroth et al. (1982), whereby an extensive submarine mafic lava plain or plateau becomes conformably overlain by subaqueous and/or subaerial, subduction-related stratovolcanic centers of intermediate to

felsic composition. These volcano-sedimentary sequences are dominated by tholeiitic and komatiitic volcanism that form a submarine lava plain and capped by arc-related intermediate to felsic volcanism. The composition, stratigraphy, flow morphology, and geochemistry of this submarine plain/plateau implies a mid-ocean ridge setting derived from plume-generated magmas (Desrochers et al., 1993; Jackson et al., 1994; Thurston, 1994). In contrast, an arc setting forms a complex stratigraphy of overlapping and coalescence of multiple discrete subaqueous vents, generally measuring less than 5 km in diameter and between 400-800 m high (De Rosen-Spence, 1976; Dimroth et al., 1982). Furthermore, arc splitting or rifting can be synchronous with arc volcanism (Carey and Sigurdsson, 1984; Orton, 1996).

7.1 Subaqueous Volcanism

The prominence of interstratified pillowed sequences throughout the study area affirms a subaqueous environment of deposition. Furthermore, the lack of background sedimentation, such as sandstones and argillites, along with the absence of wave induced structures suggest not only continuous volcanic activity, but deposition at water depths greater than 200 m. Given such an environment, it is necessary to consider the physical properties of water (e.g., density) and the hydrostatic pressures generated by the overlying water column (1 bar = 10 m), which dramatically affect fragmentation, transportation, and deposition of pyroclastic material.

Several controlling factors affecting volcanic fragmentation are magma chemistry, vent geometry, and volatile content of the magma. Of these factors, it is the volatile content, in particular volatile exsolution, which is largely influenced by the hydrostatic pressure. While volatile exsolution decreases with depth, deep-sea submersible studies have documented highly vesiculated fragments at depths in excess of 1800 m (Gill et al., 1990; Eissen et al., 2003) and even below critical depths (Clague, 2003). Thus, hydrostatic pressure probably acts more to inhibit the rapid expansion of volatiles that lead to explosive fragmentation (Kano, 1996), with the lower limit defined as the volatile fragmentation depth (VFD; Fisher and Schmincke 1984; p. 265). Consequently, any lava erupted below the VFD can vesiculate, but explosive disruption is suppressed (Kano, 1996). This situation probably explains the deposition of subrounded, breccia-sized pumiceous fragments (see **Figure 55B**) within the VDF, since such high degrees of volatile exsolution typically result in explosive eruptions producing finer grained fragments. In addition, larger fragments can retain heat more effectively, thereby forming a self-generating steam cupola that insulates the fragment from the cooling effects of water (White, 2000), thereby preserving their subrounded morphology.

A subaqueous milieu modifies the mechanics of explosive pyroclastic-forming eruptions as the inevitable ingestion of water into the expanding eruption column and/or the subsequent pyroclastic flow, transforms the support mechanism and temperature of ensuing sedimentary gravity flows. Further complicating this is the absence of documented subaqueous explosive eruptions. Only near-surface events have been observed (Surtsey, Iceland – cf. Kokelaar, 1983 and references therein), which cannot emulate deep-water

events. Water-supported pyroclastic flows exhibit graded and stratified beds and are well sorted due to effective hydraulic sorting related to the viscosity of water being two orders of magnitude greater than that of air (Stix, 1991).

7.2 Geochemical and Geochronological Support

Geochemical and geochronological data provide crucial support for the interpretation of the geodynamic environment (**see Table 22**). Major element geochemistry illustrates general compositional trends, whereas multi-element diagrams, depicting the characteristics of incompatible elements for the various formations, provide invaluable information on inter- and intra-formational variations related to the possible evolution of the study area. Geochronology establishes the temporal link between the various formations in order to elucidate the time line for their deposition; which is necessary when reconstructing the geodynamic environment.

Examination of Zr/Y ratios demonstrates that a progressive change occurred from tholeiitic to calc-alkaline affinities between the Jacola and Val d'Or formations, with a return to tholeiitic affinity for the HF. Moreover, it is possible to subdivide the VDF into lower and upper sections based on geochemical affinity and incompatible elements (**Table 22; Figures 175B, 177, and 1789**). In addition, trace elements and REE discrimination diagrams provide information on the possible tectonic environment and their magmatic source (**Table 22**).

Table 22: Chart comparing different geochemical data for each formation, CH (chondrite) and PM (primordial mantle).

Formation	Major elements	Geochemical Affinity	REE	Trace Elements	Th-Hf-Ta	Setting
JF	Ultramafic-mafic	Tholeiitic	Weak HREE enrichment (X4 to X8, CH)	Flat, near unity trend	N-MORB	Ocean floor or plateau
VDF Playground	intermediate	Tholeiitic	Flat trend (X11 , CH)	Weak Ta-anomaly; relatively flat trend (X3 to 4, PM)	Tholeiitic arc	Proto-arc; possible contamination with JF
PDN	intermediate	Transitional	Fractionated HREE (X70 to X10, CH)	Strong Ta-anomaly Fractionated (X80 to X10, PM)	Calc-alkaline arc	Proto-arc
East Sullivan	intermediate	Tholeiitic	Flat trend, (X12, CH)	Weak Ta-anomaly; relatively flat trend (X10 to 7, PM)	Tholeiitic arc	Proto-arc; possible contamination with JF
Camnet	Intermediate – Felsic	Calc-alkaline	Fractionated HREE; (X100 to X30, CH)	Strong Ta- and moderate Ti-anomalies Fractionated (X80 to X10, PM)	Calc-alkaline arc	Proto-arc
Upper VDF	Intermediate – Felsic	Calc-alkaline	Fractionated HREE; (X 110 to X 20, CH)	Strong Ta- and weak Ti-anomalies Fractionated (X70 to X10, PM)	Calc-alkaline arc	Arc construction
HF Spherulitic dacite	Felsic	Tholeiitic	Flat (X100, CH)	Flat (X30), with strong Ti-anomaly	N-MORB	Rifting
Tex-Sol	Intermediate-felsic	Transitional – calc-alkaline	Fractionated HREE (X70 to X10, CH)	Strong Ta-anomaly; fractionated (X 40 to X5)	Calc-alkaline arc	Eroded arc
Tuffs	Felsic	Calc-alkaline	Fractionated HREE (X70 to X10)	Strong Ta-anomaly; fractionated (X 30 to X5)	Calc-alkaline arc	Arc volcanism
Lavas + gabbro	Mafic	Tholeiitic	Flat (X20, CH)	Flat (X4, PM)	N-MORB	Extension

The JF is interpreted as a subaqueous lava plain/plateau developed from fissural eruptions fed by a mantle plume. A plume source is indicated by the predominance of komatiitic and Mg-rich basaltic lavas as well as REE and trace element characteristics (**Figure 176**). This primitive nature is further supported by its N-MORB character on a Th-Hf-Ta tectonomagmatic discrimination diagram (**Figure 182A**). The renewed debate is whether komatiites themselves are evidence enough to support a mantle plume origin. One unique property of komatiites was the high temperatures considered necessary for large volumes of partial melting, however, it has been demonstrated that water can lower the melting point (Allegre et a., 1982). Furthermore, Wilson and Versfeld (1994) studied geochemical evidence from komatiites in South Africa that suggested that they were deposited in a subduction zone environment. Modern lavas compared to komatiites are boninites, a high magnesia andesitic lava (Le Maitre, 2002) that is associated with incipient extension of a volcanic island arc (Wilson, 1989). Boninites are geochemically distinct by their "V-shaped" REE patterns, negative Nb-Ta anomalies, which are characteristic of arc-related volcanism (Wilson, 1989), and enrichment of Zr and Hf relative to REE with depleted Ti (cf. Parman and Grove, in press). Parman et al. (2001) analyzed basaltic komatiites that had similar geochemical profiles to boninites and Parman and Grove (in press) outlined numerous localities, such as the Barberton komattites, in an effort to lobby for hydrous melting within a subduction zone. The ultramafic-mafic lavas analyzed (cf. Champagne et al., 2002) for the JF do not show "V-shaped" REE patterns (**Figure 176**), nor is there any coupling between Hf and Ti in regard to REE, thus they are not similar to boninite lavas. Moreover, lavas from the JF have no arc-signature, such as a negative Ta-

anomaly. The low abundances of incompatible elements, however, suggest moderate to high degrees of partial melting (Sproule et al., 2002). This, together with the high-Mg content (up to 29 wt%) and spinifex textures requires a long-term depleted mantle source (Sproule et al., 2002), therefore a mantle plume is advocated.

Volcanic rocks from the lower VDF are characterized by a tholeiitic to transitional geochemistry (**Figure 175B**) and have negative Ta anomalies and low Zr abundance relative to their neighboring elements (**Figures 179A/B**). Negative Ta (or Nb) anomalies suggest subduction-related petrogenesis (Wilson, 1989; Kerrich and Wyman, 1996; Pearce, 1996), whereas low Zr abundances may be attributed to the immature nature of these arc lavas (i.e., Camnet; Figure 182C), which also may explain the absence of a negative Ti anomaly typical of an arc-signature (Kerrich and Wyman, 1996). In addition, as the arc matures, these volcanic rocks evolve from tholeiitic to transitional geochemistry (Wilson, 1989; p. 168), becoming more enriched in trace elements (**Figures 177 and 179**).

Lavas from the upper VDF have prominent negative Ta and Ti anomalies (**Figure 179D**) characteristic of subduction-related volcanism (Kerrich and Wyman, 1996; Pearce, 1996). In comparison to the lower VDF, the enriched nature of incompatible elements along with the evolution from transitional to calc-alkaline lavas suggests increased maturity of the arc (Wilson, 1989). Observed negative trace element anomalies are probably not due to crustal contamination, as geochemical and isotopic studies of volcanic and plutonic suites within the Archean greenstone belt demonstrate that while isotopic inheritance is significant (Ayer et al., 1999), assimilation of older crust is not widespread in their petrogenesis (Bédard and Ludden, 1997; Dostal and Mueller, 1997). All these lavas plot

within the calc-alkaline volcanic arc field within the Th-Hf-Ta discrimination diagram (**Figure 182A**).

The contact between the Val d'Or and Héva formations is defined geochemically by an abrupt shift from calc-alkaline to tholeiitic affinity (**Figure 175**). Nevertheless, the Tex-Sol volcaniclastic tuff breccia deposits, which stratigraphically overlie the basal tholeiitic spherulitic dacite lava flow(s), are characterized by calc-alkaline-to-transitional fragments (**Figure 175C**) that have HREE depletion trends (**Figure 178B**) and arc-signatures (**Figures 180B and 181B**) reminiscent of lavas from the VDF (see **Figure 181B**). This association suggests a coeval and spatial relationship between these formations, which is considered here to be *conformable* in nature. This is further supported by localized intercalated calc-alkaline (**Figure 175C**) felsic tuff beds that have fractionated HREE patterns (**Figure 178C**) and negative Ta anomalies (**Figure 180C**) analogous to the VDF, implying possible contemporaneous deposition from small volume eruptions of Val d'Or-related arc-volcanism (see **Figure 170**) juxtaposed to the HF. Such contemporaneous back-arc rifting and continued arc-volcanism is probably common in active regions (Carey and Sigurdsson, 1984; Orton, 1996). Incompatible element diagrams show that lavas from the HF probably originated from a slightly enriched MORB-like source (**Figures 178A-C and 180A-C**), which supports an arc-rifting interpretation. These lavas plot within the N-MORB field of Woods (1980) Th-Hf-Ta discrimination diagram, approaching E-MORB (**Figure 182B**). These geochemical characteristics are summarized in Table 22 and related to a possible magma source.

The apparent age overlap between the JF (2703.8 ± 1.3 Ma; Pilote et al., 1999) and the base of the VDF (2704 ± 2 Ma; Scott et al., 2002) suggests nearly contemporaneous volcanism between these formations. This interpretation is supported by the geochemical characteristics of volcanic rocks from the base of the VDF, which have a conspicuous tholeiitic-transitional-tholeiitic pattern between the playground-Placer Dome North - East Sullivan regions, respectively. This association is repeated on REE (**Figures 177A/B**) and multi-element (**Figures 179A/B**) diagrams. The tholeiitic deposits are similar to lavas from the JF, but Ta anomalies (**Figures 179A/B**) and Th-Hf-Ta discrimination diagrams (**Figure 182A**) imply subduction-related processes were dominant. Thus, these particular deposits were probably contaminated and/or mixed with mantle-derived rocks from the JF, which indicate a *temporal* and probably a *conformable* relationship between these formations. The age of the HF (2702 ± 2 Ma; Scott et al., 2002) and the apparent interstratified, erosional Tex-Sol deposits, composed of fragments originating from the VDF, imply a depositional continuum rather than a structural relationship.

The synvolcanic 2699.8 ± 1.0 Ma (Wong et al., 1991) Bourlamaque Pluton was probably the principal subvolcanic magma chamber that had numerous fractures that resulted in the construction of numerous small volcanic vents, which formed a large central volcanic complex. Volcanic complexes, such as in the Lesser Antilles or Izu-Bonin Arc, typically form chains of subaqueous vents or islands separated by 20-50 km (Dimroth et al., 1982; Riggs and Busby-Spera, 1990; Fiske et al., 1998).

7.3 Paleogeographic Reconstruction

Paleogeographic reconstruction of this complex region is based on several methods, which include detailed and regional mapping, along with supportive geochemistry and geochronology, which enable the construction of formation-wide stratigraphic sections (**Figure 183**). Stratigraphic correlation illustrates the complexity of the volcano-sedimentary stratigraphy within the various formations. The JF is characterized by thin, laterally extensive massive to pillowed basalts with subordinate intercalations of fragmental facies (**Figure 183B**). The southern HF has morphologically similar thin, extensive basaltic lavas, but with some interstratified andesitic lavas, as well as gabbroic sills and dykes (**Figure 183B**). Fragmental material is locally abundant and typically more felsic in composition (**Figure 183B**). In contrast, the VDF has complex intercalations of andesitic to rhyolitic lavas and associated interbedded fragmental lithofacies. These volcano-sedimentary flow sequences typically form small-volume deposits that are laterally restricted, with flow lengths on the order of 6-8 km, which commonly overlap or terminate with adjacent flow sequences (**Figure 183B**). These interstratified and/or discontinuous flow sequences possibly represent small isolated volcanic centers; eight such centers are identified, with seven located in the VDF and one in the HF (**Figure 183B**).

All the physical attributes of mappable lithofacies, together with supporting geochemistry and geochronology, are relevant to a specific geotectonic setting for each formation (**Tables 22 and 23**). Moreover, there is a temporal evolution for these formations that commences with a proto-arc stage and ending with arc rifting; such that these

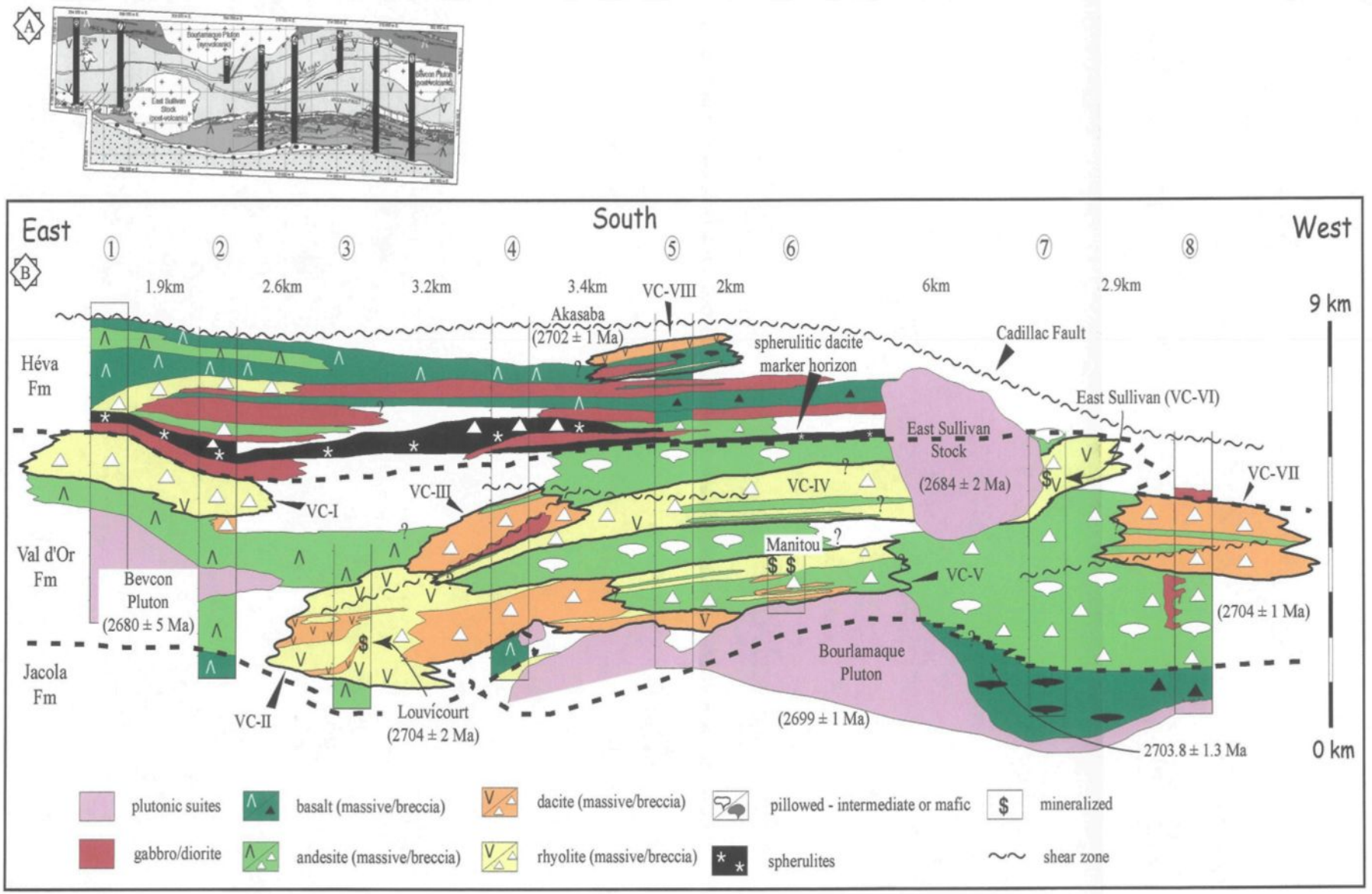

Figure 183. Simplified geology defined by regional stratigraphic columns. A. Locations of eight contructed stratigphic columns through the Jacola, Val d'Or and Héva formations. B. Detailed stratigraphic columns depicting the vertical and lateral variations in the various formations, along with presumed contacts. Eight possible volcanic centers are identified; VC-I - Sleepy Lake; VC-II - Louvicourt; VC-III - Relais; VC-IV - Columbiere; VC-V - Manitou; VC-VI - East Sullivan; VC-VII - Lamaque; and VC-VIII - Akasaba.

Table 23. Volcanic characteristics of the Jacola (JF), Val d'Or (VDF) and Héva (HF) formations (fm) related to possible geotectonic setting.

Fm	Morphology	Thickness	Length	Composition	Affinity	Setting
JF	Massive to pillowed lavas	1-200 m	> 5 km	Komatiite – basalt	Tholeiitic	Fissural – Plume?
VDF base	Massive to pillowed lavas	10 cm – 100 m	2 – 5 km	Andesite – dacite – rhyolite	Tholeiitic – transitional	Vents – Proto-Arc
top	Abundant volcaniclastic	5 cm – 100 m			Transitional - calc-alkaline	Vents – Arc
HF	Massive to pillowed lavas	5 cm – 400 m	> 5 km	Dacite – basalt	Tholeiitic	Fissural – Rifting?

formations define the evolution of a subaqueous arc, hereafter called the Val d'Or Arc. The Val d'Or Arc is restricted to the eastern segment of the SVZ and is concerned with a single complex system that extends for approximately 30 km along strike with a maximum thickness of 9 km thick, which is analogous to modern day volcanic islands within a larger subduction zone (i.e., Lesser Antilles). Field relationships, geochemistry, and geochronology also suggest that this segment of the SVZ is monoclinal, whereby the Val d'Or Arc evolved from the JF southward to the HF in three stages from arc inception and construction, to final rifting over 1-4 my.

The initial arc inception stage records a change in the geotectonic environment from plume- to arc-related volcanism, represented by the JF and the lower VDF, respectively. Observed komatiitic volcanic rocks, characterized by HREE enrichment patterns (**Figure 176A**), within the JF suggest high degrees of partial melting at mantle depths probably originating from a mantle plume source (Campbell and Griffiths, 1990; Barnes et al., 1995; Arndt et al., 1997). Massive flows, lack of interflow sedimentary units, and low relief of paleovolcanic slopes are the typical flow architecture and edifice style consistent with high eruptive rates (Griffiths and Fink, 1992), associated with ultramafic eruptions (Storey et al., 1991). These voluminous eruptions result from extensional processes and formed a subaqueous lava plain analogous to a mid-ocean ridge (**Figures 184A/B**). Meanwhile, concurrent subduction to the south (**Figure 184A**), during the *proto-arc* phase, is manifested by the appearance of low-Ti tholeiitic basalts (Wyman, 1999) interstratified with ultramafic lava flows. Moreover, contemporaneous plume-arc volcanism is supported by an apparent age and stratigraphic overlap (**Figures 183 and 184A**). Transitional

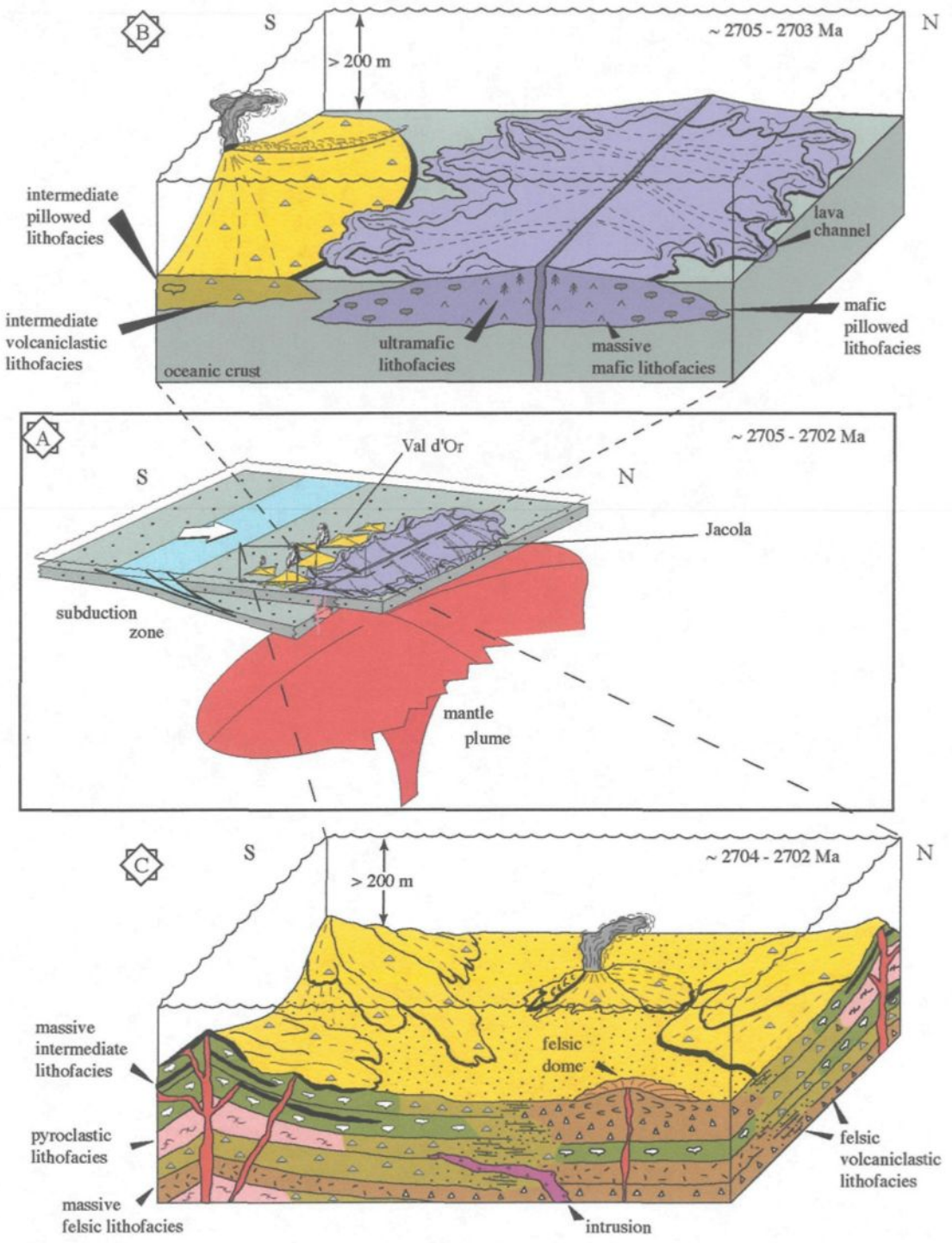

Figure 184. Series of 3-D diagrams illustrating the different stages in the geologic evolution of the Val d'Or Arc. Modified from unpublished data of Daigneault (2002). A. Three-dimensional representation depicting the temporal and spatial relationship between mantle plume- and arc-related volcanism of the Jacola and Val d'Or formations, respectively.B. Closeup 3-D diagram of plume-arc interaction between 2705-2703 Ma, during arc inception. C. Closeup 3-D diagram illustrating the arc construction phase of the Val d'Or Formation. Construction is characterized by interstratified and overlapping volcanic facies originating from small, isolated volcanic vents formed between 2704-2702 Ma.

intermediate to felsic volcanic and volcaniclastic rocks of the lower VDF signal the beginning of arc construction; however basal deposits and those from East Sullivan have flat trace element and REE profiles similar to plume-related lavas, but are characterized by negative Ta-anomalies (**Figure 179B**). Thus, these deposits probably record possible contamination from mantle-derived magmas, but originate from subduction-related processes. Plume-arc interaction is envisaged to result where voluminous eruptions of low viscosity komatiites intercalate with proto-arc deposits during possible subduction zone step-back (Wyman, 1999), in this case from an earlier subduction zone to the north (Daigneault et al., 2002). The Tonga arc is a modern day example of plume-related volcanism being located only 50 km from an active subduction zone, such that low viscosity lavas could flow into an arc setting (Wyman, 1999).

The second stage involved continued arc construction with the formation of numerous, small isolated volcanic edifices (**Figures 184A-C**). The complex, interstratified and overlapping nature of discontinuous subaqueous lavas and volcaniclastic flows suggest contemporaneous eruptions from numerous volcanic vents within an intra-arc basin (Carey, 2000) or the construction of a multi-vent volcanic complex (Riggs and Busby-Spera, 1990). These small volcanic vents are delineated by laterally restricted volcanic and volcaniclastic flows that outline vents that are 2-5 km in diameter and become juxtaposed with neighboring vents or coalesce to form a composite volcano (cf. Riggs and Busby-Spera, 1990; de Rosen-Spence, 1976). Such central volcanic complexes (cf. Dimroth et al., 1982) are typical of oceanic arcs. The presence of pillowed flows throughout the formation

(**Figure 183**) and lack of shallow water primary structures suggests that these vents remained submerged below water-base (> 200 m).

The final stage records extension within the arc that resulted in subaqueous effusive eruptions of voluminous tholeiitic lavas of the HF, which flood the calc-alkaline volcanic deposits of the underlying VDF (**Figures 184D/E**). The extensive nature and dominance of mafic volcanic and intrusive rocks are particular to an extensional environment, whereby volcanic activity is focused along km-scale fissures or deep-seated fractures (Wharton et al., 1995); in this case, rifting of an active arc (VDF). It is during this stage that the mantle plume may have become removed from the plumbing system (**Figure 184D**). Sproule et al. (2002) envisaged several such scenarios, one in which the plate may have moved off the plume source or the subducting slab interacted with the plume, effectively stalling it. Subduction step-back or forearc rifting could cause plate motion away from the plume source. Arc rifting is accompanied by increased levels of erosion (Carey, 2000; Clift and Party, 1995) of volcanic and volcaniclastic rocks, which can transport and deposit reworked volcanic debris originating from the underlying VDF. This may explain the mafic-felsic fragment populations within the Tex-Sol tuff breccia deposits, which have subduction-related geochemical signatures (**Figure 180B**). Localized felsic lapilli tuff to tuff beds intercalated with mafic lavas probably represent a small isolated volcanic vent(s) that may have overcome hydrostatic pressure to disintegrate explosively due to shoaling. Their calc-alkaline nature and subduction-related geochemical trends indicate that these flows probably originated from the VDF, which further supports a temporal and spatial relationship between these formations.

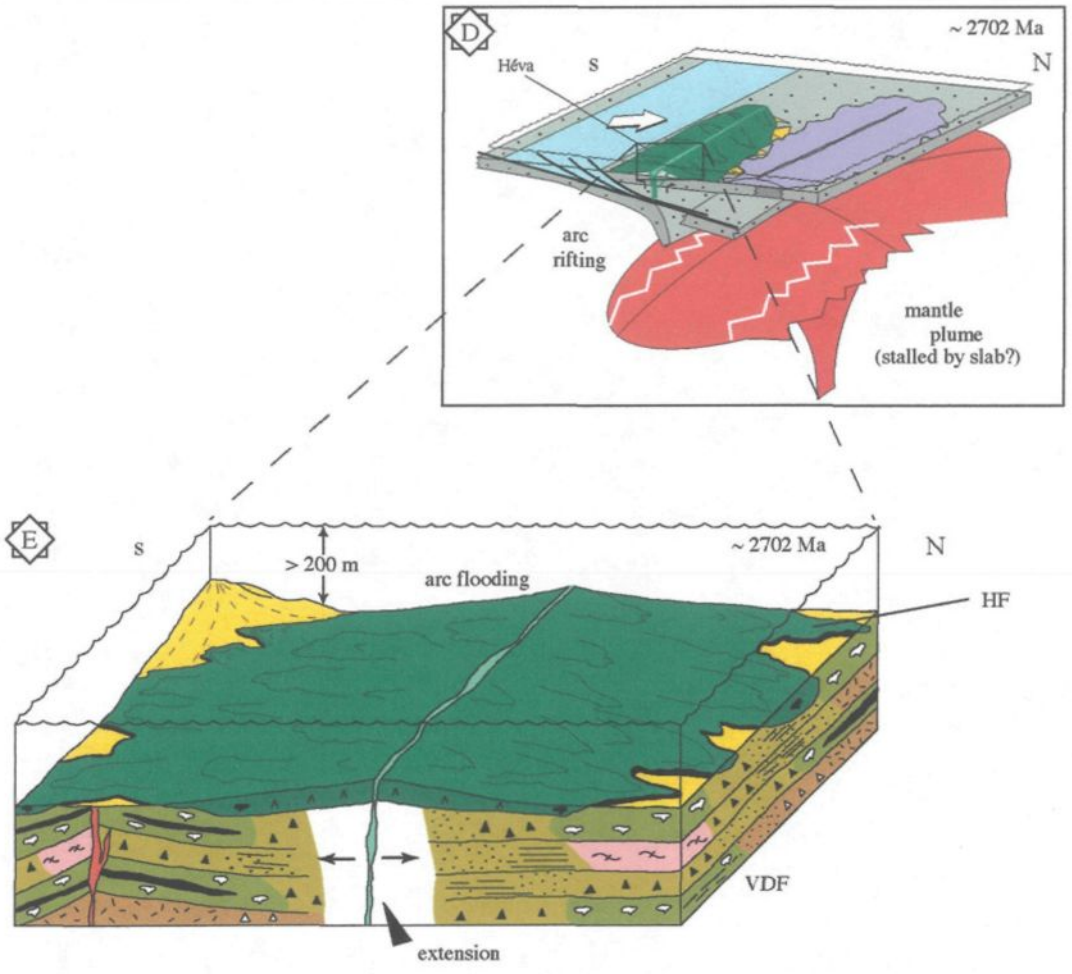

Figure 184 (con't). D. 3-D representation of arc-rifting. The mantle plume is probably being impinged or stalled as it interacts with the subducting slab. Lava of the Héva Formation floods the volcanic arc deposits of the Val d'Or Formation. Modified from unpublished work of Daigneault (2002). E. Closeup of 3-D diagram of arc-rifting as extension-related processes generatae extensive lavas that flood the arc at approximately 2702 Ma.

Structural over-thickening of the Val d'Or Arc is not indicated, particularly within the HF, which is underlain by the extensive spherulitic dacite unit (**Figure 183**). Reviewing the past composite interpretative columns for the Malartic Block, it is now possible to recognize a new geologic group within the Malartic Block, based on tectonic settings (**Figure 185**). The Malartic Group represents an oceanic floor formed from mantle-plume related volcanism, which is dominated by ultramafic-mafic effusive lavas. The JF is included with this group (**Figure 185**). The new *Louvicourt Group* represents the volcanic arc phase, which includes the Val d'Or and Héva formations, from arc construction to rifting, respectively (**Figure 184**).

7.4 VMS Deposition

The VMS deposits in the VDF are associated with felsic volcanic rocks and the locations of mineralization exhibit a westward shift from the Louivcourt to the East Sullivan mine as well as a shift up-section (**Figure 183**). This lateral and up section shift may represent a series of en-echelon faults, commonly developed in arc environments, which formed one stratigraphic horizon that is preferentially mineralized within the VDF, or simply two distinct mineralized horizons. En echelon faults may act as conduits that focus the hydrothermal fluids necessary to promote base metal precipitation during fluid discharge on the seafloor (Smith et al., 1990; Iizasa et al., 1999). The Louvicourt, Manitou, East Sullivan, and Akasaba mines are known deposits that probably represent zones of former hydrothermal discharge on the seafloor associated with felsic volcanism (**Figure**

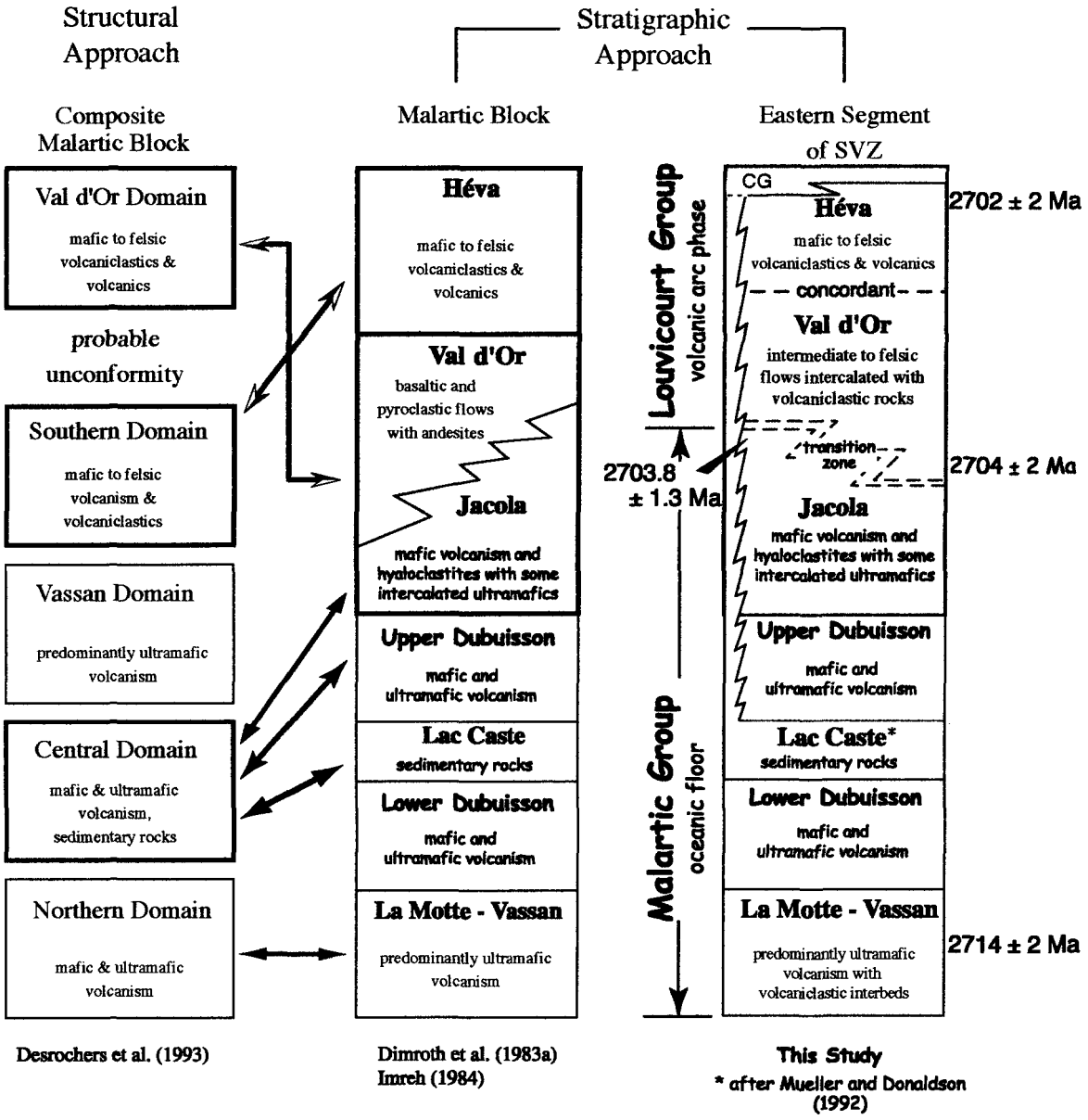

Figure 185. Series of composite columns representing previous structural and stratigraphic methods in constructing the Composite Malartic and Malartic Block, respectively. Equivalent domains and formations are linked by tie lines with the shaded blocks representing the focus of this study. The stratigraphic approach for this work subdivides the Malartic Block into two groups based on tectonic affiliation; Malartic Group represents oceanic floor and the Louvicourt Group represents a volcanic arc. The Cadillac Group (CG) forms a forearc sedimentary package of flysch-type deposits that is the lateral equivalent to the Héva Formation along strike to the west (see Figures 5B & 6). This links this region with the Blake River Block indicating a complete allochthonous assemblage.

183). Other probably volcanic centers include the Sleepy Lake (VC-I; **Figure 183**), Rainville (VC-IV; **Figure 183**), and southern Lamaque (VC-VII; **Figure 183**) zones, all of which have associated mineralization, but at sub-economic values. The Relais region (VC-III; **Figure 183**), located southwest of the Louvicourt Mine, represents a potential target for further mineral exploration hosted within multiple dacitic domes.

7.5 Comparison between Modern and Archean Island Arc Systems

This project offers an excellent opportunity to summarize salient features of modern-day volcanic island arcs and compare them to this and other work done in Archean.terranes. Comparison between their respective stratigraphical and depositional histories suggests similar tectonic mechanisms from an initial platform sequence composed of mafic lavas, a subaqueous proto-arc phase, early arc-rifting and continued or renewed arc construction with further backarc extension (**Table 24**). Geochemically, modern arcs evolve from tholeiitic to calc-alkaline lavas as a result of maturation (Wilson, 1989), but all have negative Nb-Ta-Ti anomalies that characterize arc-related volcanism (Orton, 1996). These geochemical signatures are mirrored in Archean sequences, suggesting an arc setting (Scott et al., 2002). The general size of observed subaqueous vents are similar to mapped Archean areas (**Table 24**). The style of volcanism is a function of physicochemical principles in a subaqueous realm for both modern and ancient arcs, ranging from explosive to effusive (**Table 24**). The temporal evolution of modern arc systems is variable, but Wharton et al. (1995) envisaged 25my from the proto-arc, initial rifting, and renewed arc

Table 24: Comparison between modern and Archean Island Arcs.

ISLAND ARC FEATURES	MODERN	ARCHEAN
Stratigraphy	(1) Initial sequence is composed of pillowed to massive basalts and gabbroic intrusions.[1] (2) Eruption of basaltic to rhyolitic lavas intercalated with abundant fragmental material.[2,3,4] (3) Eruption of boninitic and tholeiitic basalt lavas[1] intercalated with tuff breccias to tuff deposits.[3] (4) Pillowed to massive basaltic lavas[1] with finer tuff deposits.[3] (5) Andesitic to rhyolitic volcanism with associated volcaniclastic and pyroclastic deposits.[1,5]	(1) Initial sequence is composed of pillowed to massive flows of mafic-ultramafic lavas.[8,9] (2) Intercalation of mafic-ultramafic lavas and andesitic to dacitic lavas with associated tuffs and mass flow deposits.[8,10] (3) Thicker andesitic to rhyolitic lavas and their associated tuff and debris flow deposits.[11,12,13] (some boninitic lavas have been reported[14,15]) (4) Pillowed to massive basaltic lavas and synvolcanic sills and dyles with minor tuff deposits.[16]
Depositional Environment	(1) Oceanic crust serves as a subaqueous platform, with effusive eruptions.[1] (2) Proto-arc phase characterized by numerous small subaqueous vents.[2,6] (3) Intra-arc extension-rifting forming narrow, steep fault-scarp margins.[1,3,5] (4) Continued rifting forming backarc basin bounded by normal faults.[3,7] and (5) Renewed arc volcanism from subaqueous to subaerial activity.[1,5]	(1) Formation of a subaqueous mafic-ultramafic platform-plain.[8,9] (2) Contemporaneous subaqueous eruptions of mafic-ultramafic lavas and incipient arc-related vents.[8,10] (3) Construction arc-phase from high-relief stratovolcanoes[12], subaqueous to subaerial.[11] Evidence of intra-arc rifting with associated boninites[14,15] along with epiclastic mass flow deposits.[16] (4) Extension-related volcanic and intrusive-activity with possible formation of back-arc basin.[16]
Geochemistry	Tholeiitic to calc-alkaline evolution during maturation of arc.[1,4] Negative Nb-Ta and Ti anomalies characterizes arc-signature.[4] Oceanic crust and backarc basalts have MORB signatures.[4]	Tholeiitic mafic and komatiites intercalated with tholeiitic-transitional, arc-related volcano-sedimentary facies indicating spatial and temporal plume-arc activity.[10,16] Tholeiitic to calc-alkaline evolution during maturation of arc.[1,4] Negative Nb-Ta and Ti anomalies characterizes arc-signature.[4] Rift-related basalts have MORB signatures and intercalated epiclastic deposits have arc-signature.[16]
General Size	Subaqueous vents are characterized by numerous small vents 50-600m in relief and 300-3000m in diameter[6]; the larger the edifice the larger the spacing, which ranged from 15-75km for subaqueous vents.[2]	Numerous subaqueous vents measuring 1-4 km wide and 1-3 high in cross-section over a 30km distance.[16]
Volcanic Morphology	Single to multiple vents forming low aspect, shield-like structures, evolving upwards to more steeper stratovolcanoes and caldera structures.[1,2,6]	Fissural eruptions forming low-aspect structures[8] that become more steep-sided up section[16] with some caldera structures reported.[17]
Style of Volcanism	Subaqueous activity varies from effusive pillow lavas, magmatic and phreatomagmatic explosive and autoclastic fragmentation. Subaerial is dominantly pyroclastic to lava flows.[1,4]	Subaqueous activity varies from effusive pillow lavas, magmatic (fire fountain) and phreatomagmatic explosive and autoclastic.fragmentation.[8,9,12,13,16,17]
Age	Temporal evolution varies from around 25my[5] to 2-10my[3]	Temporal evolution varies from 12-4my, with arc extension possible in the first 2my. [17]
Examples	Western Pacific, particularly Sumisu Rift, Izu-Bonin Arc.	Val d'Or Mining Camp, Joutel, Hunter Mine, Rouyn-Noranda, etc.

[1] Wilson (1989); [2] Bloomer et al. (1989); [3] Carey and Sigurdsson (1984); [4] Orton (1996); [5] Wharton et al. (1995); [6] Taylor et al. (1990); [7] Gamble and Wright (1995); [8] Thurston (1990); [9] Dimroth et al. (1982); [10] Hollings et al. (1999); [11] Thurston (1994); [12] Lowe (1994); [13] Mueller and White (1992); [14] Boily and Dion (2002); [15] Polat et al. (2002); [16] Scott et al. (2002); [17] Mueller and Mortensen (2002)

volcanism. Archean systems evolved faster, as Muller and Mortensen (2002) outlined a 4-12my window with initial rifting in the first 2my. This disparity may be an artifact of a high heat flow typically associated with this period in Earth history. Overall, modern and ancient arcs are similar (**Table 24**), suggesting comparable tectonic processes.

7.6 Autochthonous or Allochthonous? A Final Word

The assembled evidence definitely argues against an allochthonous origin for the study area. Let's review the evidence:

1. Faulted Contacts.

The proposed allochthonous model requires faulted contacts between the various domains, except for a probable unconformity between the Val d'Or and Southern (Héva) domains. Are there faulted contacts in the study area? Contact relationships between the three studied formations were not exposed, but field data imply contacts over several hundred meters and geomagnetic data, while not outlining any major interformational faults, demarcate a sharp contact between the Val d'Or and Héva formations. Such a sharp boundary could represent a fault contact! So what would this mean for the presented model? Plate boundaries are defined by faulted contacts and the stress regimes within convergent and divergent boundaries result in very complex faulting. Thus, faulted contacts, while not observed would be expected. Contact between the Jacola and Val d'Or formations could be faulted, but would be syntectonic as the observed andesitic dykes that crosscut the upper JF (**Figure 16**) are observed cutting the lower VDF (**Figures 36 and 41**)

and probably feed overlying flows, suggesting an autochthonous origin (cf. Thurston, 2002). The sharp contact between the Val d'Or and Héva formations, marked by the abrupt appearance of the spherulitic felsic unit, supports a faulted contact. In this case, a faulted contact supports the autochthonous stratigraphic model. The HF is interpreted as a rift-sequence and rifting is associated with normal faulting (Wilson, 1989). Magma would move up through these faults to form synvolcanic sills and dykes, both of which are abundant in the HF. Furthermore, normal faulting would result in the formation of a basin (Carey and Sigurdsson, 1984), a basin in which weathered material from the VDF could be deposited. This implies further evidence of an autochthonous or parauthchthonous origin, with or without fault bounded contacts, rather than an allochthonous collage of exotic terranes.

2. Geochronology

In the allochthonous model, the youngest rocks in the sequence are represented by the Val d'Or Domain (Desrochers et al. 1993). Recent age dating, however, delineated progressive southward younging direction, with the Héva Formation being the youngest. This refutes the late stage eruption of the Val d'Or Domain.

3. Deformation history

Only one regional structural deformation event was observed in the study area, which argues against each lithotectonic domain having a unique history. Furthermore, localized bedding, north of Sigma mine, were measured to be oriented N-S,almost 90° from regional trends. On further examination and extensive stripping of the outcrop, the

observed contact was between a crosscutting dyke and E-W volcaniclastic deposits. Such observations argued for folding events.

CHAPTER 8

CONCLUSIONS

Thesis objectives were to better understand the geodynamic setting of a part of the Abitibi Greenstone Belt in which arc and plume systems were active, employing the techniques of physical volcanology, geochemistry, and geochronology. Thesis objectives were met by detailed examination of three formations, namely the Jacola, Val d'Or and Héva formations, in regard to their individual tectonic setting and to detail their contact relationships in an effort to recognize any potential temporal and/or spatial correlation. The result is the construction of a regional stratigraphy that outlines the evolution of a subaqueous volcanic arc sequence, constructed on an extensive submarine plain/plateau over 1-4 m.y., between 2705-2701 Ma.

1. Stratigraphy

    a. U-Pb dating recognizes a progressive southward younging history with overlap between the Jacola and Val d'Or formations.

    b. Pillowed sequences throughout the three formations all indicated a southward younging direction.

c. Sedimentary structures and textures, such as grading and truncated bedding, indicate a southward younging direction. Only a localized area (i.e., Sleepy Lake) had a northward younging direction; which may record overturning during emplacement of the post-volcanic Bevcon Stock.

2. Physical Volcanology and Depositional Setting

a. Thin, laterally extensive, non-vesicular, pillowed to massive mafic and ultramafic lavas, with little to no interstratified fragmental material in the Jacola Formation, suggest effusive eruptions in a deep-water setting.

b. Laterally discontinuous and overlapping of adjacent felsic to intermediate lavas, characterized by abundant interbedded, amalgamated volcaniclastic sequences in the Val d'Or Formation suggest explosive to effusive volcanism from small, local volcanic vents.

c. Well-developed bedding and grading within volcaniclastic sequences in the Val d'Or Formation imply deposition from water-supported, high- to low-concentration turbidity flows. The absence of shallow-water structures suggest deposition below wave-base of 200m depth.

d. Highly vesiculated, fluidal breccia facies, deposited by normal- to reverse-graded, high-concentration turbidity flows in the Val d'Or Formation, intercalated with below wave-base deposits suggest that hydrostatic pressure suppressed explosivity and resulted in fire-fountain style volcanism.

e. Intercalated felsic lobes and lobe-hyaloclastites facies of felsic flows define subaqueous felsic dome complexes, which represent potential targets for mineral exploration.

f. A thick, laterally extensive spherulitic felsic unit composed, from base to top, of massive lavas, lobe-hyaloclastite and hyaloclastite facies at the base of the Héva Formation, suggest an extrusive eruption in a deep-water setting, whereby hydrostatic pressures suppressed volatile exsolution, which lowered the viscosity of an otherwise viscous lava.

g. A volcaniclastic tuff breccia facies in the Héva Formation, composed of arc-related bimodal fragments, stratigraphically above the spherulitic felsic unit, implies erosional forces and redeposition from the Val d'Or Formation.

h. Thick, pillowed to massive, non-vesicular, mafic lavas interstratified with gabbroic sills and dykes, with little to no intercalated fragmental material in

the Héva Formation, suggest effusive volcanism that probably erupted from fissural sources.

i. Subordinate felsic tuff turbidite sequences, interstratified with mafic lavas of the Héva Formation, indicate localized areas of explosive volcanism. These tuff beds are typically associated with peperites formed during the syn-volcanic intrusion of gabbros into unconsolidated felsic sediments, which suggest contemporaneous sedimentation and volcanism.

3. Geochemistry

a. The Jacola Formation is composed of tholeiitic basalts and komatiitic lavas that have trace element abundances similar to primordial mantle, which suggest a N-MORB source.. This is confirmed on the tectono-magmatic discrimination diagram utilizing the trace elements Th-Hf-Ta. Their low incompatible element abundances and high-Mg imply high degrees of partial melting deep in the mantle and being transported via a mantle plume.

b. The lower Val d'Or Formation contains tholeiitic to transitional volcano-sedimentary deposits of intermediate composition, some of which have $(La/Yb)_n$ ratios similar to N-MORB. Nevertheless, all samples have negative Ta-anomalies suggestive of subduction-related processes. N-MORB

characteristics may be the result of contamination or mixing with magmas from Jacola Formation, which implies a spatial and temporal relationship. The primitive nature of these arc-related deposits indicate the initial construction of a proto-arc.

c. The upper Val d'Or Formation consists of transitional to calc-alkaline volcano-sedimentary deposits of intermediate to felsic composition. These have pronounced negative Ta-anomalies indicative of subduction-generated volcanism.

d. The spherulitic felsic unit at the base of the Héva Formation is tholeiitic, with enriched trace element abundances similar to E-MORB, but with a strong negative Ti-anomaly. These characteristics are probably related to the onset of arc rifting.

e. The volcaniclastic tuff breccia, stratigraphically above the spherulitic felsic unit, is composed of rounded mafic and felsic calc-alkaline fragments with negative Ta-anomalies, indicating that they originated from the underlying Val d'Or Formation. These *epiclastic* deposits result from erosion during incipient rifting of the arc, thus imply a temporal and spatial relationship between the Val d'Or and Héva formations.

f. Basalts and gabbros from the Héva Formation are tholeiitic with slightly enriched trace element abundances similar to an E-MORB.

g. Localized felsic tuffs are calc-alkaline with negative Ta-anomalies indicative of subduction-related processes, which are analogous to deposits from the Val d'Or Formation.

4. Geodynamic Setting

The Jacola, Val d'Or, and Héva formations represent an evolutionary sequence from an extensive subaqueous plain/plateau to arc construction and then arc rifting, respectively. The Val d'Or Arc was constructed and dissected over 1-4 m.y. The Jacola Formation represents a submarine plain formed during fissural eruptions from a mantle plume source. Northward subduction resulted in initial arc construction, represented by the lower Val d'Or Formation, which overlapped and was contaminated by lavas/magmas from the Jacola Formation, indicating both a temporal and spatial association. Maturation of the arc formed more calc-alkaline lavas within the upper Val d'Or Formation, which formed a complex arc composed of numerous coalesced vents. The onset of arc rifting, represented by an effusive, deep-water eruption of tholeiitic felsic lava, forms a local basin whereby reworked volcaniclastic rocks of the Val d'Or Formation are transported, forming interstratified polymictic deposits at the base of the Héva Formation. Subsequent

voluminous mafic volcanism floods the arc with fine-grained fragmental material from adjacent calc-alkaline volcanism periodically transported into the rifting basin. The region forms a monoclinal sequence of volcano-sedimentary rocks with a southward younging direction.

BIBLIOGRAPHY

Abbott, D.A. and Hoffman, S.E., 1984. Archean plate tectonics revisited: heat flow, spreading rate, and the age of subducting oceanic lithosphere and their effects on the origin and evolution of continents. Tectonics, 3: 429-448.

Abbott, D.H. and Isley, A.E., 2002. The intensity, occurrence, and duration of superplume events and eras over geological time. Journal of Geodynamics, 34: 265-307.

Alidibirov, M. and Dingwell, D.B., 2000. Three fragmentation mechanisms for highly viscous magma under rapid decompression. Journal of Volcanology and Geothermal Research, 100: 413-421.

Allegre, C.J., 1982. Genesis of Archaean komatiites in a wet ultramafic subducted plate. In: N.T. Arndt and E.G. Nisbet (Editors), Komatiites, London, Allen and Unwin, pp. 495-500.

Allen, S.R. and McPhie, J., 2003. Phenocryst fragments in rhyolitic lavas and lava domes. Journal of Volcanology and Geothermal Research, 126: 263-283.

Arndt, N.T., Kerr, A.C. and Tarney, J., 1997. Dynamic melting in plume heads: the formation of Gorgona komatiites and basalts. Earth and Planetary Science Letters, 146: 289-301.

Ayer, J.A., Amelin, Y., Corfu, F., Kamo, S., Ketchum, J., Kwok, K, and Trowell, N., 2002. Evolution of the southern Abitibi greenstone belt based on U-Pb geochronology: autochthonous volcanic construction followed by plutonism, regional deformation and sedimentation. Precambrian Research, 115: 63-95.

Ayer, J.A., Trowell, N.F., Madon, Z., Kamo, S., Kwok, Y.Y. and Amelin, Y., 1999. Compilation of the Abitibi Greenstone Belt in Timmins-Kirkland Lake area: revisions to stratigraphy and new geochronological results. In: O.G. Survey (Editor), Summary of Field Work and other activities 199, pp. 4-1 to 4-14.

Babineau, J., 1983. Carte géologique et structurale de la région du lac Malartic. DP 83-30, carte annotée, Ministère de l'Énergie et des Ressources, Québec.

Bagnold, R.A., 1954. Experiments on a gravity-free dispersion of large solid spheres in Newtonian fluid under stress. Proc. Roy. Soc. Lond., 225: 49-63.

Barnes, S.J., Lesher, C.M. and Keays, R.R., 1995. Geochemistry of mineralized and barren komatiites from the Perseverance nickel deposit, Western Australia. Lithos, 34: 209-234.

Barrett, T.J. and MacLean, W.H., 1997. Volcanic sequences, lithogeochemistry and hydrothermal alteration in some bimodal VMS systems. In: C.T. Barrie and M.D. Hannington (Editors), Volcanic-Associated Massive Sulfide Deposits: Processes and Examples in Modern and Ancient Settings, Ottawa, Canada, pp. 105-133.

Bates, R.L. and Jackson, J.A. (Editors), 1987. Glossary of Geology. American Geological Institute, Alexandra, Virgina, 788 pp.

Batiza, R., Fornari, D., Vanko, D.A. and Lonsdale, P., 1984. Craters, calderas, and hyaloclastites on young Pacific seamounts. Journal of Geophysical Research, 89(B10): 8371-8390.

Batiza, R., Smith, T.L. and Niu, Y., 1989. Geological and petrological evolution of seamounts near the EPR based on submersible and camera study. Marine Geophysical Research, 11: 169-236.

Batiza, R. and White, J.D.L., 2000. Submarine lavas and hyaloclastite. In: H. Sigurdsson (Editor), Encyclopedia of Volcanoes. Academic Press, pp. 361-382.

Bédard, L.P. and Barnes, S.-J., 1990. Instrumental neutron activation analysis by collecting only one spectrum: results for international reference samples. Geostandards Newsletter, 14: 479-484.

Bergh, S.D. and Gudmunder, E.S., 1991. Pleistocene mass-flow deposits of basaltic hyaloclastite on a shallow submarine shelf, South Iceland. Bulletin of Volcanology, 53: 597-611.

Best, M.G. and Christiansen, E.H., 2001. Igneous Petrology. Blackwell Science, Inc., 458 pp.

Bevins, R.E. and Roach, R.A., 1978. Pillow lava and isolated-pillow breccia of rhyodacite composition from the Fishguard Volcanic Group, Lower Ordovician, S.W. Wales, United Kingdom. Journal of Geology, 87: 193-201.

Bickle, M.J., 1978. Heat loss from the earth: a constraint on Archean tectonics from the relation between geothermal gradients and the rate of plate production. Earth and Planetary Science Letters, 40: 301-315.

Blake, S., 1981. Eruptions from zoned magma chambers. J. Geol. Soc. London, 138: 281-287.

Bonatti, E. and Harrison, C.G.A., 1988. Eruptive styles of basalt in oceanic spreading ridges and seamounts: effect of magma temperatures and viscosity. Journal of Geophysical Research, 93: 2967-2980.

Bonnichsen, B. and Kauffman, D.F., 1987. Physical features of rhyolite lava flows in the Snake River Plain volcanic province, southwestern Idaho. In: J.H. Fink (Editor), The Emplacement of Silicic Domes and Lava Flows. Geological Society of America, pp. 119-145.

Branney, M.J. and Suthren, R.J., 1988. High-level peperitic sills in the English Lake District: Distinction from block lavas, and implications for Borrowdale Volcanic Group stratigraphy. Geological Journal, 23: 171-187.

Brooks, E.R., 1995. Paleozoic fluidization, folding, and peperite formation, northern Sierra Nevada, California. Ca, Journ. Earth Sci., 32: 314-324.

Buchanan, D.J. and Dullforce, T.A., 1973. Mechanism for vapor explosions. Nature, 245: 32-34.

Busby, C.J., Kessel, L., Schulz, K., Foose, M. and Slack, J., 2003. Very deepwater silicic explosive volcanic setting of the Ordovician Bald Mountain massive sulfide deposit, Northern Maine. In: S.R.M. W.D. Goodfellow, and J.M. Peter (Editor), Economic Geology Monograph: Massive Sulphide Deposits of the Bathurst Mining Camp, New Brunswick, and Northern Maine.

Busby-Spera, C.J. and White, J.D.L., 1987. Variation in peperite textures associated with differing host-sediment properties. Bulletin Volcanology, 49: 765-775.

Calvert, A.J. and Ludden, J.N., 1999. Archean continental assembly in the southeastern Superior Province of Canada. Tectonics, 18(No. 3): 412-429.

Calvert, A.J., Sawyer, E.W., Davis, W.J. and Ludden, J.N., 1995. Archean subduction inferred from seismic images of a mantle suture in the Superior Province. Nature, 375: 670-674.

Campbell, I.H. and Griffiths, R.W., 1990. Implications of mantle plume structure for the evolution of flood basalts. Earth and Planetary Science Letters, 99: 79-93.

Campbell, I.H., Griffiths, R.W. and Hill, R.I., 1989. Melting in an Archean mantle plume: heads it's basalts, tails it's komatiites. Nature, 339: 697-699.

Capdevila, R., Goodwin, A.M., Ujike, O. and Gorton, M.P., 1982. Trace-element geochemistry of Archean volcanic rocks and crustal growth in south western Abitibi Belt, Canada. Geology, 10: 418-422.

Card, K.D., 1990. A review of the Superior province of the Canadian shield, a product of Archean accretion. Precambrian Research, 48: 99-156.

Carey, S., 2000. Volcaniclastic sedimentation around island arcs. In: H. Sigurdsson (Editor), Encyclopedia of Volcanoes. Academic Press, pp. 627-642.

Carey, S. and Sigurdsson, H., 1984. A model of volcanogenic sedimentation in marginal basins. In: B.P. Kokelaar and M.F. Howells (Editors), Marginal Basin Geology. Spec. Publ. Geological Society of London, pp. 37-58.

Carey, S.N. and Sigurdsson, H., 1980. The Roseau Ash: Deep-sea tephra deposits from a major eruption on Dominica, Lesser Antilles arc. Journal of Volcanology and Geothermal Research, 7: 67-86.

Cas, R., 1978. Silicic lavas in Paleozoic flyschlike deposits in New South Wales, Australia: Behavior of deep subaqueous silicic flows. Geological Society of America Bulletin, 89: 1708-1714.

Cas, R.A.F., 1992. Submarine volcanism: Eruption styles, products, and relevance to understanding the host-rock successions to volcanic-hosted massive sulfide deposits. Economic Geology, 87: 511-541.

Cas, R.A.F. and Wright, J.V., 1987. Volcanic Successions: Modern and Ancient: a Geological Approach to Processes, Products and Successions. Allen-Unwin, London, 528 pp.

Cas, R.A.F. and Wright, J.V., 1991. Subaqueous pyroclastic flows and ignimbrites: an assessment. Bulletin of Volcanology, 53: 357-380.

Cashman, K., Pinkerton, H. and Stephenson, J., 1998. Introduction to special section: Long lava flows. Journal of Geophysical Research, 103(B11): 27,281-27,289.

Champagne, C., Pilote, P. and Mueller, W.U., 2002. Volcanologie physique et geochimie des komaiites archeenes: Groupe de Malartic, Abitibi, Québec. MB-2002-04, Ministere des Ressources naturelles du Québec.

Chartrand, F. and Moorhead, J., 19**. Geology of the central pyroclastic belt, Val d'Or, Field guide.

Chough, S.K. and Sohn, Y.K., 1990. Depositional mechanics and sequences of base surges, Songaksan tuff ring, Cheju Island, Korea. Sedimentology, 37: 1115-1135.

Chown, E.H., Daigneault, R., Mueller, W. and Mortensen, J.K., 1992. Tectonic evolution of the Northern Volcanic Zone, Abitibi belt, Quebec. Canadian Journal of Earth Sciences, 29: 2211-2225.

Clague, D.A., Davis, A.S., Bischoff, J.L., Dixon, J.E. and Geyer, R., 2000. Lava bubble-wall fragments formed by submarine hydrovolcanic explosions on Lo'ihi Seamount and Kilauea Volcano. Bulletin of Volcanology, 61: 437-449.

Clague, D.A., Davis, A. S., Dixon, J.E., 2003. Submarine strombolian eruptions on the Gorda Mid-Ocean Ridge. In: J.D.L. White, J.L. Smellie and D. Clague (Editors), Explosive Subaqueous Volcanism. American Geophysical Union, Monograph 140.

Clift, P.D. et al., 1995. Volcanism and sedimentation in a rifting island-arc terrain: an example from Tonga, SW Pacific. In: J.L. Smellie (Editor), Volcanism Associated with extension at Consuming Plate Margins. Geological Society Special Publication, pp. 21-51.

Condie, K.C. (Editor), 1994. Archean Crustal Evolution. Developments in Precambrian Geology, 11. Elsevier, 525 pp.

Corcoran, P.L., 2000. Recognizing distinct portions of seamounts using volcanic facies analysis: examples from the Archean Slave Province, Northwest Territories, Canada. Precambrian Research, 101: 237-261.

Corfu, F., Krogh, T.E., Kwok, Y.Y. and Jensen, L.S., 1989. U-Pb zircon geochronology in the southwestern Abitibi greenstone belt, Superior Province. Can. J. Earth Sci., 26: 1747-1763.

Cousineau, P. and Dimroth, E., 1982. Interpretation of the relations between massive, pillowed and brecciated facies in an Archean submarine andesite volcano - Amulet andesite, Rouyn-Noranda, Canada. Journal of Volcanology and Geothermal Research, 13: 83-102.

Cousineau, P.A. and Bedard, J.H., 2000. Sedimentation in a subaqueous arc/back-arc setting: the Bobby Cove Formation, Snooks Arms Group, Newfoundland. Precambrian Research, 101: 111-134.

Dadd, K.A., 1992. Structures within large volume rhyolite lava flows of the Devonian Comerong Volcanics, southeastern Australia, and the Pleistocene Ngongotaha lava dome, New Zealand. Journal of Volcanology and Geothermal Research, 54: 33-51.

Dadd, K.A. and Van Wagoner, N.A., 2002. Magma composition and viscosity as controls on peperite texture: an example from Passamaquoddy Bay, southeastern Canada. Journal of Volcanology and Geothermal Research, 114: 63-80.

Daigneault, R., Mueller, W.U. and Chown, E.H., 1994. Accretion of the northern and southern volcanic zones along the Manneville fault zone, Abitibi Subprovince, Québec. In: G.A.o.C.w. Abstracts (Editor), pp. A25.

Daigneault, R., Mueller, W.U. and Chown, E.H., 2002. Oblique Archean subduction: accretion and exhumation of an oceanic arc during dextral transpression, Southern Volcanic Zone, Abitibi Subprovince Canada. Precambrian Research, 115: 261-290.

Davis, B.K. and McPhie, J., 1996. Spherulites, quench fractures and relict perlite in a Late Devonian rhyolite dyke, Queensland, Australia. Journal of Volcanology and Geothermal Research, 71: 1-11.

De Rosen-Spence, A.F., 1976. Stratigraphy, development and petrogensis of the central Noranda volcanic pile, Noranda, Quebec. Unpub. Ph.D. Thesis, Univ. Toronto, 166 pp.

De Rosen-Spence, A.F., Provost, G., Dimroth, E., Gocnauer, K. and Owen, V., 1980. Archean subaqueous felsic flows, Rouyn-Noranda, Quebec, Canada, and their quarternary equivalents. Precambrian Research, 12: 43-77.

Decker, R. and Decker, B., 1989. Volcanoes. W.H. Freeman and Company, New York, 285 pp.

Desrochers, J.-P. and Hubert, C., 1996. Structural evolution and early accretion of the Malartic composite block, southern Abitibi greenstone belt, Quebec, Canada. Canadian Journal of Earth Sciences, 33: 1556-1569.

Desrochers, J.-P., Hubert, C., Ludden, J. and Pilote, P., 1993. Accretion of Archean oceanic plateau fragments in the Abitibi greenstone belt, Canada. Geology, 21: 451-454.

Desrochers, J.-P., Hubert, C. and Pilote, P., 1996. Geologie de la region de Val d'Or - Malartic (Abitibi-est). ET 96-01, Government du Quebec.

Dimroth, E., Cousineau, P., Leduc, M. and Sanshagrin, Y., 1978. Structure and organization of Archean subaqueous basalt flows, Rouyn-Noranda area, Quebec, Canada. Canadian Journal of Earth Sciences, 15: 902-918.

Dimroth, E., Imreh, L., Rocheleau, M. and Goulet, N., 1982. Evolution of the south-central part of the Archean Abitibi Belt, Quebec. Part I: stratigraphy and paleogeographic model. Canadian Journal of Earth Sciences, 19: 1729-1758.

Dimroth, E., Imreh, L., Rocheleau, M. and Goulet, N., 1983a. Evolution of the south-central segment of the Archean Abitibi Belt, Quebec. Part II: tectonic evolution and geomechanical model. Canadian Journal of Earth Sciences, 20: 1355-1373.

Dimroth, E., Imreh, L., Rocheleau, M. and Goulet, N., 1983b. Evolution of the south-central segment of the Archean Abitibi Belt, Quebec. Part III: plutonic and metamorphic evolution and geotectonic model. Canadian Journal of Earth Sciences, 20: 1374-1388.

Dimroth, E. and Lichtblau, A.P., 1979. Metamorphic evolution of Archean hyaloclastites, Noranda area, Quebec, Canada. Part I: Comparison of Archean and Cenozoic sea-floor metamorphism. Canadian Journal of Earth Sciences, 16(7): 1315-1340.

Dimroth, E. and Yamagishi, H., 1987. Criteria for the recognition of ancient subaqueous pyroclastic rocks. Geological Survey of Hokkaido(No. 58).

Donaire, T., Sáez, R. and Pascual, E., 2002. Rhyolitic globular peperites from the Aznalcóllar mining district (Iberian Pyrite Belt, Spain): physical and chemical controls. Journal of Volcanology and Geothermal Research, 114: 119-128.

Dostal, J. and Mueller, W.U., 1997. Komatiite flooding of a rifted Archean rhyolite arc complex: geochemical signature and tectonic significance of the Stoughton-Roquemaure Group, Abitibi Greenstone Belt, Canada. Journal of Geology, 105: 545-563.

Doucet, P., Mueller, W. and Chartrand, F., 1994. Archean, deep marine, volcanic eruptive products associated with the Coniagas massive sulfide deposit, Quebec, Canada. Canadian Journal of Earth Sciences, 31: 1569-1584.

Doyle, M.G. and McPhie, J., 2000. Facies architecture of a silicic intrusion-dominated volcanic centre at Highway-Reward, Queensland, Australia. Journal of Volcanology and Geothermal Research, 99: 79-96.

Duffield, W.A., 1990. Eruptive fountains of silicic magma and their possible effects on tin content of fountain-fed lavas. Geological Society of America, Special Paper 246: 251-261.

Eichelberger, J.C., Carrigan, C.R., Westrich, H.R. and Price, R.H., 1986. Non-explosive silicic volcanism. Nature, 323: 598-602.

Eissen, J.-P., Fouquet, Y., Hardy, D. and Ondréas, H., 2003. Recent MORB volcaniclastic explosive deposits formed between 500 and 1750 m.b.s.l. on the axis of the Mid-Atlantic Ridge, South of the Azores. In: J.D.L. White, J.L. Smellie and D. Clague (Editors), Explosive Subaqueous Volcanism. American Geophysical Union, Monograph 140, pp. 143-166.

Fan, J. and Kerrich, R., 1997. Geochemical characteristics of aluminum depleted and undepleted komatiites and HREE-enriched low-Ti tholeiites, western Abitibi greenstone belt: A heterogeneous mantle plume-convergent margin environment. Geochimica et Cosmochimica Acta, 61(22): 4723-4744.

Fink, J.H., 1983. Structure and emplacement of a rhyolitic obsidian flow: Little Glass Mountain, Medicine Lake Highland, northern California. Geological Society of America Bulletin, 94: 360-380.

Fisher, R.V., 1961. Proposed classification of volcaniclastic sediments and rocks. Geological Society of America Bulletin, 72: 1409-1414.

Fisher, R.V., 1966. Rocks composed of volcanic fragments and their classification. Earth Science Reviews, 1: 287-298.

Fisher, R.V., 1983. Flow transformations in sediment gravity flows. Geology, 11: 273-274.

Fisher, R.V. and Schmincke, H.-U., 1984. Pyroclastic Rocks. Springer-Verlag, Berlin, 472 pp.

Fisher, R.V. and Smith, G.A. (Editors), 1991a. Sedimentation in Volcanic Settings, Special Publication No. 45. SEPM (Society for Sedimentary Geology), Tulsa, Oklahoma, 257 pp.

Fisher, R.V. and Smith, G.A., 1991b. Volcanism, tectonics and sedimentation. In: R.V. Fisher and G.A. Smith (Editors), Sedimentation in Volcanic Settings. SEPM (Society for Sedimentary Geology), Tulsa, Oklahoma, pp. 1-5.

Fiske, R.S., 1994. Caldera-forming submarine pyroclastic eruption at Myojin Knoll, Izu-Bonin Arc, Japan. EOS, 75: 729-730.

Fiske, R.S., Cashman, K.V., Shibata, A. and Watanabe, K., 1998. Tephra dispersal from Myojinsho, Japan, during its shallow submarine eruption of 1952-1953. Bulletin of Volcanology, 59: 262-275.

Fiske, R.S. and Matsuda, T., 1964. Submarine equivalents of ash flows in the Tokiwa Formation, Japan. American Journal of Science, 262: 76-106.

Fornari, D.J., 1986. Submarine lava tubes and channels. Bulletin of Volcanology, 48: 291-298.

Fowler, A.D., Berger, B., Shore, M., Jones, M.I. and Ropchan, J., 2002. Supercooled rocks: development and significance of varioles, spherulites, dendrites and spinifex in Archaean volcanic rocks, Abitibi Greenstone belt, Canada. Precambrian Research, 115: 311-328.

Fowler, A.D., Jenson, L.S. and Peloquin, S.A., 1986. Varolites in Archean basalts: Products of spherulitic crystallization. Canadian Mineralogist, 25: 275-289.

Franklin, J.M., Lydon, J.W. and Sangster, D.F., 1981. Volcanic associated massive sulphide deposits. Econ. Geol. 75th Anniv. Volume: 485-627.

Furnes, H., Fridleifsson, I.B. and Atkins, F.B., 1980. Subglacial volcanoes - on the formation of acid hyaloclastites. Journal of Volcanology and Geothermal Research, 8: 95-110.

Garner, A. and McPhie, J., 1999. Partially melted lithic megablocks in the Yardea Dacite, Gawler Range Volcanics, Australia: implications for eruption and emplacement mechanisms. Bulletin of Volcanology, 61: 396-410.

Gaudreau, R., Lacoste, P. and Rocheleau, M., 1986. Géologie et gîtologie du secteur de Louvicourt - Vauquelin, Abitibi. MB 86-67, Ministère de l'Énergie et des Ressources.

Gélinas, L., Brooks, C. and Trzcienski, W.E., 1976. Archaean variolites - quenched immiscible liquids. Canadian Journal of Earth Sciences, 13: 210-230.

Gibson, H.L., 1999. Subaqueous rhyolitic flows and domes, Physical volcanology: felsic volcanic process, deposits and mineralization. Geological Association of Canada, Short Course Notes, Sudbury, Ontario, pp. 1-31.

Gibson, H.L. et al., 1999. Physical volcanology: felsic volcanic processes, deposits and mineralization. Geological Association of Canada, Short Course Notes, Sudbury, Ontario.

Gibson, H.L., Morton, R.L. and Hudak, G.J., 1997. Submarine volcanic processes, deposits and environments favourable for the location of volcanic-associated massive sulfide deposits. In: C.T. Barrie and M.D. Hannington (Editors), Volcanic-Associated

Massive Sulfide Deposits: Processes and Examples in Modern and Ancient Settings, Ottawa, Canada, pp. 13-51.

Gibson, H.L., Morton, R.L. and Hudak, G.J., 2000. Submarine volcanic processes, deposits and environments favorable for the location of volcanic-hosted massive sulfide deposits. In: C.T.B.a.M.D. Hannington (Editor), Reviews in Economic Geology: Volcanic-Associated Massive Sulfide Deposits: Processes and Examples in Modern and Ancient Settings, pp. 13-51.

Gill, J. et al., 1990. Explosive deep water basalt in the Sumiso Backarc Rift. Science, 248: 1214-1217.

Goodwin, A.M. and Ridler, R.H., 1970. The Abitibi orogenic belt. In: A.J. Baer (Editor), Symposium on Basins and Geosynclines of the Canadian Shield. Geological Survey of Cananda, Special Paper, pp. 1-30.

Griffiths, R.W. and Fink, J.H., 1992. Solidification and morphology of submarine lavas: a dependence on extrusion rate. Journal of Geophysical Research, 97: 19,729-19,737.

Gunning, H.C. and Ambrose, J.W., 1940. Malartic area, Québec. Memoir 222, Geological Survey of Canada.

Hamilton, W.B., 1988. Plate tectonics and island arcs. Geological Society of America Bulletin, 100: 1503-1527.

Hamilton, W.B., 1993. Evolution of Archean mantle and crust. In: J.C. Reed et al. (Editors), Precambrian Conterminous U.S. Geological Society of America, Boulder, CO, pp. 597-614.

Hamilton, W.B., 1995. Subduction systems and magmatism. In: J.L. Smellie (Editor), Volcanism associated with extension at consuming plate margins. Geological Society (London), Special Publication 81, pp. 3-28.

Hanson, R.E. and Hargrove, U.S., 1999. Processes of magma/wet sediment interaction in a large-scale Jurassic andesitic peperitic complex, northern Sierra Nevada, California. Bulletin of Volcanology, 60: 610-626.

Head, J.W., III and Wilson, L., 2002. Deep submarine pyroclastic eruptions: Theory and predicted landforms and deposits. Journal of Volcanology and Geothermal Research, submitted.

Heiken, G. and Wohletz, K., 1985. Volcanic Ash. University of California Press, Berkeley, 246 pp.

Hekinian, R. et al., 2000. Deep sea explosive activity on the Mid-Atlantic Ridge near 34°50'N: magma composition, vesicularity and volatile content. Journal of Volcanology and Geothermal Research, 98: 49-77.

Helmstaedt, H., Padgham, W.A. and Grophy, J.A., 1986. Multiple dykes in lower Kam group, Yellowknife greenstone belt: evidence for Archean sea floor spreading? Geology, 14: 562-566.

Hess, K.-U. and Dingwell, D.B., 1996. Viscosities of hydrous leucogranitic melts: A non-Arrhenian model. American Mineralogist, 81: 1297-1300.

Hill, R.E.T., Barnes, S.J., Gole, M.J. and Dowling, S.E., 1995. The volcanology of komatiites as deduced from field relationships in the Norseman-Wiluna greenstone belt, Western Australia. Lithos, 34: 159-188.

Hollings, P., Wyman, D. and Kerrich, R., 1999. Komatiite-basalt-rhyolite volcanic associations in Northern Superior Province greenstone belts: significance of plume-arc interaction in the generation of the proto continental Superior Province. Lithos, 46: 137-161.

Hunns, S.R. and McPhie, J., 1999. Pumiceous peperite in a submarine volcanic succession at Mount Chalmers, Queensland. Australia. Journal of Volcanology and Geothermal Research, 88: 239-254.

Iizasa, K., Fsike, R.S., Ishizuka, O., Yuasa, M., Hashimoto, J., Ishibashi, J., Naka, J., Horii, Y., Fujiwara, Y., Imai, A. and Koyama, S., 1999. A Kuroko-type polymetallic sulfide deposit in a submarine silicic caldera. Science, 283: 975-977.

Imreh, L., 1974a. L'esquisse géologique de sillon serpentinitique archéen de La Motte-Vassan. DP 232, Ministère de l'Énergie et des Ressources du Québec.

Imreh, L., 1974b. L'utilisation des coulées ultrabasiques dans la recherche minière: esquisse structurale et lithostratigraphique de La Motte-Vassan, Abitibi-Est, Québec, Canada. 38-2, Ministère de l'Énergie et des Ressources du Québec.

Imreh, L., 1974c. Le sillon serpentinitique de La Motte, comté d'Abitibi-Est. DP 215, Ministère de l'Énergie et des Ressources du Québec.

Imreh, L., 1976. Nouvelle lithostratigraphie à l'ouest de Val d'Or et son incidence gîtologique. DP 349, Ministère de l'Énergie et des Ressources du Québec.

Imreh, L., 1985. Sillon de La Motte-Vassan et son avant-pays méridional: Synthèse volcanologique. lithostratigraphique et gîtologie. MM-82-04, pp. 72, Ministère de L'Énergie et des Ressources, Québec.

Jackson, S.L., Fyon, J.A. and Corfu, F., 1994. Review of Archean supracrustal assemblages of the southern Abibiti greenstone belt in Ontario, Canada: products of microplate interactions within a large-scale plate-tectonic setting. Precambrian Research, 65: 183-205.

Jensen, L.S. and Pyke, D.R., 1982. Komatiites in the Ontario portion of the Abitibi Belt. In: N.T. Arndt and E.G. Nisbet (Editors), Komatiites. George Allen and Unwin, pp. 147-157.

Kano, K., 1989. Interactions between andesitic magma and poorly consolidated sediments; examples in the Neogene Shirahama Group, south Izu, Japan. Journal of Volcanology and Geothermal Research, 37: 59-75.

Kano, K., 1991. Miocene pillowed sills in the Shimane Peninsula, SW Japan. Journal of Volcanology and Geothermal Research, 48: 359-366.

Kano, K., 1996. A Miocene coarse volcaniclastic mass-flow deposit in the Shimane Peninsula, SW Japan: a product of a deep submarine eruption? Bulletin of Volcanology, 58: 131-143.

Kano, K., Takahiro, K., Yamamoto, T. and Hoshizumi, H., 1991. Subaqueous rhyolite block lavas in the Miocene Ushikiri Formation, Shimane Peninsula, SW Japan. Journal of Volcanology and Geothermal Research, 46: 241-253.

Kano, K., Yamamoto, T. and Takeuchi, K., 1993. A Miocene island-arc volcanic seamount: the Takashibiyama Formation, Shimane Peninsula, SW Japan. Journal of Volcanology and Geothermal Research, 59: 101-119.

Kerrich, R. and Wyman, D.A., 1996. The trace element systematics of igneous rocks in mineral exploration: An overview. In: D.A. Wyman (Editor), Trace Element Geochemistry of Volcanic Rocks: Applications for Massive Sulphide Exploration. GAC Short Course Notes, Winnipeg, Manitoba, pp. 1-50.

Kimura, G., Ludden, J.L., Desrochers, J.-P. and Hori, R., 1993. A model of ocean-crust accretion for the Superior Province, Canada. Lithos, 30: 337-355.

Kokelaar, B.P., 1982. Fluidization of wet sediments during the emplacement and cooling of various igneous bodies. Journal of the Geological Society of London, 139: 21-33.

Kokelaar, B.P., 1983. The mechanism of Surtseyan volcanism. Journal of the Geological Society of London, 140: 939-944.

Kokelaar, B.P. and Durant, G.P., 1983. The submarine eruption of Surtle (Surtsey, Iceland). Journal of Volcanology and Geothermal Research, 19: 239-246.

Kokelaar, P., 1986. Magma-water interactions in subaqueous and emergent basaltic volcanism. Bulletin of Volcanology, 48: 275-289.

Kusky, T.M. and Polat, A., 1999. Growth of granite-greenstone terranes at convergent margins, and stabilzation of Archean cratons. Tectonophysics, 305: 43-73.

Lafrance, B., Mueller, W.U., Daigneault, R. and Dupras, N., 2000. Evolution of a submerged composite arc volcano: volcanology and geochemistry of the Normétal volcanic complex, Abitibi greenstone belt, Québec, Canada. Precambrian Research, 101: 277-311.

Latulippe, M., 1966. The relationship of mineralization to Precambrian stratigraphy in certain mining areas of Ontario and Quebec. Geological Association of Canada(Special Paper 3): 21-41.

Legault, M., Gauthier, M., Jébrak, M., Davis, D.W. and Baillargeon, F., 2002. Evolution of the subaqueous to near-emergent Joutel volcanic complex, Northern Volcanic Zone, Abitibi Subprovince, Québec, Canada. Precambrian Research, 115: 187-221.

Le Maitre, R.W. (Editor). Igneous rocks: IUGS classification and glossary of terms. London, Cambridge University Press, 236 pp.

Lofgren, G., 1971a. Experimentally produced devitrification textures in natural rhyolitic glass. Geological Society of America Bulletin, 82: 111-124.

Lofgren, G., 1971b. Spherulitic textures in glassy and crystalline rocks. Journal of Geophysical Research, 76: 5635-5648.

Lofgren, G., 1974. An experimental study of plagioclase crystal morphology: isothermal crystallization. American Journal of Science, 274: 243-273.

Lonsdale, P. and Batiza, R., 1980. Hyaloclastite and lava flows on young seamounts examined with a submersible. Geological Society of America Bulletin, 91: 545-554.

Lowe, D.R., 1982. Sediment gravity flows: II. depositional models with special reference to the deposits of high-density turbidity currents. Journal of Sedimentary Petrology, 52: 279-297.

Lowe, D.R., 1988. Suspended-load fallout rate as an independent variable in the analysis of current structures. Sedimentology, 35: 765-776.

Ludden, J. and Hubert, C., 1986. Geologic evolution of the Late Archean Abitibi greenstone belt of Canada. Geology, 14: 707-711.

Maicher, D., 2002. Deep-sea Limu o Pele: the signifiance of bull-wall shards in hyaloclastite deposits. In: A.G. Union (Editor), Explosive Subaqueous Volcanism. American Geophysical Union, Dunedin, New Zealand, pp. 19-20.

Maicher, D., White, J.D.L. and Batiza, R., 2000. Sheet hyaloclastite: density currents deposits of quench and bubble-burst fragments from thin, glassy sheet lava flows, Seamount Six, Eastern Pacific Ocean. Marine Geology, 171: 75-94.

Mandeville, C.W., Carey, C.N., Sigurdsson, H. and King, J., 1994. Paleomagnetic evidence for high-temperature emplacement of the 1883 subaqueous pyroclastic flows from Krakatau Volcano, Indonesia. Journal of Geophysical Research, 99: 9487-9504.

Mandeville, C.W., Carey, S. and Sigurdsson, H., 1996. Sedimentology of the Krakatau 1883 submarine pyroclastic deposits. Bulletin of Volcanology, 57: 512-529.

Manley, C.R., 1992. Extended cooling and viscous flow of large, hot rhyolite lavas: implications of numerical modeling results. Journal of Volcanology and Geothermal Research, 53: 27-46.

Manley, C.R. and Fink, J., 1987. Internal textures of rhyolite lava flows as revealed by research drilling. Geology, 15: 549-552.

McBirney, A.R., 1963. Factors governing the nature of submarine volcanism. Bulletin of Volcanology, 26: 457-469.

McBirney, A.R. and Murase, T., 1984. Rheological properties of magmas. Annual reviews Earth and Planetary Sciences, 12: 337-357.

McDonough, W.F. and Sun, S.-s., 1995. The composition of the Earth. Chemical Geology, 120: 223-253.

McPhie, J., 1993. The Tennant Creek porphyry revisited: A synsedimentary sill with peperite margins, Early Proterozoic, Northern Territory. Australian Journal of Earth Science, 40: 545-558.

McPhie, J., 1995. A Pliocene basaltic seamount: Ba Volcanic Group at Rakiraki, Fiji. Journal of Volcanology and Geothermal Research, 64: 193-210.

McPhie, J., Doyle, M. and Allen, R., 1993. Volcanic textures: A guide to the interpretation of textures in volcanic rocks. University of Tasmania, Centre for Ore Deposit and Exploration Studies, 198 pp.

Meinert, L.D., 1998. A review of skarns that contain gold. In: D.R. Lentz (Editor), Mineralized intrusion-related skarn systems. Mineralogical Association of Canada, Quebec City, pp. 359-414.

Minakami, T., Ishikawa, T. and Yagi, K., 1951. The 1944 eruption of Volcano Usu in Hokkaido, Japan. Bulletin of Volcanology, 11: 45-160.

Miyabuchi, Y., 1999. Deposits associated with the 1990-1995 eruption of Unzen Volcano, Japan. Journal of Volcanology and Geothermal Research, 89: 139-158.

Moore, J.G., 1975. Mechanism of formation of pillow lava. American Scientist, 63: 269-277.

Moore, J.G., 1985. Structure and eruptive mechanisms at Surtsey volcano, Iceland. Geological Magazine, 122: 649-661.

Moore, J.G., Phillips, R.L., Grigg, R.W., Peterson, D.W. and Swanson, D.A., 1973. Flow of lava into the sea 1969-1971, Kilauea Volcano, Hawaii. Geological Society of America Bulletin, 84: 537-546.

Moore, J.G. and Tepley, L., 1974. Fire Under the Sea: the Origin of Pillow Lavas. Moonlight Productions.

Morrissey, M., Zimanowski, B., Wohletz, K. and Buettner, R., 2000. Phreatomagmatic fragmentation. In: H. Sigurdsson (Editor), Encyclopedia of Volcanoes. Academic Press, pp. 431-446.

Mortensen, J.K., 1993a. U-Pb geochronology of the eastern Abitibi Subprovince. Part 1: Chibougamu-Matagami-Joutel region. Canadian Journal of Earth Sciences, 30: 11-28.

Mortensen, J.K., 1993b. U-Pb geochronology of the eastern Abitibi Subprovince. Part 2: Noranda-Kirkland Lake area. Canadian Journal of Earth Sciences, 30: 29-41.

Mueller, W., Chown, E.H., Sharma, K.N.M., Tait, L. and Rocheleau, M., 1989. Paleogeographic and paleotectonic evolution of a basement-controlled Archean

supracrustal sequence, Chibougamau-Caopatine, Quebec. Journal of Geology, 60: 273-300.

Mueller, W. and Donaldson, J.A., 1992. Development of sedimentary basins in the Archean Abitibi belt, Canada: an overview. Canadian Journal of Earth Sciences, 29: 2249-2265.

Mueller, W. and White, J.D.L., 1992. Felsic fire-fountaining beneath Archean Seas: pyroclastic deposits of the 2730 Ma Hunter Mine Group, Quebec, Canada. Journal of Volcanology and Geothermal Research, 54: 117-134.

Mueller, W.U., Chown, E.H. and Thurston, P.C., 2000a. Processes in physical volcanology and volcaniclastic sedimentation: modern and ancient. Precambrian Research, 101: 81-85.

Mueller, W.U., Daigneault, R., Mortensen, J.K. and Chown, E.H., 1996. Archean terrane docking: upper crust collision tectonics, Abitibi greenstone belt, Quebec, Canada. Tectonophysics, 265: 127-150.

Mueller, W.U., Garde, A.A. and Stendal, H., 2000b. Shallow-water, eruption-fed, mafic pyroclastic deposits along a paleoproterozoic coastline: Kangerluluk volcano-sedimentary sequence, southeast Greenland. Precambrian Research, 101: 163-192.

Mueller, W.U. and Mortensen, J.K., 2002. Age constraints and characteristics of subaqueous volcanic construction , the Archean Hunter Mine Group, Abitibi greenstone belt. Precambrian Research, 115: 119-152.

Németh, K. and White, J.D.L., 2003. Reconstructing eruption processes of a Miocene monogenetic volcanic field from vent remnants: Waipiata Volcanic Field, South Island, New Zealand. Journal of Volcanology and Geothermal Research, 124: 1-21.

Norman, G.W.H., 1943. Bourlamaque Township, Abitibi county, Québec. Paper 43-2, Geological Survey of Canada.

Norman, G.W.H., 1947a. Dubuisson, Bourlamaque, Louvicourt, Abitbi County, Québec, Geological Survey of Canada, paper 47-20.

Norman, G.W.H., 1947b. Vauquelin, Pershing and Haig Townships, Geological Survey of Canada, paper 47-12.

Orton, G.J., 1996. Volcanic environments. In: H.G. Reading (Editor), Sedimentary Environments; Processes, facies, and Stratigraphy. Blackwell, Oxford, pp. 485-567.

Parman, S.W. and Grove, T.L., in press. Komatiites in the plume debate. In; Penrose Conference, Plume IV: Beyond the Plume Hypothesis, Geological Society of America, Iceland.

Parman, S.W., Grove, T.L., and Dann, J.C., 2001. The production of Barberton komatiites in an Archean subduction zone. Geophysical Research Letters, 28, pp. 2513-2516.

Parker, S.P. (Editor), 1997. Dictionary of Earth Science. McGraw-Hill, 468 pp.

Pearce, J.A., 1996. A user's guide to basalt discrimination diagrams. In: D.A. Wyman (Editor), Trace Element Geochemistry of Volcanic Rocks: Applications for Massive Sulphide Exploration. GAC Short Course Notes, Winnipeg, Manitoba, pp. 79-113.

Pearce, J.A. and Cann, J.R., 1973. Tectonic setting of basic volcanic rocks determined using trace element analysis. Earth and Planetary Science Letters, 19: 290-300.

Pearce, J.A. and Peate, D.W., 1995. Tectonic implications of the composition of volcanic arc magmas. Annual Reviews of Earth and Planetary Science, 23: 251-285.

Péloquin, A.S., Verpaelst, P. and Ludden, J.N., 1996. Spherulitic rhyolites of the Archean Blake River Group, Canada: Implications for stratgraphic correlation and volcanogenic massive sulphide exploration. Economic Geology, 91: 343-354.

Pichler, H., 1965. Acid-hyaloclastites. Bulletin of Volcanology, 28: 293-310.

Pilote, P., Scott, C.R., Mueller, W.U., Lavoie, S. and Riopel, P., 1999. Géologie des formations Val-d'Or, Héva et Jacola: nouvelle interprétation du Groupe de Malartic, Ministere de l'Energie et des Ressources, Quebec, pp. 52.

Polat, A. and Kerrich, R., 2001. Geodynamic processes, continental growth, and mantle evolution recorded in late Archean greenstone belts of the southern Superior Province, Canada. Precambrian Research, 112: 5-25.

Polat, A., Kerrich, R. and Wyman, D.A., 1998. The late Archean Schreiber-Hemlo and White River-Dayohessarah greenstone belts, Superior Province: collages of oceanic plateaus, oceanic arcs, and subduction-accretion complexes. Tectonophysics, 289: 295-326.

Prothero, D.R. and Schwab, F., 1996. Sedimentary Geology. W.H. Freeman and Company, 575 pp.

Prud'Homme, N., 1996. Report on Power Stripping Program, Bourlamaque Township, Québec. Project 526A/526B, New Bidlamaque/Union Gold Option, Placer Dome Canada Limited, Val d'Or.

Riggs, N.R. and Busby-Spera, C.J., 1990. Evolution of a multi-vent volcanic complex within a subsiding arc graben depression: Mount Wrightson Formation, Arizona. Geol. Soc. Amer. Bull., 102: 114-1135.

Rittman, A., 1962. Volcanoes and their activity. John Wiley and Sons, New York, 305 pp.

Rollinson, H., 1993. Using Geochemical Data: evaluation, presentation, interpretation. Longman Geochemistry Series. Longman Scientific & Technical, Harlow, England, 352 pp.

Sauvé, P., 1995. Les dacites sphérolitiques de Norman.

Schumacher, R. and Schmicke, H.-U., 1995. Models for the origin of accretionary lapilli. Bulletin of Volcanology, 56: 626-639.

Scott, C.R., Mueller, W.U. and Pilote, P., 2002a. Inferred deep-water eruptive processes from the Archean Val d'Or Formation, Abitibi Greenstone Belt, Québec, Canada. In: A.G. Union (Editor), Explosive Subaqueous Volcanism. American Geophysical Union, Dunedin, New Zealand, pp. 28-29.

Scott, C.R., Mueller, W.U. and Pilote, P., 2002b. Physical volcanology, stratigraphy, and lithogeochemistry of an Archean volcanic arc: Evolution from plume-related volcanism to arc-rifting of SE Abitibi Greenstone Belt, Val d'Or, Canada. Precambrian Research, 115: 223-260.

Scott, C.R., Richard, D. and Fowler, A.D., 2003. An Archean submarine pyroclastic flow due to submarine dome collapse: the Hurd deposit, Harker Township, Ontario, Canada. In: J.D.L. White, J.L. Smellie and D. Clague (Editors), Explosive Subaqueous Volcanism. American Geophysical Union, Monograph 140, pp. 317-328.

Scutter, C.R., Cas, R.A.F., Moore, C.L. and de Rita, D., 1998. Facies architecture and origin of a submarine rhyolitic lava flow-dome complex, Ponza, Italy. Journal of Geophysical Research, 103(B11): 27,551-27,566.

Sharpe, J.I., 1968. Canton de Louvicourt. Rapport Géologique 135, Ministére des Richesses Naturelles du Québec.

Shaw, H.R., 1974. Diffusion of H_2O in granitic liquids. Part I. Experimental data: Part II. Mass transfer in magma chambers. In: B.J.G. A.W. Hofmann, H.S. Yoder, Jr, R.A. Yund (Editor), Geochemical transport and kinetics. Carn, Inst. Wash., pp. 139-170.

Shelly, D., 1993. Igneous and metamorphic rocks under the microscope: classification, textures, microstructures and mineral preferred orientations. Chapman & Hall, 445 pp.

Sheridan, M.F. and Wohletz, K.H., 1983. Hydrovolcanism: basic considerations and review. Journal of Volcanology and Geothermal Research, 17: 1-29.

Simpson, K. and McPhie, J., 2001. Fluidal-clast breccia generated by submarine fire fountaining, Trooper Creek Formation, Queensland, Australia. Journal of Volcanology and Geothermal Research, 109: 339-355.

Skilling, I.P., White, J.D.L. and McPhie, J., 2002. Peperite: a review of magma-sediment mingling. Journal of Volcanology and Geothermal Research, 114: 1-17.

Sleep, N.H. and Windley, B.F., 1982. Archean plate tectonics: constraints and inferences. Journal of Geology, 90: 363-379.

Smith, J.R., Taylor, B., Malahoff, A. and Peterson, L., 1990. Submarine volcanism in the Sumisu Rift, Izu-Bonin arc: submersible and deep-tow camera results. Earth and Planetary Science Letters, 100: 148-160.

Smith, R.L., 1960. Ash flows. Geological Society of America Bulletin, 71: 795-842.

Smith, T.L. and Batiza, R., 1989. New field and laboratory evidence for the origin of hyaloclastite flows on seamounts summits. Bulletin of Volcanology, 51: 96-114.

Sproule, R.A., Lesher, C.M., Ayer, J.A., Thurston, P.C., and Herzberg, C.T., 2002. Spatial and temporal variations in the geochemistry of komatiites and komatiitic basalts in the Abitibi greenstone belt. Precambrian Research, 115: 153-186.

Staudigel, H. and Schminke, H.-U., 1984. The Pliocene seamount series of La Palma/Canary Islands. Journal of Geophysical Research, 89(No. B13): 11195-11215.

Stern, R.A., Percival, J.A. and Mortensen, J.K., 1994. Geochemical evolution of the Minto block: A 2.7 Ga continental magmatic arc bulit on the Superior protocraton. Precambrian Research, 65: 115-153.

Stern, R.J. and Bloomer, S.H., 1992. Subduction zone infancy: Examples from the Eocene Izu-Bonin-Mariana and Jurassic California arcs. Geological Society of America Bulletin, 104: 1621-1636.

Stix, J., 1991. Subaqueous, intermediate to silicic-composition explosive volcanism: a review. Earth-Science Reviews, 31: 21-53.

Storey, m., Mahoney, J.J., Kroenke, L.W. and Saunders, A.D., 1991. Are oceanic plateaus sites of komatiite formation? Geology, 19: 376-379.

Swanson, S.E., Naney, M.T., Westrich, H.R. and Eichlberger, J.C., 1989. Crystallization history of Obsidian Dome, Inyo Domes, California. Bulletin of Volcanology, 51: 161-176.

Taira, A., Pickering, K.T., Windley, B.F. and Soh, W., 1992. Accretion of Japanese island arcs and implications for the origin of Archean greenstone belts. Tectonics, 11(No. 6): 1224-1244.

Tanner, L.H. and Calvari, S., 1999. Facies analysis and depositional mechanisms of hydroclastite breccias, Acicastello, eastern Sicily. Sedimentary Geology, 129: 127-141.

Tanner, L.H. and Hubert, J.F., 1991. Basalt breccias and conglomerates in the lower Jurassic McCoy Brook Formation, Fundy Basin, Nova Scotia: differentiation of talus and debris-flow deposits. Journal of Sedimentary Petrology, 61: 15-27.

Taylor, B. et al., 1990. ALVIN-SeaBeam studies of the Sumisu Rift, Izu-Bonin arc. Earth and Planetary Science Letters, 100: 127-147.

Thurston, P.C., 1994. Archean volcanic patterns. In: K.C. Condie (Editor), Archean Crustal Evolution. Elsvier, pp. 45-84.

Thurston, P.C. and Chivers, K.M., 1990. Secular variations in greenstone sequence development emphasizing Superior Province, Canada. Precambrian Research, 46: 21-58.

Ui, T., Matsuwo, N., Sumita, M. and Fujinawa, A., 1999. Generation of block and ash flows during the 1990-1995 eruption of Unzen Volcano, Japan. Journal of Volcanology and Geothermal Research, 89: 123-137.

Vergniolle, S. and Mangan, M., 2000. Hawaiian and strombolian eruptions. In: H. Sigurdsson (Editor), Encyclopedia of Volcanoes. Academic Press, pp. 447-461.

Walker, G.P.L., 1992. Morphometric study of pillow-size spectrum among pillow lavas. Bulletin of Volcanology, 54: 459-474.

Wallace, P. and Anderson, J., A.T., 2000. Volatiles in magmas. In: H. Sigurdsson (Editor), Encyclopedia of Volcanoes. Academic Press, pp. 149-170.

Wharton, M.R., Hathway, B. and Colley, H., 1995. Volcanism associated with extension in an Oligocene-Miocene arc, southwestern Viti Levu, Fiji. In: J.L. Smelli (Editor), Volcanism associated with extension at consuming plate margins. Special Publication of the Geological Society of London, pp. 95-114.

White, J.D.L., 1996a. Impure coolants and interaction dynamics of phreatomagmatic eruptions. Journal of Volcanology and Geothermal Research, 74: 155-170.

White, J.D.L., 1996b. Pre-emergent construction of a lacustrine basaltic volcano, Pahvant Butte, Utah (USA). Bulletin of Volcanology, 58: 249-262.

White, J.D.L., 2000. Subaqueous eruption-fed density currents and their deposits. Precambrian Research, 101: 87-109.

White, J.D.L., Clague, D. and Houghton, B., 2002. Explosive Subaqueous Volcanism. In: A.G. Union (Editor), Chapman Conference. American Geophysical Union, Dunedin, New Zealand, pp. 40.

White, J.D.L., Smellie, J.L. and Clague, D.A. (Editors), 2003. Explosive Subaqueous Volcanism. Geophysical Monograph, 140. AGU, 370 pp.

White, M.J. and McPhie, J., 1996. Stratigraphy and palaeovolcanology of the Cambrian Tyndall Group, Mt Read Volcanics, western Tasmania. Australian Journal of Earth Science, 43: 147-159.

Whitham, A.G. and Sparks, R.S.J., 1986. Pumice. Bulletin of Volcanology, 48: 209-223.

Wilson, M., 1989. Igneous Petrogenesis. Unwin Hyman, London, 466 pp.

Wilson, A.H. and Versfeld, J.A., 1994. The early Archaean Nondweni greenstone belt, southern Kaapvaal Craton, South Africa; Part II, Characteristics of the volcanic rocks and constraints on magma genesis. Precambrian Research, 67: 277-320.

Wohletz, K., 2002. Water/magma interaction: some theory and experiments on peperite formation. Journal of Volcanology and Geothermal Research, 114: 19-35.

Wohletz, K.H., 1983. Mechanisms of hydrovolcanic pyroclast formation: grain-size, scanning electron microscopy, and experimental studies. In: M.F. Sheridan and F. Barberi (Editors), Explosive Volcanism. Journal of Volcanology and Geothermal Research, pp. 31-63.

Wohletz, K.H., 1986. Explosive magma-water interactions: Thermodynamics, explosion mechanisms, and field studies. Bulletin of Volcanology, 48: 245-264.

Wohletz, K.H. and McQueen, R.G., 1984. Experimental studies in hydromagmatic volcanism, Studies in Geophysics: Explosive volcanism: Inception, evolution and hazards. National Academy Press, Washington, pp. 158-169.

Wohletz, K.H. and Sheridan, M.F., 1983. Hydrovolcanic explosions II: Evolution of basaltic tuff rings and tuff cones. American Journal of Science, 283: 385-413.

Wong, L., Davis, D.W., Krogh, T.E. and Robert, F., 1991. U-Pb zircon and rutile chronology of Archean greenstone formation and gold mineralization in the Val d'Or region, Quebec. Earth and Planetary Science Letters, 104: 325-336.

Wood, D.A., 1980. The application of a Th-Hf-Ta diagram to problems of tectonomagmatic classification and to establishing the nature of crustal contamination of basaltic lavas of the British tertiary volcanic province. Earth Planetary Science Letters, 50: 11-30.

Wright, I.C., de Ronde, C.E.J., Faure, K. and Gamble, J.A., 1998. Discovery of hydrothermal sulfide mineralization from southern Kermadec arc volcanoes (SW Pacific). Earth and Planetary Science Letters, 164: 335-343.

Wright, I.C. and Gamble, J.A., 1999. Southern Kermadec submarine caldera formation by effusive and pyroclastic eruption. Marine Geology, 161: 207-227.

Wyman, D.A., 1999. A 2.7 Ga depleted tholeiite suite: evidence of plume-arc interaction in the Abitibi Greenstone Belt, Canada. Precambrian Research, 97: 27-42.

Wyman, D.A., Bleeker, W. and Kerrich, R., 1999a. A 2.7 Ga plume, proto-arc, to arc transition and the geodynamic setting of the Kidd Creek deposit: evidence from precise ICP MS trace element data. Economic Geology Monograph, 10.

Wyman, D.A., Kerrich, R. and Groves, D.I., 1999b. Lode gold deposits and Archean mantle plume-island arc interaction, Abitibi Subprovince, Canada. Journal of Geology, 107: 715-725.

Yamada, E., 1984. Subaqueous pyroclastic flows: their development and their deposits. In: B.P. Kokelaar and M.F. Howells (Editors), Marginal Basin Geology. Spec. Publ. Geol. Soc. London, pp. 29-35.

Yamagishi, H., 1987. Studies on the Neogene subaqueous lavas and hyaloclastites in southwest Hokkaido. Hokkaido Geological Survey Report 59.

Yamagishi, H. and Dimroth, E., 1985. A comparison of Miocene and Archean rhyolite hyaloclastites: evidence for a hot and fluid rhyolite lava. Journal of Volcanology and Geothermal Research, 23: 337-355.

Zimanowski, B. and Buttner, R., 2002. Dynamic mingling of magma and liquefied sediments. Journal of Volcanology and Geothermal Research, 114: 37-44.

Zimanowski, B., Buttner, R. and Lorenz, V., 1997. Premixing of magma and water in MFCI experiments. Bulletin of Volcanology, 58: 491-495.

Zimanowski, B., Frohlich, G. and Lorenz, V., 1991. Quantitative experiments on phreatomagmatic explosions. Journal of Volcanology and Geothermal Research, 48: 341-358.

APPENDICES

A-1

Sample ID: CS97-246A

Formation: Jacola Formation

Location: Highway 117, west of Val d'Or

Lithology: Massive flow

Significance: Part of submarine lava plain

Physical Description: Massive, highly crystalline flow

PETROGRAPHY

Constituents	Description	Amount
Olivine(?)	Completely altered to a bluish mineral phase; equant crystals that measure upwards to 500 μm.	> 30%
Pyroxene	Tabular- to lath-shaped microphenocrysts that are completely altered. Measure upwards to 1 mm with an average of 600-700 μm.	> 30%
Chlorite	Comprises the groundmass.	> 30%

Important Characteristics (textures, etc.)

Massive, crystalline structure that is highly altered. Some relict blades of pyroxene that are altered to amphibole that may represent stringbeef spinifex (?).

Interpretation(s)

Part of an ultramafic flow that was slightly lower temperature that only permitted growth of pyroxene spinifex.

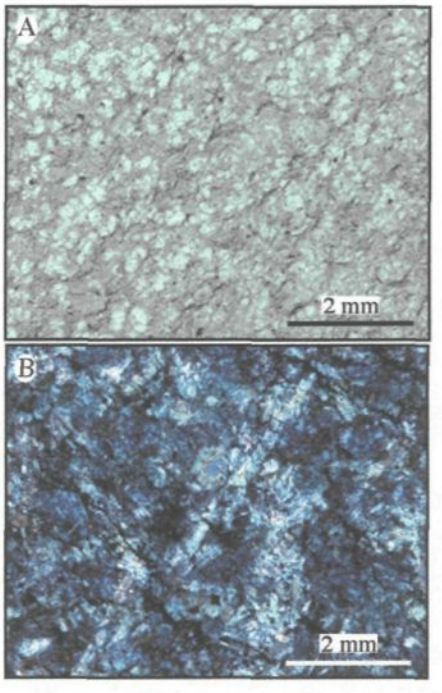

Microphotograph(s)

(A) Plane polarized light (2.5X) photo of equant altered microphenocrysts of olivine (?) in a chloritized matrix.

(B) Cross-Nicols photo of same field of view as (A) depicted bladed amphibole that may represent former stringbeef pyroxene.

A-2

Sample ID: CS97-246C

Formation: Jacola Formation

Location: Highway 117, east of Val d'Or

Lithology: Massive mafic/ultramafic flow

Significance: Forming part of submarine lava plain

Physical Description: Highly crystallized lava

PETROGRAPHY

Constituents	Description	Amount
Pyroxene	Tabular to blocky, mm-sized phenocrysts	> 30%
Plagioclase	Highly altered tabular to blocky, mm-sized crystals. Altered to sericite. Albite and Carlsbad twinning common.	> 30%
Olivine (?)	Bluish alteration patches of possible former olivine.	< 5%

Important Characteristics (textures, etc.)

Near complete crystalline structure.

Interpretation(s)

Massive lava flow; probably central part where cooling was significantly lower, which permitted near complete crystallization of mm-sized crystals.

Microphotograph(s)

(A) Plane polarized light photo (2.5X) showing crystalline structure of massive flow with plagioclase and pyroxene.

(B) Cross-Nicols photo of same field of view in (A).

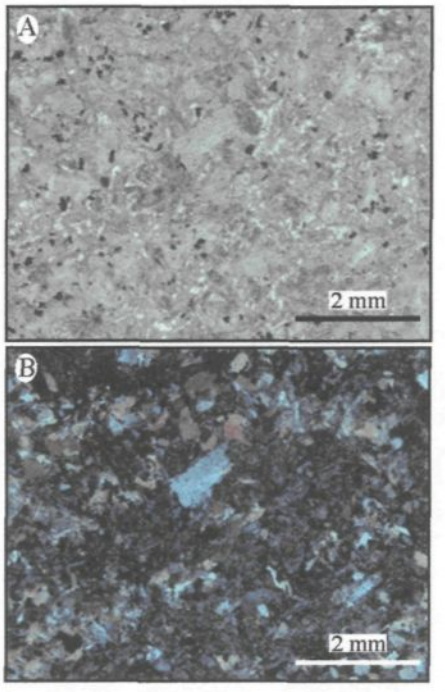

A-3

Sample ID: CS99-2497A

Formation: Jacola Formation

Location: West of Val d'Or

Lithology: Autoclastic tuff breccia

Significance: Water-interaction

Physical Description: In situ breccia.....

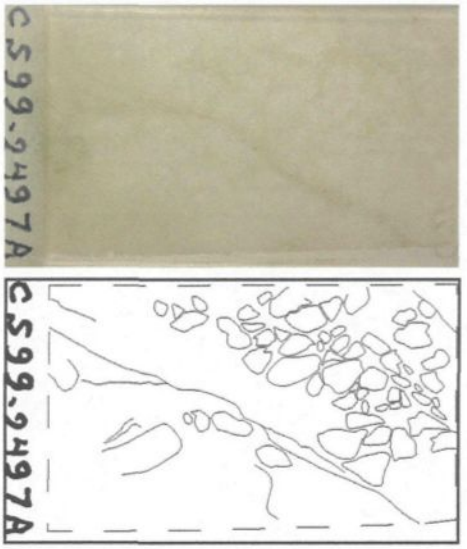

PETROGRAPHY

Constituents	Description	Amount
Groundmass	Carbonate + chlorite ± albite ± quartz	> 70-vol%
Chloritoid	High-relief, bluish-yellow birefringence. Euhedral to subhedral, μm-sized tabular microphenocrysts.	< 2-vol%
Feldspar (?)	Completely altered to sericite, only ghost crystal forms visible that may have been feldspar.	< 2-vol%

Important Characteristics (textures, etc.)

Very fine-grained, re-crystallized groundmass of an in situ breccia of possible ultramafic lava.

Interpretation(s)

Fine-grained nature and in situ character suggest a possible margin of ultramafic lava that interacted with water.

Microphotograph(s)

(A) Plane polarized light (5x) photo showing fine-grained groundmass and high-relief, euhedral microphenocrysts.

(B) Plane polarized light (2.5x) photo showing in situ character.

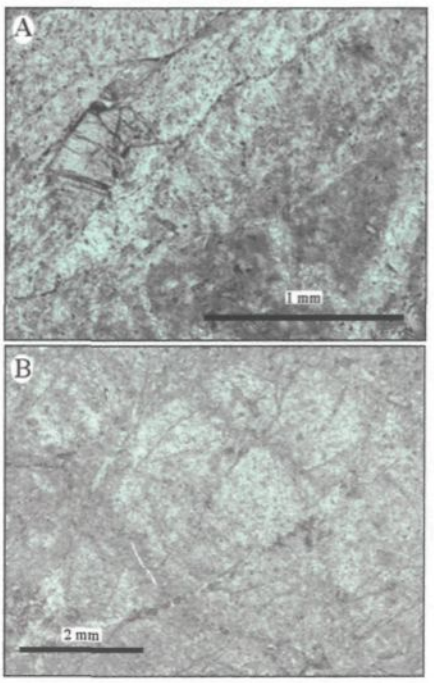

A-4

Sample ID: CS99-2466A

Formation: Val d'Or Formation (base)

Location: Playground - Val d'Or

Lithology: Breccia-sized fragment

Significance: Volatiles & hot emplacement

Physical Description: Part of clast-supported tuff breccia facies with slighly flattened amygdules in a feldspar-phyric fragment.

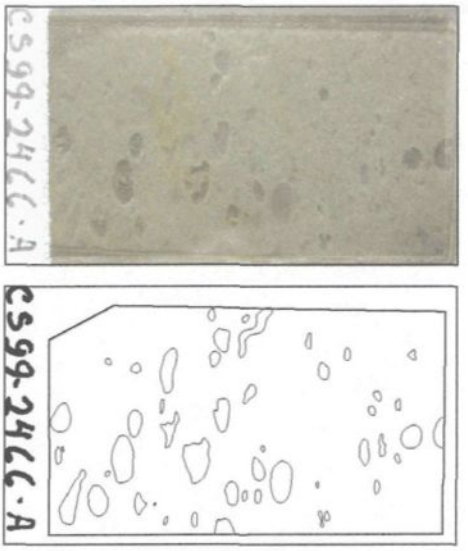

PETROGRAPHY

Constituents	Description	Amount
Plagioclase	Lath-shaped, sieved textured microphenocrysts measuring up to 1 mm in length	~ 5-vol%
Amygdules	Chlorite + quartz + carbonate filled vesicles. All are oval to slightly ellipisoidal in form and oriented in the same direction.	~ 5-10-vol%
Groundmass	Mosaic of acicular feldspar and anhedral, equant quartz with chlorite filling the interstices (> 40%)	~ 85-90-vol%

Important Characteristics (textures, etc.)

Completely chloritized section (piece of fragment) with slightly flattened vesicles. Fragment has ~5% microphenocrysts of sieved plagioclase. Thin section image shows oval shaped vesicles.

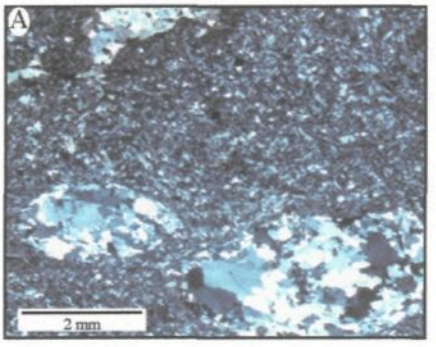

Interpretation(s)

Weakly volatile-rich fragment that was still hot after emplacement that underwent subsequent compaction.

Microphotograph(s)

A. Cross-Nicols image showing the oval nature of quartz amygdules hosted in fine-grained groundmass of feldspar and quartz.

A-5

Sample ID: CS99-2466B

Formation: Val d'Or Formation (base)

Location: Val d'Or Playground

Lithology: Intermediate volcaniclastic

Significance: Vesicular fragment with vitrophyric shards molded around feldspar.

Physical Description: Matrix and fragment

PETROGRAPHY

	Constituents	Description	Amount
FRAGMENT	Amydules	Quartz and carbonate filled vesicles.	2 -vol%
	Plagioclase	Blocky to lath-shaped, sieved 1-2 mm microphenocrysts.	5-7-vol%
	Groundmass	Quartz + chlorite + feldspar fine-grained mosaic.	
MATRIX	Feldspar	Lath- to blocky-shaped, sieved 2-8 mm microphenocrysts that have a slight orientation. Epidote is a common inclusion.	5-10-vol%
	Chlorite	Wisps that are flattened and contorted around feldspar.	>50-vol%
	Remainder	Mosaic of carbonate + quartz + feldspar + epidote	

Important Characteristics (textures, etc.)

Fragment margin characterized by fine-grained chloritized matrix. Chloritic bands are contorted and molded around denser feldspar phenocrysts in matrix.

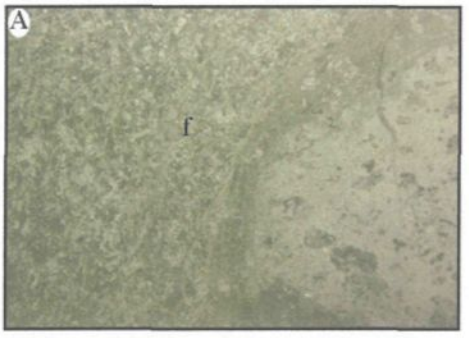

Interpretation(s)

Fine-grained, chloritized matrix along edge of fragment may be a baked contact.
Chloritic bands are possible former vitrophyric shards that are welded around denser feldspar crystals.
Crystal-rich nature of matrix suggests they have been liberated during a minor explosive event.

Microphotograph(s)

A. Macroscopic digital photo of thin section showing the nature of the contact between the vesicular fragment and matrix. Also possible to see chloritic bands molded around feldspar (f) phenocrysts in the matrix. Image is approximately3 cm-across.

A-6

Sample ID: CS98-242

Formation: Val d'Or Formation

Location: Placer Dome North

Lithology: Intermediate pillowed facies

Significance: Representative sample of lava

Physical Description: Two distinct zones based on the degree of epidote alteration.

PETROGRAPHY

Constituents	Description	Amount
Amygdules	Trace amounts of quartz amygdules within both alteration zones.	< 5-vol%
Feldspar	Trace amounts of anhedral crystals in epidote zone; groundmass of acicular feldspar microlites in non-epidote zone.	< 1 / 25-30-vol%
Epidote zone	Alteration assemblage of epidote + quartz + chlorite +/- carbonate +/- albite	
Non -epidote	Alteration assemblage of chlorite + quartz + epidote +/- albite.	

Important Characteristics (textures, etc.)

Important to note the existance of vesicles (amygdules) in these intermediate lavas. Overall fine-grained to aphyric nature is important.

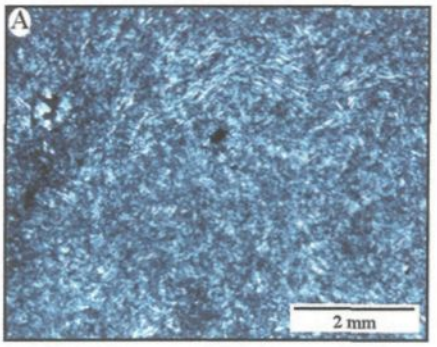

Interpretation(s)

Vesicularity indicates some exsolution of gas, which is necessary for the possible explosive fragmentation of the overlying tuff facies. The fine-grained nature suggests a high temperature flow that erupted close to the solidus for feldpsar crystallization, which is reflected in the low viscosity textures of these lavas (i.e., amoebodial).

Microphotograph(s)

A. Cross-Nicols image of non-epidotized zone characterized by acicular feldspar microphenocrysts. A single quartz amygdules is also in the field of view.

A-7

Sample ID: CS98-027

Formation: Val d'Or Formation

Location: Placer Dome North

Lithology: Lapilli tuff

Significance: Vesiculated lapilli fragments

Physical Description: Finer-grained part that overlies coarser tuff breccia, part of single depositional facies.

PETROGRAPHY

Constituents	Description	Amount
Feldspar	Subhedral (?) phenocrysts that are completely altered to form relict outlines of sericite + epidote (?) liberated in the matrix.	
Matrix	Highly altered to epidote + chlorite + quartz + carbonate +/- sericite +/- albite.	
Fragment 1	Vesicular (> 35% quartz-amygdules) aphyric epidotized fragment with distinct margins (see below).	
Fragment 2	Possible relict glass fragments that are altered to the same alteration assemblage as matrix.	

Important Characteristics (textures, etc.)

Highly altered section composed of vesicular fragments, possible former vitrophyric fragments, and liberated feldspar crystals. Veiscular fragments are characterized by a μm-thick margin that is non-vesicular.

Interpretation(s)

Vesicular fragments were probably emplaced in a hot state due to the interpreted chilled margin. The quantity of amygdules and liberated feldspar crystals suggest violent disruption of a vesiculating magma, which probably followed an initial suppressed eruption forming the basal tuff breccia.

Microphotograph(s)

A. Plane polarized light photo on vesicular fragment and its distinctive chilled margin.

B. Plance polarized light photo of core of vesicular fragment.

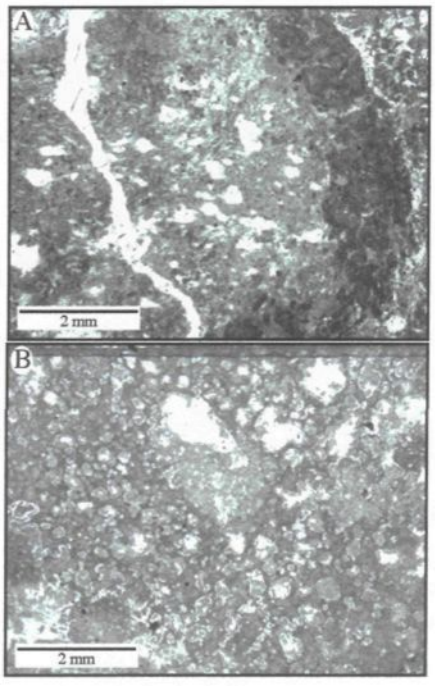

A-8

Sample ID: CS97-039

Formation: Val d'Or Formation

Location: East Sullivan outcrops

Lithology: Tuff breccia

Significance: Fragment from tuff breccia

Physical Description: Feldspar phyric, vesicular fragment from tuff breccia

PETROGRAPHY

Constituents	Description	Amount
Feldspar	Tabular to blocky, euhedral to subhedral phenocrysts that commonly are grouped to form glomerocrysts. Carlsbad twinning is common.	12.5 +/- 1.8-vol%
Amygdules	Quartz and carbonate amygdules that are typically flattened (see below)	19.9 +/- 4.4-vol%
Groundmass	Composed of alteration assemblage of fine-grained quartz + chlorite + albite.	67.7 +/- 4.2-vol%

Important Characteristics (textures, etc.)

Amount and the morphological characteristics of amygdules record pre- and post-eruptive conditions of magma/fragment. The feldspar population may be related to pillowed facies and other volcaniclastic deposits in sequence to determine, if any, a genetic relationship.

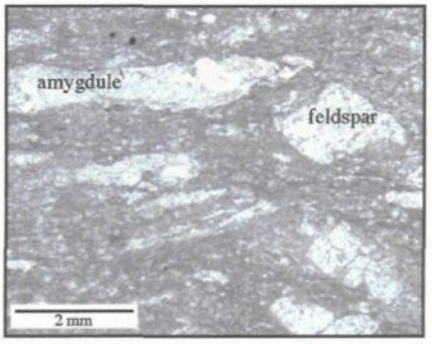

Interpretation(s)

The percentage of amygdules indicate that the magma had exsolved gas that could drive a volcanic eruption, whereas flattening probably records post-eruptive plastic deformation indicating that the fragment was still hot after deposition. Not tectonic as phenocrysts are not affected - see photo.

Microphotograph(s)

Plane polarized photo illustrating flattened character of quartz amygdules in relation to non-oriented feldspar.

A-9

Sample ID: CS97-051

Formation: Val d'Or Formation

Location: East Sullivan Outcrops

Lithology: Lapilli tuff

Significance: Fragment morphology

Physical Description: Part of vesicular lapilli fragment and matrix.

PETROGRAPHY

Constituents	Description	Amount
Feldspar	Tabular to blocky morphology with euhedral habit. Highly altered, with sericite cores. Crystals liberated in matrix are broken into smaller aggregates.	~30-vol%
Fragment	Lapilli-sized vesicular fragment re-crystallized to quartz + chlorite +/- carbonate. Edges are serrated with weak flattening.	
Matrix	Composed of fine-grained quartz + chlorite + carbonate +/- albite. Chloritic 'shards' are molded around liberated feldspar crystals	

Important Characteristics (textures, etc.)

Serrated edges (see photo) and molded features are important in regard to the fragments history. Broken, liberated feldspar crystals relate to the origin of the deposit.

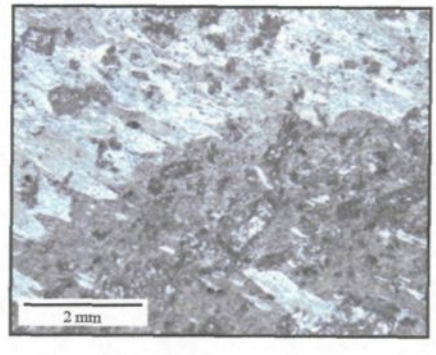

Interpretation(s)

Serrated edges of a fragment are typically related to vesicular fragments, in this case alteration has erased evidence of former vesicles, which may be further hidden by weak welding, as collapsed vesicles are molded around denser feldspar crystals. Molded tuff-sized fragments in the matrix are probably former glass shards that are also deformed around denser feldspar crystals. Broken feldspar crystals attest to violent volcanic origin.

Microphotograph(s)

Plane-polarized light photo of serrated edge of lapilli fragment with smaller flattened wisps in the matrix.

A-10

Sample ID: CS98-260A

Formation: Val d'Or Formation

Location: Pole Line

Lithology: Tuff breccia - matrix

Significance: Characterization of matrix

Physical Description: Tuff breccia with subrounded fragments that are jigsaw shaped.

PETROGRAPHY

Constituents	Description	Amount
Fragment	Subangular, lapilli-sized, feldspar-phyric fragment. Feldspar phenocrysts are tabular to blocky, with subhedral to euhedral habits hosted in quartz + albite groundmass.	
Matrix	Fine-grained mosaic of quartz + chlorite + sericite + epidote with abundant liberated, tabular to blocky, euhdral to subhedral feldspar phenocrysts, some of which appear broken.	

Important Characteristics (textures, etc.)

Feldspar phenocrysts along the fragment margin appear to be 'sticking' out into the matrix and broken edges/parts of feldspar phenocrysts liberated in the matrix appear to fit together.

Interpretation(s)

Protruding and jigsaw fitting feldspar phenocryts suggest that brecciation is probably in situ, as former crystals would be broken off during deposition and latter fragments dispersed.

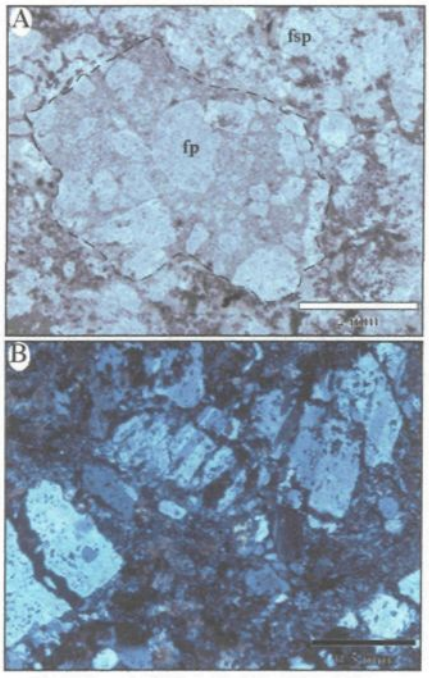

Microphotograph(s)

A. Plane polarized light photo of subangular feldspar-phyric (fp) lapilli fragment with phenocrysts protruding into the matrix, while the matrix is rich in liberated feldspar (fsp).

B. Crossed-Nicols photo of in situ fragmentation of feldspar phenocrysts hosted in the matrix.

A-11

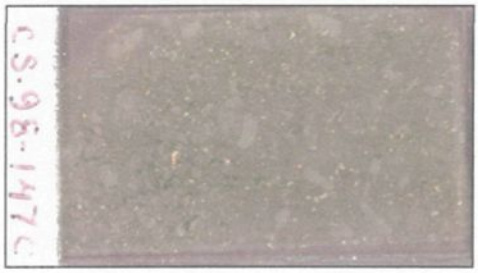

Sample ID: CS98-147C

Formation: Val d'Or Formation

Location: Camnet

Lithology: Mafic facies

Significance: Mafic facies in VDF?

Physical Description: Feldspar-phyric massive mafic facies

PETROGRAPHY

Constituents	Description	Amount
Pyroxene?	Tabular, euhedral to subhedral phenocrysts.	2-3-vol%
Feldspar	Tabular/blocky, euhedral to subhedral phenocrysts. Sericite alteration in cores and overprinting by ampibole/epdiote.	10-12-vol%
Groundmass	Re-crystallized to fine-grained mosaic of quartz + albite + chlorite.	

Important Characteristics (textures, etc.)

Presence of pyroxene....

Interpretation(s)

Pyroxene suggests a more mafic composition in comparison to other lavas in Val d'Or Formation.

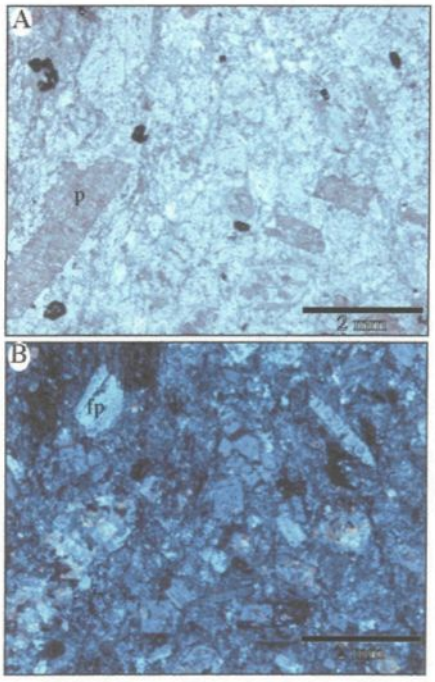

Microphotograph(s)

A. Plane polarized light photo of groundmass showing tabular pyroxene (p).

B. Crossed-Nicols photo of same view as (A), only now it is possible to discern feldspar phenocryts (fp).

A-12

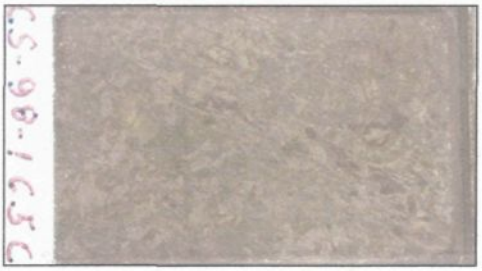

Sample ID: CS98-165C

Formation: Val d'Or Formation

Location: Camnet

Lithology: Intermediate tuff breccia

Significance: Evidence of low grade metamorphism

Physical Description: Subrounded porporphyric vesicular fragment from tuff breccia.

PETROGRAPHY

Constituents	Description	Amount
Feldspar	Tabular/blocky; euhedral/subhedral phenocrysts with Carlsbad and albite twinning. Some epidote and sericite alteration, but very fresh looking.	8-vol%
Hornblende	Tabular euhedral phenocrysts, probably former pyroxene	<2-vol%
Groundmass	Fine-grained mosaic of quartz + albite +/- chlorite. Vesicles (2-4 vol%) are filled by quartz and fibrous prehnite-pumpellyite.	

Important Characteristics (textures, etc.)

Fibrous infilling of prehnite-pumpellyite, probably after zeolites.

Interpretation(s)

Prehnite-pumpellyite alteration indicates low-grade metamorphism.

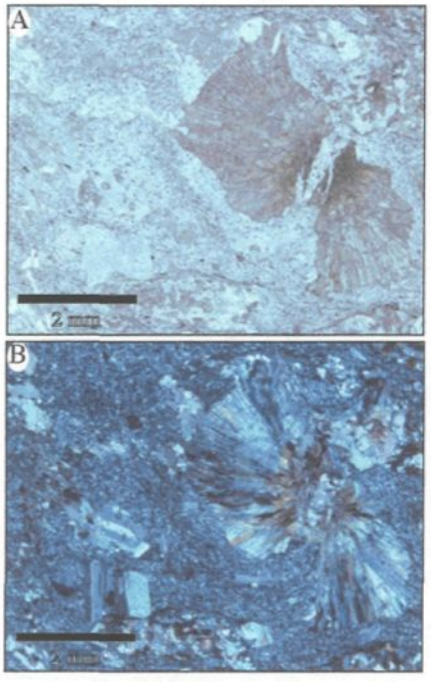

Microphotograph(s)

A. Plane polarized light photo of quartz and prehnite-pumpellyite filling vesicles.

B. Crossed-Nicols photo of same view as (A). The fibrous nature of prehnite-pumpellyite is depicted, as well as blocky feldspar and hornblende.

A-13

Sample ID: CS98-154A

Formation: Val d'Or Formation

Location: Camnet

Lithology: Intermediate lapilli tuff breccia

Significance: Character of lapilli fragments

Physical Description: Matrix-supported lapilli tuff breccia with subrounded to subangular fragments.

PETROGRAPHY

Constituents	Description	Amount
Feldspar	Broken, tabular/blocky, euhedral/subhedral phenocrysts liberated in the matrix.	15-vol%
Matrix	Fine-grained mosaic of quartz + chlorite + albite.	

Important Characteristics (textures, etc.)

Numerous lapilli-sized fragments that have been completely altered; possible to observe rare microphenocrysts of feldspar hosted in these fragments. Subrounded to subangular forms. Abundance of broken feldspar phenocrysts in matrix are important in understanding the genesis of facies.

Interpretation(s)

Broken phenocrysts suggest a violent origin for this facies.

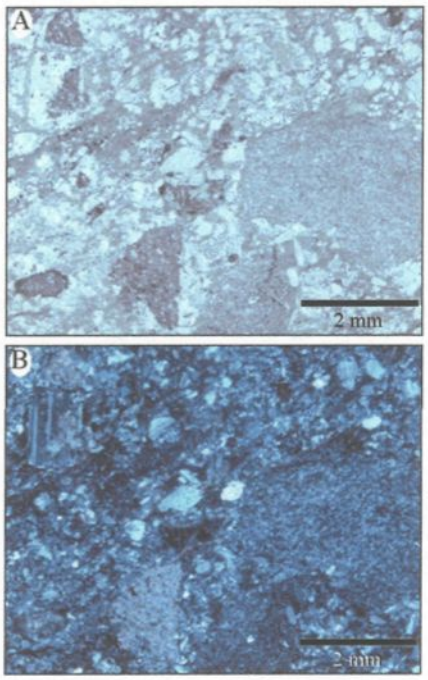

Microphotograph(s)

A. Plane polarized light photo illustrating two lapilli sized fragments and broken feldspar phenocrysts in matrix.

B. Crossed-Nicols photo of same field of view as (A).

A-14

Sample ID: CS98-154D

Formation: Val d'Or Formation

Location: Camnet

Lithology: Laminated FP facies

Significance: Abundance of broken feldspar phenocrysts

Physical Description: Fine-grained bed capping tuff breccia

PETROGRAPHY

Constituents	Description	Amount
Feldspar	Blocky/tabular, euhedral/subhedral broken phenocrysts. Albite twinning common. Carbonate + epidote + sericite alteration, but appear relatively fresh.	25-vol%
Matrix	Fine-grained mosaic of quartz + albite + carbonate + chlorite.	

Important Characteristics (textures, etc.)

Oriented phenocrysts of broken feldspar within laminated facies. High concentration of feldspar phenocrysts capping tuff breccia facies.

Interpretation(s)

Abundance of broken phenocrysts liberated in the matrix indicate an explosive fragmentation mechanism. The fact that they cap the sequence suggests these fine grained fragments were lofted above the vent and settled to form a low-concentration turbidity current.

Microphotograph(s)

A. Plane polarized light photo depicting the abundance and broken morphology of feldspar phenocrysts.

B. Crossed-Nicols photo of same field of view as in (A).

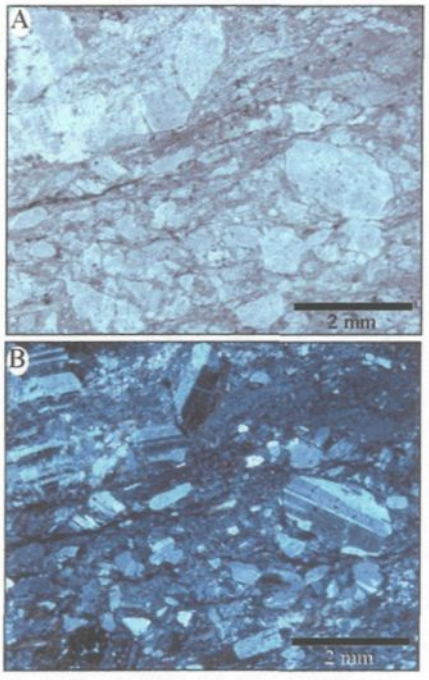

A-15

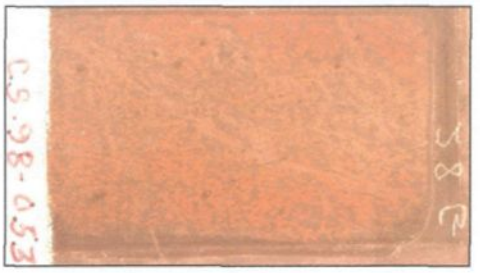

Sample ID: CS98-053

Formation: Val d'Or Formation

Location: Relais

Lithology: Massive felsic lava

Significance: Mineralogy and character of lava

Physical Description: Slightly vesicular, massive felsic facies with elongated vesicules close to contact with underlying massive lava.

PETROGRAPHY

Constituents	Description	Amount
Feldspar	Tabular to blocky, euhedral phenocrysts.	5-vol%
Vesicles	Oval to circular quartz-filled amygdules.	< 5-vol%
Quartz	Anhedral microphenocrysts.	1-vol%
Groundmass	Microlites of feldspar and intergranular quartz + sericite + carbonate +/- chlorite.	

Important Characteristics (textures, etc.)

Slightly vesicular felsic lava facies. Characterizes felsic facies of the Relais region.

Interpretation(s)

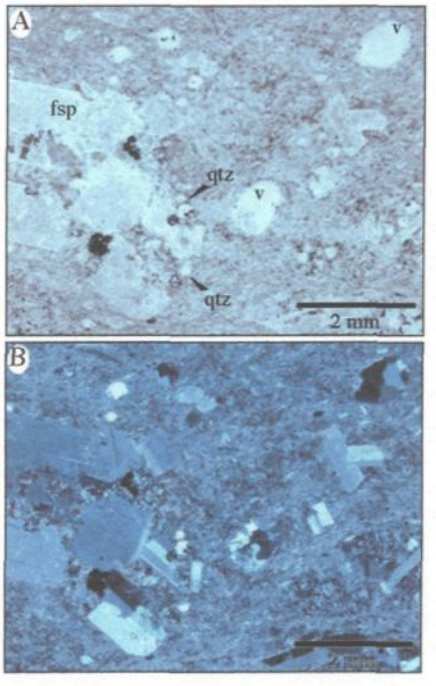

Microphotograph(s)

A. Plane polarized light photo illustrating tabular, euhedral feldspar (fsp) phenocrysts along with anhedral quartz (qtz) and oval-shaped quartz amydules (v).

B. Crossed-Nicols photo of same field of view in (A).

A-16

Sample ID: CS98-232

Formation: Val d'Or Formation

Location: Dunraine East

Lithology: Massive felsic lava

Significance: Shearing and mineralogy

Physical Description: Massive felsic lava that is fractured with sericite filling in fractures.

PETROGRAPHY

Constituents	Description	Amount
Quartz	Anhedral habit with blobby morphology; up to 2 mm in size with undalatory extinction patterns. Some may be amygdules, but shearing precludes clear evidence of primary nature.	30-vol%
Feldspar	Highly altered to sericite; mostly relict tabular forms - euhedral?!	Rare
Groundmass	Fine-grained mosaic of sericite + chlorite with rare blades of muscovite.	

Important Characteristics (textures, etc.)

Slight fabric present in thin section. Unmineralized section, which is important as the facies caps a mineralized volcaniclastic sequence.

Interpretation(s)

In situ brecciation probably due to subsequent movement of lava resulting in fractures due to high viscosity of felsic facies.

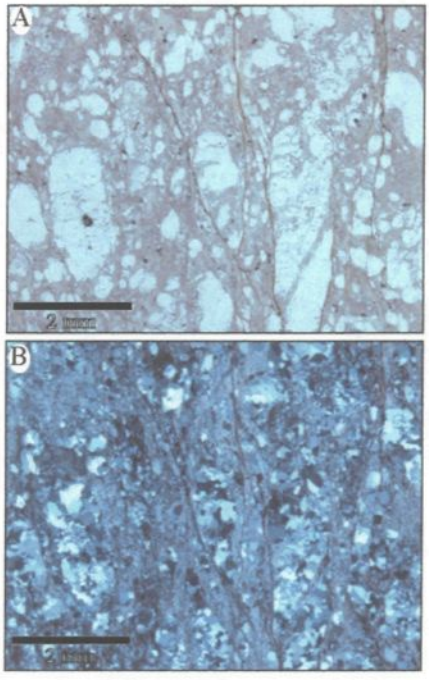

Microphotograph(s)

A. Plane polarized light image of fractures with abundant quartz oriented in same plane fractures.

B. Crossed Nicols image in same field of view as (A).

A-17

Sample ID: CS98-202B

Formation: Val d'Or Formation

Location: Dunraine (east)

Lithology: Tuff breccia

Significance: Characterization of in situ brecciation

Physical Description: Part of subrounded vesicular feldspar-phyric fragment

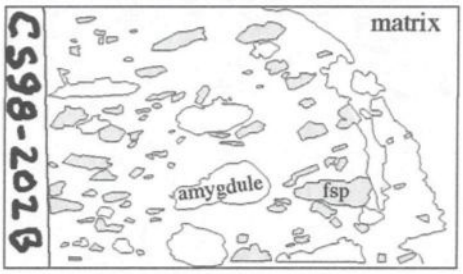

PETROGRAPHY

Constituents	Description	Amount
Fragment	Mm-sized, carbonate/quartz amygdules (20-vol%); mm-sized, tabular, euhedral feldspar phenocrysts that are completely altered to sericite; glomerocrysts are common.	
Matrix	Mosaic of quartz + albite + sericite + carbonate +/- chlorite.	

Important Characteristics (textures, etc.)

Large fracture that cuts fragment and phenocryst.

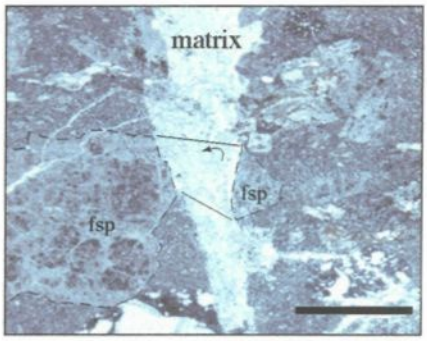

Interpretation(s)

Demonstrates in situ fragmentation of breccia-sized fragments in tuff breccia.

Microphotograph(s)

Plane polarized light image illusrtating wedge of matrix that has invaded fracture, with parts of altered feldspar (fsp) phenocryst on both sides of crack. Arrow outlines the rotation of fragment in order to piece feldspar phenocryst back together. Scale bar is 2 mm in length.

A-18

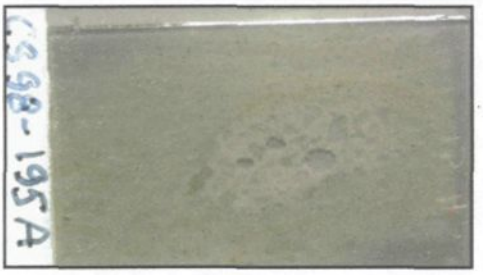

Sample ID: CS98-195A

Formation: Val d'Or Formation

Location: Dunraine (East)

Lithology: Tuff breccia

Significance: Subaqueous eruptive processes

Physical Description: Volcaniclastic sequence composed of angular lapilli- to tuff-sized fragments and subrounded vesicular breccia-sized fragments.

PETROGRAPHY

Constituents	Description	Amount
Fragment	Lapilli-sized, feldspar-phyric, vesicular subrounded fragment. Euhedral, tabular feldspar phenocrysts (15-vol%) are completely altered to sericite and vesicles (10-vol%) are filled by quartz. Groundmass altered to fine-grained sericite + quartz + chlorite +/- albite mosaic. Contact with matrix is sharp, but irregular with wispy/serrated terminations.	
Matrix	Highly altered to a fine-grained mosaic of quartz + albite + sericite + chlorite. Relict outlines of tabular, euhedral feldspar (2-5%).	

Important Characteristics (textures, etc.)

Serrated fragment terminations and feldspar-phyric and quartz-amgydules are important to the genesis of deposit. Also important are the relict feldspars liberated in matrix.

Interpretation(s)

Fragment morphology and contact relationships suggest that it was emplaced at elevated temperatures indicating that this facies was probably deposited by a primary subaqueous pyroclastic flow(s), but water-supported (based on grading). Liberated crystals in the matrix support violent disintegration of the lava. The vesicularity of the fragments indicate that the lava had exsolved violatiles necessary to drive an explsoive eruption.

Microphotograph(s)

A. Plane polarized light photo of feldspar-phyric nature and contact relationship between fragment and matrix.

B. Sketch of photo A.

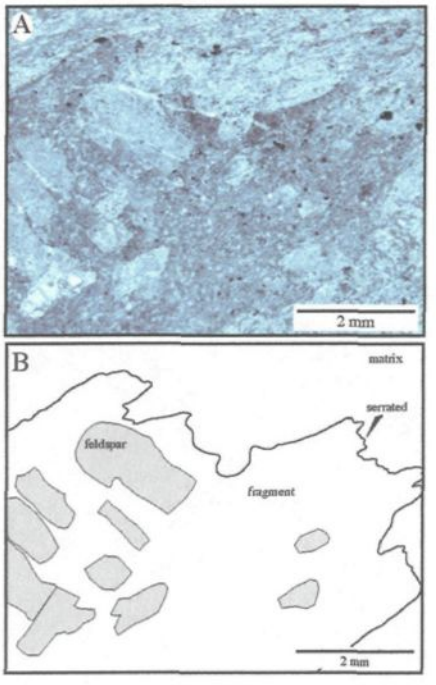

A-19

Sample ID: CS99-2250

Formation: Val d'Or Formation

Location: Abitibi Copper

Lithology: Felsic lava

Significance: In situ brecciation

Physical Description: Massive gray felsic facies with ~10% Fe-staining and highly silicified.

PETROGRAPHY

Constituents	Description	Amount
Feldspar	Fresh, 1-2 mm, blocky/equant/tabular forms with euhedral habits. Carlsbad and albite twinning common.	5-vol%
Ankerite	Alteration product.	5-vol%
Groundmass	In situ brecciated appearance, with chlorite along fractures. No apparent movement. Completely re-crystallized to a fine-grained mosaic of quartz and albite (?).	90-vol%

Important Characteristics (textures, etc.)

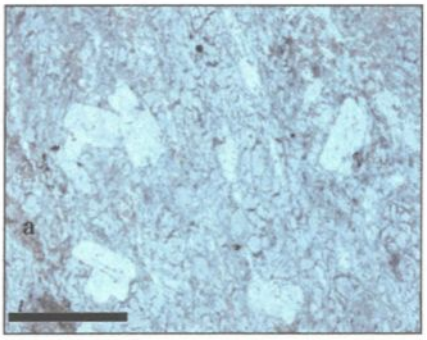

Interpretation(s)

In situ brecciation with no apparent movement suggests that this is part of the outer margin of the felsic flow, with moderate alteration due to subsequent low-temperature fluids.

Microphotograph(s)

Plane polarized light image of fracturing with no separation and evidence of alteration along other fractures outlined by ankerite (a). Scale bar is 2 mm long.

A-20

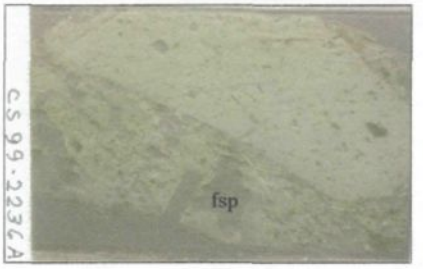

Sample ID: CS99-2236A

Formation: Val d'Or Formation

Location: Abitibi Copper

Lithology: Lapilli tuff

Significance: Characterization of eruptive processes

Physical Description: Vesicular lapilli fragments hosted in a matrix rich in liberated feldspar (fsp) phenocrysts.

PETROGRAPHY

Constituents	Description	Amount
Fragment	Subrounded morphology, weakly vesicular with < 1-vol% blocky feldspar phenocrysts and spiral fracture patterns. Groundmass is altered to a fine-grained mosaic of quartz and albite.	
Matrix	Large cm-sized feldpar laths and smaller broken phenocrysts. Also has wispy chloritic shapes throughout.	

Important Characteristics (textures, etc.)

Spiral fracture patterns, cuspate fragments and broken crystals within matrix are important in characterizing the origin of the deposit.

Interpretation(s)

Spiral fractures are probably perlitic cracks of formerly glassy groundmass of fragment. Cuspate- and wedge-shaped tuff fragments are considered to be former glass shards, whereas broken crystals and the concentration of liberated phenocrysts attest to an explosive genesis.

Microphotograph(s)

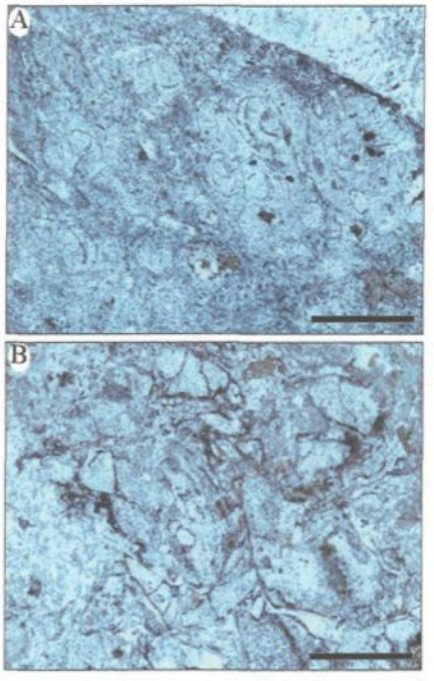

A. Plane polarized light image of perlitic cracks in fine-grained groundmass of fragment. Scale bar is 0.5 mm long.

B. Plane polarized light image of numerous tuff-sized former glass shards in the matrix. Scale bar is 0.5 mm long.

A-21

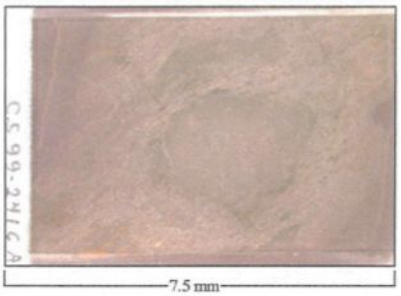

Sample ID: CS99-2416A

Formation: Val d'Or Formation

Location: Sleepy Lake

Lithology: Lapilli tuff

Significance: Characterization of lapilli fragment

Physical Description: Coarse lapilli tuff bed as part of tuff turbidite sequence.

PETROGRAPHY

Constituents	Description	Amount
Fragment	Aphyric subrounded fragment with > 50-vol% quartz/carbonate filled vesicles. Groundmass is completely altered to sericite + chlorite + quartz.	
Matrix	Completely re-crystallized to carbonate + quartz + sericite + chlorite.	

Important Characteristics (textures, etc.)

Coarse (lapilli-sized) vesicular fragments with chloritized margins.

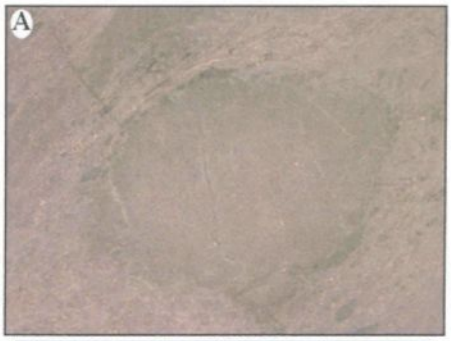

Interpretation(s)

The vesicularity of these lapilli fragments, in an otherwise, tuffaceous sequence suggests that these deposits may have originated from an explosive eruption where fragmentation was efficient. The chloritized margin may be an artifact of chilling with amibient water.

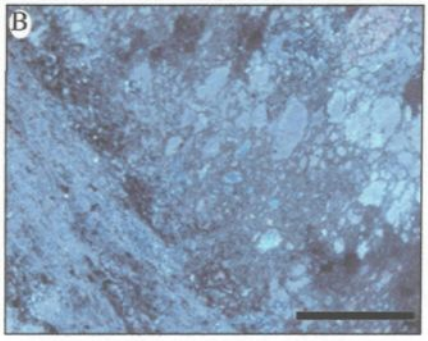

Microphotograph(s)

A. Macroscopic photo of vesicular lapilli fragment with chloritized rim. Fragment is 3 mm long.

B. Cross-Nicols image showing carbonate amygdules and sharp contact with sericitized matrix. Scale bar is 2 mm-long.

A-22

Sample ID: CS98-083B

Formation: Val d'Or Formation

Location: Dunraine (west)

Lithology: Intermediate pillowed facies

Significance: Sheared nature

Physical Description: Foliated intermediate feldspar-phyric pillowed facies

PETROGRAPHY

Constituents	Description	Amount
Feldspar	Mm-sized, blocky to tabular, euhedral/subhedral microphenocrysts; rough margins with speckled cores due to sericite.	10-vol%
Groundmass	Strong alteration to very fine-grained sericite + quartz with fine chlorite bands (in plane of schistosity).	

Important Characteristics (textures, etc.)

Strong fabric observed on outcrop and in thin section.

Interpretation(s)

Microphotograph(s)

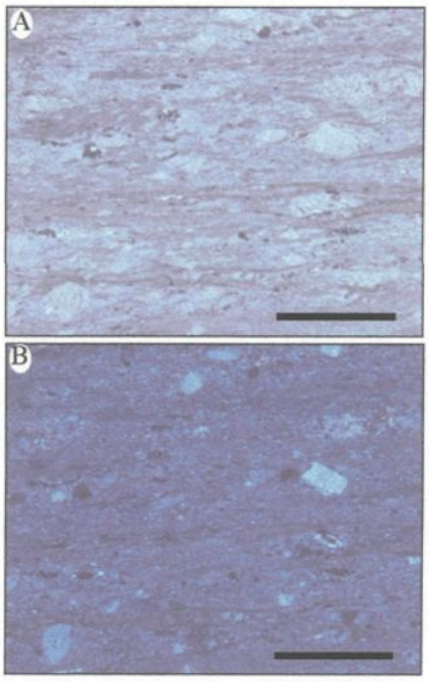

A. Plane polarized light image of feldspar-phyric nature and sheared character of facies. Scale bar is 2 mm long.

B. Crossed-Nicols image of same field of view as (A).

A-23

Sample ID: CS99-2136

Formation: Val d'Or Formation

Location: Dunraine (west)

Lithology: Tuff breccia

Significance: Character of lapilli fragment

Physical Description: Intermediate tuff breccia with subangular, feldspar-phyric fragments.

PETROGRAPHY

Constituents	Description	Amount
Feldspar	Relict, mm- to cm-sized tabular, euhedral phenocrysts; highly altered to sericite + carbonate.	10-vol%
Vesicles	Quartz + carbonate filled - small circular forms.	< 5-vol%
Groundmass	Highly altered to sericite + quartz + chlorite + carbonate.	

Important Characteristics (textures, etc.)

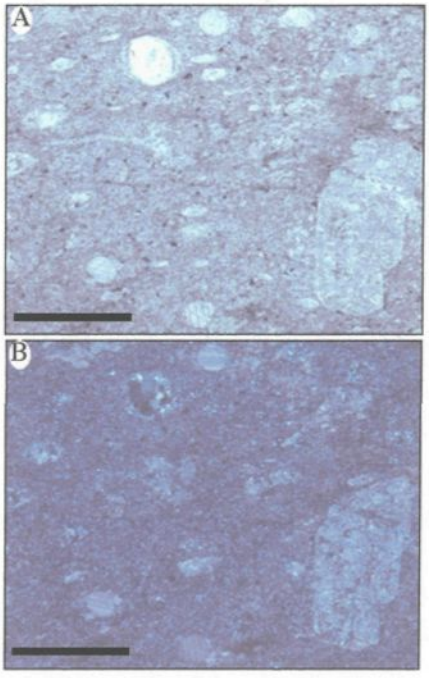

Interpretation(s)

The crystallinity and vesicularity of the lapilli-sized fragment is similar in mineralogy to spatially deposited pillowed lavas suggesting a probable autoclastic origin.

Microphotograph(s)

A. Plane polarized light image of quartz amygdules and altered feldspar phenocrysts within groundmass of lapilli fragment. Scale bar is 2 mm long.

B. Crossed Nicols image of same field of view as in (A).

A-24

Sample ID: CS98-123

Formation: Val d'Or Formation

Location: Dunraine (west)

Lithology: Tuff breccia

Significance: Evidence of in situ fragmentation

Physical Description: Matrix of tuff breccia

PETROGRAPHY

Constituents	Description	Amount
Feldspar	Tabular, euhedral phenocrysts, some are fragments of crystals and others are broken in situ. Albite twinning is common or core is completely sieved.	25-vol%
Matrix	Completely altered to grungy mosaic of sericite + quartz.	

Important Characteristics (textures, etc.)

Abundance of broken feldspar liberated in the matrix and in situ nature of some phenocrysts, as well as sieved cores attest to origin of deposit.

Interpretation(s)

Broken, liberated phenocrysts suggest an efficient fragmentation mechanism for this facies, whereas sieved cores indicate a complex crystallization history, which may have involved magma mixing.

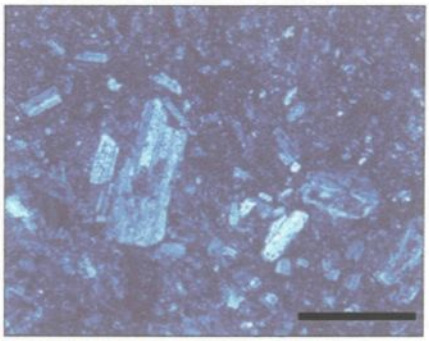

Microphotograph(s)

Cross-Nicols image of in situ fragmentation of tabular, euhedral feldspar phenocryst, as well as a sieved feldspar. Scale bar is 2 mm long.

A-25

Sample ID: CS99-2212A/B

Formation: Héva Formation

Location: Anamaque

Lithology: Massive felsic spherulite

Significance: Flow bands and spherulite growth

Physical Description: Bleached, flow banded to massive facies

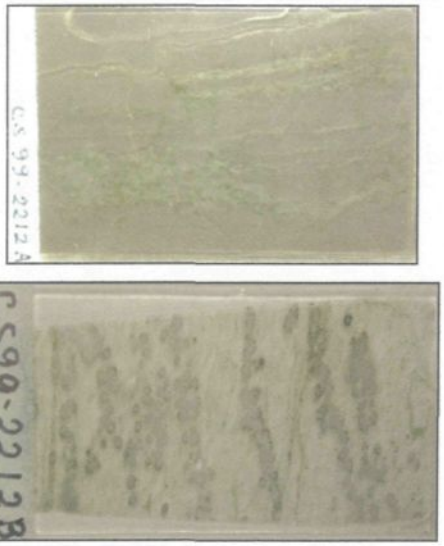

PETROGRAPHY

Constituents	Description	Amount
Spherulites	Mm- to cm-sized and spherical-shaped; composed of fine-grained albite within thin to thick bands of amalgamated spherulites.	> 35-vol%
Groundmass	Altered to chlorite + sericite + quartz, along with arrested spherulite growth and incipient fragmentation.	
Vesicles	Quartz-amygdules that are within bands and groundmass. Some serve as nucleation points for spherulites.	rare

Important Characteristics (textures, etc.)

Amalgamation of spherulites as single or groups forming flow bands.

Interpretation(s)

Flow bands indicate spherulitic growth along former glass inhomogeneities. Thinner bands are hosted in groundmass that has arrested spherulites and incipient fragmentation suggesting sudden quenching below glass transition temperature due to thermal stress; probably induced by interaction with water.

Microphotograph(s)

A. Plane polarized light image of thicker flow band with fine spherulites (dashed lines) that form a crystalline mass. Field of view is 7 mm.
B. Plane polarized light image of larger, individual spherulites forming bands with rare vesicles (V) and arrested spherulite growth in groundmass.

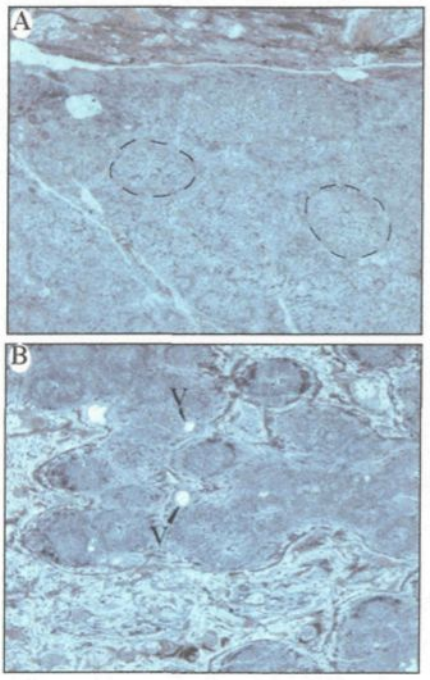

A-26

Sample ID: CS97-237

Formation: Héva Formation

Location: Highway 117 - Louvicourt

Lithology: Massive felsic spherulite

Significance: Spherulite growth

Physical Description: Isolated to groups of mm-sized, spherical spherulites

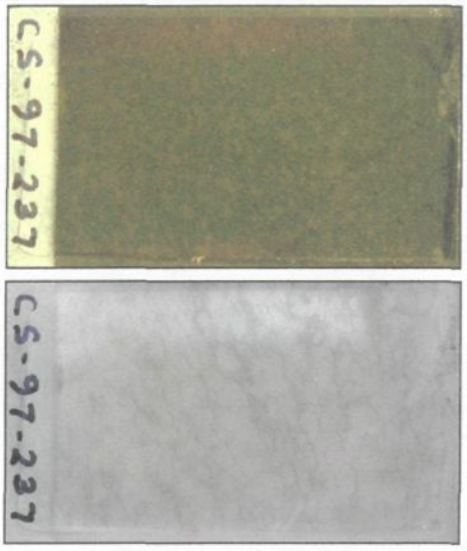

PETROGRAPHY

Constituents	Description	Amount
Spherulites	Millimeter-sized, spherical forms with slight elongation in a preferred orientation, rare examples of acicular/tabular feldspar serving as nucleaton point.	60-vol%
Groundmass	Quartz + chlorite +/- albite mosaic.	
Feldspar	Acicular to tabular, euhedral microphenocryts.	rare

Important Characteristics (textures, etc.)

Oriented fabric and isolated to grouped nature of aphyric spherulitic facies.

Interpretation(s)

Large undercooling of low viscosity felsic lava, with devitrification being probably stopped due to a sudden cooling event.

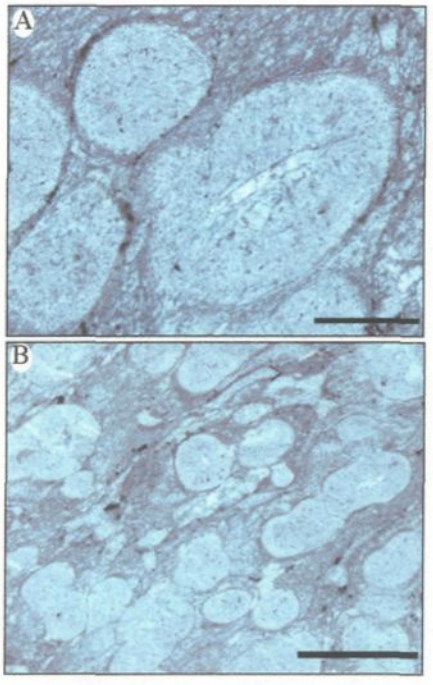

Microphotograph(s)

A. Plane polarized light image of isolated spherical spherulites with tabular feldspar microphenocryst serving as nucleation point. Scale bar is 0.5 mm.
B. Plane polarized light image of isolated groups of spherical spherulites in a groundmass showing slight orientation. Scale bar is 2 mm.

A-27

Sample ID: CS99-2174B/2176B

Formation: Héva Formation

Location: Tex-Sol area

Lithology: Hyaloclastite

Significance: In situ nature

Physical Description: In situ breccia of lapilli tuff with a boxwork texture on surface.

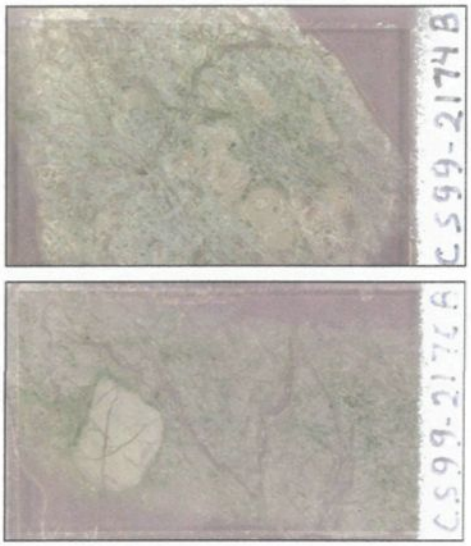

PETROGRAPHY

Constituents	Description	Amount
Shards	Chloritic and oxide altered cuspate-forms and feldspar and quartz curvilinear forms.	
Matrix	Quartz + chlorite + albite mosaic.	

Important Characteristics (textures, etc.)

Jigsaw fitting textured hyaloclastite and curvilinear shards

Interpretation(s)

Carapace hyaloclastite facies with glassy shards that have undergone devitrification as evident by perlitic fractures.

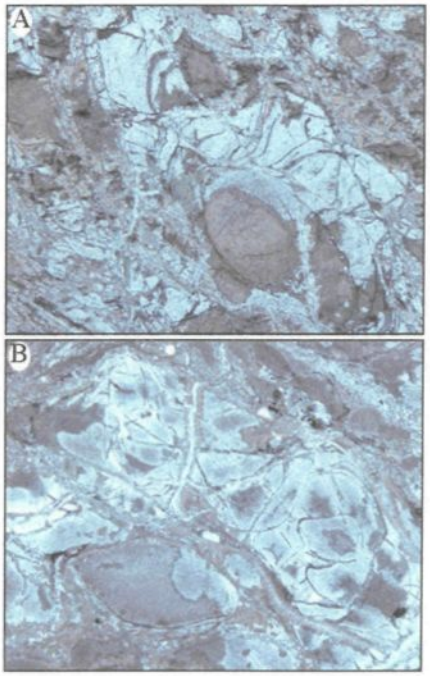

Microphotograph(s)

A. Plane polarized light image of in situ shards and curvilinear nature of hyaloclastite. Field of view 7 mm.

B. Plane polarized light image of in situ and perlitic nature of feldspar/quartz re-crystallized shards. Field of view is 7 mm.

A-28

Sample ID: CS98-288B2

Formation: Héva Formation

Location: Highway 117 - Louvicourt

Lithology: Hyaloclastite

Significance: Carapace breccia

Physical Description: Little to no movement of hyaloclastite

PETROGRAPHY

Constituents	Description	Amount
Hyaloclastite	In situ fragmentation - altered to chlorite.	
Spherulites	Coarse-grained texture showing chess-board albite features.	
Groundmass/ matrix	Mosaic of quartz + albite	

Important Characteristics (textures, etc.)

Similar to CS98-288B1, except there is little to no movement between fragments and shards are NOT as angular - spherulitic feldspar are coarser grained.

Interpretation(s)

Coarser-grained fibro-radial texture suggests replacement of a fibro-radial mineral phase (e.g., zeolite?). In situ carapace that has not separated - transitional to overlying carapace of CS98-288B1.

Microphotograph(s)

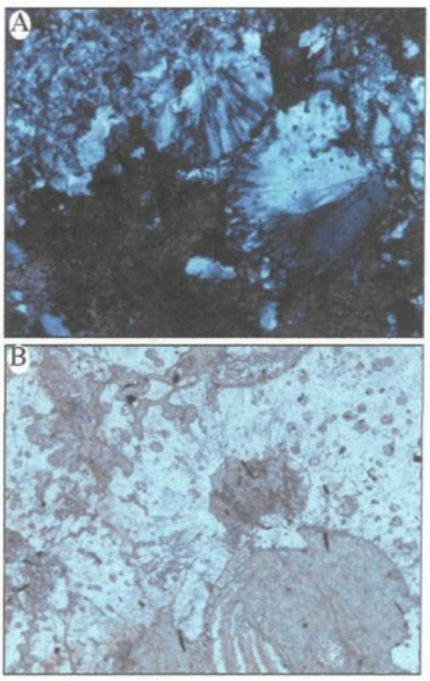

A. Cross-Nicols image of chess-board albite forming a fibrous texture in chloritic shard. Field of view 2 mm.

B. Plane polarized light image of coarser-grained albite replacing former fibro-radial mineral (e.g., zeolite). Field of view is 7 mm. See Figure 153 for cross-Nicols image of same field of view.

A-29

Sample ID: CS98-263C

Formation: Héva Formation

Location: Tex-Sol Outcrops

Lithology: Felsic fragment

Significance: Felsic fragment within polymictic facies

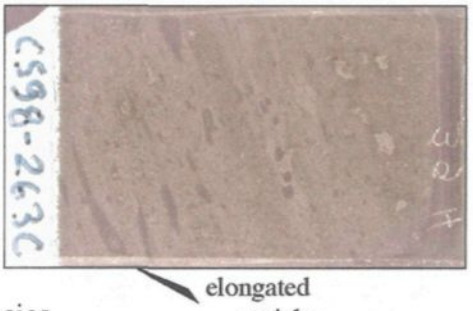

Physical Description: Rounded, vesicular breccia-sized fragment

PETROGRAPHY

Constituents	Description	Amount
Feldspar	Tabular, euhedral feldspar characterized by Carlsbad twinning.	5-vol%
Vesicles	Oval to elongated quartz amygdules. The larger the amygdule, the more stretched it appears. Some deformation between jutaposed vesicles and some that have coalesced.	15-20-vol%
Groundmass	Fine-grained mosaic of albite + quartz + chlorite.	

Important Characteristics (textures, etc.)

Felsic nature (and geochemistry), vesicularity, and rounded morphology are important in interpreting its origin.

Interpretation(s)

All these characteristics suggest an epiclastic origin. The vesicular and felsic nature would suggest an explosive origin, but there is no evidence of hot emplacement or heat retention, therefore the rounded morphology of the fragment is due to abrasion subsequent to erosion from a felsic lava.

Microphotograph(s)

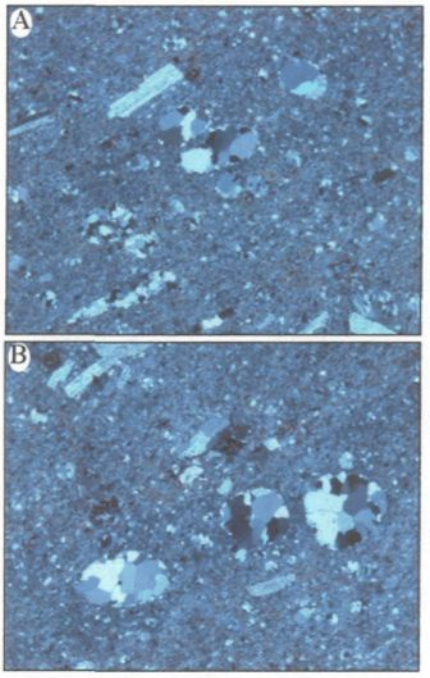

A. Cross-Nicols image of deformation between justapozed mm-sized oval quartz amygdules. Tabular, euhedral feldspar phenocrysts are also in field of view (7 mm).

B. Cross-Nicols image of vesicle coalescence. See Figure 158B for plane polarized image. Field of view is 7 mm.

A-30

Sample ID: CS98-263G

Formation: Héva Formation

Location: Tex-Sol Outcrops

Lithology: Gabbro

Significance: Evidence of synvolcanic intrusion

Physical Description: Variolitic margin of gabbro in contact with volcaniclastic sediments

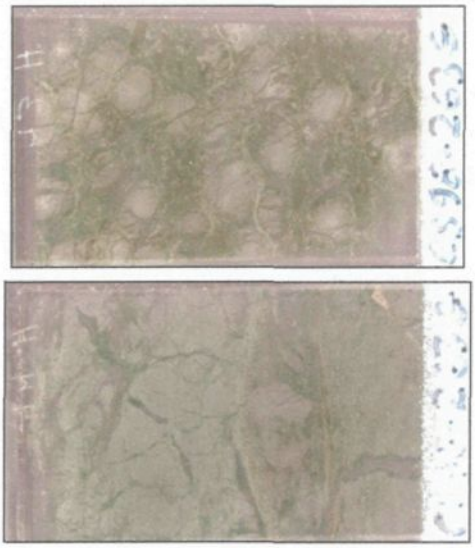

PETROGRAPHY

Constituents	Description	Amount
Variolites	Subspherical masses of fibrous feldspar microlites with chlorite margins.	70-80-vol%
Matrix?	Intersitial material to varioles is composed of chlorite and μm-sized, highly birefringent euhedral microphenocryts that appear to be relict pyroxene.	

Important Characteristics (textures, etc.)

Varioles....

Interpretation(s)

Formation of varioles are suggestive of rapid cooling, probably induced by intrusion into unconsolidated sediments. Variole formation is associated with peperite development.

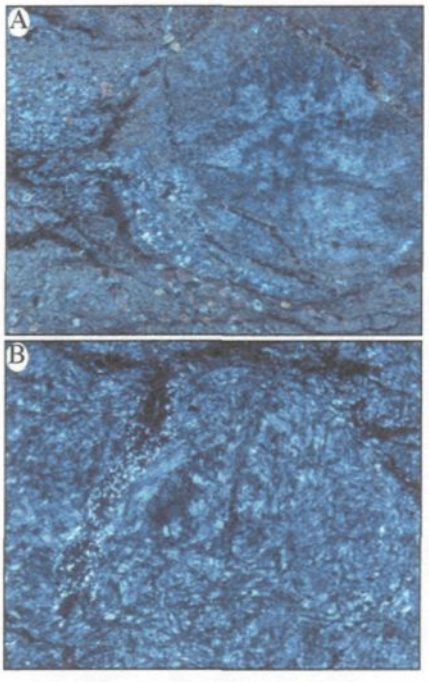

Microphotograph(s)

A. Cross-Nicols image of cm-sized, subspherical variolite composed of fibrous microlites of feldspar with a chlorite margin and euhedral microphenocrysts of pyroxene? Field of view 7 mm.

B. Cross-Nicols image of fibrous nature of feldspar variolites. See Figure 161B for plane polarized image. Field of view is 7 mm.

A-31

Sample ID: CS98-266J

Formation: Héva Formation

Location: Akasaba North

Lithology: Slightly mineralized lapilli tuff

Significance: Proximity to mineralized zone and matrix composition

Physical Description: Massive felsic lapilli tuff within a meter of mineralized zone

PETROGRAPHY

Constituents	Description	Amount
Feldspar	Tabular-blocky, euhedral-subhedral, broken microphenocrysts. All crystals have a speckled appearance due to sericite alteration.	~40-vol%
Matrix	Very fine-grained mosaic of quartz and feldspar	
Quartz	Anhedral blobs	rare
Sphalerite	Irregular outlines, but seems to have a preferred orientation along veins/stringers.	1-2-vol%

Important Characteristics (textures, etc.)

Cannot recognize feldspar in PPL due to resolution with matrix. Veins/stringers of sphalerite hint at origin.

Interpretation(s)

Porous lapilli tuff permitted hydrothermal fluids to pass through this facies, which precipitated sulfides.

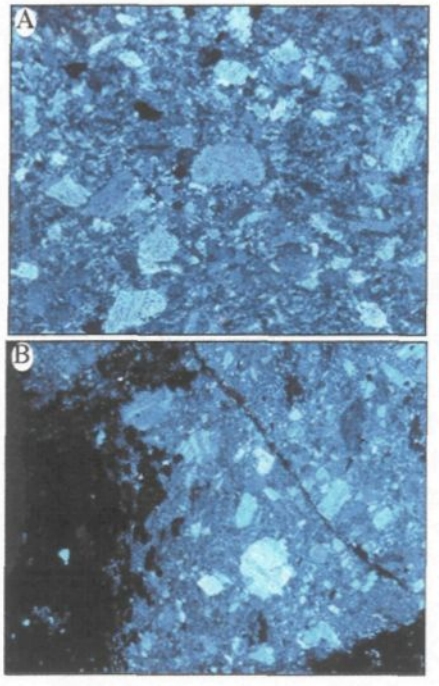

Microphotograph(s)

Crossed polarized images with a field of view 7mm.
A. Feldspar-rich and broken nature of lapilli tuff.

B. Irregular outline of sphalerite (opague) in lapilli tuff.

A-32

Sample ID: CS99-2142D

Formation: Héva Formation

Location: Akasaba North

Lithology: Peperite

Significance: Contemporaneous mixing between felsic sediment and mafic magma

Physical Description: Featureless tuff and amoeboidal gabbro clast

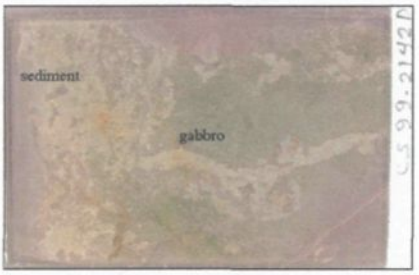

PETROGRAPHY

Constituents	Description	Amount
Feldspar (sed)	Tabular, euhedral/subhedral phenocrysts that are broken and hosted in a fine-grained mosaic of quartz and albite(?).	~15-vol%
Feldspar (gab)	Tabular, euhedral, mm- to cm-sized phenocrysts	Exact estimate of percentage is difficult due to alteration
Pyroxene (hbl)	Tabular, euhedral/subhedral mm- to cm-sized phenocrysts	
Matrix	Associated with sediment - mosaic of fine-grained quartz and albite with tabular biotite throughout.	

Important Characteristics (textures, etc.)

Commingling of apparent sediment and coarse-grained pyroxene.

Interpretation(s)

Peperite formation - mixing between a wet unconsolidated sediment and hot fluidal mafic magma.

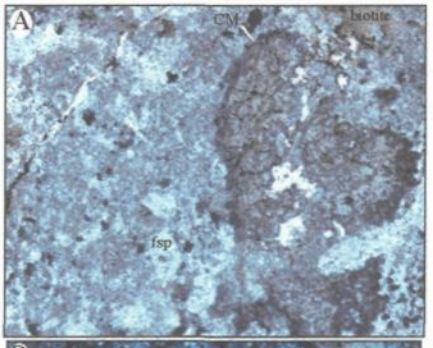

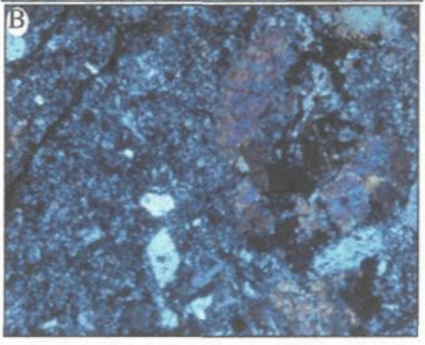

Microphotograph(s)

A. PPL image of relationship between lapilli tuff (with broken feldspar phenocrysts and gabbro, which has a possible chilled margin (CM). Field of view is 7mm.

B. Crossed polarised image of same field of view as (A).

A-33

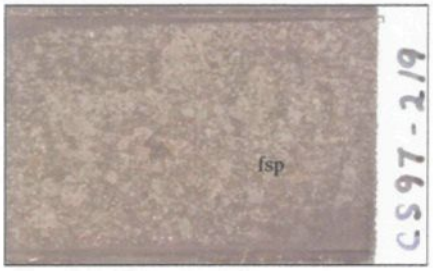

Sample ID: CS97-219

Formation: Héva Formation

Location: Akasaba North

Lithology: Pyroclastic lapilli tuff

Significance: Crystal-rich nature

Physical Description: Massive lapilli tuff

PETROGRAPHY

Constituents	Description	Amount
Feldspar	Blocky, euhedral/subhedral broken crystals. Albite twinning common and most crystals have sieved cores.	~20-vol%
Quartz	Anhedral phenocryts.	rare
Altered phase	Highly altered, high birefrigent phase with irregular outlines in matrix.	
Matrix	Mosaic of quartz and albite with subordinate chlorite blobs.	

Important Characteristics (textures, etc.)

Crystal-rich nature with broken character. Large and sieved character of feldspar population and altered phases differs from felsic tuffs.

Interpretation(s)

Pyroclastic phase is different from underlying felsic tuffs in phenocryst assemblage and alteration.

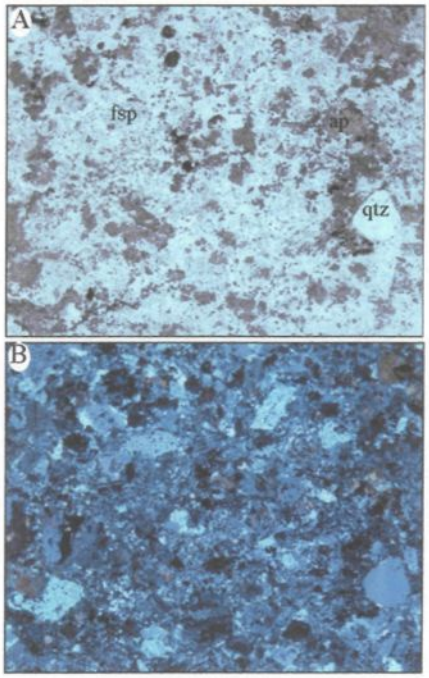

Microphotograph(s)

A. PPL image illustrating feldspar-phyric nature, as well as the altered phase (ap) and anhedral quartz (qtz). Feldspar (fsp) appears dirtly looking. Field of view is 7mm.

B. Cross polarised of same field of view in (A).

A-34

Sample ID: CS97-218

Formation: Héva Formation

Location: Akasaba North

Lithology: Fine-grained gabbro

Significance: Characterter of crystalline gabbro not in contact with sediment

Physical Description: Chloritized, fine-grained gabbro

PETROGRAPHY

Constituents	Description	Amount
Chlorite (pyx?)	Chlorite after pyroxene (?); forms relict tabular crystal forms. Medium to light green appearance.	~60-vol%
Plagioclase	Tabular phenocrysts that have a corroded appearance.	~30-vol%

Important Characteristics (textures, etc.)

Fine-grained gabbro with crystalline nature, but highly altered.

Interpretation(s)

Rapid, near co-crystallization of plagioclase and pyroxene.

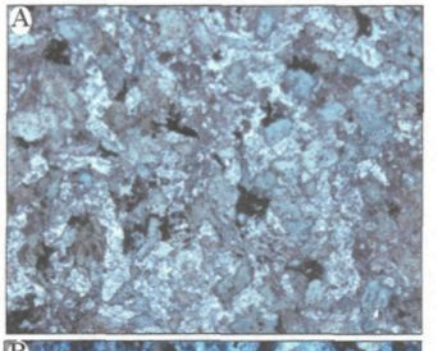

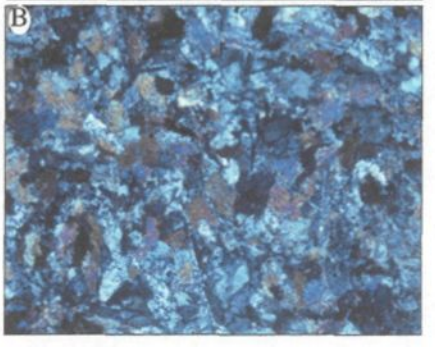

Microphotograph(s)

A. PPL image of section illustrating the intergrown pyroxene (chl) and plagioclase. Field of view is 7 mm.

B. Crossed polarized view of (A).

GEOCHEMISTRY

B1 – JACOLA FORMATION
B2 – LOWER VAL D'OR FORMATION
B3 – UPPER VAL D'OR FORMATION
B4 – HÉVA FORMATION

Table B1: All geochemical data from the Jacola Formation.

Sample	CS97-246A	CS97-246C	CS99-2496	CS99-2497B	CS99-2482A	CS99-2487A	CS99-2193A	CS99-2193B
Location	HW 117	HW 117	Val d'Or town	Val d'Or town	Val d'Or town	Val d'Or town	N.Bidlamaque	N.Bidlamaque
Formation	JF	JF	JF	JF	JF	JF	JF	JF
Description	ultramafic	ultramafic	basalt	basalt	basalt	ultramafic	basalt	Intermed. Dyke
SiO_2 (wt%)	42.80	46.50	40.9	45.3	51.9	40.1	48.4	55.8
TiO_2	0.38	1.06	0.34	0.36	0.79	0.26	0.45	0.73
Al_2O_3	5.47	15.70	4.89	21.1	13.5	3.81	14.6	16.9
Fe_2O_3	10.90	11.40	11.5	9.49	15	10.8	11	7
MnO	0.20	0.18	0.16	0.16	0.24	0.19	0.15	0.1
MgO	27.60	9.64	29.3	8.89	6.16	25.5	10.5	4.89
CaO	5.16	9.65	3.55	7.35	7.85	7.38	9.9	8.93
Na_2O	0.17	2.11	0.16	2.04	1.95	0.13	2.31	3.56
K_2O	0.01	0.62	0.01	0.33	0.24	0.02	0.05	0.07
P_2O_5	0.03	0.24	0.01	0.01	0.06	0.01	0.03	0.12
Cr_2O_3			0.35	0.01	0.02	0.27	0.08	0.02
LOI	7.30	2.62	8.62	4.61	2.03	10.4	2.74	1.75
TOTAL	100.02	99.72	99.79	99.65	99.74	98.87	100.21	99.87
Zr (ppm)	19	75	21	23	59	19	35	114
Y	8	21	7	13	38	8	20	20
Cu	22	43	63	3	100	35	11	85
Zn	62	92	55	87	87	43	30	17
Ba	3	99	ND	ND	ND	ND	ND	ND
Co	107	47	110	53	51	90	46	21
Cr	2300	377	2300	75	96	1800	500	84
Ni	1600	225	1600	130	80	1300	220	40
Rb	4	23	3	18	7	3	3	3
Sr	10	182	3	86	108	22	77	144
Sc	22	40	22	51	82	21	50	33
Zr/Y	2.38	3.57	3.00	1.80	1.60	2.40	1.75	5.70

* ND = no data or below detention limits; CC = sampled by C. Champagne; PP = sampled by P. Pilote; PR = sampled by P. Riopel; SL = sampled by S. Lavoie

Table B2: All geochemical data from the Lower Val d'Or Formation

Sample	CS98-290	CS99-2466D	CS97-233	CS97-234	CS97-235	CS97-239	CS97-240	CS97-242	CS97-243
Location	playground	Playground	PDN	PDN	PDN	PDN	PDN	PDN	PDN
Formation	VDF	VDF	VDF	VDF	VDF	VDF	VDF	VDF	VDF
Description	xtal tuff	Int. lava	Lamprophyre	mafic dyke	Felsic dyke	Felsic dyke	Mafic lava	Int. lava	Feeder dyke
SiO_2 (wt%)	44.1	41.8	63.10	47.00	60.60	57.00	50.50	63.80	46.40
TiO2	0.83	0.83	0.41	0.50	0.73	0.59	0.85	0.68	0.62
Al_2O_3	17.3	18.7	15.30	18.70	16.70	18.00	16.60	15.00	20.80
Fe_2O_3	9.82	10	4.36	10.90	5.85	7.57	7.81	4.21	10.10
MnO	0.14	0.18	0.07	0.19	0.08	0.09	0.22	0.08	0.18
MgO	3.98	6.69	2.49	8.14	2.64	3.08	5.62	3.85	8.50
CaO	12.4	11	4.11	8.85	6.63	6.80	11.60	5.41	5.42
Na_2O	2.82	1.69	4.55	0.66	3.77	2.62	3.16	4.35	1.27
K_2O	0.06	0.63	1.87	0.68	0.93	1.59	0.64	0.35	1.45
P_2O_5	0.08	0.09	0.18	0.06	0.27	0.12	0.16	0.16	0.05
Cr_2O_3	0.02	0.02	ND	ND	ND	ND	ND	ND	ND
LOI	7.98	8.8	3.64	4.30	1.83	2.55	2.98	2.24	5.11
TOTAL	99.53	100.43	100.08	99.98	100.03	100.01	100.14	100.13	99.90
Zr (ppm)	70	68	129	40	156	109	104	99	49
Y	24	25	12	19	15	18	21	20	20
Cu	15	38	9	48	9	14	49	70	115
Zn	ND	73	56	78	42	64	92	46	120
Ba	52	ND	728	221	453	514	223	114	443
Co	ND	34	11	54	14	15	46	18	57
Cr	73	96	75	99	22	20	670	45	93
Ni	ND	43	31	70	20	2	319	59	84
Rb	4	18	43	19	28	39	19	11	49
Sr	72	148	311	197	371	401	293	181	197
Sc	ND	44	9	57	13	13	40	29	64
Zr/Y	2.92	2.70	10.75	2.11	10.40	6.06	4.95	4.95	2.45

* ND = no data or below detention limits; CC = sampled by C. Champagne; PP = sampled by P. Pilote; PR = sampled by P. Riopel; SL = sampled by S. Lavoie

CS97-244 PDN VDF Felsic dyke	CS97-245 PDN VDF Lapilli tuff	CS98-001 PDN VDF Int. lava	CS98-003 PDN VDF pyx dyke	CS98-088 PDN VDF feeder dyke	CS97-001 E. Sullivan VDF Felsic dyke	CS97-023 E. Sullivan VDF Felsic dyke	CS97-028 E.Sullivan VDF Int lava	CS97-039 E. Sullivan VDF Lapilli breccia	CS97-040 E. Sullivan VDF Lapilli breccia
57.00	55.40	54.00	44.60	48.50	60.20	59.60	47.80	51.00	52.50
0.86	0.66	0.6	0.48	0.56	0.64	0.67	0.98	0.71	0.85
18.10	16.40	19	9.56	18.4	16.50	16.40	19.70	16.00	18.80
7.28	7.27	6.15	12.1	9.21	5.48	6.26	9.73	6.15	8.01
0.12	0.10	0.09	0.21	0.15	0.11	0.10	0.17	0.17	0.13
3.48	4.83	4.93	16.7	7.77	2.68	2.60	5.07	3.83	5.01
5.30	4.95	6.57	8.34	7.76	4.98	5.47	7.55	8.13	5.41
5.04	3.85	1.18	0.25	1.37	4.82	4.31	4.45	6.06	4.87
0.09	0.38	2.8	0.24	1.16	0.86	1.10	0.02	0.18	0.13
0.33	0.12	0.16	0.12	0.06	0.27	0.27	0.11	0.09	0.09
ND	ND	0.03	0.17	0.03	ND	ND	ND	ND	ND
2.51	5.94	3.86	6.78	4.37	3.43	3.56	4.21	7.83	4.15
100.11	99.90	99.37	99.55	99.34	99.97	100.34	99.79	100.15	99.95
150	107	90	56	53	144	141	101	71	91
22	20	20	14	20	15	16	33	22	27
12	11	1	2.6	1	1	1	90	143	42
100	72	34	96	50	79	77	78	51	76
50	126	630	50	1000	639	418	26	41	93
19	21				14	13	26	21	23
20	103	82	1100	99	20	20	29	20	44
19	57	163		59	17	17	47	36	60
3	10	80	10	26	23	29	3	6	5
309	152	161	70	224	217	220	243	79	215
17	20	38	33	59	12	11	52	33	43
6.82	5.35	4.50	4.00	2.65	9.60	8.81	3.06	3.23	3.37

CS97-042 E. Sullivan VDF Felsic dyke	CS97-049 E. Sullivan VDF Lapilli breccia	CS97-052 E. Sullivan VDF Lapilli breccia	CS97-054 E.Sullivan VDF Int lava	CS97-060 E. Sullivan VDF Felsic dyke	CS97-064 E.Sullivan VDF Int lava	CS97-065 E.Sullivan VDF Int lava	CS97-069 E.Sullivan VDF Int. lava	CS98-080 E.Sullivan VDF tuff	CS99-2506 E. Sullivan VDF Int. lava
48.50	53.30	57.80	51.90	49.40	51.00	48.50	53.50	51.20	58.9
0.71	0.43	0.41	0.85	0.63	0.84	0.82	0.85	0.87	0.49
15.10	15.40	16.20	19.80	13.50	19.50	19.70	19.00	19.2	15.8
8.32	6.58	5.89	7.82	7.15	7.85	8.70	8.31	9.54	13.6
0.17	0.15	0.12	0.14	0.29	0.14	0.14	0.13	0.15	0.68
5.37	4.44	3.09	4.62	4.15	5.08	4.63	4.46	5.3	3.06
8.13	8.38	8.64	4.03	10.50	5.92	7.21	3.94	4.46	0.02
3.82	4.41	3.73	6.65	3.05	5.25	2.87	6.02	4.46	0.39
0.48	0.01	0.02	0.01	0.58	0.06	1.28	0.03	0.11	2.04
0.44	0.07	0.07	0.08	0.38	0.09	0.09	0.10	0.11	0.11
ND	ND	ND	ND	ND	ND	ND	ND	0.02	0.01
8.92	6.85	4.16	4.27	10.40	4.32	5.87	3.79	4.35	4.28
99.96	100.02	100.13	100.17	100.03	100.05	99.81	100.13	99.77	99.38
143	66	81	85	129	87	88	86	91	96
20	10	12	26	21	26	26	25	28	15
8	36	21	54	71	74	55	53	56	10
87	59	43	71	70	75	75	68	67	610
65	12	21	18	108	24	260	16	65	ND
29	30	24	28	26	24	28	28	ND	14
81	231	112	29	60	49	39	20	43	45
47	93	59	45	42	45	47	101	65	21
15	3	3	3	17	5	33	4	5	41
64	183	314	188	102	197	208	189	215	18
22	23	20	43	22	42	42	42	49	15
7.15	6.60	6.75	3.27	6.14	3.35	3.38	3.44	3.25	6.40

CS98-260A Pole Line VDF Int. lava	CS98-260B Pole Line VDF aphy dyke	CS99-2452 Pole Line VDF Int. lava	CS99-2453A Pole Line VDF Int. lava	CS98-140a Camnet VDF Lapilli breccia	CS98-140b Camnet VDF FP dyke	CS98-141 Camnet VDF Felsic lava	CS98-146b Camnet VDF mafic dyke	CS98-147c Camnet VDF Mafic lava	CS98-149 Camnet VDF Felsic lava
55.6	53.4	56.2	53.4	71.40	58.30	68.20	51.70	58.70	75.00
0.7	0.6	0.69	0.89	0.65	0.83	0.86	0.87	0.91	0.28
18.3	14.6	16.9	18.7	13.8	16.8	13.3	15.7	16.5	13.1
7.35	7.91	7.25	8.79	4.33	6.85	6.05	14.7	7.33	2.19
0.12	0.13	0.11	0.15	0.05	0.07	0.05	0.21	0.11	0.04
4.11	2.38	3.92	4.64	2.35	2.85	3.17	8.34	3.18	0.62
6.11	15	4.48	4.84	0.62	5.35	0.79	0.36	5.04	1.5
4.38	0.72	4	5.01	5.33	3.03	4.28	0.13	4.5	5.55
0.2	0.06	0.47	0.02	0.06	0.93	0.04	1.31	0.15	0.2
0.12	0.37	0.12	0.1	0.23	0.17	0.2	0.18	0.22	0.05
0.02	0.02	0.01	0.01	0.01	0.02	0.02	0.02	0.02	0.01
2.45	4.2	5.79	3.59	1.85	4.44	2.62	5.86	3.12	1.28
99.46	99.39	99.94	100.14	100.68	99.64	99.58	99.38	99.78	99.82
104	162	112	93	133	157	275	152	156	193
23	18	21	30	31	24	35	31	26	46
28	31	11	51	1	6	1	1	24	1
ND	ND	69	84	20	18	27	140	77	19
76	50	ND	ND	50	80	50	340	65	65
ND	ND	22	26	ND	ND	ND	ND	ND	ND
89	66	62	35	20	43	20	50	39	20
ND	ND	21	31	34	23	20	ND	ND	39
5	3	14	3	3	21	3	31	5	3
132	1100	177	156	50	252	32	3	274	137
ND	ND	22	50	33	27	19	33	31	9.5
4.52	9.00	5.30	3.10	4.29	6.54	7.86	4.90	6.00	4.20

CS98-153 Camnet VDF Felsic lava	CS98-154e Camnet VDF Felsic lava	CS98-156b Camnet VDF Felsi dyke	CS98-158B Camnet VDF Felsic lava	CS98-165A Camnet VDF FP	CS98-165b Camnet VDF Felsic lava	CS98-170 Camnet VDF Felsic lava	CS98-171B Camnet VDF Felsic lava	CS98-172A Camnet VDF Int. lava	CS98-173B Camnet VDF Lapilli tuff
73.9	69.20	69.00	65.9	57.6	68.90	69.7	69.3	52.9	50.6
0.4	0.78	0.81	0.72	1.02	1.04	0.65	0.74	0.72	1.12
13.3	13.3	13.7	14.6	16	13.4	14.9	14.5	17.6	14.6
2.64	5.58	5.93	3.21	8.76	4.73	3.46	4.18	5.67	13.7
0.04	0.11	0.13	0.14	0.27	0.12	0.04	0.05	0.13	0.15
1.23	1.15	1.33	1.2	3.54	1.65	1.3	1.25	4.74	6
0.87	3	1.59	3.9	4.32	3.09	1.05	1.36	5.58	6.86
3.3	4.69	4.54	6.25	3.43	4.48	5.74	4.76	3.24	2.99
1.8	0.06	0.5	0.05	0.29	0.04	0.71	1	1.85	0.07
0.3	0.19	0.2	0.16	0.18	0.29	0.36	0.35	0.15	0.5
0.01	0.02	0.02	0.01	0.02	0.01	0.01	0.01	0.01	0.1
1.64	1.65	1.99	3.17	3.87	1.88	1.53	1.9	6.8	3.03
99.43	99.73	99.74	99.31	99.3	99.63	99.45	99.4	99.39	99.72
257	280	287	203	160	272	268	213	97	194
50	43	50	28	29	36	38	38	15	31
61	15	1	29	4	1	30	1	18	6
	59	60	ND	ND	82	ND	ND	ND	ND
460	50	170	50	88	50	78	360	740	100
ND	ND	ND	ND	ND	ND	ND	ND	ND	ND
20	20	20	20	79	20	20	20	43	630
ND	20	47	ND	ND	20	ND	ND	ND	ND
42	3	12	3	7	3	18	24	35	3
69	180	82	116	124	193	139	161	277	414
ND	22	25	ND	ND	23	ND	ND	ND	ND
5.14	6.51	5.74	7.25	5.52	7.56	7.05	5.61	6.47	6.26

CS98-172C Camnet VDF mafic dyke	CS98-174 Camnet VDF Mafic lava	CS98-179B Camnet VDF Int. lava	CS98-183 Camnet VDF Int. lava	CS98-184 Camnet VDF FP	CS98-185A Camnet VDF Int. lava	CS98-186B Camnet VDF Mafic lava	CS98-188B Camnet VDF Mafic lava	CS98-189B Camnet VDF Int. lava	CS98-192A Camnet VDF FP
44.4	48.5	55.5	56.2	58.2	66.3	56.2	59.7	69.1	55.2
1.08	1.16	0.69	0.88	0.82	1.1	0.96	0.89	0.76	0.87
13.6	15.4	17.7	16.6	16.6	14.4	16.9	15.5	12.9	16.2
22	10.5	6.55	7.85	7.69	4.86	7.73	7.29	7.4	7.45
0.2	0.15	0.11	0.1	0.08	0.07	0.09	0.11	0.09	0.12
9.1	7.2	5.14	3.94	4.15	1.9	4.38	3.43	3.62	3.78
1.68	9.42	6.98	3.85	3.44	4.45	3.67	3.78	0.15	4.95
0.1	2.05	2.72	4.53	4.57	4.53	4.48	2.57	2.66	4.72
0.07	2.52	0.97	0.8	0.59	0.05	0.26	1.3	0.71	0.47
0.28	0.52	0.17	0.17	0.15	0.23	0.18	0.19	0.17	0.14
0.08	0.1	0.02	0.02	0.02	0.01	0.02	0.02	0.01	0.02
6.83	2.05	2.77	5.59	4.91	1.55	4.59	4.95	2.68	5.6
99.42	99.57	99.32	100.53	101.22	99.45	99.46	99.73	100.25	99.52
174	204	111	143	147	218	162	192	269	140
54	27	22	26	25	35	29	27	36	26
4300	40	8	1	1	180	1	43	17	55
0.5	3.1	ND	ND	ND	ND	0.5	1.6	ND	ND
50	1400	520	310	50	80	92	390	180	170
ND	ND	ND	ND	ND	ND	ND	ND	ND	ND
480	650	90	58	61	22	39	67	20	83
79	680	ND	ND	ND	ND	17	21	ND	ND
5	48	23	19	13	3	5	28	19	10
46	628	385	127	197	314	304	179	40	177
199	220	ND	ND	ND	ND	150	160	ND	ND
3.22	7.56	5.05	5.50	5.88	6.23	5.59	7.11	7.47	5.38

CS98-192B Camnet VDF Felsic lava	CC98-384 Camnet VDF Felsic lava	CS99-2504 E. Camnet VDF Felsic lava	CS98-194 Cambior VDF Felsic lava	CS98-198B Cambior VDF Matrix	CS98-199B Cambior VDF Fragment	CS98-200 Cambior VDF Int. lava	CS98-202A Cambior VDF Fragment	CS98-203 Cambior VDF Felsic lava	CS98-210 Cambior VDF Felsic lava
71.9	72.1	64.8	68.9	70.2	69.8	64.5	65.5	73.7	73.7
0.37	0.34	0.82	0.77	0.87	0.89	1.21	1.14	0.65	0.78
11.5	15.7	15.8	12.7	13.7	14	13.9	15.1	14.2	13.1
1.9	2.38	5.64	4.73	5.5	4.81	6.85	2.11	1.01	2.43
0.06	0.03	0.04	0.1	0.07	0.07	0.09	0.08	0.03	0.01
0.59	0.51	2.37	0.74	0.74	0.88	1.64	0.49	0.06	0.38
3.98	1.33	0.49	2.68	1.36	1.56	5.46	5.41	1.54	1.33
4.91	7.63	5.77	4.96	4.46	2.6	2.52	3.19	4.63	5.27
0.46	0.28	0.79	0.64	1.09	2.57	1.34	2.36	1.88	0.58
0.07	0.05	0.39	0.19	0.19	0.22	0.23	0.28	0.15	0.21
0.01	0.01	0.02	0.01	0.01	0.01	0.02	0.04	0.01	0.02
3.58	1.01	1.99	2.98	1.12	2.15	2.88	3.68	2.03	1.7
99.33	101.37	98.92	99.4	99.31	99.56	100.64	99.38	99.89	99.51
235	234	236	246	278	273	207	152	284	250
38	59	35	42	42	43	34	36	47	41
12	8	14	56	36	42	51	49	15	70
ND	ND	51	ND	ND	ND	ND	ND	ND	ND
74	50	ND	130	170	640	410	470	410	130
ND	ND	20	ND	ND	ND	ND	ND	ND	ND
20	20	64	20	20	20	31	200	20	20
ND	ND	24	ND	ND	ND	ND	ND	ND	ND
9	5	21	17	33	74	41	68	39	15
116	103	64	241	96	174	211	210	130	86
ND	ND	22	ND	ND	ND	ND	ND	ND	ND
6.18	3.97	6.74	5.86	6.62	6.35	6.09	4.22	6.04	6.10

CS98-213 Cambior VDF Matrix	CS98-217 Cambior VDF Int. lava	CS98-222 Cambior VDF Felsic lava	CS98-229 Cambior VDF Tuff breccia	CS98-250 Cambior VDF Int. lava	CS99-2137 Boul. River VDF Int. lava	CS98-156D Camnet VDF Int. lava	CS99-2096 E. Bourlama VDF Int. lava	CS99-2131 S. Manitou VDF Int. lava	CS99-2137 E. Bourlama VDF Int. lava
71.3	55.9	74.5	69.9	63.9	59.1	58.4	69.5	53.5	58
0.78	0.87	0.73	0.89	0.78	0.83	0.82	0.59	1.09	0.84
13.5	15.6	11.7	13.8	14.7	16.5	15	13.6	16.5	17.1
5.01	7.42	1.71	5.03	7.02	6.68	8.02	5.05	10	6.67
0.07	0.11	0.03	0.06	0.08	0.12	0.21	0.05	0.15	0.11
0.89	3.13	0.7	0.82	5.89	3.51	4.29	2.53	5.13	3.45
1.45	5.07	2.03	1.6	0.33	7	3.99	1.38	6.45	7.49
5.59	2.98	1.86	2.18	0.2	3.74	3.4	5.03	3.07	3.67
0.42	1.61	2.86	2.33	2.06	0.42	0.74	0.56	0.01	0.2
0.19	0.17	0.16	0.21	0.36	0.18	0.16	0.13	0.11	0.18
0.01	0.02	0.02	0.01	0.04	0.01	0.02	0.01	0.02	0.01
1.17	6.63	3.03	3	4.25	2.39	4.75	2.04	4.45	2.22
100.38	99.51	99.33	99.83	99.61	100.48	99.8	100.47	100.48	99.94
254	138	155	269	224	136	164	302	89	139
42	26	23	43	30	23	24	44	26	24
40	1	55	30	1	130	250	3	76	12
ND	ND	ND	ND	ND	78	110	32	80	58
50	410	580	420	580	ND	ND	ND	ND	ND
ND	ND	ND	ND	ND	17	23	8	27	18
20	54	34	20	92	55	120	20	72	59
ND	ND	ND	ND	ND	17	50	5	22	17
12	43	77	58	38	10	19	14	3	5
107	70	107	91	15	324	139	66	202	362
ND	ND	ND	ND	ND	31	27	18	50	30
6.05	5.31	6.74	6.26	7.47	5.91	6.80	6.90	3.40	5.80

CS99-2442 Camnet VDF Int. lava	CS98-156E Camnet VDF Mafic dyke	PR99-4330A E. Camnet VDF Felsic lava	CS99-2196 S. Manitou VDF Felsic lava	CS99-2101 Manitou Wes VDF Int. lava	CS99-2104C Manitou Wes VDF Int. dyke	PR99-4089 SW Manitou VDF Int. lava	99SL-3391 S. Manitou VDF Int. lava	99SL-3398 S. Manitou VDF Int. lava	CS99-2109 Manitou VDF Int. lava
54	59.2	72.3	57	61.5	52.6	50.8	59.9	58.4	53.4
0.8	0.83	0.44	0.84	0.96	0.67	0.78	0.98	0.78	1.01
16.5	16.6	13.7	16.1	14.9	13.6	18	14.4	15.8	18.8
7.62	9.29	2.9	5.33	6.45	8.42	10	6.65	6.91	7.41
0.11	0.16	0.04	0.11	0.1	0.17	0.18	0.07	0.05	0.1
4.41	5.24	1.2	2.55	3.82	6.85	7.6	3.78	5.35	4.2
5.23	1.07	0.77	6.17	4.55	8.66	4.98	2.82	5.04	7.73
4.4	2.2	3.68	5.04	4.1	3.34	3.11	4.92	3.71	2.97
0.43	1.72	2.04	0.49	0.25	0.33	0.04	0.29	0.27	0.26
0.14	0.15	0.29	0.15	0.2	0.38	0.08	0.2	0.14	0.16
0.02	0.03	0.01	0.01	0.02	0.05	0.02	0.02	0.02	0.01
5.97	3.93	2.24	5.65	2.77	5.13	4.82	5.81	3.39	3.41
99.63	100.42	99.61	99.44	99.62	100.2	100.41	99.84	99.86	99.46
129	164	263	150	213	137	65	196	122	178
22	26	48	28	30	20	18	29	31	31
33	100	34	45	69	10	42	6	2	67
70	93	44	66	64	70	78	67	30	90
ND	ND	ND	ND	ND	ND	ND	ND	ND	ND
24	30	4	19	19	34	35	26	21	31
66	150	20	33	96	290	130	96	71	37
25	60	1	16	35	56	31	37	24	19
11	33	58	14	6	8	3	9	6	8
238	48	93	114	274	337	160	76	183	330
31	31	19	28	27	33	52	27	29	30
5.90	6.30	5.48	5.36	7.10	6.90	3.60	6.80	3.90	5.70

CS99-2116A Manitou VDF FP facies	CS99-2123 S. Manitou VDF Int. lava	CS99-2141 S. Manitou VDF Int. lava	CS99-2104B West Manitou VDF Felsic dyke	99SL-3388 Camnet West VDF Felsic lava	CS99-2196 S. Manitou VDF Felsic lava	99SL-3421 Lamaque VDF Felsic lava	CS99-2400 Lamaque VDF Int. lava	99SL-3442 Lamaque VDF Int. lava
50.7	48.6	62	69.9	55.6	56.7	68.6	59.3	65.5
1	0.95	1.28	0.55	0.88	0.86	0.85	1.15	0.79
17.7	18.7	14.2	13	17.2	16.4	12.3	16	14.4
8.25	7.77	8.07	4.35	6.91	5.38	3.02	10.2	4.98
0.13	0.11	0.1	0.04	0.13	0.11	0.06	0.29	0.1
5.17	4.06	2.44	0.7	4	2.56	0.86	3.4	2.88
7.6	6.1	1.98	3.51	8.97	5.94	4.99	2.05	2.73
2.74	3.89	5.59	4.13	3.71	5.05	4.59	3.93	5.55
0.28	1.6	0.59	1.24	0.26	0.53	0.35	0.69	0.11
0.21	0.15	0.3	0.12	0.14	0.15	0.22	0.13	0.18
0.02	0.01	0.01	0.01	0.02	0.01	0.02	0.01	0.01
5.12	7.69	2.72	1.6	1.72	5.38	3.71	2.84	2.55
98.92	99.63	99.28	99.15	99.54	99.07	99.57	99.99	99.78
178	88	198	292	139	150	198	86	105
32	17	33	43	30	25	31	20	20
48	36	120	30	1	61	95	2	140
110	62	73	14	37	65	42	230	44
ND	ND	ND	ND	ND	ND	ND	ND	ND
24	23	16	1	20	19	11	21	17
69	64	20	20	69	31	76	20	20
35	40	5	5	18	15	7	4	18
6	52	13	28	8	15	15	23	6
330	137	147	128	215	114	205	141	147
43	36	33	20	33	28	19	52	33
5.60	5.20	6.00	6.79	4.63	6.00	6.39	4.30	5.30

Table B3: All geochemical data from the Upper Val d'Or Formation

Sample	CS98-062	CS99-2017	CC98-305B	CC98-308A	CC98-308B	CC98-321	CC98-324B	CC98-328	CS99-2013
Location	Relais	Relais	Relais	Relais	Relais	Relais	Relais	Relais	Relais
Formation	VDF	VDF	VDF	VDF	VDF	VDF	VDF	VDF	VDF
Description	Int. lava	lobe FP facies	Tuff breccia	Int. lava	felsic dyke	Int. lava	Felsic lava	Tuff breccia	Int. lava
SiO_2 (wt%)	58.50	65.2	77.8	67.2	62.8	66.3	66.3	61.4	59.1
TiO2	0.8	1.06	0.83	0.98	0.98	1.05	1.2	1.39	0.88
Al_2O_3	14.4	14.2	10.8	14.7	15.5	14.4	13.2	15.5	15
Fe_2O_3	5.91	6.09	1.71	4.71	6.3	5.57	7.38	8.25	6.78
MnO	0.11	0.09	0.05	0.04	0.07	0.05	0.11	0.11	0.1
MgO	4.66	1.38	0.39	0.55	1.27	1.75	2.33	2.31	5.06
CaO	4.52	1.62	1.16	2.05	2.53	1.07	1.1	1.69	3.13
Na_2O	4.14	6.22	2.44	4.2	4.43	6.11	4.45	4.62	5.33
K_2O	0.38	0.84	2.42	2.45	2.14	1.02	1.85	2.52	0.07
P_2O_5	0.2	0.29	0.24	0.49	0.49	0.29	0.35	0.4	0.2
Cr_2O_3	0.03	0.01	0.01	0.01	0.01	0.01	0.01	0.01	0.03
LOI	6.08	2.95	1.75	2.42	2.98	1.48	1.24	1.29	4.67
TOTAL	99.73	99.95	99.6	99.8	99.5	99.1	99.52	99.49	100.35
Zr (ppm)	145	211	175	296	313	220	250	292	150
Y	25	34	29	37	39	37	42	49	27
Cu	93	21	65	3	59	63	190	120	47
Zn	67	110	ND	0.5	ND	ND	ND	ND	55
Ba	220	ND	1000	750	600	160	330	820	ND
Co	ND	8	ND	ND	ND	ND	ND	ND	22
Cr	140	20	20	20	20	20	20	20	160
Ni	143	1	ND	2	ND	ND	ND	ND	68
Rb	9	22	37	61	60	25	42	56	3
Sr	169	92	67	112	172	64	48	118	241
Sc	27	33	ND	75	ND	ND	ND	ND	30
Zr/Y	5.80	6.21	6.03	8.00	8.03	5.95	5.95	5.96	5.56

* ND = no data or below detention limits; CC = sampled by C. Champagne; PP = sampled by P. Pilote; PR = sampled by P. Riopel; SL = sampled by S. Lavoie

99-SL-3032 Relais VDF Int. lava	PR99-4027 Relais VDF Int. lava	PR99-4049 Relais VDF Felsic lava	CS98-006 Dunraine VDF xtal tuff	CS98-020c Dunraine VDF fine tuff	CS98-024 Dunraine VDF Int. lava	CS98-031 Dunraine VDF Int. lava	CS98-033 Dunraine VDF xtal tuff	CS98-035B Dunraine VDF Int. lava	CS98-037 Dunraine VDF Int. lava
64.6	58.7	70.6	54.00	69.10	50.30	49.2	49.90	53.2	53.00
1.2	0.84	0.73	1.08	0.81	0.99	1.14	0.69	1.06	1.07
13.6	14.5	11.8	20.7	17.3	17.5	16.6	17.3	16.6	16.1
7.95	5.41	4.84	6.53	2.56	8.61	9.7	8.33	10.1	9.11
0.1	0.11	0.08	0.09	0.06	0.13	0.13	0.15	0.15	0.13
2.48	1.93	1.22	3.4	0.44	4.94	4.98	5.5	6.08	5.94
1.6	6.8	1.99	4.78	1.31	7.64	9.57	8.75	3.9	4.58
4.55	2.27	4.07	4.59	2.75	2.75	2.81	1.85	3.54	3.62
2.06	1.4	0.75	0.91	2.09	0.5	0.04	0.23	0.03	0.06
0.35	0.24	0.4	0.19	0.39	0.11	0.11	0.1	0.11	0.13
0.01	0.03	0.01	0.02	0.02	0.03	0.03	0.03	0.02	0.03
1.31	7.75	3.27	2.91	2.83	6.17	5.39	6.97	4.72	6.06
99.81	99.98	99.76	99.2	99.66	99.67	99.7	99.8	99.51	99.83
250	141	238	183	321	83	87	68	91	90
40	25	30	31	40	25	25	16	25	28
ND	61	3	120	88	38	21	46	48	73
ND	52	61	77	30	56	ND	52	ND	75
ND	ND	ND	380	350	180	50	50	50	50
15	21	8	ND	ND	ND	ND	ND	ND	ND
20	160	20	48	20	99	92	140	75	72
ND	47	2	20	35	60	ND	129	ND	74
46	43	26	20	68	13	3	7	3	3
89	190	47	194	301	231	256	212	139	145
30	30	19	33	14	39	ND	40	ND	51
6.25	5.60	7.93	5.90	8.03	3.32	3.48	4.25	3.64	3.21

CS98-040 Dunraine VDF Int. lava	CS98-040b Dunraine VDF Int. lava	CS98-041 Dunraine VDF Int. lava	CS98-041 Dunraine VDF Int. lava	CS98-045 Dunraine VDF Int. lava	CS98-081a Dunraine VDF Int. lava	CS98-084 Dunraine VDF Int. lava	CS98-093 Dunraine VDF mass. FP	CS98-098 Dunraine VDF mass. FP	CS98-101 Dunraine VDF Int. lava
54	52.00	51.2	52.20	51.50	60.70	70.50	54.00	59.5	48.90
0.77	0.72	0.8	0.75	1.01	1.38	0.61	0.81	0.88	0.81
17.4	17	16.7	15.9	21	13.5	15.2	16	16.7	16.5
7.48	6.8	7.9	7.06	6.08	6.05	2.97	5.69	6.02	9.23
0.12	0.1	0.16	0.19	0.1	0.1	0.03	0.1	0.07	0.16
5.44	4.98	7.75	7.2	2.97	1.23	0.6	1.63	3.52	5.48
8.46	8.92	8.8	9.5	6.92	5.92	1.46	8.85	5.76	10.2
1.8	1.95	2.52	2.36	3.82	2.36	3.62	3.24	3.64	1.65
0.07	0.75	0.2	0.11	1.19	1.46	2	0.52	0.28	0.05
0.11	0.12	0.09	0.11	0.14	0.27	0.46	0.15	0.15	0.11
0.02	0.03	0.13	0.13	0.03	0.01	0.01	0.02	0.01	0.05
4.51	6.26	3.65	3.93	4.53	6.21	2.27	8.58	3.01	6.26
100.18	99.63	99.9	99.44	99.29	99.19	99.73	99.59	99.54	99.4
85	76	78	75	112	196	288	140	148	81
23	19	18	18	34	30	41	25	29	21
40	97	6	7.4	71	40	78	18	47	38
ND	51	ND	59	64	70	45	51	ND	64
50	90	130	74	390	350	440	140	50	50
ND	ND	ND	ND	ND	ND	ND	ND	ND	ND
98	95	760	800	76	20	20	32	42	260
ND	20	ND	373	43	55	27	20	ND	250
3	27	8	4	32	58	81	17	7	3
212	159	163	184	176	164	158	158	196	177
ND	42	ND	39	34	31	20	26	ND	43
3.70	4.00	4.33	4.17	3.29	6.53	7.02	5.60	5.10	3.86

CS98-115 Dunraine VDF Fragment	CS98-118b Dunraine VDF Mafic lava	CS98-119 Dunraine VDF FP	CS98-137 Dunraine VDF Fragment	CS98-235 Dunraine VDF Felsic lava	CS98-236 Dunraine VDF FP	CS98-246 Dunraine VDF FP	CS98-249 Dunraine VDF FP	CS99-2326 Dunraine E VDF Felsic lava	CS99-2113 Dunraine W VDF Int. lava
62.00	52.20	49.8	77.2	65.9	60.9	66.3	58	65.4	62.8
1.62	1.01	1.01	0.74	1.05	1.36	0.77	1.05	0.79	1.16
14	15.6	21.1	12.2	12.7	16.3	15.4	14	15.4	14.1
5.93	8.44	8.47	0.98	5.9	3.88	5.05	6.49	5.57	5.26
0.1	0.17	0.13	0.01	0.09	0.09	0.02	0.04	0.09	0.08
1.24	5.31	3.55	0.34	1.41	2.67	3.43	6.12	5.35	0.83
4.94	6.36	5.5	0.39	3.95	5.61	0.64	3.62	0.35	5.42
3.23	3.7	3.53	2.25	2.85	4.43	6.37	3.91	0.28	4.16
0.67	0.11	1.54	3.54	1.25	0.38	0.43	0.05	2.2	0.9
0.24	0.19	0.11	0.39	0.24	0.24	0.37	0.35	0.37	0.24
0.02	0.03	0.03	0.01	0.02	0.05	0.04	0.07	0.02	0.01
5.1	6.43	4.58	1.28	4.83	3.54	2.31	5.68	4.13	4.84
99.09	99.55	99.35	99.33	100.19	99.45	101.13	99.38	99.95	99.8
190	104	104	235	260	175	227	217	234	178
29	24	28	41	42	26	33	29	31	27
160	110	1	22	92	66	1	110	14	110
96	120	ND	ND	ND	ND	ND	ND	230	73
670	65	760	770	250	450	160	260	ND	ND
ND	ND	ND	ND	ND	ND	ND	ND	5	12
20	103	140	20	20	220	94	390	90	20
44	79	ND	ND	ND	ND	ND	ND	26	16
33	5	59	62	41	11	10	3	40	42
251	205	299	61	107	309	82	388	223	115
35	44	ND	ND	ND	ND	ND	ND	24	52
6.55	4.33	3.71	5.73	6.19	6.73	6.88	7.48	7.55	6.59

CS99-2123 Dunraine W VDF Int. lava	CS99-2317 Dunraine E VDF Int. lava	CS99-2386B Dunraine E VDF Int. lava	CS99-2195 Dunraine W VDF Felsic lava	CS99-2385B Dunraine E VDF Felsic lava	CS99-2208B Dunraine W VDF Felsic lava	CS99-2318 Dunraine E VDF Felsic lava	CS99-2298C Dun. E -core VDF Felsic lava	CS99-2377C Dun. E -core VDF Felsc tuff	CS99-2329 Dunraine VDF Felsic lava
49	53.6	54.8	59.8	72.9	60.6	62.2	63	46.1	64.5
0.93	1.13	0.91	0.91	0.9	0.8	1.33	0.31	0.7	0.66
18.1	14.1	11.9	17.4	11.8	15.9	15.6	16.9	17.2	12.9
7.86	5.55	4.86	4.45	0.84	5.16	2.21	2.72	6.89	6.47
0.11	0.13	0.19	0.06	0.06	0.11	0.08	0.04	0.26	0.11
4.2	3.93	0.68	1.79	0.1	1.28	0.36	2.01	6.65	8.22
6.5	6.5	11.1	4.71	3.77	5.51	5.8	3.41	6.09	0.3
4.31	3.1	4.74	3.62	5.58	3.04	5.11	5.56	2.35	0.25
1.17	1.25	0.62	0.83	0.57	1	0.92	1.43	1.17	0.76
0.15	0.2	0.19	0.15	0.27	0.14	0.27	0.09	0.13	0.32
0.02	0.03	0.01	0.01	0.01	0.02	0.01	0.01	0.05	0.02
7.84	10.7	9.85	6.13	2.91	6.52	5.72	4.18	12.2	4.64
100.19	100.22	99.85	99.86	99.71	100.08	99.61	99.66	99.79	99.15
87	141	175	151	170	136	223	82	89	190
21	22	34	25	30	22	38	4	19	26
47	ND	ND	110	68	64	160	1	55	9
54	ND	ND	78	7	54	37	44	48	330
ND	ND	ND	ND	ND	ND	ND	ND	ND	ND
23	25	9	23	5	9	6	11	24	5
64	180	20	38	20	70	32	62	290	76
44	ND	ND	15	4	20	6	31	120	38
36	33	18	24	15	32	26	39	25	17
144	163	232	185	117	162	143	381	177	62
37	28	20	29	13	27	23	7	25	16
4.14	6.41	5.15	6.04	5.67	6.18	5.87	20.50	4.68	7.31

CS99-2325 Dunraine Ea VDF Int. lava	99SL-3160 Dunraine We VDF Int. lava	CS99-2295C Dun. E core VDF Mafic lava	CS99-2311C Dun. E core VDF Int. lava	CS97-092 Abitibi-Cu VDF Int lava	CS97-095A1 Abitibi-Cu VDF lapilli breccia	CS97-106 Abitibi-Cu VDF Gabbro	CS97-108 Abitibi-Cu VDF Mafic lava	CS97-110 Abitibi-Cu VDF Mafic lava	CS97-111 Abitibi-Cu VDF Felsic lava
55.9	51.5	44.1	63.6	53.50	60.00	54.40	52.40	53.80	70.80
0.89	0.76	0.77	1.14	0.69	1.13	0.82	0.82	0.88	0.68
17.3	16.6	11.5	14.9	16.50	15.00	14.10	14.30	15.90	13.50
5.53	8.44	8.29	4.35	6.59	5.50	6.24	8.96	8.64	6.67
0.17	0.15	0.16	0.06	0.16	0.08	0.12	0.06	0.12	0.05
1.27	5.15	7.74	1.89	5.34	3.30	8.83	6.43	7.60	1.37
6.25	7.6	9.18	3.46	4.84	3.86	6.23	5.77	3.03	0.31
4.36	2.71	2.63	1.14	6.46	6.86	3.46	3.45	2.66	3.46
0.96	0.13	0.33	2.56	0.18	0.02	0.01	0.26	0.79	1.16
0.15	0.08	0.48	0.23	0.17	0.30	0.23	0.25	0.26	0.12
0.04	0.02	0.06	0.01						
7.18	6.41	13.9	6.7	5.56	4.08	5.64	7.45	6.30	1.79
100	99.55	99.14	100.04	99.99	100.13	100.08	100.15	99.98	99.91
141	69	143	295	113	177	154	162	162	206
24	19	24	39	21	30	27	25	24	22
71	83	86	44	5	144	59	144	12	8
54	60	85	43	84	63	70	62	109	33
ND	ND	ND	ND	98	17	17	71	187	257
16	29	41	12	28	18	34	36	31	11
220	81	420	25	140	23	332	263	266	20
45	41	62	9.3	135	67	224	192	182	7
27	5	10	61	6	3	3	10	22	31
186	244	353	222	155	124	222	147	81	55
31	52	28	23	26	28	28	26	27	31
5.90	3.60	5.96	7.56	5.38	5.90	5.70	6.48	6.75	9.36

CS97-113 Abitibi-Cu VDF Mafic lava	CS97-114A1 Abitibi-Cu VDF Felsic lava	CS97-215 Abitibi-Cu VDF Gabbro	CS97-114A1 Abitibi-Cu VDF Felsic lava	CS99-2250 Abitibi-Cu VDF Felsic lava	CS99-2270 Abitibi-Cu VDF Felsic lava	CS99-2337 Abitibi-Cu VDF Felsic lava	CS99-2236B Abitibi-Cu VDF Int. lava	CS99-2278 Abitibi-Cu VDF Int. lava	PR99-4213 Abitibi-Cu VDF Int. lava
56.80	72.40	52.80	71.00	66.4	66.8	75.1	68.7	65.2	72
0.82	0.58	0.79	0.61	0.81	0.64	0.79	1.18	0.72	0.57
14.70	12.20	14.00	13.00	14	13	10.8	13.3	14.5	13.3
6.79	5.51	7.70	5.60	4.82	5.8	2.71	5.34	9.16	6.19
0.17	0.05	0.12	0.05	0.06	0.16	0.03	0.03	0.05	0.04
4.90	1.50	9.14	1.56	0.69	1.45	1.43	1.17	3.47	0.74
5.62	1.13	6.07	1.17	2.06	2.92	1.61	1.51	0.3	0.31
2.66	2.81	3.23	3.15	6.27	2.51	4.65	5.62	0.1	4.69
0.15	1.12	0.01	1.26	0.81	1.51	1.37	0.5	2.65	0.74
0.23	0.26	0.22	0.28	0.17	0.27	0.24	0.35	0.32	0.11
				0.01	0.01	0.02	0.04	0.01	0.02
6.88	2.48	5.85	2.44	3.18	4.92	0.99	2.09	3.51	1.45
99.72	100.04	99.93	100.12	99.28	99.99	99.74	99.83	99.99	100.16
156	150	144	154	248	157	141	235	176	147
26	27	24	26	36	32	25	31	32	30
19	5	50	1	170	2	100	80	1	230
113	37	74	38	110	61	30	79	40	19
94	301	12	305	ND	ND	ND	ND	ND	ND
23	8	36	9	8	8	8	10	16	9
92	20	349	20	20	20	93	20	20	20
73	6	230	2	1	2	31	1	1	1
4	25	3	29	20	40	34	13	55	19
198	35	216	38	68	78	105	48	20	37
28	26	28	24	21	31	22	22	34	31
6.00	5.56	6.00	5.92	6.89	4.91	5.64	7.58	5.50	4.90

CS99-2234 Abitibi-Cu VDF Int. lava	CS99-2288 Abitibi-Cu VDF Mafic lava	CS99-2265 Abitibi-Cu VDF Int. lava	CS99-2251 Abitibi-Cu VDF Felsic lava	CS99-2335 Abitibi-Cu VDF Felsic lava	CS99-2417 Sleepy Lake VDF Int. lava	99SL-3330 Sleepy Lake VDF Felsic lava	CS99-2409 Sleepy Lake VDF Felsic lava	CS99-2412 Sleepy Lake VDF Felsic lava	CS99-2414 Sleepy Lake VDF Felsic lava
53.5	63.5	64.8	70.1	63.6	60.2	65.6	75.3	63.5	77.1
0.69	0.66	1.15	0.78	1.19	0.8	1.28	0.83	0.96	0.74
13.3	12	13.1	13.6	14.8	15.3	15.3	11	12.8	11
6.01	16	6.49	4.94	6.87	6.54	2.49	4.48	7.59	2.59
0.1	0.1	0.12	0.03	0.04	0.1	0.07	0.02	0.19	0.06
7.08	2.08	2.88	1.81	3.1	4.54	0.47	1.45	1.32	2.31
6.02	0.07	2.69	0.3	1.08	2.54	2.78	0.02	2.7	0.77
3.65	0.1	2.12	5.93	5.59	3.16	4.98	0.46	1.7	0.47
0.03	1.45	1.37	0.44	1.15	1.46	1.76	2.1	2.43	1.66
0.2	0.14	0.34	0.16	0.32	0.2	0.32	0.1	0.24	0.19
0.05	0.01	0.01	0.01	0.01	0.01	0.01	0.01	0.01	0.01
8.59	2.93	4.28	1.67	2.25	5.02	4.01	3.23	5.41	2.88
99.22	99.04	99.35	99.77	100	99.87	99.07	99	98.85	99.78
130	193	227	241	217	133	211	144	170	205
22	30	38	38	34	24	33	14	27	35
36	1500	270	210	190	9	110	12	130	120
58	50	120	86	100	82	47	240	45	65
ND	ND	ND	ND	ND	ND	ND	ND	ND	ND
27	30	13	8	17	17	5	9	14	5
310	20	20	20	20	47	20	20	20	20
120	26	4	1	13	19	2	2	3	1
3	30	35	13	29	43	40	39	44	33
119	3	44	79	81	69	109	88	60	92
25	20	27	23	26	30	31	29	37	21
5.90	6.40	6.00	6.34	6.38	5.50	6.39	10.29	6.30	5.86

CS99-2460B E. Sleepy L VDF Felsic lava	CS97-216A1 Sleepy Lake VDF Felsic lava	CS97-127 Sleepy Lake VDF Felsic lava	CS98-256 Sleepy Lake HF Mafic lava	CS97-072A Sleepy Lake VDF Felsic lava	CS97-076 Sleepy Lake VDF Int lava	CS97-078 Sleepy Lake VDF Felsic lava
76.2	69.00	69.30	48.2	70.60	58.20	67.80
0.76	1.24	0.53	1.27	1.04	0.62	1.28
12	13.90	11.60	14.1	13.00	14.70	15.00
4.49	6.18	4.73	14.5	3.48	7.40	3.52
0.05	0.11	0.10	0.2	0.10	0.33	0.08
1.59	3.15	1.25	6.09	0.58	2.17	0.38
0.15	0.44	3.80	9.95	2.44	4.72	2.37
0.6	0.29	3.40	2.03	4.76	2.48	4.99
1.83	2.28	1.03	0.07	0.81	1.16	1.36
0.16	0.32	0.11	0.08	0.27	0.13	0.29
0.01			0.03			
2.31	3.07	4.23	2.65	2.96	7.72	3.28
100.15	99.98	100.08	99.17	100.04	99.63	100.35
168	230	179	59	199	123	209
30	34	29	26	27	20	33
5	55	92	98	84	133	130
39	492	72	0.6	46	65	17
ND	781	187	50	228	137	215
9	7	3	ND	11	39	19
20	20	20	95	20	247	20
7	1	2	69	14	140	21
40	41	27	3	20	22	34
64	165	42	95	106	107	106
21	34	19	310	21	24	22
5.60	6.76	6.17	2.27	7.37	6.15	6.33

Table B4: All geochemical data from the Héva Formation

Sample	CS97-030	CS97-043	CS97-217	CS97-218	CS97-220	CS97-224	CS98-256	CS98-263A	CS98-263B
Location	Sigma II	End of SL rd	Akasaba 2	Akasaba 2	Akasaba 2	Akasaba 1	Sleepy Lake	Tex-Sol	Tex-Sol
Formation	HF	HF	HF	HF	HF	HF	HF	HF	HF
Description	Gabbro	Gabbro	Gabbro	Gabbro	tuff	Gabbro	mafic lava	fel. Fragment	maf. Fragment
SiO_2 (wt%)	50.10	49.60	45.60	49.50	78.30	50.50	48.2	73.4	56.8
TiO2	1.22	1.34	1.43	1.56	0.59	2.23	1.27	0.56	0.77
Al_2O_3	14.40	13.70	12.00	13.40	9.93	13.40	14.1	11.4	16.8
Fe_2O_3	12.90	15.10	14.00	15.40	2.57	13.90	14.5	2.94	9.25
MnO	0.18	0.21	0.16	0.19	0.05	0.17	0.2	0.06	0.06
MgO	6.59	6.12	5.07	5.25	1.45	4.81	6.09	1.51	4.8
CaO	9.42	8.36	9.56	10.70	1.90	9.75	9.95	2.36	0.8
Na_2O	2.86	3.03	2.06	2.01	4.22	3.36	2.03	5.21	5.59
K_2O	0.04	0.08	0.70	0.53	0.03	0.75	0.07	0.35	2.45
P_2O_5	0.08	0.08	0.08	0.09	0.13	0.08	0.08	0.1	0.2
Cr_2O_3	ND	ND	ND	ND	ND	ND	0.03	0.01	0.07
LOI	2.27	2.46	9.29	1.48	0.84	0.92	2.65	2.24	1.89
TOTAL	100.06	100.08	99.95	100.11	100.01	99.87	99.17	100.14	99.48
Zr (ppm)	61	54	60	68	135	70	59	197	122
Y	27	24	25	26	17	23	26	25	23
Cu	29	167	131	111	26	3	98	32	1
Zn	82	80	75	78	64	70	0.6	ND	1.4
Ba	16	22	68	40	6	66	50	77	660
Co	42	45	47	55	11	43	ND	ND	ND
Cr	128	59	20	27	40	20	95	20	380
Ni	104	81	53	61	42	13	69	ND	120
Rb	3	3	29	18	3	28	3	10	86
Sr	90	113	75	119	35	109	95	53	119
Sc	44	47	44	49	16	56	310	ND	170
Zr/Y	2.26	2.25	2.40	2.62	7.94	3.04	2.27	7.88	5.30

* ND = no data or below detention limits; CC = sampled by C. Champagne; PP = sampled by P. Pilote; PR = sampled by P. Riopel; SL = sampled by S. Lavoie

CS98-263C Tex-Sol HF fel. Fragment	CS98-263D Tex-Sol HF maf. Fragment	CS98-263E Tex-Sol HF fel. Fragment	CS98-263H Tex-Sol HF fel. Dyke	CS98-263I Tex-Sol HF Gabbro	CS98-263J Tex-Sol HF tuff	CS98-266A Akasaba 3 HF gabbro	CS98-266C Akasaba 3 HF xtal tuff	CS98-266D Akasaba 3 HF FP	CS98-270 Akasaba w HF mafic pillow
75	57.9	66.4	69.3	58.2	71.9	47.8	53	60.1	50.5
0.82	0.74	0.93	0.74	1.36	0.77	0.93	0.78	0.64	1.74
11.4	17.2	13.4	14	13	13.6	15.2	17.6	18.2	13.9
2.36	6.35	4.87	5.17	13.1	3.85	12.3	9.04	5.51	13.1
0.02	0.08	0.05	0.04	0.12	0.02	0.17	0.1	0.04	0.19
1.18	3.98	2.69	1.18	2.99	0.29	7.85	4.76	2.8	5
2.11	2.26	2.44	1.75	4.36	0.8	11.6	9.18	4.22	11.2
4.93	6.1	5.03	4.97	3.1	4.55	0.83	1	4.99	2.97
0.8	1.96	1.88	0.94	0.82	2.02	0.15	0.25	0.63	0.25
0.21	0.18	0.2	0.17	0.43	0.16	0.04	0.11	0.09	0.1
0.01	0.09	0.01	0.01	0.02	0.01	0.06	0.03	0.01	0.02
0.92	2.39	1.6	1.12	1.97	1.44	3.19	3.32	2.25	1.07
99.76	99.23	99.5	99.39	99.47	99.41	100.12	99.17	99.48	100.04
177	119	162	203	224	202	45	81	105	78
30	24	32	36	83	32	17	21	25	28
2	2	62	25	13	1	130	38	41	2
ND	0.5	ND	ND	2	ND	0.5	ND	ND	0.5
210	420	460	780	230	750	50	50	86	50
ND	ND	ND	ND	ND	ND	ND	ND	ND	ND
20	540	32	20	56	20	300	100	27	31
ND	130	ND	ND	5	ND	120	ND	ND	28
25	64	60	27	27	50	6	13	15	5
92	105	74	145	185	80	106	180	48	98
ND	130	ND	ND	54	ND	260	ND	ND	420
5.90	4.96	5.06	5.64	2.70	6.31	2.65	3.86	4.20	2.79

CS98-288A HW 117 HF Sp. Dacite	CS98-288C HW 117 HF Sp. Dacite	CS98-289 HW 117 HF diabase	CS99-2055A Lapaska HF Sph. unit	CS99-2066 Tex-Sol HF felsic dyke	CS99-2067 Tex-Sol HF V1-2 massif	CS99-2153B Val-doria HF tuff (oriented)	CS99-2161A Goldfields HF massive lobe	CS99-2174D Goldfields HF Sph. unit	CS99-2216 Anamaque HF Sph. unit
73.9	70	58.5	62.6	75.7	65.8	55.5	58.8	55.1	64.6
0.45	0.46	1.36	0.83	0.58	0.93	0.89	1.04	1.46	1.13
11.6	11.8	12.3	12	11.9	13.7	17.9	13.2	11.7	14.9
4.17	7.29	15.9	8.14	2.75	6.42	9.48	10.9	13.6	5.83
0.06	0.11	0.22	0.1	0.02	0.06	0.08	0.11	0.2	0.09
2.36	4.33	1.85	1.86	0.23	2.14	3.04	3.41	1.36	1.26
1.18	0.25	4.31	4.55	2.43	4.13	6.32	6.91	6.7	3.59
3.69	0.3	3.75	3.38	5.45	4.34	3.94	1.1	4.05	3.14
0.07	1.67	0.46	0.64	0.17	1.37	0.47	0.88	0.08	2.9
0.06	0.06	0.49	0.21	0.13	0.2	0.14	0.23	0.62	0.27
0.01	0.01	0.01	0.05	0.01	0.01	0.01	0.02	0.01	0.01
1.91	3.31	0.31	5.25	0.48	1.13	2.36	3.68	5.05	2.41
99.46	99.59	99.46	99.61	99.85	100.23	100.13	100.28	99.93	100.13
383	397	251	314	141	158	182	297	190	266
143	134	103	114	26	29	48	108	82	50
3	31	1	12	58	120	1	29	3	94
ND	ND	0.8	81	9	32	36	43	110	28
50	500	230	ND	ND	ND	ND	ND	ND	ND
ND	ND	ND	9	5	13	21	11	15	7
20	20	20	320	20	40	34	130	20	20
ND	ND	1	6	5	15	12	11	1	1
3	35	21	17	6	36	15	31	4	87
73	6	98	134	76	232	199	229	79	83
ND	ND	9	23	31	31	27	27	33	40
2.68	2.96	2.44	2.75	5.42	5.45	3.79	2.75	2.32	5.32

CS99-2180E sph facies HF Sph. unit	CS99-2212A Anamaque HF Sph. unit	99SL-3366 Lapaska HF Sph. unit	99SL-3160 Tex-Sol HF Sph. unit	PR99-4055 Lapaska HF Sph. unit	CS99-2225 Anamaque HF Sph. unit	CS99-2051 Lapaska HF Sph. unit	CS99-2077B Tex-Sol HF V2	CS99-2085C Tex-Sol HF Int. lava	CS99-2209 Anamaque HF Sph. unit
65.7	69.7	71.5	60.8	64.6	66.9	57.9	58.9	60.8	56.3
0.74	0.49	0.47	1.11	0.87	0.96	1.08	1.42	1.02	0.87
15.6	11.9	13	15	12	13.9	10.5	11.7	16.3	17.6
4.09	6.31	4.21	7.35	8.59	6.4	12.9	14.6	6.36	9.13
0.06	0.05	0.02	0.07	0.1	0.05	0.26	0.22	0.09	0.07
1.33	1.76	1.08	3.28	2.29	1.06	1.01	3.16	2.89	2.92
2.24	1.63	0.9	2.16	3.53	2.22	6.26	4.04	3.67	6.27
7.58	4.61	6.47	5.65	3.73	5.49	3.79	2.78	5.74	3.9
0.06	0.4	0.04	2.16	0.01	1.03	0.01	0.37	1	0.48
0.14	0.07	0.06	0.24	0.21	0.24	0.38	0.59	0.23	0.14
0.03	0.01	0.01	0.01	0.02	0.01	0.01	0.01	0.01	0.01
1.96	2.07	1.35	1.19	2.82	1.1	5.71	2.22	1.57	2.29
99.53	99	99.11	99.02	98.77	99.36	99.81	100.01	99.68	99.98
101	387	391	180	339	234	182	186	163	174
21	118	134	32	126	33	76	72	28	45
140	62	24	95	22	170	14	77	92	4
52	63	38	24	78	26	130	100	33	34
ND	ND	ND	ND	ND	ND	ND	ND	ND	ND
46	7	6	19	11	13	7	21	13	22
150	20	20	41	150	20	20	20	35	30
98	6	3	19	8	1	1	1	27	13
3	17	3	65	3	46	3	12	35	16
105	57	72	108	221	97	78	77	131	199
28	11	10	37	23	33	34	32	33	25
4.81	3.28	2.92	5.63	2.69	7.10	2.40	2.60	5.80	3.90

CS99-2225 Anamaque HF Int. lava	CS99-2397B Valdora HF Int. lava	PR99-4176 Anamaque HF Int. lava	CS99-2158A Tex-Sol HF Gabbro	CS99-2147 Tex-Sol HF mafic lava	CS99-2164A Goldfields HF mafic lava
66.4	64.1	47.8	49.9	50.9	48.7
1.01	0.85	0.75	1.24	1.19	1.29
14.2	14.5	14.8	13.6	13.4	13.9
6.89	7.3	5.32	14.8	13.7	15.8
0.06	0.14	0.14	0.2	0.19	0.24
1.11	3.93	4.3	6.23	6.37	6.37
2.51	2.14	13.5	9.13	9.07	8.97
5.33	3.75	2.03	1.76	1.98	1.6
1	0.57	0.69	0.08	0.52	0.11
0.25	0.14	0.16	0.1	0.09	0.07
0.01	0.01	0.07	0.02	0.02	0.02
1.28	2.93	9.84	2.58	2.48	3.19
100.05	100.36	99.4	99.64	99.91	100.26
242	85	106	82	77	53
38	19	24	33	29	22
99	62	12	160	99	140
26	94	52	94	50	150
ND	ND	ND	ND	ND	ND
15	25	24	53	38	53
20	20	430	88	86	93
1	15	170	66	63	78
40	16	34	3	20	5
102	109	188	81	76	93
31	40	30	50	45	53
6.40	4.50	4.40	2.50	2.66	2.41